OPEN ACCESS

University of BRISTOL

This electronic thesis or dissertation has been downloaded from Explore Bristol Research, http://research-information.bristol.ac.uk

Author:
Radonjic, Mileva

Title:
Application of surface analysis in a study of the mechanism of alkali-carbonate reaction in concrete.

General rights
The copyright of this thesis rests with the author, unless otherwise identified in the body of the thesis, and no quotation from it or information derived from it may be published without proper acknowledgement. It is permitted to use and duplicate this work only for personal and non-commercial research, study or criticism/review. You must obtain prior written consent from the author for any other use. It is not permitted to supply the whole or part of this thesis to any other person or to post the same on any website or other online location without the prior written consent of the author.

Take down policy
Some pages of this thesis may have been removed for copyright restrictions prior to it having been deposited in Explore Bristol Research. However, if you have discovered material within the thesis that you believe is unlawful e.g. breaches copyright, (either yours or that of a third party) or any other law, including but not limited to those relating to patent, trademark, confidentiality, data protection, obscenity, defamation, libel, then please contact: open-access@bristol.ac.uk and include the following information in your message:

• Your contact details
• Bibliographic details for the item, including a URL
• An outline of the nature of the complaint

On receipt of your message the Open Access team will immediately investigate your claim, make an initial judgement of the validity of the claim, and withdraw the item in question from public view.

Application of surface analysis in a study of the mechanism of alkali-carbonate reaction in concrete

MILEVA RADONJIC

Interface Analysis Centre and Department of Earth Sciences, University of Bristol, UK.

A dissertation submitted to the University of Bristol in accordance with the requirements of the degree of Ph.D. in the Faculty of Science

December 1998

Abstract

The main aim of this study was to understand the mechanism of Alkali-Carbonate Reaction (ACR), applying a novel approach in combining surface chemistry and conventional microscopes. The empirical data has proved an evident association between the ACR and the transformation of dolomite to calcite, a process known as dedolomitisation. Therefore the study of the behaviour of a single dolomite crystal in an alkaline environment, simulating concrete conditions, in order to establish if the dedolomitisation process was of an expansive nature. The combination of spectroscopic and microscopic techniques enabled the modelling of Mg-Ca exchange in the crystal lattice and the allocation of the preferential nucleation sites within dolomite minerals.

Experimental data of this study reveals that Dolomite mineral in high pH environments transforms to two new phases, calcium carbonate and magnesium hydroxide. These changes take place along cleavage planes or similar defect planes within the crystal-lattice, such as ion-displacement and elemental impurities Fe, Mn etc. However, once established, nucleation sites initiate another sequence in the reaction which is the deposition of newly formed Mg and Ca phases. From the chemically unbalanced system, delicate (sub-micron) size brucite crystals and well developed calcium carbonate crystals are deposited on the surface of a single dolomite crystal. The same observations were also obtained in a more complex system of argillaceous dolomitic limestone, where carbonate fractions (calcite and dolomite) are surrounded by silicates (quartz and clays), with the crystal-growth taking place in a confined space. Dedolomitisation will cause expansion if the fabric of the rock is such that no sufficient space is available to accommodate the volume change. On an even higher level of complexity, with the aggregate embedded in cement paste and various admixtures, such a crystallisation within a confined space will generate sufficient force to cause a physical expansion, therefore it will have deleterious effect on the whole concrete.

Thermodynamic modelling and molar volume calculations for reactions involved also supported the volume change. However, since the concrete environment is dynamic, there are several reactions taking place sequentially, from dissolution, precipitation to hydration.

Publications

The research undertaken in this thesis resulted in the following publications:

1)Radonjic, M.; Allen, G.C., Ragnarsdottir, K.V., and Livesey, P., (1996)
Spectroscopic studies of alkali induced reactions at cement carbonaceous aggregate interfaces.
Proceedings of the 10th International Conference on Alkali-Aggregate Reaction in Concrete, Melbourne, Australia

2)Radonjic, M., Allen, G.C., Heard PJ, Ragnarsdottir V, Livesey P (1997)
Applications of focussed ion beam optical spectroscopy (FIBOS) to alkali aggregate reactivity in concrete
Proceedings of the 19th International Conference on Cement Microscopy, April 27-May1, Cincinnati, USA, pp94-102

3)Radonjic, M., Allen, G.C., ,Ragnarsdottir V, Livesey P (1997)
Study of the expansion mechanisms of alkali carbonate reaction
Proceedings of the 19th International Conference on Cement Microscopy, Cincinnati, USA, pp320-330

4) Radonjic, M., Allen, G.C., ,Ragnarsdottir V, Livesey P (1997)
Applications of focussed ion beam optical spectroscopy (FIBOS) to alkali aggregate reactivity in concrete
Proceedings of the European Conference on Microscopy of Building Materials, Reykavik, Iceland, 316-324

5) Radonjic, M, Ragnarsdottir V, Allen, G.C., Livesey P (1997)
Mineralogical changes occurring within aggregates affected by alkali-carbonate reactivity
Proceedings of the European Conference on Microscopy of Building Materials, Reykavik, Iceland, pp177-186

6) Radonjic, M., Allen, G.C., ,Elton N., Livesey P (1998)
The stability of dolomite in high pH environments
Proceedings of the 20th International Conference on Cement Microscopy, Guadalajara, Mexico, pp.357-366

7) Radonjic, M., Allen, G.C., ,Elton N., Livesey P and Farey M. (1998)
ESEM study of physico-chemical reactions at grain boundaries in concrete/mortar
Proceedings of the 20th International Conference on Cement Microscopy, Guadalajara, Mexico, pp.221-231

8) G.C.Allen, K.R.Hallam M.Radonjic, (1996)
XRD of ancient mortars
Proceedings of the 3rd International Conference on Environmental Pollution, Thessaloniki, Greece

TO MY PARENTS, SLAVOLJUB AND RADA, AND THE FAMILY BACK IN SERBIA

EXPERIMENT IS THE INTERPRETER OF SCIENCE, EXPERIMENT NEVER DECEIVES, IT IS ONLY OUR JUDGEMENT WHICH SOMETIMES DECEIVES ITSELF WHEN IT EXPECTS RESULTS WHICH EXPERIMENT REFUSES.

LEONARDO DA VINCI

Acknowledgements

During the last six years since my arrival in the UK many people have played important roles in my transformation from an *au pair* to a doctor. The list of those involved presented below is chronological as it would be very difficult to give preference.

My friends: Olga Gorjackovski, Eillen, Lindsey Staniforth, Marie Collis, Joan and David Coombs, Elena Bassi, Peter Hardy, Ann Watson, Caroline Oyedepo, Mariaelena Trivella, Haida Liang, Julie Grey and Wills Hall SCR and staff members.

The academic and scientific achievements would have been impossible without my colleagues: Sinan Al-Jassar, Stuart Kearns, Graham Meaden, Keith Hallam, Charles Younes, Peter Heard, Jaya Chakrabarti, Leon Black, Mike Holt and Ricki Williamson.

The workshop in Geology Department helped in preparing my samples. My thanks are due to Fred Wheller and Gary Weber. Many thanks to Brenda at the Castle Cement Ltd. for obtaining the literature for me at such short notices.

I must also thank Prof. Jack Gillott, Chris Rogers, and Dr. Nick Elton for their understanding and suggestions at crucial moments of my work.

Special thanks to my supervisors Dr.Vala Ragnarsdottir, Professor Geoffrey Allen, and Paul Livesey for their supervision, shared enthusiasm and for putting up with me all these years.

The research would have been impossible without the University of Bristol scholarship, the Castle Cement Ltd. sponsorship and English China Clays Ltd. travelling grant and use of their Environmental SEM and finally The Natural History Museum Mineralogy group with Dr. Gordon Cressey, to all of whom I am grateful.

Finally, many thanks to John Nicholson for **brutal** editing of this thesis. A gallon of beer is on its way.

Author's Declaration

I declare that the work presented in this dissertation was carried out in accordance with the Regulations of the University of Bristol. The work is original except where indicated by special reference in the text and no part of the dissertation has been submitted for any other degree.

Any views expressed in the thesis are those of the author and in no way represent those of the University of Bristol.

The dissertation has not been presented to any other University for examination either in the United Kingdom or overseas.

Signed: Mirela Pagoreni

Date: 3/12/1998.

Table of Contents

List of Figures

List of Tables

Abbreviations

AAR	Alkali-aggregate reaction
ACR	Alkali-carbonate reaction
ASR	Alkali-silica reaction
BE	Binding energy
BEI	Backscattered electron imaging
BSE	Backscattered electron
CSH	Calcium Silicate Hydrate
EDX	Energy dispersive x-ray analysis
EPMA	Electron probe microanalysis
ESCA	Electron spectroscopy for chemical analysis
eV	Electron volt
SEI	Secondary electron image
SEM	Scanning electron microscope / microscopy
SIM	Scanning ion microscopy
SIMS	Secondary ion mass spectroscopy
WDX	Wavelength dispersive x-ray analysis
XPS	X-ray photoelectron spectroscopy
XRD	X-ray diffraction
ZAF	Atomic number / absorption / fluorescence (correction factors in quantitative energy dispersive x-ray analysis)

Chapter 1 Evolution of Cementitious Materials in Building Construction

The human endeavour to build dwellings or houses represents one of the most basic needs for their existence. The ability to build has evolved over the years not just in skills but in the materials used. The spectrum of building materials from stone and wood on one hand, to steel and concrete on the other, has not changed. The improved properties of those building materials brought advances in the construction industry. These have been achieved by various combinations of compounds, pre-treatments of those materials, and by introducing different curing conditions of concrete.

1.1 Cement

Cements are adhesive compounds with the ability to embed and hold together fragments and particles of rocks, reinforcement and other solid materials, in any required morphology and dimension. Modern Portland cement was named after Portland stone, owing to the similarities in appearance of Portland cement concrete to the Portland building stone (Stanliey 1979). It is important to distinguish between cementing materials and cements, as there are various cementing materials: cements, limes and gypsum. However, in this study the main interest is in cement. Neville (1997) states that 'cement is to concrete what flour is to a fruit cake, and the quality of the cake depends on the cook. Cement is hence not the building material: concrete is'.

1.1.1 History

Some existing ancient structures, such as those of the Cyclopean masonry in Greece or the brick walls of ancient Egypt, can prove that the early construction works contained no cementing materials. The first examples of cement as adhesive materials were mainly composed of gypsum (Stanley 1979, St John *et al.* 1998). The term 'cement' was originally used for mortar, which in Roman times was made from a mixture of lime

[$Ca(OH)_2$] and a reddish volcanic earth (pozzolanic) found near the Bay of Naples, Pozzuoli, St John *et al.* 1998. Today's analysis reveal that the Roman mortars possessed a dense texture, almost impermeable to gases, as there are still non-carbonated lime particles present. For a long time the main classical authorities quoted on cement work were Pliny, Vitruvius and St. Augustine approximately 20 AD (St John *et al.* 1998). In more recent history, John Smeaton discovered hydraulic limes, by adding clay to lime mixture to achieve water-resistance, while rebuilding Eddystone Rock Lighthouse in 1756. The next important discovery was a cement, produced by calcining nodules of argillaceous limestone which was patented in 1796.

Hydraulic cements were replaced by Portland cements from 1850. Portland Cement, made by heating a crushed limestone with a clay material until CO_2 is expelled, was patented by Joseph Aspdin in 1824. This cement also known as proto-Portland cement, was a hydraulic lime, since due to low burning temperatures, there was no interaction between CaO and SiO_2 (Stanley 1979). The transitional product towards normal Portland cement was meso-Portland cement. The Portland cement used today is a synthetic mixture of calcium silicates, manufactured from a mixture of calcareous and argillaceous materials within a apparatus called the rotary kiln (Lea 1970).

1.1.2 Composition and manufacturing of cements

Portland cement is a mixture of limestone and clay whose chemical composition can commonly be expressed as CaO, SiO_2, Al_2O_3, Fe_2O_3 and MgO (Lea 1970, Taylor 1990). CaO and SiO_2 are the primary components of cement whereas Al_2O_3, Fe_2O_3 and MgO are minor components. The rate of setting, strength, durability and other properties of the cement produced vary considerably with the proportion of basic and acidic components in the raw materials used in its manufacture. Therefore they are subjected to careful prior analysis and selection.

In modern cement production, the starting material is a mixture of about 80 % limestone and approximately 20 % clay (Lea 1970). This mixture is ground to a slurry and then passed through the kiln. The first transformation upon the influence of heat is water loss followed by calcination; CO_2 liberation. This process reduces the primary material to 35-40 wt % of the initial amount. The material is finally heated to 1200 - 1500° C, a process

known as sintering. At this stage, the cement clinker is formed, which occurs by the adhesion of adjacent particles due to an exchange and penetration of atoms. After cooling, the clinker is ground to a fine powder together with a small amount of gypsum, $CaSO_4.2H_2O$ (2-5 wt %). The proportion of limestone in the mixture is carefully controlled, so that the cement clinker formed contains approximately 50 wt % alite ($3CaO.SiO_2$; tricalcium silicate), and 25 wt % of belite ($2CaO.SiO_2$; dicalcium silicate). There are also two less abundant components, present in no more than 10 wt %. They are: tricalcium aluminate ($3CaO.Al_2O_3$; aluminate phase), and tetracalcium aluminoferite ($4CaO.Al_2O_3.Fe_2O_3$; ferrite phase). Trace compounds are present in the form of free lime (CaO), magnesium oxide (MgO), sodium and potassium sulphates (Na_2SO_4, K_2SO_4). These are extremely important as they can influence the final product disproportionally to their amount. Another important parameter of the newly formed cement powder is the surface area, as this determines its speed of reaction with water during the manufacture of concrete (Taylor 1990; Hewlett 1998; St John *et al.* 1998).

1.1.3 Hydration and setting of cements

In cement science, it is important to understand the effect of adding water to the individual compounds. The rates of reactivity for different components differ, as well as the heat liberated by exothermic hydration reactions. The hydration also changes the thermal conductivity and diffusivity of each phase, creating a complex process of physicochemical changes (Neville 1995, Lea 1970). This results in the formation of mineralogical characteristics that give cement-paste microstructural and macrostructural properties. Figure 1.1 is a schematic presentation of sequential development of a such structure (Garboczi 1998).

Looking back through the history of cement, it becomes evident that the present understanding of the setting and hardening of cement paste originates from the work of Lavoisier. In 1756 he postulated that the hardening of Plaster of Paris could be attributed to the crystallisation of small, entangled crystals, resulting in a hard newly formed product (Lavoiser 1765, in Lea 1970). However, this theory was replaced a century later when Michaelis proposed that the colloidal gel formation was responsible for the hardening of wet cement paste (Michaelis 1893, in Lea 1970). Baykoff completed and updated this hypothesis; he suggested that the initial gel formation was

completed and updated this hypothesis; he suggested that the initial gel formation was responsible for the setting followed by crystallisation of CSH and consequent hardening of the cement paste (Baykoff in Lea 1970). Much later, in the 1970s, with the use of the scanning electron microscope (SEM) this was confirmed and a more descriptive and accurate mechanism of hydration was established. It was discovered that the initial hydration involves alite which exisat for only a few minutes. This is followed by the formation of a colloidal gel at the water/cement-grain interfaces which is composed of aluminate and silicate phases. Calcium ions diffuse into the pore solution, from which Portlandite [$Ca(OH)_2$] precipitation proceeds, leaving silica gel and creating an osmotic pressure between the two (Lea 1970). The formation of Portlandite buffers the pore solutions at a very high pH (pH 13.5).

The cement setting process takes approximately five hours at the end of which the cement paste has a heterogeneous structure (Taylor 1990). The hydration process continues for up to a month, with concurrent multiplication and growth of Portlandite and fine fibrils of CSH (Mehta 1986). The above mentioned process requires extra volume in order to accommodate the interactions of the individual components which consequently produce the strength of the end product. A brief description of the water/cement reaction will be given in the next paragraph. Alite reacts with water to form a calcium silicate hydrate and Portlandite. The hydration of alite gives cement paste the dominant mechanical properties and involves a moderate release of heat (Lea 1997). The process involves an acquisition of 40 wt % of water, whether as chemically bound or physically absorbed.

In order to accelerate the alite hydration, additional aluminate or gypsum can be added to the cement (Taylor 1990, Bye 1983). The addition of water to belite causes an almost identical hydration process to that of alite. The same reaction products are formed, the only difference being that the kinetics of the reaction is much slower and the amount of Portlandite is only two thirds of that formed during hydration of alite. The ultimate strength of concrete, although gained over a much longer period of time (up to a year), is on the same order of magnitude as that of alite.

The interaction of aluminates ($3CaO.Al_2O_3$) with water is more vigorous, and illustrated in terms of kinetics, takes only a few hours. The heat emission is almost double that of alite, which explains why the intake of water amounts up to twice its own weight (Lea 1997). Initially, C_3A and $CaSO_4$ react and as a result ettringite is formed (hydrated

calcium sulfoaluminate). The role of ettringite is to prevent rapid hydration of C_3A by enveloping those un-hydrated particles. In terms of mechanical properties, aluminates have relatively little impact on the overall strength of cement paste, and are susceptible to attack by dissolved sulphates. The other minor component – ferrite ($4CaO.Al_2O_3.Fe_2O_3$), only has a small influence on hydration process and contribution to final concrete strength. However, ferrite has a rather different role on the aesthetic level in being used to determine the colour of the hardened cement-paste.

The influence of gypsum on the hydration of cement-paste is enormous bearing in mind that it is present in only a few percent. The importance of gypsum is that it slows the activity of the aluminate compound by forming ettringite as a surface coating on the aluminate particles, providing prolonged workability of the cement paste. Two additional effects of ettringite are reducing heat liberation and thus lowering the temperatures in the cement paste. Moreover, gypsum controls the volume change of the aluminate phase under varying moisture conditions (Taylor 1990).

Finally, the free oxides of Ca and Mg react with water forming hydroxides which cause an increase in volume, leading to the appearance of micro-cracks and weakening of the final product. Sodium and potassium sulphates have an opposite effect on setting to that of gypsum, in that they speed up the process resulting in rapid setting of the wet paste. The hydration of Portland cement and formation of various phases are presented in the Table 1.1.

In conclusion, Portland cement is composed of a number of phases that react in specific ways with water. The consequences of the summation of those reactions are the setting and hardening of cement paste.

In cement chemistry, a shorthand notation is used to represent complex compounds e.g. C-calcium oxide, S-silica, H-hydrate and A-alumina. For example, CSH refers to calcium silicate hydrate gel.

The following table published in Concrete Petrography handbook of investigative techniques (*St John et al. 1998*) shows the main hydration reactions, established theoretically and some of them experimentally.

Table 1.1 Hydration reactions for Portland cement mineral phases (from Czernin 1980)

Tricalcium silicate:	$2(3CaO.SiO_2) + 6H_2O = 3CaO.2SiO_2.3H_2O + 3Ca(OH)_2$
Dicalcium silicate:	$2(2CaO.SiO_2) + 4H_2O = 3CaO.2SiO_2.3H_2O + Ca(OH)_2$
Tricalcium aluminate and Gypsum:	$3CaO.Al_2O_3 + 3(CaSO_4.2H_2O) + 26H_2O = 3CaO.Al_2O_3.3CaSO_4.32H_2O$
further developed into:	$2(3CaO.Al_2O_3) + 3CaO.Al_2O_3.3CaSO4.32H_2O + 4H_2O = 3(3CaO.Al_2O_3.CaSO_4.12H_2O)$
and finally forming:	$3CaO.Al_2O_3 + Ca(OH)_2 + 12H_2O = 4CaO.Al_2O_3.13H_2O$
Tetracalcium aluminofeerrite:	$4CaO.Al_2O_3.Fe_2O_3 + 4Ca(OH)_2 + 22H_2O = 4CaO.Al_2O_3.13H_2O + 4CaO.Fe_2O_3.13H_2O$

1.2 Concrete

The origin of the word 'concrete' comes from the Latin 'concretus' meaning compounded. In this context it is interesting to note that it is a material classified in terms of strength within the range of ordinary limestone, approximating 70 Mpa (Waltham 1994).

1.2.1 History and applications

Concrete has been described as an artificial stone made from cement, sand and various kinds of aggregates. The oldest known concrete-like material on Earth dates from approximately 5600 BC and was found in Lepenski Vir, near the River Danube in Eastern Serbia. This extraordinary material thus has great archaeological and historic value (Stanley 1979), some of examples are shown in Figure 1.2. Since then it has had its periods of glory and great use during Roman times. The Greeks used it as did the Egyptians. The Romans used a conglomerate of gravel, sand and lime or cement, for some of their buildings and pavements. The most famous of these is the Pantheon in

was cast solid, using boards as moulds.

It was, however, the invention of Portland cement in the 19th Century that established concrete as the synthetic stone in the form we know today. It has since become a most versatile building material, superior to some other building materials such as stone, wood, glass and steel, in terms of suitability, durability and cost. Almost all large structures rest on concrete foundations and there are many dedicated applications for building dams, dry docks, reservoirs, roads, piers, arches, bridges. With light-weight aggregates, concretes are made that are suitable for sound and heat insulation; for partitions that can be cut, sawn or nailed; posts, blocks, tiles and pipes. With special surface treatment, it can be used as a sculptural and decorative medium. Finally, the Trans-Tokyo Bay Project includes two 10 km undersea tunnels at one end and a 5 km bridge at the other end with two man-made islands in the middle (Dhir 1996). Figure 1.3 shows the use of concrete in modern times with examples of the Opera house and Petronas Towers.

Concrete at the beginning of the 21st century has a prosperous future ahead, being the most substantial manufactured product on the planet, second only to water in the amount used. Demands for more complex, durable and stronger structures will increase not just production but also the research and development of its properties. In his presentation entitled 'Concrete in the Modern World' at a conference in Dundee, Professor K. Mehta concluded that 'in the foreseeable future, there seems to be no alternative to concrete as a volume construction material for most structural purposes. In addition to low cost, universal availability and adequate engineering properties, Portland cement concrete has a better environmental-friendly profile than metals, polymers and ceramic materials' (Mehta 1996).

In spite of all this, concrete has its weak aspects and problems that need to be overcome. These include corrosion of reinforcement, carbonation, sulphate attack, delayed ettringite formation (DEF), and different forms of alkali-aggregate reactivity (AAR). As a composite, the properties of concrete depend on the quality and performance of its individual components namely; aggregate, cement, water, admixtures and the environment in which they are used. According to Mehta (1996) the predicted 'Golden Age of Concrete' might therefore be affected by the following;

1) Shortages of natural aggregates, caused not only by limited sources but also by

environmental constraints.

2) Increasing amounts of reinforcement steel, required for high-strength concretes, which could lead to concrete being priced out of the construction industry.
3) Perceived lack of concrete durability and expensive repair work, which could force a change of criterion from a low initial cost to that of a low life-cycle cost.
4) Aesthetics, probably the last on the list of problems that concrete faces, but will in future, be a very important issue.
5) Finally, it is necessary to mention the contribution that concrete makes to environmental enhancement/protection, which is probably once again best described by Mehta. He referred to concrete as the 'Lord Siva' (the poison-drinking God of Hindu mythology), of construction materials because of its ability to relatively safely incorporate millions of tonnes of toxic and radioactive waste (Mehta 1996).

1.2.2 Composition and chemistry of concrete

The three main components of concrete are graded aggregate particles, bound together by a mixture of the other two constituents, cement and water. The conglomeration process is achieved by hydration and hardening of cement paste around aggregate grains. Concrete, as a final product is required to be strong and durable. The strength of concrete is determined by the water/cement ratio, and so is its permeability. On the other hand, durability is derived from resistance to chemical attacks and water penetration. Therefore, the causes of concrete failure are accidental overload, intrinsic changes and environmental attack. Sulphate attack, alkali-aggregate reaction (AAR) and the corrosion of reinforcement can cause the intrinsic deterioration of concrete. An environmental attack is the result of the penetration of CO_2 (carbonation) or Cl ions (corrosion). Another important cause of deterioration is freeze-thaw (St. John *et al.*1998).

In order to have a complete understanding of any process that has a damaging effect on concrete, it is essential to combine the analytical data from the laboratory with the empirical information obtained from the field. Some of the processes are slow and long-lasting such that their prediction cannot be accurately made by simply observing laboratory specimens, where curing conditions, the sample size and other controlling parameters could interfere in with the mechanism and kinetics of the reactions

concerned. The demonstration of the importance of building materials is best expressed in the amount of yearly production, which is approximately 1.2-1.5 billion tonnes for cement and around 5-7 billion tonnes for concrete world-wide. At the end of the 20th century, Portland cement concrete is the most commonly used building material because of its low cost, availability, versatility, adaptability and ability to meet the requirements of a demanding construction industry (Dhir 1996).

1.2.3 Prospects

Although there is no other economic alternative to cement as a binder in concrete for modern structures, the production of Ordinary Portland Cement (OPC) faces opposition from environmental groups. The reasons are that cement production is an energy-intensive process, and also it produces world-wide one billion tonnes of CO_2 per year. This amounts to approximately 5 % of the worlds' CO_2 emission. A partial resolution to this problem is to use blended cements which contain up to 50 % of supplementary cementing materials (SCEM) such as pulverised fuel ash (PFA) and silica fume (SF) (Dhir 1996). Blended cements are already used in the UK, Belgium and France, with a growing tendency for their production world-wide.

1.3 The role of Aggregate in formation of concrete's properties

1.3.1 Minerals and Rocks used as Concrete Aggregates

The aggregate particles in concrete are dispersed through and held together by the matrix of hardened cement paste. Some of the first definitions of aggregates suggested their use in concrete mainly for economic reasons, being cheaper than cement. However, with present understanding of concrete, it is obvious that aggregate increases the volume stability and durability of concrete (Neville 1995). Almost three quarters of concrete's volume are occupied by aggregates. Therefore it is obvious that the quality and performance of an aggregate will determine the overall durability of concrete (Smith and Collis 1993). The essential property of an aggregate is to promote within the concrete the required strength and abrasive resistance. The aggregate should preferably be chemically inert or, if reactive, should have no adverse effect on the setting, strength and durability of the concrete (Neville 1995).

Based on their origin, aggregates can be divided into three main sources (Manning 1995).

a) Sand and gravel, derived from quarries and dredging.

b) Crushed rock, derived from hard-rock quarries, and

c) Recycled or secondary aggregates derived from building demolition or refurbishment.

Heavy aggregates include natural sand, gravel and crushed rocks, which have been shown to be weather-resistant. Artificial aggregate materials include broken bricks and air-cooled blast furnace slag. The latter is widely used to produce reinforced concrete and large pre-cast concrete objects (Smith and Collis 1993). The air-cooled slag is in effect cooled slowly, in order to develop a crystalline rather than glassy, structure. Crushed concrete from demolished structures is used more and more as a source of aggregate. Light aggregates include natural pumice, furnace clinker, shale, slate, exfoliated vermiculite, foamed slag, asbestos and saw-dust (Smith and Collis 1993).

The annual consumption of aggregate is 5 billion tonnes world-wide (St John *et al.* 1998). Because of this, it is an increasing problem to obtain good aggregate. It is therefore important to learn how to use marginal natural aggregates and to increase the utilisation of aggregates produced from industrial wastes.

In this study, only natural concrete aggregates which compositions are defined as calcareous will be considered. Only some of the carbonate rock-forming minerals actually have a significant effect on the quality of concrete. The properties of these minerals, such as their stability in alkaline environments, can affect concrete. Therefore mineral identification is a necessary step for predicting the properties which may influence the behaviour of the material for the intended use (Mather 1950).

1.3.2 Testing

A thorough examination and assessment of aggregates is conducted by petrographic methods and various technological tests. Petrographic methods are used to determine the properties of rocks and their constituent minerals that may affect the performance of

concrete in the intended application (Dolar-Mantuani 1983). Of particular interest are properties that might influence the durability of concrete. The durability of an aggregate is dictated by its interaction with the matrix components in which it is embedded, and also other elements in the surrounding environment. Durability in this context is defined as a material's resistance to deterioration and disintegration when in contact with various agents, whether in micro-environmental conditions in concrete (high pH pore solution) or climatic conditions around the structure.

Most reactions within the aggregate that are induced by cement-pore solutions are due to the presence of undesirable phases within aggregate. This explains why their identification is very important. As fully acknowledged by Smith and Collis (1993) in the following statement; 'If a material is detrimental, the petrographer should indicate in what way and to what degree it will be detrimental to the intended use'. The importance of adequate testing of aggregate prior to its use in concrete, can be reflected by the following lengthy list of properties, each of which needs to be evaluated. Some of these properties are particle shape, bond, strength, specific gravity, bulk density, porosity and absorption, moisture content, deleterious substances in aggregate, soundness, thermal properties and grading of fine and coarse aggregates (Dolar-Mantuani 1983).

1.3.3 Carbonate rocks as concrete aggregates

Quarried carbonate rocks are commonly used as aggregates throughout the world and in some countries (e.g. Canada) over 90% of the crushed rock aggregate is of carbonate origin (Grattan-Bellew 1978). In the UK, almost 60% of quarried carbonate rock is used as concrete aggregate (Smith and Collis 1993). Limestone and dolomite are widely used as aggregates in concrete, and their record of performance has so far been satisfactory in most cases. There are, however, a few argillaceous dolomitic limestones that produce excessive expansion and breakdown of the concrete when present as coarse aggregates, and also when a Portland cement contains a relatively high percentage of alkalis. This phenomenon is known as the alkali-carbonate rock reaction and is abbreviated ACR (Swenson and Gillott 1967). Therefore it should be stated that only some dolomitic limestones cause expansive reactions when used as an aggregate in concrete (Gillott 1964, Rogers 1986). In general, Dolomitic rocks wear quickly due to their softness, but can also take a good polish.

1.3.4 Classification of dolomitic limestone

Carbonate rocks form one of the most diverse groups within sedimentary rocks in terms of petrographical characteristics. Depending on which carbonate fraction is predominant they form different types of rocks (Deer *et al.* 1995). *Dolomitic Limestone* is a rock where the dominant carbonate fraction is calcium carbonate $CaCO_3$, present in more than 50 mol %. The progressive addition of magnesium carbonate will however form *dolomite* $CaMg(CO_3)_2$, the ideal composition being equal portions $CaCO_3$ and $MgCO_3$. On the other hand, if magnesite $MgCO_3$ is present as the main fraction then the rock is referred to as *magnesite* or if that percentage is less than 50 mol % *Mg-limestones*. Limestone and dolomites have a potentially good predisposition for a sound aggregate as they are the most indurated members of younger sedimentary sequences. This is especially true if they possess a dense crystalline or cemented fabric containing few cavities or high porosity, a characteristic of some dolomites. Dolomites and limestones are common concrete aggregates that originate from different polygenetic groups: detrital, chemical or biochemical. Carbonates are easily soluble in water and re-deposited. This is why their original characteristics can be transformed rapidly after deposition and lithification (Shukla and Baker 1988).

Despite considerable research and a great deal of speculation, the question of the origin of dolomite has remained one of nature's well guarded secrets (Moore 1989). Diagenesis encompasses a range of natural changes that occur in sediments from the time of their deposition to the final rock formation. The lack of an adequate understanding of carbonate diagenesis can be attributed to a prevailing tendency of earth scientists to work with newly formed or ancient sediments at a time, but not with both. As noted by Purser and his colleagues, it has been only in recent years that any significant number of scientists possessing a sufficient depth of experience in geology coupled with chemistry, physics or other cognate sciences, has attacked the problems of diagenesis (Purser *et al.* 1994). This view can similarly be applied to the dolomitic ACR problem today. In spite of the difficulties present, a sound interpretation can be based upon four factors: carbonate rocks as end products, the physical and chemical processes involved, the nature and movements of intra-stratal solutions and the starting materials. One of the aspects for an ACR study are changes within carbonate rocks that involve processes of solution and precipitation at solid-liquid interfaces, and solid state transformations.

Impurities in the original rock quarried for aggregate can also cause disruption. From ACR expansive nature and association of pyrite crystals with alkali-reactive dolomitic-limestone, as some forms of iron sulphide after oxidation can cause expansion when situated at or near concrete surfaces. Another contaminant that may have a deleterious effect on aggregate durability is clay. The two principal detrimental effects these fine materials have on concrete are increasing the water demand of the concrete and reacting with the alkaline pore solutions if present as sub-micron inter-granular inclusions in dolomite (Smith and Collis 1993).

1.4 Aims of this research

The overall aim of this study was to elucidate the complex nature of ACR by using an interdisciplinary approach. Particular emphasis was placed on defining the origin and nature of ACR expansive forces, their association with the mechanism of the chemical reactions involved and a prediction of the practical consequences that they could have on concrete structures. In order to make progress in the understanding of the ACR mechanism, it was necessary to monitor any mineralogical, chemical and physical changes within the aggregate, surrounding cement paste and most important of all, within the boundary/transition zone between the two components (Mather *et al.* 1964). The project was designed only after much compilation work on already existing data from researchers involved in ACR and related AAR studies. The compilation of experimental data obtained in various scientific fields was necessary because it provided a better understanding of the dedolomitisation process as well as the associated volume changes that are a result of this reaction. As the research and experiments progressed, further needs evolved, suggesting other directions for the research project that could not have been predicted at the beginning and even involved omitting some of the original steps thought to be necessary.

Experiments completed in this study were:

1) Monitoring of time-dependent changes such as expansion measurements based on ASTM C-586 for potentially reactive aggregate samples;

2) Microstructural changes within carbonate fraction of aggregate calcite and dolomite)

as well as possible influence of silicate and pyrite in the mechanism of chemical reactions present;

3) The detection of surface deposits in mineral/rock/concrete samples produced under laboratory conditions, compared to those obtained from concrete structures with evident ACR;

4) Establishing whether or not application of surface sensitive techniques would be adequate in cementitious materials.

The aim was to find the correlation between materials used in concrete production *(cement + aggregate + water)* and the environmental parameters, such as *temperature* and *relative humidity* as the key factors for initiating ACR. Moreover, it was desirable to produce a proposal or a model for the expansive physico-chemical reaction that was resulting in already described ACR deterioration.

This thesis therefore reports the results of a comparative study of reactions occurring in the dedolomitisation process in concrete affected by ACR compared to laboratory reacted samples and reactions observed in the natural environment.

1.5 Outline of the thesis

The thesis consists of the following chapters: Chapter 1 contains the evolution and characterisation of materials used in this study, including their composition and physico-chemical changes to which they might be subjected in real concrete. Chapter 2 gives an insight into the main achievements in the field of concrete deterioration and alkali-carbonate reactivity, particularly during the last 50 years. At the same time, it further clarifies the dilemma and controversy surrounding the mechanism of ACR. The experimental procedure, methods, standards and sample preparation techniques as well as a list of samples used are the contents of Chapter 3. The main aspects of micro-analytical and spectroscopic techniques are described in Chapter 4, concentrating on their applicability to analysing building materials.

The results obtained are presented in the next three chapters, based on the materials analysed. The dedolomitisation process and its correlation to the expansive nature of

ACR was studied on a single dolomite crystal. The experimental data related to this is given in Chapter 5 with the additional novelty of ESEM micrographs together with AFM images, used for the first time in this type of study. To a certain degree, a more complex system of a dolomitic-limestone aggregate and its behaviour in a highly alkaline environment is summarised in Chapter 6. This chapter also tries to correlate the geochemistry of carbonate rocks with their behaviour in the alkaline environment of Portland cement concrete simulated by the use of NaOH solutions. Another important part of this chapter is the attempt to use spectroscopic techniques (XPS, TOF SIMS) for detection of rapid changes at the aggregate/solution interface. Chapter 7 is aimed at a concrete case study, with data obtained on ACR affected concrete from Canada (laboratory and *in situ* samples) and China (*in situ*).

Discussion and conclusions concerning the expansion mechanisms and mineralogical transformation are presented in Chapter 8. This part of the thesis contains a broader view of the complexity of the reactions, their synergism and the effect they may have on the degradation of concrete when ACR is in question. A brief summary of the thesis with the suggestions for further research are given in Chapter 9.

1.6 Conclusions

As early as the writings by Vitruvius in De Architectura, the importance and influence of aggregates as well as other cementitious materials on concrete was described (Vicat 1837). Concrete is a major construction material of present times and all the components that make concrete will have an impact on the quality, strength and durability of concrete structures. In itself, the quest for understanding the properties of concrete is a justification for extensive and detailed study and testing of each constituent as well as their interactions, whether chemical, physical or mechanical. Only the characteristics, properties and processes that are relevant and could have an impact on ACR have been described, from as varied fields of carbonate petrology, mineralogy, surface chemistry and geochemistry, as well as cement and concrete science.

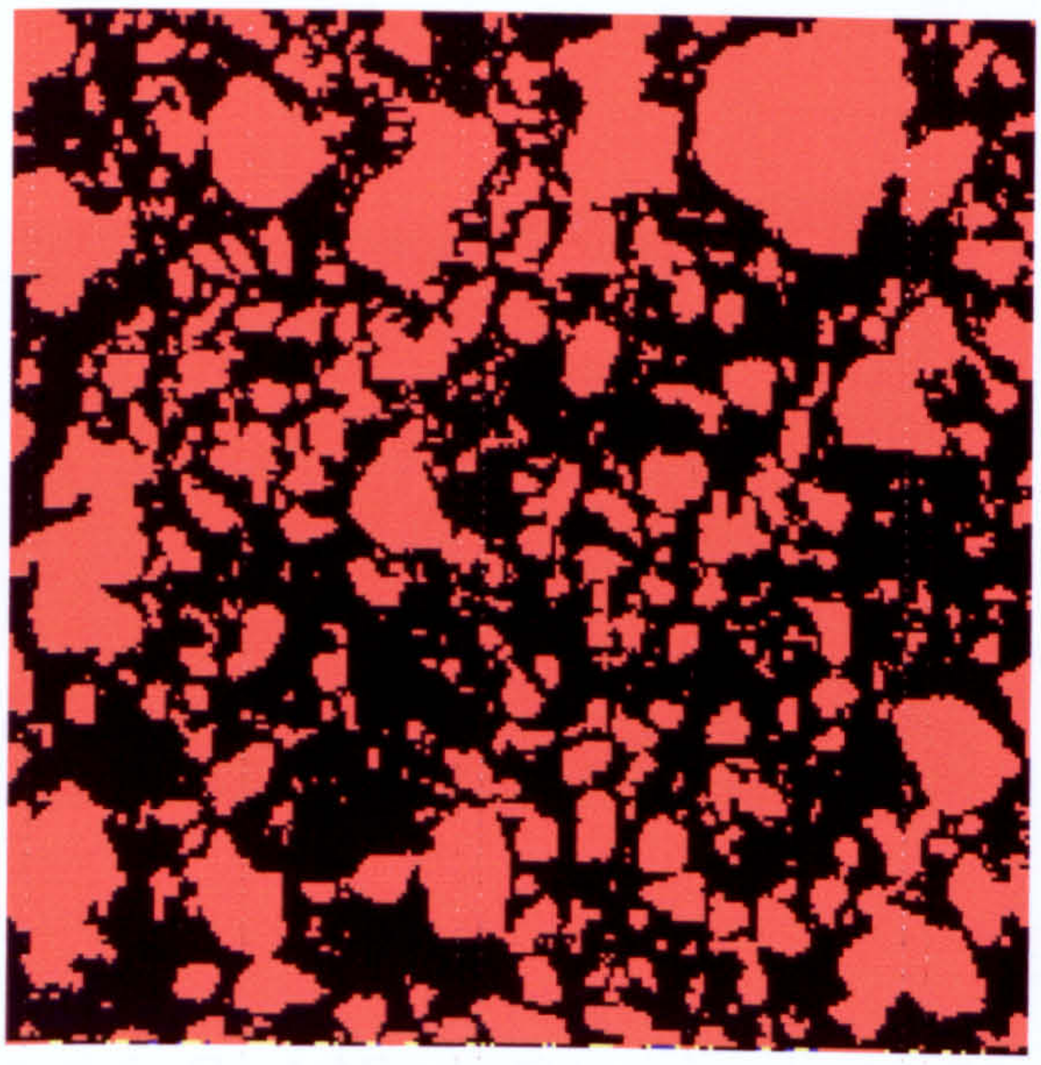

Stage 1 with 0% hydration.

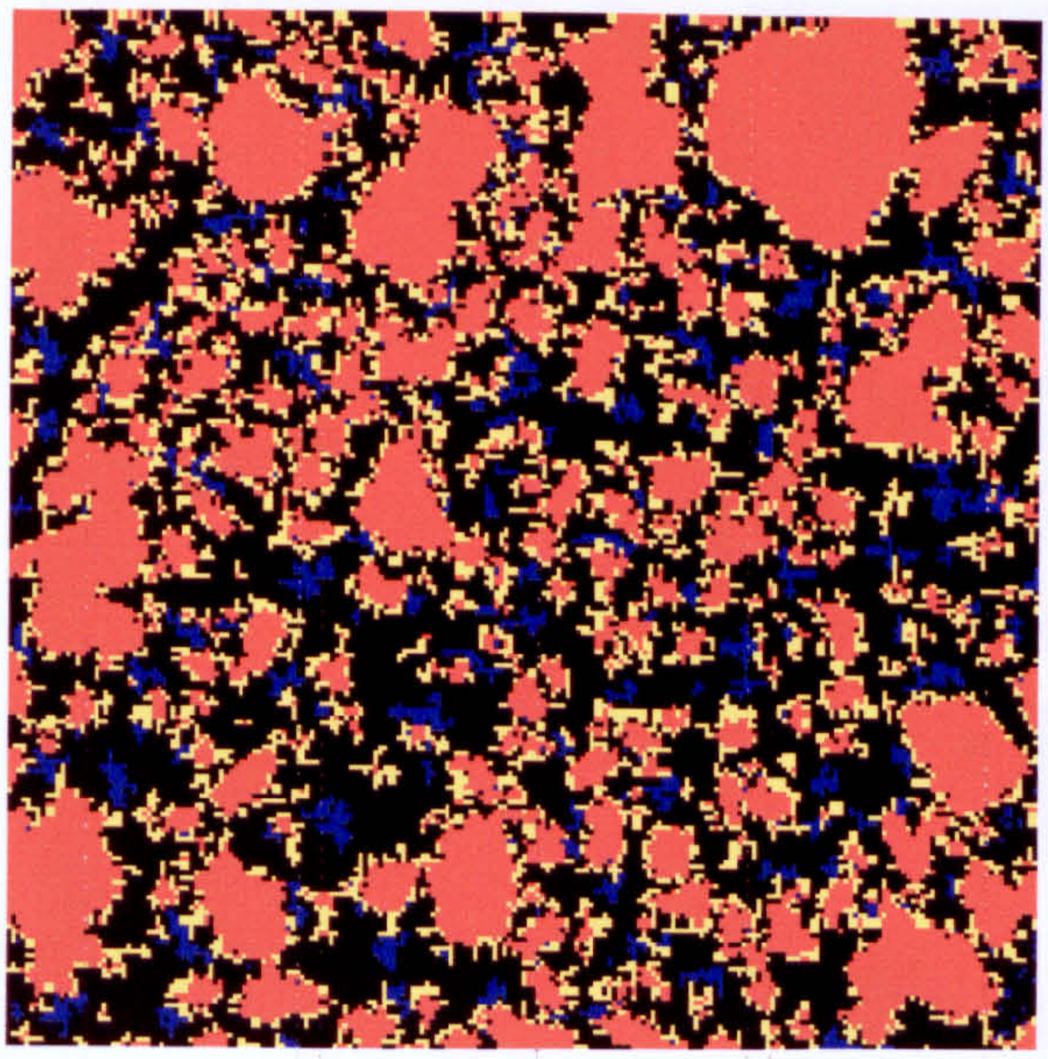

Stage 2 with 20% hydration.

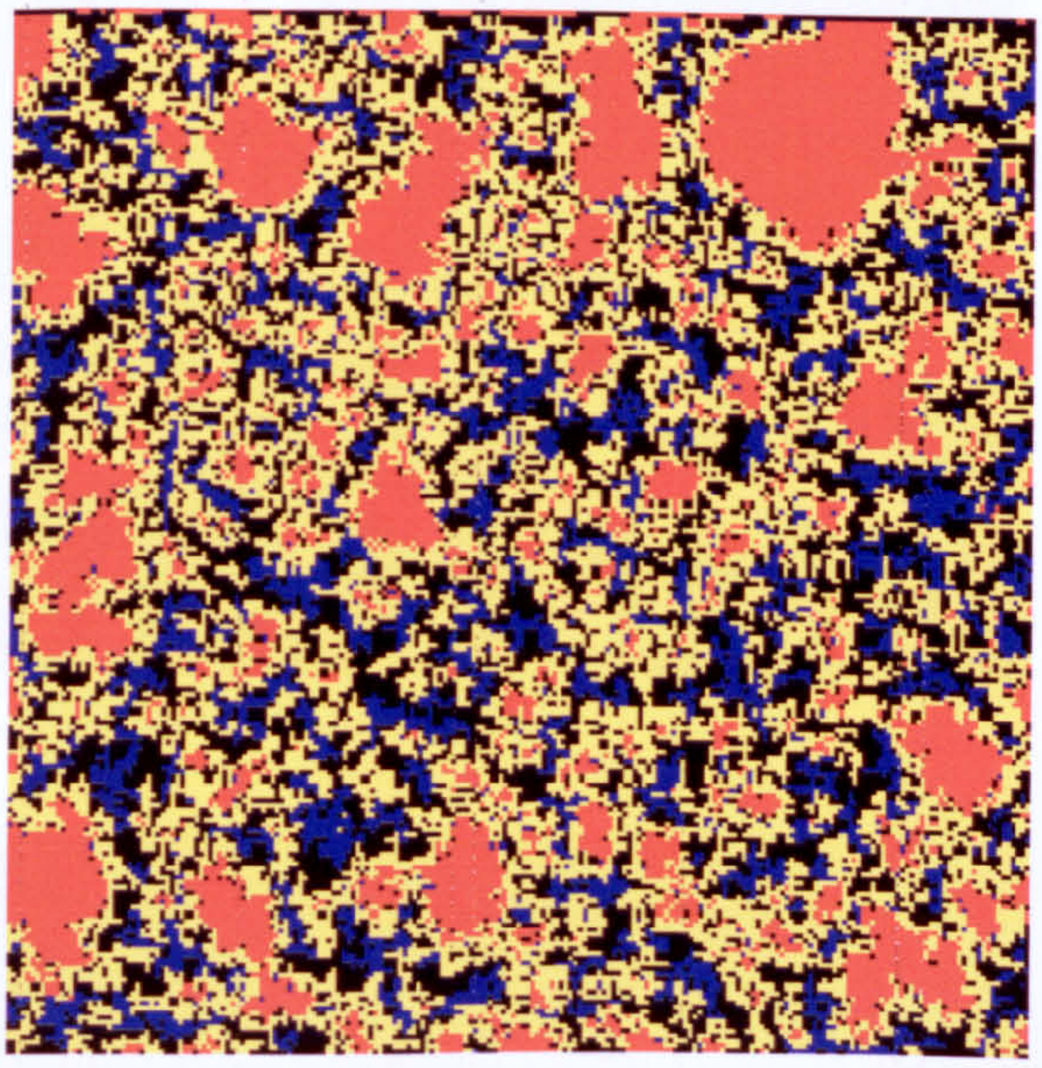

Stage 3 with 50% hydration.

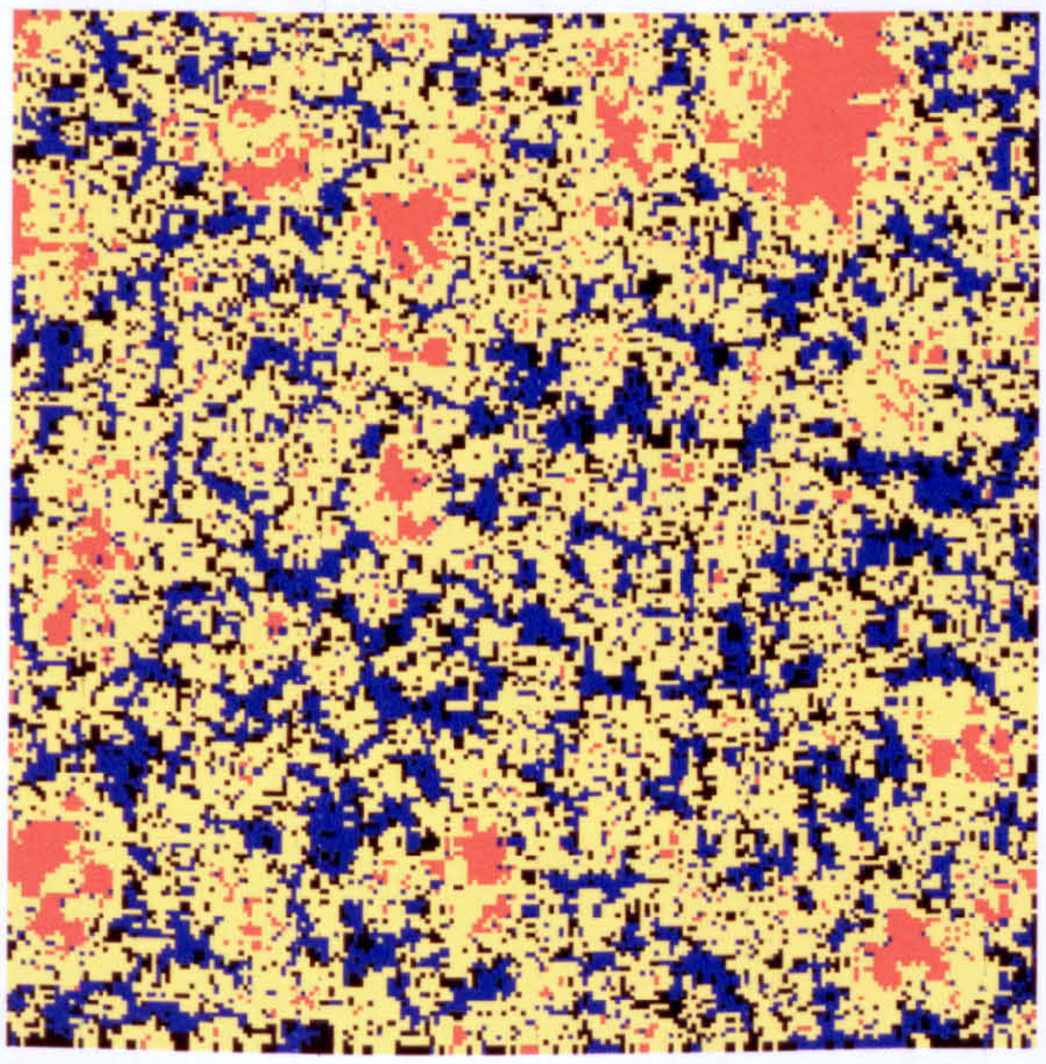

Stage 4 with 87% hydration

Red=unreacted cement grains,	**Blue=C H,**
Yellow=C-S-H	**Black=porosity**

Figure 1.1 Hydration of portland cement showing chemical hydration as a basis for the microstructure of cement (after Garboczi 1998).

Pont du Gard, Nimes, France, example of Roman construction using masonry and lime Pozzolana concrete.

Colloseum, Rome, Italy.

Panthenon, Athens, Greece.

Chichenitza Mayan Pyramid, Mexico.

Figure 1.2 Examples of Ancient building structures using cementitious materials

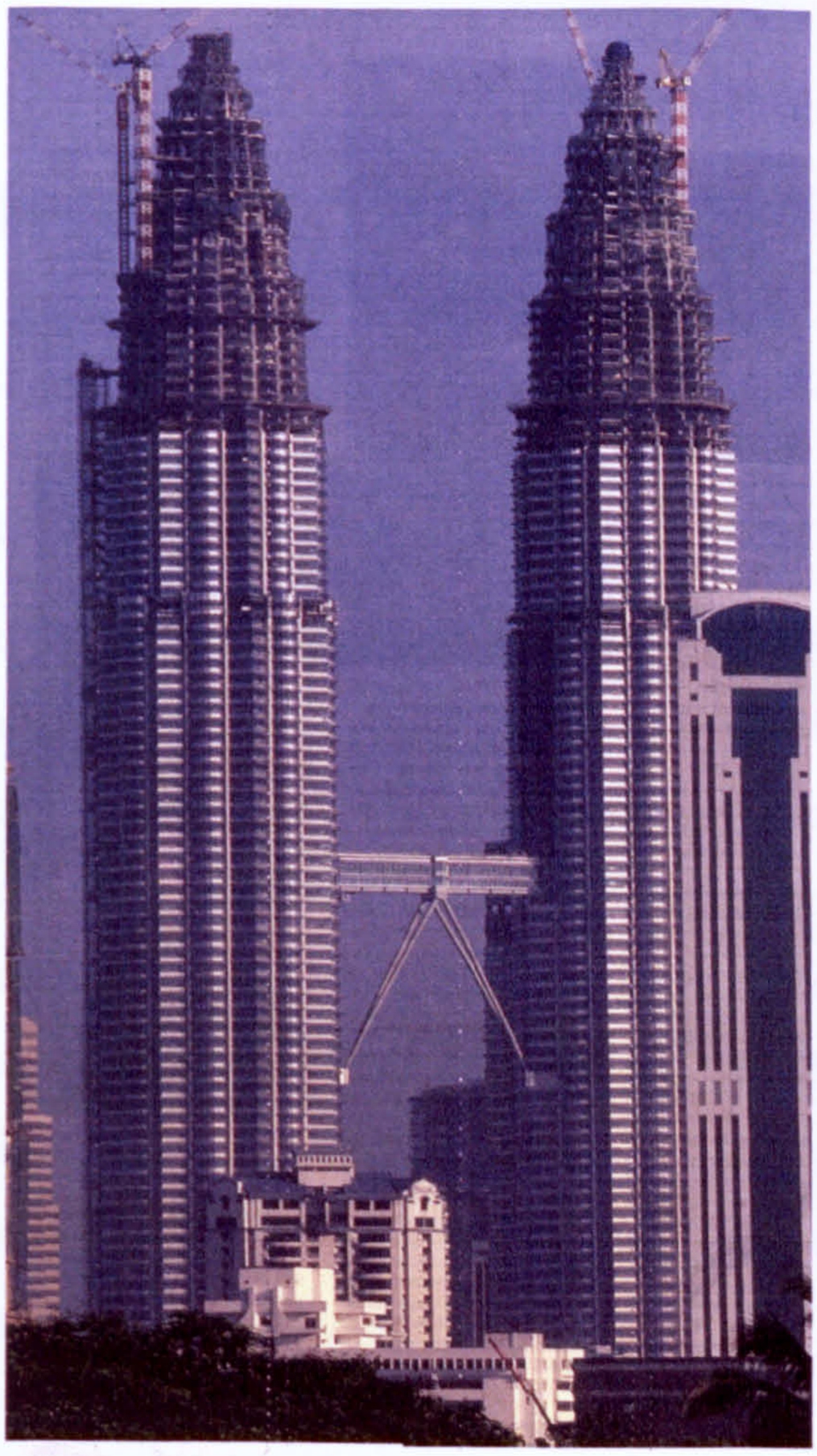

Figure 1.3 The Petronas Towers, Malaysia, the tallest building in the world at the present (453m), top image;
The Opera House (Sydney), one of the land marks of the planet is also a fine example of concrete use (lower images).

Chapter 2 Mechanisms of concrete degradation

2.1 Introduction

Concrete is defined in the Oxford dictionary (8th Edition 1990) as 'a composition of gravel, sand, cement and water, used for building' and in the Roman times the word 'concreteus' meant 'to grow together'. The durability and performance of concrete depends on the properties of its constituents, major and minor, as well as the parameters of the environmental setting in which the material is being used. The complexity of concrete as a material is best illustrated in terms of the chemical reactions and mineralogical and physical changes that take place during its manufacture and endurance. Some of these reactions are beneficial while others are harmful, causing deterioration and undesirable characteristics in the concrete structure.

In a complex material such as concrete, many chemical and physical reactions are taking place simultaneously, therefore it is sometimes almost impossible to extract an exact cause of unwanted changes. However, among other reactions such as carbonation, sulphate attack, delayed ettringite formation and corrosion of steel etc., alkali-aggregate reactions (AAR) are unique as they occur between the two major components of concrete: aggregate and cement paste (Neville 1995).

2.2 Alkali-Aggregate Reaction

Aggregate is the most abundant component of concrete, occupying approximately two thirds of its volume. Therefore its soundness is of great importance for the overall performance of concrete. There are several types of aggregates, and various classifications are used to describe their origin, composition, size and role in concrete (Smith and Collis 1993). This study is mainly concerned with the chemical interactions between aggregate and cement paste as a medium in which they are embedded, and also the consequential physical reactions. Specifically, as these reactions can be beneficial, innocuous or deleterious, with sometimes a very fine dividing line (Neville 1995), only

the later will be considered. All aggregates will react in an ordinary Portland cement (OPC) environment. On one hand, they are positive reactions, such as the grain boundary interactions and epitactic growth of portlandite at the cement paste/aggregate interface that gives concrete desirable strength and durability, or on the other hand, deleterious reactions causing deterioration of concrete. Most of the unwanted reactions will result in the poor performance of concrete, due to physical changes within the aggregates themselves or the formation of reaction products that affect the microscopical and macroscopical characteristics of the aggregate/cement interface.

The first records of aggregate/cement reactions date from the early 1940s, and were brought to the attention of the civil engineering world by Stanton. The name coined for this type of reaction was alkali-aggregate reaction (AAR), as the changes were the result of a chemical reaction between an aggregate and alkaline pore solutions of cement paste (Stanton 1942). Various types of AARs were discovered later due to the presence of a wide spectrum of aggregates used across the world. Today the most important types of AAR are distinguished based on the type of aggregate susceptible to reactivity, the mechanism of the reaction and its products (Neville 1995). These are:

1) Alkali-Silica Reaction (ASR), is a chemical process that results when some forms of silica react with alkalis from cement, producing expansive silica-gel, presence of which is manifested in map-cracking and displacement of concrete. The expansive materials are opal, tridymite, cristobalite, chalcedony and microcrystalline quartz. Figure 2.1 presents an ASR affected concrete structure.

2) Alkali-Carbonate Reaction (ACR), mainly appears when a dolomitic limestone of specific compositional and textural characteristics is used as the aggregate. Since ACR is the main topic of this study its nature and mechanisms involved will be described in detail later. Figure 2.2 shows a bridge in Canada where concrete has undergone ACR.

3) Alkali-Silicate Reaction, is yet another type of AAR, where phyllites, greywackes, and silicate glass from volcanic rocks are unstable in a high pH environment. These can cause slow and late reactions with the products, which will consequently result in a deleterious expansion.

2.2.1 Manifestations of AAR - field/laboratory observations

All AARs cause directly or indirectly, the poor performance of concrete by inducing a degree of cracking or weakening of the aggregate/cement bond, either of which is reflected by diminution of the overall strength of concrete structure. As previously mentioned, the causes of a concrete's physical deterioration are not easily identifiable, which is why the effect of an AAR can only be diagnosed after a thorough chemical and microscopical examination. Henceforth, this study will concentrate on the second type of AAR described, with only a brief discussion of any relation between ACR and the other AAR types. Deterioration of concrete structures in more than 50 countries has been attributed to AAR.

2.3 Alkali-Carbonate Reaction (ACR)

The aim of this section is to review the present state of knowledge regarding alkali-carbonate reaction (ACR). The most important case studies are summarised in accordance with their geographical occurrence in order to give a better description of the variability within the reaction and its effects. The alkali-carbonate reaction, is a type of alkali-aggregate reaction occurring in concrete containing aggregates susceptible to expansion in high pH environments (Gillott 1964, Swenson and Gillott 1967). Extensive research over the years has resulted in an accumulation of data that have provided a better understanding of AAR, especially of ASR as the major AAR sub-type. Historically, the scientific foundation of ACR was laid in the 1960s in North America. It become well researched in the Middle East in the 1970s and finally in the 1980s China and Argentina became two established strongholds of ACR research. ACR today has an enormous scientific and academic interest at an international level, based not so much on the expensive repair work and practical problems induced as in the case of ASR, but due to its controversial expansion mechanism which is still not clearly defined.

2.3.1 Alkali Carbonate Reaction in North America

The first known report on the reactivity of carbonate aggregate involved a magnesium rich limestone, containing >20 wt % of Mg with a relatively high specific gravity (2.62g cm^{-3}), low absorption (1.7 wt %) and high sodium sulphate resistance (2.8%). The

aggregate caused expansion even when the amount of the aggregate was as low as 2% and the cement used had 0.98 wt % alkali content (Stanton 1940).

The second publication from Stanton was in a report by American Society of Civil Engineers, describing various reactive aggregates: shales, cherts and impure limestones, later classified as undergoing ASR (Stanton 1942). The ASR causes were described by different investigators and attributed to: sand, unsound cement, excess water, extreme variations in temperature, faulty curing, defective concrete design, variable coefficient of expansion between different parts, electrolysis, over-stressing and rusting of metal components/elements.

The first mortar tests showed that specimens kept in sealed containers, protected against drying and leaching of salts, were undergoing a chemical reaction which caused an excessive expansion of mortar and ultimate failure. In support of the expansive theory of the Mg-rich phase, shale and chert samples containing no Mg were subjected to the same experimental procedure. Results different from those of siliceous magnesian limestone observed in that the samples did not produce any expansion when cured in sealed containers. This was unlike the curing regime in water where substantial expansion was demonstrated (Stanton 1942). It has not been determined whether the reaction in the case of this impure limestone was due entirely to some form of silica or in part to the magnesium carbonate. Based on the comparison with other ACR cases, the most likely reaction would be:

$$MgCO_3 + 2Na^+ + 2OH^- + (7\text{-}10)H_2O \Leftrightarrow Mg(OH)_2 + Na_2CO_3.\ (7\text{-}10)H_2O$$

Magnesite + Alkaline solution ⇔ Brucite + Hydrated sodium carbonate

The sodium carbonate crystallises with seven to ten molecules of water, produces an increase in volume, and thus causes an expansion of considerable magnitude, which results in stress sufficient to rupture the concrete. The molar volumes of this reaction are presented in Table 2.1. Thus, a combined volume of reacting components produce a total volume of reaction products which causes an overall increase in volume of 239% as shown in Table 2.1.

Table 2.1 Molar volumes of reactants and products for magnesite reaction with sodium hydroxide, data from Stanton 1942.

Phase	Molar weight [g/mole]	Specific gravity [g/cm^3]	Molar volume [cm^3/mole]	Sums of molar volumes
$MgCO_3$	84.33	3.04	27.70	Reactants
NaOH	80.02	2.13	37.60	65.3
$Mg(OH)_2$	58.34	2.30	25.36	Products
$Na_2CO_3.H_2O$	286.17	1.46	196.00	221.36

This mechanism was further supported by the proof that sodium hydroxide reacts with certain forms of magnesium carbonate but not with calcium carbonate. Another conclusion from these early studies is the effect of the particle size of the rock on the amount of expansion. The finely grained aggregate showed no expansion. It was postulated that the expansion was taken up in the interstices and by the gel (Stanton 1942).

The main conclusion from Stanton's work was that the principal ingredient contributing to the volume change was the $MgCO_3$ in this rock along with the NaOH from cement paste. The reactive gel typical for ASR developed in this Mg-rich aggregate and was composed of almost 50wt % $Na_2CO_3.10\ H_2O$ of the form of white deposits or incrustations. Although the paper by Stanton is considered as one of the first documentation of ASR, it would be more appropriate to describe it as a concurrent ASR and ACR reactions. The aggregate involved was Mg-limestone and the reaction that caused expansion was assigned to the reaction of magnesite and alkaline pore solutions. Previous cases of ACR, if they existed, were most likely to have been perceived as an ASR occurrence until their recognition in the late 1950s (Swenson 1957). Argillaceous dolomitic-limestone from Kingston, Canada has now become the most controversial ACR-susceptible aggregate and the reference material for researchers world-wide studying ACR.

One of the first papers attempting to describe the ACR mechanism, studied the Kingstone dolomitic limestone from Canada, (Swenson and Gillott 1960), and is seen today as the pioneering work on ACR. The reaction was reported as causing excessive expansion and cracking of concrete with none of the surface effects or evidence of any

newly formed gel-like material, that was typical for ASR. The early conclusion was that cracking within aggregate would occur at planes of weakness with the expansion of reactive rock. Parameters controlling the reaction were demonstrated to be: moisture, temperature, aggregate size and high-alkali Portland cements. Attempts to find expansion inhibitors based on experiences with ASR were unsuccessful (Rogers 1990). A partial replacement of cement by pozzolanic materials produced negligible effect on the rate of expansion. In order to explain the ineffectiveness of admixtures (BFS, SF) used, it is useful to select characteristics common to both reactions as well as those typical for ACR.

According to Gillott and Swenson, work on ACR and ASR during the 1960's showed the following:

1) Both mechanisms require a high pH, high temperature and high moisture content.

2) Both have similar rates and degrees of expansion, reduction in expansion rates with decreasing aggregate size, occurrence of rim-formation although different in appearance and evidence of microcracking in both aggregate and cement paste.

3) Differences were: an absence of silica-gel in ACR affected concrete, ineffectiveness of ASR inhibitors, and water/cement ratio had no impact. A very intriguing point of note was that uncracked parts of concrete affected by ACR remained intact, unless they had been subjected to other aggressive agents.

The interest in carbonate aggregates, mainly limestone and dolomite, was increasing as it was not always easy to distinguish between ACR and ASR. Walker 1974 carried out a general study on the chemical reactivity of carbonate aggregates in Portland cement concrete, and described the rim-formation within aggregates and a deleterious dedolomitisation reaction. The manifestation of ACR was evident in the presence of distinctive pseudo-hexagonal cracking, so-called map-cracking. The quarried rock was middle ordovician dolomite of low porosity and good physical properties.

Similar reactions were reported by Hadley (1964) on aggregates from Iowa, Illinois and Indiana, while Newlon and Sherwood (1962) found rocks susceptible to ACR in Virginia. A further report was published in the early 1960s on ASR and ACR occurring in aggregates from South Dakota, Kansas and Missouri (Mather *et al.* 1961). Aggregates in all the above mentioned cases had some common characteristics. The

microstructure of the rock was made up of fine rhombs of dolomite floating in a micron sized, aphanocrystalline calcite matrix containing disseminated clay material, with approximately equal amounts of calcite and dolomite. The rock's insoluble residue content ranged from 5wt% for early expanders to 45wt% for late-expanding aggregate.

Apart from analysing of affected concrete samples, during the early 1960s, testing procedures were being developed, and the rock cylinder method reduced the aggregate screen-testing time(ASTM). Rock prisms prepared from potentially reactive carbonate aggregates, were treated with high alkaline solutions simulating the high pH of Portland cement and their change in length was monitored in order to establish potential expansion. The only mineralogical or chemical change detectable in an ACR affected aggregate, as stated by Gillott, Swenson, Lemish and Poole in above reviewed papers, was the transformation of dolomite to calcite, brucite and alkali carbonates or hydrated alkali-carbonates, accompanied by an increase in volume that could cause disruption and crack-development .

The dedolomitisation phenomenon almost became a synonym for ACR but inspite it being the only detectable change within the aggregate affected by ACR, it could not provide explanation for the generation of expansive forces, since it was thought to be a solid volume reducing process, according to cell-volume calculations. The mineralogical change where one dolomite molecule is replaced by one calcite and one brucite is volume reducing. Data published by Hadley (1961, 1964) produced even more controversy around ACR. He proposed that dedolomitisation on the contrary was a volume increasing reaction and supporting it with the experiment on a single crystal of dolomite immersed in alkaline solution and measured for volume change. The basis of Hadley's research was to explain the role of chemical and physical factors which could influence the performance of aggregates in an unwanted direction. In an attempt to isolate parameters influencing the expansion, and the effect of alkali on each individual component (carbonates, clay and silicates), the aggregate concerned had to be studied in detail.

Since the dolomite phase was the only one 'undergoing' complete transformation, (the dedolomitization process), its chemistry and kinetics were of primary importance. In this study the dolomite composition and crystallinity were also considered, since it is rare for dolomite to appear in its ideal crystal form with a regular alteration of Ca and Mg

carbonate sheets. Most naturally occurring dolomites are well known for isomorphous substitution and imperfect ordering of Ca and Mg components within the crystal structure. However, the euhedral dolomite crystals used in Hadley's study (Hadley 1961, 1964) displayed a high degree of crystal disorder in both reactive and inert carbonate rocks.

The single crystal experiment was accompanied by a sample suite of several hundred carbonate rocks of different mineralogical and chemical composition as well as different textural characteristics. Once more, the conclusion was that the dolomite/calcite ratio was playing an important role, and the well described texture of Kingstone dolomitic limestone was present in almost all reactive rocks. Measurement of expansive forces showed that the expansion of the rock was sufficient to disrupt and fracture a hardened cement-paste. The postulated characteristics of potentially reactive rocks according to Hadley (1961) were as follows:

1) Carbonate mineralogy: dolomite is present in 40-60% wt of the total carbonate fraction;

2) Clay mineralogy: 10-20 wt % clay minerals;

3) Texture: partially dolomitized calcilutities (limestone which consists of detritial calcite particles of silt or clay size) with small isolated dolomite rhombs in a matrix of microcrystalline calcite and clay.

It is of interest to note that Hadley's experiment on the expansion of single dolomite crystal in NaOH solution has never been reproduced in any laboratory test till today. In this experiment Hadley has proved that dedolomitisation is a volume increasing reaction by measuring the length of a single dolomite crystal immersed in alkaline solution. One of the main reason for it is the slow kinetics and difficulties in measuring volume change.

Experiments on ACR rocks from Virginia gave results that agreed with those from Hadley's work on Kingston rock (Newlon and Sherwood, 1962). The rock prism test established during 1960s, produced the evidence for a linear relationship between concrete expansion and a prism made from the coarse aggregate rock, suggesting that the prism test was indicative and able to predict concrete performance. The other new observation was that there was a decrease in reaction after 2-3 years.

A detailed study of the petrology of the Kingston rock was given by Gillott during

1960s, showing the importance for the understanding of the rock characteristics for ACR susceptibility. This study included a comparison between expansive and non-expansive rocks of similar composition and additional observations on reactive rocks prior to and after the treatment with alkaline-solutions. The untreated rock was composed of a carbonate fraction, where the calcite contained Mg in solid solution with Ca resulting in smaller lattice spacing. In contrast, dolomites that were enriched in Ca ions above the optimum 50 mole %, causing an extended lattice spacing due to the larger ionic radius of Ca substituting for Mg ions. The clay content was dominated by illite and chlorite, typical non-swelling sheet-silicates.

The other noticeable component of the carbonate rock was the presence of sulphur of organic origin as well as pyrite crystals. Textural characteristics are represented by well formed dolomite euhedra up to 0.05mm in diameter with symmetrically arranged inclusions of calcite and silicate grains. The dolomite crystals are evenly distributed on microscopic scale, which dissimilar to the macroscopic segregation of dolomite and larger crystals of spary calcite are easily observed (Gillott 1964, 1967). Porosity is 0.5%. The reactive beds of the Kingston dolomitic limestone differ from their non-reactive equivalents. They are less dolomitic, less detrital quartz is present and they are less porous. The Ottawa Valley dolomitic limestone, another also reactive aggregate is less dolomitic, formed in a more energetic sedimentary regime in contrast to the low-energy environment deposition of the Kingston rock. Gillott concluded that the main changes detectable in the dolomite component of the rock after the rock/alkaline solution interaction for various lengths of time (6 months to several years) and ambient to elevated temperatures (25-80°C) are:

1) An increase in unit cell size of dolomite induced by alkaline environment and established by using XRD measurements;
2) A weakening of 3-order reflections, supported by XRD diffractograms;
3) Diffuseness in reflections with strong c-axes components.

According to Gillott these criteria are all based on the changes detected on dolomite crystals within reacted carbonate rock. They suggest that dedolomitisation is the only reaction present and therefore that ACR mechanism is related to the dedolomitisation reaction. However, crystallographic calculations at that time suggested that dedolomitisation is a volume reducing process.

When the aggregate of the same rock was analysed after being extracted from concrete, the presence of silicification rims were noted, which suggests Si migration from cement paste into the outer regions of aggregate particles (Gillott 1964).

In a review paper on ACR published in 1964, Swenson and Gillott presented results from the study that included ASTM tests, concrete beams expansion test, rock prism test, powder cell test and petrographic criteria as the main methods for the testing and identification of potentially reactive aggregates. Another novel point made in this paper was the experimental evidence against the release of residual elastic strains as an explanation for the expansion mechanism, since powdered Kingston rock, also expanded in NaOH solution.

Dedolomitisation as a possible cause of expansion showed that the products of complete dedolomitisation such as pirssonite ($CaNa(CO_3)_2.2H_2O$), and gaylusite ($Na_2CO_3.CaCO_3.5H_2O$) were unlikely to form in concrete, as they would require a saturated solution to precipitate from, and they were the only phases demanding a much higher volume than dolomite. The alkaline carbonates are also soluble and there was no XRD data to support their presence. The powdered compound of the same mineralogical composition as the reactive rock, was completely dedolomitised by alkaline treatment, although neither expansion nor water imbibition was observed. An important observation was that the treated rock did show an increased surface area accompanied by an increased capacity for water uptake. In a summary of the review, Swenson and Gillott (1964) postulated that active clay in the form of inclusions in dolomite crystals, released by dedolomitisation, will be susceptible to water uptake and the swelling forces induced will cause the expansion.

The mechanism and kinetics of expansion processes within carbonate aggregates undergoing ACR soon became an academic research topic. This is particularly well illustrated in Gillott's paper on the comparison between the cell test, which monitors changes in the solid volume, and the dilatometer test, which registers the change in volume of the entire system (liquid and solid). The results obtained by Gillott (Gillott 1964) showed that dedolomitisation caused a volume increase of the entire system, but not of the solid fraction only.

The density of water at the surface of the solid phase was different from the bulk liquid, probably due to the ordering of water molecules taken up by clays. The possibility of the

fine crystal deposition newly formed as a result of dedolomitisation within restricted spaces was not supported by XRD. The conclusion was drawn that the expansion of the Kingston rock resulted from the formation of a hydrous double layer on the surface of clay minerals, after they have been freed by the dedolomitisation process from their incapsulating dolomite hosts. This was further supported by the experiment in which Kingston rock was powdered down to 1μm and immersed in an alkaline solution. The experiment showed no detectable expansion (Gillott 1964).

Swenson and Gillott (1967) also investigated the relevance of the geological age of the rock on its expansive nature, suggesting that the burial pressures involved in sedimentological processes would result in dehydrated clay minerals locked within interlocking dolomite and calcite crystals. This was supported by an experiment on rock wafers preheated to 490°C, used to simulate the formation of channel-microcracks, similar to those produced by dedolomitisation. The amount of expansion was considerable. A good correlation was also established between expansive reactivity and the specific surface area of dolomite, as well as calcite to dolomite ratio with the optimum at the value of 50/50 mole wt%, except for the coarse grained samples.

The ground work on the mechanism of ACR and probably one of the most referenced hypothesis on the ACR expansion, was summarised by Gillott and Swenson (1969) and it is as follows:

1) The dedolomitisation reactions open up channels for the pore solution, and the imbibition of previously dry clay inclusions will generate sufficient force to cause the expansion of aggregate and distress in concrete;
2) Dolomite grain size must be less than 75μm in order to provide a sufficient specific surface area;
3) Most of the clay component is distributed close to the dolomite grains;
4) The rate of reaction is affected by temperature (T), moisture content as relative humidity (RH), alkalinity (pH) and aggregate particle size;
5) The crystalline order of the dolomite fraction, rock porosity and permeability, amount and type of clay minerals in the matrix have no significant impact on the reaction

UNIVERSITY OF BRISTOL LIBRARY

In 1980, Gillott confirmed once more that although dedolomitisation was not responsible for aggregate expansion, the two processes were related and the rate and kinetics of dedolomitisation showed a linear relationship with the expansion. The cause of the expansion was suggested to be moisture uptake of illite and chlorites from their dry state, and the development of expansive forces was explained as surface hydration and build up of double hydrous layers around clay minerals.

In the late 1970s there was an increased number of ACR cases observed in Ontario, Canada. Rogers (1979) provided an explanation for these ACR cases. He attributed them to the increased usage of alkali enriched dust in cement which was recycled into the kiln to keep the cement clinker firing temperature low. A maximum alkali-level of 0.6 wt % (Na_2O equivalent) was introduced as a preventive measures, since some of the aggregates were generally slow/late expanders.

Pagano and Cady (1982) also approached the problem of alkali-reactive carbonate aggregates from a different angle. They agreed that all already established hypothesis for the ACR mechanism (chemical mode, mechanical model and osmotic mechanism model) had a common factor, the dedolomitisation reaction. Their research resulted in the proposal of the potential admixtures for combating expansion, based on preventing the following mechanisms by using the suggested admixtures:

1) Hadley's osmotic swelling mechanism based on concentration: here it would be desirable to equalize the ion concentration on either side of the clay semi-permeable membrane, thus eliminating the swelling potential. However, this cannot be easily done as there must not be any interference or alteration of hydration, setting and strength of the cement paste on one side, or contribution towards the dedolomitisation process or any other deleterious expansive reaction products on the other side. The suggested admixtures were LiCl and Li_2CO_3.

2) Swenson and Gillott's mechanism: here it would be necessary to prevent the double hydrous layers formation on clay surfaces. If the reaction was responsible for the expansion, then to inhibit the process it would be necessary to incorporate ions of smaller ionic radii with higher valence, since the swelling potential of clays depend on the pH of the solution, valence of cation species, ion size and ion concentration.

Increasing the ionic concentration, or valence of cations available to the clay mineral and decreasing the ionic radius with a reduction in the pH value will tend to decrease the swelling potentials.

The conclusion was that a high-valence cation with a small ionic radius therefore high mobility to migrate through rock-pores to the exchange sites on clay surfaces, such as $FeCl_3$ (iron chloride) or DMSO (dimethyl sulfoxide), would be effective. Although $FeCl_3$ outperformed Li_2CO_3 in terms of its effectiveness on the reduction of the expansion, the disadvantages were that it caused accelerated setting time and corrosion of the reinforcement (steel).

To support 'the clay-swelling' model as a cause of expansion, Gillott (1986) demonstrated that clay-water interactions depend on the nature of water and the composition and microstructure of clays, (personal communications with Gillott on 'not swelling but absorption' process involving clay fractions). The reason for the high reactivity of clays in aqueous solutions is due to their high specific surface area, which is a result of the small grain size, platy and fibrous clay crystals. If these type of crystals are present as inclusions within dolomite, their stability will be sufficient in order to react with alkaline solution. To illustrate this the following example is used smectite generally has 760m^2/g and kaolinite 14-40m^2/g) as well as the polar nature of water molecules. Gillott (1986) concluded that the expansive nature of aggregate in Portland cement concrete was closely related to the presence of a sufficient amount of water, since potentially highly expansive concrete and mortar specimens stored at low relative humidity show no expansion. He suggested that because of a large number of controlling factors, the effectiveness of preventive measures for ACR will have to be extended over a significant time interval and to include all the relevant parameters for a potential expansion/deterioration.

In 1986, Rogers reported that over 130 structures were affected by ACR in Ontario, and in some cases the life of ACR concrete was reduced to five years. The reason for this was that ACR caused the development of initial cracking, later used by other aggressive agents such as chlorides and moisture for their access paths. He further explained that the penetration of such species into the concrete accelerated the damaging effects of ACR. In spite of all the precautions and some 100 papers published on ACR during the

early 1980s, the number of ACR cases in Ontario alarmingly increased, especially with aggregates from the newly open quarries. A quick chemical test was used to determine their reactivity, showing that the weight percentage of CaO, MgO and Al_2O_3 could effectively be used for screening potentially reactive rocks, since alumina was only present within the clay fraction (Rogers, 1986a).

During the 8th International Conference on AAR in Kyoto, 1989, results were reported from samples where cement paste was casted in contact with a single aggregate particle previously polished (Carles-Gibergues *et al.* 1989). Observations of a two-year old composite-sample revealed the following:

1) Large amounts of secondary calcite were present within the transition zone on the cement side, suggesting that precipitation of calcite as a dedolomitisation product can occur at a large distance from the reaction site, probably as a result of the dissolution-diffusion precipitation mechanism.
2) At the same time the aggregate side of the transition zone was enriched with Mg phases, thought to be brucite, another dedolomitisation product, which is unlike calcite insoluble under high pH. Therefore an '*in situ*' solid residue after dedolomitisation was formed. These results were confirmed by microscopic observation on field concrete samples (extracted aggregate particles) (Fournier 1986).

The problem present in Canada was the discrepancy between the results obtained from the samples subjected to the Canadian Standard Analysis (CSA) and the field performance of concrete. It was observed that the expansion in the conventional CSA was only half of the expansion measured in the field after 5 years. The reason for this was thought to be the leaching of alkalis from the concrete in laboratory conditions, which suspended the expansion process. It was suggested that the storage of concrete prisms in 5wt % NaCl solution or at 38°C in moist environment would give more accurate results of potential expansion in the field. The same study also revealed that the cracking of concrete due to ACR would increase water access as well as reduce the average compressive strength to 55% of its original value after 5 years (Williams and Rogers 1991, Rogers and Hooton 1992).

2.3.2 Alkali-Carbonate Reaction in The Middle East

During the mid-seventies alkali-carbonate reactivity was reported to be causing problems in the Middle East, and some of the features there were slightly different from the North American cases described earlier (French and Poole 1974).

The most important novelties in Middle Eastern ACR were the different types of aggregates as well as the severe climate to which the structures were exposed. It became obvious that under certain conditions, dolomites other than Kingston-like rock, would be susceptible to ACR. The second important point was that there were more than one type of ACR present, according to the composition of rim-products and the effect of their expansive nature on concrete. Detailed, mineralogical and chemical data were produced and compared with similar data already available on well-known ACR aggregates. Satisfactory methods of identification and evaluation of aggregates were suggested, partially based on the empirical data from the concrete structures from Middle Eastern countries (French and Poole 1976).

The petrographic examinations conducted by French and Poole (1976, 1976a), revealed that dolomitic aggregates from Bahrain were 5-60μm grain sized particles with palygorskite and illite in the clay fraction and dolomite or gypsum lining the voids present in the rock. It appeared that additional sulphates within the aggregate and chlorides from the surroundings, together with excess hydroxyl ions and porosity, promoted ACR in a more complex fashion than in previously described ACR studies.

The evidence for ACR found in the 14 year old concrete sample was manifested in a friable, decomposed appearance in extreme cases, or soft and porous patches in less affected structures. In recent construction works the reaction was only detectable, under microscopic observation, as reaction rims around aggregate. The amount of reaction would increase in finer-grained rocks although the presence of reaction products was more evident in coarser grained rocks.

Typical features that developed as a result of ACR, reported by French and Poole (1976), were broken up aggregate particles with the marginal zone dominated by isotropic gel. Some of the aggregate fragments had bleached zones up to 1mm wide that were associated with gypsum. The carbonate fraction of the rock experienced a reduction in grain size near the interface with cement paste, and changes occurring on

dolomite grains which showed rapid dedolomitisation and growth of calcite, with fritting that was indicative of corrosion and mechanical disintegration.

According to French and Poole (1976), the above described petrographic evidence of ACR was accompanied by several chemical changes:

a) Alteration of gypsum to portlandite;
b) Alteration of dolomites, with Mg decreased markedly relative to Ca within a 1mm wide outer rim where the Mg/Ca ratio is half of the value present in the rock;
c) The liberation of silicate gel;
d) Mg-rich, Ca-deficient almost sub-μm size crystals within the reaction rim enriched in sulphur;
e) Line-profile analysis revealed that the Ca/Mg ratio in cement paste is approximately 12, and inside the aggregate the ratio is 1.19, with controversial value of 4 at the aggregate cement interface on the aggregate side.

The conclusion was that some of the reactions present were difficult to distinguish since they had products or reactants in common, but that it was probably the result of ASR, ACR and sulphate attack reactions occurring simultaneously.

Another important outcome of the Middle Eastern study was the discovery of several different ACR reaction rims. The first type involves the formation of a siliceous rim zone. The second type is manifested with a rim zone that contains no mineralogical changes but has a specific white colour. The third type, which is more common, involves the removal of Mg from dolomite fraction and formation of calcite, brucite and sodium-carbonate. The fourth type appears in a form of dark reaction rims, which occurs only in fine grained rocks that contain clays as the result of dedolomitisation reaction taking place (Sims and Poole 1980).

A further study on samples from the Middle East using a more sophisticated EPMA analysis revealed that the observed ACR may be summarised into three groups, based on the amount of expansion and the composition of the reaction rims developed (Poole 1981):

1) A non-dolomitic carbonate rock aggregate that produces no expansion when used in concrete with entirely beneficial reaction products for the aggregate cement/paste bond.

2) Reactions involving dolomitic aggregate particles embedded in cement paste, with

development of reaction rims within the aggregate that are of the same composition but discoloured but without evidence of expansion.

3) Alkali-Carbonate reaction where aggregates are from quarried fine grained dolomitic limestone, demonstrated with reaction rim zones enriched in silica at the margins and accompanied by disruptive expansions that consequently leads to map-cracking of concrete.

The EPMA data in Poole and French experiments indicated that the expansive ACR generally proceeds as shown in the equation below with subsidiary reactions involving silica and regenerated alkali assumed that the sodium carbonate was in solution:

$$CaMg(CO_3)_2 + 2Na^+ + 2OH^- = CaCO_3 + Mg(OH)_2 + Na_2CO_3$$

According to works of Poole and Sotiropoulos (1980) and Poole (1981), the reaction rim at the aggregate/cement interface is composed of three zones:

1) A dark-coloured zone that occupies the peripheral volume of the aggregate particle, and has an irregular inner margin which is enriched with Si and depleted in Mg;
2) This zone is followed by an adjacent zone of cement-paste and is light-coloured;
3) The third zone is of a darker colour, rich in silica and embedded in cement-paste on one side.

The summary was that there was clear evidence of Mg^{2+} migration into both the inner parts of the aggregate as well as the cement paste, much further from the reaction rim. At the same time, Si ions clearly migrated through the reaction rim from the cement paste and were deposited within the aggregate (Poole and Sotiropoulos 1980, Poole 1981).

2.3.3 Alkali-Carbonate Reaction in China

The alkali-carbonate reaction was also reported to be the cause of the failure of many concrete structures in China, which was brought to the attention during 1970s, and even more in the 1980s and 1990s. It is important to mention that China is one of the leading countries in the World in the amount of cement and concrete produced each year; therefore the scale of the problem was alarming. In some cases in Northern China, 80% of the structures were affected by ACR within a period of 3 years from building. The manifestations of the reaction were 0.2 mm wide and several meters long with

longitudinal cracks parallel to the reinforcement which sometimes extended 10-15 mm into the bulk concrete. In older structures, even deeper -up to 180 mm - cracks were observed (Deng *et al.* 1993). An example of the deterioration in Chinese concrete due to the ACR is shown in Figure 2.3, and the combination of ACR and ASR affected concrete is the sample in Figure 2.4.

Tang and his co-workers made a significant contribution towards the understanding of the mechanism of ACR as well as developing a rapid autoclave test procedure for identifying potentially expansive carbonate aggregates (Tang *et al.* 1983). The advantage of the new procedure was mainly in the amount of time saved, as all the test methods known required months and years for reliable results. The rapid method, using elevated temperatures and pressures enabled preliminary test results in two days. It was also valuable in assessing additional information about the mechanism of this reaction and its expansive nature.

As a result of studious work the Chinese researchers proposed a new hypothesis as an explanation for the expansive mechanism, based on the autoclave method and new experimental techniques such as STEM, TEM and Argon-ion etching for thinning samples. The STEM analyses revealed that dolomite rhombs were surrounded by a ring, composed of parallel oriented 2μm crystals that were separated by a significant amount of pore-space. Their chemical composition suggested that the interior rim was lined with brucite crystals and the outer ring contained calcite and clay minerals (Tang *et al.* 1986).

The hypothesis in the Chinese study was that dedolomitisation as such could cause expansion due to the rearrangement and growth of brucite within a restricted space, especially when the expansive forces exceed the strength of the fine-grained calcite skeleton that surrounds the space previously occupied by dolomite grain (Tang *et al.* 1986). It is important to mention that in this study not only surfaces of dolomite grains were affected by dedolomitisation but their interior spaces as well. The evidence showed that a porous product layer developed during restricted growth, therefore acquiring additional space. This suggested a rise of crystallisation pressure due to the reduction of Gibbs free energy of the reacting system.

The mechanism proposed as a result of research in China was as follows. During reaction attack with alkaline solutions, dolomite dissolves into Ca^{2+}, Mg^{2+}, and CO_3^{2-} which become hydraulic in the surrounding aqueous medium. The initial crystallisation of

brucite and calcite takes place at the boundary of a dolomite crystal, and as the dedolomitization process proceeds it has a tendency to spread towards the inner parts of the crystal. Local heterogeneous distribution of new phases occurs because new nucleation sites form at some distance from already growing crystals, due to the higher energy required by nucleation than by crystal growth. The additional complexity of this process is that portlandite-rich cement paste will consume CO_3^{2-} ions to form calcite and regenerate OH^- ions, providing the required amount of species required for dedolomitisation to proceed. This is thought to be providing a reverse character for the ACR's chemical reaction.

Calcite and brucite are fine grained and enclose voids, which results in an increased occupation volume than the reacted dolomite grain. In rocks with such texture where dolomite crystals are restrained by the matrix, secondary calcite and brucite formed in situ will grow in confined space, causing the expansive nature of the dedolomitisation reaction. As a result of this, the rate of dedolomitization will depend on pH, the grain size of dolomite crystals and the textural characteristics (Deng 1993).

Similar results were also obtained when experimented on specially prepared compacted powders with controlled composition, simulating natural dolomite and magnesite. There was a linear correlation between the molar fraction of dolomite reacted and calcite formed. Some excess amount of secondary calcite is present due to dedolomitisation induced carbonation of portlandite. The final result again suggested the generating of expansive forces due to the crystallisation in restricted space at the dolomite/matrix interface (Liang 1995). The same authors in their next publication proposed that the expansive nature of ACR in concrete was a result of two interfacial reactions:

1) The first interface was within the aggregate particle at the dolomite/matrix interface, already described above.
2) The second interface was at the aggregate/cement boundary, which was well supported by observations of microstructural changes at the surface of alkali treated rock specimen that revealed the presence of secondary calcite with an underlining Mg-rich film, probably brucite.

At the aggregate/cement interface a presence of calcite crystals of rather different morphology was detected, possibly due to the carbonation process. The difference

between the two reaction sites was a confined space in the first case and an unrestricted growth space in the second. This mechanism was also valuable in explanation of CaO and MgO hydration and ettringite formation as volume demanding reactions (Liang 1995). The conclusion was that the volume increasing processes were indispensable to their expansion, therefore the dedolomitisation process could cause expansion in concrete affected by ACR (Liang 1995).

2.3.4 Alkali Carbonate Reaction in Argentina

In the early 1990s reports came out on ACR cases in Argentina when the aggregate used was argillaceous dolomitic limestone (Milanesi *et al.* 1994). The manifestation was familiar: expansion, crack-formation, rim-zones containing well known reaction products and aggregate particle boundary corrosion.

A study was carried out on three compositionally different rocks, confirming that clay-swelling is unlikely to cause expansion since ethylenglycol treatment of samples gave no XRD peaks for expansive clays. Preliminary results revealed the existence of secondary calcite and brucite; therefore the degree of mineralogical alteration was dictating the level of expansion (Milanesi *et al.* 1994).

More thorough results were published in a subsequent paper (Milanesi *et al.* 1996), based on experiment with Argentinean dolomites. The data published agreed with the already established scientific convention that ACR expansion was always accompanied by the dedolomitisation process. They concluded that an excessive increase, either in the specific surface of reactants or in the concentration of solution, may have a catalytic effect on the rate and type of chemical reaction and its products, which could be applied to the dedolomitisation reaction. The behaviour of Argentinean dolomitic rocks subjected to a high pH medium, as summarised in the above publications, shows:

1) The intensity and the degree of dedolomitisation depended on mineralogical and microstructural characteristics of the rock, such as porosity, texture, grain size, and percentage of insoluble residue.

2) A comparative XRD study of compositionally different powdered rocks (<75μm) immersed in NaOH solution, showed no difference; all of them were completely dedolomitised after alkaline treatment.

3) At higher pH, 2N and 10N NaOH, uncommon reaction products were formed, such as pirsonite and portlandite, not likely to occur in concrete.

4) The expansion mechanism proposed by Deng (1993), based on the tightest pile of particles, could not be applied in the case of one of the rocks used in this study, which did not expand in spite of the reduced compactness of the rock's fabric.

5) The data obtained in this study seemed to be in agreement with Headley's expansion mechanism model, mainly due to the controlling parameters that were similar to those in real concrete (T, aggregate and pH of~ 13) (Milanesi 1996).

2.3.5 The French ACR Mechanism model

At the 9th International Conference on AAR held in London in 1992, Prince and Perami reported their understanding of the ACR mechanism using a novel approach where they attempted to explain the role of alkali's in the dedolomitisation process (Prince and Perami 1992, 1992a). The results obtained on the reactivity of dolomite in lime, alkali or lime-alkali solutions, suggested that dedolomitisation as a chemical reaction was directly linked to the alkali concentration not only in an indirect catalyst role but in the sense that it intervenes directly in the nature of newly formed phases.

Accordingly this alkali-dolomite reaction can be written as the two stage reaction:

1) dissociation of dolomite

$$CaMg(CO_3)_2 \Leftrightarrow Ca^{2+} + Mg^{2+} + 2CO_3^{2-}$$

2) dedolomitisation

$$Ca^{2+} + Mg^{2+} + 2CO_3^{2-} + 2Na^{+} + OH^{-} \Leftrightarrow Mg(OH)_2 + Ca^{2+} + 2Na^{+} + 2CO_3^{2-}$$

Dedolomitisation is a result of a displacement of the equilibrium of dolomite dissolution. With additional OH^{-} ions reaction products will differ, and brucite will precipitate. The reminder of the ionic species (Ca^{2+}, Na^{+} and CO_3^{2-}) will form different compounds, depending on the environment.

Calcium carbonate fraction (aragonite, calcite or viterite), sodium carbonates ($Na_2CO_3.H_2O$, $NaHCO_3$, $Na_2CO_3.HCO_3.2H_2O$) and double carbonates of Ca and Na (pirsonite, gaylusite). Dedolomitisation was complete only in alkaline solutions and the products were pirsonite and brucite. The dolomite-lime reaction gave only partial dedeolomitisation, with different products:

$$CaMg(CO_3)_2 + Ca(OH)_2 \Leftrightarrow Mg(OH)_2 + 2CaCO_3$$

Finally, when both alkalis and Ca^{2+} are present the phases formed will depend on the relative activities of Ca and Na ions. A high $[Ca^{2+}]/[Na^{+}]$ value will cause preferrential crystallisation of calcite and brucite, which is in accordance with the Portland cement concrete environment. Laboratory conditions where the above value is lower will result in precipitation of brucite and pirsonite.

2.3.6 The Japanese interpretation of the ACR Mechanism

Katayama (1992), reported a controversial explanation of the alkali-carbonate reactivity. He suggested that the expansion was due to cryptocrystaline quartz, bearing in mind that alkali-reactive silica is a common constituent in limestone aggregate, although the final results would cause not only expansion but the formation of easily observed silica-gel. However, this hypothesis that ACR is just a modified form of ASR, is still being debated.

2.4 Conclusion of the literature review

Suggested conclusions of this world-wide review is that the AAR is no longer a local problem. As can be seen from the discussion above, AAR affects Portland cement concrete structures world-wide (Gillott 1995). The best illustration for the seriousness of the problem is that some £500 million are spent each year on concrete maintenance and repairs in UK only, and a large number of those damages were directly or indirectly induced by AAR.

As early as the writings by Vitruvius in De Architectura (1960-translation), the importance and influence of aggregates as well as other cementitious materials on concrete was described. Concrete is a major building construction material of present times, and all the components that make concrete have an impact on the quality, strength and durability of concrete structures. The properties of concrete are very important and therefore extensive and detailed studies and testing of each constituent as well as their interactions, whether chemical, physical or mechanical is justified. Only the characteristics, properties and processes that are relevant and could have an impact on alkali-carbonate reactivity have been mentioned. These range from carbonate rock petrology, mineralogy, chemistry, geochemistry, cement and concrete science.

Lucinda Jetty as a structure, photographed during the field work with 10th AAR Conference, Australia, August 1996.

Map-cracking surface of the concrete, close look.

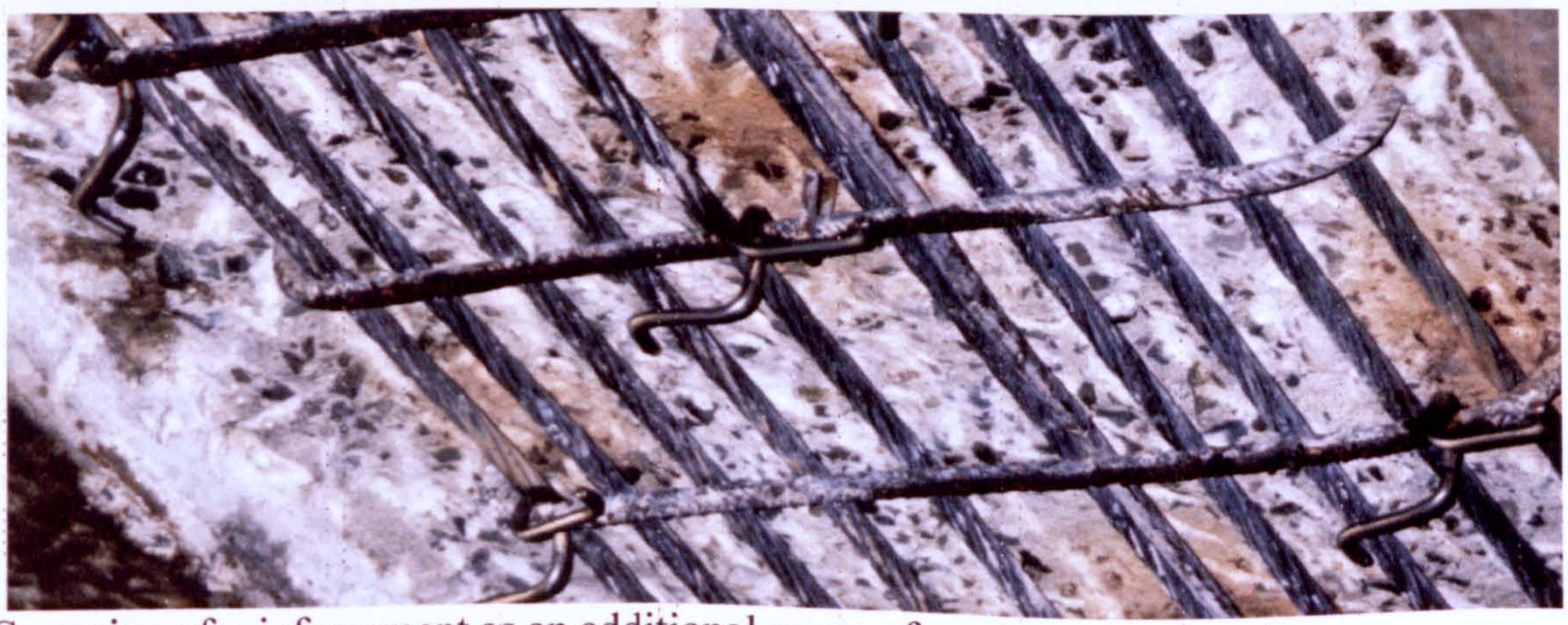

Corrosion of reinforcement as an additional cause of concrete deterioration.

Figure 2.1 ASR affected concrete of Lucinda Jetty (6km), Queensland, Australia.

PAGE
NUMBERS
CUT OFF
IN
ORIGINAL

Figure 2.2 An ACR affected concrete bridge showing typical map-cracking. Gananaque, Ontario, Canada, built 1934.

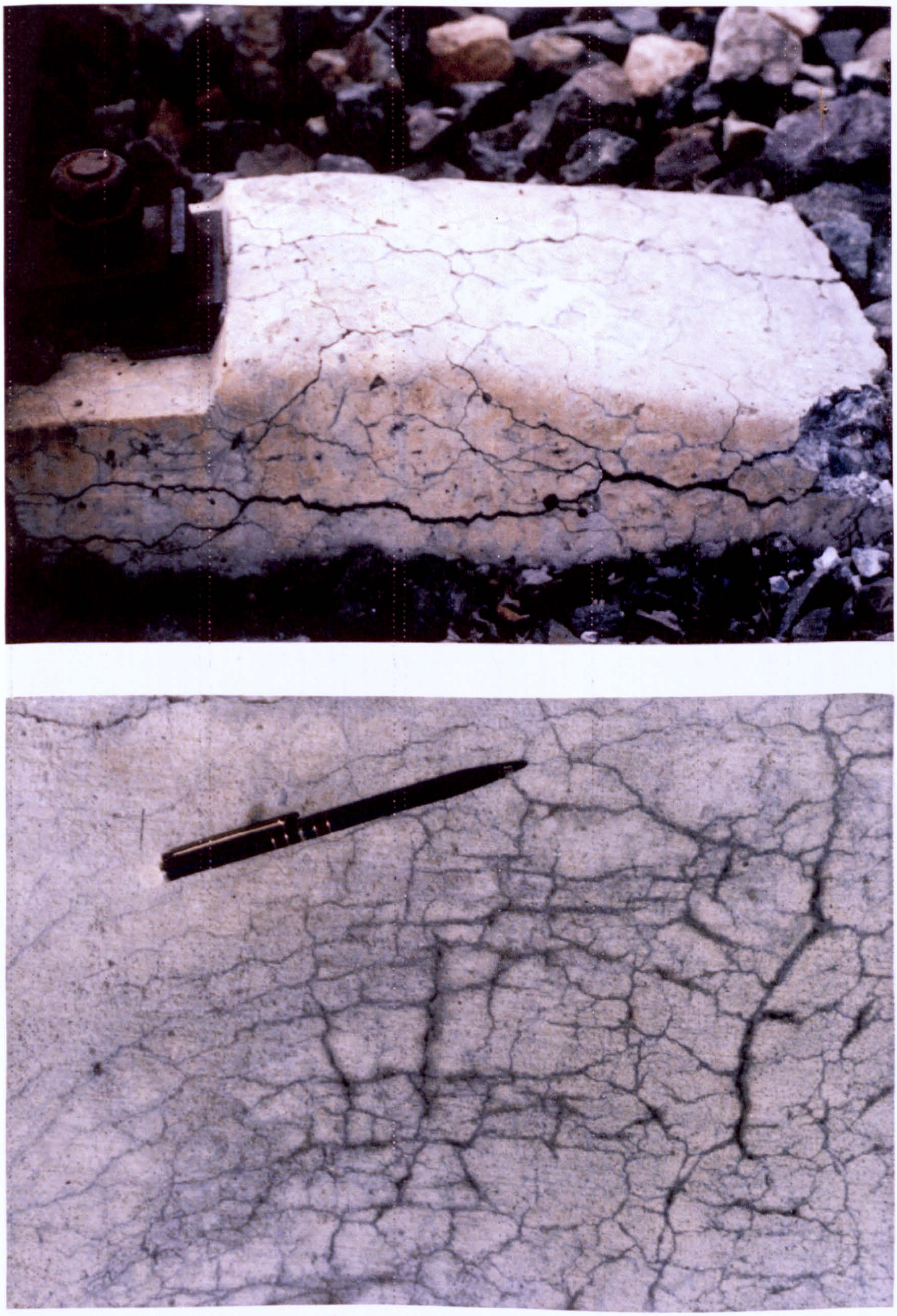

Figure 2.3 ACR affected concrete in China. Top image shows a railway track while the lower image displays a similar condition of an airport pavement.

Figure 2.4 Bridge pier in Tianjin, China, affected by both ACR and ASR reactions.

Chapter 3 Materials and methods used

3.1 Introduction

This chapter describes a series of independent experiments undertaken towards analysing the ACR mechanism. It also presents a description of the main samples of study, including their origins, compositions and preparation for instrumental study. The operation and setting modes of the various instruments will not be described here since such information can be found in the accompanying manufacturer's manual.

As a part of the planning process, a review of the experimental methods used by other concrete researchers was undertaken. This was necessary to avoid repetition in the first instance. Furthermore, the development and availability of new instruments such as the ESEM, enabled a novel approach was employed in studying the two main reacting components of concrete, simulating *in-situ* conditions.

The first of these components, the alkaline pore solution originating from cement paste, was replaced with NaOH at different pH concentrations in order to simulate *in-situ* concrete environments. The second component, aggregate, from carbonate rock, was also treated with NaOH. From this initial and previous investigations, it became obvious that dolomite was the only mineral of the studied carbonate rocks undergoing significant transformations (dedolomitisation) during the experiment. As a result of this, a single dolomite crystal was studied in detail in order to determine its stability under alkaline conditions, and the role dedolomitisation plays in aggregate volume changes. It was envisaged that the outcome of these two primary studies would contribute towards establishing the physical and chemical changes involved in the ACR mechanism.

3.2 Nature, origin and composition of samples studied

A good selection of both aggregate and concrete samples, affected by ACR, was gathered. This was mainly achieved through personal contacts with prospective donors encountered at various international conferences. Tables 3.1-3.3 list samples used in this study.

Table 3.1 Samples of single minerals used in this study and the purpose of their use

Sample No.	Minerals	Origin and supply	Description and sample conditioning	Purpose and experiments
MR01	Dolomite	Spain, Taylor's minerals	Single crystal, brown-black colour suggesting Fe, Mn impurities, grain size 3mm long, 2mm wide, perfect rhombic structure and cleavage.	Standard for XPS, SEM and EDX
MR02	Dolomite	Spain, Taylor's minerals	Single crystal, Fe-rich, silicate inclusions, grain size 3.5 by 2.5mm, rhombic, one fractured corner with Q, treated with 15ml 1N NaOH solution at room T for 3months in a sealed PVC bottle, no coating or drying was required.	Dedolomitisation reaction and formation of calcite and brucite, ESEM &EDX.
MR03	Dolomite	Spain, Taylor's minerals	Single crystal, 4 by 3mm, the same composition as above, ultrasonically washed in pure water prior to first analysis, immersed in 5ml 3N NaOH for 3weeks at room T in a sealed PVC bottle, removed from solution thoroughly washed in pure water before the second analysis allowing drying of the surface.	Crystal structure and changes at atomic level, observation of dissolution of dolomite and nucleation of brucite, AFM
MR04	Brucite	The NHM London, origin from Zimbabwe	Fine, platy colourless crystals, 2-3mm in diameter easily cleaved into thin fragments. SEM samples were Au coated and XPS, ESEM as received.	Standard for SEM and ESEM& EDX and XPS
MR05	Brucite	The NHM London, origin from Zimbabwe.	A thin plate ($1cm^2$) removed from a cluster of brucite crystals and immersed in 1N NaOH for several weeks at room T, removed from solution and rinsed with pure water, dried at room T before XPS spectrum was acquired.	Changes induced by alkaline solution SEM, EDX
MR06	Natron	The NHM Melbourne, Australia	Fine fibrous and powdery growth of natron on carbonate substrate, very fragile and hygroscopic unstable in the air.	Comparison standard, SEM, BEI EDX
MR07	Calcite	Pittsburgh Quarry, Rogers	Calcite crystals from calcinised veins within argillaceous dolomitic limestone from Kingston, used as a fractured sample Au coated for SEM observations and comparison with cc matrix in as received and alkali treated .	Distinguishing primary from secondary-calcite or pseudo-calcite SEM BEI

* Single dolomite crystal containing chemical impurities was used as a standard in order to simulate dolomite from reacting Kingston aggregate, where the dolomite fraction is known to contain Fe/Mn impurities.

3.2.1 Single crystals

In this study, single dolomite crystals approximately 3mm long and 2.5mm wide were used. They possessed almost perfect rhombic structure, but their dark appearance suggested the presence of Fe and Mn enrichment, and clay and quartz impurities. The presence of such imperfections in crystals was ideal for this study as one of the aims was to establish impact of clays and quartz on dolomite stability and expansion. The crystals

as received (supplied by Taylor-Crystals) were examined for microstructural features that could be of interest later as a part of the dedolomitisation reaction. This material was used for AFM, XPS and ESEM analysis to establish changes induced by alkaline solution on various levels of depth resolution (few atomic layers to micron depths) and analysing conditions (with high vacuum in XPS and SEM and non-vacuum in ESEM and AFM). Samples are listed and described in Table 3.1 (sample no. MR02, MR03, MR05, MR07) and the results obtained are presented in Chapter 5 on Mineral/solution reactions.

Table 3.2 Samples of carbonate rocks used in this study (origin, composition and aim)

Sample No.	Carbonate Rocks	Origin and supplier	Description, sample conditioning and susceptibility to ACR	Experimental Purpose
MR08	Kingston dolomite	Kingston, Canada, supplied by C. Rogers	Grey, fine grained argillaceous dolomitic limestone with pyrite, low porosity non-uniformly dispersed dolomite, easily split along layers, as received (sound) and alkali treated discoloured, ACR expansive.	Rock cylinders 35 by 9mm and cone ends at 120°for expansion test ASTM C586.
MR09	Kingston dolomite	Pittsburg Quarry	The appearance of the rock as above, known to be expansive when used as aggregate, also used for concrete test.	SEM & EDX, XRD.
MR10	Kingston dolomite	Kingston, outcrop by the motorway	Samples collected from different beds on a face exposed to weathering for several years, grey-expansive and greenish-non-expansive, crumbly.	XPS, ESEM, TOF SIMS fresh and alkali-treated.
MR11	Kingston dolomite	Pittsburg Quarry, Gillott	Ordovician dolomitic-limestone but higher 4N NaOH solution, for 3yrs. With visible 2mm dark reaction rim on the edge of the 20mm diameter core.	EPMA, XRD, comparison with non-expansive reaction rims.
MR12	Nelson dolomite	Canada, Calgary, Gillot	Pale-grey, coarse grained-dolomite, treatment as above, sound inner part and 2mm white reaction rim no expansion recorded.	EPMA, XRD, SEM & EDX.
MR13	Massachs. dolomite	From US, supplied by Gillott	White, well crystallised coarse grained dolomite, 2mm reaction rim and semi-expansive in ASTM C586 test.	EPMA, XRD, SEM & EDX.
MR14	Chinese dolomite	Nanjing, by Tang	Grey, shells, intermediate grain size, dol. limestone fresh and alkali-treated	TOF SIMS, XPS, EPMA.
MR15	Limestone/ dolomite	SW England Quarries	Grey/brown, fine grained quartz veins, Carboniferous age, dolomitic-limestone, no ACR record, one bed Fe-rich.	SEM &EDX, XRD.
MR16	Dolomitic limestone	S. Wales, Quarries.	Brown, fine grained dolomite with quartz veins and no record of ACR.	SEM, XRD.
MR17	De-dolomitic Limestone	Durham, England	Brown-yellow, highly porous limestone formed by dedolomitisation process.	SEM &EDX.
MR18	Dolomite	Swedish aggr.	White, marble-like, coarse grained	SEM, XPS.

Table 3.3 Classification of carbonate rocks used in this study based on their record

ERSITY OF BRISTOL

and susceptibility to ACR when used as aggregate in concrete.

ACR expansive rocks	Potentially ACR expansive rocks	Non-expansive rocks
Pittsburg Quarry (MR09), all from first lift in the quarry.	Whatley dolomitic limestone Fe rich bed in Quarry (MR15).	Non-reactive beds from Kingston dolomitic limestone.
Pittsburg Quarry (MR09a) *	Halecombe Quarry , grey dolomite, (MR15a).	Nelson dolomite (MR12)
Pittsburg Quarry (MR09b)	Mearhead dolomite, (MR15b).	Swedish white dolomite (MR18).
Pittsburg Quarry (MR09c)	Cheddar dolomite, (MR15c).	Ordovician dolomite, Scotland.
Kingston dolomite parallel to the bedding, (MR10a).	Dolomitised limestone, Chepstow (MR15d).	Spanish dolomite.
Kingston dolomite (MR10b) perpendicular to the bedding.	Fe-rich dolomitic limestone, South Wales, (MR16).	French dolomite.
Chinese dolomite (MR14)	Massachusetts dolomite, compact, (MR13).	South African dolomite.
	Mg-limestone, Yorkshire	Limestone, Zimbabwe.

*Samples are further divided within one set of samples, labelled as a, b, c, additionally to the MR00, to show that they belong to the same group of samples but with different composition or sample preparation procedure.
Some of the samples are the same as in Table 3.2.

3.2.2 Standards

***Minerals*:** Single natural minerals were used as reference materials for microscopic and spectroscopic analysis. They were of different origin and contained a variety of impurities and inclusions, ideal for the simulation of laboratory conditions as close as possible to the naturally occurring processes (Table 3.1 sample MR01). In this study the brucite minerals used were supplied by the Natural History Museum, London, and consisted of fine, platy, colourless crystals, approximately 1-2cm^2 in plane surface, which originally came from a mine in Zimbabwe (Table 3.1 samples MR04). Samples of Natron from Melbourne Natural History Museum, were used for comparison with some of the phases observed and aided in identifying one secondary phase as natron ($Na_2CO_3.H_2O$), Table 3.1, sample MR06. Calcite sample used a standard was from a calcite vein within Kingston Dolomite, Table 3.1, sample MR07.

3.2.3 Rock samples/aggregates

Although the actual deterioration of concrete structures is not often caused by AAR, the products of the reaction between aggregate and cement-paste, such as map-cracking, will

initiate other reactions and effects of aggressive agents (corrosion, carbonation, sulphate attack). A susceptibility of any aggregate to alkali aggregate reactivity is closely related to the compositional and textural characteristics of the rock used. Deleterious substances present in an aggregate can enhance chemical instability when in contact with highly alkaline pore solutions, or a part of an aggregate can develop a harmful chemical reaction with the cement paste. The second aspect of an aggregate's contribution towards undesired AAR is the alkali content that can be released into the pore solution and therefore increase pH of the surrounding cement-paste pore solution. The source of alkalis in aggregates are salts that can liberate sodium and potassium ions, or some of the rock forming minerals such as feldspars and phyllosilicates that contain appreciable amounts of Na_2O and K_2O. The deleterious reactions involving carbonate aggregate appear to be rare on a world scale, having only been identified in Canada, the Middle East, North Africa, China and Argentina.

In this study carbonate rocks of different origin, composition, texture, age and ACR susceptibility were observed. All the rocks used are as shown in Tables 3.2 and 3.3. More detailed description of carbonate rock samples is important as the majority of experiments were conducted on the rock/solution system.

1) The most important set of samples were from argillaceous dolomitic limestone from Kingston Canada, mainly from the well known Pittsburg Quarry. This dolomitic limestone is of prime interest because the first reported case on ACR (Swenson 1957) was construction in Barriefiled Barracks, which had aggregate supplied from the first lift of the Pittsburg Quarry. As is specified by Rogers (1990), reactive beds dominating the lower half of the first lift of the Pittsburg Quarry. Figure 3.1 presents the view of one of outcrops in Pittsburg Quarry, revealing the layered structure of the rock formation with expansive (grey) and non-expansive (green and brown) formations. A more detailed view of one of the reactive dolomitic beds again using the scale shows finer compositional layers, Figure 3.1.

   For more detailed studies of this rock see: Swenson (1958), Legget (1960), Swenson and Gillott (1960), Hadley (1961), Gillott (1963), Smith (1964), Hadley (1964), Swenson and Gillott (1964 and 1967), Dolar-Mantuani (1972), Smith (1974), Pagano and Cady (1982), Dolar-Mantuani (1983), Rae (1984), and Rogers

(1986, 1990). The rock was found to be an argillaceous (illitic) dolomitic limestone and expansive when used as aggregate in concrete. Detailed studies of the expansive rock samples prior to and after immersion in NaOH, were carried out in this study (samples MR08-MR11 from Table 3.2).

2) Carboniferous dolomitic limestone, from Southwest England and Wales, formed a large proportion of the sample collection, because these areas produce a high percentage of UK carbonaceous aggregate. The composition of the rock varies from limestone to a pink dolomitic limestone and dolomite. None of the UK aggregates used in this study were reported as being susceptible to ACR. Sample collection contained specimens from sites in the UK from the following quarries: Chepstow, Halecombe, Whatley Figure 3.2 (Table 3.2, sample MR15), Drybrook, Merehead, Cheddar, Stancombe Figure 3.2, Taff Well Region Wales (Table 3.2 sample MR16), Mg-Limestone from Yorkshire (two quarries), limestone from Castle Cement Quarry Clitheroe, Lancanshire. Samples that are not listed in Table 3.2 and have been used in this study such as Mg-limestone did not produce significant results.

3) Chinese dolomites, known to be ACR expansive when used as concrete aggregates, were supplied by Tong Liang, Nanjing University. (Table 3.2 sample MR14).

4) Samples of Massachusetts (Table 3.2 sample MR13) dolomite US and Nelson (Table 3.2 sample MR12) dolomite from Canada, were used for comparative studies. This was carried out in order to investigate the causative role of dedolomitisation on expansion, as they were all undergoing different degrees of dedolomitisation and expansion. Both Nelson dolomite and white dolomite from Sweden (marble dolomite) (Table 3.2 sample MR18) have been successfully used as concrete aggregates owing to their non-expansive property, even though the Nelson dolomite had undergone partial dedolomitisation. Massachusetts dolomite (MR13) by comparison, is a semi-expansive rock when immersed in alkaline solution.

5) ***Rock standards:*** Dedolomitic limestone, from Durham, England (Table 3.2 sample MR17) was used as reference material for easier identification of specific textural and mineralogical characteristics produced by dedolomitisation process (naturally

occurring). The characterisation was obtained by SEM and EPMA analysis. These samples showed the presence of secondary calcite which could be distinguished from primary calcite matrix Similar occurrence was expected in ACR affected carbonate aggregate (concrete environment). The material was supplied by Professor Tucker from the Department of Earth Sciences at Durham University.

3.2.4 Concrete samples

The aim was to observe the changes in aggregates undergoing ACR in real structures and compare it with laboratory cured concrete specimens also affected by ACR. Samples are presented in Table 3.4. Two sources from Canada and China provided a variety of aggregates and cements used. In addition to this ASR concrete samples were observed as reference materials for potential overlapping of the two reactions.

ACR Field concrete from Canada: Concrete from constructions in Canada (two dams and on purpose built pavements), primarily collected with the intention to assess the condition of the structure and to identify the factors contributing to an unsatisfactory performance. The samples are listed with main specification in Table 3.4. These samples were used in this study as a part of collaboration with the University of Toronto, in order to define the mechanism that led to the undesirable transformation of the material. Parallel research is being carried out in Canada but with more physical tests such as expansion, strength and phase identification using optical microscopy (personal communication with J. Gillott, Calgary University, M. Thomas, Toronto University and C. Rogers-Ministry of Transport Ontario).

Most of the ACR affected structures in Canada were demolished and repaired in recent years, apart from a bridge built in 1934, (Chapter 2, Figure 2.1). Therefore it was difficult to obtain samples from a ACR damaged structure. However, the Ministry of Transportation and University of Toronto in Canada, have built concrete pavements at the MOT headquarters in Kingston, in order to monitor concrete expansion under *in-situ* conditions, monitoring temperature and humidity that would affect real structures. Concrete mixtures were designed accordingly, with high alkali content, low alkali content, with Portland cement, and with partial replacements of cement by silica fume and blast furnace slag admixtures. Core samples were drilled from some of the expanded, ACR affected pavements after 10 years of their manufacture, (Figure 3.3a and

3.3b). Even those samples with partial replacement of cement by supplementary cementitious materials (SCM) had map-cracking and obvious symptoms of ACR, (Rogers 1990). Field conditions allowed for thawing-freezing cycles and different temperature and moisture content to have an active role in concrete deterioration, not present in laboratory samples. Samples from this material are numbered in this study as sets samples MR19 from Kingston pavements, and MR20, from dams where concrete was undergone deterioration and requiring repair works, with adequate a, b, c, d and e.

Laboratory concrete from Canada: Concrete samples cured under laboratory conditions were important because they could help relate environmental parameters/conditions to the actual reaction products and the kinetics of those reactions. They were a part of ongoing research at the Ministry of Transportation, Ontario, Canada, mainly following concrete prism tests for the expansion monitoring. The aggregate used was already known as ACR reactive argillaceous dolomitic limestone from Pittsburg Quarry in Kingston (samples MR08-11, Table 3.2). Two types of cements were used, highly alkaline cements and the low alkali contents blended cements. It is important to mention that laboratory cured concrete prisms have some disadvantages due to the sample size, and controlling parameters such as temperature (T) and relative humidity (RH).

This was demonstrated by Rogers, (1990), who claimed a discrepancy between laboratory and *in-situ* measurements were the result of different environmental conditions. In other words results obtained in the laboratory cannot be applied to predict the behaviour of field concrete. He suggested that an increase in alkalinity and relative humidity (RH) will improve the applicability of the test results from laboratory-mixed concrete. The laboratory concrete samples used in this study were of the same mix-design as the concrete pavements in Kingston (above paragraph). Samples from this set are numbered as sets MR21 and MR22 with individually prepared a, b, c, d and e samples for each individual analytical technique.

ACR concrete from China: A sample of ACR concrete was obtained from the Nanjing Materials Science Research Centre, kindly supplied by Professor Tang. It consisted of an aggregate very different in composition and texture to that obtained from Canada. Unfortunately, there was not much additional information about the mix design of the concrete. However, the sample was presented as a representative of the ACR reaction in concrete in China, where the scale of ACR problem is greater than anywhere else in the

world. Some of the typical ACR affected concrete structures in China can be observed in Figure 3.4, supplied by Nanjing Centre. Sample numbers MR23 Table 3.4

Table 3.4 Concrete samples used in this study

Sample No.	Concrete	Origin, supplier	Description, composition and AAR test results/records	Purpose of experiment
MR19	ACR field samples, Canada	Kingston Pavements Rogers	A concrete core from a pavement after 10yrs, expansive coarse aggregate from Pittsburgh Quarry and Portland cement with the same mix/design as in Lab. prism test. Aggregate/cement interface and aggregate grains removed from cement were studied.	*In-situ* changes in mineralogy, microstructure. Using techniques SEM, XRD EPMA, XPS
MR20	ACR field samples, Canada.	Dam in Canada, Thomas	Concrete partially made with Pittsburg aggregate as well as limestone rich in silicate. Aggregate grains have dark reaction rims developed and microcracks radiating from cement into aggregate.	*In-situ* changes in a structure of larger concrete mass, using SEM, EPMA.
MR21	ACR lab samples, Canada	Prism expansion test material Rogers	The same concrete mix as in MR19 but stored at Laboratory conditions as expansion prism test with coarse aggregate particles visible developing reaction rims and typical map cracking of concrete.	Effect of T, moisture, sample size and alkali-supply, SEM & EDX
MR22	ACR lab samples, Canada	Prism test Gillott, Calgary.	Laboratory concrete sample using Pittsburg aggregate and cured in moist room and alkali solutions.	Effect of T, RH, sample size and alkali-supply.
MR23	ACR laboratory samples, China	Prism test, Tang Nanjing, China.	Concrete sample from a laboratory controlled conditions also subjected to a high T=150°C and alkaline solution using test developed by Tang. Cement source is different as well as water, map-cracking developed.	Different source of aggregate, cement, stored in laboratory conditions, EPMA, XRD.
MR24	ASR field samples, UK	Not for publishing data.	Samples (commercial) UK, with reaction products typical for ASR but also un-identified reactions, micro-cracking	Relation between ACR/ASR
MR25	ASR laboratory samples, UK	Prism test, Castle Cement Ltd., UK.	ASR expansion prism test with Portland cement and limestone susceptible to ASR. Also gel-like products typical for ASR were observed and used as a reference features in observations.	ASR gel and microstructural appearance, cracks development.

Additional concrete samples: ASR/ACR concrete samples from a structure in UK (sample MR24, Table 3.4) and ASR concrete samples from Castle Cement Laboratory study (sample MR25, Table 3.4) were used as reference materials for typical ASR features such as silica-gel, micro-cracking and mineralogical and chemical changes in limestone aggregate.

3.2.5 Solutions, curing and storage conditions used

The relevance of any research in materials science is best tested when compared with data obtained in field examinations. This is especially true for concrete more than in any other material as the performance of concrete depends on several parameters, nearly all of which cannot be simulated in the laboratory (climate both temperature and humidity that will oscillate, sample size and various working conditions). The reverse also applies, as laboratory conditions cannot fully reflect real life concrete.

3.3 Sample preparation procedures

Procedures of sample preparations are vital because depending on their impact on the sample composition and structure the accuracy of analysis can be affected. Table 3.5 and 3.6 present the two main types of sample techniques used in this study, mechanical and chemical and the disadvantage/advantage of their use on the accuracy of final experimental results. Figures 3.5-3.7 schematically present sequential sample preparation procedures, (cutting, drilling), used in this study.

Table 3.5 Mechanical preparations and their effect on accuracy of analysis

Mechanical/physical preparations	Experimental requirement involving specific sample preparation techniques
Cutting, discs and thin samples, Figure 3.7	For spectroscopy 1mm thin disc from previously treated rock cores and the same size samples from untreated rocks.
Drilling cores, cone-end shaping at 120°, Figures 3.5	For expansion measurements ASTM C-586, cone end used for SEM without coating as the charge effect was reduced due to the slope angle, limiting electron penetration.
Fracturing of rock samples before and after the alkaline treatment.	For interfaces, planes of weakness, help avoid contamination of polishing, SEM micrographs were taken from coated fractured surfaces, with EDX characterisation before and after the treatment with alkaline solutions, ESEM samples freshly fractured.
Polishing, thin sections and flat surfaces of grain boundaries.	Chemical (EPMA) and microstructure (BEI) analysis. Concrete rock samples previously embedded in epoxy resin for impregnation were than polished/ground to 0.25μm for BEI and EPMA observations.
Extracting, peeling off of aggregate particles from cement matrix.	Immediate *in-situ* study in ESEM and XPS, for transition zone, aggregate/cement-paste interface, ESEM Aggregate samples were removed from concrete specimens prior to examination and analysed in high humidity.
Grounding powders	Detailed mineralogical observation using XRD were also carried out before and after alkaline treatment.
Drying, vacuum condition	For all analysis but ESEM.

Table 3.6 Chemical treatments and preparations, their effect on accuracy of analysis

Chemical preparation	Samples subjected and experiment requirement
1N NaOH solution to simulate cement, approximately 35ml per rock-core (9 by 35mm), replaced every 3months, kept at room temperature in a sealed plastic bottle.	Expansion monitoring to distinguish ACR susceptibility of rock samples, mineralogical and chemical changes induced by alkalis determine the mechanism of the reaction by correlating chemical, physical and mineralogical changes, establish the chronology of processes involved (all minerals and rock samples were used in alkaline treatments, MR01-18).
NaOH + D_2O, tracer for monitoring the role of hydroxyl ions at the room T for 1 month.	Depth penetration of OD ions into the structure of newly formed phases in carbonate rock, to help understand the ACR mechanism using TOF-SIMS, samples MR09 & 14.
Ion-etching, bombardment with Ar (XPS) and Ga (TOF-SIMS) sources	For surface cleaning, depth profiling in spectroscopy, small area mapping at different depths (sample no. MR09-14).
Rinsing, and ultrasonic bathing.	Removing impurities and excess solution for AFM XPS, SEM, EPMA analysis of single crystals and rock samples
Glycol treatment, where rock powders were filtered, oriented on a glass slide, immersed in glycol	For XRD clay analysis of rock-samples that reacted and expanded to different degree for establishing their role in ACR (sample no. MR11-15).
Epoxy resins were used to impregnate samples before polishing procedures and agents	Maintain fragile fractions intact during preparation of EPMA and BE samples especially to detect reaction rims at grain boundaries, (all concrete samples, MR19-25).

3.4 Design of systems analysed

As stated in the introduction, the design of the experimental procedure was aiming to obtain data on the three main interfacial systems: mineral/solution, rock/solution and aggregate/cement paste. The combination of the three data sets were expected to help design a model for the ACR mechanism. Tables 3.7, 3.8 and 3.9 provide a summary of the main areas of interest during the investigation of each of the systems.

Table 3.7 Type of data acquired from single mineral/ solution system

Step	Action	Aim
ESEM & EDX	Before and after alkaline treatment.	Mineralogical changes on the surface of dolomite.
SEM & EDX	Before and after alkaline treatment.	Changes in microstructure, new texture, cracks.
AFM	Before and after alkaline treatment.	Volume change/nucleation, using atom-assemblages.
XPS	Before and after alkaline treatment.	Chemical changes using binding energy shifts.

*samples used were single dolomite and brucite crystals listed in Table 3.2.

Table 3.8 Type of data required from carbonate rock/ solution system

Step	Action	Aim
XRD, EPMA, SEM	Before & after alkaline treatment	Detect new phases composition
SEM & BEI, ESEM, EPMA	Before & after alkaline treatment	Textural changes, crystal growth and micro-cracks
EPMA, XPS, TOF SIMS	Before & after alkaline treatment	Elemental distribution, migration and quantitative and qualitative chem. composition
Expansion measurements	Before &after alkaline treatment	ASTM C-586, length change

*samples used were carbonate rocks listed in Table3.3.

Table 3.9 Type of data required from aggregate/cement paste system

Step	Action	Aim
ESEM & BEI	Peeling/extracting cement paste attached to reacted aggregate grain.	Interface phases, composition, porosity.
XRD, EPMA	Cutting, grounding impregnation, polishing.	Mineralogical changes in aggregate and aggregate/cement transition zone.
SEM & BEI	Fractured, polished coated.	Development of cracks and new phases.
EPMA, XPS	Aggregate/cement interface, chemical changes.	Impact of bulk cement paste on aggregate weathering and grain boundaries formation.

* samples used were concrete samples (MR19-25) listed in Table 3.4.

Alkaline solutions: Cement as a component can influence AAR to a great extent mainly due to its alkali-content. The amount of alkalis recommended in Portland cement used in concrete today is $Na_2O + K_2O = 0.6$ wt%. In this study, the alkaline environment of Portland cement concrete was simulated by using 1N NaOH or 2-4N NaOH according to ASTM C-586. The alkaline solution of increased pH 4N was used for studies on single dolomite crystal to enhance the rate of dedolomitisation. Solution was replaced every 3 months. The water used was de-ionised.

All the samples were stored in sealed plastic bottles and kept at room temperature for various lengths of time. For spectroscopic and surface studies the time was reduced as the resolution allowed detection of minor changes. However, ASTM C586 rock cores

were measured over 3.5 years, which enabled detection even on a slow / late expanding rocks.

Tracer-monitoring using deuterium oxide (D_2O): D_2O was used to monitor alteration reaction and depth of penetration of hydroxyl ions into reactive rocks. These were traced using spectroscopic techniques (TOF-SIMS). The experiment was aimed to establish the role of hydroxyl ions in the ACR mechanism. The solution used was of 1N NaOH where H_2O was replaced with D_2O. Two ACR reactive carbonate rocks (9mm by 2mm discs as in Figure 3.5) were immersed in 5ml solution per sample and kept in a sealed plastic bottle at room temperature for 4 weeks. Samples were removed from solution and rinsed with pure water and dried immediately at 105°C prior to analysis.

The drying at such temperature would evaporate any water/solution present in pores, therefore the expectations were to see depth of incorporation of OD^- ions into the mineral-structure, whether into swelling clays or formation of first brucite phases. Both rock used, Chinese and Kingston dolomite, did not contain any apparent fractures or cavities which would allow easy access for the solution; both were well packed and fine grained dolomites. The results of this experiment are presented in Chapter 6.

3.5 Methods of analysis

The data obtained on materials analysed in this study provided a collection of valuable information often with complementary character. This was achieved by using methods that acquired data in different scientific fields such as mineralogy, crystallography, surface chemistry and geochemistry, with adequate levels of accuracy and resolutions. In this study a number of different techniques were used to characterise the samples. They are presented in Tables classified based on the resolution obtained into surface, near surface and bulk analysis (Tables 3.10, 3.11, and 3.12) with the sample used and the aim behind their use.

Table 3.10 Methods used for Bulk material analysis (>1μ depth resolution)

Method	SEM and EDX	ESEM and EDX	EPMA and BEI	XRD
Aim	Microstructure, increased depth of field information on grain structure components	Observation of samples in similar to *in-situ* conditions of high RH, no sample alterations	Qualitative compositional data of various reaction rims, spatial elemental distribution	Mineralogical composition and ratios of main components

Experiment	Rocks and minerals stability in NaOH solution	Aggregate remove. from cement, mineral/solution	rock/solution and concrete's grain boundaries	Rocks before and after NaOH solution

Table 3.11 Methods used for Near-surface analysis (several top atomic layers)

Method	**X-ray Photoelectron Spectroscopy (XPS or ESCA)**	**Time of Flight Secondary Ion Mass Spectroscopy (TOF-SIMS)**
Aim	Establishing chemical state changes and ionic exchange	Penetration of OD^- ions by using Ga ion etching for depth profiling
Experiment	Rock and mineral interaction with NaOH solution, the dedolomitisation reaction	Tracer experiment for establishing the role of OH^- ions in ACR mechanism

Table 3.12 Methods used for Surface analysis, (top atomic layer analysed)

Method	**Atomic Force Microscopy (AFM)**
Aim	For observing top atom layer of dolomite crystal surface and detecting nucleation sites for the dedolomitisation reaction.
Experiment	Crystal surface observed before and after alkaline treatment.

3.5.1 Expansion measurements (ASTM C-586)

The standard test (ASTM C-586 or Rock Cylinder Method) for determining the potential alkali reactivity of carbonate rocks for use as concrete aggregates was followed for distinguishing between expansive and non-expansive carbonate rocks. This test was designed to determine the expansive properties of carbonate rocks when immersed in alkaline solutions at room temperatures. Any length changes taking place during the test would indicate the rock's general level of reactivity. This in turn provides information on the possible expansive nature of the rock if used as an aggregate in concrete.

The procedure involves length measurements of small rock cylinders immersed in pure water till no length change is observed. Samples are then transferred to the reagent used (1N NaOH solution) with a minimum of 35 ml of solution per sample, sealed in plastic containers and kept at room temperature. The solution was replaced every 3 months. The comparator used for length measurements was the Mitutoyo Digimatic Indicator, graduated to read down to 0.001 mm.

A standard reference bar made of steel, 31.5 mm in length, was used to calibrate the measuring device. The specimens used were in the form of circular cylinders with conical ends at approximately 120° angles, as shown in Figure 3.5. The overall length of each rock specimen was 35 mm ±5mm and 9 mm diameter, prepared as in Figure 3.5. Measurements were performed once a week for 6 weeks, then monthly for 6 months, reducing to every 3 months for 2 years and finally once every six months. The measurement was always performed at the same temperature (~17–23°C), whenever possible. Samples were removed from the solution, rinsed with pure water, allowed to dry on the surface and immediately measured.

The aim of the test was to detect potentially ACR expansive rocks, using NaOH solution to simulate environment for the alkaline cement paste in which an aggregate would be embedded once used in concrete. The method has so far been successfully used in research and preliminary screening of aggregate sources to discard potentially expansive material. However, the time required for the reliable results is too long, especially for late-expanding aggregates, which tend to start expanding after 2 years or even later.

3.5.2 Petrographic and mineralogical observations

Examination and assessment of aggregates is generally conducted by petrographic methods and various technological tests. Petrographic methods are used to determine the properties of rocks and their constituent minerals, that may affect the performance of concrete in the intended application. The particular interest is in properties that might influence the durability of concrete. The durability of aggregate is dictated by its interaction with species of matrix in which they are embedded and elements from the surrounding environment. Durability is the resistance to deterioration and disintegration in contact with various agents, whether in the micro-environmental conditions in concrete or the climatic conditions around the structure. Most of reactions within the aggregate that are induced by cement-pore solution are due to the presence of undesirable phases within aggregate, which is why their identification is very important.

Petrographic examination in this study was carried out using microscopy for textural and microstructural properties, from preliminary optical microscopy to the higher resolution in SEM and ESEM. Figure 3.6 shows a schematic description of the importance of

sample thickness and slope for un-coated SEM observation. Phase identification was conducted by using XRD and EPMA.

3.5.3 Surface chemistry and micro-architecture

More detailed studies of chemical and microstructure changes were investigated applying sophisticated AFM, XPS and TOF SIMS analysis. Spectroscopic techniques were used to observe changes on the surface of a single dolomite crystal immersed in alkaline solution as a simulation for concrete or OPC environment. This offered the possible detection of mineralogical changes, surface deposition or dissolution occurring at atomic level. Moreover, using XPS for elemental mapping of the different chemical states to distinguish the amounts of Mg in brucite and dolomite was important to support the microstructural findings from SEM & EDX observations. The Figure 3.7 shows the rock-tablets used. In addition to this AFM was used to establish the correlation between atomic structure of dolomite crystal lattice and the location of calcite nucleation sites on its surface during dedolomitisation process.

3.6 Conclusion

In order to have an overview of processes that have damaging effects on concrete, it is essential to combine the analytical data from the laboratory with the empirical information from the field. Some of the processes are slow and long-lasting and their forward prediction cannot be made accurately by simply observing laboratory specimens. This is because curing conditions, the sample size and other controlling parameters could interfere in the mechanism and kinetics of the reactions concerned.

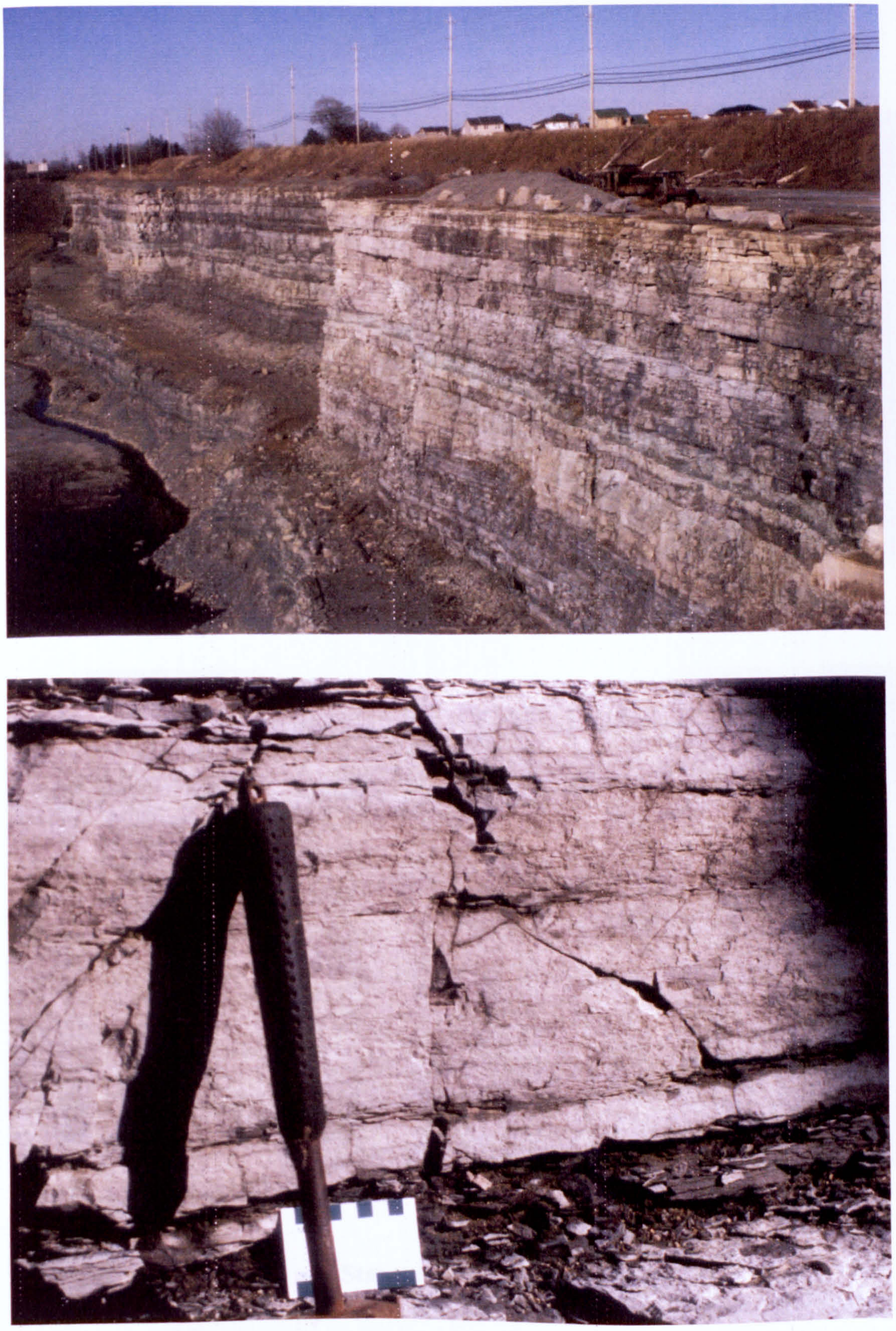

Figure 3.1 Pittsburg Quarry, Kingston Canada. Top image displays a layered formation of argillaceous dolomitic limestone showing expansive (grey) and non-expansive (pale brown and green layers). Lower image shows a close-up of the expansive layer.

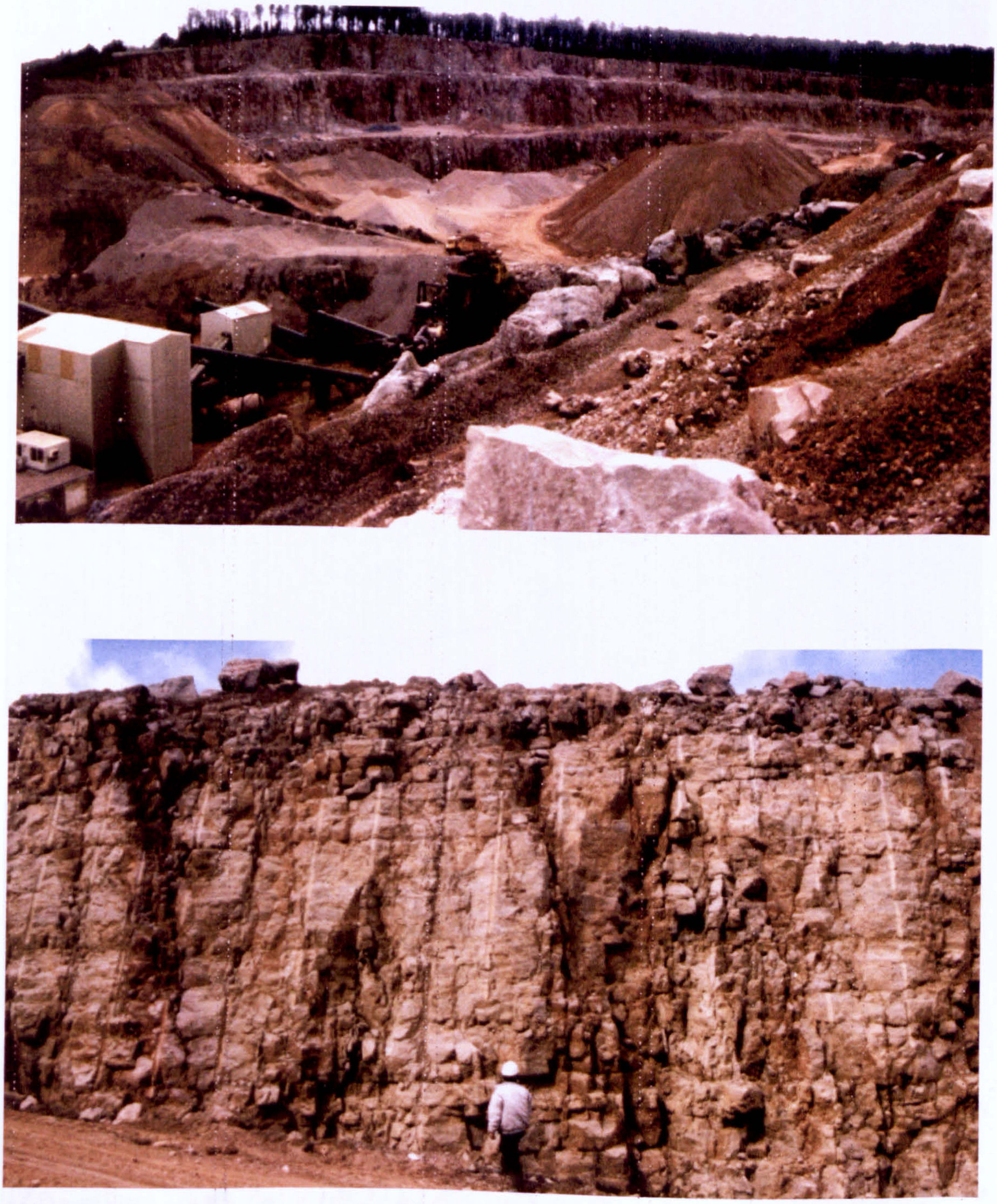

Figure 3.2 Whatley (top) and Stancombe (bottom) Quarries, SW England. Both quarries contain dolomitic limestone and limestone used in aggregate production.

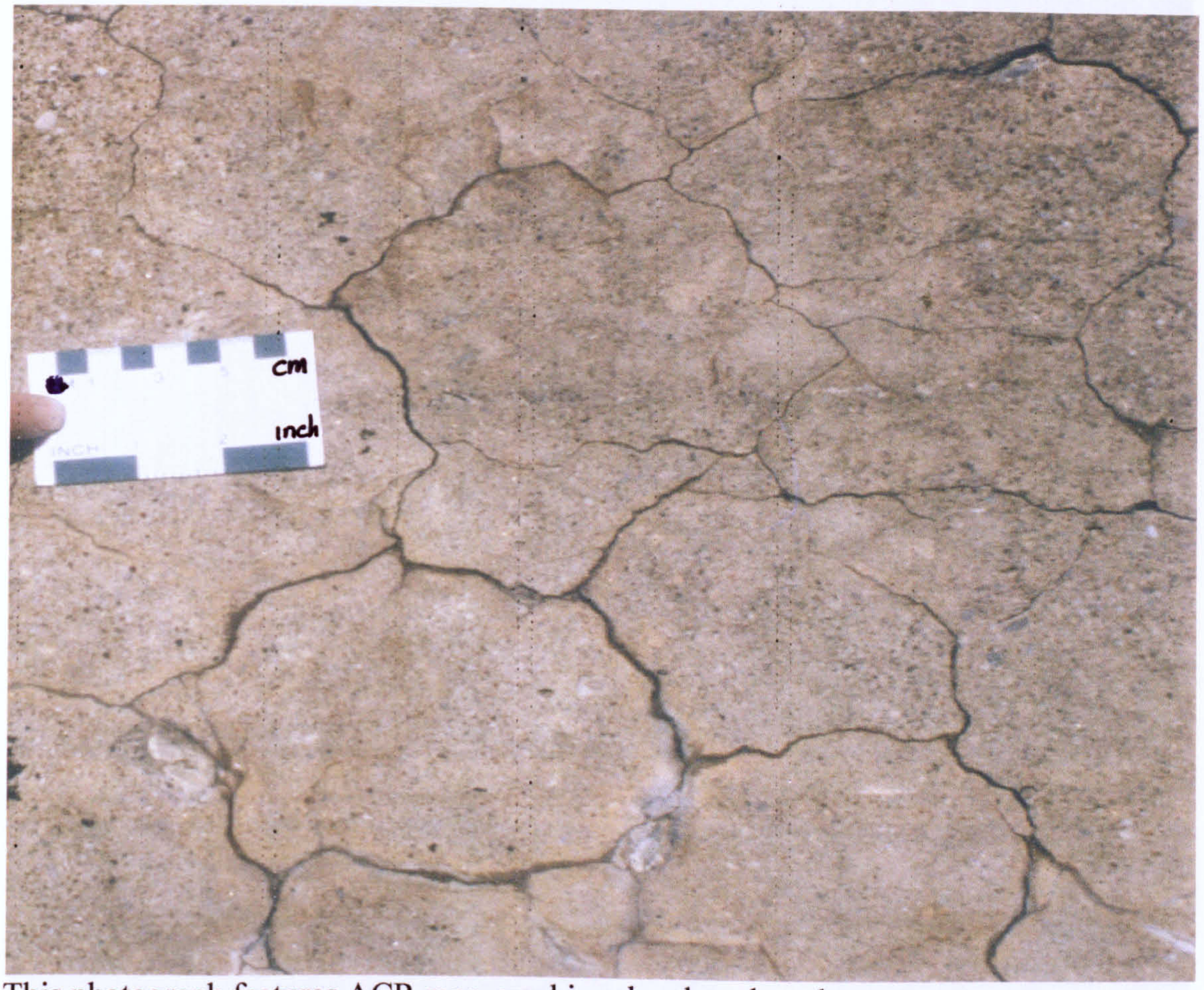

This photograph features ACR map-cracking developed on the pavement.

This image shows the same concrete mixture placed within a concrete pipe, which subsequently reveals cracking due to expansion.

Figure 3.3 ACR concrete samples at the test site in Kingston, Ontario, Canada. These samples were made in 1980 with Kingston dolomite used as the coarse aggregate and as a result of that this concrete has undergone ACR.

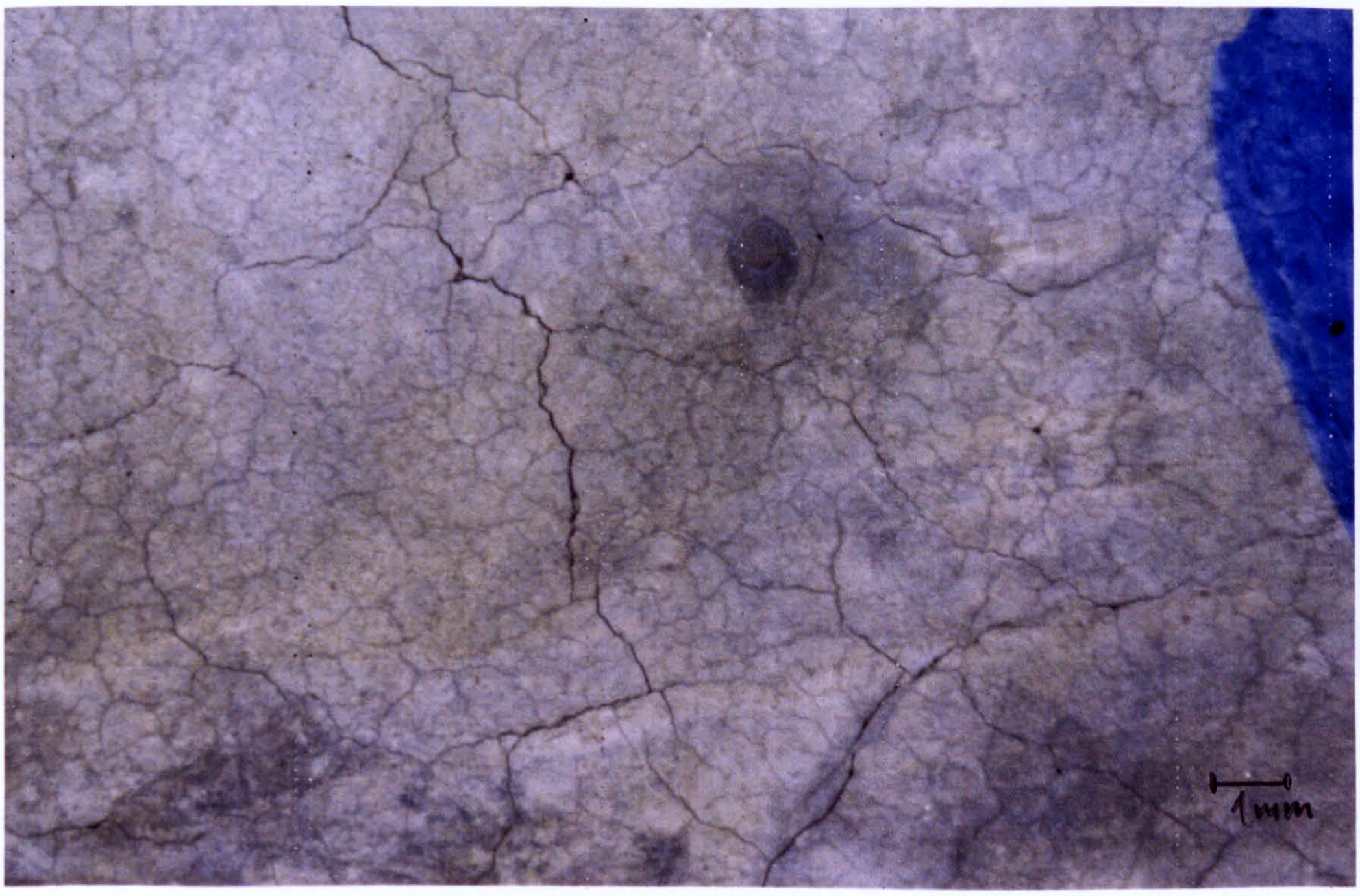

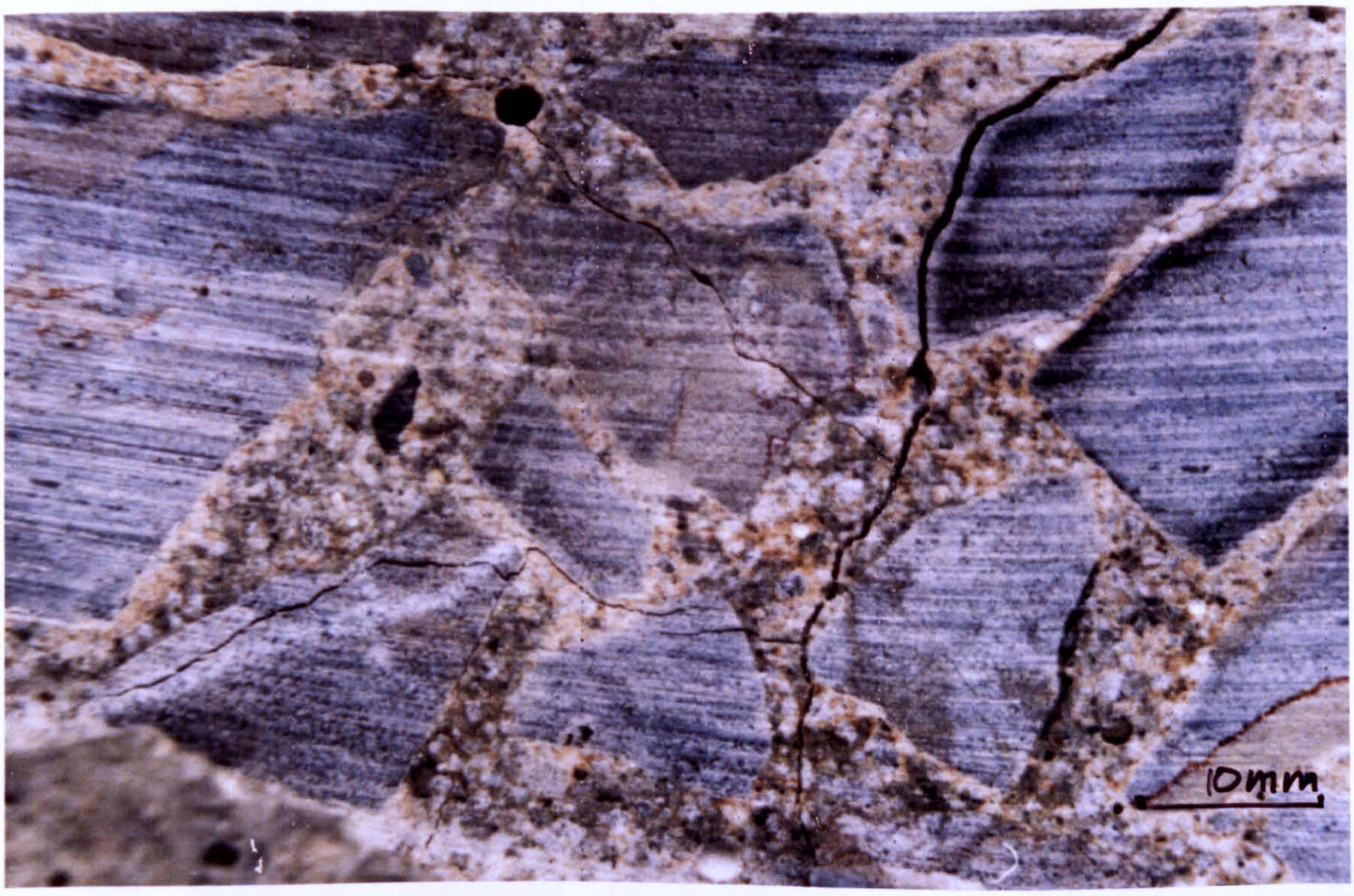

Figure 3.4 Tianjin bridge pier, China. The top image shows the area affected by AAR (alkali-dolomite and alkali-silica reactions). A cross-section close-up view (lower image) highlights the inner cracks and aggregate reaction rims.

a) rock sample (expansive Kingston dolomite). Scale: mm

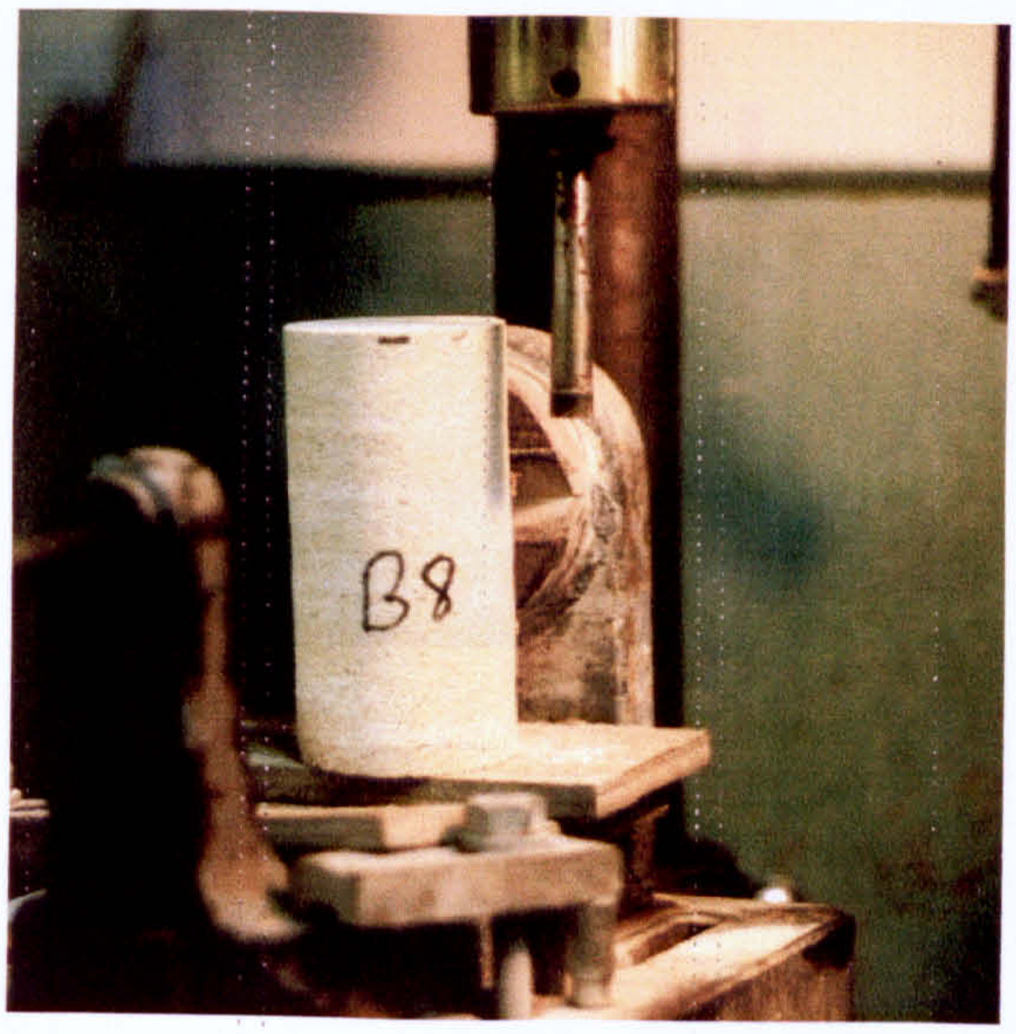

b) drilling equipment

c) rock cylinders (5-6 cm length, 9mm diameter)

d) cone-ends (angle 120^0)(ASTM C586) 35mm length

e) Variety of samples studied

Figure 3.5 Sequence of rock sample preparation. Rocks are first cut down to manageable sizes. These are then drilled into cylinders as shown.

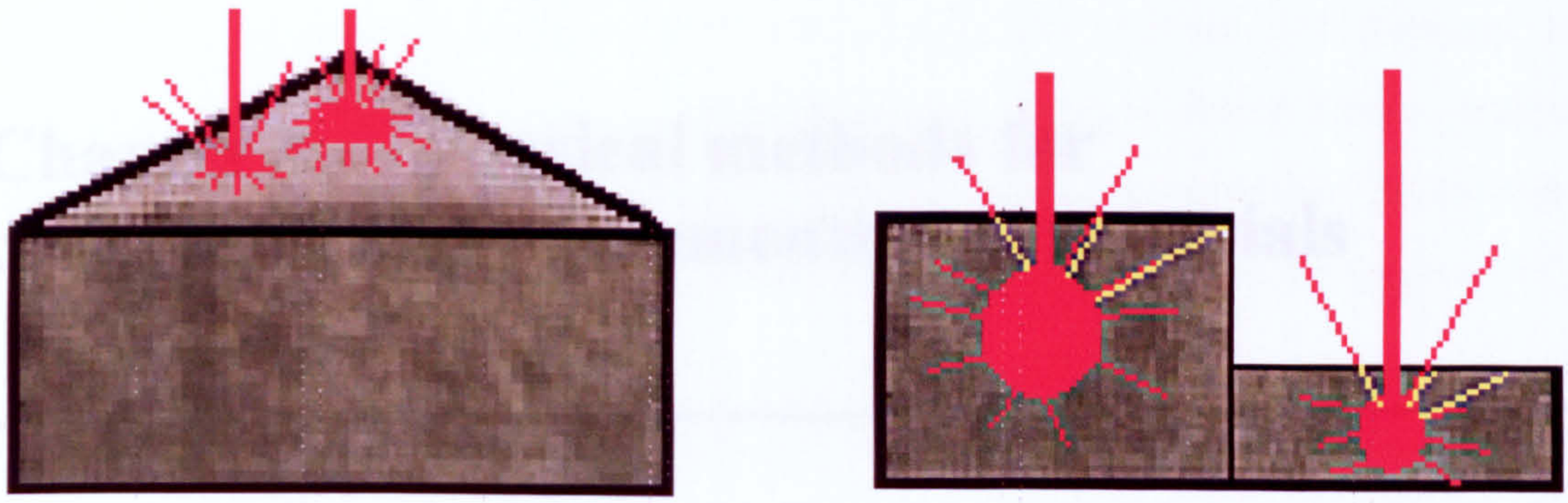

a) Cone ends of rock cylinders have been used for SEM observations without the coating, since their slope angle prevented the build up of electrons.

b) Thickness of samples also plays important role in SEM&EDX.

Figure 3.6 The shape of the sample was important for SEM studies. It was found that un-coated rock samples with slopes gave better images due to lower e^- charge build-up. This is compatible with samples of small thickness also having less e^- charge build-up then larger ones.

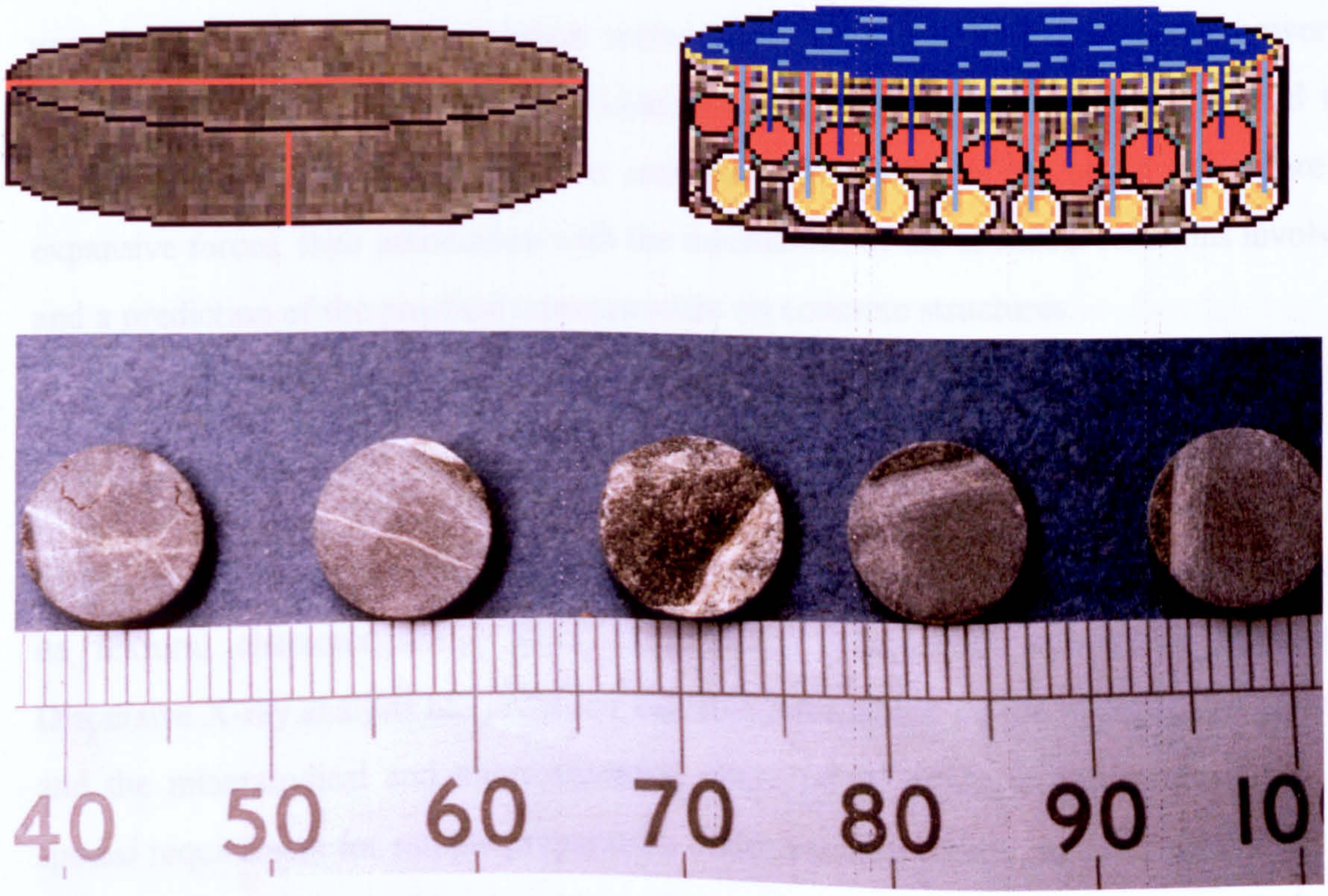

Figure 3.7 Thin rock tablets that were used for spectroscopic observations, allowing faster solution penetration.

Chapter 4 Physical methods for characterisation of cementitious materials

4.1 Introduction

Improving the properties of building materials, particularly concrete and mortars, is one of the most challenging activities within current construction research. For a long time, micro-characteristics were neglected and poorly understood. Instead, priority was given to testing physical qualities, such as strength, resistance to fracture and environmental factors. In the last few decades however scientific interest in concrete has increased and due to the application of novel instrumental techniques the field of scientific activity now includes micro properties and interactions at the atomic scale.

In view of their complexity, the characterisation of cementitious materials requires the use of sophisticated micro-analytical techniques. Thus establishing the most powerful techniques for the study of ACR in concrete based on surface chemistry, formed the beginning of a much greater task, i. e. including a definition of the origin and nature of expansive forces, their association with the mechanism of the chemical reactions involved and a prediction of the practical consequences on concrete structures.

4.2 Microscopy

Microscopic analysis provides valuable information on the microstructure of material and its textural characteristics. Scanning Electron Microscopy coupled with Energy Dispersive X-ray analysis has provided valuable information on the hydration of cements and the mineralogical and microstructural character of concrete and mortars, but has special requirement for sample preparation under vacuum conditions. More recently, the instrumentation for SEM has been improved and a new era of Environmental Scanning Electron Microscopy (ESEM) has begun, allowing for the first time analysis of a sample in an '*in-situ*' environment. For concrete, the ability to monitor the progress of reactions as they occur without any artificially introduced changes, is a crucial factor.

Microstructural characterisation has also been improved in terms of chemical and mineralogical analyses, by the introduction of the Electron Probe Micro Analyser (EPMA) in this field. The ultimate goal of materials scientists is to relate microproperties of a material to its macroscopic characteristics and performance

This section of the chapter presents aspects of analytical techniques used from a materials scientist point of view and their application in this study. Further details on the techniques and their operating principles maybe found in a wide number of scientific publications (Goldstein *et al.* 1991, Williams 1984, Reimer 1985, Heinrich 1981, Heinrich and Newbury 1991, Scott and Glove 1994, Potts *et al.* 1995).

4.2.1 Optical Microscopy (OM)

The examination of samples by optical microscopy is the stage after field observations and use of magnifying lenses. Thin sections or glass slides are necessary for this kind of work, but it is still a first line of identification of any physical or mineralogical disturbances in the concrete aggregate. Stereo and a high magnification optical microscope) were used for this purpose. A recent publication by St John, Poole and Sims (1998), 'Concrete Petrography' contains some of the most representative thin section images, featuring most of the phases/minerals common in concrete and mortar.

4.2.2. Scanning Electron Microscopy (SEM)

Today the Scanning Electron Microscope (SEM) is used extensively in materials science and finds many aspects applications in cement and concrete petrography. Although the instrument can have various attachments and several possible operational modes, the most important and widely used is the imaging facility, where micrographs are produced of surfaces in the range of 50-100,000 times magnification. The micrographs have a good depth of field due to the use of X-rays, generated by the interaction of the sample atoms and the electron beam. The latter permits the analysis of sample volumes down to a few μm^3, where the X-rays emitted reflect the chemical composition of the surface in these regions.

The SEM is primarily used for imaging. It consists of an electron source, lenses that focus electrons into an adequate beam and a scanning system that enables the beam to be rastered across the sample. A Everhart-Thornle type detector is used to collect electrons

emitted from the specimen, with an image display facility (Reed 1996). The mode of detection dictates the type of image produced, either topographic, which uses secondary electrons (SE) or compositional contrast based on the atomic number (Z) of the elements composing the sample, where back-scattered electrons (BE) are used for imaging (BEI). Secondary electrons are ejected from the specimen following electron bombardment and posses relatively low energies (few eV) compared with the back-scattered electrons. The fact that their energy is very low, limits their origin to not more than a few nm of the sample surface. The emission of secondary electrons results not only from the primary electron beam, but also from the interaction of backscattered electrons with surface atoms as they emerge from the sample. For a schematic description of a SEM instrument see Figure 4.1.

The main advantages of scanning electron microscopy over its optical counterpart are:- its high spatial resolution, large depth of field and low requirements for sample preparation. Spatial resolution in the range of 10nm can be achieved in topographic mode, and 100nm in compositional but the 100 times greater depth of field offers the most significant advantage. Although the SEM can be operated at very high magnifications, the maximum useful magnification is dictated by the resolution. Spatial resolution is the size of the smallest feature clearly visible in the image, and is limited by the diameter of the electron beam and by the interaction of the incident electrons with the specimen. SEM images of three-dimensional objects are for the most part amenable to intuitive interpretation (Reed 1996), which is what makes SEM one of the necessary tools in materials science in general.

4.2.2.1 Back-Scattered Electron Imaging (BEI)

The so-called 'back-scattering' phenomenon occurs when incident electrons are deflected through an angle greater than 90° to re-emerge from the surface of the specimen, or as a result of multiple deflections through several smaller angles. The back-scattering coefficient depends on the atomic number of the elements present in the sample, as the probability for high-angle deflection increases with value of Z. Back-scattered electrons possess energy with a maximum value equivalent to that of the incident beam energy. Single high-angle back scattered electrons from a high Z element will retain most of their initial energy and therefore produce a stronger signal (brighter image). By contrast, the lower atomic numbers and greater energy loss in multiple-angle

scattering will result in a lower output energy and therefore a darker image. The BEI can also be affected by the morphology of the surface and the voltage used. Recommended operating conditions are a voltage of 15-30 keV, a fine polished target surface and a short working distance. However, it is important to bear in mind that increasing the voltage will deteriorate spatial resolution in BEI, and result in less well-resolved images, (Reed 1996). In the work described in this thesis the BEI facility in the SEM proved to be especially valuable in distinguishing between dolomite and calcite grains within aggregates. It was also useful for observing the transition zone between aggregate and cement paste and any new phases present due to their different chemical states/atomic masses of components.

4.2.2.2 Energy Dispersive X-ray Analysis (EDX)

Various analytical attachments to the SEM have greatly improved its flexibility and applicability. The most important additional information to be gained is the chemical characterisation of the images obtained, through the introduction of Energy Dispersive X-ray Spectrometry (EDS). The energy dispersive X-ray spectrometer (EDX) produces the spectrum in a solid state detector according to the X-ray photon energy received and the acquisition is parallel for the whole spectrum. A semiconductor with an electronic band structure with the valence band fully occupied by electrons acts as a detection medium in an ED system. The absorption of an X-ray photon generates Auger and photo-electrons, which distribute a portion of their energy by raising valence electrons to the conduction band level. The detector is held at a certain voltage and when the photons initiate movements of electrons and holes in opposite directions, a brief pulse of current is generated. Therefore, X-rays photons presenting different energies can be differentiated by the measurement of the output pulses. The detection efficiency is determined by the solid angle subtended by the detector, or alternatively the detector may be mounted on a mechanism that provides variable working distances from the source. The level of efficiency can be altered by the absorption effect at the window or in the gold layer of the detector, as described (Russ 1984).

4.2.2.3 Application of Electron Microscopy in ACR

The advent of the scanning electron microscope, with its good depth of focus, has been important to cement and concrete science. SEM as an imaging instrument enables the

observation of microstructure, in terms of presence of micro-cracks, textural changes, micro-pores, weathering and the dissolution of crystal grains together with changes in surrounding matrix within aggregates. In addition to this it is possible to observe the morphology of individual grains as well as their inter-growths. Perhaps the area of special interest is the transition zone between aggregate and cement/paste and need to determine the starting point for the development of micro-cracks or the exchange of Mg and Ca ions during the process of dedolomitisation.

For SEM observations a Hitachi S2300 scanning electron microscope was used, with attached link system for EDX measurements. Among the difficulties present in concrete samples in addition to the complex nature is their out-gassing in the high vacuum. Therefore it is necessary to subject samples to an overnight degassing procedure prior to SEM analysis. Sample size and shape are only dependent on the analysing-chamber space. However, it is important to know that samples are stable under high vacuum conditions and the amount of heat produced in the electron beam. In case of non-conducting materials such as concrete and rocks it is necessary to coat samples, with carbon or gold, in order to avoid charge build-up at the surface. The sample morphology is also important and it is essential to have a flat, polished surface without smearing and contamination for a reliable X-ray analytical results. This requirement is also essential for BEI imaging. For the surface polished to ¼ micron it is possible to detect elements present as low as 0.1% from a volume 1-2μm in diameter. Light element detection requires a window-less detector, or a light element detector and is in general more difficult to achieve the same precision. It was also important to be able to use line analysis or spot analysis to detect changes following ACR expansion.

4.2.3 Electron Microprobe Analysis (EMA)

An electron beam micro analyser comprises of: a probe-forming system, WD&ED X-ray spectrometers, an optical microscope, a specimen stage, scanning mode, and the analysis are conducted in a vacuum system. The vacuum of 10^{-1} Torr is necessary to prevent the absorption of the X-rays in air. The specimen stage usually holds standards and several samples, and allows x, y, z, movements for point, line scan or map automatic acquisition, while the beam is stationary, and modern instruments are computerised. The role of the optical microscope is to be able to find areas of significant interest. In order to avoid

interference and operate simultaneously optical observation and carry out analysis, the optical microscope is positioned so that the reflecting microscope objective has a central hole to allow free path for the electron beam. The secondary electron imaging or back-scattered electron imaging are used as secondary modes, to assist in the primary function of an EPMA, which is a chemical identification of elements present, and possibly correlate morphological, microstructure features with the composition.

The electron microprobe analyser uses the X-ray spectrum emitted from the sample surface bombarded by a focused electron beam to characterise the chemical composition of the targeted area. Two types of analysis may be obtained, qualitative analysis of the elements present by the identification of the lines in the spectrum produced (using EDS) and quantitative analysis where the concentration of those elements is determined, by measuring the intensities of the sample spectrum against calibration standards (using WDS). The X-ray spectrometers are arranged so that the distance between the crystal and the X-ray source is equal to the distance between the crystal and the X-ray detector. The use of an electron beam with a miniature probe diameter provides a very small area of analysis. Imaging facility is carried out as in SEM, where a secondary electron image provides topographic information and a backscattering electron image reflects the atomic number of each phase present. Element distribution images may also be produced by scanning the electron beam in a TV-like raster and displaying the intensity of a selected X-ray line.

The electron micro-probe instrumentation principle is very similar to that for SEM, but the electron beam is ten times larger (about 1μm) than in SEM (10 nm), and higher beam currents are used. The probe current is emitted from the filament, within the electron gun. A set of magnetic lenses focuses the beam into approximately a 0.2-1μm diameter probe and 1-100 nA current. Two or three electron lenses are used to de-magnify scanning images. Most of EPMA are equipped with two or more wavelength dispersive and an energy dispersive spectrometer, each of which possesses electronics for amplifying and counting the pulses from the detector. The EPMA used in this study was equipped with both wavelength and energy dispersive X-ray detectors (WDS and EDS). As a result of a larger beam and higher voltage, the penetration of the beam into the sample is deeper, up to 15μm, compared to 1-2μm in SEM. These changes offer higher accuracy and detection for the lighter elements sometimes which are often difficult to

analyse in the SEM. The detection of major elements has a high level of accuracy, with an overall analytical accuracy of approximately +/- 2%. The spatial resolution is a result of the penetration and spreading of the incident electrons in the sample, which is ultimately governed by the density of the specimen and its thickness.

4.2.3.1 Wavelength Dispersive Spectrometers (WD)

The second type of X-ray spectrometers was in use before ED and is called wavelength-dispersive, based on the Bragg reflection of crystals. These type of spectrometers are usually incorporated within an electron microprobe instrument. Unlike ED, were a simultaneous production of signals is achieved for the whole spectrum, WD spectrometer operates in serial mode, where the detector can recognise only one wavelength at the time. Advantage of WD over ED is that it has a better spectral resolution, even though ED requires much shorter acquisition time. The operating principal of WD is that the X-rays are dispersed relevant to their wavelength. The atoms from the crystal structure are then dispersing X-rays that infringe on a crystal (Reed 1996).

An electron probe instrument is usually equipped with up to five vertical WD spectrometers around the column. The count-rate per unit beam current obtained with WD spectrometers are lower than those given by a typical ED spectrometer. Another important parameter is the peak to background ratio, which is related to resolution since the background count-rate depends on the width of the band of continuum which is recorded by the spectrometers. The values obtained by WD are approximately a factor of ten higher than those of ED spectrometry (Agarwal 1991).

4.2.3.2 Element mapping

Another mode of operation available using X-ray analysis, was mapping for elemental composition, in spatial distribution as well as line profiles and scans made to plot changes in element concentration. The above mentioned were of particular importance in the observation of reaction rims and grain interfaces, enabling a detection of any distribution changes of chemical elements due to the chemical-physical reactions that might have taken place. These were complemented by the use of the spectroscopic techniques, with the application of ion-etching that enabled the acquisition of the depth-profile chemical

analysis, which provided the information on the depth-extent of the changes that occurred.

4.2.3.3 Applications of EPMA in this study

The illustration of how important is a choice of adequate technique for the desired information, especially for unknown materials, is listed in the following paragraph for an EPMA:

1) Investigation of any inhomogeneity present on a point-by-point level with high accuracy and precision.

2) The distribution of inhomogenieties in the form of an elemental distribution map, but with lower accuracy.

3) The determination of the compositional variations along one or more line traverses.

4) Averaging the data obtained from an area by enlarging the probe diameter or by scanning, on the expense of resolution quality.

The reason for the wide use of EPMA in fields of mineralogy and petrology, therefore concrete petrography and processes that lead to various phase changes within concrete compound are:

1) EPMA and SEM are non-destructive techniques, with minor alterations in volatile elements due to heat release from high voltage electron beam.

2) Elements with atomic number higher than 10 are determined with acceptable accuracy and sensitivity, and lighter elements apart from H, He and Li are undetectable.

3) Minor and trace elements have detection limits of approximately 50 ppm.

4) The time required for analysis usually 1-5minutes enables reliable sample characterisation within a short time period.

5) A high spatial resolution in the order of 1μ allows identification of almost sub-micron features

6) EPMA can provide compositional information in form of atomic mass weight that

can be used for mineral identification.

7) Experimental studies of co-existing phases and the associated elemental partitioning as well as phase relationships.

8) Creatures such as a zoning within minerals and the elemental exchange can be monitored in detail as a result of a high spatial resolution.

9) Fabric Analysis is yet another aspect of SEM use, revealing the orientation and arrangements of individual grains or agglomerates, presence of micro-cracks and cavities (Gillott 1976, Reed 1993).

Reed (1996) describes Electron probe analysis as a standard technique in mineralogy and petrology, thanks to its capability for a rapid non-destructive *in-situ* analysis with high spatial resolution, good accuracy, and a reasonably low detection limits, and the fairly simple specimen preparation requirements. Other micro-analytical techniques described elsewhere can offer better performance in specific aspects, but none compares for all round usefulness and convenience.

4.2.4 Environmental Scanning Electron Microscopy (ESEM)

A need for the modification of the traditional high vacuum operating conditions in the scanning electron microscopy, resulted in a series of preliminary designs during 1970's (Lane 1970, Robinson 1974, Spivak 1977, Shah and Beskett 1979, Danilatos 1979). Specialised scanning microscopes available today do not require specimen-coating, and can perform analysis in wet state, making the SEM applicable in areas of materials science and biological sciences more than ever before. Only recently the use of an ESEM system has become more accessible and applicable, due to the manufacture of the first commercial instruments. The two most important aspects of an ESEM, a brief instrumentation description and the more detailed application of it in the cement and concrete science, will be presented in this section (Danilatos 1993).Figure 4.2 presents the schematic description of an ESEM with all individual components as mentioned in the above section. The instrumentation principles will be given on the example of the updated version of an ESEM instrument, so-called Electro-Scan ESEM (E-S/ESEM), which was used in this study (Danilatos 1993a). The main units that provide effective functioning of the E-S/ESEM are: the electron optics, pressure stages, the environmental

parameters control system, and the accessories for EDS, BEI and SEI operational modes. An environmental scanning microscope is in reality a conventional SEM with a sample chamber with pressure as low as 4.6 Torr, separated from the electron optics column and the gaseous secondary electron detector by the differential pumping systems.

In practice this means that the samples do not have to be dried, they can even be flooded with water or exposed to various degrees of humidity. Different gases can also be used as the sample chamber is isolated from the high vacuum of the electron gun with the multiple Pressure Limiting Apertures (PLA). The diagram in Figure 4.2 shows the details of the electron optics column and stages with different pressure levels that secure undisturbed path for the electron beam, by using differential pumping system, incorporation of several pumps and valves. Another advantage of the E-S/ESEM is the ability to observe insulating samples without coating, due to the presence of a positive ion supply from the ionised gas, which suppresses the negative charge build-up on the sample. Moreover, the gaseous species are used as a detection medium, whether in form of gaseous ionisation or gaseous scintillation.

The gas that carries the information about the sample surface flows through the apertures depending on the aperture size and the differential pressure present, and is admitted to the column where the detection process starts. The detection takes place in the gaseous secondary electron detector (GSED), where ionised gas is used to detect and amplify the secondary electron signal, or back-scattered electrons, allowing production of SEI and BEI. The gaseous detection device (GDD), is the main detection mode of an E-S/ESEM. Secondary electrons emitted from the specimen undergo acceleration between consecutive collisions with the gas present in the chamber (usually water vapour). As a result of that additional electrons are freed from the surrounding atoms, creating an avalanche process. With the increased pressure and the working distance (more than 2mm below PLA1), the ejection of back-scattered electrons is predominant, and they too cause the primary gas ionisation. The back-scattered electron detector used in the ESEM is of a different design than in SEM and is effective at a long working distance, at low pressure and a high keV, for a better electron collection angle (Danilatos 1990).

However, because of their nature and the operating conditions, there are some limitations on the resolution and analytical capability of this instrument, mainly due to the limitations in achieving a small probe diameter. The disadvantage of the presence of gas is that it causes skirting effects, another word the interaction of gas species and electrons from the electron beam resulting in a broad electron skirt around the original beam spot. The modern type of E-S/ESEM can obtain the resolution of a conventional SEM under adequate operating procedures (Danilatos 1991). Figure 4.2 presents the schematic description of an ESEM with all the individual components as mentioned in the text above.

4.2.4.1 Energy Dispersive X-ray Analysis (EDX) in ESEM

As in a conventional scanning electron microscope (CSEM), back-scattered electron imaging and X-ray microanalysis were used to obtain the complete sample transformation evaluation. The resolution in EDX is to a certain degree affected by what is known 'skirting effect'-scattering of beam electrons by the presence of various gas molecules. To negate effects of the charge build-up in the operating low-vacuum mode (>270Pa) the analysing chamber contains gas and that causes beam skirting. This problem can be overcome by various EDX modifications to the X-ray detector used, such as the working-distance at which analysis are carried out.

4.2.4.2 Application of ESEM in this study

The Philips ESEM-Environmental Scanning Microscope at English China Clays, St. Austel, Cornwall, was used for all the observations in this study. It enabled measurements to be performed without prior treatment or sample alteration. No coating was required. This was of particular importance for the analysis of the dolomite crystal after the treatment with alkaline solution. The sample was observed straight from the solution allowing investigation of the hydrated phases and their structure unaltered. The non-destructive nature of ESEM examinations and the possibility to view even delicate sub-micron deposits that would have been otherwise removed during sample preparation or coating was beneficial. By using the ESEM interference effects of sample preparation techniques on the analysis and imaging were minimised, which automatically helped in achieving main aims of the study, an accurate description of the mechanism of dedolomitisation reaction. The advantages of the Environmental Scanning Microscopy are discussed below.

Firstly, the process of hydration, the essential part of concrete setting can be now monitored in time with full imaging and chemical characterisation (Jennings 1992, Kjellsen and Jennings 1996). Samples of lime and cements can be treated with various agents such as CO_2 and the effect observed almost instantly. The effects of different compositional ratios on crystallisation are especially valuable in observing the impact of new supplementary cementitious materials added to concretes and mortars for specific requirements, (Radonjic *et al.* 1998). Unlike in a CSEM, the possible physical or chemical transformation of the sample surface under the electron beam, were completely avoided.

Secondly, field concrete samples could be analysed without any alteration and apart from the sample size limitations all characteristics remain intact. This is of particular importance for study of damaged concrete structures, where diagnosis must not be confused with other side effects. These could be produced due to the sample preparation, as concrete is well known for hosting various synergetic reactions, such as AAR, DEF, carbonation, sulphate attack and many other minor processes. Thirdly, in case of the expansion mechanism of ACR, powdered samples were used for smectite hydration monitoring (Mehta 1991).

4.2.5 Atomic Force Microscopy (AFM)

Introduction

The atomic force microscope (AFM) belongs to a family of microscopes called the scanning force microscopes (SFM) also known as scanning probe microscopes. Since its invention in 1986 by Binning, Quate and Gerber it has evolved into a valuable imaging technique with the resolution in the micrometre to subnanometre scale. In this particular study the main advantage of AFM over SEM was the ability to image insulating samples without prior coating, and under different environments.

Principles and instrumentation

Typical for all scanning probe microscopes, an AFM utilises a sharp probe which when by moving over the examined surface produces an image of the topography of the top atomic layer. The movement is a simple raster scan of the probe that consists of tip at the end of a cantilever, see Figure 4. 3.a . The cantilever bends responding to the force between the tip and the analysed surface. Modern AFM microscopes employ an optical

lever technique although the first AFM used a scanning tunnelling microscope to detect the bending of the lever. As it is shown in Figure 4.3a, as the cantilever flexes the light emitted from a laser is reflected onto the split photo-diode. This measurement of the difference signal is reflective of the bending of the cantilever. An accurate positioning device made from piezo-electric ceramics carries out the movement of the tip or a sample stage. The precision of this device is such that allows sub-angstrom resolution in all three axes (x, y and z).

Image Acquisition

An AFM image is a topographic presentation of the sample surface, therefore the tip-sample interaction is of the main importance for image contrast. There are three main types of imaging: contact mode, tapping mode and a non-contact mode. In this study contact and tap-mode were used. The contact mode (Figure 4.3b) is the most used operational mode, where the tip and the sample surface remain in contact during the scanning. However, with particular surfaces that contain unstable, fine deposits, the contact mode can produce images as a result of a multiple probing due to the tip-contamination. The tapping mode (Figure 3.4c) is used for imaging of such surfaces. The cantilever is oscillated during tapping mode imaging allowing the contact of the probe with the sample for a short time. In this study a third type of imaging that used was the phase imaging. This involves the measurement of difference between the oscillations of the cantilever driving piezo and the detected oscillations. It is suggested that the image contrast obtained during such imaging reflect the compositional difference, stiffness and viscoelasticity. The resolution of the image depends on the sharpness of the scanning tip. The best probes can have a radius of only 5nm.

An AFM image is usually displayed as a three-dimensional image, using the colour mapping for height, where black presents low features and white or light colours in general are used for high features. The AFM instrument used in this study was in Physics Department, University of Bristol.

4.3 Spectroscopy

Surface chemistry and near surface chemistry have been used in materials science over the last few decades (since 1960s), enabling improvements in fields as diverse as anti-corrosion coatings, conservation and grain-boundary analysis. However, the application

of this branch of physics and chemistry to the characterisation of building materials has been limited to NMR (Groves and Richardson 1995), Raman and FTIR analysis for cement-minerals. In this thesis an attempt has been made to introduce, X-ray photoelectron spectroscopy (XPS) and time of flight secondary ion mass spectrometry (TOF-SIMS) to the study of the ACR mechanism.

The reactions taking place at the surface may be on an atomic scale, but their impact will reflect on the material as a whole system in a given environment and function. Practically, the structure and chemistry of the top atomic layers will be to a great degree dependent on the behaviour of the atoms immediately below the surface (Vickerman 1997). An illustration given by Vickerman is that in $1cm^3$ of a metal there are 10^{23} atoms, so the top layer of a surface analysed is approximately 10^{-6}%.

Surface techniques in general are based on the same principle, where the analysed surface is bombarded by electrons, ions or photons, and the detection is carried out on the emitted subatomic particles (Woodruff and Delchar 1994). Bearing in mind the spatial resolution it is evident that theses techniques have limitations for a bulk characterisation of a specimen, but are able to provide important complementary information for SEM, EPMA, XRD. Another difficulty with surface techniques is that they operate in UHV, in order to prevent interactions and scattering of electrons with gas molecules, complicating their application to porous materials such as rocks and concrete.

The present study is an example of the parallel application of microscopy and surface techniques in building materials, aiming at a better understanding of ACR. In the following three sections of this chapter a more detailed description of the techniques used is given, with the theory, instrumentation, applications and advantages they offer.

4.3.1 Electron Spectroscopy for Chemical Analysis (ESCA)

The range of applications and information gathered, are the two aspects on which electron spectroscopy for chemical analysis (ESCA) or X-ray Photoelectron Spectroscopy (XPS) can be defined as the most popular contemporary surface technique (Vickerman 1997). The foundation for modern ESCA dates back to the 1880s (Hertz 1880, Hallwachs 1888 and Thomson 1899) and first observation of light emissions from solid surfaces, the major contribution of which was the quantisation of energy by Planck (1900), was followed by the explanation of photoelectric effect by Einstein (1905).

However, it was not before 1951 Steinhardt and Serfass (1951) that the first photo-emission was applied as an analytical tool.

The surface analytical method ESCA is simply the identification of electrons emitted from the surface previously bombarded by a photon, shown in Figure 4.4 The photo-emission is a process involving a total transfer of the energy from an in-coming photon to the atomic orbital electron, resulting in an electron emission from the interacting atom (Vickerman 1997). The minimum energy required for the emission of electrons from irradiated sample surface is called the work function. Under the X-ray bombardment, electrons ejected from the specimen are collected and their kinetic energies determined, from which binding energies are calculated. The basic physics is described by Einstein equation where E_b is the binding energy of the ejected electron, $h\nu$ is the energy of the X-ray source and E_k is the kinetic energy of the emitted electron that is measured in the analyser (Berkowitz 1979, Feldman and Mayer 1986). ,

$$E_b = h\nu - E_k$$

When the work function for the instrument (ϕ) is incorporated the above equation is corrected to the following:

$$E_b = h\nu - E_k - \phi, \quad \text{where } \phi = E_f - E_{vac}$$

Figure 4.4 presents a schematic description of the ESCA.

4.3.2 Binding energy

An electron is bound to an atomic nucleus, and the distance between the electron and nucleus within an atom governs the energy needed for the electron to escape. In addition, the binding energy will depend on any covalent or ionic bonds between constituting atoms, giving valuable information, referred to as chemical shifts or binding energy shifts, used to establish the chemical states of elements analysed. For example the energy shift between the electron of an element in an oxidised state and a carbonate state can be a few KeV. The energy resolution of an ESCA instrument is 0.2eV, making it possible to detect the binding energy shifts for most chemical elements (Briggs 1977). From the above-mentioned it is evident that the XPS can provide qualitative elemental and chemical state information. The obvious next step is the quantification, which is mainly obtained from the peak heights/widths.

It is also important to explain the sampling depth in XPS. The X-rays used in ESCA are approximately 1KeV and can penetrate up to 1000 nm, unlike electrons (EPMA) whose penetration depth is 10nm. Analysis based on emitted electrons will therefore have a depth resolution of an average length of the ejection path of an electron, during which there will not be any energy loss. Electrons from the bulk of the sample lose their kinetic energy, resulting in a reduced kinetic energy, adding to the background of the spectrum or simply never reach the surface in case of a complete energy loss (Briggs 1977).

4.3.3 Interpretation of spectrum

In order to understand and to extract the required information from an ESCA spectrum it is necessary to differentiate the various spectral features. The typical ESCA analysis will involve first of all an acquisition of a wide scan spectrum, 0-1000eV, with more detailed narrower scans of the areas of a particular interest. An average spectrum is composed of the background or inelastic scattering caused by photoelectrons subjected to energy loss, but which remaining energy was sufficient to escape the work function of the surface. The dominant part of a spectrum includes two types of peak: the photo-emission and Auger electron peaks, and they are easy distinguished by changing the X-ray source, as the Auger lines will remain the same. Photoelectron lines are usually intense and symmetric and may be identified by reference to standard spectra. Lines that are of less importance are X-ray satellites, X-ray ghost lines, Shake-up lines, energy loss lines and those from spin-orbit coupling (Briggs 1997).

4.3.4 Instrumentation

An ESCA instrument is composed of a vacuum system, X-ray source, electron energy analyser and data system. The instrument used in this study was a Vacuum Generators ESCASCOPE photoelectron spectrometer with a Mg-Kα X-ray source operated at 400W, with a 3mm entrance slit. Wide scans were recorded at 50eV pass energy and regional scans at 30eV. The mapping was carried out at 700 μm, zoom 2. An ultra high vacuum system (UHV) of 10^{-10} Torr is required in order to enable undisturbed travelling of photoelectrons, prevent contamination of the sample surface and finally provide the optimum operating conditions for the X-ray source. The X-ray source is an anode (Mg or Al were used) bombarded by a high energy electrons (10 keV) as a result of which fluorescence X-rays are produced. The analyser is made of a collection lens, energy analyser and the detector.

4.3.5 Application of ESCA in this study

The main advantage of ESCA analysis in this study was that it was the only technique that potentially was able to identify chemical changes after much shorter time due to its atomic layer sensitivity. Another advantage was that there was no need for coating or any other sample preparation, apart from long out-gassing procedures. The most important of all was the possibility to monitor transition of Mg from its carbonate to hydroxide state. There was also the potential to observe the interaction of cementitious phases with species of interest, leading to application in nuclear waste disposal and monitoring of the effect of supplementary cementitious materials on concrete properties. In the case of ASR it would be possible to detect the change in the form of reactive silica component and save time on time demanding conventional testing procedures such as prism tests etc. However, an established data base of standards/reference spectra for cementitious materials is required.

4.4 Time of Flight Secondary Ion Mass Spectroscopy (TOF-SIMS)

Secondary Ion Mass Spectrometry (SIMS) is a technique involving ionised particles emitted from the surface bombarded by ions, electrons, neutrons or photons (1-15keV). The secondary particles analysed are atoms, molecules or their clusters. There are two types of SIMS: dynamic used for depth profiles and static which application is in chemical characterisation of the surface. In this study only dynamic SIMS was used. Although SIMS techniques are in principal destructive techniques as they involve sputtering of top atomic layers of the sample, in 1970s Benninghoven and his Munster group showed that with a relatively low primary particle flux density, the surface will remain static (Briggs *et al.* 1989, Vickerman *et al.* 1989).

A SIMS instrument consists of three components: the primary beam source, the mass spectrometer and an ion optical selection system (see Figure 4.5 for a schematic description of the instrument). The instrument used in this study was equipped with a liquid gallium field ionisation source, able to achieve the highest spatial resolution (200-20nm) (Vickerman 1997). This beam source is also adapted for the pulsing mode, with a set of deflection blanking plates that sweep the beam across an aperture, which is important for TOF SIMS molecular ion imaging for the high spatial resolution (Briggs and Seah 1992).

The mechanism of secondary ion generation is a complex one. First of all there is a dynamic process during which atoms and their clusters are desorbed, followed by the ionisation process when some of the secondary particles receive a positive or negative charge. The incident beam transfers its energy to the targeted surface, initiating a chain of collision cascades between the atoms within 30A of the top layers (Briggs and Seah 1992). Only 1% of the sputtered particles is ionised. In spite all of this static SIMS can generate a valuable information on the chemical structure of the surface analysed. The main advantage of static SIMS over other surface techniques is its ability to study polycrystalline surfaces, with products that usually involve compounds of more than three atoms (Vickerman 1997). This again could be potentially useful in study of cementitious materials.

The operational concept of the Time of Flight Mass Spectrometer is based on the time the particles need to reach the detector. Basically the ions leaving the surface will poses the same kinetic energy, so the time they spend 'travelling' will depend on their mass. In order to have the ions of the same mass reaching the detector simultaneously, an ion mirror is introduced so that reflected ions of the same mass leave with the same energy. Although the charging effect is reduced comparing to the continuous beam analyser, sample charging can still be a problem for insulating samples. Additional charge compensation is achieved when the extraction field is reduced to zero between the primary ion pulses, producing a pulse of electrons directed at the sample surface that can effectively neutralise the positive charge (Briggs and Seah 1992). This aspect of the technique was particularly useful when bearing in mind the nature of material analysed in this study, which is categorised as highly insulating. The acquisition of the negative spectrum was of vital importance in the experiment with D_2O tracer and the depth penetration of OD^- ions. For the accurate information it is important to acquire both negative and positive spectrum. SIMS studies employed a Vacuum Generators Ionex Time-of-Flight Mass Spectrometer with 30kV liquid metal gallium source.

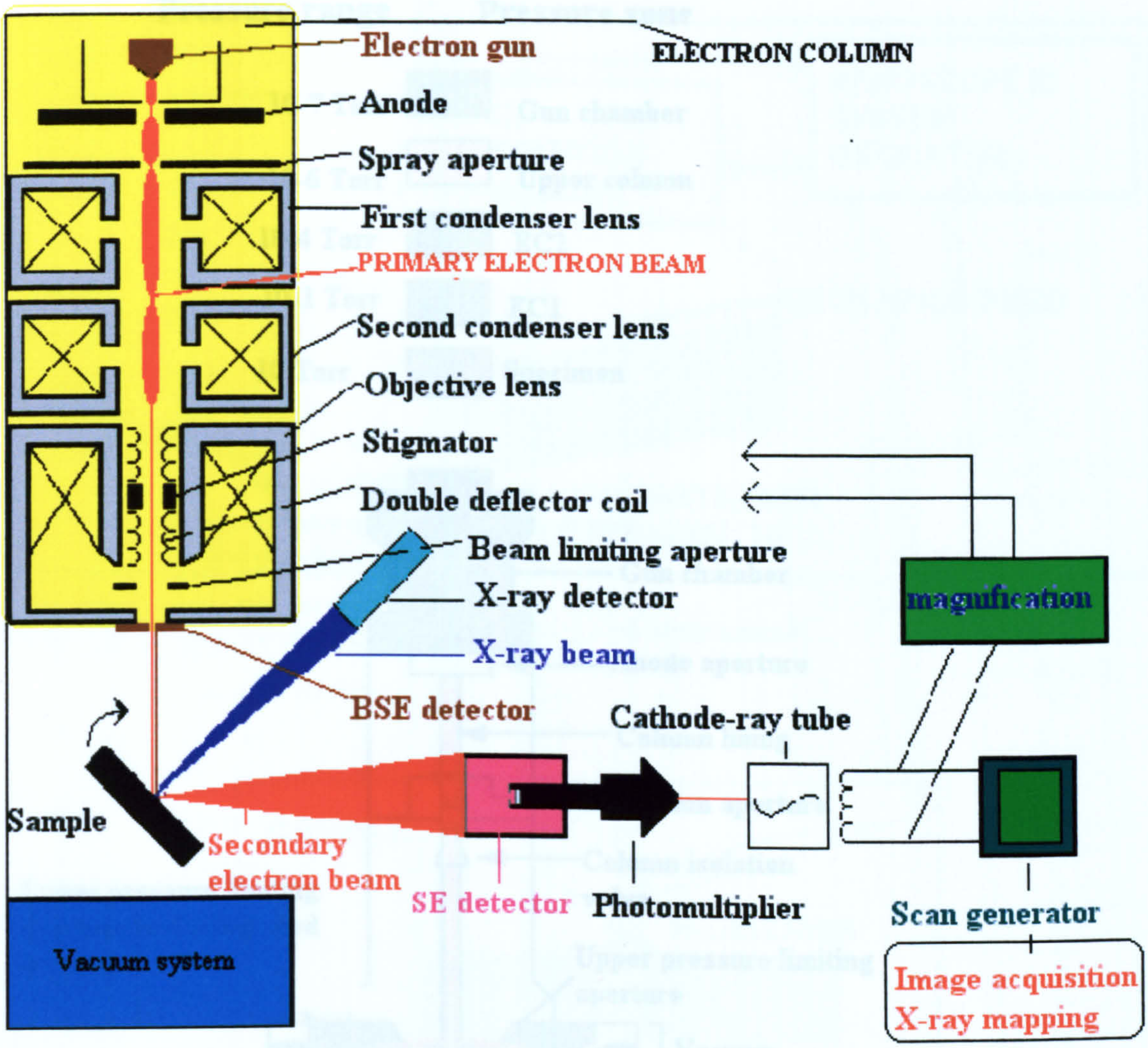

Figure 4.1 Schematic presentation of an SEM

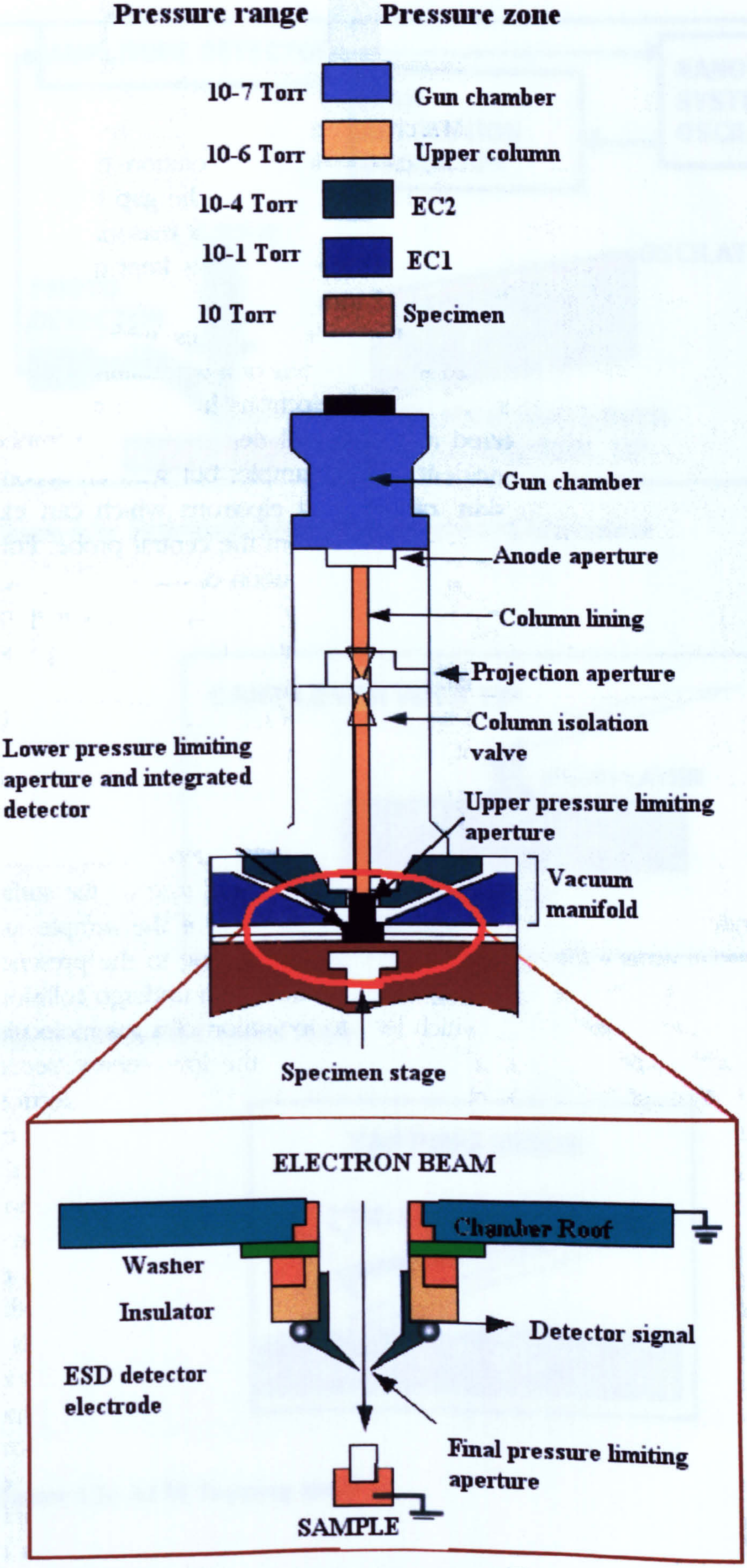

Figure 4.2 Schematic representation of an ESEM instrument

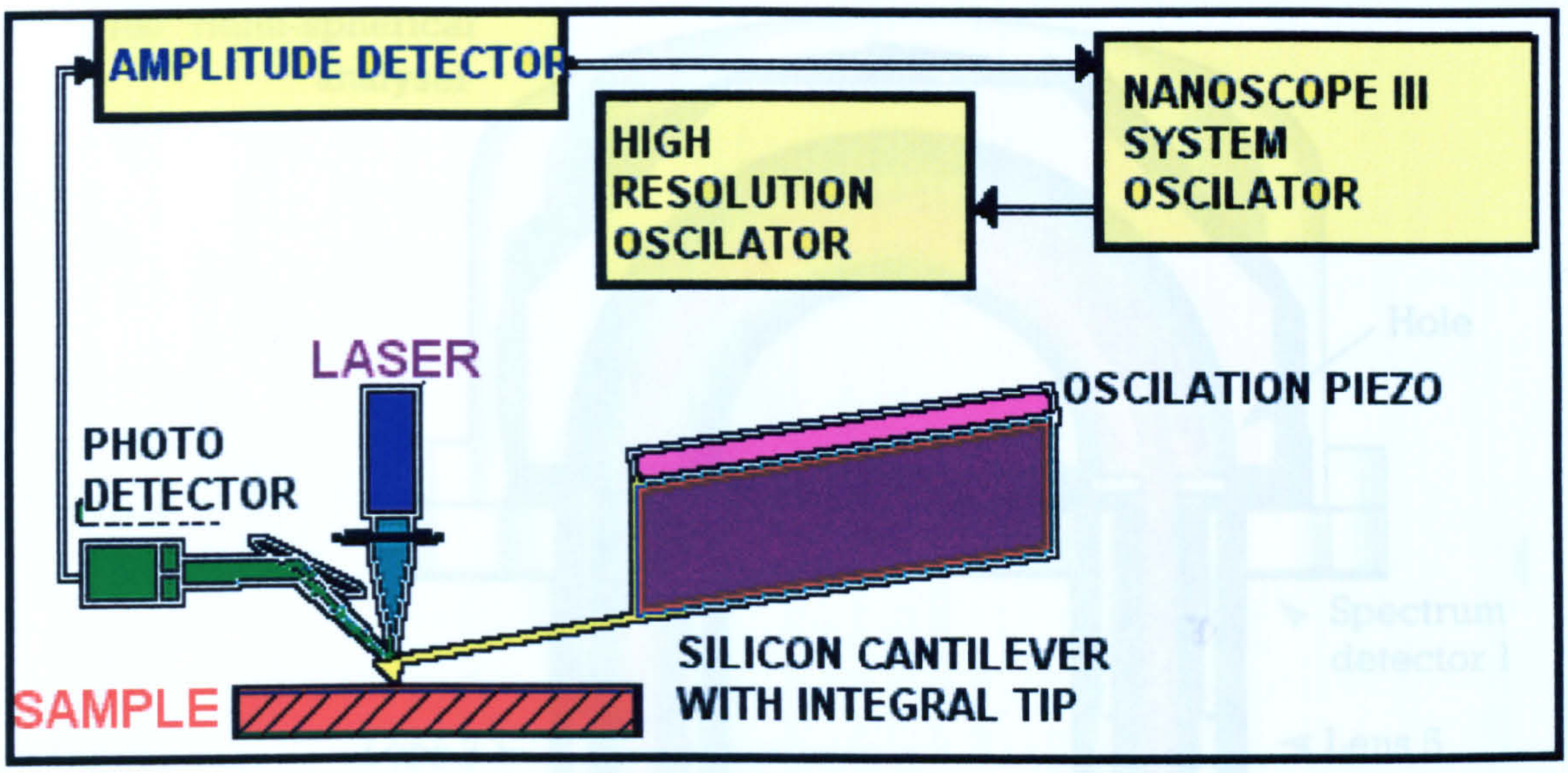

Figure 4.3a Schematic description of an AFM instrument

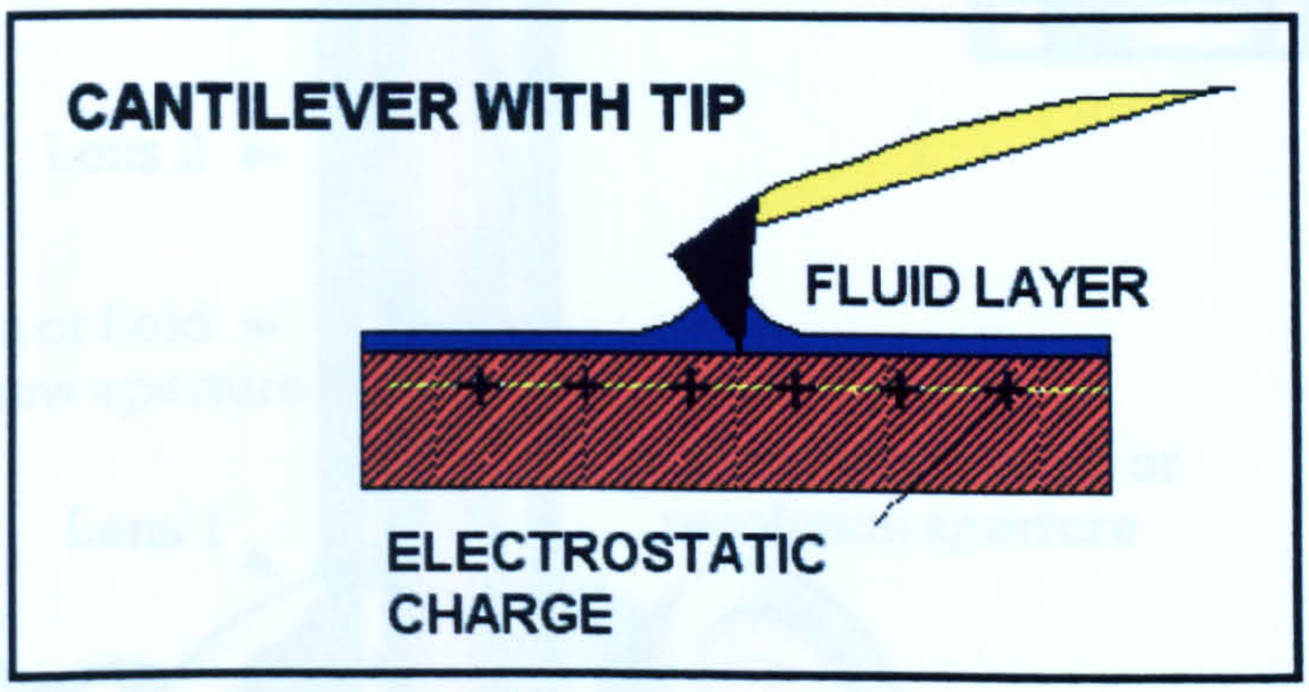

Figure 4.3b AFM Contact mode

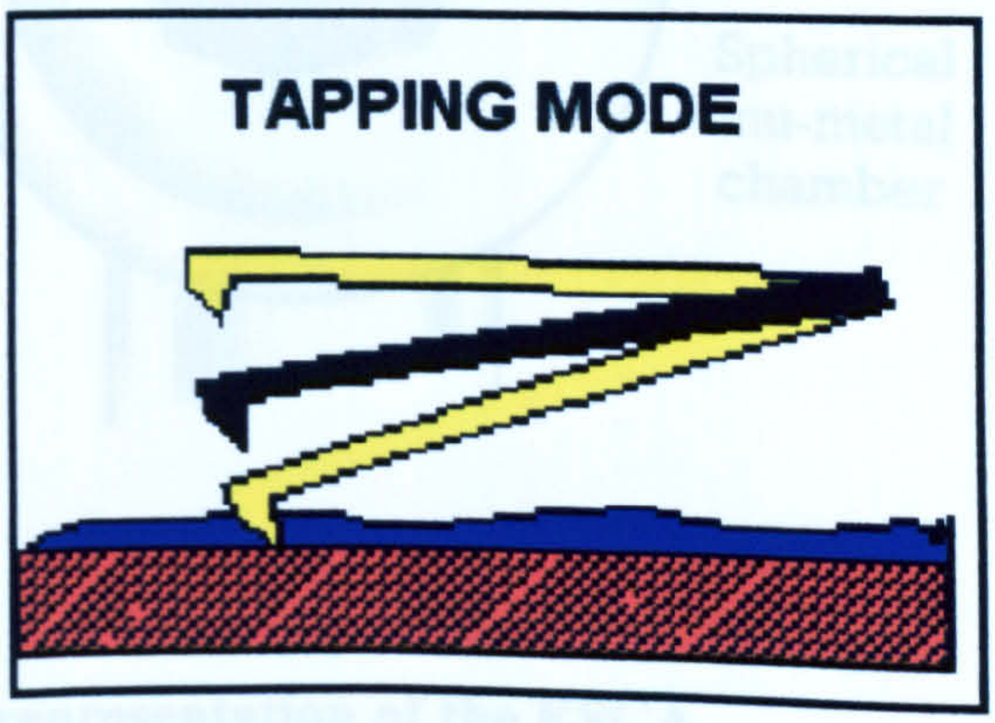

Figure 4.3c AFM Tapping mode

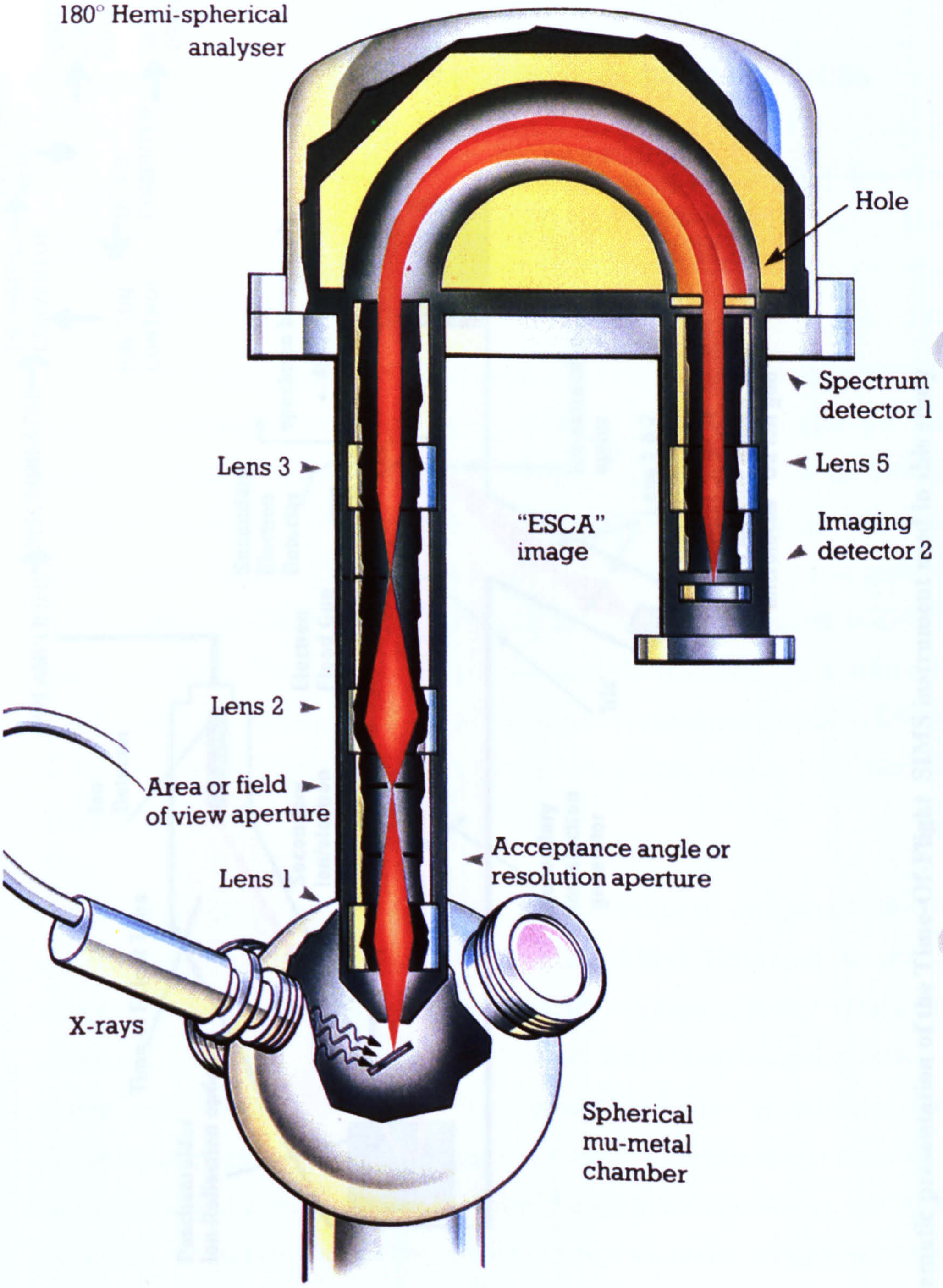

Figure 4.4 Schematic representation of the ESCA

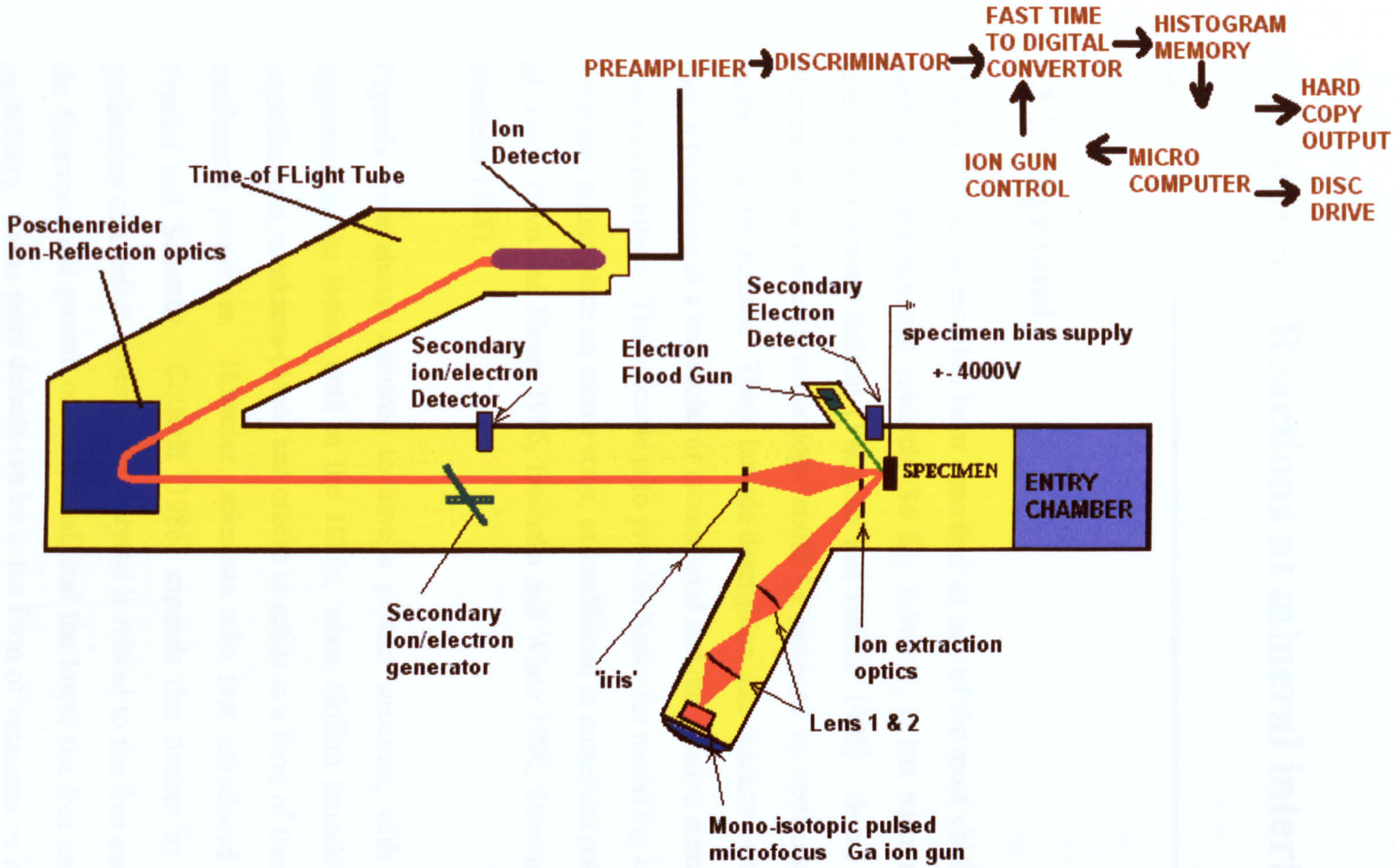

Figure 4.5 Schematic presentation of the Time-Of-Flight SIMS instrument used in this study

Chapter 5 Reactions at mineral interfaces

5.1 Background

Mineral surface science has been described as one of the most challenging areas in the earth and environmental research. So far, however, it has been applied to concrete science in a limited fashion (Vaughan and Patrick 1995). Some of the challenging phenomena in concrete mineralogy could be resolved by applying the techniques of mineral surface science. These include description and characterisation of surfaces and their interactions at a molecular or atomic level and quantitative elemental analysis under various conditions. The outcome is to provide basics for modelling and prediction of the processes taking place on macro scale, as established in numerous publications (Coyne *et al.* 1989, Davis and Hayes 1986, Hochella and White 1990, Stumm 1992, Berry 1985, Hochella 1988).

Crystals were always assumed to have a perfect structure, with atoms permanently appointed in the lattice until in the 1920s, when Griffith introduced the concept of imperfections, weakness-planes and cracks in solids in a form of theory relating flaws to mechanical properties. However, scientists who first introduced point defects were Frenhel and Schotthy. Cotterill (1986) expands this further by explaining that the probability of a defect appearing in a crystal is related to the free energy associated with the formation and growth of the crystal, and the lower the free energy, the higher the probability. These point defects can be in the form of vacancies or interstitial impurities, and may can take part in different diffusion processes (vacancy-mediated process and interstitial diffusive process).

Other possible point defects may take the form of impurity atoms which can occupy a regular lattice space or an interstitial impurity, depending on the thermodynamics of the chemical state. More influential though are the line defects, represented by the dislocation or disruption of the crystal lattice, stacking faults, twin boundaries, grain boundaries and free surfaces (Cotterill 1986).

5.2 Carbonate minerals

Weathering and dissolution of carbonate minerals is one of the most advanced research areas in mineral sciences, mainly due to their wide range of applications, from the oil industry to pure scientific enigmas such as the 'dolomite problem' (Shukla and Baker 1988). Mineral/solution reactions involve dissolution of certain carbonate minerals and precipitation/growth of others. For a system in an equilibrium between a solid and a solution, dissolution and precipitation are of the same rate (e.g. Morse and Mackenzie 1990). However, the solubility of the carbonate minerals can be further complicated by their compositional heterogeneity or the presence of excess free energy as a result of lattice strain, various defects in the lattice and the surface free energy. The solubility will increase exponentially with an increase of the reactive surface area.

In order to gain a better understanding of the mechanism of alkali-carbonate reactivity in concrete, it was necessary to establish the role of one of the most important components involved in this reaction, the mineral dolomite, and its replacing phases brucite and calcite. The main aim of this chapter is to present the findings of this work regarding changes on single minerals during ACR and to establish their correlation with the existing data.

5.3 Mineral dolomite

The French mineralogist and scientist Dolomieu (1750-1801) was one of the first to notice the mineral dolomite in the Italian Alps and to recognise some of its main characteristics. Since the 1700's there has been much research into the crystallographic, chemical and physical properties of dolomite, although still some of the most controversial mineralogical transformation are related to this mineral, such as its formation, or the so-called dolomitisation process.

Much compilation work has been necessary on the crystallographic and chemical properties of dolomite, and its susceptibility to changes in aqueous solutions. The well-researched field of the role of dolomite in sedimentological processes as a rock forming mineral was used for the interpretation of similar reactions involving dolomite and its behaviour in concrete.

5.3.1 Crystal chemistry of dolomite

The chemical composition of dolomite is $CaMg(CO_3)_2$ with the Ca/Mg ratio varying between the minerals, calcite $CaCO_3$ at one extreme and magnesite $MgCO_3$ at the other. As in other carbonate minerals the CO_3^{2-} group as a structural unit remains the same, in the form of an equilateral triangle with carbon in the centre and oxygen at corners (characterised with O-C-O bonds at an angle of 120°, and bond-lengths of 1.284 +/- 0.004A), demonstrated in Figure 5.1a Due to different cations present in neighbouring layers (typical for dolomite) the C atom is displaced from the plane of 3 oxygen atoms. Because of the difference in Ca-O (2.38Å) and Mg-O (2.08Å) bond lengths the CO_3^{2-} groups are rotated at an angle of 6.5° around the 3-fold axis. Both Ca and Mg octahedra are less distorted in dolomite compared to the crystal lattice of calcite and magnesite, resulting in the enhanced stability of dolomite (Reeder 1990).

The layered structure usually contains impurities and imperfections due to ion exchange of Mg^{2+} by other elements (Ca, Fe, Mn), resulting in minerals such as ferroan dolomite and ankerite $Ca(Mg,Fe)(CO_3)_2$. Ferroan dolomite contains sites A completely filled by Ca and smaller B sites taken by Mg, Fe and excess Ca. If the number of A (Ca layer in Figure 5.1a) and B (Mg layer in Figure 5.1a) sites is equal, non-stoichiometry results from Ca atoms occupying the smaller B sites. This will be of particular interest for the mechanism of ACR in Kingston dolomite where there is a high amount of Fe in dolomite grains. The relevance of atomic/ionic radius of elements involved is presented in Table 5.1.

Table 5.1 Parameters of elements involved in cation exchange in dolomite which will cause different volume occupancy

Element	Ionic Radius Å	Atomic Radius Å	Atomic Volume
Calcium [Ca]	0.99 (for 2+)	1.97 A	29.9 w/d
Magnesium [Mg]	0.65 (for2+)	1.60 A	14.0 w/d
Iron [Fe]	0.76 (for 2+)	1.26 A	7.1 w/d

5.3.2 The Dolomite microstructure

The mineral dolomite has a rhombic crystal lattice with consecutive layers of Mg and Ca atoms, between planes of CO_3^{2-} group common to both (Figure 5.1a). An easy description is simple substitution of Ca ions with Mg atoms in every other cation layer.

During crystal growth various types of lattice defects can be introduced into the structure consequentially forming the following growth microstructures (Wenk *et al.* 1990).

1) Dislocations caused by incorporation of foreign ions of particles, can facilitate growth along steps, typical of crystal growth from aqueous solutions.

2) Growth bands, reflecting local chemical compositional variations or impurities.

3) Faults, separating distinct growth regimes in a crystal.

4) Modulated structures are the most common heterogeneous structures. They are the result of excess $CaCO_3$ in dolomites of all ages. Lamellar spacing is usually 100-200Å, with modulations parallel to one of the cleavage rhomb faces. These modulations are well established in cases where replacement of a precursor occurs, so that the dissolution-re-precipitation mechanism might include deposition of thin solution films between dissolving and precipitating layers. These are influenced by the environment where the crystallisation is taking place, such as limited space, pressures, temperatures.

These features are important as they will explain some of the changes or susceptibility to alteration within dolomite in an alkaline regime as studied here.

5.3.3 Stability and Mineralogical-Transition of Dolomite

The relative reactivity of carbonate minerals depends on a given set of conditions. The main factors influencing the rate of reactivity are: the saturation state of the solution with the respect to carbonates and availability of inhibiting species, the relative surface areas/microstructure, degree of structural ordering, chemical heterogeneity and irregularities within the lattice of a crystal concerned. The two most important chemical processes involving dolomite minerals are dolomitisation (its formation) and dedolomitisation (transformation to calcite).

5.3.3.1 Dolomitisation

One of the most controversial questions in the mineralogical world - the so-called dolomite problem, concerns the mechanism of its formation (Purser *et al.* 1994). The mode of formation of dolomites remains controversial because it is kinetically hindered

by the complex and well-ordered crystal structure (Morse and Mackenzie 1990). The most obvious reason for the lack of understanding of the dolomitisation mechanism is the slow kinetics of the reaction that make most of laboratory data (acquired under exaggerated conditions of high T, P or pH) inapplicable to real sedimentary conditions. Morse stated that dolomite has been found to be relatively non-reactive and attempts to study its reaction kinetics under earth-surface conditions have been largely unsuccessful (Morse 1990).

A main consideration in the geochemistry of dolomite, is its stability and susceptibility to ion incorporation and the Mg to Ca ratio as well as its structural ordering. Carpenter (1980) postulated that if calcite and dolomite are in equilibrium with the same solution then they must be in equilibrium with each other. Although dolomite is a common and well researched mineral the process of dolomitisation, which may be affected by various inclusions and the elemental substitution of Ca or Mg with Fe, Mn, Sr, Ti, may introduce additional complicating factors, including the degree of crystallinity and defect structure (Deer *et al.* 1995). Some of the above inclusions can be explained by diagenetic processes such as decomposition of Fe-rich biotite in an environment with decaying organic matter resulting in formation of kaolinite, silica and pyrite, and as suggested by Galliher (1939) these would be alkaline black mud furnished conditions. These are also referred to as organogenic dolomites and studies related to the role of sulphate reduction on dolomite formation and the controlling factors for their major and minor chemistry are of particular interest (Burns and Baker 1988, Compton 1988).

The origin of dolomite has long remained not only one of the great mysteries of sedimentary geology, but it is also an important scientific problem since the mineral is so common it represents an important part of geologic record with an additional economic connotation (oil reservoirs, Mg-source, building material). Dolomitisation is considered to be a replacement process, and as such dolomitisation generates a carbonate rock with improved permeability (Tucker and Wright 1990). However, it is well established that dolomite is being formed today in the supratidal flats of arid and semi-arid climates in association with waters that have been evaporated to the stage of precipitation of gypsum (Tucker and Wright 1990). The significance of gypsum precipitation on the formation of dolomite is that it creates a significant rise in the magnesium to calcium ratio in the solution, therefore favouring the replacement of calcite by dolomite and even a free growth of dolomite matrix. There are undoubtedly kinetic factors that inhibit or

accelerate the dolomitisation process (Morse and Mackenzie 1990, Brady *et al.* 1996). Great importance is given to the dolomitisation process and an understanding of its mechanism, because one of the main topics of this study is dedolomitisation, the reverse process of dolomitisation. The objective was to draw some conclusions from the dolomitisation process and to apply it to the dedolomitisation mechanism, kinetics, controlling parameters and possible consequences such as the volume change, that might occur as a result of this reaction taking place in concrete aggregate.

5.3.3.2 Dedolomitisation

The diagenetic change that leads to transformation of dolomite to calcite was first reported in study by Von Morlot (1847), suggesting that he process involved dissolution and reprecipitation and was written as following chemical reaction:

$$CaSO_4 + CaMg(CO_3)_2 = 2CaCO_3 + MgSO_4$$

This mechanism was adopted by Shearman *et al.* (1961), Ewamy (1963) and Goldberg (1967), who additionally to previous also proposed that the sulphate ions needed for the dedolomitisation reaction are released during the oxidation reaction of pyrite. This process known as the dedolomitisation process involves chemical substitution of Mg by Ca. The dedolomitisation that occurs at the crystal surface was experimentally studied by De Groot (1967) and can be written as follows:

$$CaMg(CO_3)_2 + Ca^{2+} \Leftrightarrow 2CaCO_3 + Mg(OH)_2$$

In which the mineralogical transformation is:

$$\textit{Dolomite} \Leftrightarrow \textit{Calcite} + \textit{Brucite}$$

This reaction takes place under the following conditions (DeGroot 1967):

1) With a high Ca/Mg ratio, from circulating waters;

2) Low partial pressures of CO_2;

3) Low temperatures;

4) High water flow rate (DeGroot 1967).

If dolomite is of a different composition such as $Ca(Mg,Fe)(CO_3)_2$, dedolomitisation proceeds due to the oxidation of pyrite (Ewamy 1963). This reaction was chemically formulated by Al-Hashimi and Hemingway (1973) in a study of dedolomitisation and crust formation in Northumberland:

$$4[Ca(Mg,Fe)(CO_3)_2] + 2H_2O + 1/2O_2 = 4CaCO_3 + Fe_2O_3 + 2Mg + 2CO_3 + 2H_2CO_3$$

$$Fe_2O_3 + H_2O = 2FeOOH$$

with the mineralogical transformation as follows:

$$\textit{Dolomite} \Leftrightarrow \textit{Calcite} + \textit{Goethite}$$

In nature goethite is meta-stable and it transforms to hematite upon ageing:

$$FeOOH \Leftrightarrow Fe_2O_3 + H_2O$$

$$\textit{Goethite} \Leftrightarrow \textit{Hematite}$$

Another type of dedolomitisation is of metamorphic nature, and occurs at high T and P, although this is not of direct interest in this study, and can be written:

$$CaMg(CO_3)_2 + SiO_2 = 2CaCO_3 + MgSiO_4 + 2CO_2$$

$$\textit{Dolomite} \Leftrightarrow \textit{Calcite} + \textit{Olivine}$$

Calcite replacing dolomite can occur on a large scale and up to 95% of porous dolomite can be exchanged for calcite (Deer 1995). Dedolomitisation can affect peripheral or central portions of dolomite crystals. Another interesting point is that dolomite can be replaced by non-carbonate minerals, and those that are very common replacement are: pyrite (FeS_2), marcasite (ZnS) and galena (PbS), (Tucker and Wright 1990). Another common replacement is kaolinite. Cementing or replacing kaolinite crystals are lamellar, anhedral to pseudo-hexagonal euhedral, 2-60μm in diameter, that commonly form book-like grain sequences. In relation to the expansive nature of argillaceous dolomitic limestone from Kingston, and given the possibility that the origin of this rock might play an important role ,it was thought to be valuable to compare shrinkage processes during diagenesis of carbonate rocks. It was found that in some cases iron silicates, present in

the rock as a matrix, can lose up to 50% of their original volume.

5.3.4 A study of single dolomite crystal

An experiment was carried out to observe the changes on a single dolomite crystal induced by an alkaline environment (sample MR02, Table 3.1). SEM micrographs were taken before immersion in 1N, NaOH solution, and spectroscopic measurements were carried out prior to and after three months exposure to alkaline environment. AFM measurements were performed before and at the end of three weeks period exposure to an alkaline environment (4N NaOH solution), since reactions on the atomic scale were expected to produce much faster changes in the crystal structure (Table 3.1).

5.3.4.1 Microscopic observations

An ESEM was used for microscopical observations, allowing for no sample alteration due to preparation processes, which was of great advantage for analysing samples from solution. Prior to immersion in a NaOH solution, the single dolomite crystal was characterised under the microscope. Figure 5.2a presents the surface observed. One of the corners of the crystal was fractured for observation of an unaltered fracture surface with alkaline solution. Quartz inclusions and some silicates were observed as shown in Figure 5.2b,c. It was concluded that the sample was a non-stoichiometric dolomite with Ca/Mg is not 50/50wt%, as can be seen from EDX spectrum in Figure 5.2e presents the chemical composition of an unaltered dolomite surface.

After removal from a 1N NaOH solution the sample was rinsed in pure water several times. The sample was put into the ESEM chamber for analysis immediately, to avoid phase changes due to drying and migration of pore solutions. Growth of uniform crystals with preferential orientation was observed on the surface as it can be seen in Figure 5.3-5.5. Images were also acquired at higher magnification hoping to resolve the mysterious preferential growth direction and their relation with the dolomite substrate. There were no signs of any physical changes such as micro-cracks and larger crystals growing along defined lines were surrounded with underlying patches of fine platy crystals (Figure 5.4). These elongated Ca-rich crystals were up to 20μ in size, and twinned (Figure 5.5b). From the crystal habit these were identified as calcite, which, also appear to be of epitaxy arrangement on the dolomite surface. EDX analysis (spectrum in Figure 5.3c) indicates that the calcite contains some magnesium. The comparison

between the dolomite composition and the composition of newly formed calcite crystals (Figures 5.2e and 5.3c) reveals the difference in Ca/Mg ratio, suggesting that the new phases contain enough Mg to be categorised as Mg-calcite. On the other hand, a second observed phase was fine grained and appears to grow perpendicularly to the dolomite surface. These Mg rich crystals were identified as brucite $Mg(OH)_2$ (Figure 5.5a) from crystal habit and are appearing to be of topotaxy arrangement (as a result of ionic exchange), resulting in non-oriented appearance on the surface. However, brucite crystals do grow perpendicularly to the cleaved dolomite surface.

Another set of images were taken from the fractured corner of dolomite rhombohedra (the same area was imaged before the treatment in NaOH (Figure 5.2c). As it was expected such a surface would allow an access of solution species to all of the structural layers (Ca, Mg and CO_3 groups). Such fracturing was preferred to cleavage of the dolomite since the cleavage plane would expose just only one type of atoms to the solution. This approach has proven to be particularly successful because secondary crystals were observed to be growing from dolomite substrate (point 1 on Figure 5.6). The fine surface coating of brucite was evident (point 3 in Figure 5.6).

5.3.4.2 Surface characterisation

As shown above the resolution of an electron microscope was not sufficient to observe changes on sub-micron level. It was therefore decided to use an Atomic Force Microscope (AFM), which enabled characterisation of the crystals surface at an atomic scale, giving more detailed information on the nucleation sites and the reason for preferential growth direction of calcite. An identical dolomite crystal to that used in the ESEM study (sample MR03) was ultrasonically washed with pure water for 3 minutes and thoroughly rinsed several times with pure water to obtain a surface free of any loose particles and impurities. After drying the crystal was examined under AFM. As it can be seen in Figure 5.7 and 5.8, the surface is composed of two main types of atomic ordering. Dominant features are lower, uniformly arranged atoms (Figure 5.7) with no specific depth or shape, whose average height is 25nm.

The second feature consists of morphologically higher (approximately 750nm) atomic segregation with a more definite shape and orientation (Figure 5.8). Other specific characteristics of these features is that they have a length of 2.0151μm, height

approaching 1000nm, with the angle of 5.018° and appearing in rows which are of uniform distance of approximately 5μm (Figure 5.8). The other difference between the two described phases was also the hardness - with the second phase being much harder. In order to be able to examine the same area after treatment a freshly cleaved edge was used as one fixed point (750μm north) and corners of the crystal as other two fixed points. The sample was then immersed in 5ml 4N NaOH solution and kept in a sealed plastic container at room temperature for 3 weeks. After removal from the solution the sample was rinsed several times with pure water and examined under the AFM as soon as the surface had dried. The aim was to observe the area examined before the treatment, which was done within a 20-40 μm^2 field.

First of all it was obvious that the secondary phases on the surface were much more unstable and therefore it proved difficult to obtain images, although the same instrumental settings were used (contact mode AFM). This suggested that the surface was covered with crystals poorly-attached to the dolomite surface. Therefore the tap mode AFM imaging was introduced. Images obtained were stable and revealed that the surface was covered with a network of layered platy-crystals that intersected and were growing almost perpendicularly to the surface (Figure 5.9) identical to the brucite observed under ESEM &EDX after months of exposure. The AFM imaging that provided the phase information, (resulting in a different shade of a colour image), revealed that the cross section of those plates was of a different composition from their side-faces. This partially explained the unstable nature of the crystals if they were covered with thin films of water-rich deposits (Figure 5.11).

In order to be sure that the morphology of phases observed was accurate (suspecting changes such as the contamination of the tip) different set of images was acquired after the change of tip, and it proved to be effective. The phase observed was a single plate rather than three-layered plates, although the rest of the information observed earlier was valid (the orientation, height and amount). As it can be observed from Figure 5.10 these crystals are identical to the brucite observed in ESEM study, suggesting that the formation of brucite can appear after 2-3 weeks of alkaline treatment. None of the original features of untreated dolomite were present and the entire dolomite surface was covered with brucite. It was also observed that calcite as a second dedolomitisation product has not precipitated at this stage of the reaction.

5.3.4.3 Spectroscopic measurements for near surface changes

Microscopic observations showing the change on the surface of an alkali treated dolomite crystal needed a confirmation in terms of chemical analysis. ESCA measurements of the near-surface (sensitivity 20nm), were undertaken in an attempt to support the chemically supported the previously observed changes and transformation of dolomite from ESEM and AFM studies.

A single dolomite crystal (sample MR01) was used to acquire the XPS data before as well as after the treatment with alkaline solution. Although the main interest were on the chemical states of Ca, Mg, C, and O, a wide spectra was obtained from fresh and treated surfaces (400 by 400μm), showing general differences in the chemical state (Figure 5. 12a). As it can be observed the alkaline environment causes a change in the crystal chemistry. These changes can be observed at an early stage by ESCA, since it is required for only a few top atomic layers to react in order to detect the alterations. The wide scan shows the mineralogical changes in the presence of new peaks, but also some of the peaks present in the crystal prior to treatment can not be observed on the treated surface, Figure 5.12a. Another important observation is the change in the relative height of the peaks.

Regional XPS scans can reveal more detail and can be used for the determination of chemical shifts. First of all the carbonate peak height decreased after NaOH treatment and the peak is shifted from 290.05 eV to 289.13 eV due to the formation of another carbonate phase on the surface, most likely $CaCO_3$ (figure 5.12b). The position of the O*1s* peak also suggests a change in chemical state, with the treated O*1s* at binding energies in a range of O*1s* of brucite, and untreated surface possesses O*1s* of a carbonate weathered by exposure to atmosphere only (Figure 5.12c, Table 5.2).

Observation of the regional XPS spectra for Mg*2p* (Figure 5.12e) shows that there was a peak shift for Mg *2p*, from 50.59 eV typical for Mg-carbonates to 49.38 eV as in Mg-hydroxide . The same trend was observed in Ca*2p* peak which shifted from 347.62 and 351.34 eV to 346.91 and 350.34 eV (Figure 5.12d). All the XPS spectra for untreated and treated dolomite surfaces are presented in Figure 5.12 and the binding energies from this study as well as reference values are in Table 5.2.

5.4 Mineral Calcite

The reaction product with an undefined role in ACR is calcite. All carbonate rocks susceptible to ACR contain calcite in various amounts, although it was always assumed that only dolomite reacts. Since the main product of reacted dolomite in dedolomitisation reaction is calcite its contribution to ACR was also examined in this study.

Calcium carbonate is polymorphous ($CaCO_3$) and exists in five modifications, from which two are known to occur in sediments, calcite and aragonite (Deer *et al.*1996). The rhombohedral mineral, calcite, is the most abundant and is thermodynamically stable. The carbonates are a group of minerals in which the essential structural unit is the CO_3^{2-} ion. The structure of calcite can be described as similar to that of halite, in calcite Ca^{2+} and CO_3^{2-} ions form a face-centred rhombohedral cell. However, a distortion of a cube due to extra accommodating space required by the large planar CO_3^{2-} groups, composed of a carbon ion at the centre of an equilateral triangle with an oxygen ion at the apices, is present. Although many divalent cations can take a part in a partial replacement of the Ca^{2+} ion, pure calcites are close to the ideal composition of $CaCO_3$ (Deer *et al.* 1996).

An important sub-group of the $CaCO_3$ minerals is magnesian calcites, where Ca is replaced by Mg up to 20 mol % at low temperature (Deer *et al.* 1996). Their solubility is strongly influenced by the magnesium content. Magnesium carbonates present many problems in sedimentary geochemistry because of their tendency to form a variety of hydrates, as a result of the high energy of hydration of the magnesian ion. The solid solution of $MgCO_3$ in calcite is one of the most important carbonate solid solutions. The alteration of calcite is accomplished mainly by solution and replacement (Deer *et al.* 1996).

The role of calcite in the ACR mechanism has been overlooked since it is a mineral that has not been related to undesirable reactions in concrete. In spite of that it is relevant for ACR because the amount of calcite that forms takes up a volume for growth which in a rock compound will almost definitely be confined. $CaCO_3$ phases that have been observed in this study have slightly distorted cube forms with an empty space in the middle (referred to by Professor Glasser as spagheti form or hopper-shaped). Some of these crystals appear as twins (Figure 5.5b).

EDX analysis in ESEM have shown that their composition is close to a magnesian-calcite, but that could be the effect of skirting in an ESEM analytical chamber (Figure 5.3c). Further analysis would be necessary to establish a more accurate chemical composition. Apart from their distinguished appearance it was also important to understand the factors that were favouring Ca supply to the nucleation sites and establish the chronology of phase formations in the dedolomitisation reaction. What can be concluded from these results is the presence of calcite as a result of the dedolomitisation process and that crystal growth in confined spaces will produce a force.

5.5 Mineral Brucite

The second dedolomitisation product is brucite. In this study the first question was the chronology of brucite/calcite formation in the dedolomitisation reaction. However, this is not the only interest in brucite, since in this study it is also important to establish the relation between brucite deposits and the expansive nature of ACR. Therefore the aim was to monitor the formation as well as its behaviour and alterations in an alkaline environment similar to concrete, and the reason why some of the dedolomitisation reactions did not have expansive effects.

Brucite has a layered crystal structure, where Mg ions are placed between two sheets of OH^- ions that are parallel to the basal plane. Each Mg ion is surrounded with six OH^- groups as shown in Figure 5.1b. Brucite is hexagonal with OH^- groups in close hexagonal packing with an individual OH^- group attached to three Mg ions on one side and linked to three hydroxyl groups in the consecutive layer. Although brucite forms in the alteration process of periclase (MgO), it can be easily transformed to hydromagnesite ($3MgCO_3\ Mg(OH)_2\ .3H_2O$) (Deer *et al.* 1996).

Standard brucite samples were used to acquire XPS spectra before and after alkaline treatment and establish Mg*2p* binding energy values so that they can be used for evaluation of Mg*2p* peak position for newly formed brucite layer in dolomite experiment. A fraction was freshly removed from a cluster of fine platy brucite crystals (sample MR04) and analysed for Mg and O. The same sample was then exposed to 5ml 1N NaOH solution at room temperature for 3 months. The sample was removed from solution thoroughly washed in pure water and left to dry at room temperature before put

in the prep chamber for degassing. The same range regional spectra were required and these results are shown in Figure 5.13 and Table 5.2.

As it can be observed the alkali treated brucite resulted in the Mg*2p* peak position shifted slightly by 0.2 eV from that of the untreated brucite. The data obtained was used to identify the Mg*2p* observed on the surface of the alkali-treated dolomite crystal. The answer to the first question: 'What secondary phase forms first?' was obtained using AFM on a single dolomite crystal (Figures 5.9,10). It showed that only after 3 weeks the alkali-treated dolomite surface was covered with sub-micron brucite crystals, identified by morphology. No calcite was observed.

Although the single dolomite crystal immersion was not representable of dolomite grains in dolomitic limestone where their surfaces are surrounded with a silicate/carbonate matrix, it will give a simplified explanation for dolomite dissolution/transformation susceptibility.

The second study on a single dolomite crystal immersed in NaOH solution using ESEM revealed the formation of a brucite layer on the surface of reacted dolomite (Figure 5.5a). The appearance of calcite and brucite on the surface of alkali-treated dolomite grain here suggested a simmultaneous formation of both (see previous section). These ESEM images reveal that the brucite has tendency to grow at an angle of 90° from the dolomite substrate, with fine crystals tightly intersected into a blanket-like surface layer easy to observe in the 3 dimensional AFM image (Figure 5.9 AFM).

Support for the chemical transition of Mg in dolomite is evident after comparing XPS spectra of brucite from dolomite surface with regional spectra from brucite standard, (Table 5.2). It was significant to observe that the Mg *2p* peak from reacted dolomite surface was very similar to the peak of standard brucite crystals treated with alkalis. This suggests that the brucite, formed as a result of dedolomitisation in an alkaline environment, would be susceptible to a further chemical change and react with species from the solution present. These will also include Mg and Fe rich phases formed as a result of the dedolomitisation process reacting further with alkaline solution and species available in cement pore soulution such as Ca and Si ions.

5.6 Conclusion

The data presented in this chapter revealed details about the behaviour of single crystals in an alkaline aqueous environment. Most of the changes presented here were easily identified with the use of surface characterisation of the reacting material prior to and after treatment with alkaline. Together with the results from the other analytical techniques and thermodynamic calculations a model could be proposed for the mechanism involved in ACR. All these indicate that the ACR process is centred around the dedolomitisation reaction.

The conclusion from the ESEM study of a single dolomite crystal is that the $CaCO_3$ crystal growth on the surface of dolomite as a result of dedolomitisation in its initial stage will have a preferential growth along discontinuity planes or other forms of crystal lattice impurities. The chemistry involving elemental transitions during dedolomitisation might require volume change since they appear to be surface reactions. It was also discovered that the dedolomitisation process can involve not just Mg replacement but Fe replacement with Ca. However, the ESEM observations were not sufficient for the explanation of the nucleation mechanism, composition and chronology of precipitation processes. As reported AFM was used to obtain more delicate changes after shorter period of time used for the treatment.

The tendency for oriented growth of $CaCO_3$ crystals observed in the ESEM study was explained with more confidence after the AFM experiment. There was a similarity in the trend of calcite growth and the orientation in the appearance of plutonic extrusions on dolomite surface as presented by three dimensional image of dolomites surface in Figure 5.8. Using AFM analysis was also possible to establish the changes in morphology of the features observed on the crystal surface that would suggest the nature of the reaction, and as shown, the first dedolomitisation product was brucite. As it can be seen when the ESEM brucite image is compared with the AFM image, the formation of $CaCO_3$ must follow that of brucite. Another conclusion apart from chronology is that the dedolomitisation reaction would be preceded by the dissolution of dolomite.

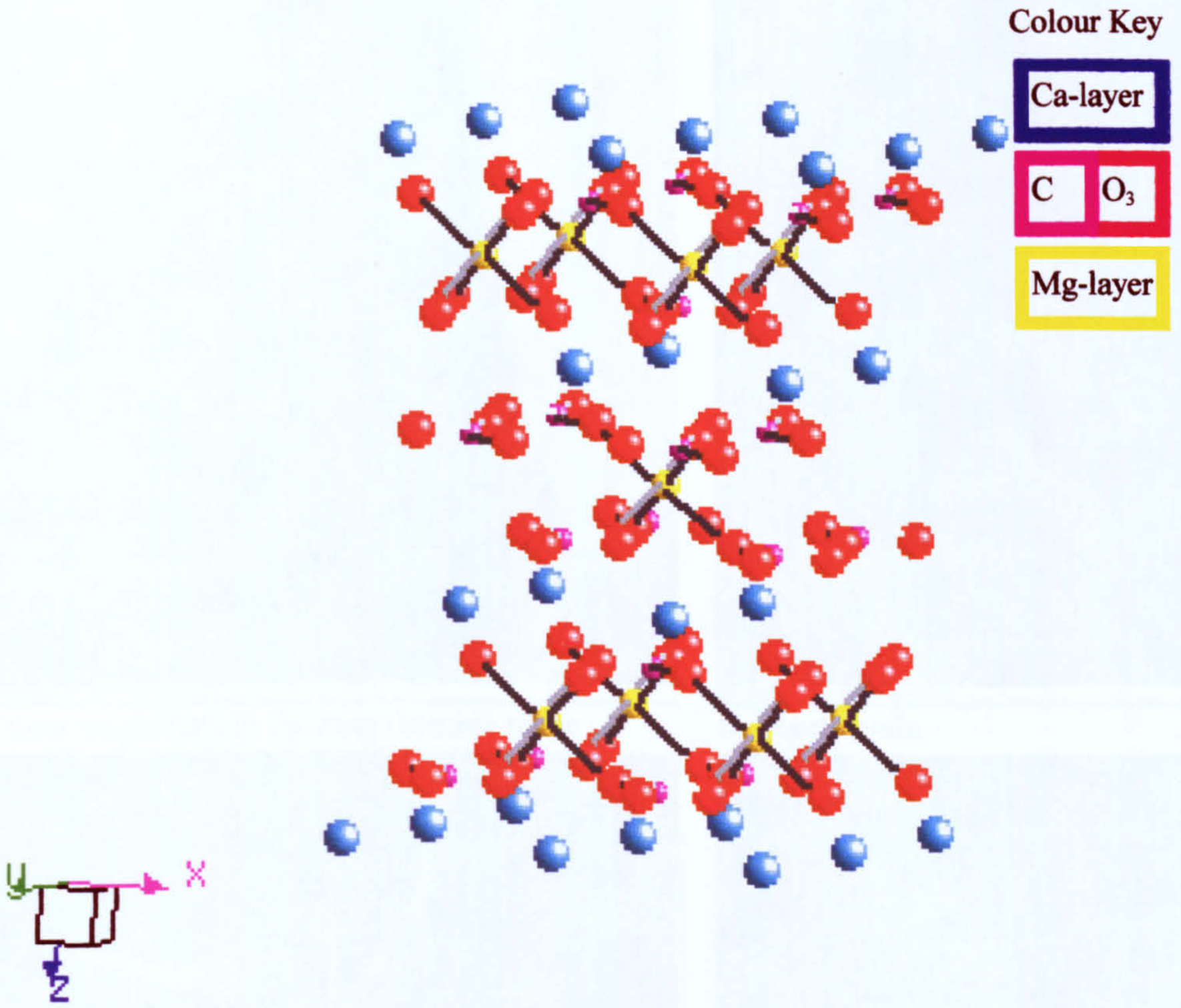

Figure 5.1a Crystal structure of mineral dolomite.

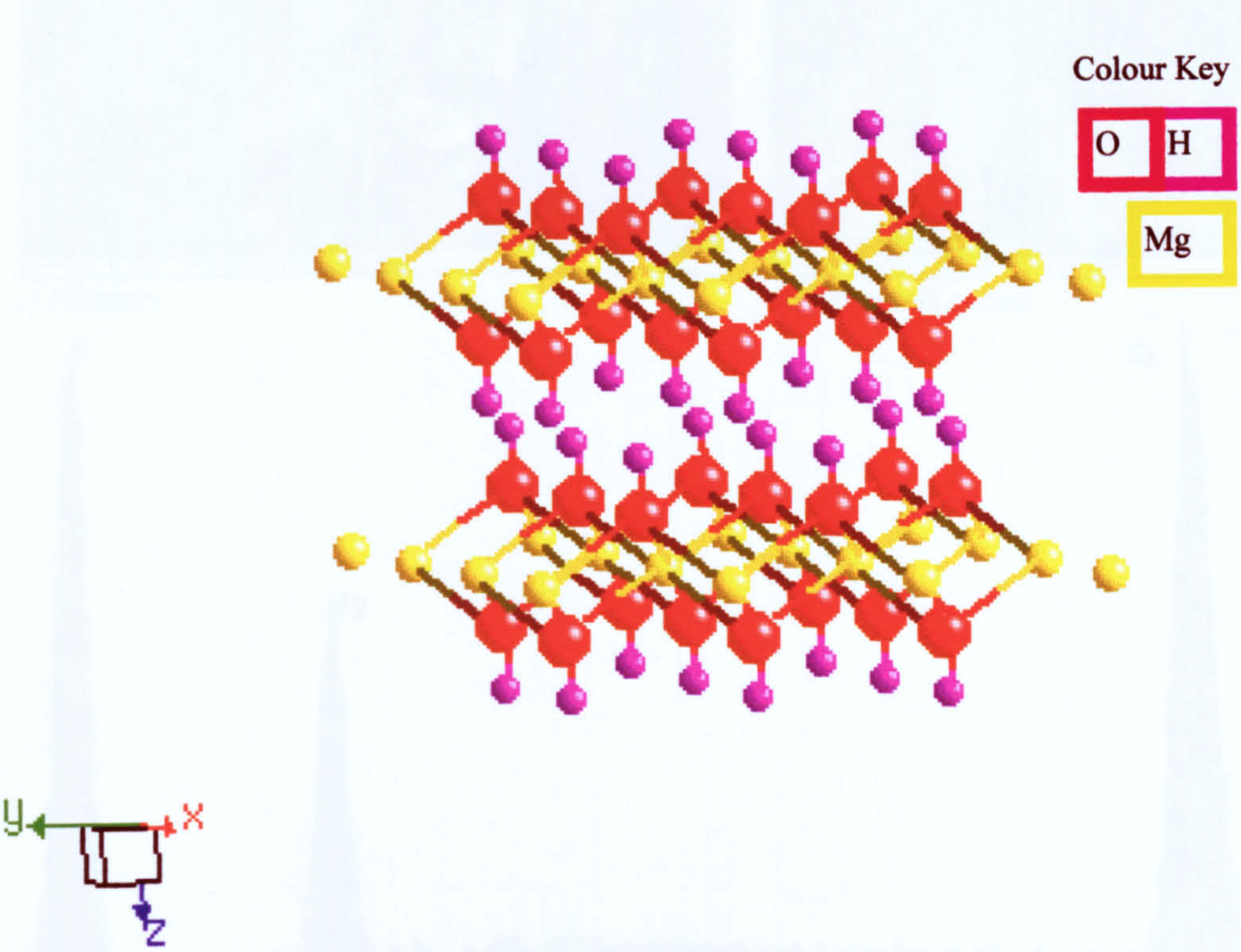

Figure 5.1b Crystal structure of mineral brucite.

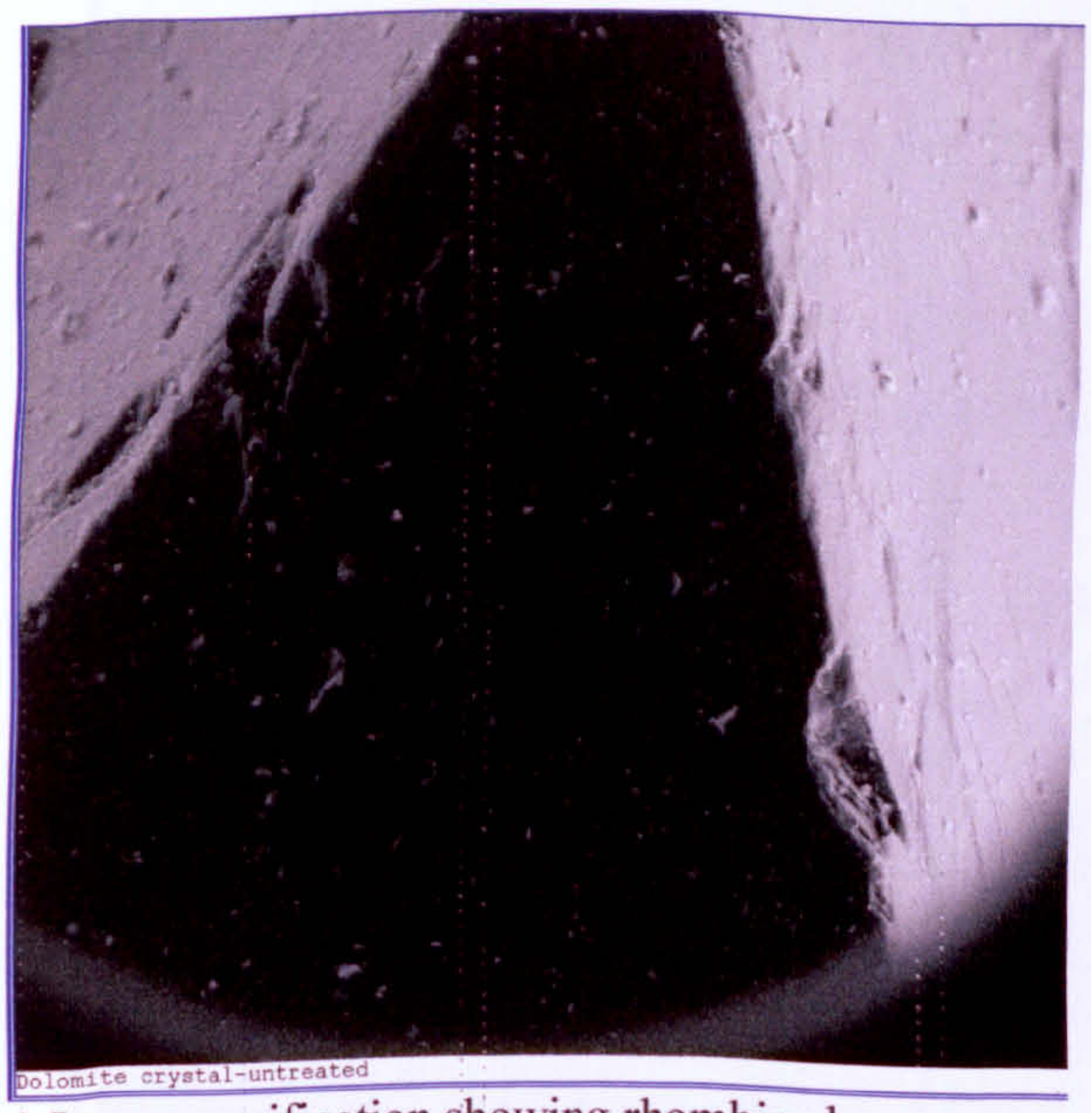

a) Low magnification showing rhombic shape

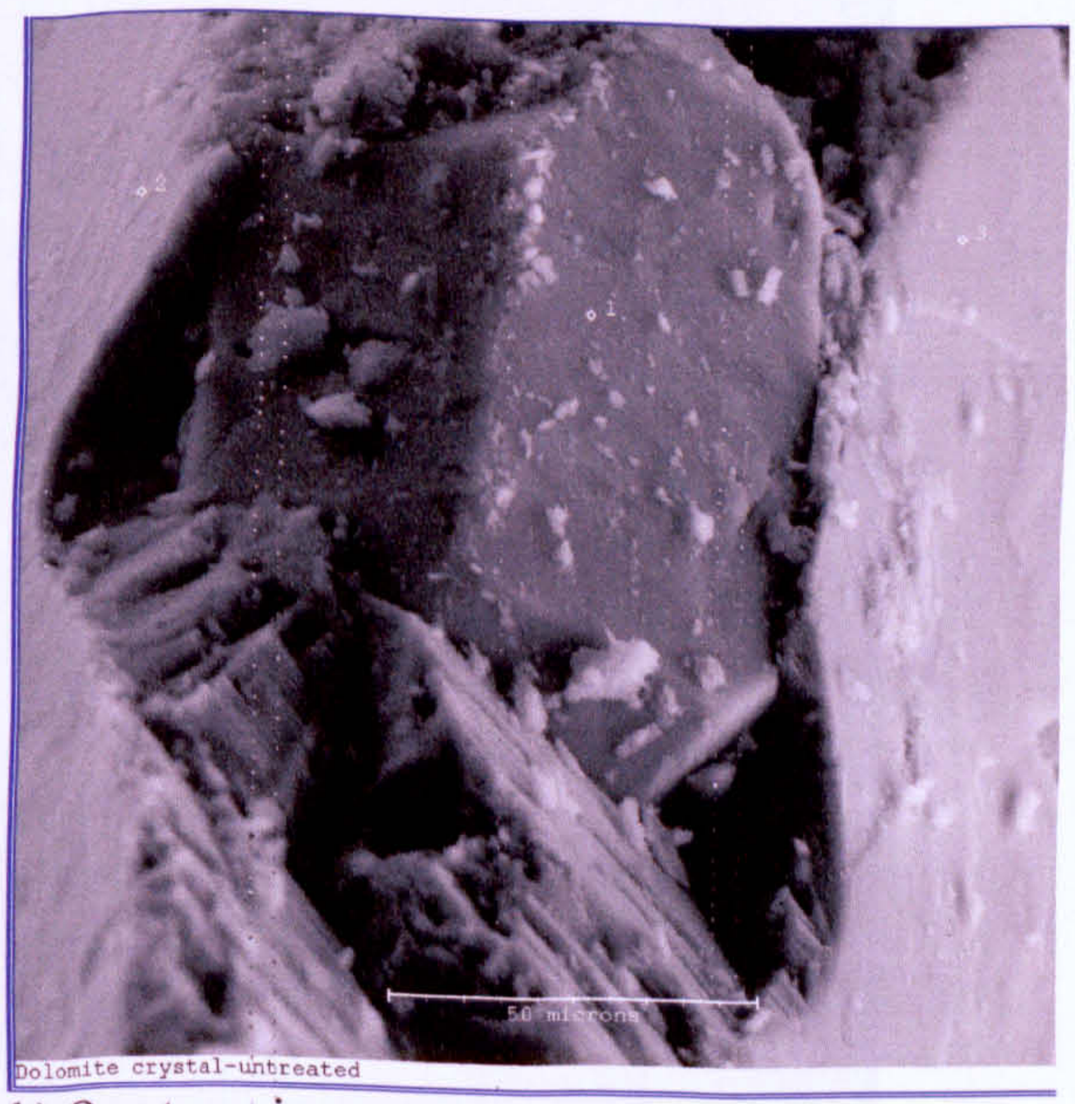

b) Quartz grain

c) Silicates

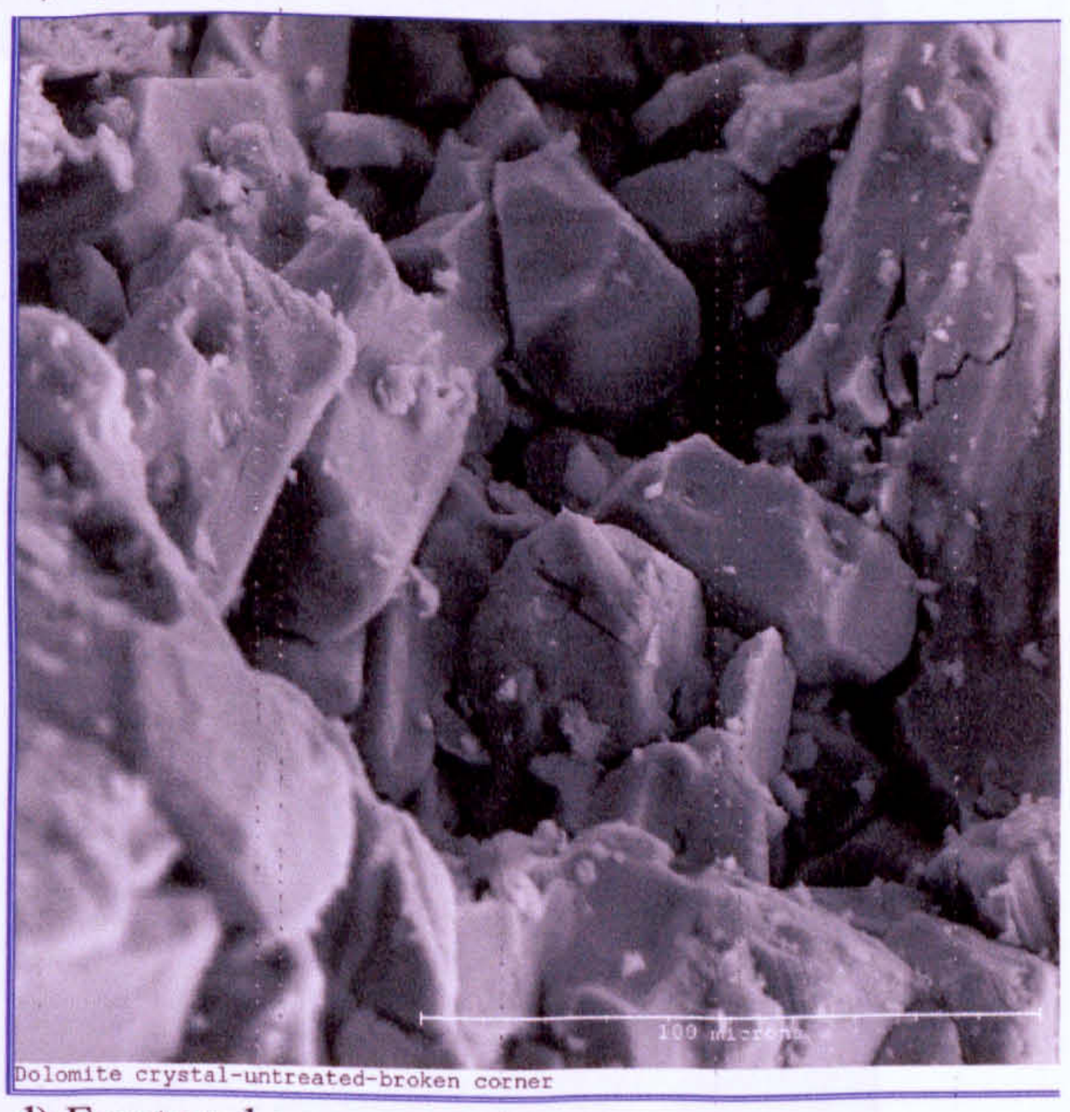

d) Fractured corner

e) EDX spectrum of untreated dolomite surface

Figure 5.2 Single dolomite prior to immersion in NaOH solution.

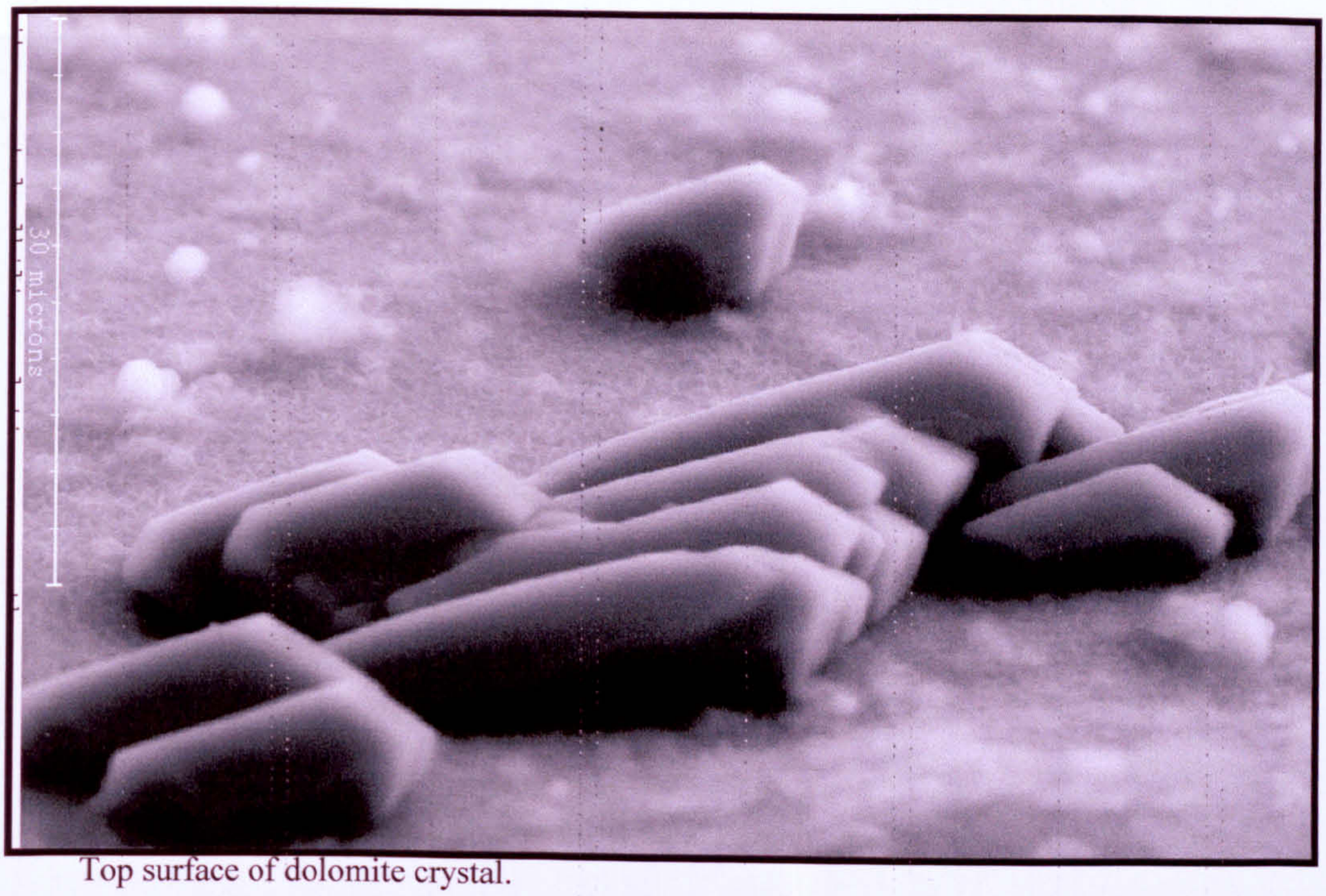

Top surface of dolomite crystal.

Surface opposite the top surface, which is the reason for up-side down effect.

Figure 5.3 Dedolomitisation reaction taking place on the surface of a single dolomite crystal after three months of alkaline solution treatment. These images reveal preferential growth and the twinning of calcite along the defect planes within the crystal structure. EDX shows absence of Mg.

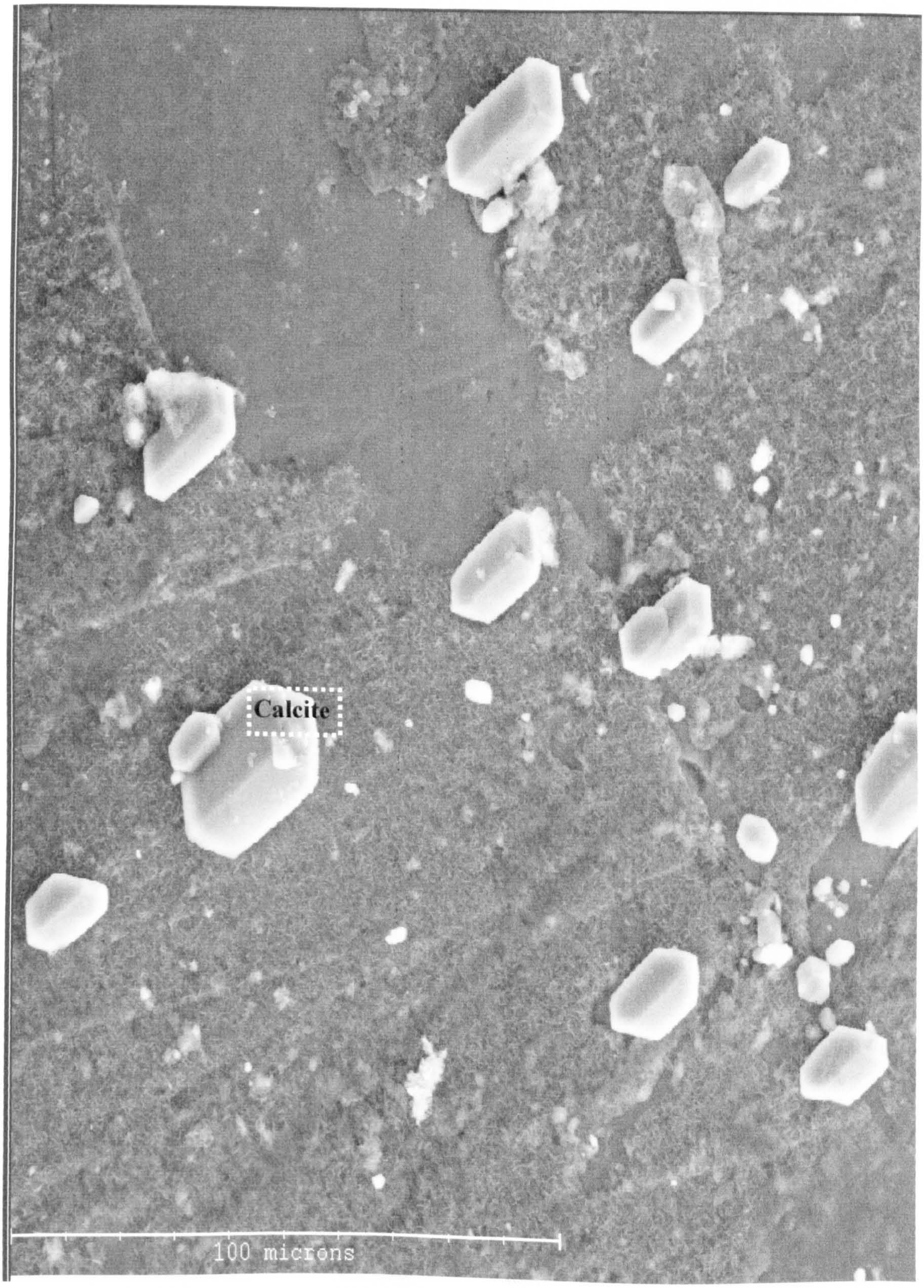

Figure 5.4 Oriented growth of calcite on the surface of a single dolomite crystal with simultaneous precipitation of fine brucite crystals underneath. As can be observed, carbonate crystals are an example of epitaxy crystal growth.

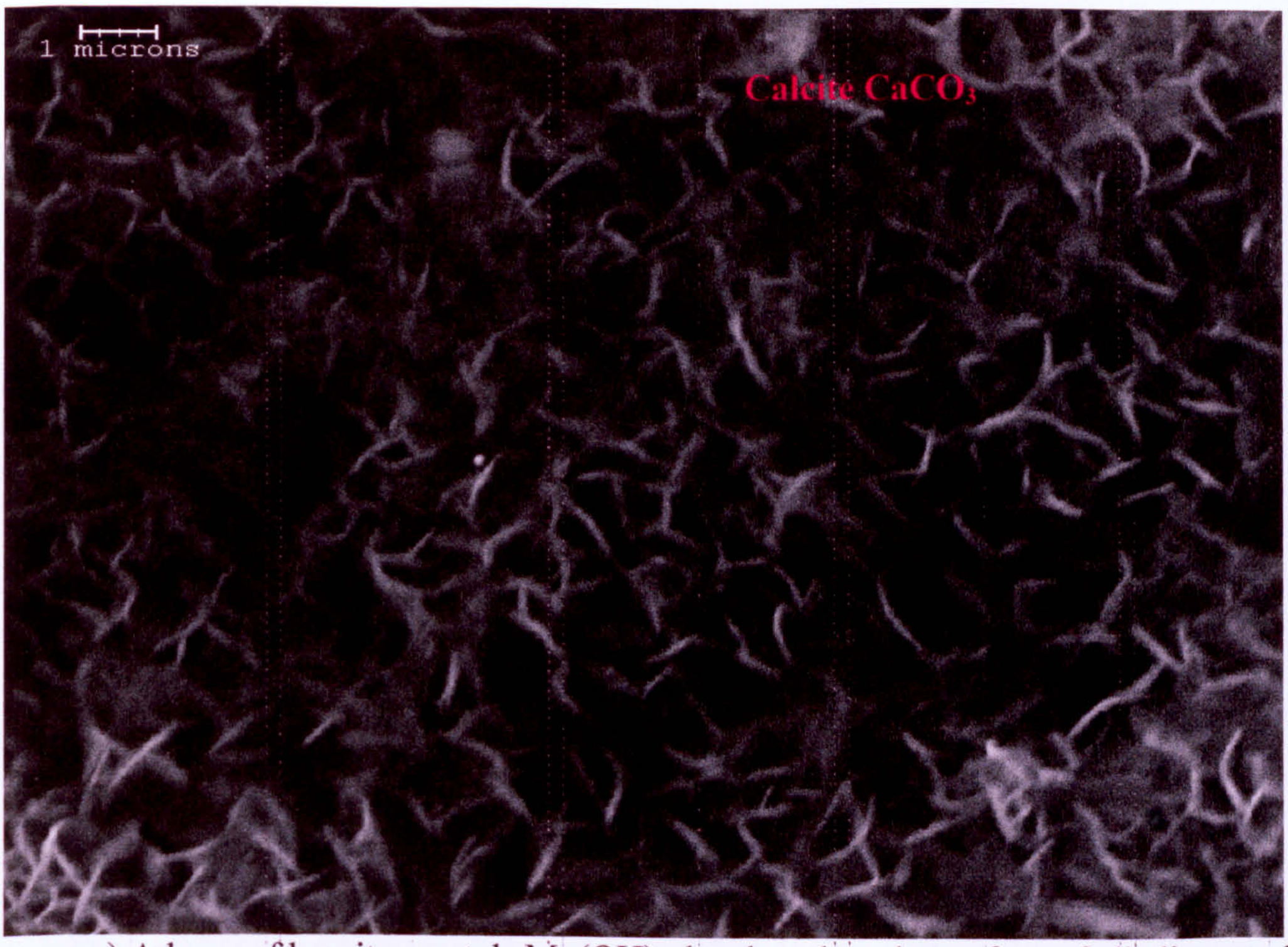

a) A layer of brucite crystals $Mg(OH)_2$ developed on the surface of alkali-treated dolomite crystal

b)Hooper-shaped calcite crystals growing on the same dolomite surface,

Figure 5.5 Higher magnification revealing brucite $Mg(OH)_2$ and calcite ($CaCO_3$)

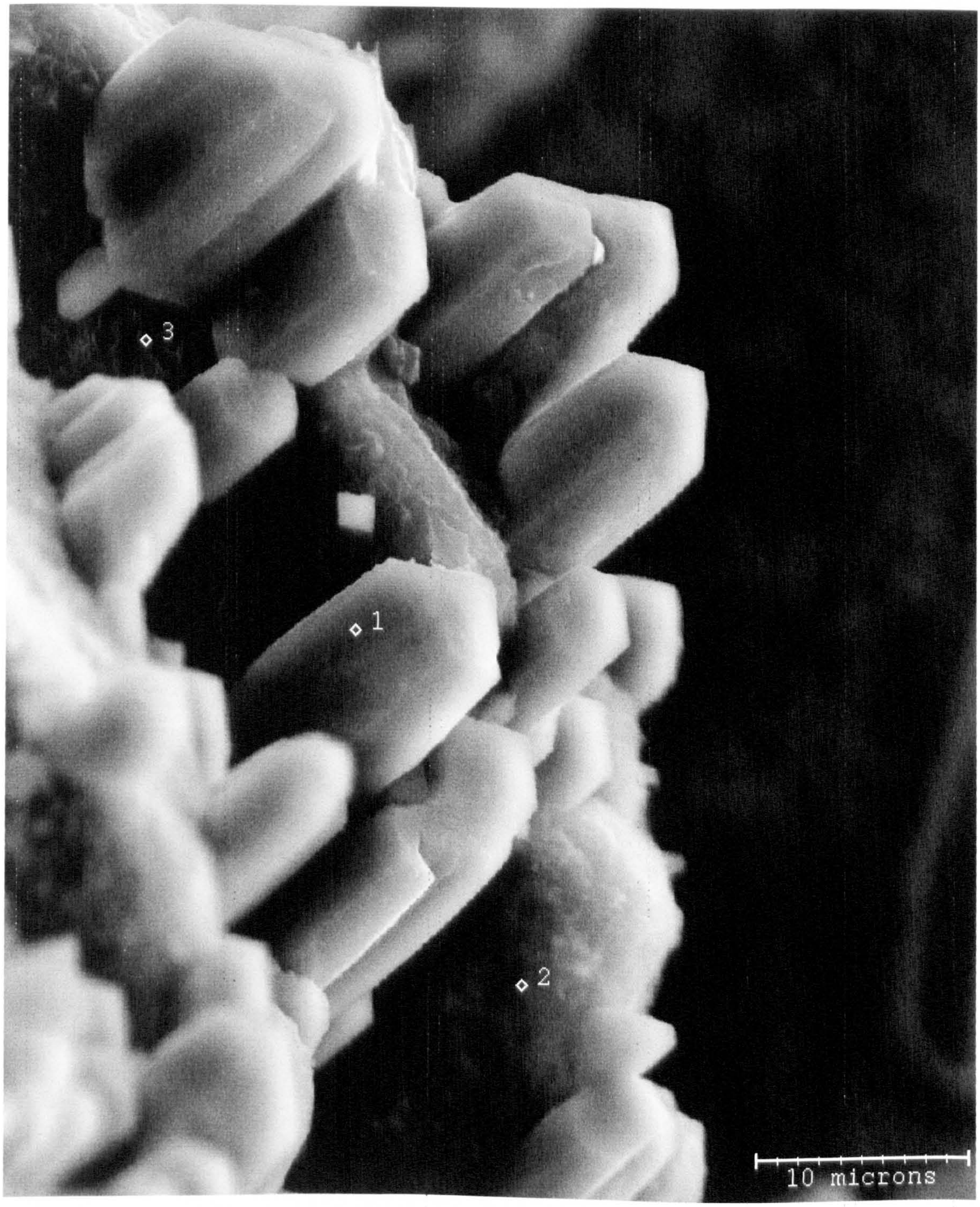

Figure 5.6 Dedolomitisation products developed on a surface of a single dolomite crystal (MR02) immersed in 3N NaOH for three months. Point 1-Ca phase (calcite/aragonite), Point 2-original dolomite substrate, Point 3-Mg phase (brucite).

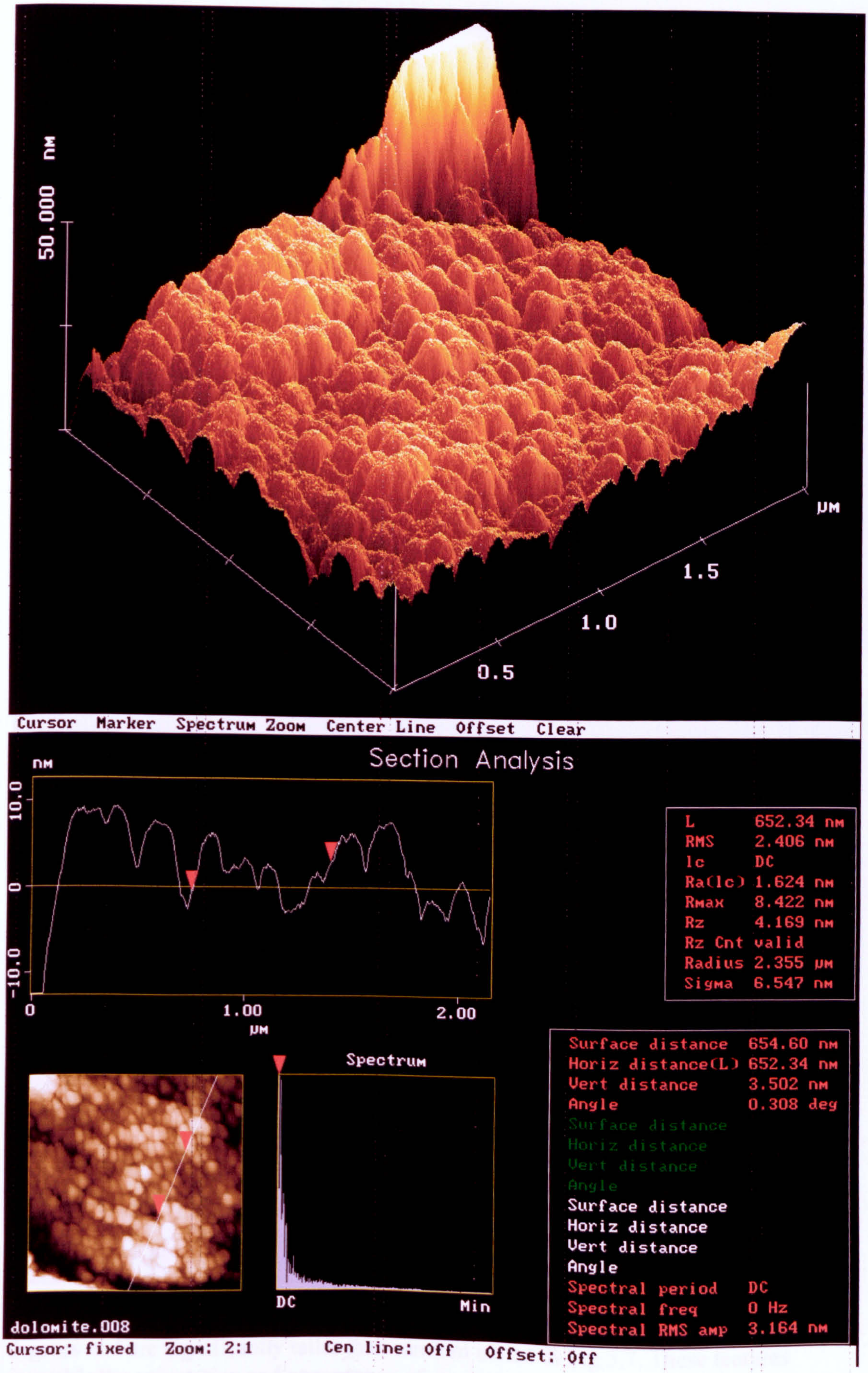

Figure 5.7 AFM (contact mode) image of untreated dolomite surface revealing the top atomic layer, topographically lower ordered atoms whose height is 10-20nm and are randomly dispersed with no orientation.

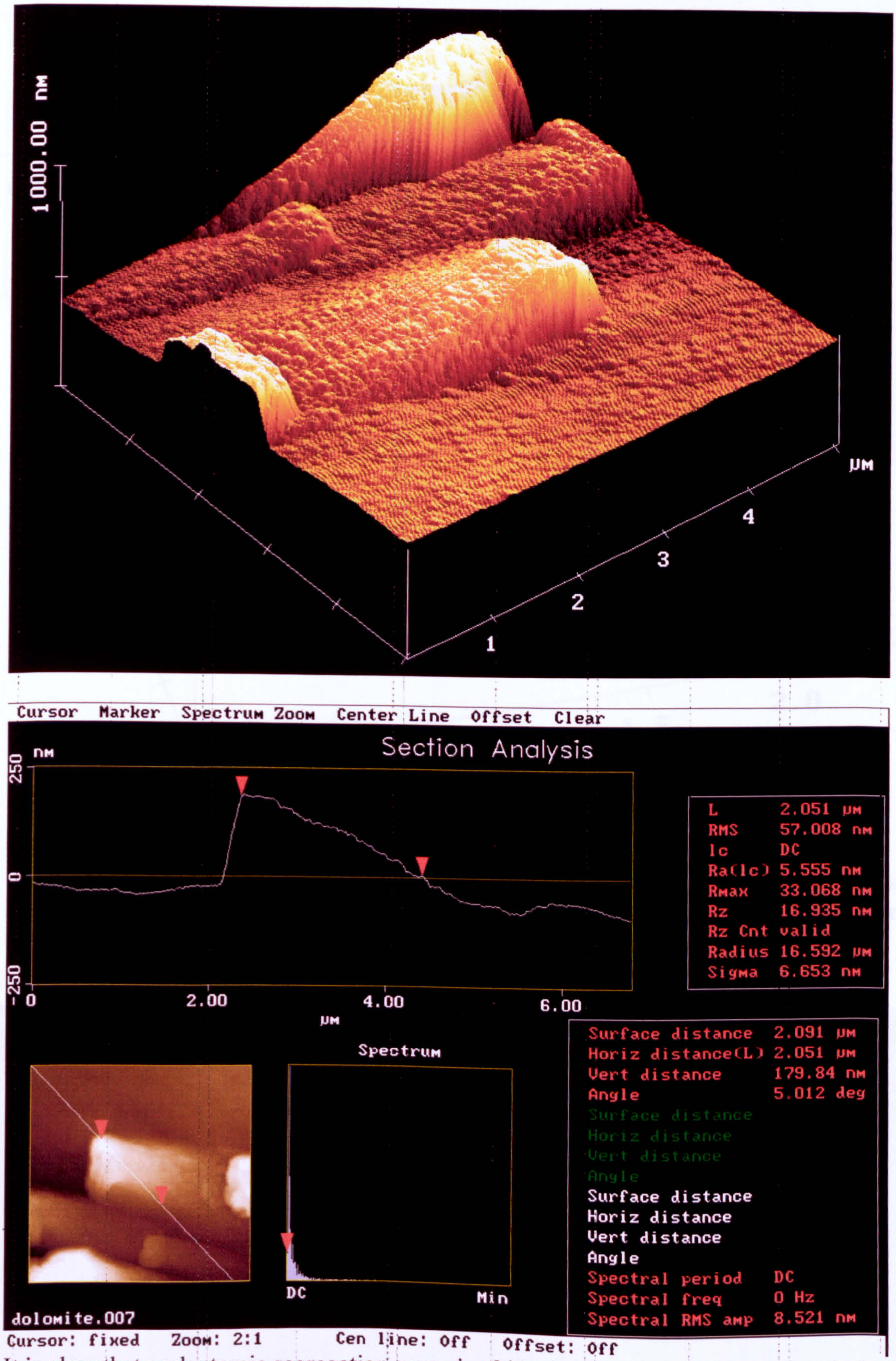

It is clear that each atomic segregation occupies 2*2micron area, and its slope angle is 5 degrees and are significantly taller than random atoms in Fig.5.7. These features resemble the orientation and appearance of cc growth during dedolomitisation (Fig.5.4).

Figure 5.8 AFM (contact mode) image of topographically higher atomic order at dolomite surface. Sample MRO3 prior to NaOH treatment.

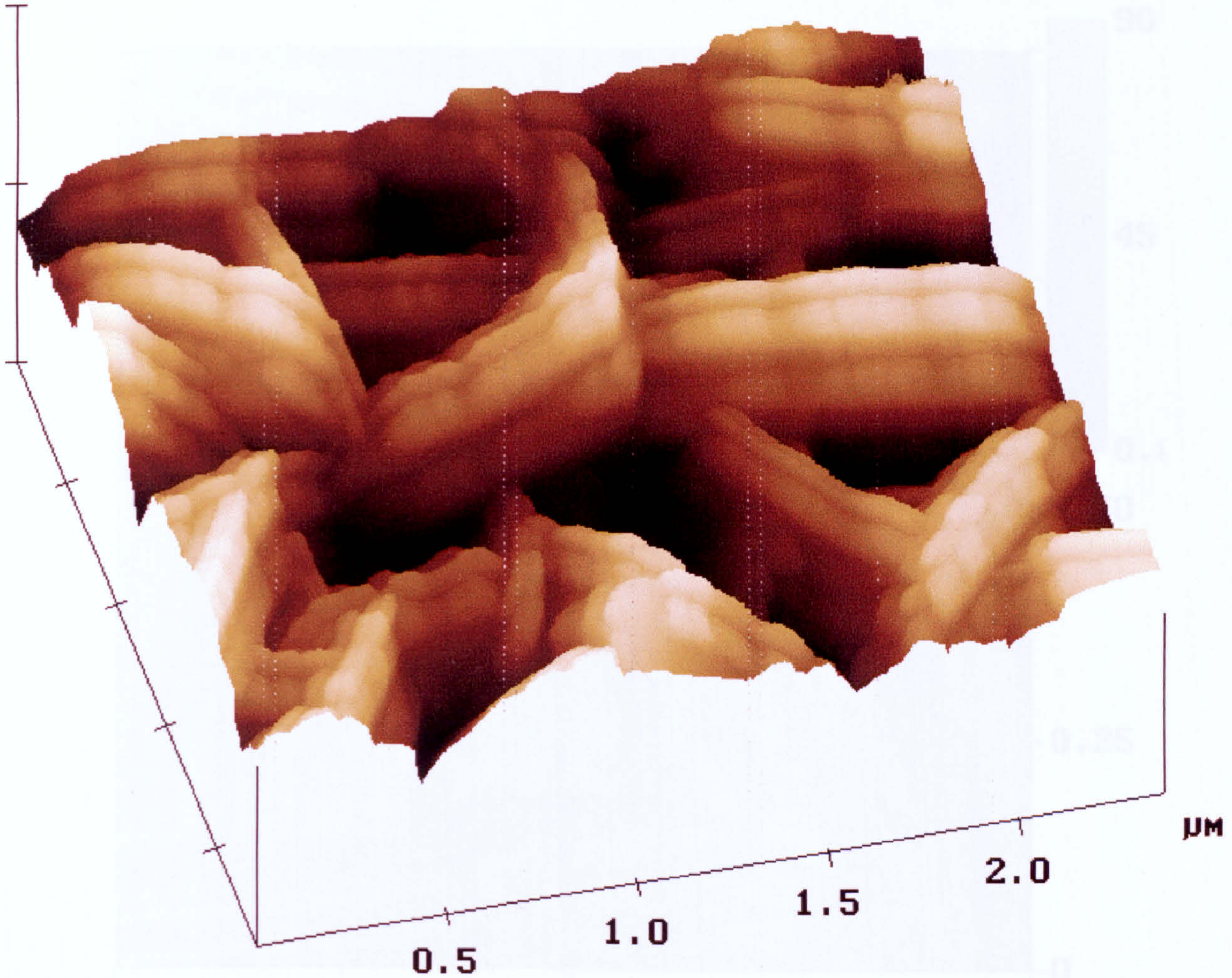

Figure 5.9 AFM (tapping mode) image showing a 3-D section of the fine network layer of brucite crystals on the surface of dolomite after 3 weeks in alkaline solution.

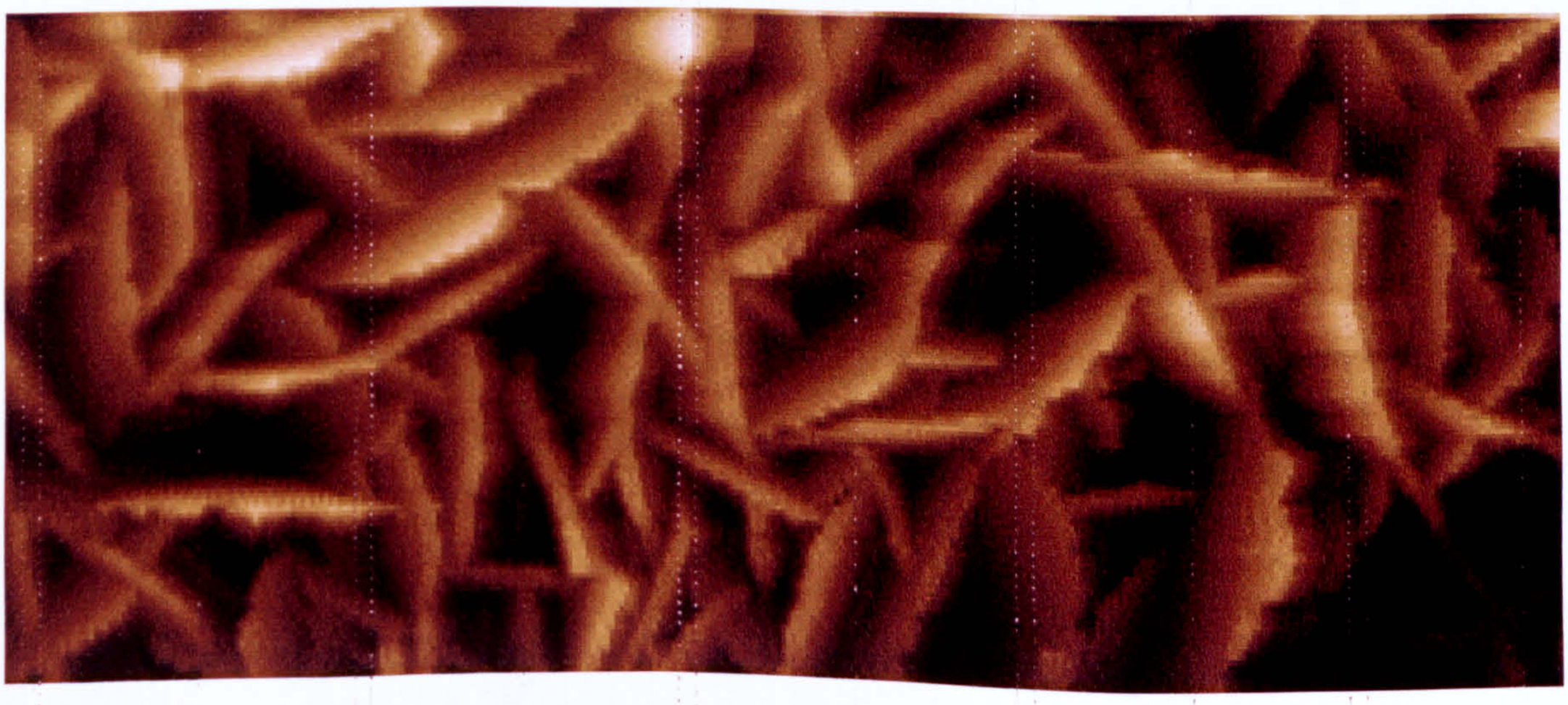

Figure 5.10 Brucite growth as above showing a 2-D section.

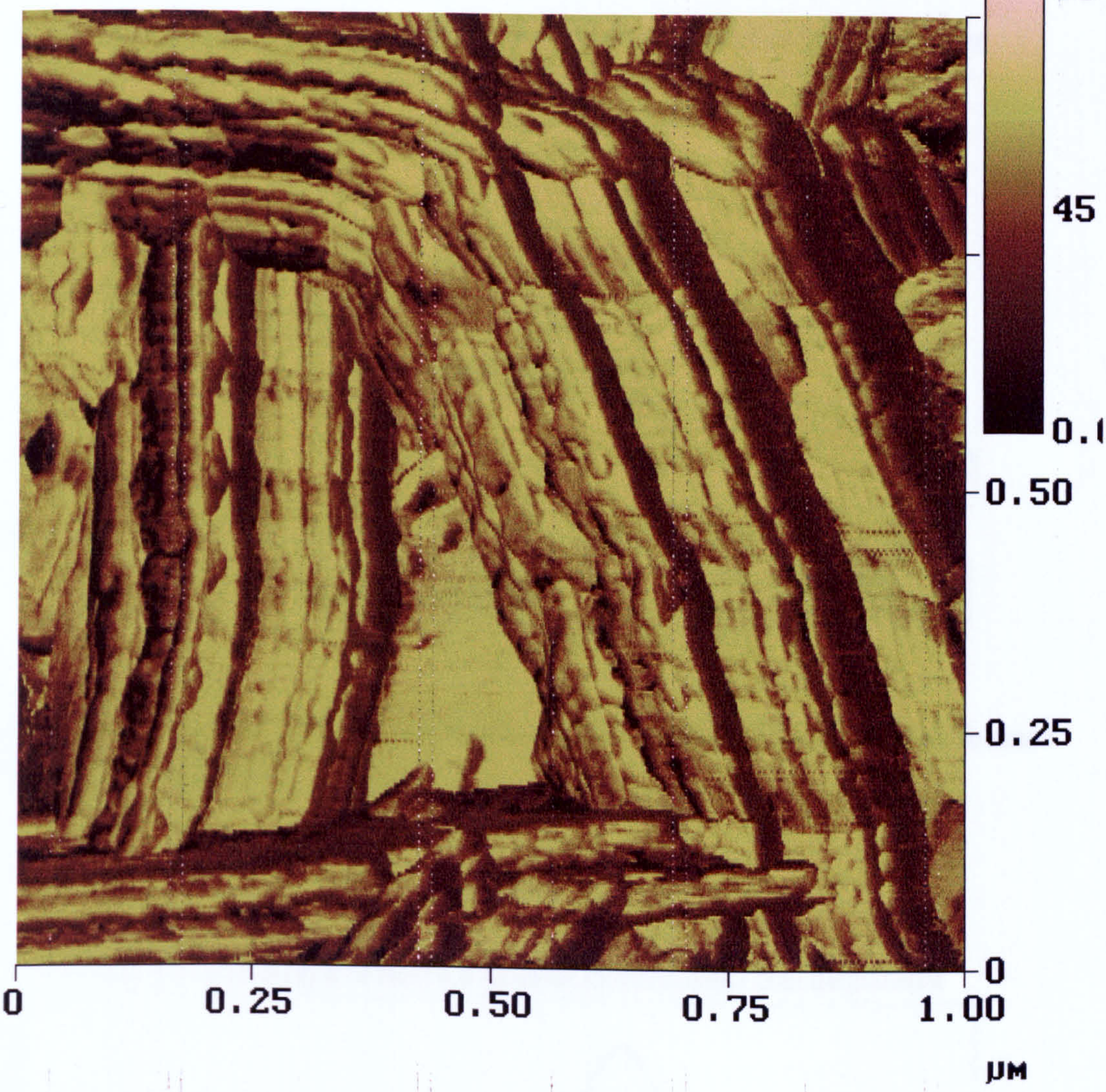

Figure 5.11 AFM phase image of brucite formation on the surface of alkali-treated dolomite crystal developed within 3weeks.

* Light colouring present brucite crystals and dark colouring refers to the clearly compositionally different phases adjacent to the brucite crystals. This new products are developed as a result of brucite/alkaline solution reaction.

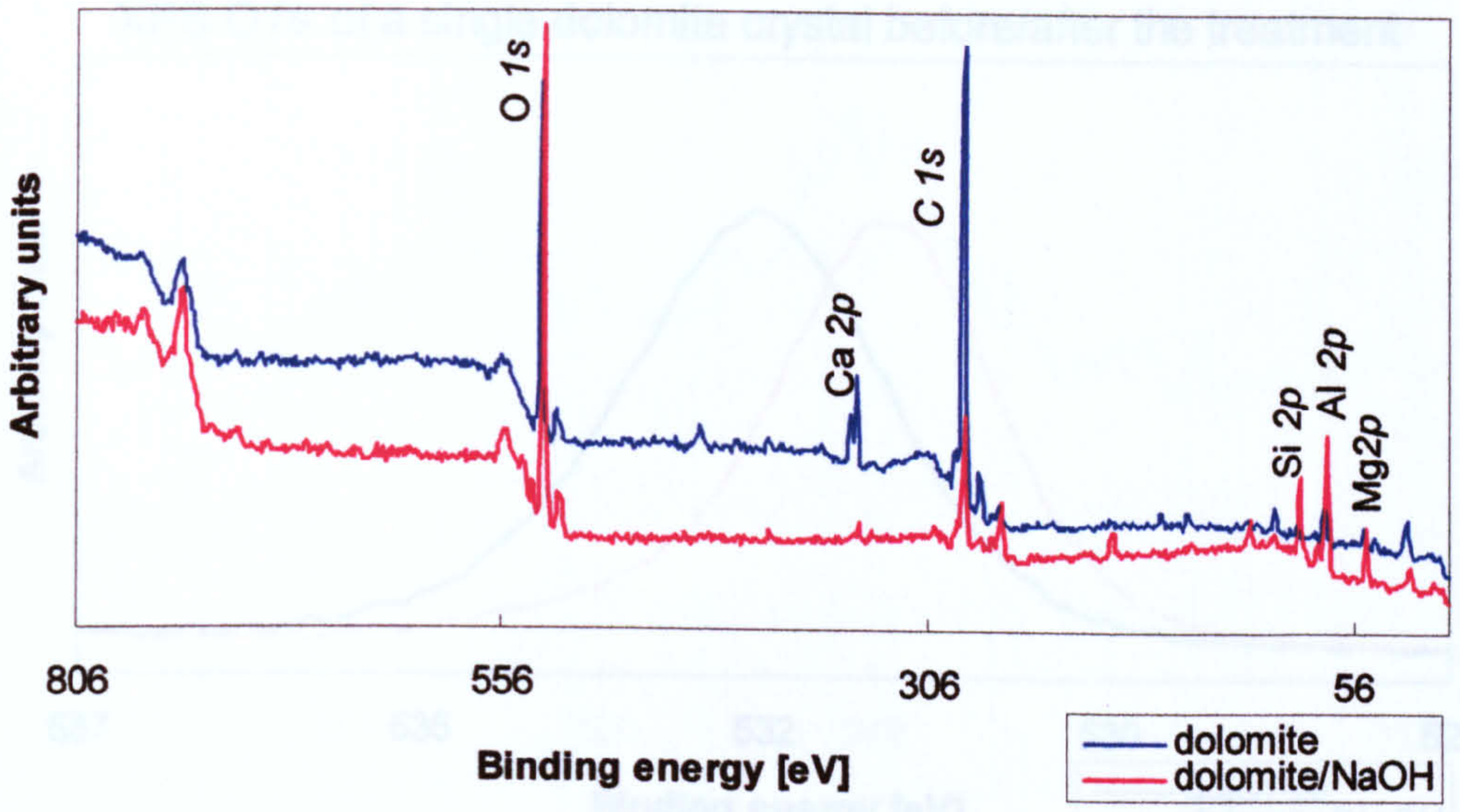

a) Wide spectra of untreated/treated dolomite surface revealing the general difference between the phases present.

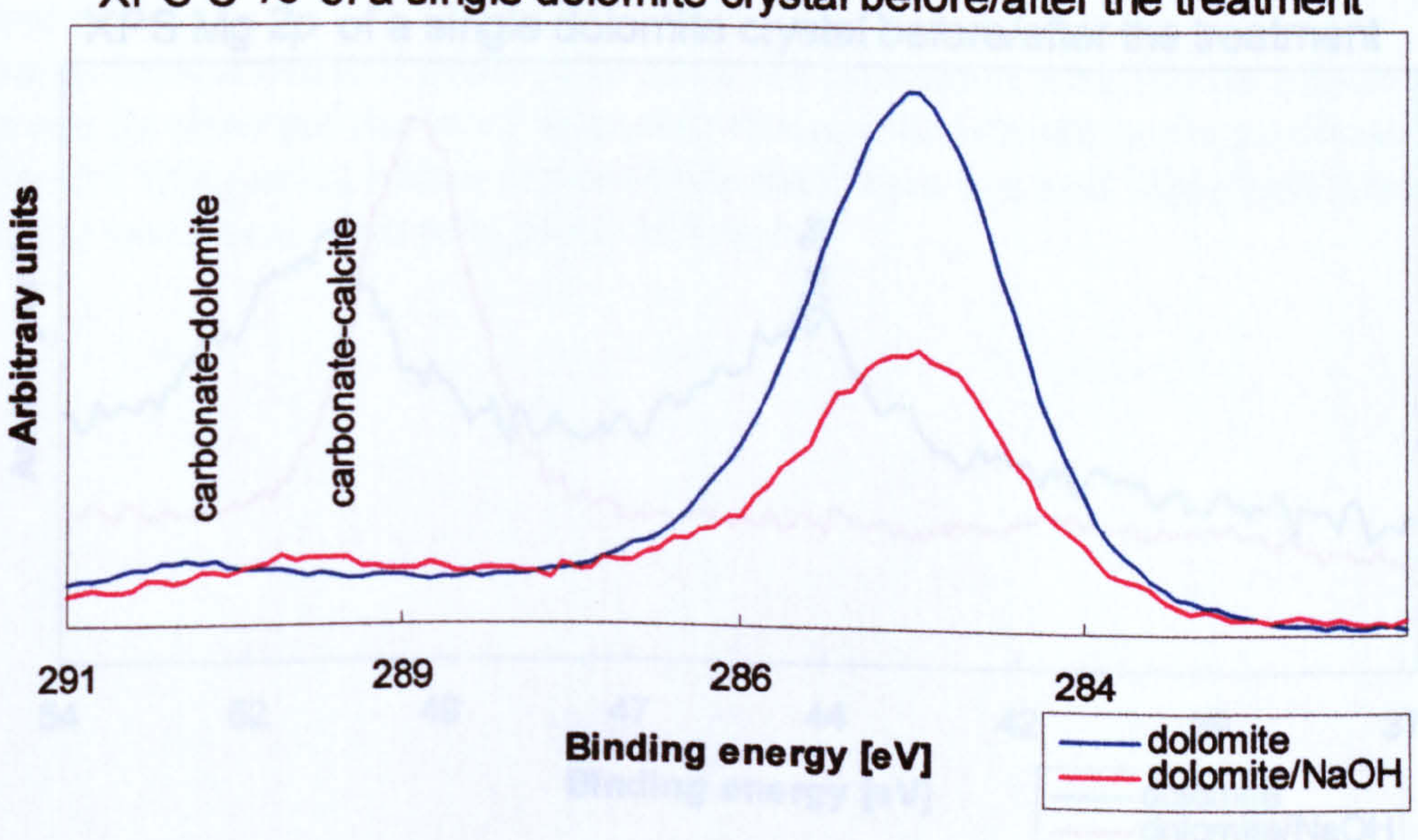

b) Regional spectrum for carbon showing the different chemical states before and after the NaOH treatment, manifested mainly by the carbonate peak shift and different peak heights (see table 5.2).

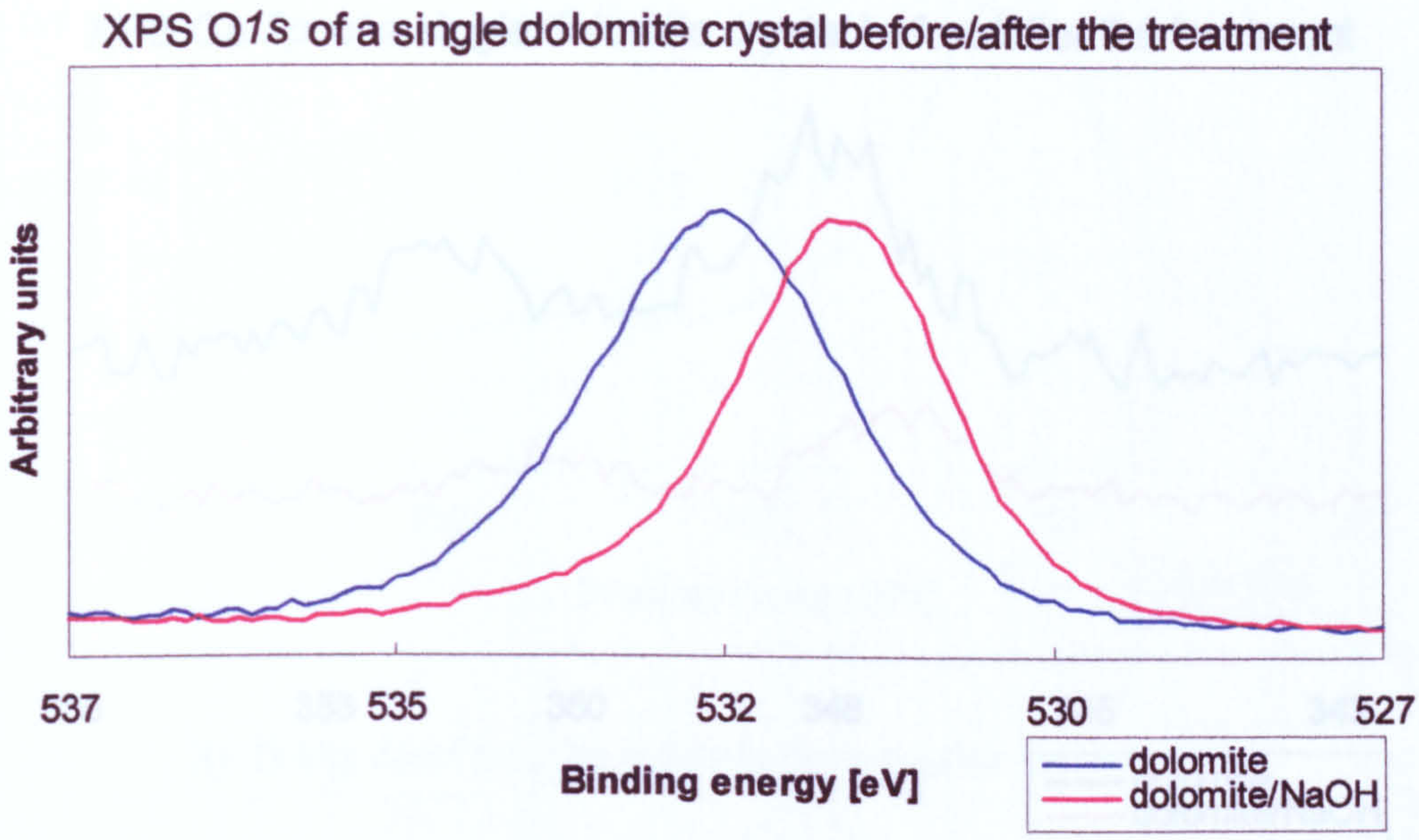

c) Peak shift in oxygen reveals the chemical change of carbonate to a hydroxide

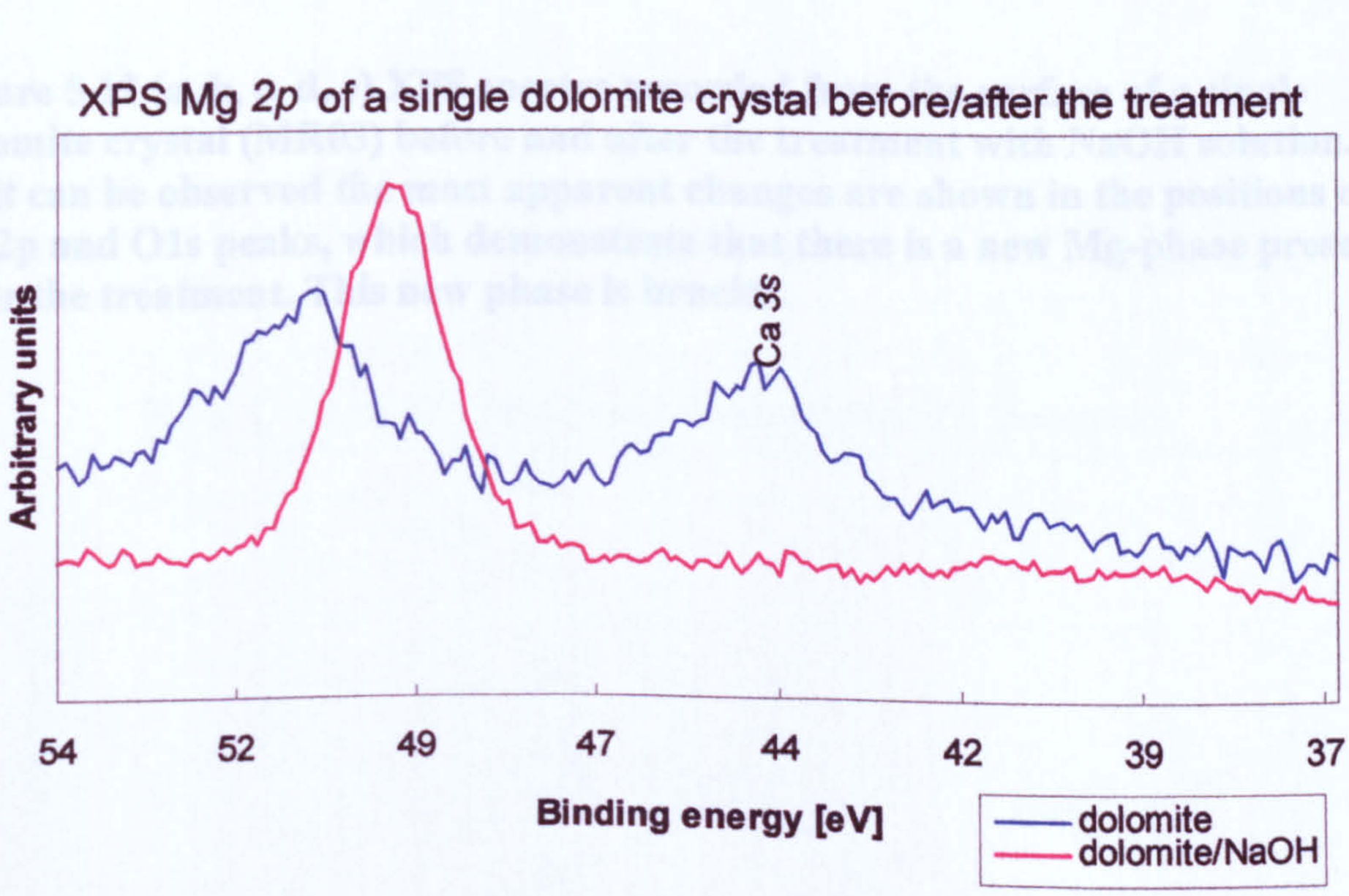

d) Mg2p region confirms the previous-change of carbonate to a hydroxide

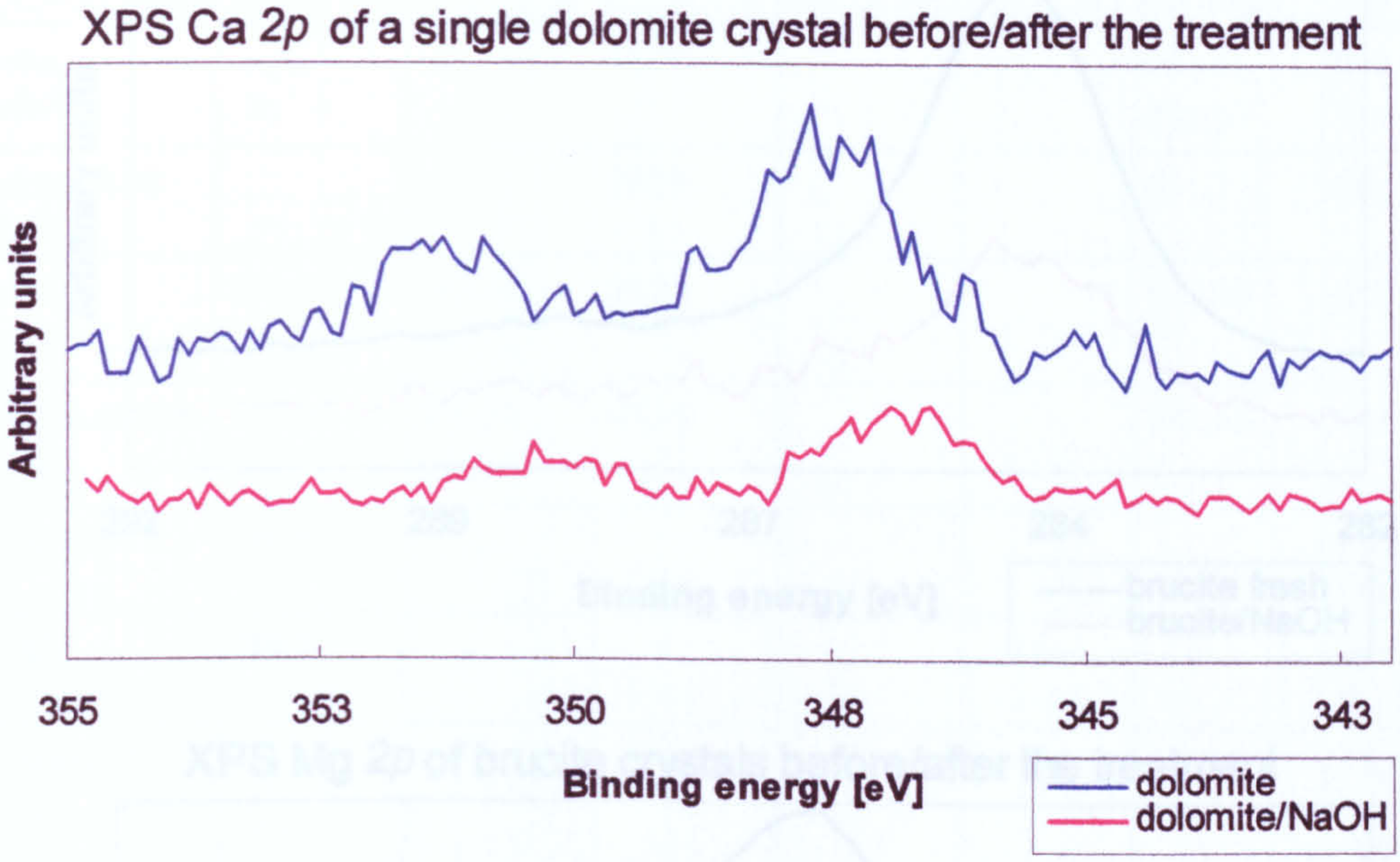

e) Regional spectrum of Ca2p before and after NaOH treatment. It is clear that although there is a change in the chemical state of Ca the rate is much slower than the rate observed in Mg.

Figure 5.12 (a, b, c, d, e) XPS spectra recorded from the surface of a single dolomite crystal (MR03) before and after the treatment with NaOH solution. As it can be observed the most apparent changes are shown in the positions of Mg2p and O1s peaks, which demonstrate that there is a new Mg-phase present after the treatment. This new phase is brucite.

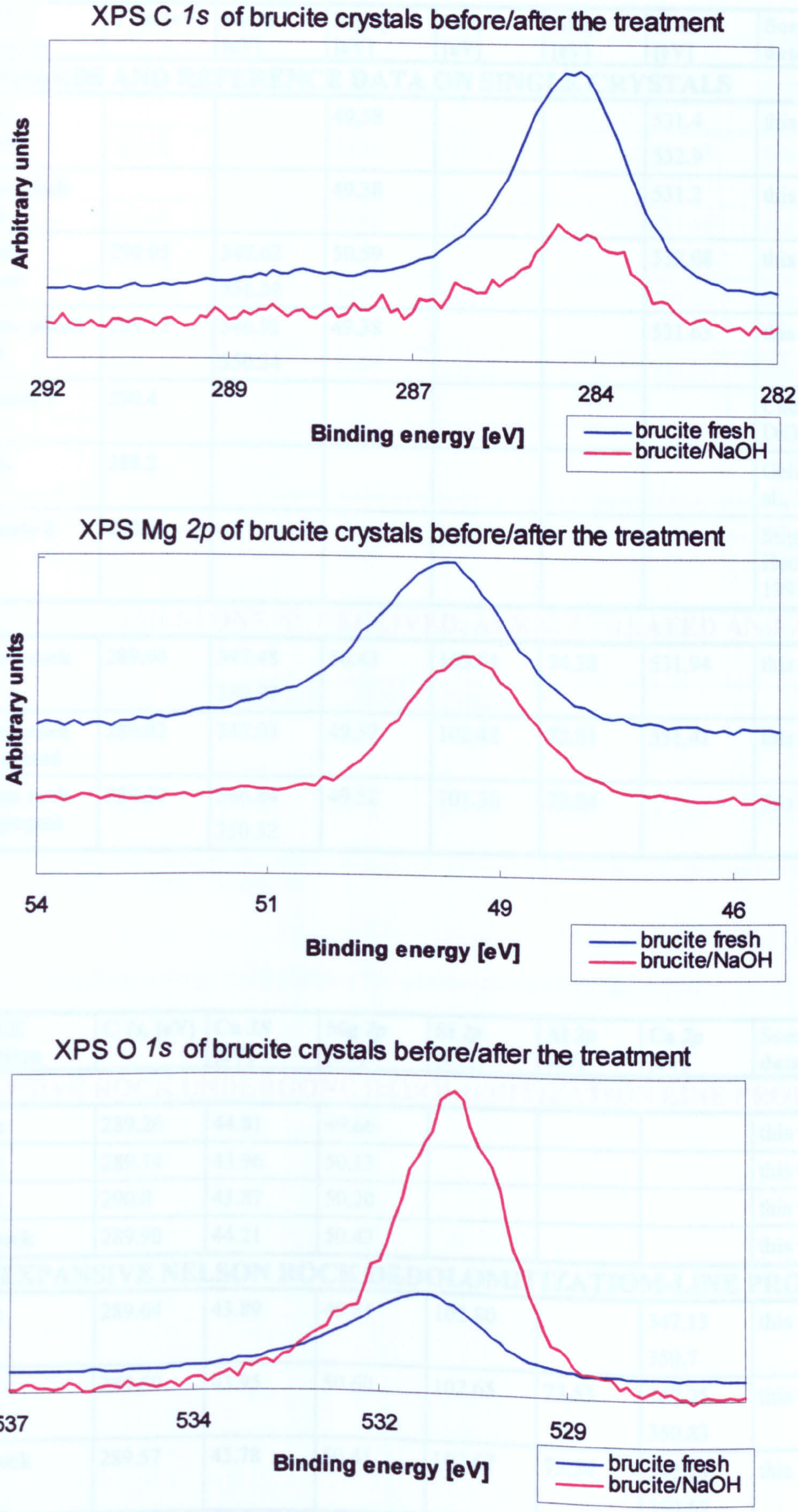

Figure 5.13 Regional XPS spectra of brucite (sample MRO4) before and after the treatment with NaOH solution showing binding energy shift (change in chemical state).

SAMPLE Description	C *1s*, [eV]	Ca *2p* [eV]	Mg *2p* [eV]	Si *2p* [eV]	Al *2p* [eV]	O *1s* [eV]	Source of data
STANDARDS AND REFERENCE DATA ON SINGLE CRYSTALS							
Brucite standard			49.58			531.4 532.9	this work
Brucite alkali treated			49.38			531.2	this work
Dolomite standard	290.05	347.62 351.34	50.59			532.08	this work
Dolomite alkali treated	289.13	346.91 350.34	49.38			531.63	this work
Carbonate 1	290.4						Clark and Dilks, 1979
Na_2CO_3	288.2						Gelius et al., 1970
Carbonate 2	290.1						Stipp and Hochella, 1991
DOLOMITIC LIMESTONE AS RECEIVED, ALKALI TREATED AND ACR							
Kingston rock	289.90	347.48 350.97	50.43	103.01	74.28	531.94	this work
Kingston rock alkali treated	289.02	347.05	49.57	102.42	72.81	531.41	this work
Kingston rock acr aggregate	289.20	346.84 350.32	49.52	101.36	73.84		this work

SAMPLE Description	C *1s*, [eV]	Ca *3S* [eV]	Mg *2p* [eV]	Si *2p* [eV]	Al *2p* [eV]	Ca *2p* [eV]	Source of data
EXPANSIVE ROCK UNDERGONE DEDOLOMITIZATION LINE PROFILE							
Surface	289.26	44.81	49.66				this work
0.7 mm	289.74	43.96	50.13				this work
4.5 mm	290.0	43.87	50.20				this work
Fresh rock	289.90	44.21	50.43				this work
NON-EXPANSIVE NELSON ROCK DEDOLOMITIZATIOM-LINE PROFILE							
Surface	289.64	43.89	49.81	102.80		347.13 350.7	this work
1-2mm	289.60	43.95	50.60	102.65	73.53	347.25 350.83	this work
Fresh rock	289.57	43.78	50.41	102.67	73.34	347.13 350.67	this work

SAMPLE Description	C *1s*, [eV]	Ca *2p* [eV]	Mg *2p* [eV]	Si *2p* [eV]	Al *2p* [eV]	O *1s* [eV]	Source of data
ACR DOLOMITIC LIMESTONE FROM KINGSTON, different beds							
Kingston 3pl	289.24	344.81 350.28	50.10	102.50		531.42	this work
Kingston 3nr	289.19	346.83 350.34	49.80	102.59		531.48	this work
Kingston 4	289.20	346.80 350.31	59.31	102.67		531.55	this work
Kingston 5	289.26	346.93 350.44	49.97	102.69		531.57	this work
Kingston 7	289.41	346.94 350.84	51.20			531.44	this work
ACR EXPANSIVE DOLOMITE FROM CHINA							
China 1	289.66	347.19 350.77	50.23			531.62	this work
China 2	289.62	347.15	50.30	103.09		531.65	this work
NON-EXPANSIVE DOLOMITIC LIMESTONES							
Spanish	289.57	342.11 350.65	49.89	102.37	72.87	531.60	this work
Swedish	289.41	347.48 350.92	50.33	102.63	72.97	531.98	this work

In text of Chapter 5 and Chapter 6

Table 5.2 Binding energy (*eV*) values for elements used in this study.

Chapter 6 Laboratory based carbonate aggregate/alkaline solution reactions

6.1 Introduction

The data obtained on single mineral/solution reactions (Chapter 5) could not have been used as a basis for the ACR mechanism unless identical processes and reaction products were detected within carbonate rocks subjected to the same treatment.

A selection of carbonate rocks (sample MR08-MR16, Table 3.2) was subjected to ASTM C586 standard tests as a first selective measure for expansive and non-expansive aggregate. Core specimens were produced from different types of carbonate rocks ranging from well known expansive Kingston dolomitic limestone from Canada to dolomite and limestone from various quarries in England, Wales and expansive dolomite from China as presented in Table 3.2 and 3.3, Chapter 3. Rock-cores were subjected to 1N NaOH solutions for up to 3 years.

Length measurements were performed on 130 cores (from samples MR08-MR16) over a 3 year period, and analyses carried out for the detection of compositional and microstructural changes that had been induced by alkaline solution. In order to define the main characteristics of the rocks expansive in alkaline solutions and establish parameters that would distinguish reactive from non-reactive rocks, each specimen was micro-analytically characterised prior to and after the NaOH treatment, and inspected during measuring procedures. The objective of this part of the study was to establish similarities and differences between reactive-expansive, reactive-non/expansive and non/reactive rocks, since the study contained rock samples known to be from all of the three categories, (Table 3.3).

6.2 Alkali induced mineralogical transformation

Untreated samples of various carbonate rocks used as aggregates were mineralogically characterised using X-ray powder diffraction. The data were subsequently acquired for samples that had been treated with alkaline solutions, ensuring that in expansive rock

specimens, XRD traces were obtained from different regions of the rock core (physically altered outer rims and unaffected inner areas), (Figure 6.1). Particular interest was given to dolomitic limestones from Canada and a Chinese dolomite, as they were potentially susceptible to ACR. However, mineralogical changes occurred during the alkaline treatment. These changes can be seen in diffractograms (Figure 6.1), mainly manifested by a change dolomite/calcite ratio. The data shown in the Figure 6.1 suggests that the amount of dolomite is decreasing or that due to an increase in calcite the dolomite intensity is changed for expansive samples (samples MR09, 11, 14), resulting in a different D/C ratio.

On the contrary, the dolomite of similar composition but of non-expansive nature from dolomite from Whatley, S.W. England (MR15) when subjected to NaOH solution, was shown to have the dolomite peak as a dominant one (Figure 6.2). The XRD analysis of the above-mentioned, alkali-treated rocks of similar composition (Kingston and Whatley dolomites) suggested the following: the dolomite/calcite ratio within the expansive Kingston rock decreased after alkaline treatment, where as the D/C ratio within non-expansive Whatley dolomite increased. This might have originated from the interference of peaks with different intensities. Although dolomite is the main peak in Whatley rock, that could have resulted from the dissolution of calcite and not the formation of extra dolomite, since the dissolution of calcite would also enhance the appearance of dolomite peak. The majority of expansive carbonate rocks contain rhombohedral dolomite in a silty and clay-rich micrite sized calcite matrix, which is why it was important to establish the role of the clay fractions (illite and chlorite) and their possible contribution to the expansive nature of ACR.

A separate XRD analysis with a different preparation of samples aimed at the identification of the clay fractions, involving glycol treatment, was also carried out. The intention was to establish whether the specimens that were treated with alkaline solutions but had different expansion records would contain qualitatively and quantitatively different clay fractions. The rock cores (Table 6.1) with different expansion rate and dedolomitisation degree were powdered, allowed to dry, filtered and using two glass slides spread in a thin film orienting clay crystals in one plane to enhance the signal for the spectrum. This is clay XRD analysis at English China Clays Laboratories, St. Austell, UK also described in XRD text books). Although with a different expansion

record these samples did not show any difference in their clay fraction. The slides were then immersed in glycol and left overnight, expecting that swelling of sheet silicates would proceed much faster with glycol than with water. The samples were then used to acquire another set of data, with the 2θ angle in the range 1-15 degrees, allowing 2 hours on each sample. The result was the same; the spectra did not show any clay peaks and there was no difference between treated and untreated rocks whether expansive or non expansive, and no significant change when reaction rims were compared to un-reacted regions of the rock cores. The evidence of any involvement of clay-fraction was absent, mainly due to the fact that XRD is a technique for bulk analysis, unable to detect phases present in less than approx. 10%. XRD-patterns for samples 1-8 (Table 6.1) are shown in Figure 6.3.

Table 6.1 The samples from which the XRD patterns in Figure 6.2 were acquired.

XRD spectrum	Description and nature of the sample
Spectrum 1	White, outer reaction rim from Nelson dolomite, non-expansive in NaOH
Spectrum 2	Nelson dolomite unaltered by NaOH solution
Spectrum 3	Kingston dolomite before the alkaline treatment
Spectrum 4	Kingston dolomite alkali treated, expanded, dried
Spectrum 5	Kingston dolomite reaction rim, removed from the core without drying
Spectrum 6	Massachusetts dolomite, alkali treated, semi-reactive
Spectrum 7	Whatley dolomite (rich in Fe), before the treatment with NaOH solution
Spectrum 8	Whatley Fe-dolom.limestone after the treatment with alkali

6.3 Microstructural changes induced by alkaline solution

It is possible that the microarchitecture of carbonate rocks influence the expansion mechanism since the rocks of similar composition have different behaviour when used as aggregate in concrete. Scanning Electron Images (SE and BE mode) from different types of carbonate rocks prior to and after the treatment with alkaline solution were used to obtain the information about the changes in microstructure.

Most of the carbonate rocks used in this investigation were dolomitic limestones in mineralogical composition and therefore the changes that potentially could have contributed towards the expansion were expected to be identified within individual grains of the rock or at the grain boundaries between main components (carbonates and silicates). The difference between the rocks involved were mainly in the calcite/dolomite ratio, the grain size of dolomite crystals and the presence of a fine calcite - silicate matrix, enveloping coarser carbonate grains.

Samples of the untreated argillaceous dolomitic limestone from Kingston were used as a reference material for expansive carbonate rocks and are thus an ideal sample for study of the mechanism of ACR. The rock is characteristic for its fine-grained calcite/silicate matrix and 20-60 μm-sized dolomite fraction. A SEM image of the edge of the core prepared for ASTM C 586 is shown in Figure 6.4.a, where the rhombohedral dolomite crystals are surrounded with calcite/silicate matrix. Microscopical observations of freshly fractured surfaces of Kingston dolomite revealed the presence of calcite crystals with sharp clean surfaces, (Figure 6.4.b).

Additional observation from polished surfaces, that complement the data from fractured surfaces of the same rock samples, were obtained under back scattered mode in SEM. This enabled an easy distinction between dolomite (darker) and calcite (brighter) regions, otherwise difficult to distinguish under SEM (Figure 6.4). From these micrographs it is obvious that the rock was not homogeneous in terms of dolomite abundance; there were some calcite rich patches with no dolomite. In addition to this, the rock contains pyrite crystals, in BE image presented by very bright areas, Figure 6.5.a,b. Dolomite grains are rich in inclusions and have zoned appearance due to the presence of Fe. Therefore the rock is referred to as ferroan dolomitic limestone. A detailed SEM image of a fractured surface of Kingston dolomite reveals the presence of layered structures with steps-like appearance and silicates inclusions (Figure 6.6).

6.3.1 Observations after treatment with NaOH solution

All the samples were investigated after alkaline treatment at various intervals, in order to establish the changes in some of the typical features described in the previous paragraph. Visually detectable changes are present in the form of a dark rim formed on the outer part of the core, with occasional cracks and fibrous surface deposits. These were

analysed to be natronite at the Natural History Museum of London (Radonjic *et al* 1996). The Kingston rock changed from a dark grey colour rock to a discoloured pale grey surface, although no visible change was observed in the soundness of the rock were produced with NaOH treatment, (samples MR08). Rock cores from the Laboratory in Calgary, Canada of the same material, but kept in 4N NaOH solution, showed formation of 1.5mm dark outer rim (sample MR11). It was observed that the macroscopically unaltered inner regions of rock cores had a different chemistry and texture from the outer of approximately 50-100 mμ. Comparison between changes in 1N and 4N NaOH solution shows that the reaction rate can be increased with an increase in pH of the solution used. Practically, the kinetics of the ACR/dedolomitisation reactions are usually slow but with an increase of alkalinity the reaction proceeds faster. This is demonstrated in the amount of reaction products formed (rims and discoloration) as well as development of microcracks.

Microscopic observations were performed on fractured as well as polished samples previously embedded in epoxy resin. The samples fractured after being taken out of NaOH solution showed disintegration of some dolomite grains. This was best demonstrated by comparing now jagged edges of crystals and evidence of dissolution, well presented in Figure 6.6.d, where the layered structure of dolomite is affected by alkalis. Other types of secondary deposits are presented in Figure 6.6.e, presenting a mineral in a form of needles or fibrous segregation attached to fine carbonate crystals. Finally, fine grained calcite crystals shown in Figure 6.6.d, developed in the proximity of some of the larger carbonate grains subjected to dissolution, could also be a newly formed phase. Back scattered imaging of polished surfaces, compared with untreated samples of Kingston dolomite, showed dissolution in peripheral regions of the rock core. Figure 6.7.a, b contains some of the typical dolomite changes. It is possible that the raw Kingston rock has undergone partial dedolomitisation, since some of the untreated BEI are similar to those from treated, containing calcite or quartz inclusions, and semi-dissolved grains.

6.3.2 Elemental mapping

When comparing the elemental distribution, using X-ray maps from treated and untreated specimens (Figures 6.8, 6.9, 6.11, 6.12 and 6.13) the following was observed: The fractured surface of untreated rock have uneven topography due to the different hardness

of the phases present, mainly carbonates, silicates and quartz. Although mapping from fractured surface with high relief is not recommended because of topographic effects, in this case it was performed so that fine intra-granular phases would be the ones giving the main signal. A sample of untreated Kingston rock (control sample MR09) was freshly fractured, carbon coated and used to obtain an elemental map. The aim was to detect the presence of elemental components of fine matrix material along the fracture plain. The result is presented in Figure 6.8, with the SEM image of the surface that reveals the plane of weakness, and elemental maps. It is obvious that the high relief areas are composed of Ca, K, Si and S. The compilation map that combines S, Si and Mg shows that there is no correlation between Mg and other two elements, since Mg is present in dolomite only, but it is clear that S is present in morphologically higher areas (Figure 6.8).

Elemental mapping was then carried out on a cone sectioned from the rock cylinder (sample MR 08) immersed in NaOH for three years. The charge effect was reduced due to the angle of the slope 120°C which meant that the electron penetration and pear effect of charge build up were reduced (Figure 3.7 with the sample shape). The sample was not coated or altered in any other way apart from drying, so that the surface deposits were preserved. This type of experiment using cone-shaped samples can be useful if coating needs to be avoided and charge effect reduced in insulators examined in conventional SEM.

As can be seen in Figure 6.9.a SEM micrograph is used to allocate boundaries between dolomite grains (white lines). Comparing X-ray maps (brighter areas represent higher concentrations) of Mg and Fe with the SEM image shows that the dolomite edges are enriched in Mg (Mg map), opposite to the central parts of dolomite grains which are mainly Ca rich. This was caused by an elemental migration which occurred as Mg and Fe are present in the outer rim of dolomite grains opposite to calcite. The role of the silicate phase is not fully understood. Therefore further studies were needed to establish the changes from untreated specimens to those altered by expansion.

Other elements of interest were Si, K, Fe and Al. The presence of Si is in the form of quartz grains as inclusions in dolomite crystals and in matrix or as silicates. Al and K are distributed in the matrix as clay minerals. When compared with the X-ray maps from untreated surfaces it can be concluded that one of the reasons for expansion is because

Mg/Fe reaction products (brucite and iron oxides/hydroxide) will form in a space originally occupied by silicates. This would than have further implications on the migration of Si, and that would involve dissolution and reactivity of Si phases. The red dot was used to follow one particular dolomite grain in individual elemental maps, revealing Mg/Fe peripheral enrichments and depletion of Ca in the same regions.

6.4 Geochemistry of carbonate rocks

Rock-forming minerals for limestone and dolomite are mainly minerals of the carbonate group (dolomite and calcite) with silicate minerals as minor constituents. Since 40-90% of the mass in an expansive dolomitic rock-aggregate are dolomite/calcite phases, full understanding of the alkaline solution/carbonate minerals interactions is required. In this section the basic principles of the behaviour of carbonate minerals during rock-alkaline solution interaction are studied.

The dolomitic limestone from Kingston Canada is of Ordovician age (Rogers 1990), formed as the Ordovician Sea advanced over the exposed Cambrian rocks of eastern North America. Since the eroded rocks were dolomites and the extent of erosion was on the large scale, the result was an increased concentration of species necessary for the precipitation of $CaCO_3$ and $MgCO_3$ in a form of dolomite. These dolomites are typically finely crystalline and contain argillaceous material or thin shale beds due to build-up of insoluble matter from the original dolomite. Argillaceous materials can also be derived from the decomposition of feldspar or Mg-biotite (Calvert 1972). The second process of dolomite formation, resulting in a dolomitic limestone with patchy dolomite abundance and varying grain size, is late diagenetic dolomitisation, referred to as the metasomatism of $CaCO_3$ by Mg, (Udowski 1968).

6.4. 1 Elemental mapping and line profiles of alkali-treated rocks

Epoxy embedded, polished and carbon coated samples were prepared for further investigation using EPMA and back scattered imaging. Rock cores subjected to ASTM C586 were cross-sectioned into 1mm thick discs for the depth profiling and elemental mapping. Two types of elemental analysis were acquired: line profiles for accurate quantitative analysis and detection of minor chemical changes, and, elemental maps which provided spatial elemental distribution in different regions of samples analysed.

The data presented in this section was selected so that comparison can be made between reactive and expansive Kingston dolomite (sample MR011), reactive but semi-expansive Massachusetts dolomite (sample MR3) and reactive but non-expansive Nelson dolomite (sample MR12), Table 3.3. It is important to define the term reactive, which means that the rocks were dedolomitised when treated with alkaline solution, but when the length measurements were recorded some were expansive and the others not. The data was gathered from altered (dedolomitised and discoloured outer rims of rock cores) and from unaltered inner regions of samples for all three rock-types.

1) Kingston dolomite is well known as a prototype for alkali-expansive carbonate rock. Line A profile of 300-microprobe-point analysis was obtained from the cross section of rock cores after 3 years in NaOH solution (samples MR11-13). The acquisition regions were chosen using BEI mode for detecting different stages of dolomite and calcite alteration as well as the presence of various inclusions. The acquired data was plotted as graphs that have accompanying tables (Appendix A) with the data points showing quantitative analysis.

The first line profile was acquired from the regions that were closer to the outer reaction rim. This line is shown in Figure 6.10a and the data are presented in Appendix A, Table A1, again at similar scale of approximately 200 mμ. There is an obvious presence of Si rich inclusions although silicon is lower in amount but present in more data points. The Ca/Mg ratio is almost unchanged and the amount of Fe is similar to the unaltered regions.

The second line profile shows the composition of unaltered dolomite grains (20-60μm), across the region of 200μm, (Figure 6.10b) with the data points listed in Table A3. As it can be observed the Ca/Mg ratio is almost 2:1 and there is a detectable presence of Si, as high as 10 wt%, probably in the form of quartz inclusions. The data also shows the presence of Fe observed in BEI as rims in dolomite structure, with 1-3 wt% of Na in the regions towards the outer part of rock core.

The third line profile, aimed to cover 200μm of the reacted discoloured region, (Figure 6.10c) and Appendix A, Table A2 includes clusters of altered dolomite crystals. As can be observed, there are much higher amount of Si, Na, Fe and a significant amount of Al_2O_3 present. The Ca/Mg ratio is generally lower than in previous analysis (3:1 and

sometimes as low as 8:1). Two types of calcite present, porous and unaltered, compact grains, present another textural observation.

The fourth line profile presents a general correlation in Ca/Mg ratio from reacted outer rim towards unaltered inner areas of the rock core, Figure 6.10d.

The fifth line profile from the region of 500μm shown in Figure 6.10e and Appendix A, Table A5, reveals the composition of a porous, fine grain size calcite phase. This region is characterised with a high percentage of SiO_2 present and uncommonly high concentrations of Al_2O_3 and Na_2O. Since no Mg or Fe was detected, the suggestion is that these are Ca-silicate dominant areas. Finally, the data acquired shows the chemical and mineralogical assemblage of inclusion and impurities within a single dolomite crystal, approximately 50μm in diameter, Figure 6.10 and Table A7.

Measurements were then performed for establishing **spatial elemental distribution** on the same samples for comparative studies with line profiles. Spatial elemental distributions which could have been induced by alkaline treatment of Kingston dolomite are presented in Figures 6.11, 6.12 and 6.13, where X-ray maps are displayed with accompanying BSE images.

In Figure 6.11, the BSE image of the outer rim shows the dissolution of dolomite crystals and porous regions within those crystals, outlined with a red dotted line. There are also much more compact large calcite grains outlined in blue. As can be seen from the Figure the boundary between these two phases is not always clear. Elemental maps of Al and Si show that these two elements surround dolomite grains probably in a form of fine silicates. Weathered, highly porous regions of dolomite grains on BSEI are not occupied by any of the major elements, suggesting dissolution and partial dedolomitisation.

The same type of data was acquired from another cross section disc of Kingston dolomite. In Figure 6.12 the BE image shows a cluster of dolomite crystals with a calcite matrix and some silicates. A pyrite grain (bright circle at the edge of the image) shows no alteration. X-ray maps of Ca and Mg demonstrate the Mg rich bands within dolomite crystals towards the edge, while Ca is present both in the carbonate matrix and calcite inclusions within dolomite crystals. The reaction leading to this type of elemental distribution is dictated by the effect of mass transport and based on the lower mass of

Mg, magnesium ions as expected are observed before Ca. This also favours Mg migration as a reaction occurring over Ca dissolution, also supported experimentally by AFM. It is difficult to decide if these features are the result of alkaline treatment only as they could be present in the original rock.

In order to establish the correlation between various elements a computer program was used to combine X-ray maps and SE images. The combined maps where each element is presented in different colour are displayed in Figure 6.13. The first map (Figure 6.13) shows the distribution of Mg, Si and Fe in the inner regions of the rock disc, revealing that quartz and pyrite are present not only in the calcite matrix but also as inclusions inside individual dolomite crystals.

In Figure 6.13(top right map), X-ray maps of Ca and Mg are combined with a SE image which makes it much easier to allocate the boundary between the grains and clearly outline inclusions in dolomite crystals as well as potential pseudo-calcite crystals that have typical dolomite shape (rhombic). The following two combined maps (6.13.c & d) are presenting elemental distribution within 150-200μm from the edge of the core. Finally maps 6.13.e&f were acquired at much lower magnification and as it can be seen in map 6.13.f that there are Mg rich phases present (bright red) but also Al enriched channel-crack formation (bright green) in the lower right hand side corner. The region covered is approximately 0.5mm.

2) Massachusetts dolomite was also analysed. This rock sample is known as semi-expansive in an alkaline solution, although susceptible to dedolomitisation. Both rocks, Kingston and Massachusetts dolomites, developed outer reaction rims, but with significantly different amount of expansion. Figure 6.14 contains a set of data presenting line profile analysis on altered rim and unaltered regions of the Nelson dolomite rock core which was immersed in NaOH solution for three years.

The first line profile presented in Figure 6.14a, shows the composition of inner regions of the core that have no visible changes such as discoloration or microcracking. As it can be observed these regions of approximately 100μm contains dolomite with Ca/Mg ratio sometimes very close to the stochiometric value of 1. The other observation is the presence of silicates (simultaneous high concentrations of Si and Al). However, more information on the nature of dedolomitisation of Nelson dolomite is shown in line profile

6.14.b, acquired from 0.5mm line, within the transition zone between white, outer rim and less reacted region. As the EPMA data shows the external reaction rim is mainly composed of Ca, probably $CaCO_3$ as a result of dedolomitisation. The intermediate reaction rim with somewhat less alteration still contains Mg as a constituent of dolomite (percentage up to 20-30 wt%), but there are also other Mg phases that contain as much as 73 wt% Mg, which can only be $Mg(OH)_2$, the second reaction product of dedolomitisation, Table A14. The line profile presented in Figure 6.14.c presents a wider region which contains porous material from discoloured reaction rim, again clearly rich in $Mg(OH)_2$ and $CaCO_3$. The data is presented in Table A15.

3) The Massachusetts dolomite results were then compared to those obtained on the Nelson dolomite sample. However, the Nelson dolomites, is known to have undergone the dedolomitisation reaction after alkaline treatment, showed no expansion. EPMA line analysis from the inner area of the disc, displays the same chemical composition of unaltered Nelson rock. The Ca/Mg ratio is closer to that of an ideal dolomite mineral (50/50mol%) than Kingston dolomite, but with a considerable amount of Si, Al, and Fe, Figure 6.15.a, Table A9. The chemical composition of the reaction rim that contained porous phases is presented in Figure 6.15.b, Table A9, revealing components along 50-60μ line of analysis. The final line presented in Figure 6.15.c, Table A10, (point 349-624, from the region of 0.5mm) shows the compositional difference between unaltered inner part of the core and the white outer rim. It can be concluded that the reacted rim is Ca-rich, as observed in previous samples. One difference between Ca rims in all dolomite samples is CaO%, with approximately 50-70% in Kingston and Nelson dolomite, and 30-35% in Massachusetts, suggesting two different phases (carbonates and hydroxides).

Spatial elemental distributions for Nelson dolomite were also acquired. Maps taken from three different regions within the disc are presented. Figure 6.16.a presents the elemental distribution within the outer reacted rim of the core, which supports the evidence from line profile of the existence of a Ca rich rim. The difference can be seen in Figure 6.16.b, which presents the elemental composition within the rim adjacent to the reacted, white rim, which could be described as semi-reacted. The main difference is in the amount of Ca, the distribution of Mg is more homogeneous as are of Si and Na present. Finally Figure 6.16.c presents the composition of the un-reacted internal part of the core. When Figures 6.16.a, b, and c were compared it was clear that the Si, Na rich grains from the

un-reacted rock are in the process of dissolving in Figure 6.16.b (semi-reacted) and do not exist in outer rim. On the other hand Ca/Mg distribution, that is layered and uneven in original rock, is rearranged into evenly spread Ca and no Si. The overall conclusion is that expansion was not only related to the dedolomitisation process, but was very much dependent on the texture of the rock as well, since the rocks susceptible to expansion have similar texture, with a fine grained matrix of calcite and silicates surrounding dolomite crystals.

6.5 Surface chemistry of rock/solution interaction

6.5.1 Introduction

The interface of a solid/solution within a system presents a form of boundary or discontinuity. These surfaces, whether of a liquid or solid phase, are different from the bulk phase, with an excess free energy. Due to the disruption in bonding and the excess free energy which bring potential instability, these areas are susceptible to changes and interactions. Two main reactions which can take place are chemisorption and physical adsorption (Stumm 1992, Davis *et al.* 1990). For carbonate geochemistry chemisorption is of central importance. The BFC (Burton *et al.* 1951) model presents a visual interpretation of potentially reactive sites on a surface and the ion interaction which might take place (Figure 6.17). It has been proved that surface sites of different energies will react at different rates with sorbates. Another interesting point that could have application in this study is the simultaneous chemisorption and precipitation in case of solutions saturated with a substrate, as a result of which adsorbed ions can be than buried in the growing layers of the mineral and become co-precipitates. (Stumm and Leckie 1970). A study of magnesium ion adsorption on carbonate surfaces has been published by Mucci and Morse (1985) and is summarised as follows:

Table 6.2 Mg/Ca concentrations on the surface of four carbonate minerals, after immersion in synthetic seawater at two different saturation states. (Ωc saturation)

Mineral	Ωc = 1.2	Ωc = 8
Aragonite	0.63	0.03
Calcite	0.83	1.34
Dolomite	3.05	2.67
Magnesite	120.00	8.00

Other relevant studies are those concerned with carbonate dissolution and precipitation kinetics and factors that influence these processes (temperature, pH, and pCO_2). The data obtained by Chou *et al.* 1989, on the dissolution of calcite, dolomite, magnesite, aragonite and witherite, showed that aragonite and calcite have higher dissolution rates comparing to dolomite and magnesite. They also noted that a decrease in pH or an increase in P_{CO_2} or T speeds up dissolution of carbonates. According to studies carried out by various researchers (Weyl 1965, Pytkowicz 1965, Berner 1975), the precipitation of calcite can be inhibited by the presence of Mg or phosphates. Due to their origin and variable composition, most of the carbonate minerals will not always have predictable behaviour. One of the most important obstacles for successful modelling and prediction of solubility/precipitation rates of carbonates is the presence of co-precipitates in concentrations higher than 1 wt%. A carbonate rock-solution reaction mechanism is even further complicated due to the fact that the chemical composition of most carbonate rock forming minerals can be classified as solid solutions (Mackenzie *et al.* 1983). However the data obtained on carbonate rock-alkaline solution reaction combined with the results obtained on single minerals (dolomite)-alkaline solution was expected to reveal more information on the dedolomitisation process and its contribution towards expansion.

6.5.2 Compositional changes using chemical shifts ESCA

Carbonate rock samples of different composition and texture (samples from Table 3.2) were examined using X-ray Photoelectron Spectroscopy technique for establishing surface and near-surface chemical changes induced by alkaline solution treatment. The detected changes in the chemical state of elements remaining in the system will be presented in this section. The main aim of this study is to be able to define changes in surface chemistry of carbonate rocks due to reactivity with solution at an early stage. As it has been mentioned earlier most of the changes and transition involving carbonate minerals have been studied at elevated temperatures, pressures and solution concentrations in order to speed up otherwise very slow reaction kinetics. An exception to this is trend is the study conducted by Brady (1996) on the formation of dolomite under room temperatures and Earth surface conditions. The advantage of spectroscopic techniques such as XPS is that even minor chemical changes and binding energy shifts can be detected at the top few atomic layers, allowing avoidance of extreme conditional parameters that could potentially interfere in chemical reactions.

In practice this means that results obtained by using XPS analysis will be more applicable to the *in-situ* conditions since it is possible to detect changes produced in a near surface environment (T=17-30^{0}C, P=1atm. and pH=12-14) as the detection limit is increased (few atomic layers). Another important factor in this type of study is time, and that too can be reduced due to an improved sensitivity to chemical changes. Two types of data were acquired using ESCA, wide and regional spectra and elemental mapping combined with depth profiling for spatial elemental distribution.

The Kingston argillaceous dolomitic limestone as a prototype of ACR expansive rock is presented first (sample MR08, 09, 10) and consists of two sets of data from the specimens examined in this study. The first set is untreated rock from four different levels of the Pittsburg Quarry, 1mm thick rock tablets from various beds in Pittsburg Quarry, exposed to 1N NaOH solution (sample from Table 3.2). A second set is of samples from the cone end of ASTM C586 cylinder treated with alkalis (sample Table 3.2). The spectra acquired from a freshly fractured surface of an untreated rock provided the information about the surface chemistry of the rock. This type of measurements were repeated several times, with different instrument settings to obtain the maximum count rate, compensate for surface charging and possible instability of some components under the radiation and UHV (Table 5.2 contains the measured binding energy-values).

XPS spectra from untreated Kingston dolomite samples are presented in Figure 6.18. As it can be observed from the wide spectra Figure 6.18.a the main difference between different beds in the quarry is in the ratio of various phases. However, more detailed information is obtainable from the regional spectra for Si*2p* and Ca*2p*, Figure 6.18.c,d. It was expected that sample (Kingston dolomite) that was produced by drilling normal and parallel to the bedding will show some difference, but the data for these two are identical, although it could be said that the signal is of different intensity for Si*2p*. The same type of measurements were produced from a cross section disc cut from ASTM rock-core that was in NaOH solution for three years. The first set of data was acquired from the surface, the second from 0.7mm and the third from 4.5mm (Figure 6.19). The regional C*1s* spectra show that there is change in C*1s* peak. As it can be observed that the carbonate peak for fresh rock is almost as high as the C*1s* reference peak, and for the surface of alkali-treated sample and 0.7mm from the surface carbonate peak does not exist, Figure 6.19.a. The same experiment also shows the chemical shift for the Mg*2p*

peak, Figure 6.19.b, where it is clear that the Mg carbonate (fresh rock) changes to Mg hydroxide (surface) binding energies, also see Table 5.2. The chemical state for Ca*3s* has almost no change from fresh rock sample to alkali-treated surface (Figure 6.19.c).

In order to be able to observe the difference between XPS spectra from expansive and non-expansive alkali-treated carbonate rocks, a set of ESCA analysis was carried out on a sample of Nelson dolomite cross section from a core treated with alkalis for 3years. A similar type of analysis was acquired from three regions: 1) the surface of the core, 2) 1-2mm from the surface inside the core and 3) from un-reacted regions of the rock, as shown in Figure 6.20. First of all the change in the carbonate peak is less drastic than in Kingston dolomite, (Figure 6.20.a), revealing that the C*1s* ratio is not as affected by NaOH when surface and fresh rock spectra are compared. However, the regional spectra for Mg*2p* clearly shows the change of binding energy between the surface and fresh rock spectra, supporting the evidence for carbonate to hydroxide transformation of Mg, (Figure 6.20.b). There is no chemical shift change for Ca*2p*, Si*2p*, Ca*3s*, shown in Figure 6.20.c.

6.5.3 Elemental mapping using ESCA

ESCA elemental maps were acquired from two sets of samples (Table 3.2): alkali treated thin tablets of Kingston dolomite, and combined depth profile-mapping of the cone end of Kingston rock core previously immersed in NaOH solution for three years.

ESCA experimental measurements were then carried out on the cone surface of a Kingston dolomite rock core exposed to 1N NaOH for three years, where white deposits were observed and discoloration was obvious in the peripheral regions. The spectra were acquired on the surface thoroughly washed with de-ionised water, and then ion etched for 5minutes and for 86 minutes. The spectra was than used to set the regions for mapping (400 by 400μm) in order to establish changes in the amount of major elements and an attempt for elemental depth profiling terms of spatial distribution after the removal of atomic layers in etching procedure. As can be observed in Figure 6.21, there is difference in the amount of Mg and Ca on the surface and after the etching procedure: bright areas represent higher elemental concentrations. Another type of XPS mapping on 1mm thick rock tablets (Table 3.2) is shown in Figure 6.22. The ESCA elemental mapping for expansive carbonate rock suggests the following: Samples that have been

exposed to NaOH for a short period of time develop Si and Fe rich layer on the surface. Also a Si layer can be seen on the cone surface as well, but only before the etching.

After 5 minutes and especially after 86 minutes etching the surface is composed mainly of Mg and Ca, probably due to the fact that a silicate phase would be more resistant to atmospheric change than the unstable $Mg(OH)_2$, but the UHV and removal of top atomic layers reveal chemical composition of an unaltered layer. This also explains why some of these changes could not have been detected by an EDX or EPMA analysis. It still remains unclear why there is an iron rich layer. A possible explanation could be that like Mg ions, Fe ions are leaching out from the dolomite crystals, which was evident from ESCA maps of Fe. This would support the theory of the higher energy sites for nucleation of secondary calcite in a linear fashion since it is obvious from the BEI and EPMA elemental mapping that dolomites in Kingston rock are rimmed/zoned with Fe rich bands. Fe depleted areas were not monitored, only enriched Fe areas.

6.5.4 Use of D_2O as a tracer for establishing the role of Hydroxyl ions

Another attempt to fully characterise the surface chemistry after rock/solution reactions was undertaken using TOF-SIMS, one of the most sensitive surface techniques. The ionic bombardment in this type of ion microscopy, although of destructive nature, was useful for obtaining complementary data for the information gained with ESCA analysis. Chemical shift observations coupled with low detection limits (ppb) of SIMS result in collection of potentially useful new data regarding ACR mechanism in a form of the subtle compositional differences between expansive and non-expansive rocks.

Several samples of untreated and treated Kingston dolomite samples were investigated and the representative spectra for both treated and fresh samples are shown in Figures 6.23. The main difference appear in the presence/absence of CH fractions (organic matter), indicating that alkaline treatment caused dissolution and removal of these components from the argillaceous carbonate rock. Other noticeable changes are the Ca/K ratio and Mg/Si and Mg/Al ratios. SIMS data was also more representative of the actual solid/solution boundary as it is more sensitive.

In some of the early studies on ACR it was established that the reaction was dependent

on the presence of moisture as one of the key factors. However, it was not clear in what capacity OH ions were involved in the reaction and how important their role was in the mechanism of the reaction. The experiment was designed to define the role of OH^- ions, by monitoring the penetration rate of OD^- ions into the rock.

Samples of dolomitic limestone of Kingston and Chinese dolomite (Table 3.2) were immersed in a 2N NaOH solution in which H_2O was replaced with D_2O. The idea behind this was that by using TOF SIMS instrument it would be possible to monitor OD^- ions that were chemically bonded in newly developed phases or absorbed to the clay fractions as a result of rock/aqueous solution interaction. Spectra were acquired from the surface, and after each ion etching procedures, removing atomic layers to produce a depth profile of OD^- ions, followed by spectrum from a fractured surface, representing bulk material. See Figure 6.24 for Kingston dolomite and Figure 6.25 for Chinese dolomite, both known as ACR expansive.

Using D_2O as a tracer in the mechanism of reactions taking place in aggregate but even more in cementitious materials can be informative and if combined with XRD and electron diffraction studies of thin specimens useful for further investigations. However from the present set of data it was evident as it can be seen in spectra in Figure 6.24-25 that the penetration rate of OD^- ions is rather rapid considering the slow kinetics of carbonate mineral interactions. It appears that OD^- penetration can be successfully monitored. This study shows that there is a hydroxide phase within the rock after solution treatment, suggesting that not all hydroxide deposits are formed on the mineral surface as observed in ESEM study of single dolomite crystals.

6.6 Conclusions

From the experimental work reported in this chapter on carbonate rock-alkaline solution reactions the following conclusions can be drawn:

1. Mineralogical transformation of dolomite to calcite was observed using XRD analysis. The reason why brucite or goethite was not detected is because of the high detection limit for small quantities of material present.
2. Using routine XRD for clay minerals, it was evident that there is no difference in the clay fraction between reacted, fresh, expansive and non-expansive carbonate rocks.
3. Changes in the microstructure of the rock samples, due to alkaline treatment and

expansion, were monitored by comparing fresh and treated samples. These changes are dissolution of grains, secondary deposits and development of microcracks.

4. BE imaging was useful for observation of dolomite grains and in particular changes in their zoning, inclusions and pore-space caused by weathering. This type of analysis also helped monitor the change in porosity across the rock sample induced by alkaline solutions.
5. Qualitative and quantitative EPMA analysis, whether as line profiles or as elemental maps, revealed information on element diffusion (Si and alkalis) and migration (Mg^{2+} and Ca^{2+}) from their original sites.
6. XPS spectra and maps supported the previous chemical analysis, and provided the evidence for actual Mg carbonate to hydroxide transformation as well as a general decrease of the carbonate fraction. These also showed the involvement of Fe^{2+} in a fashion similar to Mg^{2+}, as a result of alkaline treatment.
7. TOF-SIMS data provided information on the presence of organic components in the sample before but not after the NaOH treatment.
8. Finally, D_2O experiments provided an insight into the role of hydroxyl ions in rock-solution reactions since they were observed as species incorporated within the rock.

Calculation of the kinetics of those processes involved in dedolomitisation, could be aided by knowledge of the depth of OD^- ion penetration into the rock, after different periods of exposure to (NaOH) solutions. Clearly, transport is a critical boundary constraint on reactions in rock and /or concrete. A more porous matrix will allow higher reaction rates than one which is less porous or in which the transport is by diffusion only.

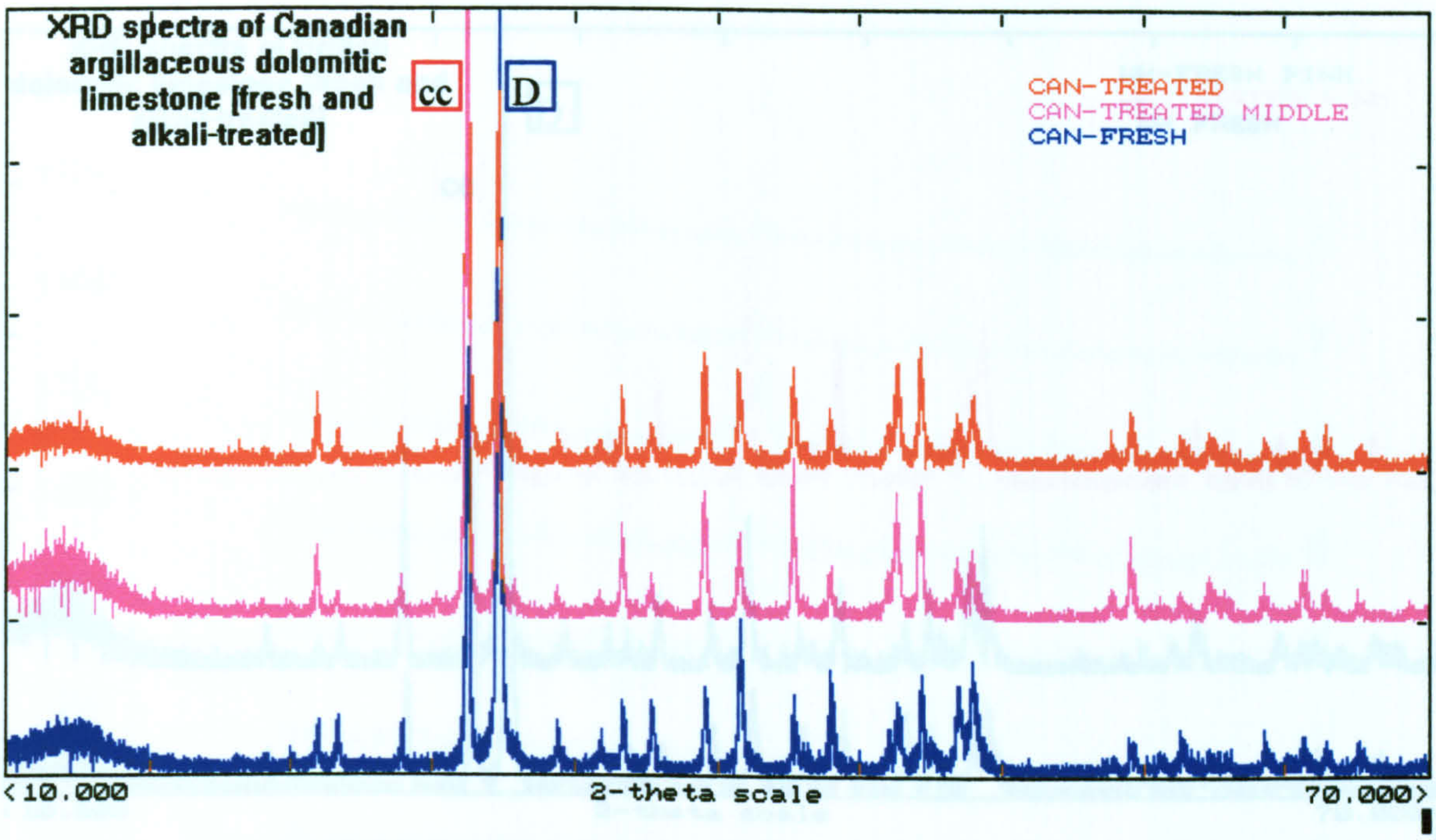

a) Figure a) is a more detailed/expanded spectra

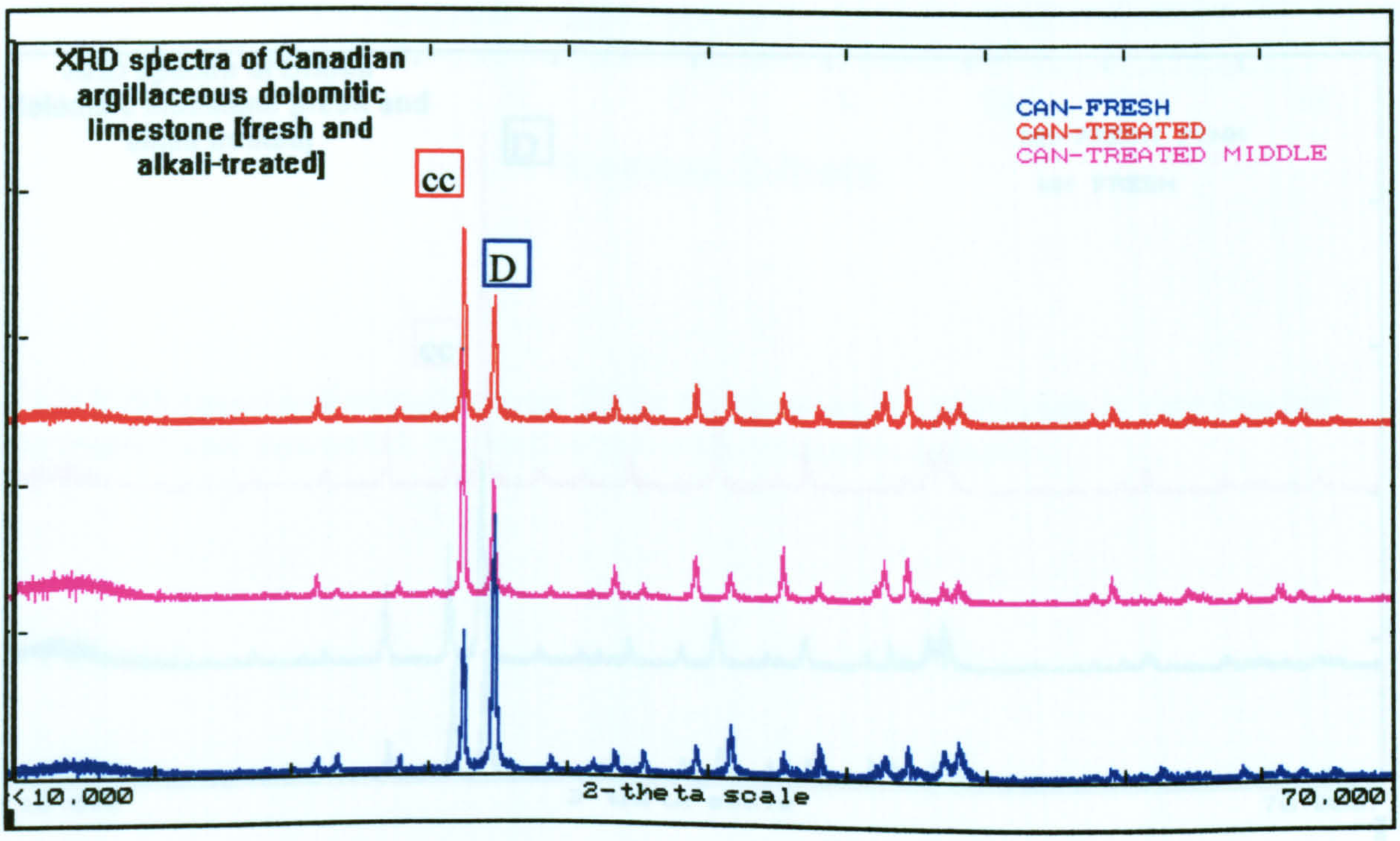

b) Figure b) presents ratios of main phases

Figure 6.1. Diffractograms showing the change in composition of Kingston dolomite (samples in Table 3.2) after 2 years in 1N NaOH, from the surface of the rock core (top spectrum), from the middle (4.5mm from the surface) (middle spectrum) and fresh rock (bottom spectrum).

Most obvious change is the difference in calcite (cc) dolomite (D) ratio.

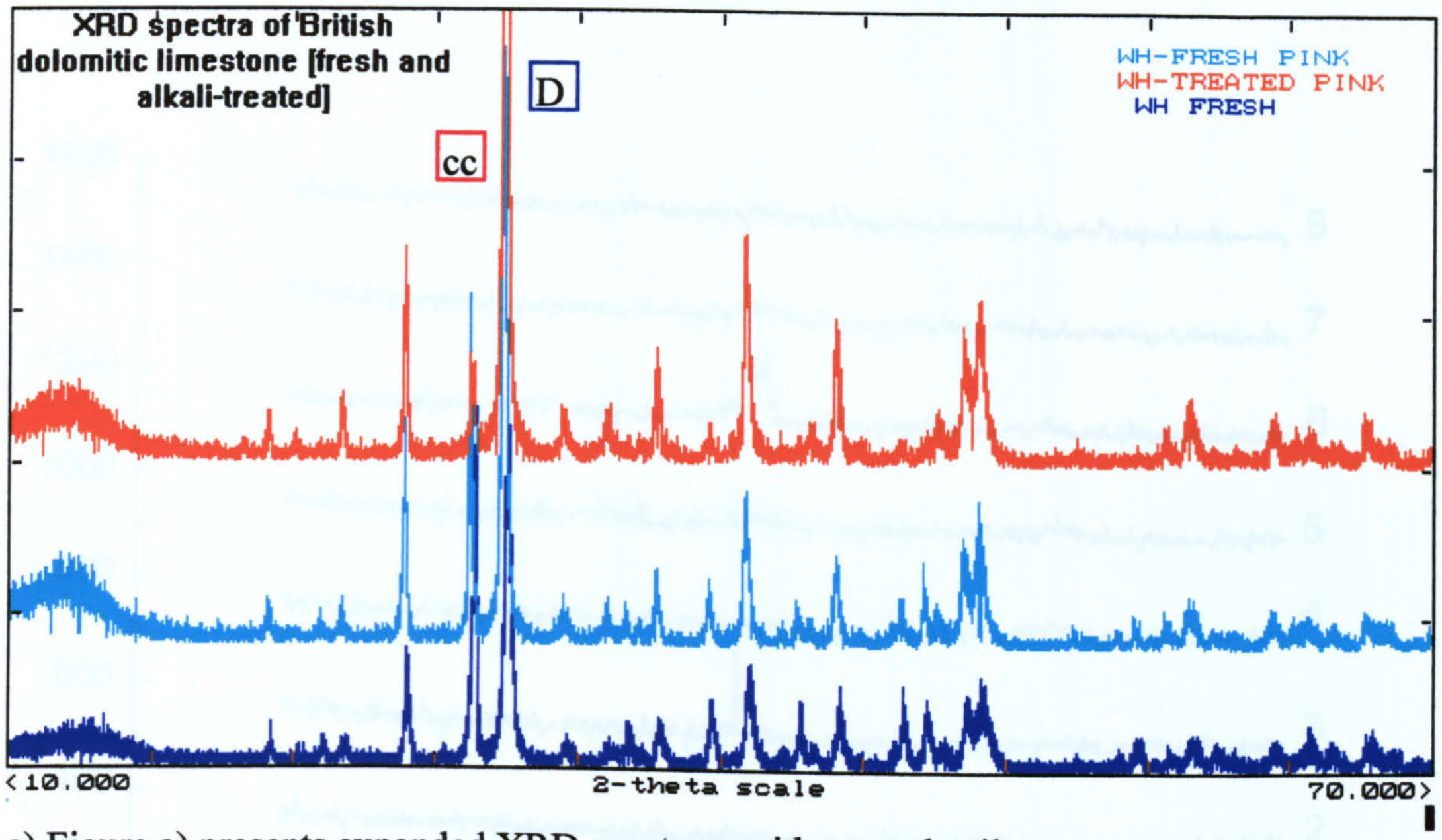

a) Figure a) presents expanded XRD spectrum with more details.

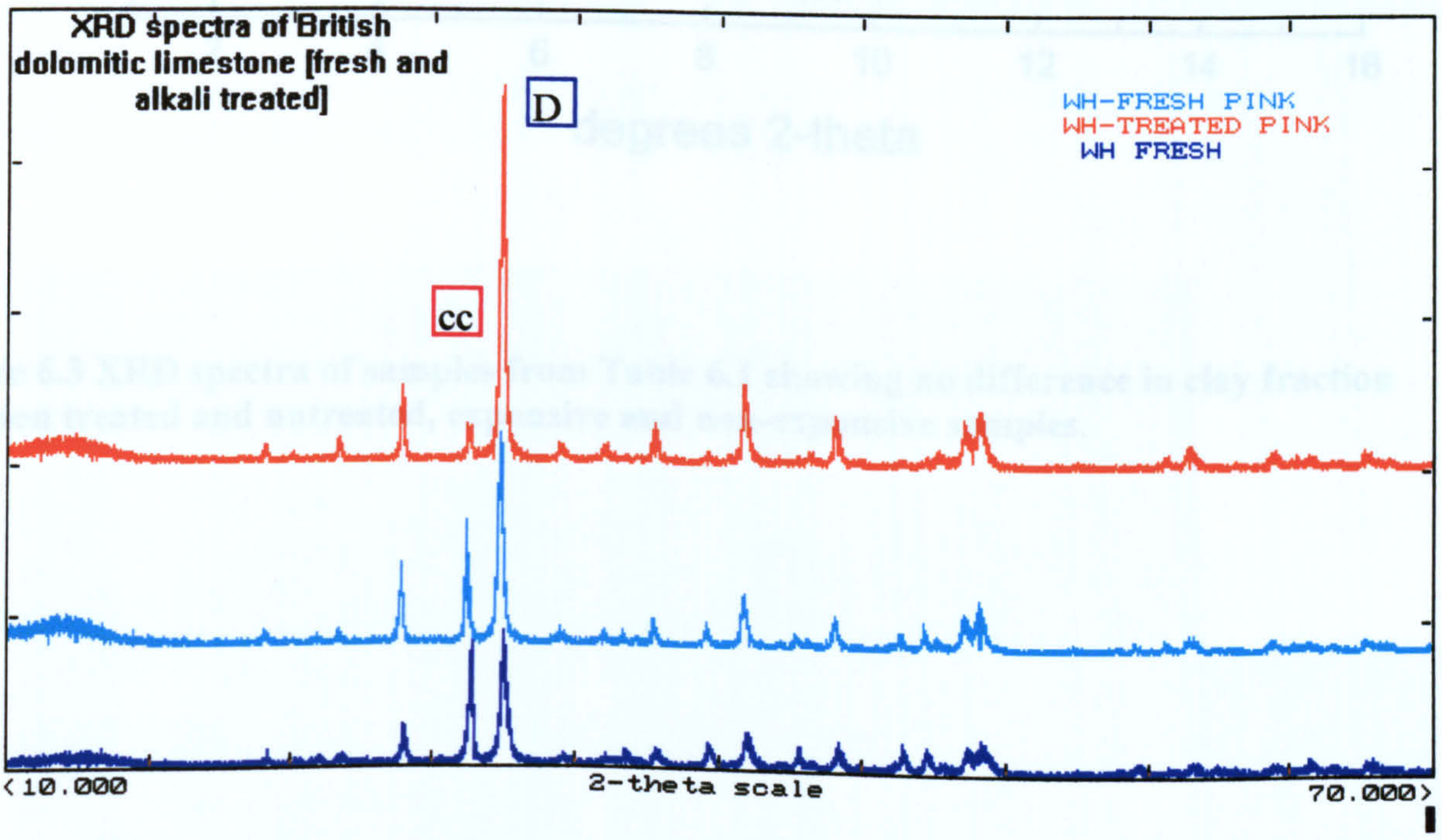

Figure b) presents ratios of dominant phases (calcite-cc and dolomite-D).

Figure 6.2 Diffractograms showing the difference in mineralogical composition of aggregates from two different beds in Carboniferous limestone quarry (samples in Table 3.2) with pink dolomite rich in Fe.

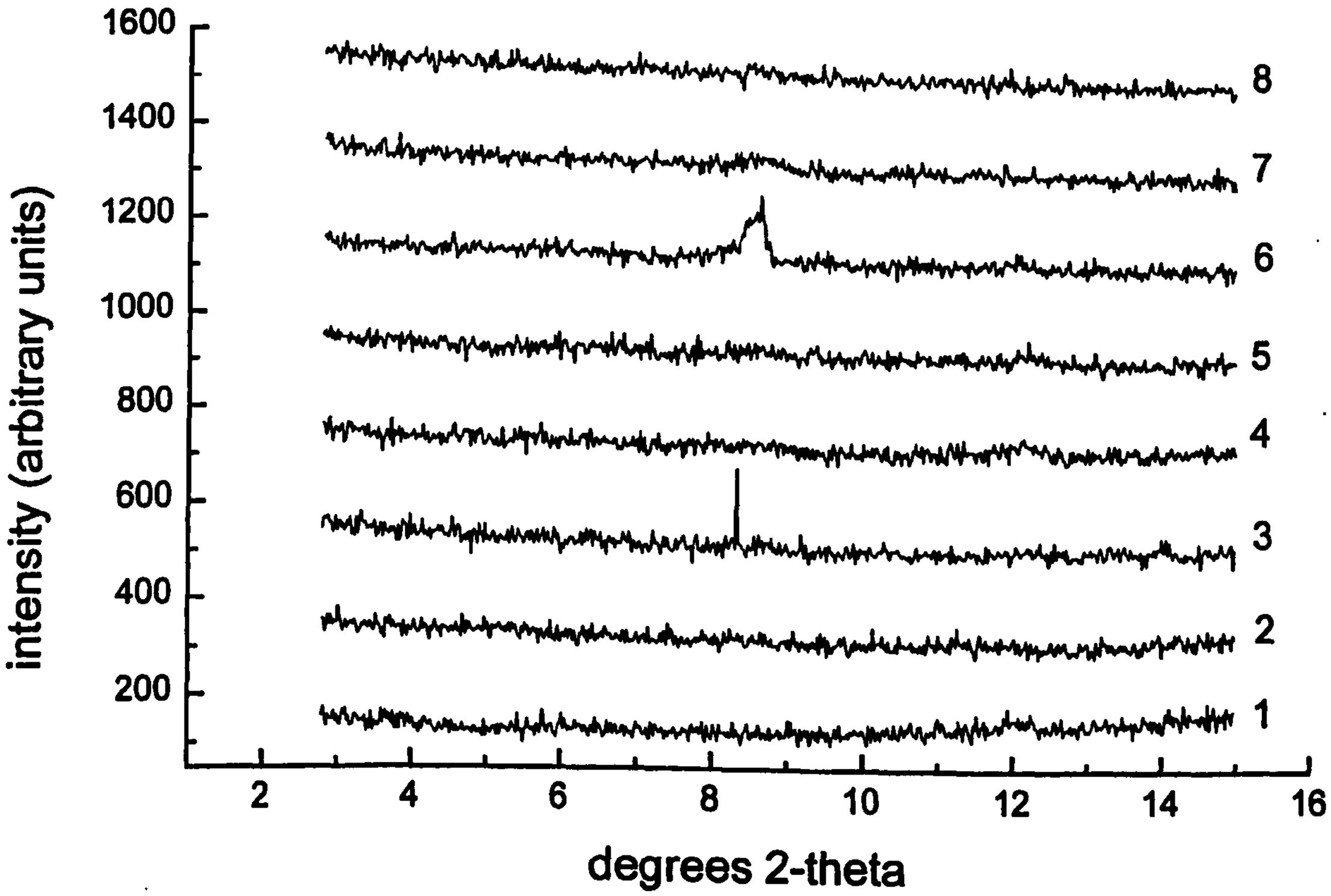

Figure 6.3 XRD spectra of samples from Table 6.1 showing no difference in clay fraction between treated and untreated, expansive and non-expansive samples.

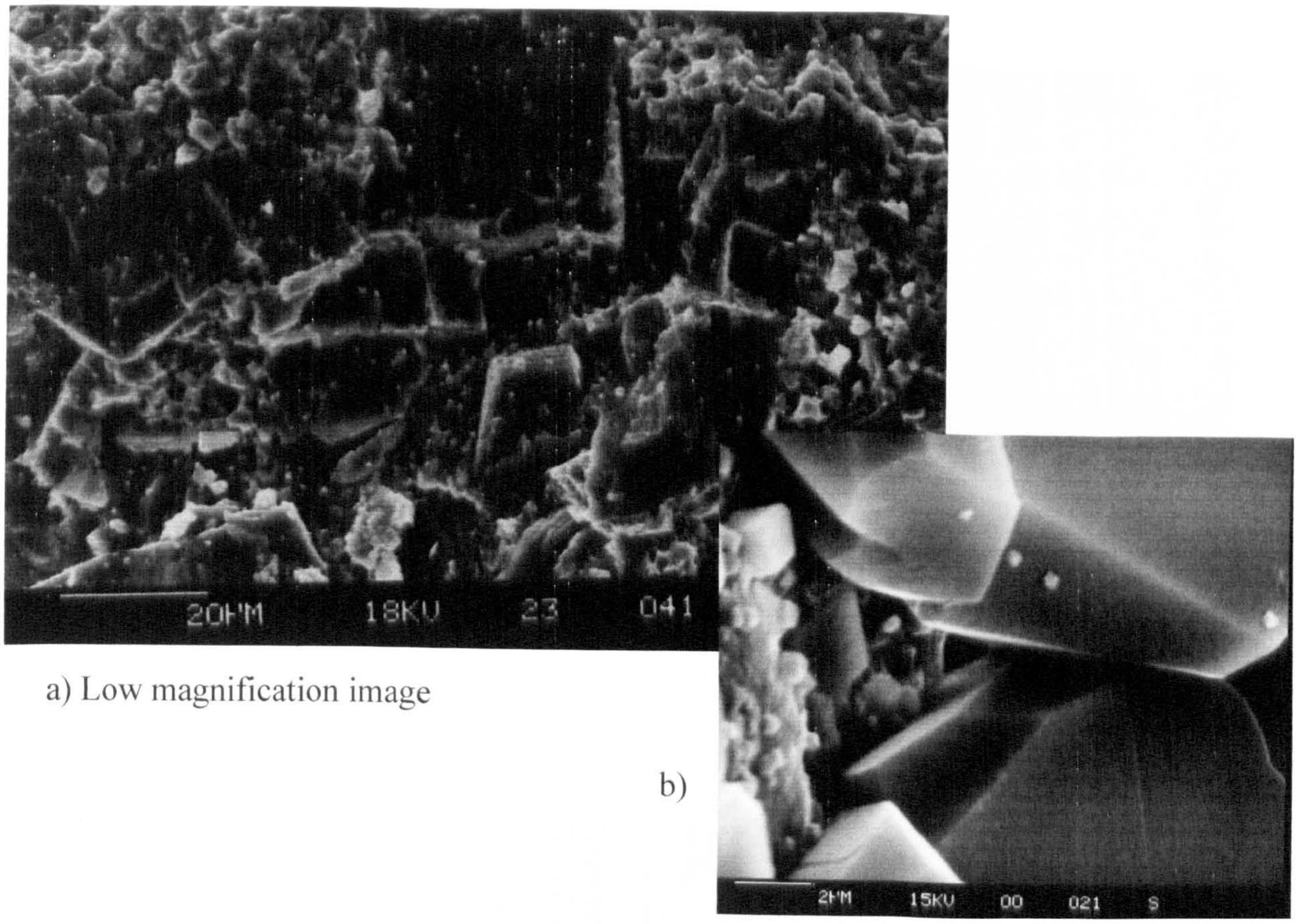

a) Low magnification image

b)

Figure 6.4 SEM secondary electron images of fresh rock (control samples),
a) Low magnification and b) higher magnification.

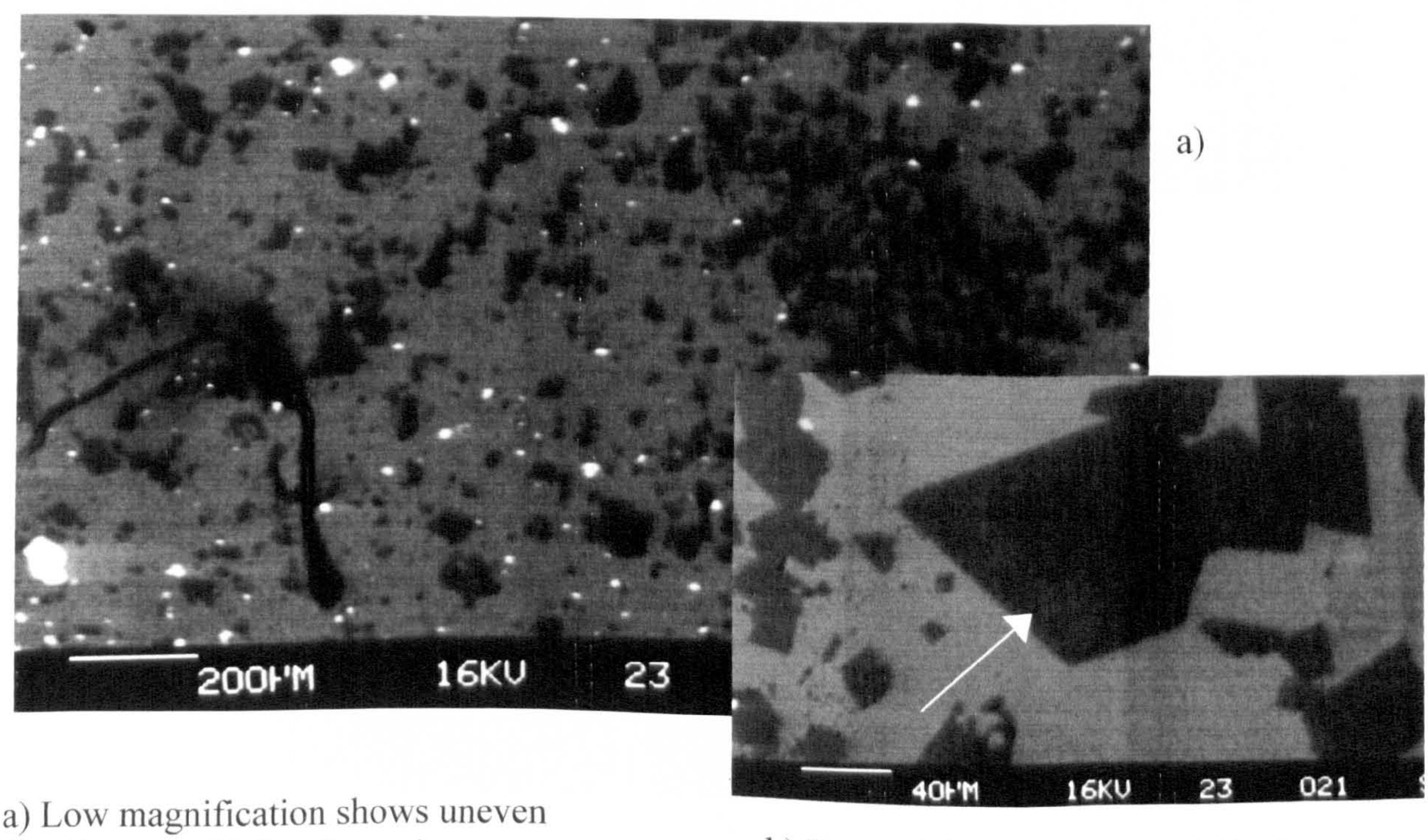

a)

a) Low magnification shows uneven distribution of dolomite grains.

b) Large dolomites appr.80-100microns

Figure 6.5 BSE image of the same sample as in Figure 6.4. It reveals dolomite (dark grey rhombs), calcite (light grey matrix) distributions as well as presence of pyrite (white areas).

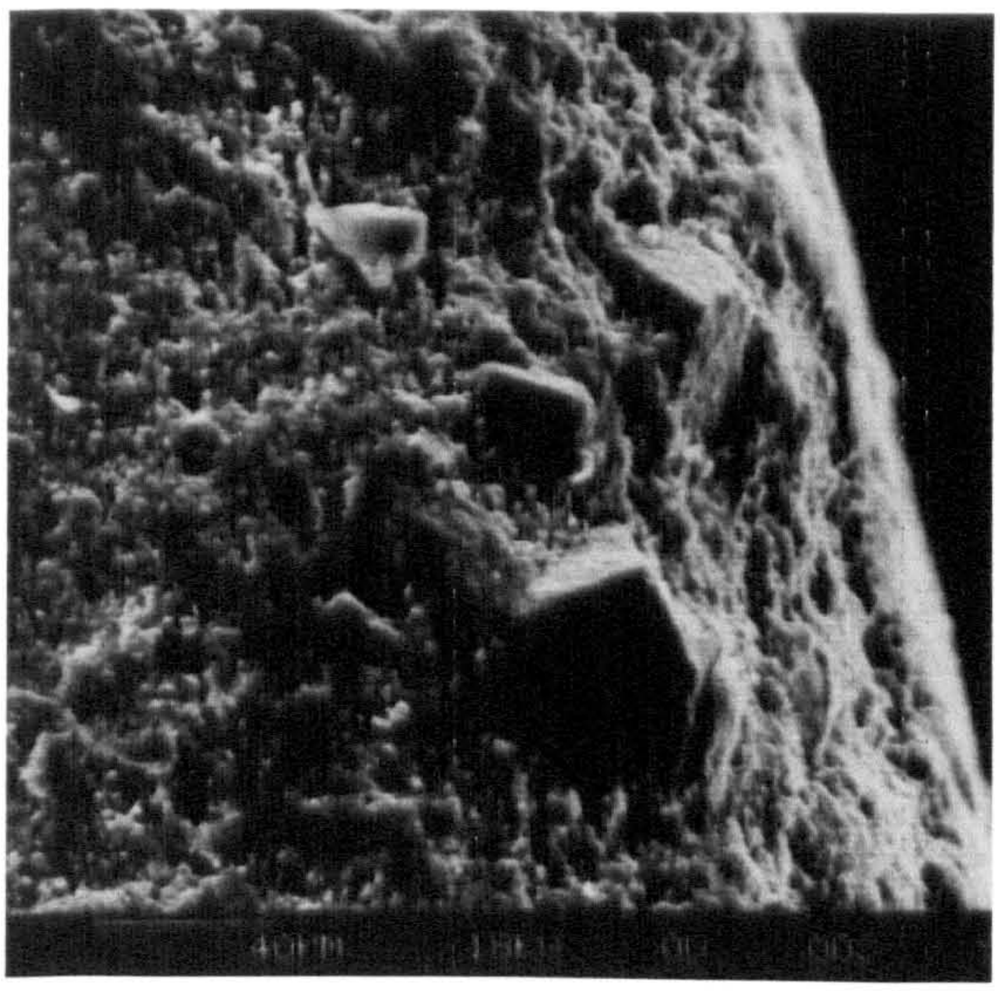

a) Treated Kingston dolomite.

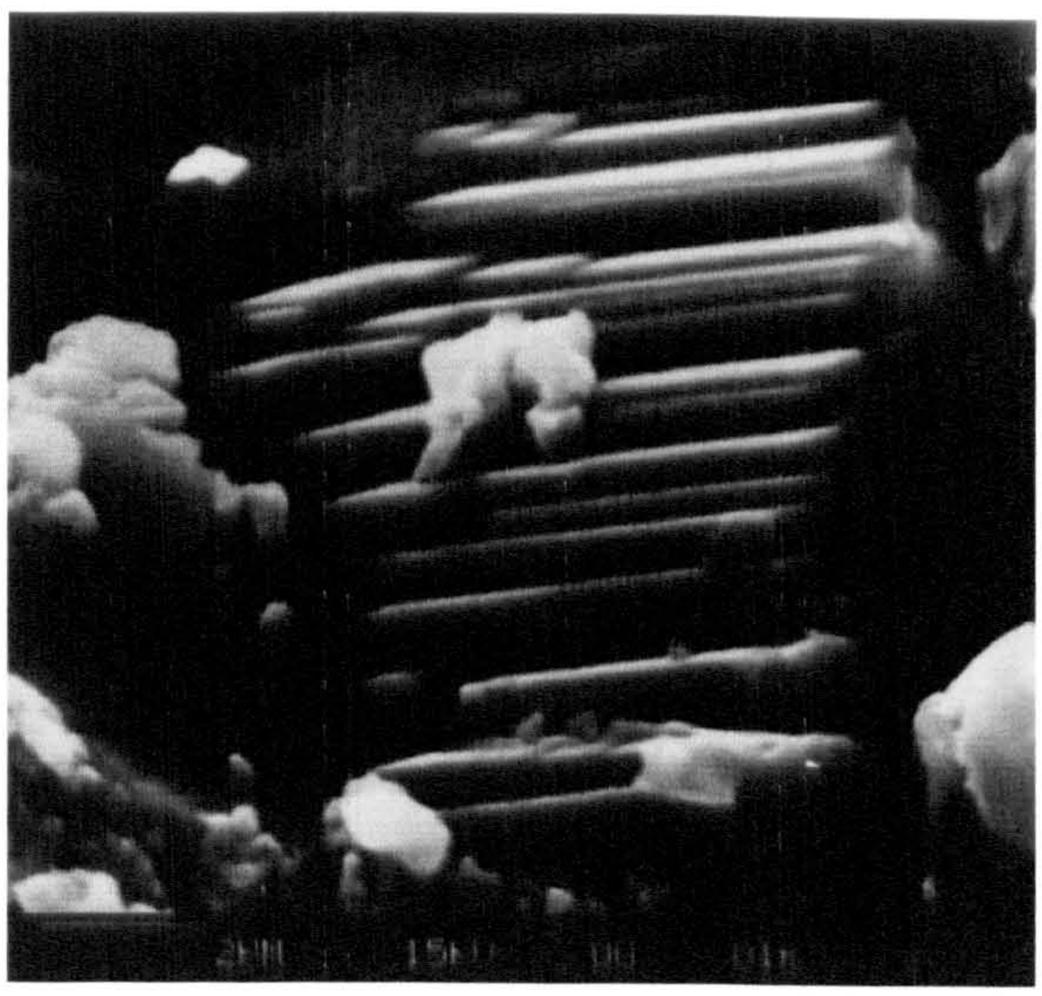

b) Untreated layered structure of dolomite

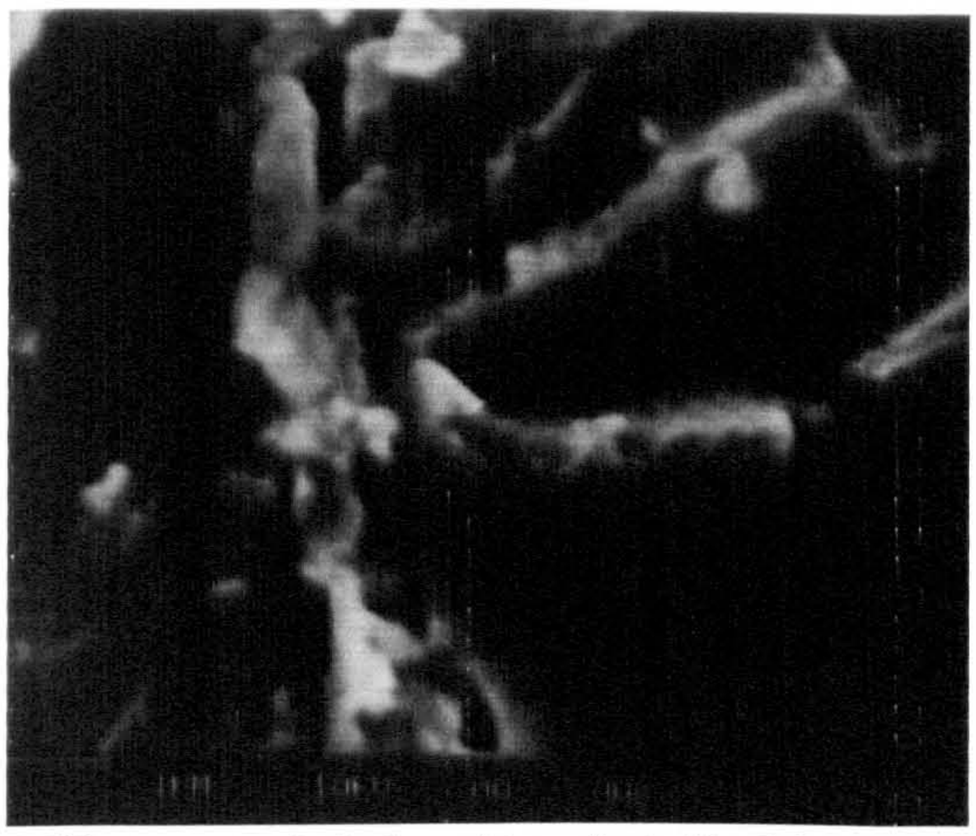

c) Untreated dolomite- detailed image

d) Treated dolomite-weathered layers

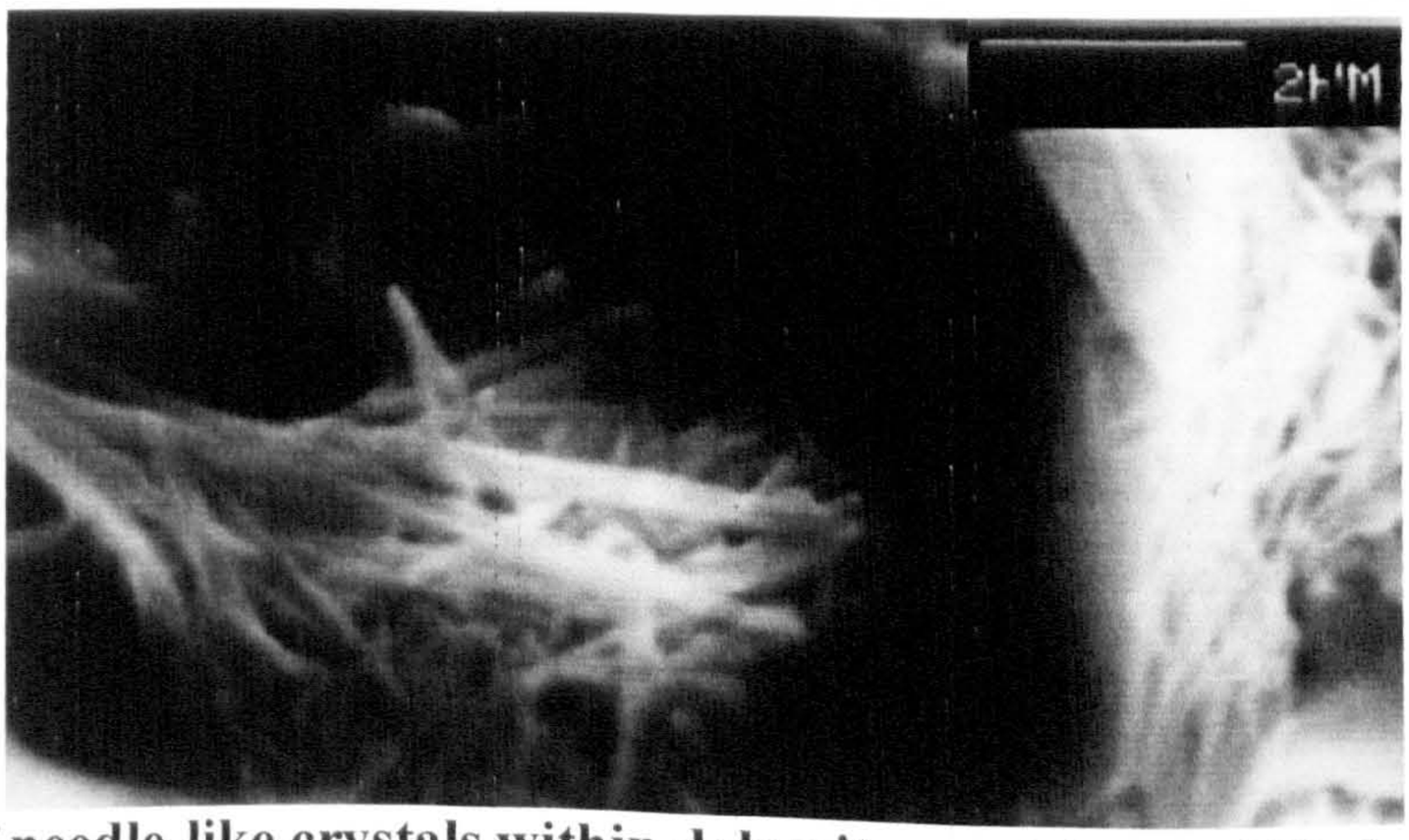

e) Formation of needle-like crystals within dolomite crystals, most likely brucite

Figure 6.6 Representative changes in the microstructure of Kingston dolomite induced by alkaline treatment and therefore nucleation and growth of secondary minerals (brucite and calcite).

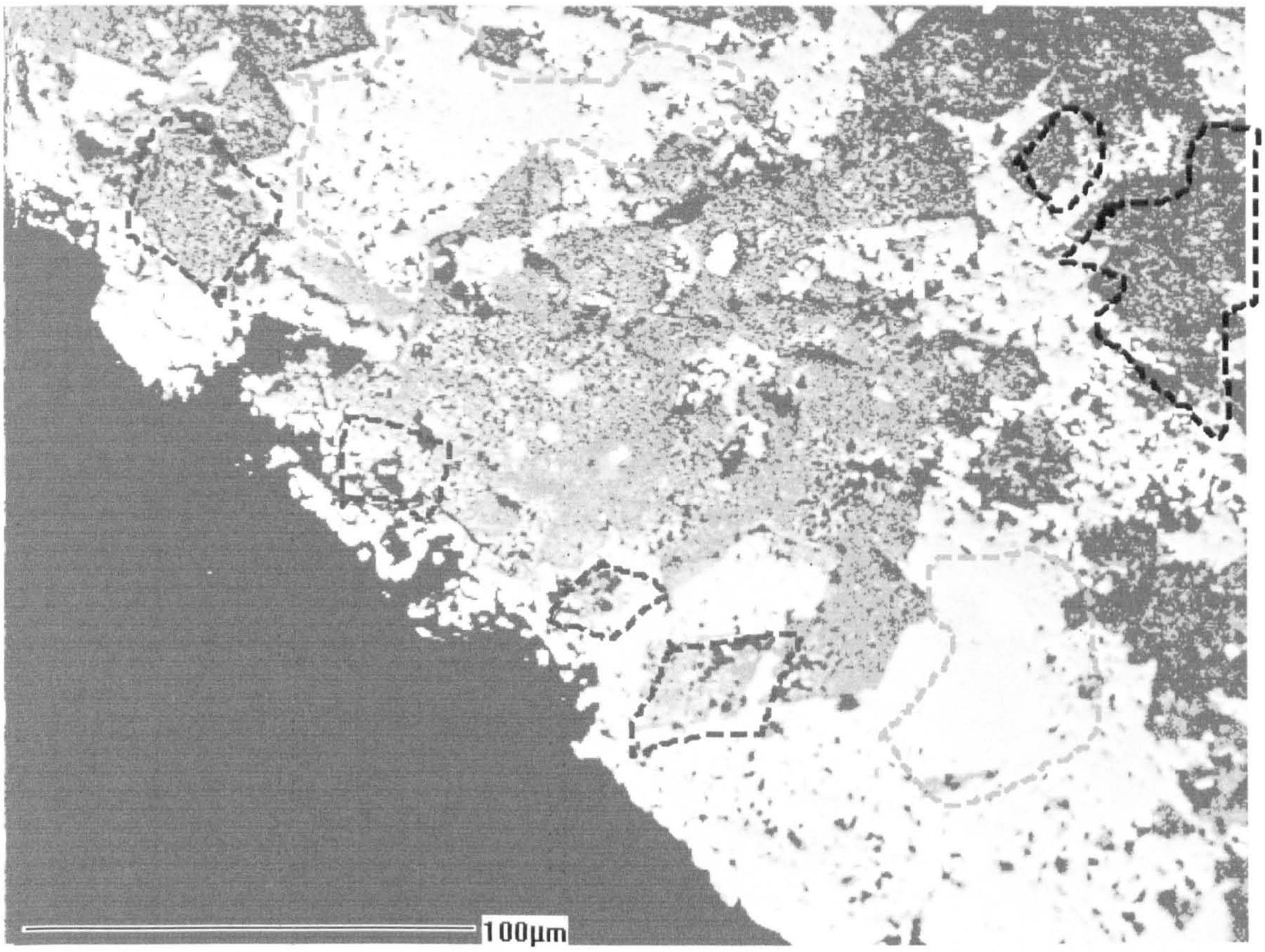

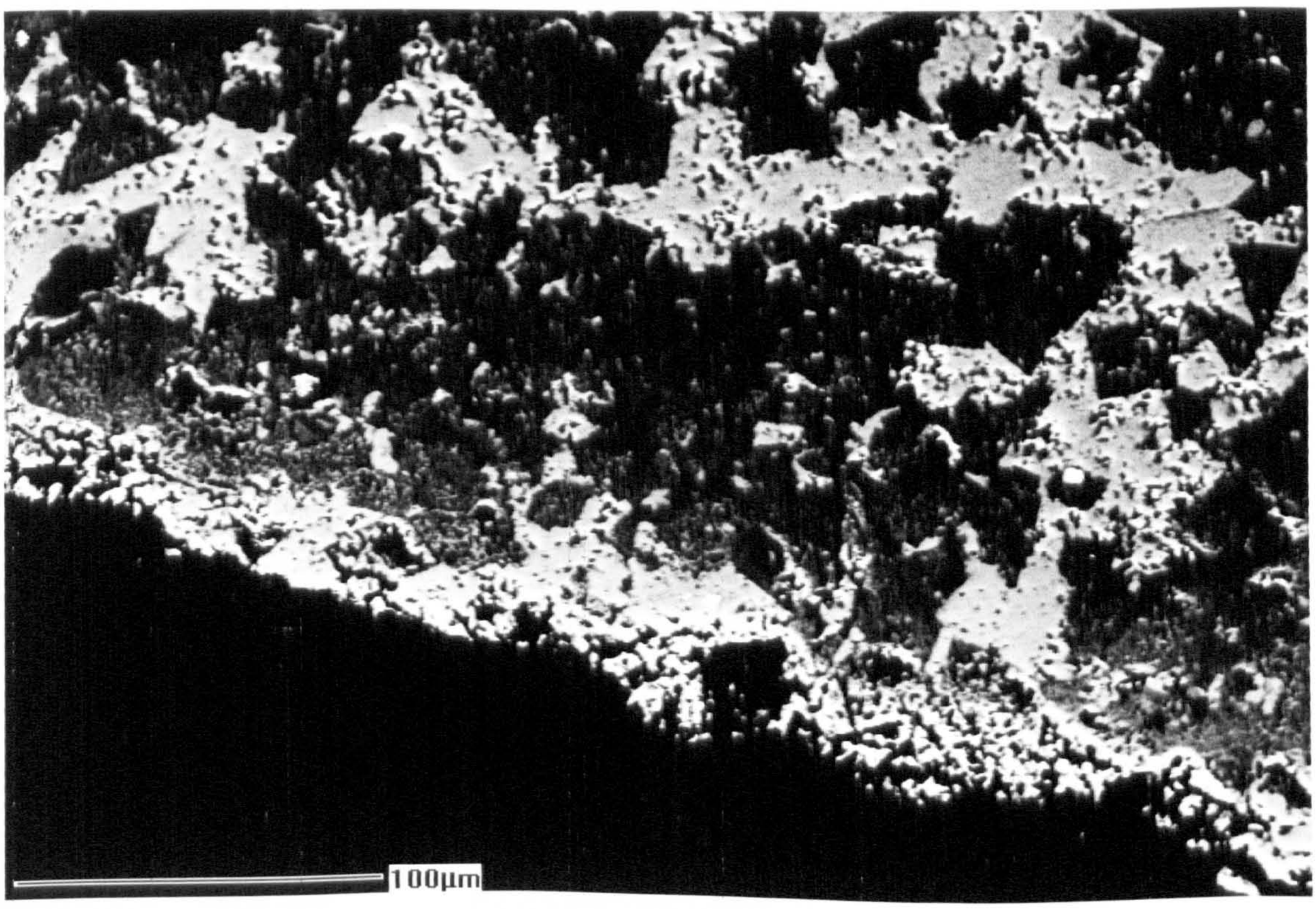

Figure 6.7 BSE image of a polished core cross section after 3yrs in NaOH solution following ASTM C586, showing the effect of alkaline solution on the carbonate minerals [dolomite (dotted red lines) and calcite (dotted green lines) within the 200-250micron range]. The blue outlined areas are of a higher porosity, due to dissolution of dolomite.

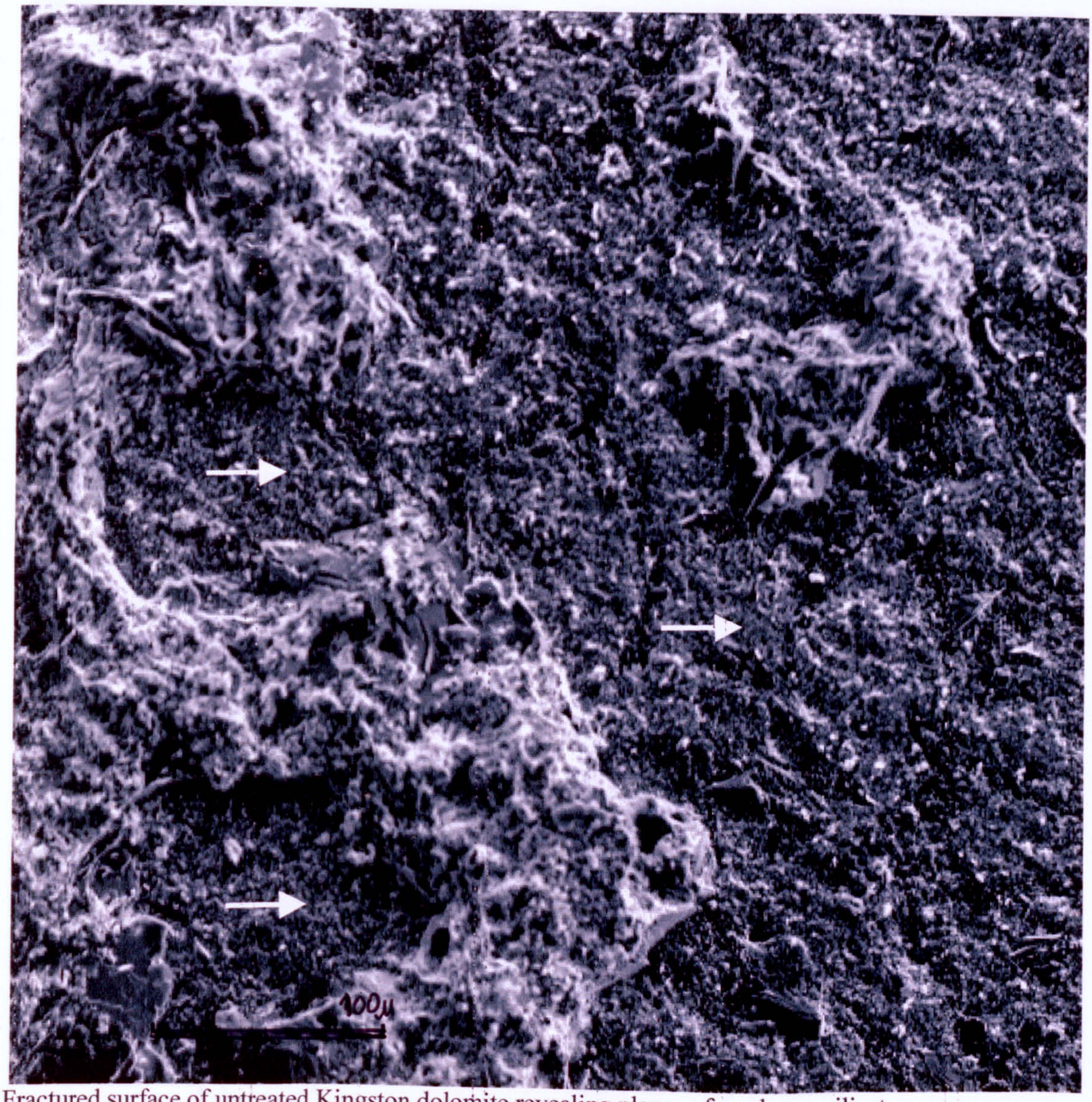

Fractured surface of untreated Kingston dolomite revealing planes of weakness-silicates

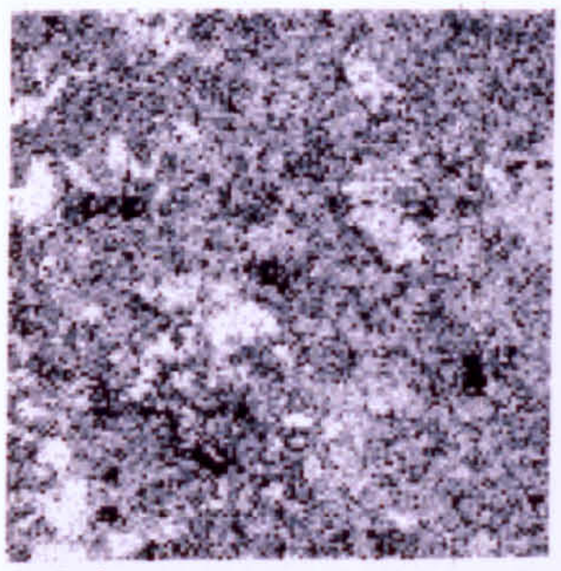

Calcium map

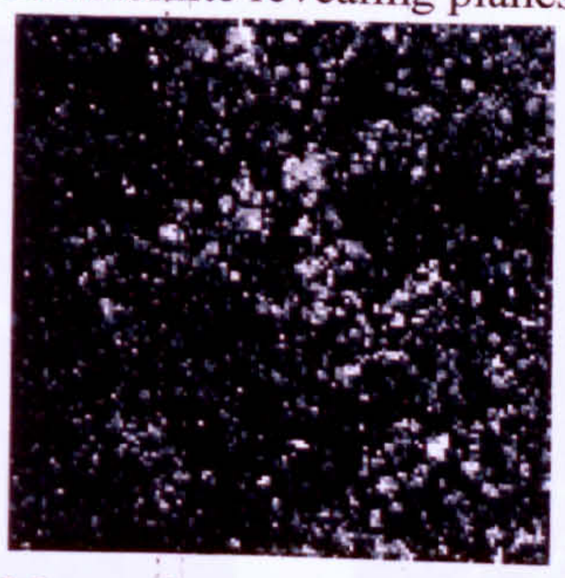

Magnesium map

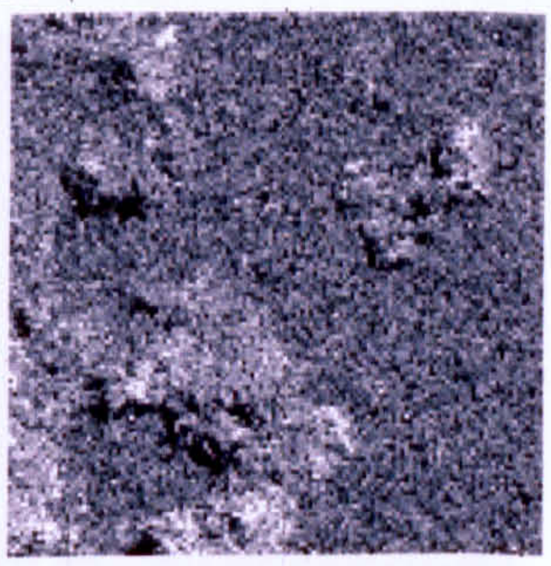

Sulphur map

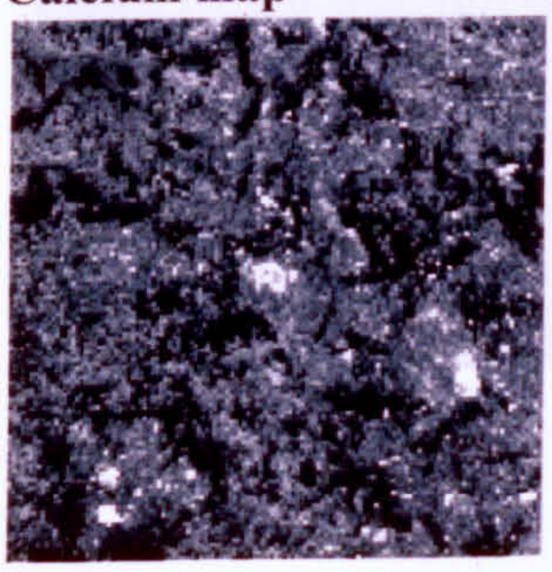

Silicon map

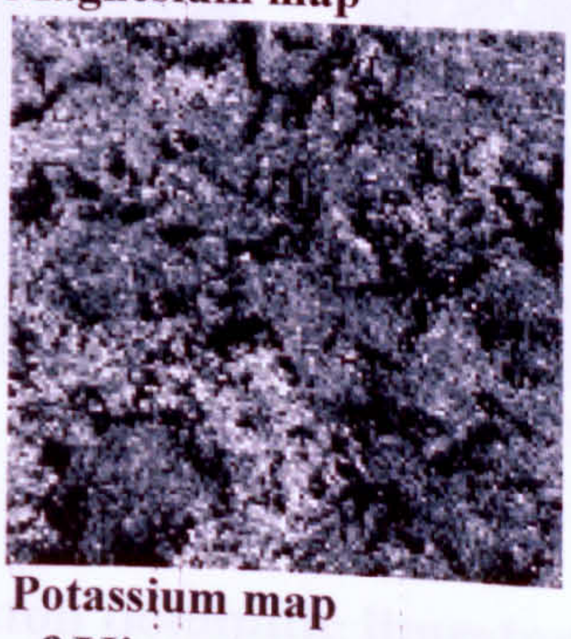

Potassium map

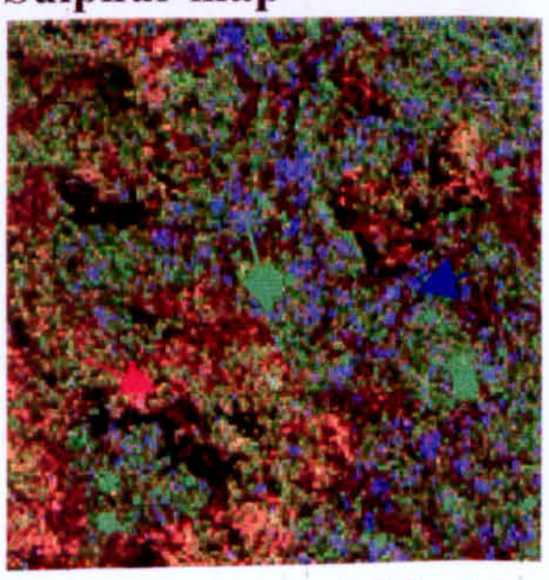

S-red, Si-green and Mg-blue

Figure 6.8 Fractured surface of Kingston dolomite with elemental maps, with Si and presence of S, (bright areas higher concentration of the element mapped).
(dolomite pointed with white arrows)

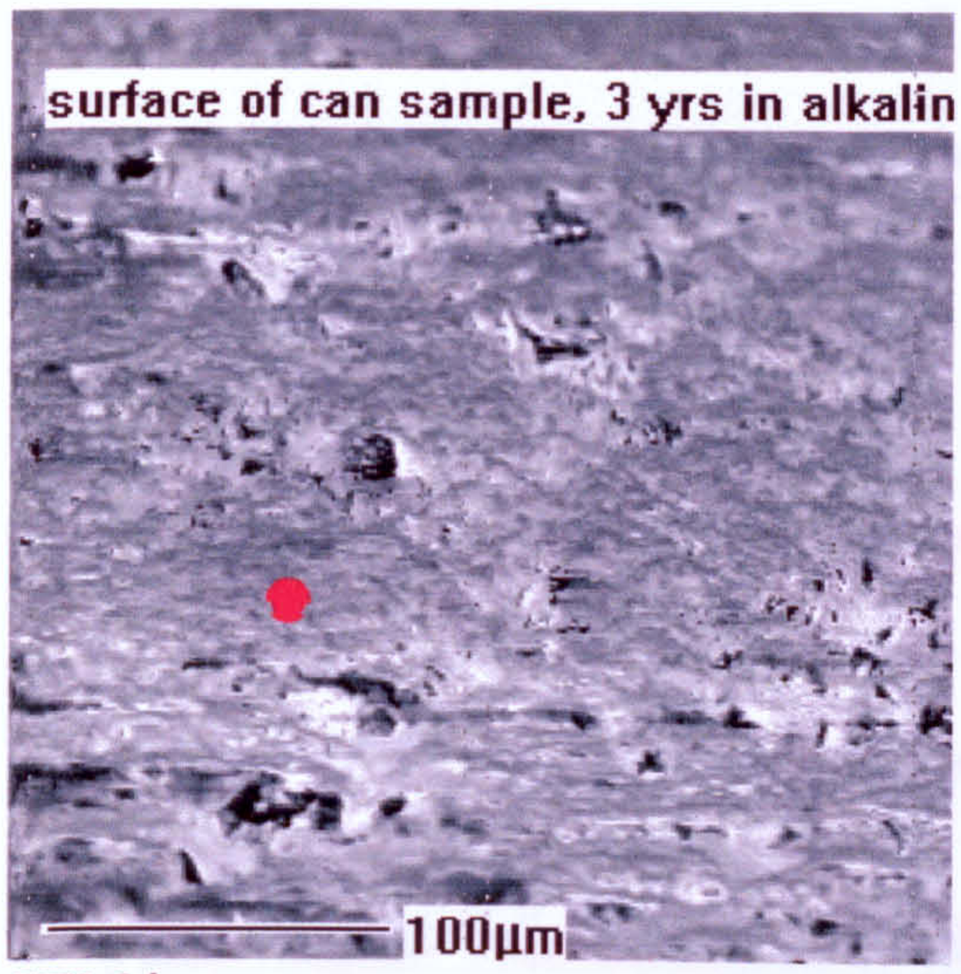

SEM image

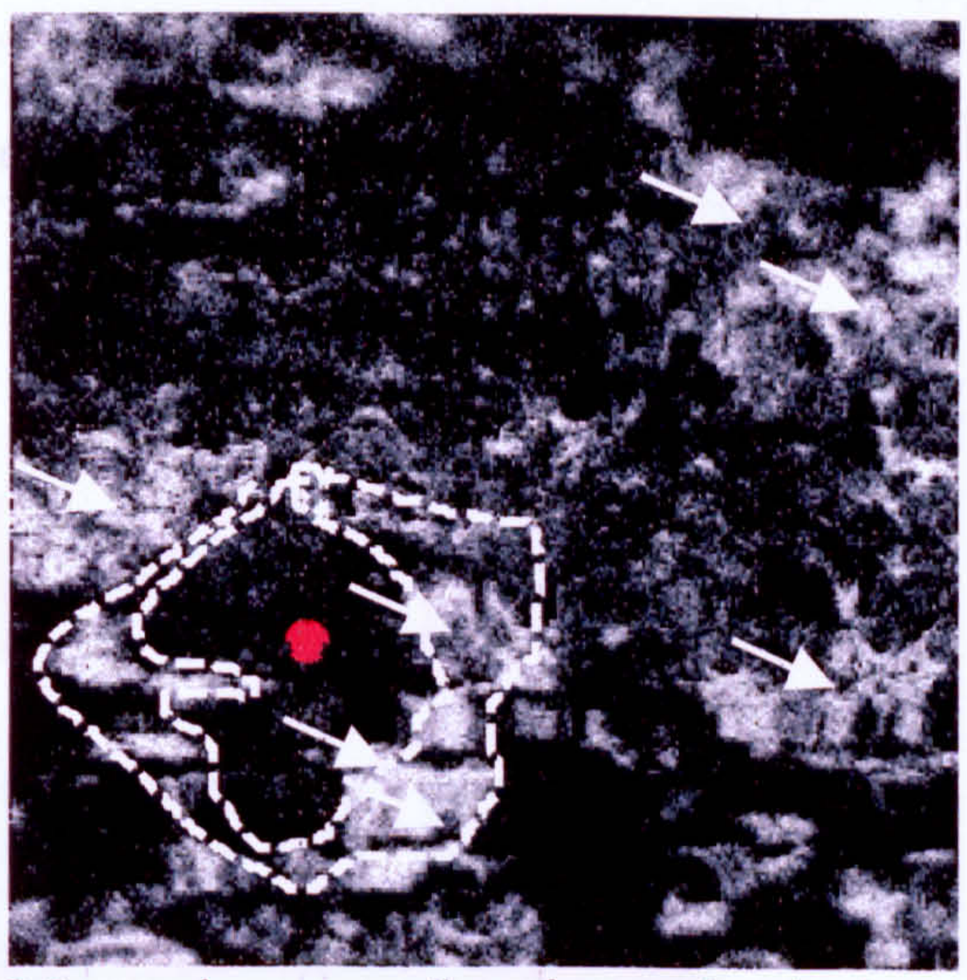

Magnesium map (brucite nucleation)

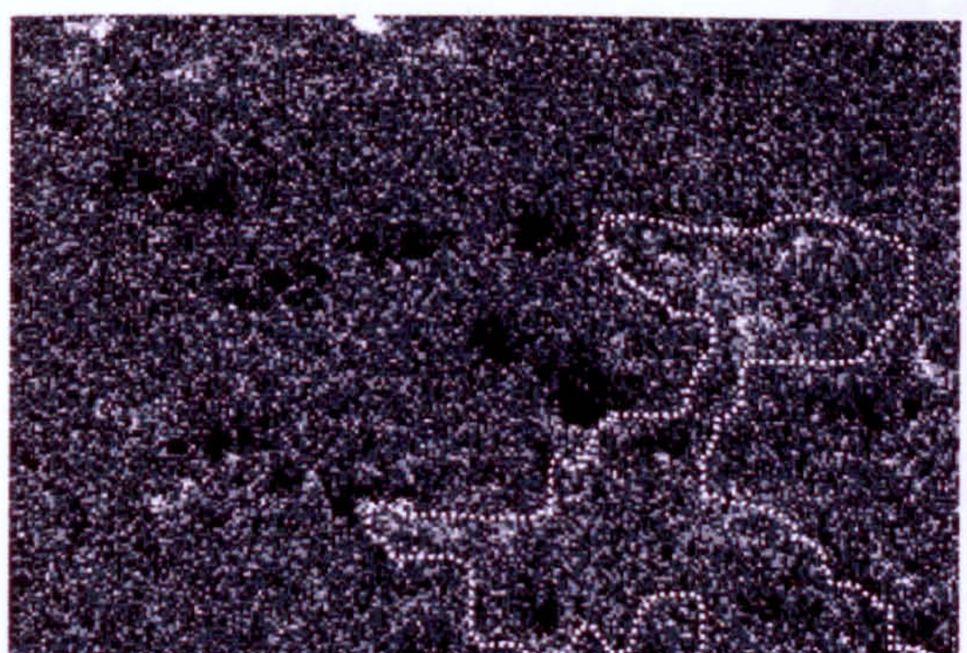

Aluminum map (matrix)

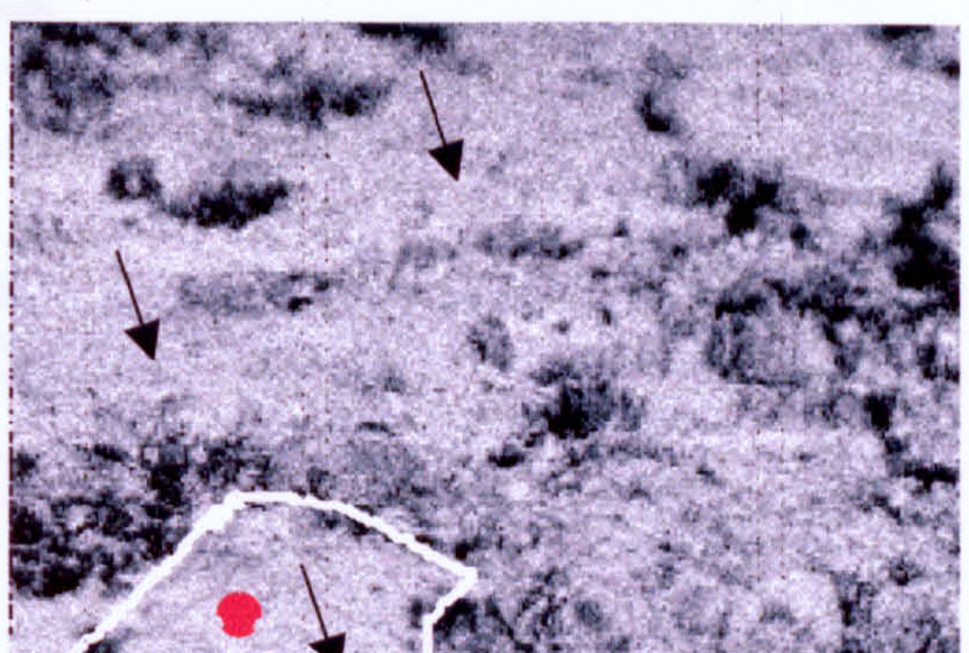

Calcium map (calcite)

Silicon map (matrix)

Iron map (outlined area, on the rim of D)

Figure 6.9 Surface of Kingston dolomitic limestone after 3yrs in alkaline solution, clearly illustrating the migration of Mg towards the edges of dolomite crystals, also followed by Fe. (White dotted lines are outlining

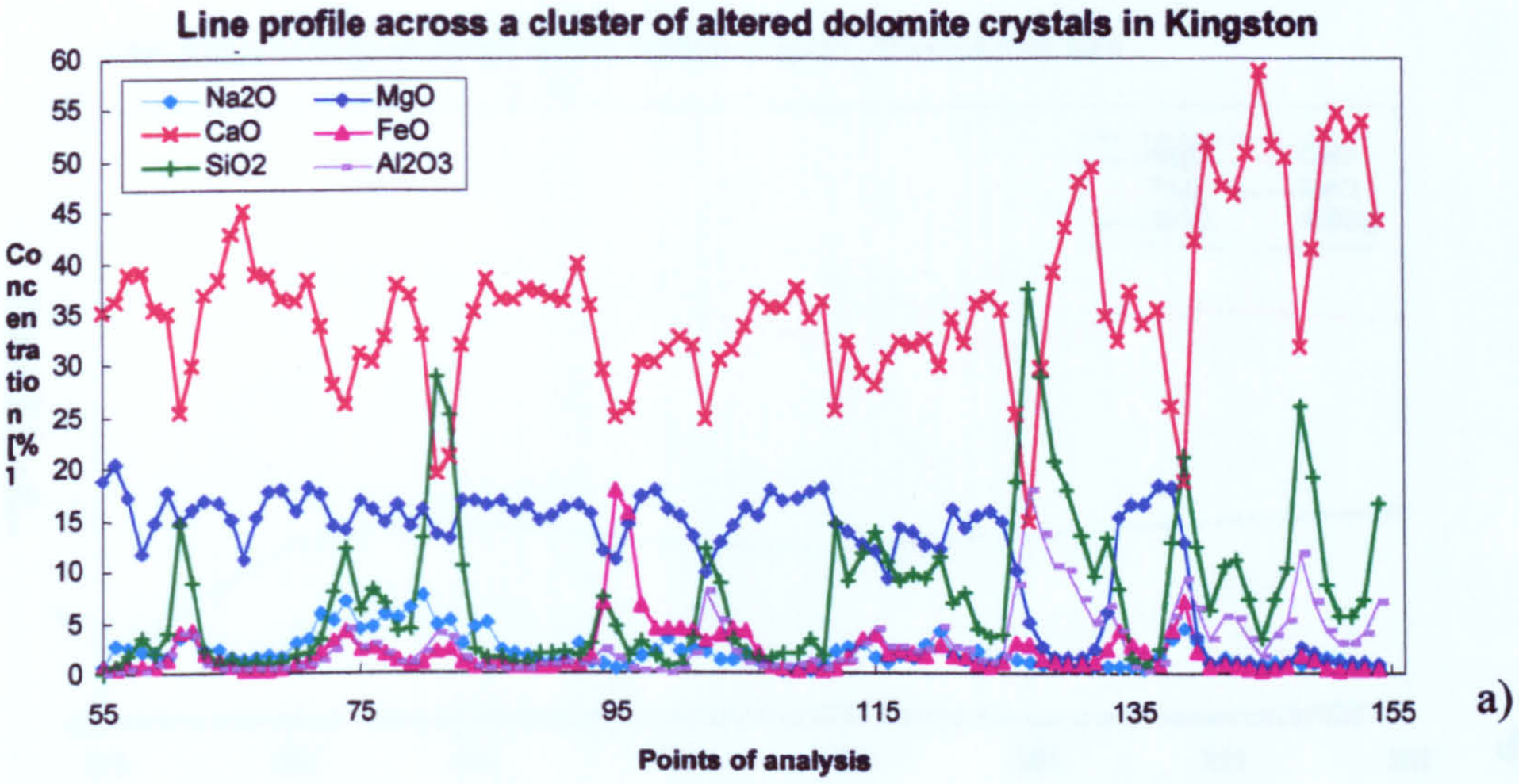
Line profile across a cluster of altered dolomite crystals in Kingston
Na2O
MgO
CaO
FeO
SiO2
Al2O3
Concentration [%]
60
55
50
45
40
35
30
25
20
15
10
5
0
55
75
95
115
135
155
Points of analysis

a)

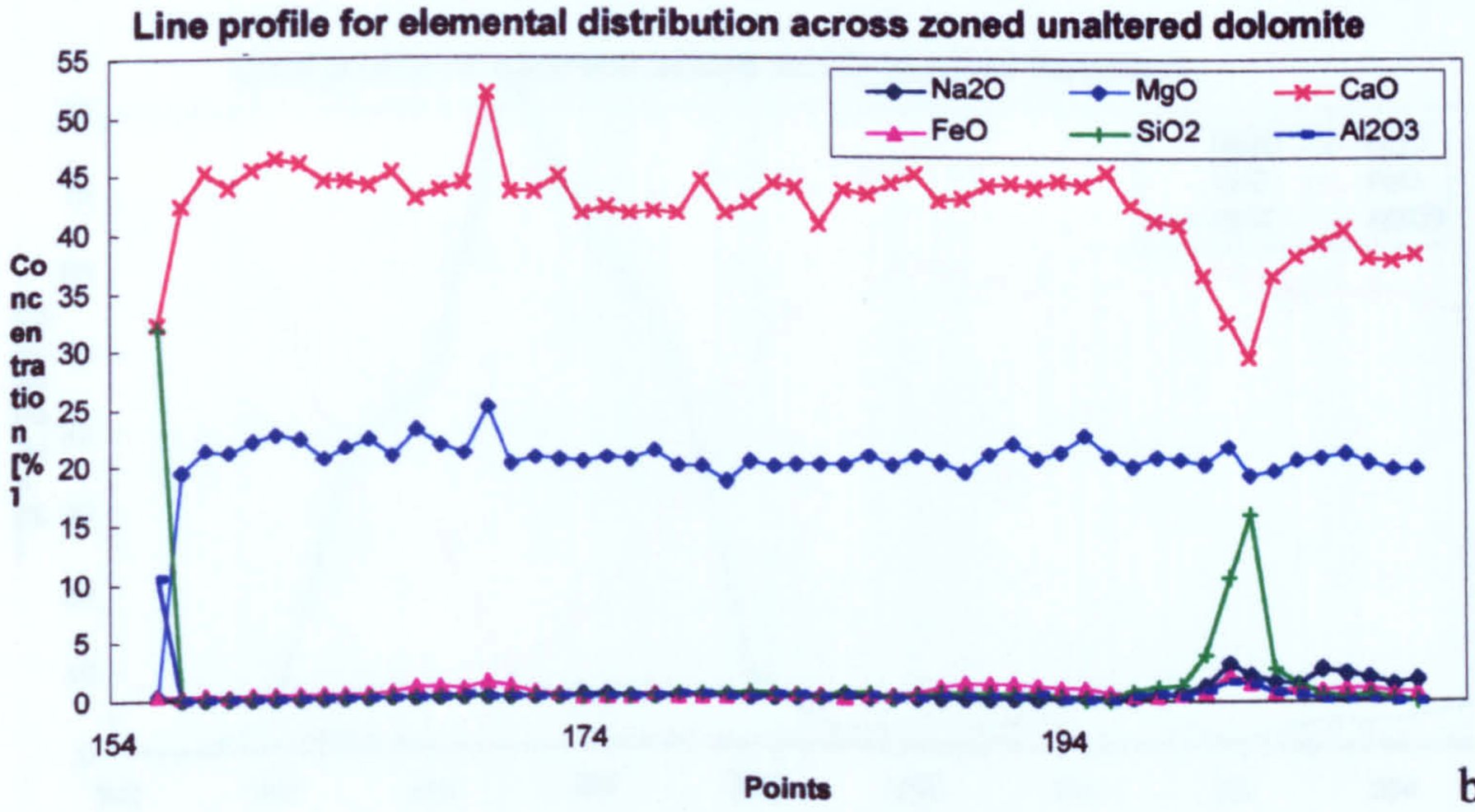
Line profile for elemental distribution across zoned unaltered dolomite
Na2O
MgO
CaO
FeO
SiO2
Al2O3
Concentration [%]
55
50
45
40
35
30
25
20
15
10
5
0
154
174
194
Points

b)

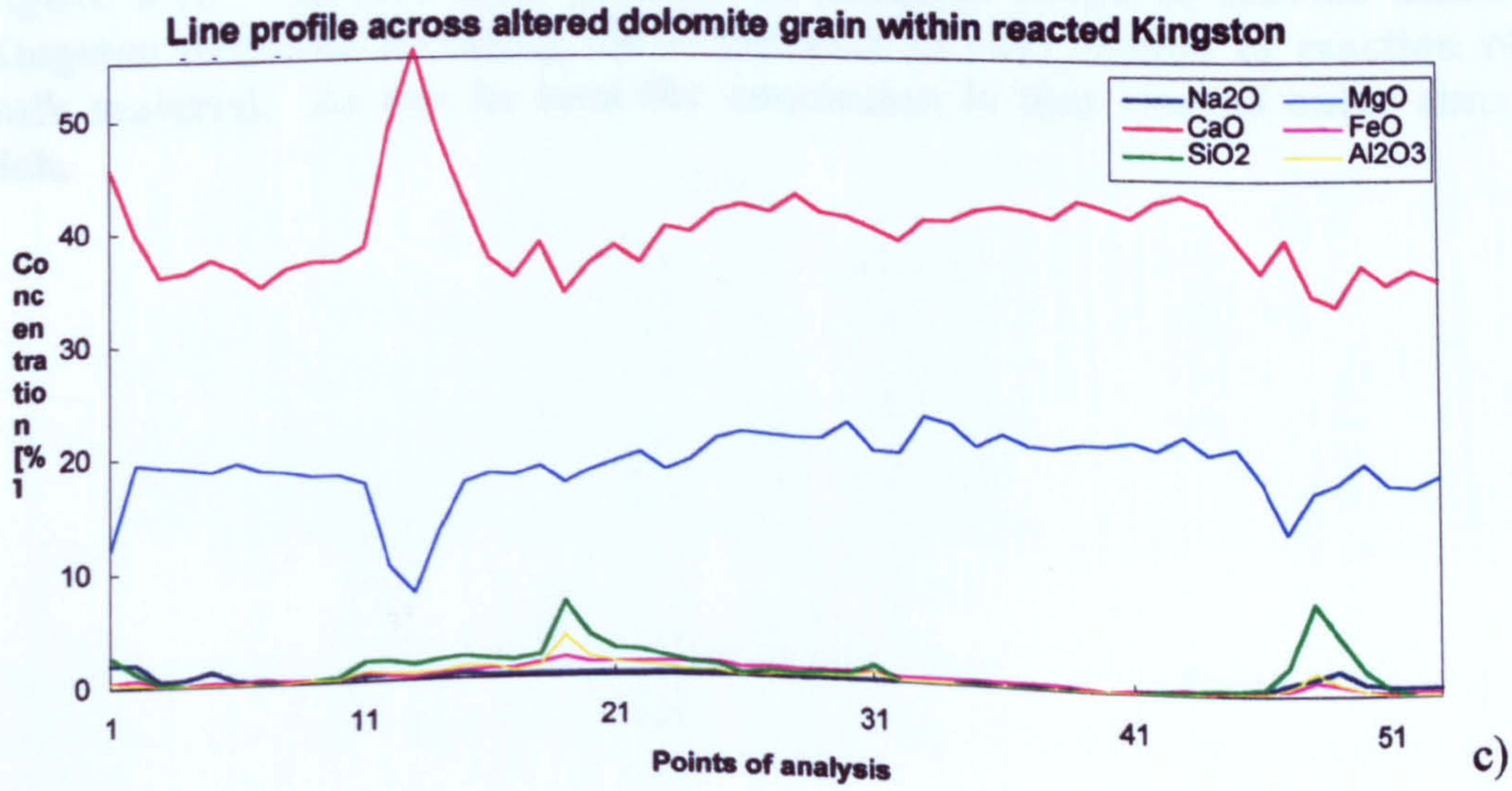
Line profile across altered dolomite grain within reacted Kingston
Na2O
MgO
CaO
FeO
SiO2
Al2O3
Concentration [%]
50
40
30
20
10
0
1
11
21
31
41
51
Points of analysis

c)

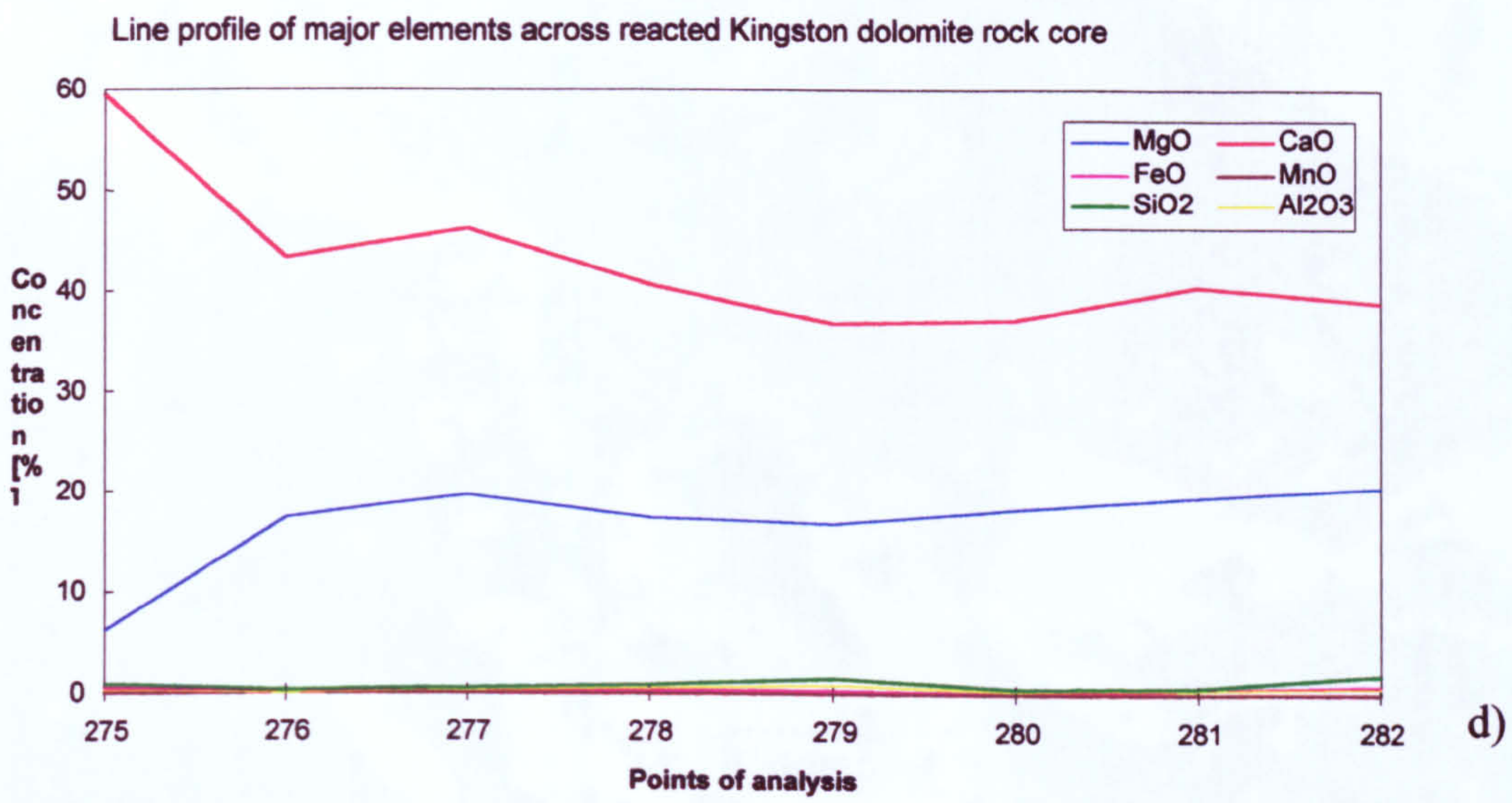

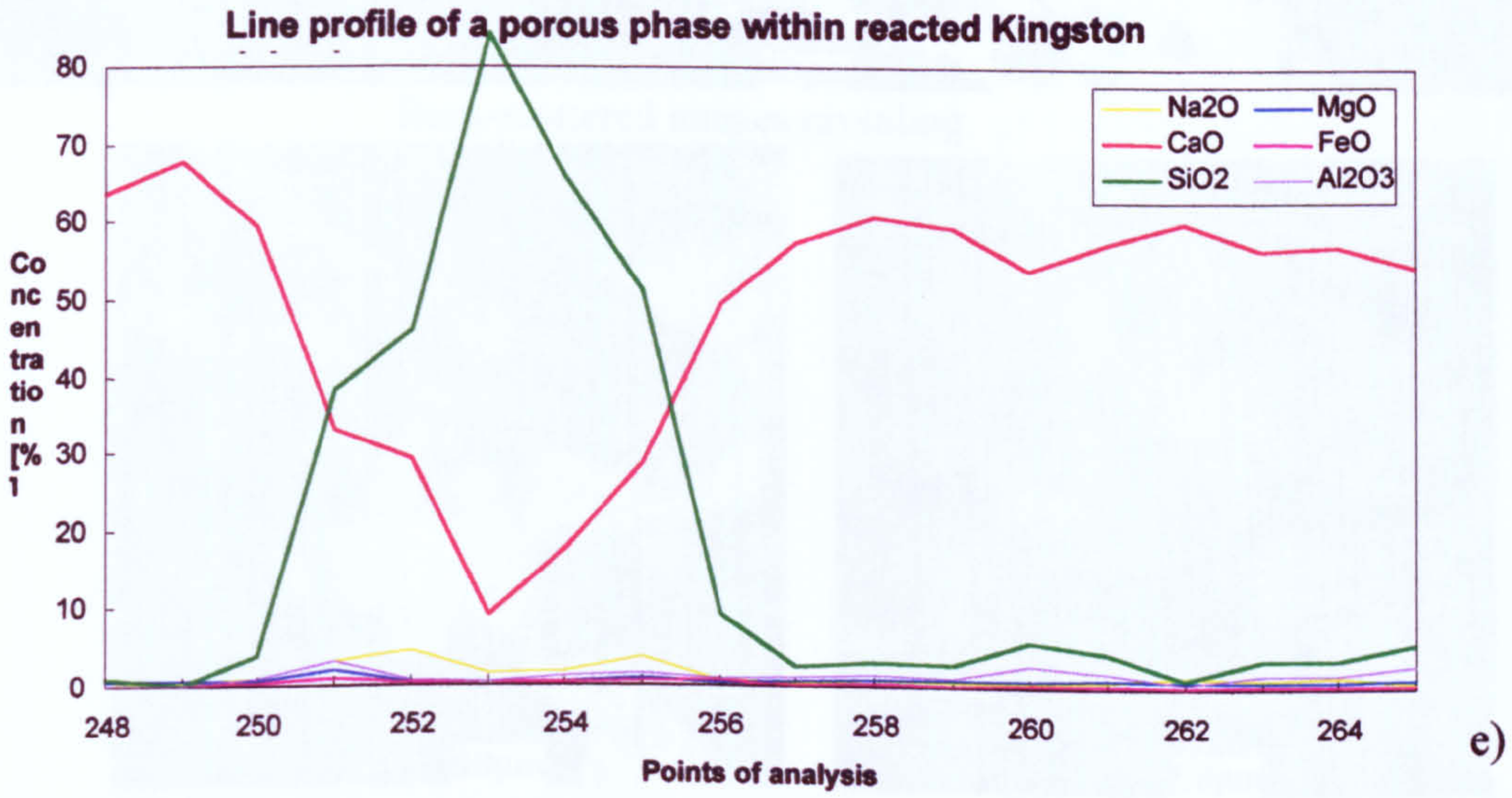

Figure 6.10 EPMA Line profiles in different areas of reacted alkali-treated Kingston dolomite revealing the differences in composition of reaction rims and bulk material. As can be seen the conclusion is that reacted outer rims are Ca rich.

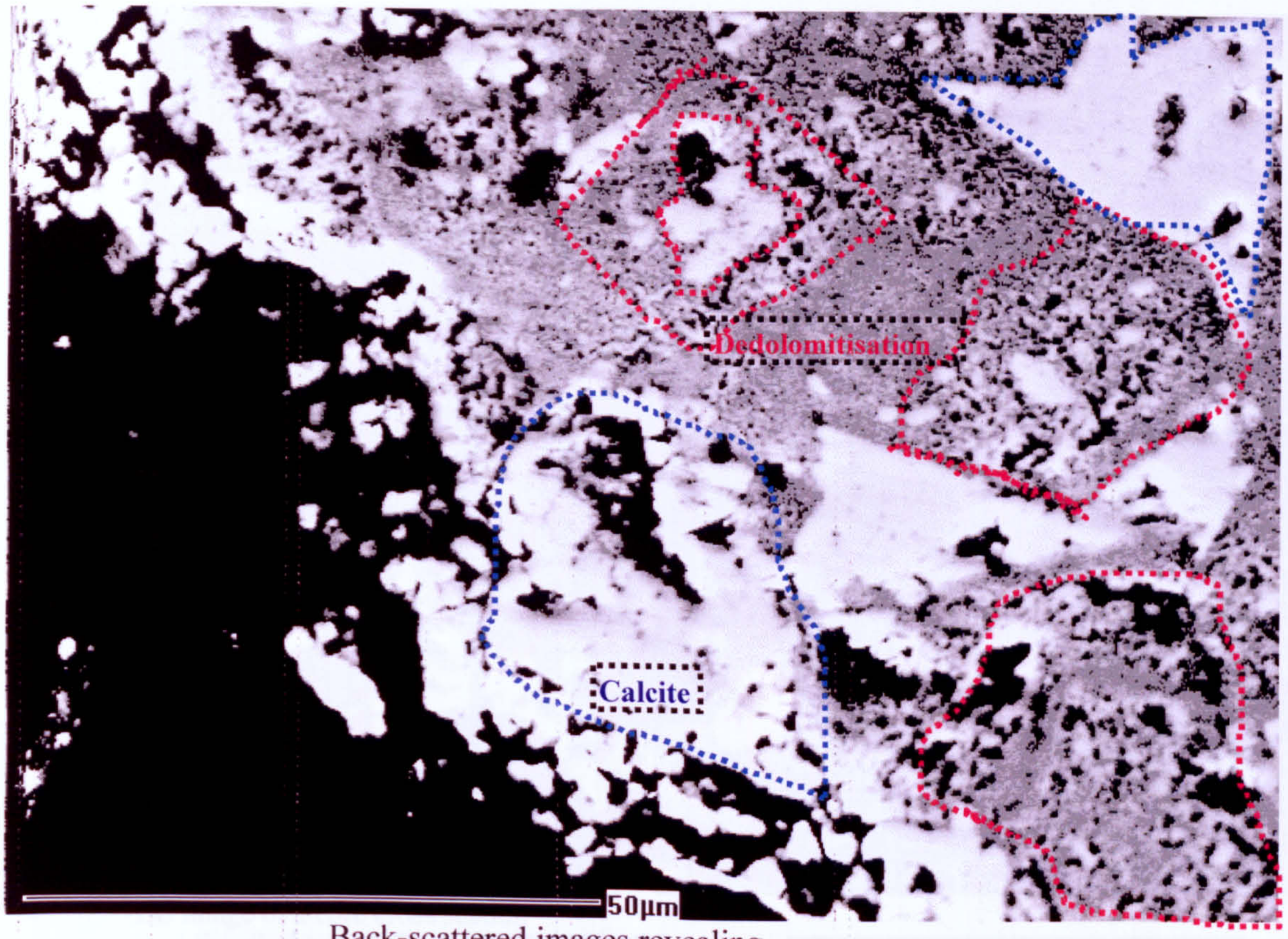

Back-scattered images revealing

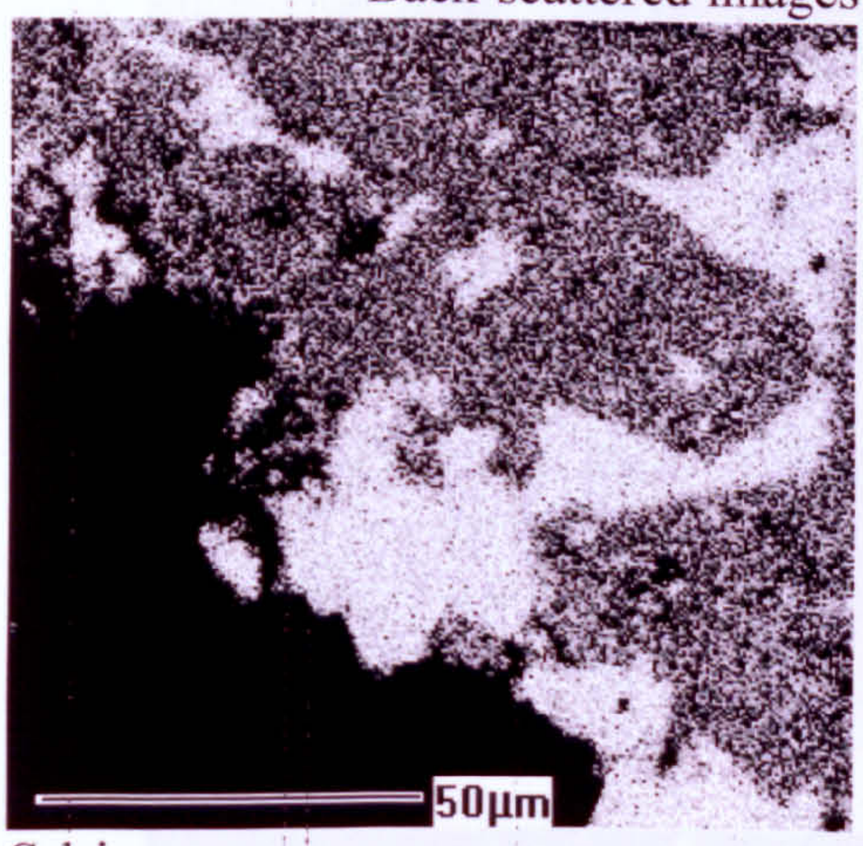

Calcium

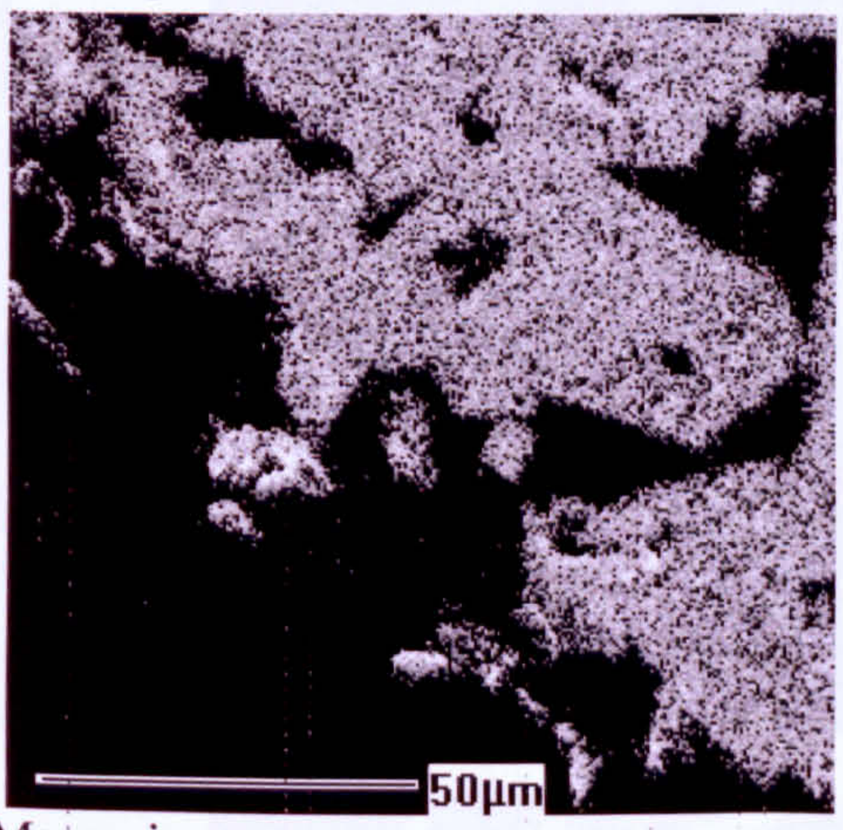

Magnesium

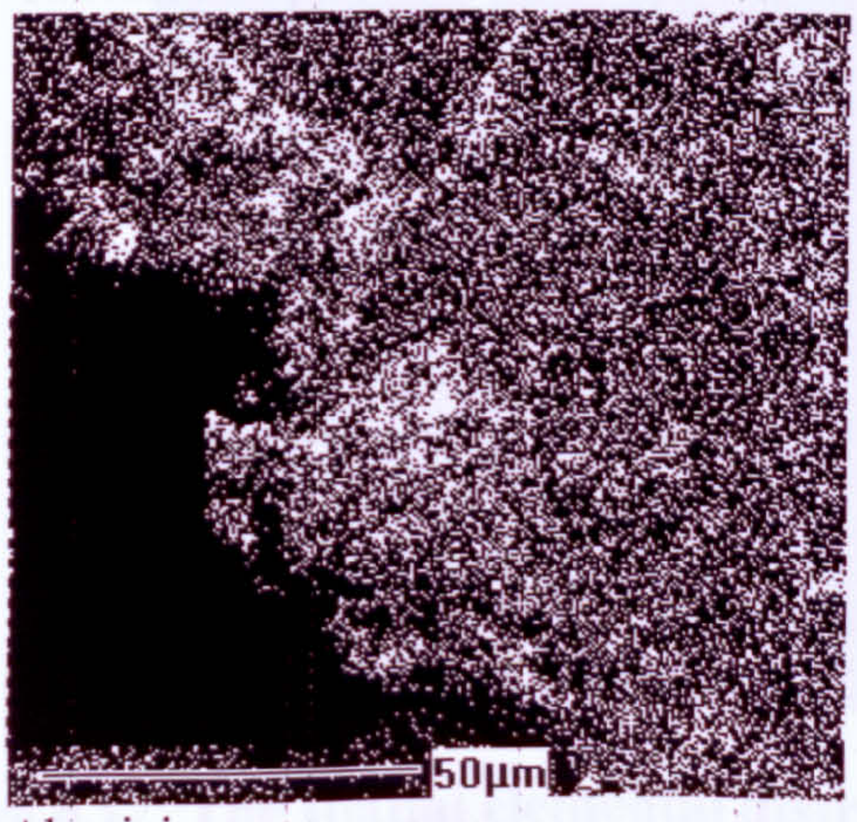

Aluminium

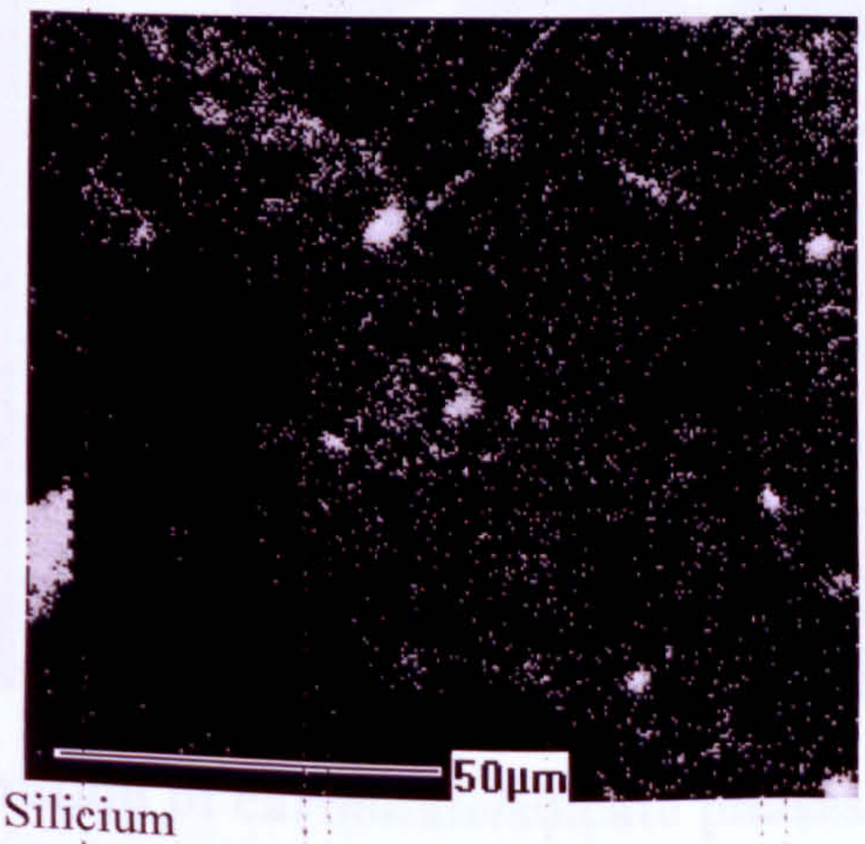

Silicium

Figure 6.11 Elemental distribution at the periphery of ASTM C586 core specimen, cross-section. Top image is the BSEI of mapped area with dolomite in red and calcite in blue.

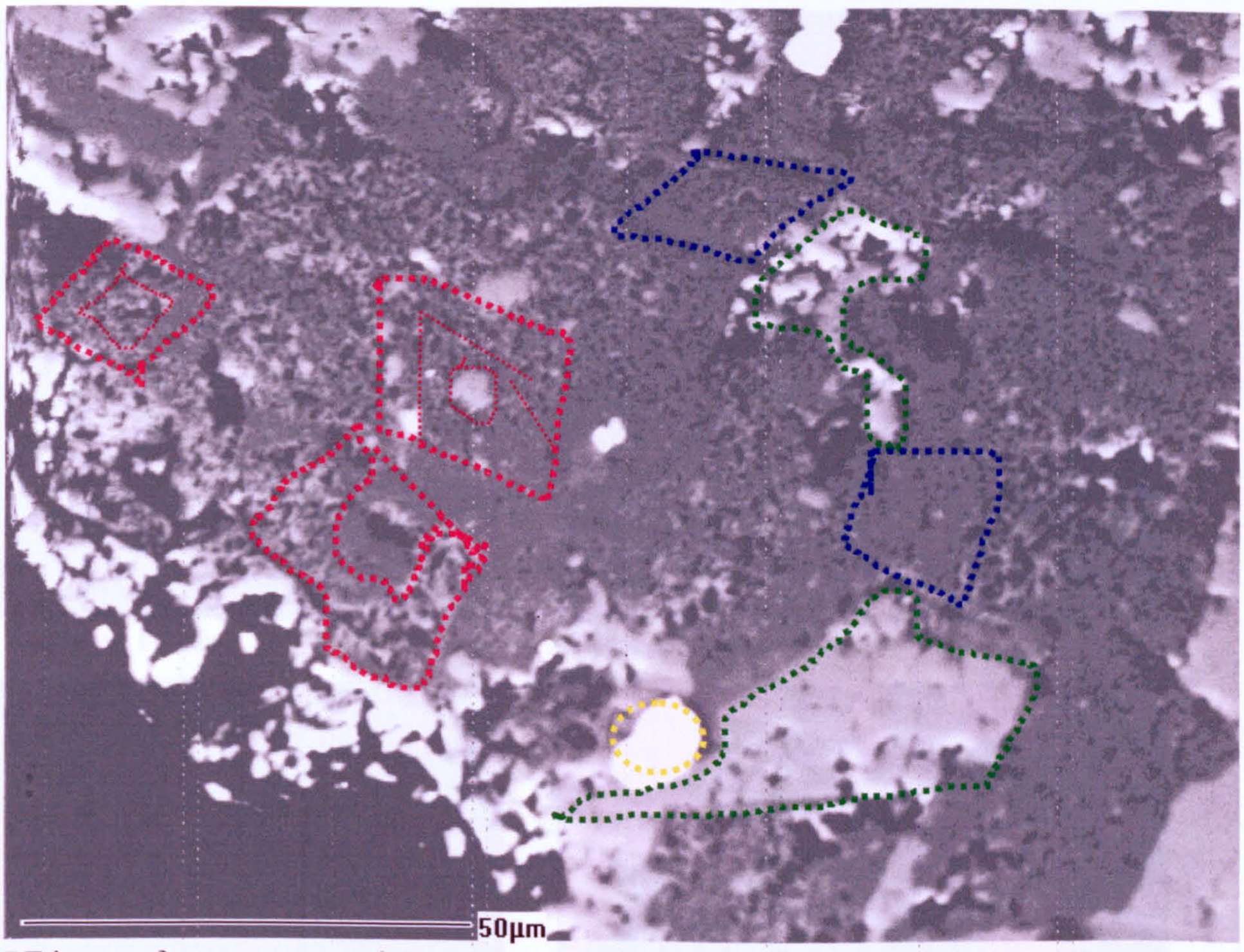

BE image of a core cross section

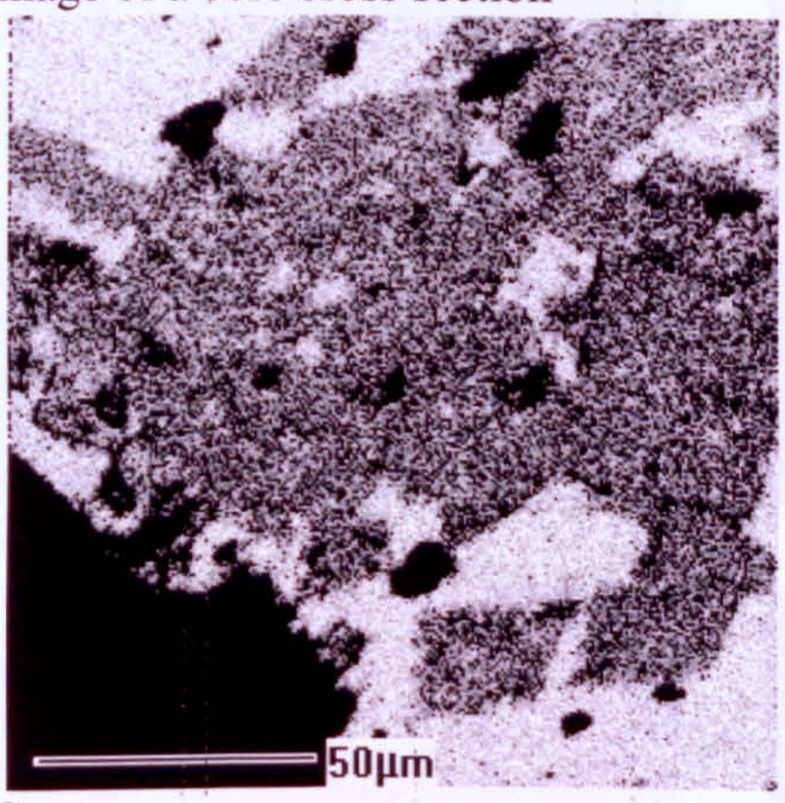

Ca map

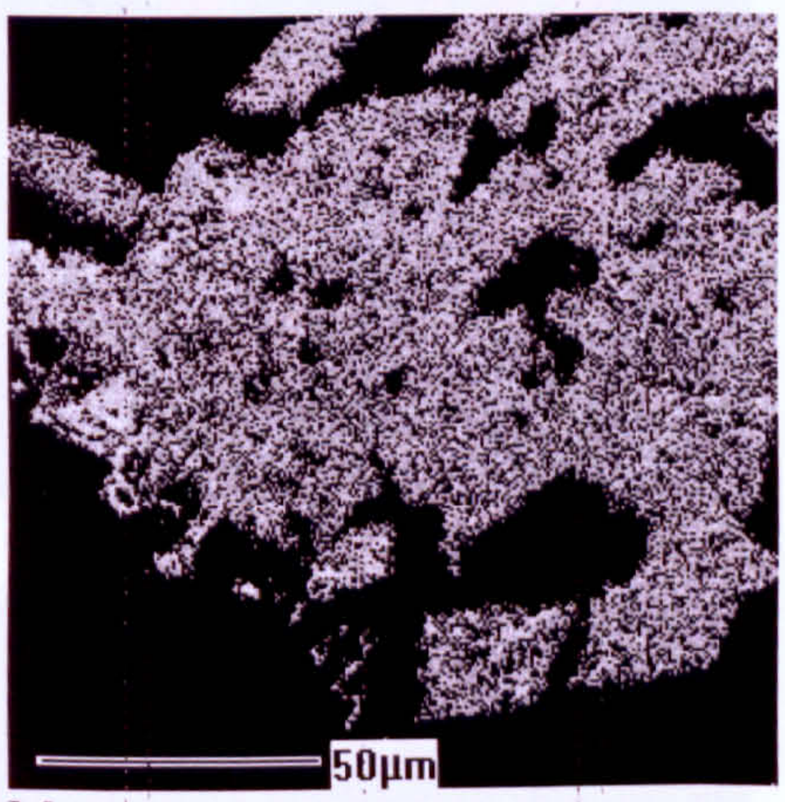

Mg map

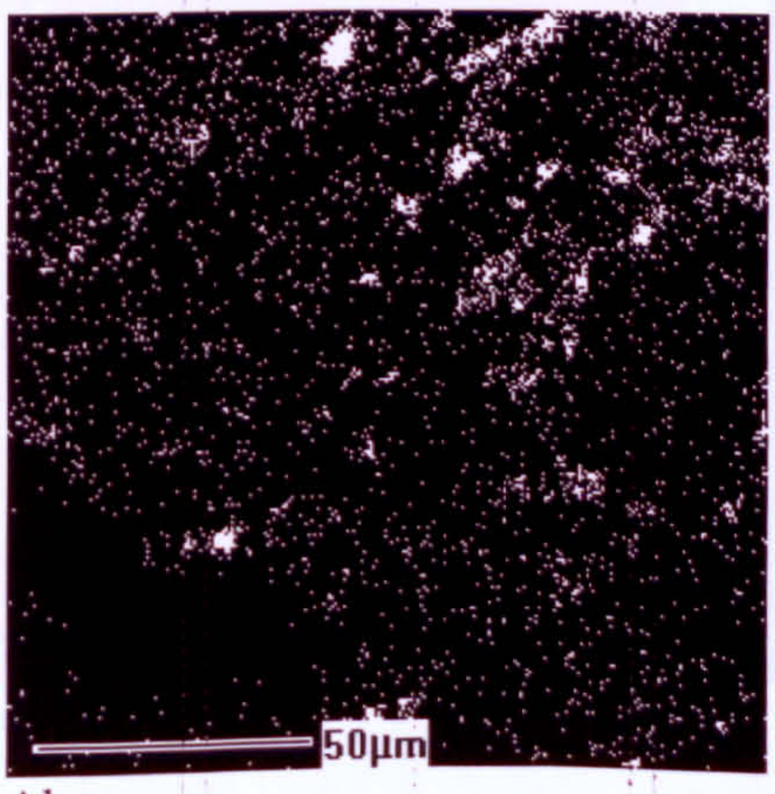

Al map

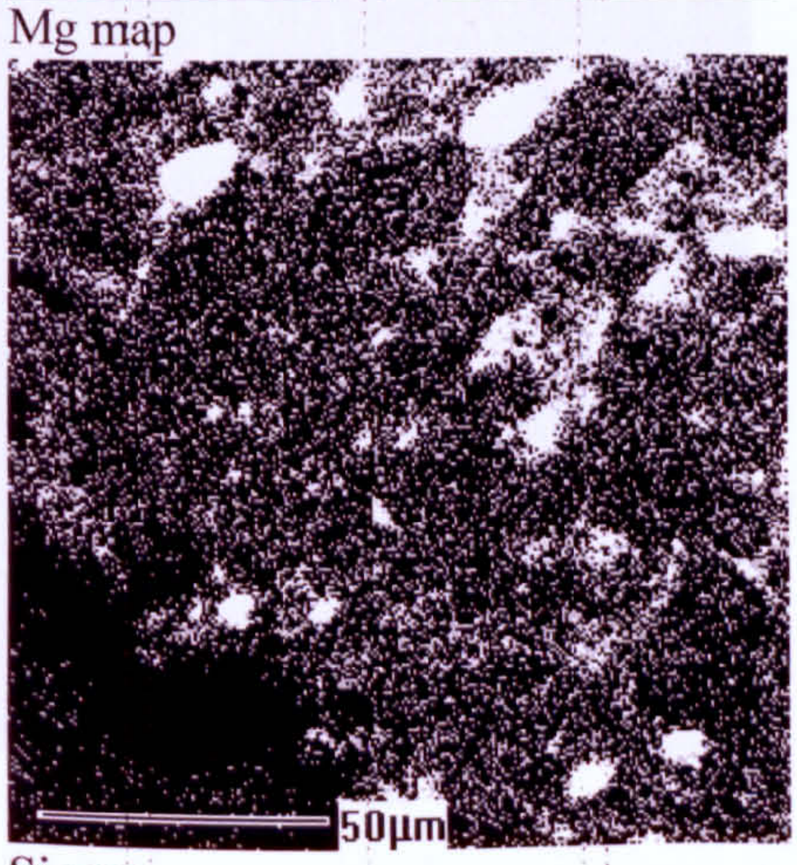

Si map

Figure 6.12 The spatial elemental distribution of carbonate/silicate phases at the edge of cross section of a core that was immersed in alkaline solution, showing Ca and Mg accumulations within reacted dolomite grains (outlined in red), suggesting migration of elements towards their nucleation sites after the dedolomitisation reaction.

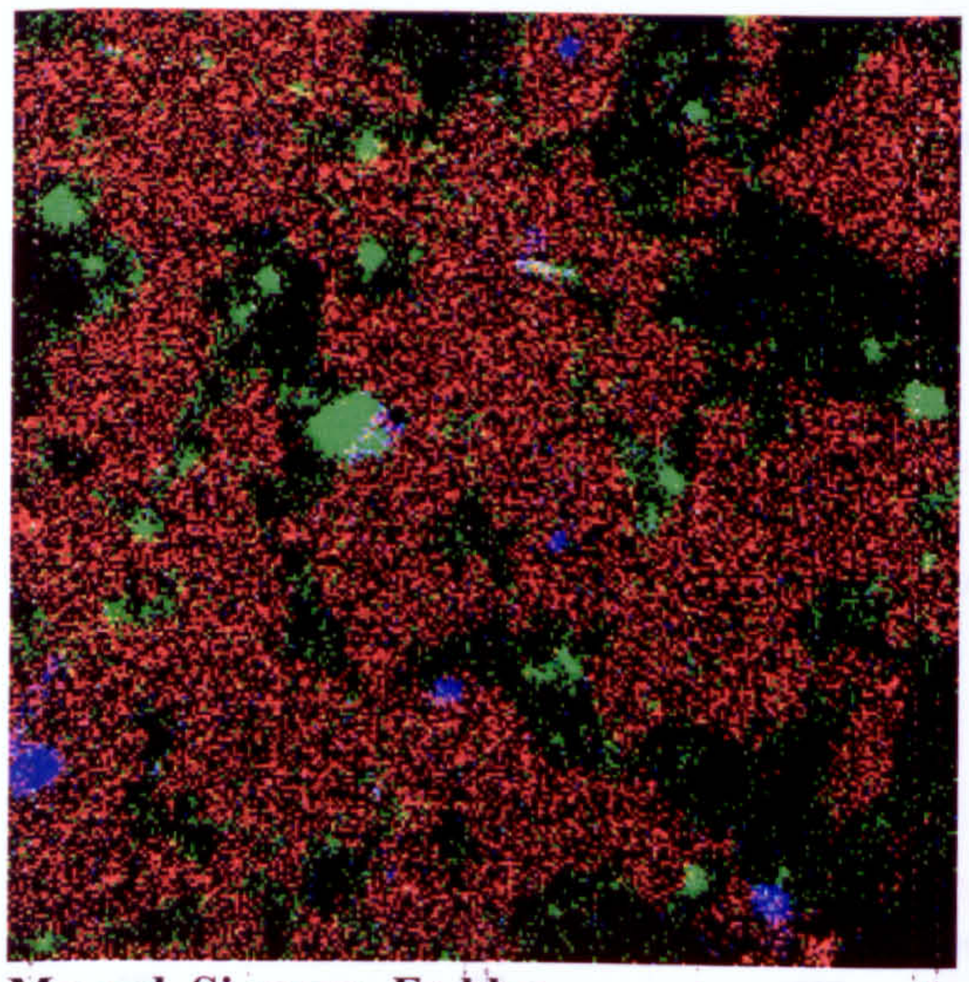

Mg-red, Si-green, Fe-blue a)

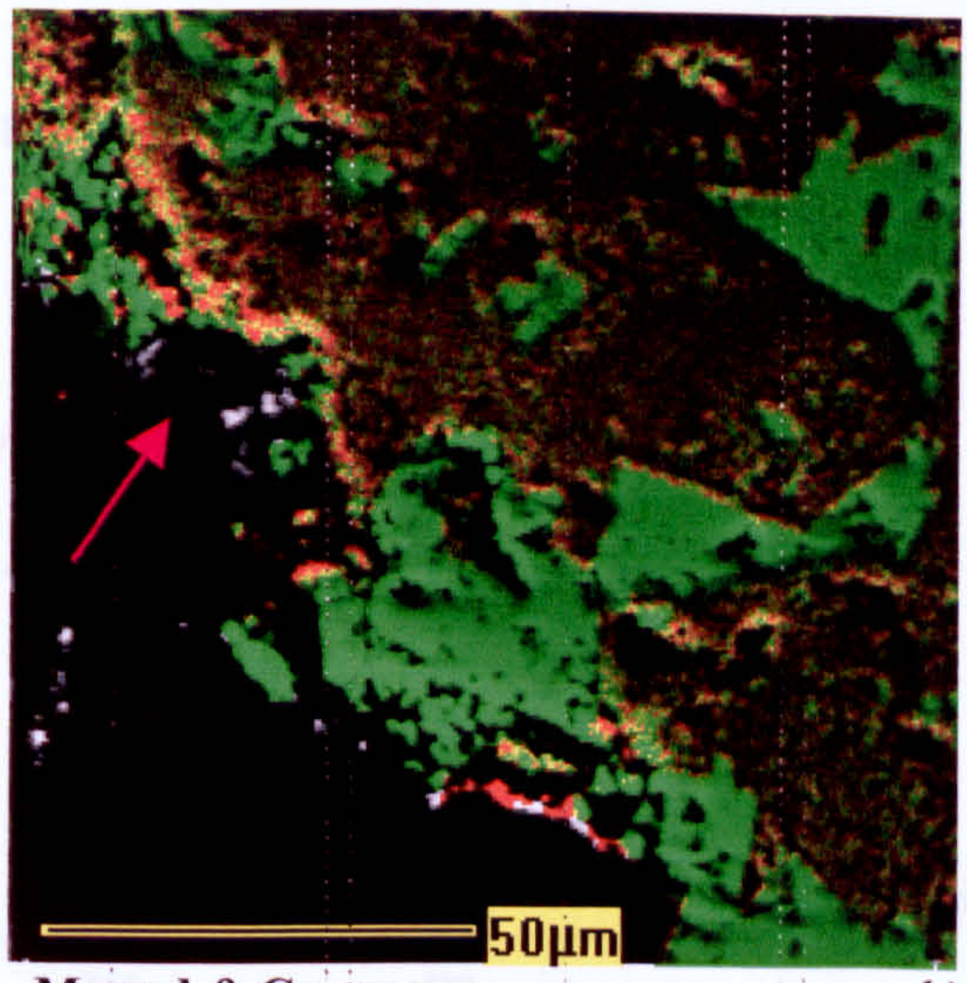

Mg-red & Ca-green b)

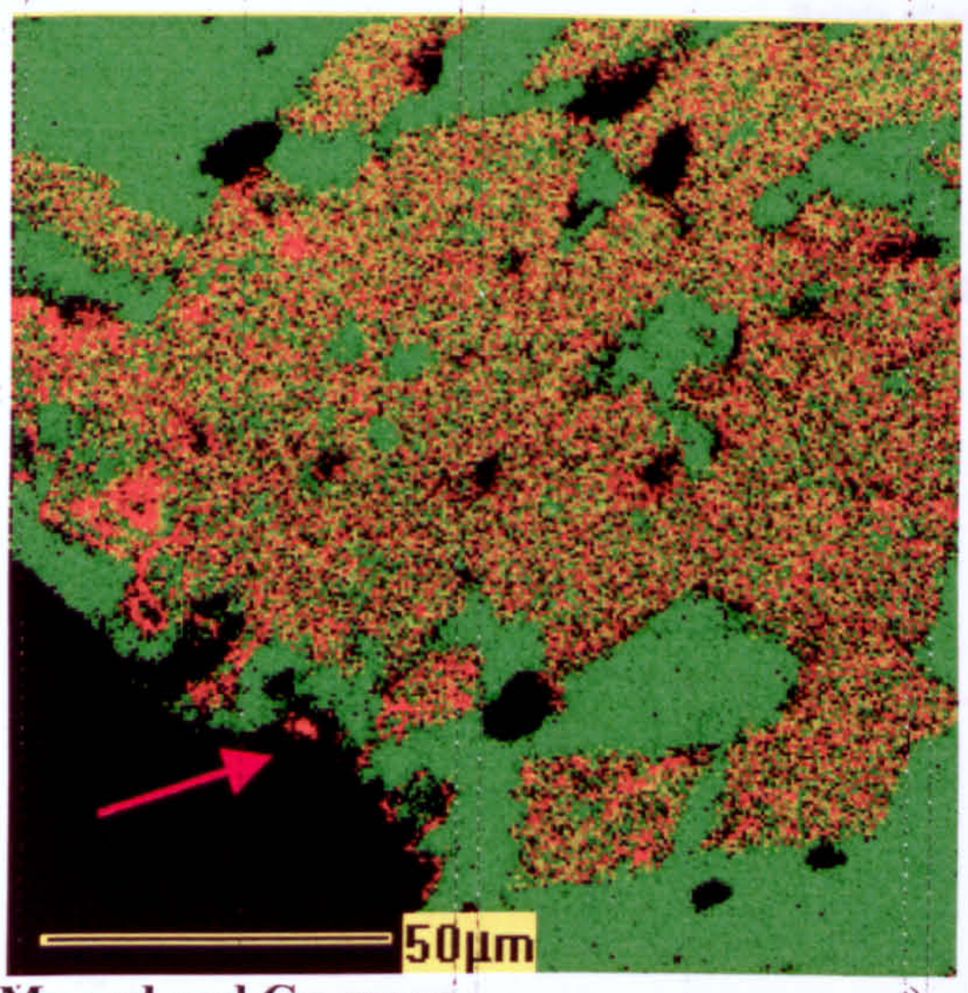

Mg-red and Ca-green c)

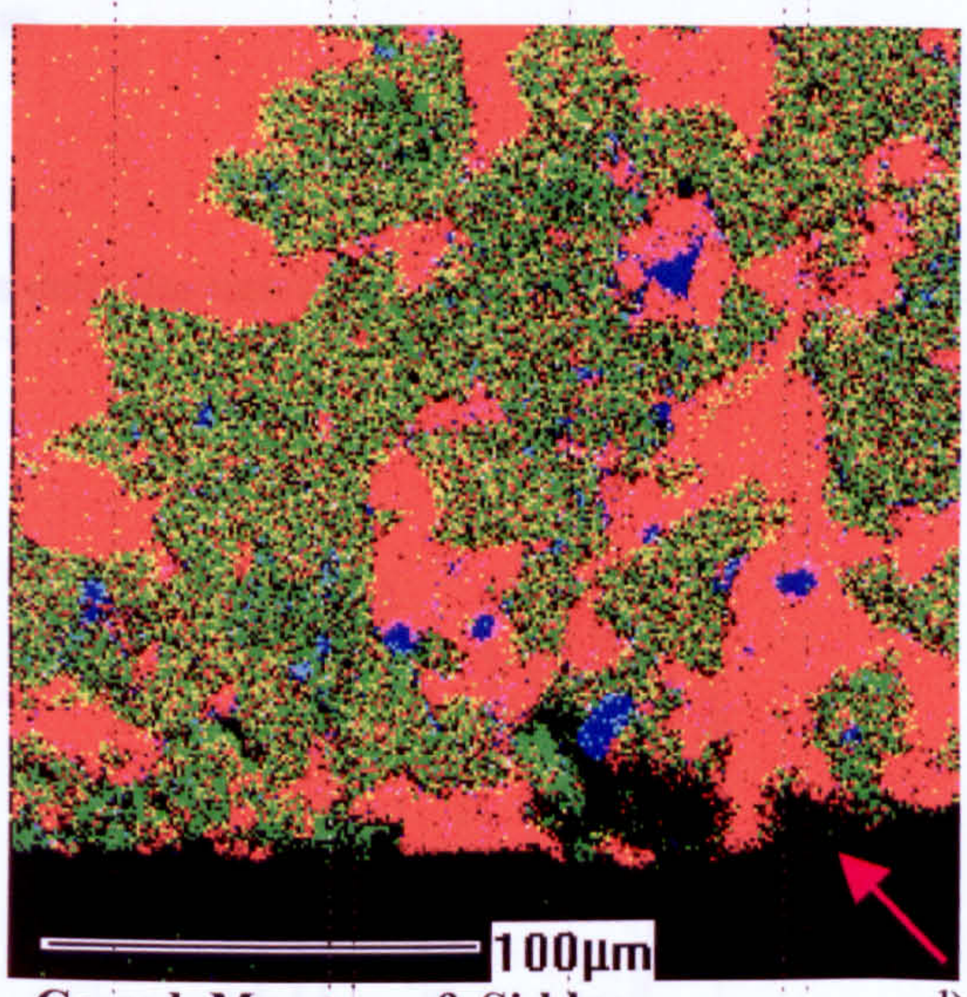

Ca-red, Mg-green & Si-blue d)

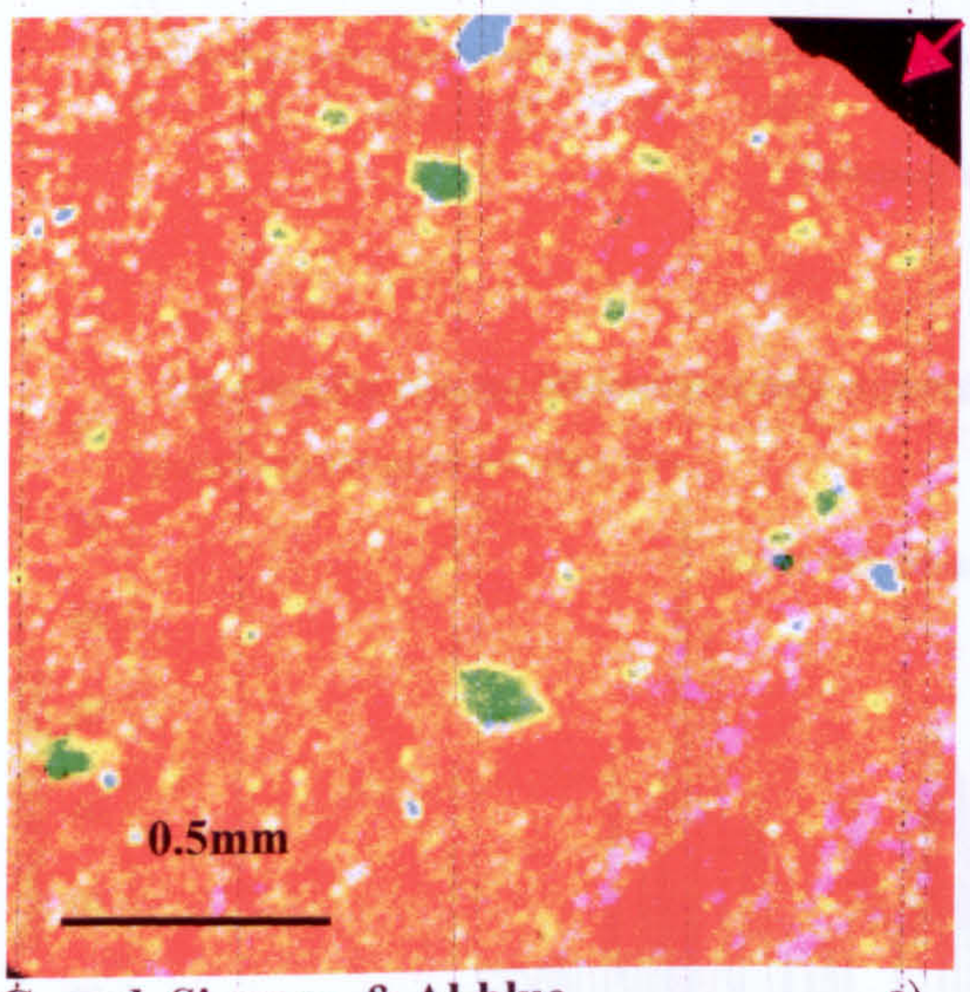

Ca-red, Si-green & Al-blue e)

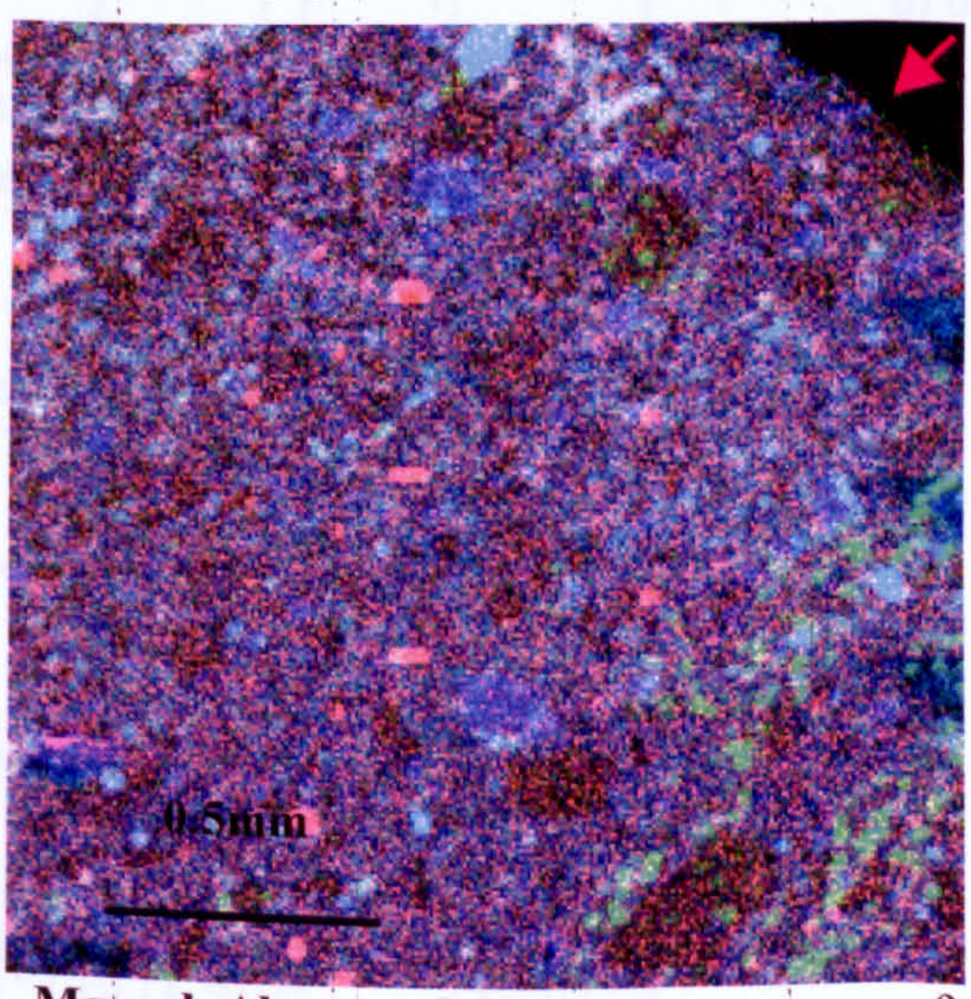

Mg-red, Al-green & Si-blue f)

Figure 6.13 Co-dependence between spatial elemental distribution in dolomite treated with alkaline solution, revealing presence of silicate matrix, dissolution effects and migration of elements induced by rock/solution reaction.
(*Red arrows are pointing the outer areas-edges; images are from different areas, apart from maps e and f)

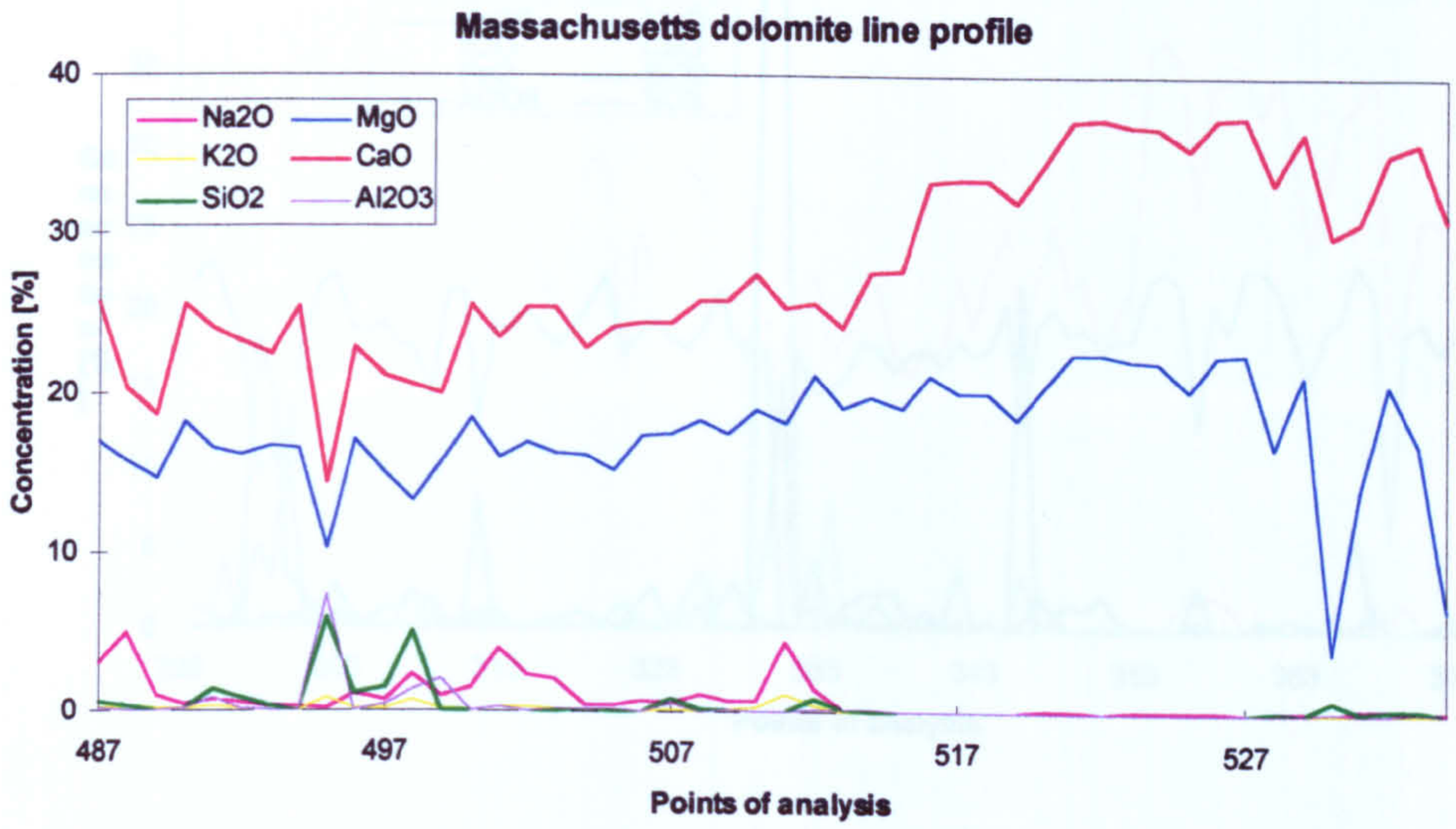

a) 100micron

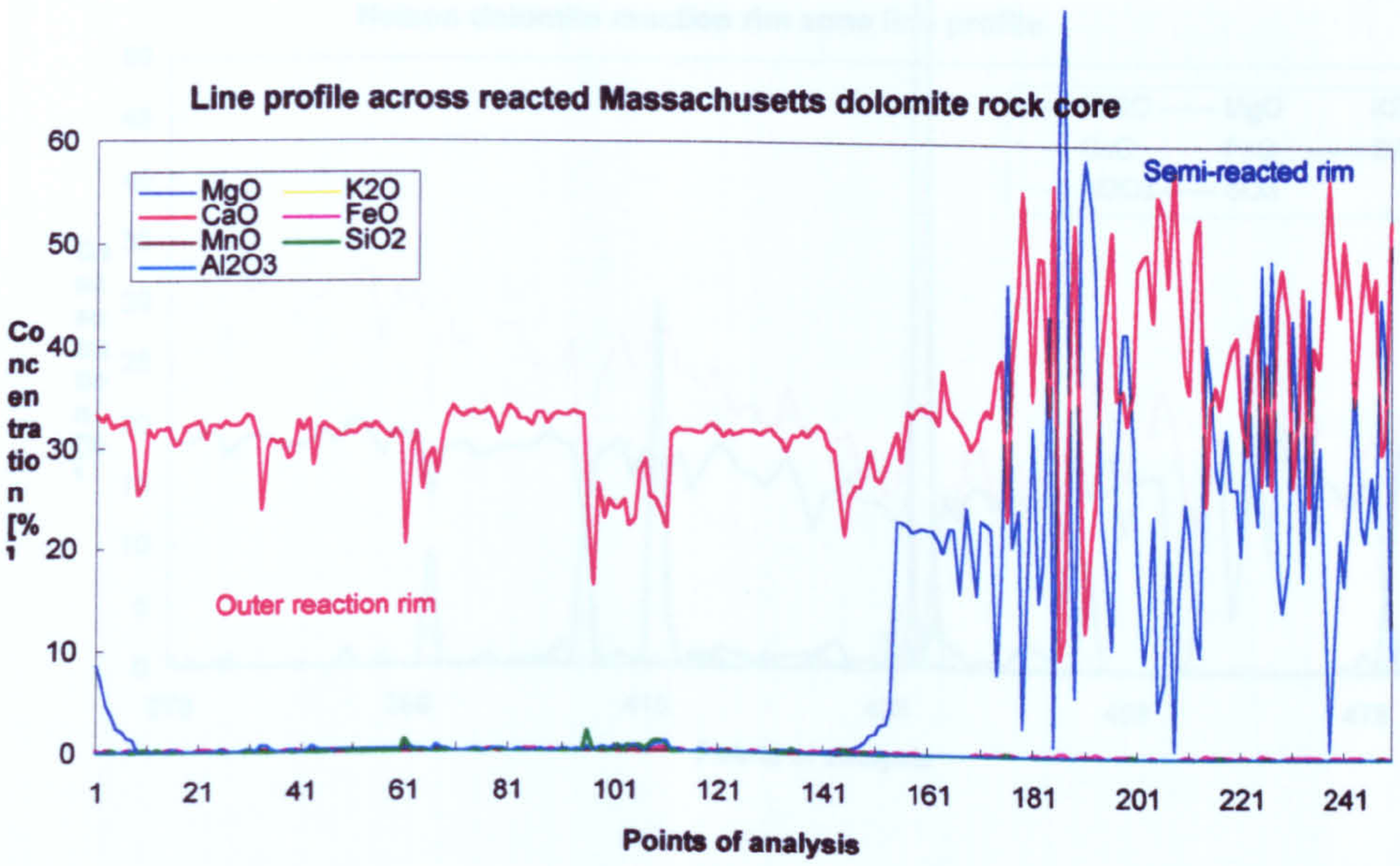

b) 0.5mm

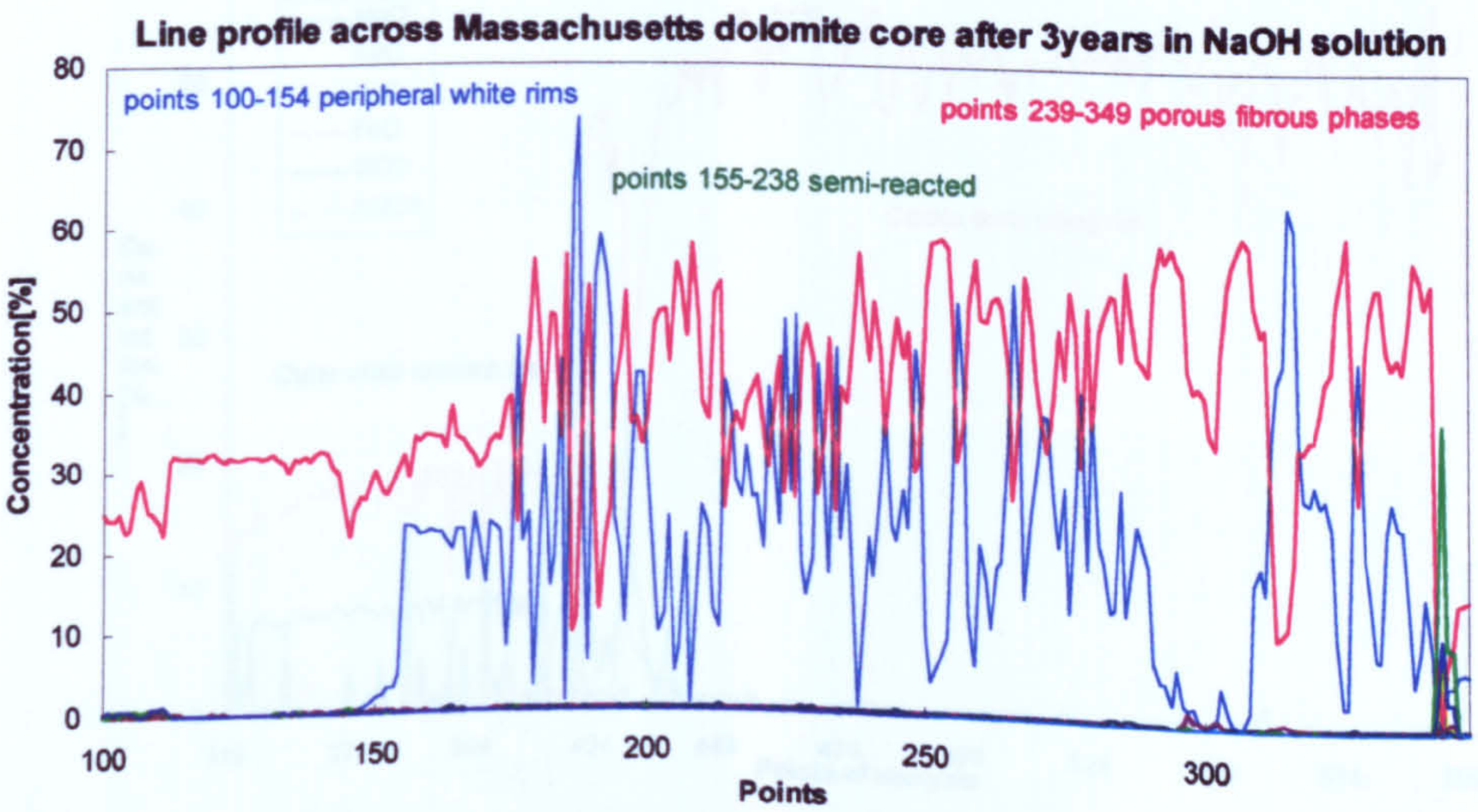

c) 1mm line

Figure 6.14 EPMA line profile analysis of reaction rims in alkali-treated Massachusetts dolomite

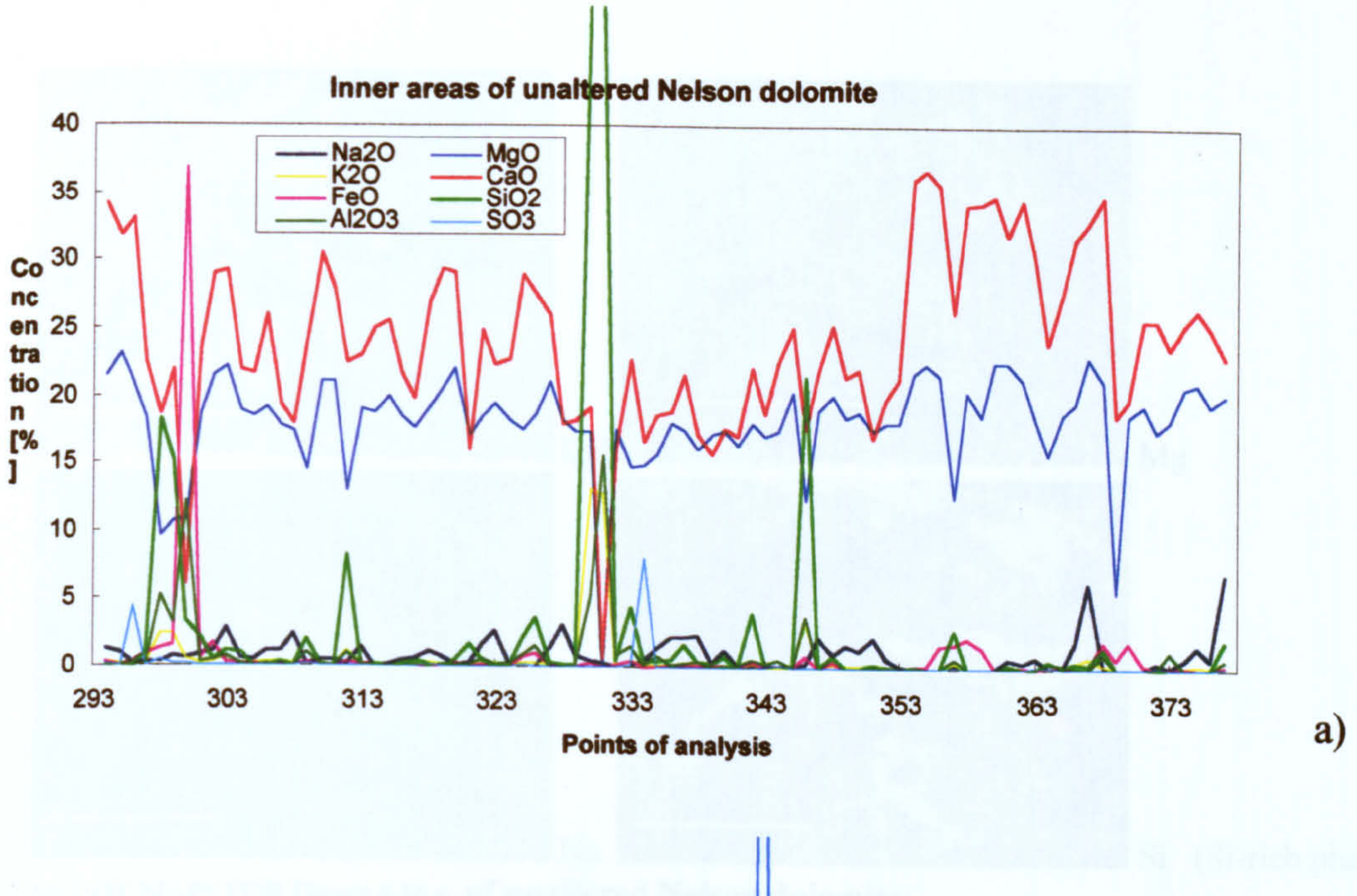

a)

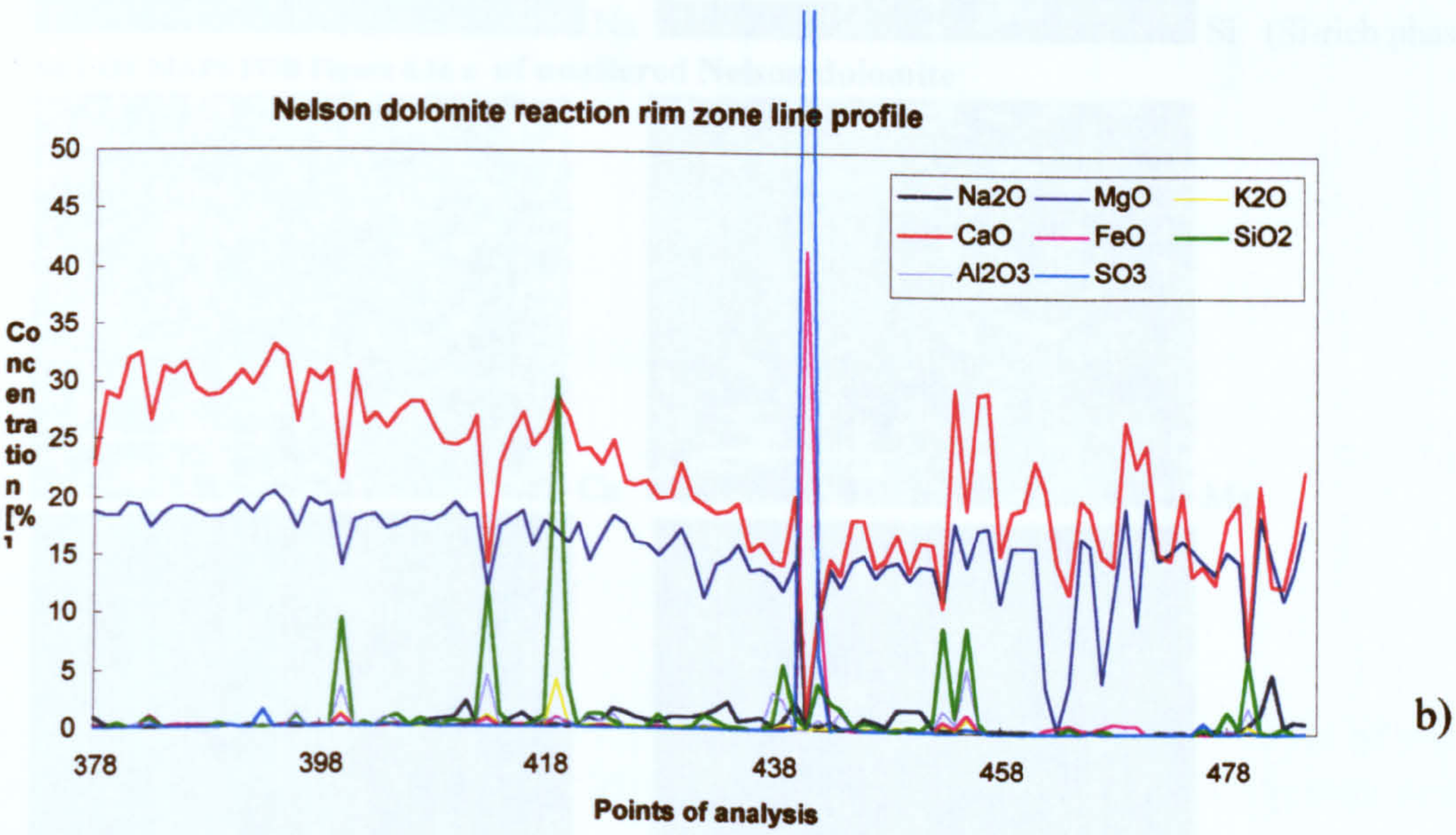

b)

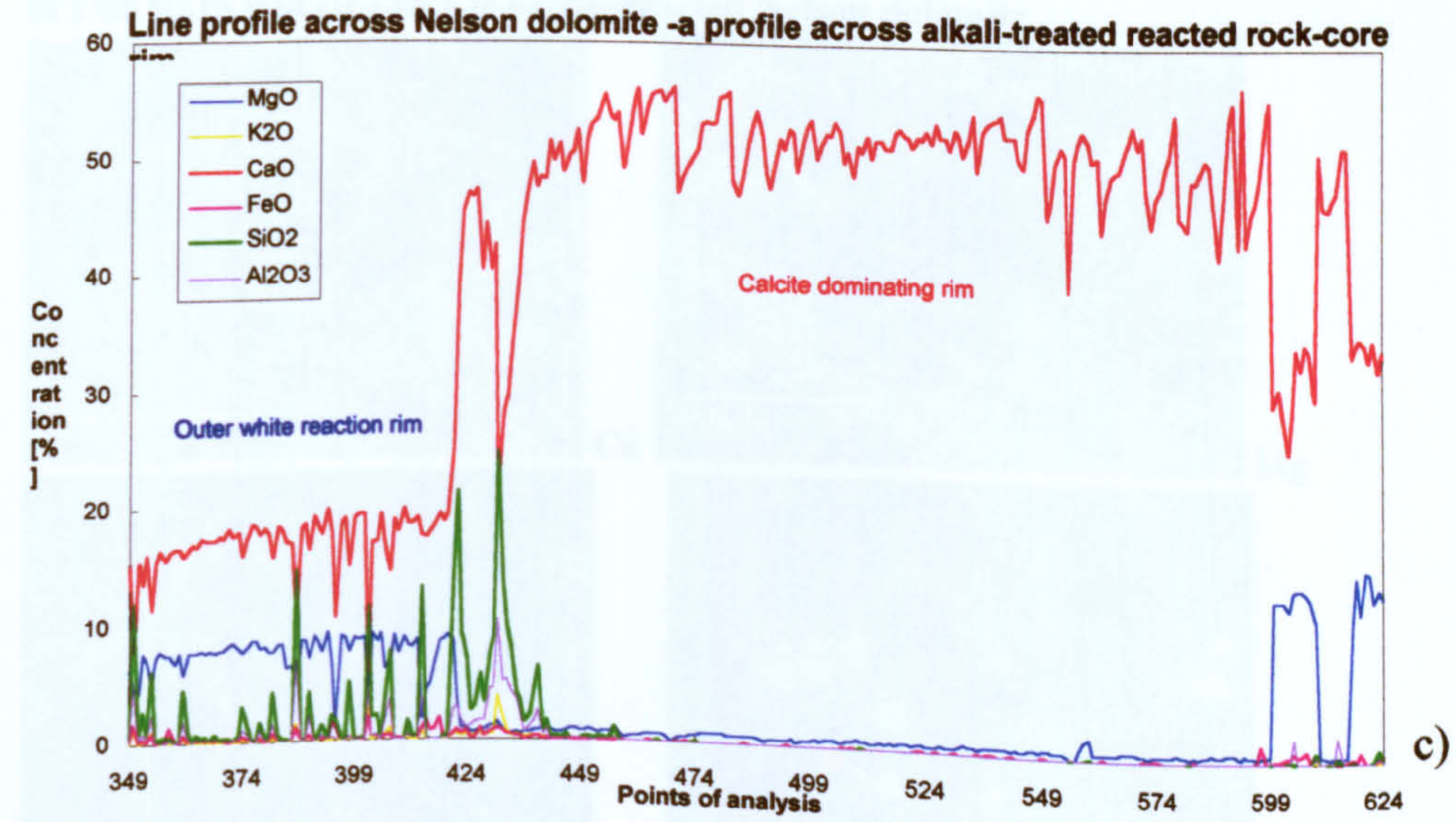

c)

Figure 6.15 EPMA line profile analysis of alkali treated semi-expansive Nelson dolomite, showing that reacted rim is composed of mainly Ca and some Mg-rich phases (calcite and brucite).

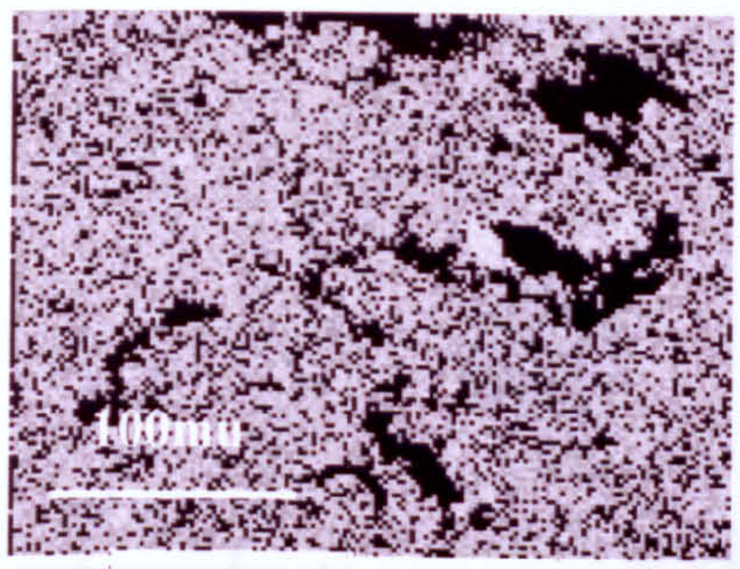

Cal

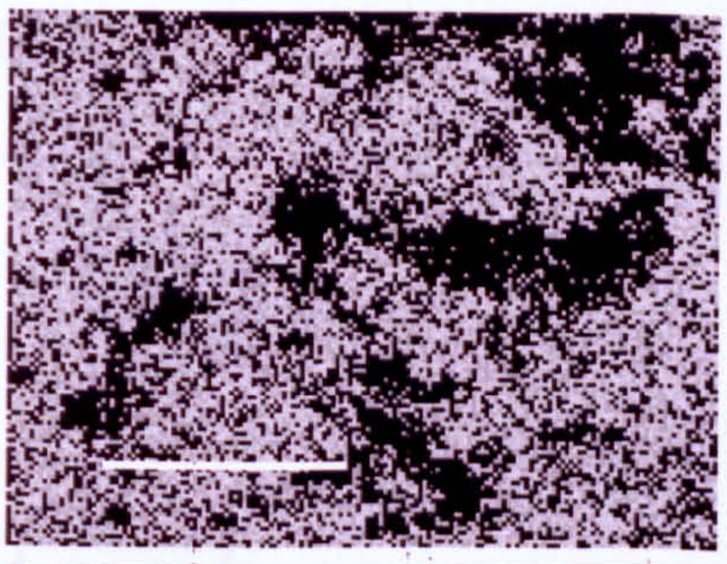

Mg

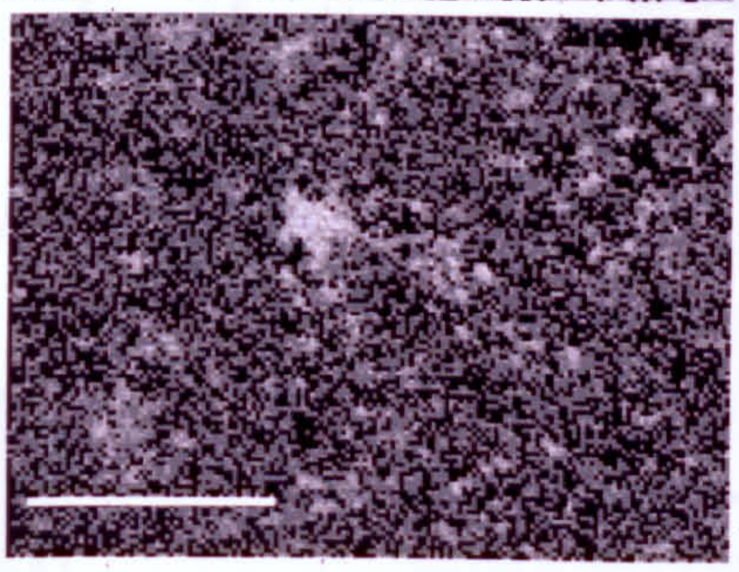

Na

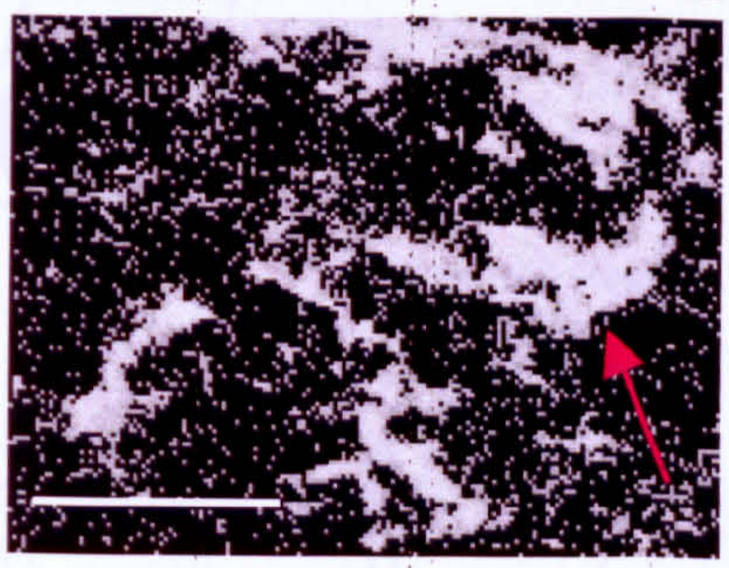

Si (Si-rich phases)

SET OF MAPS FOR Figure 6.16 a of unaltered Nelson dolomite

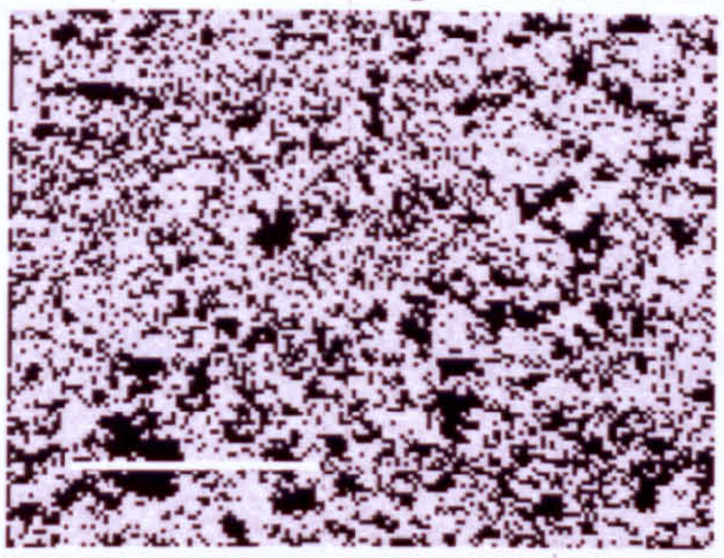

Ca

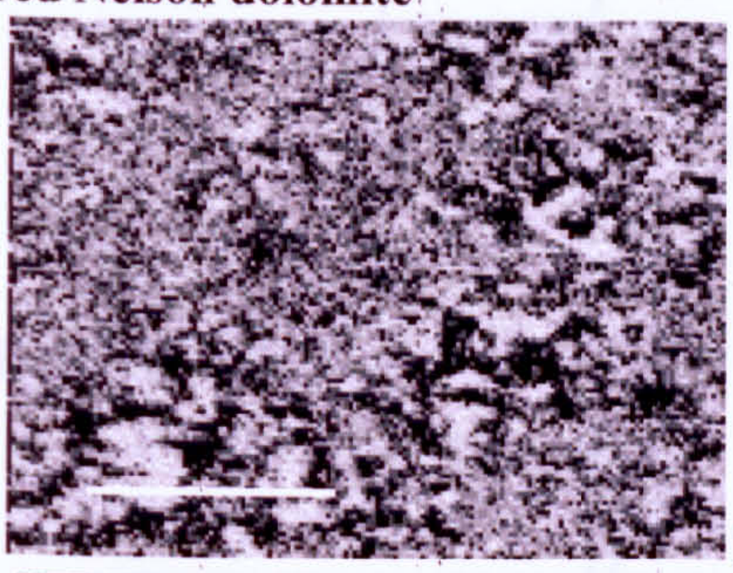

Mg

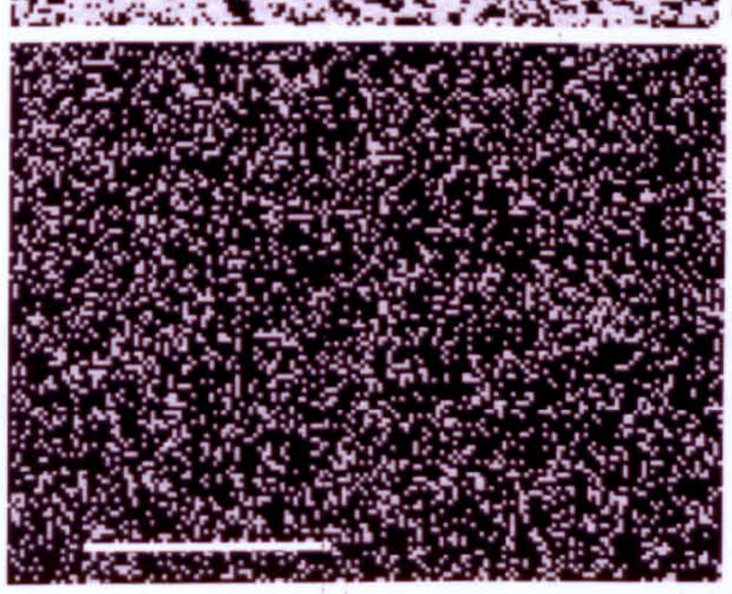

Na

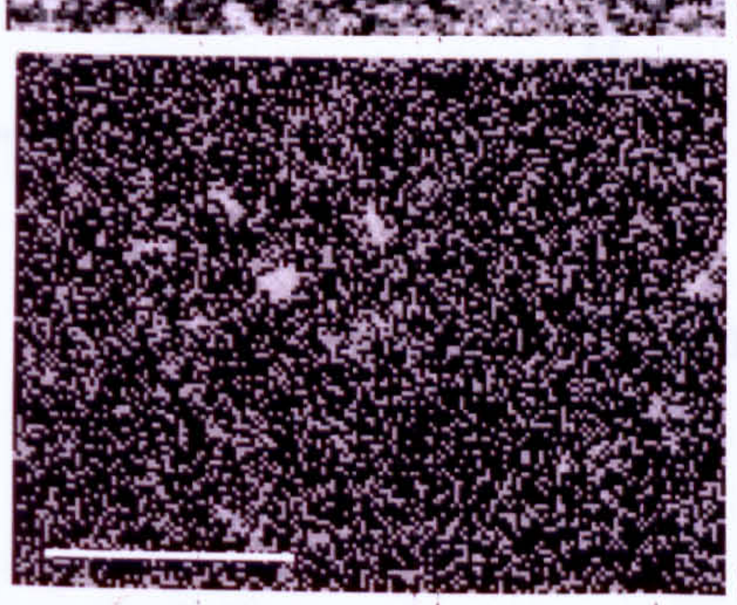

Si (lack of Si-phase)

SET OF MAPS FOR FIGURE 6.16 b semi-reacted Nelson dolomite

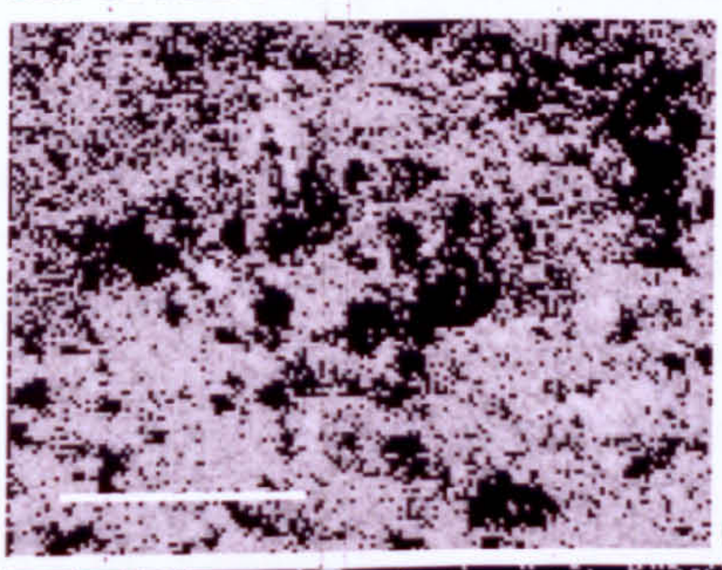

Ca

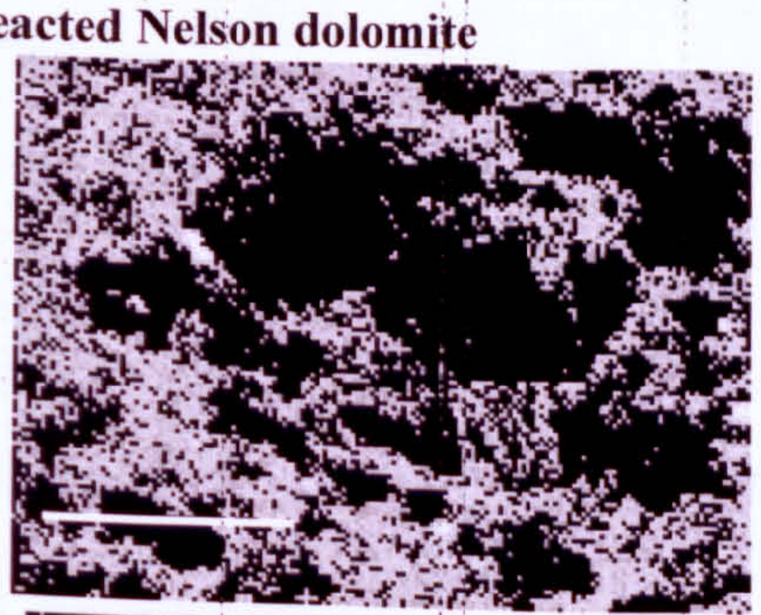

Mg

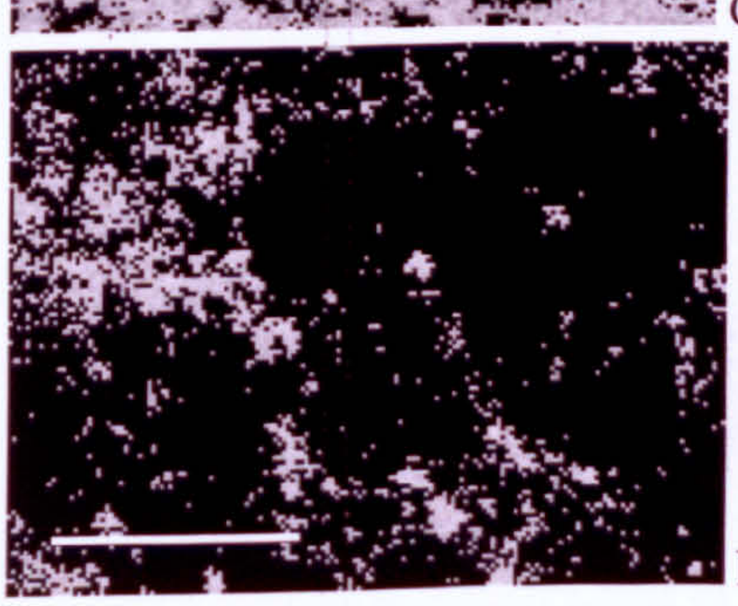

Na

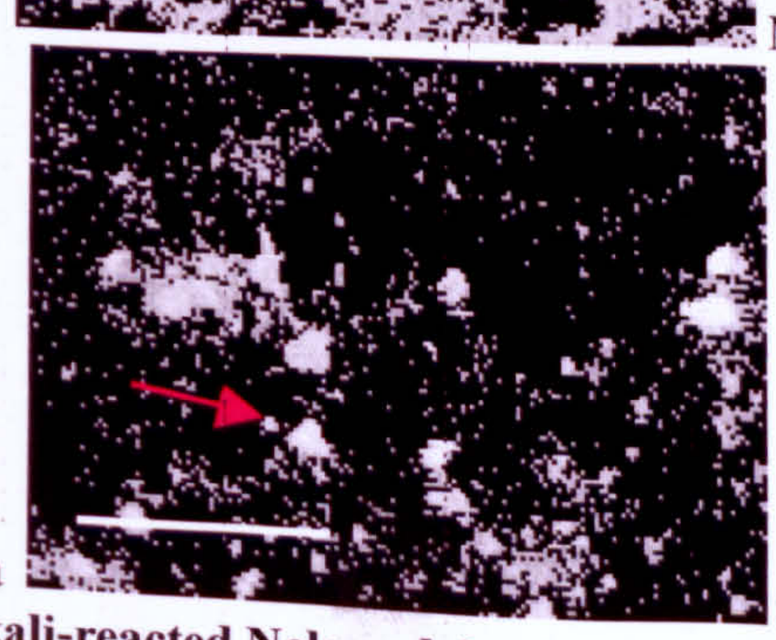

Si (only quartz)

SET OF MAPS FOR FIGURE 6.16 c for alkali-reacted Nelson dolomite

Figure 6.16 EPMA, maps of alkali treated Nelson dolomite rock.

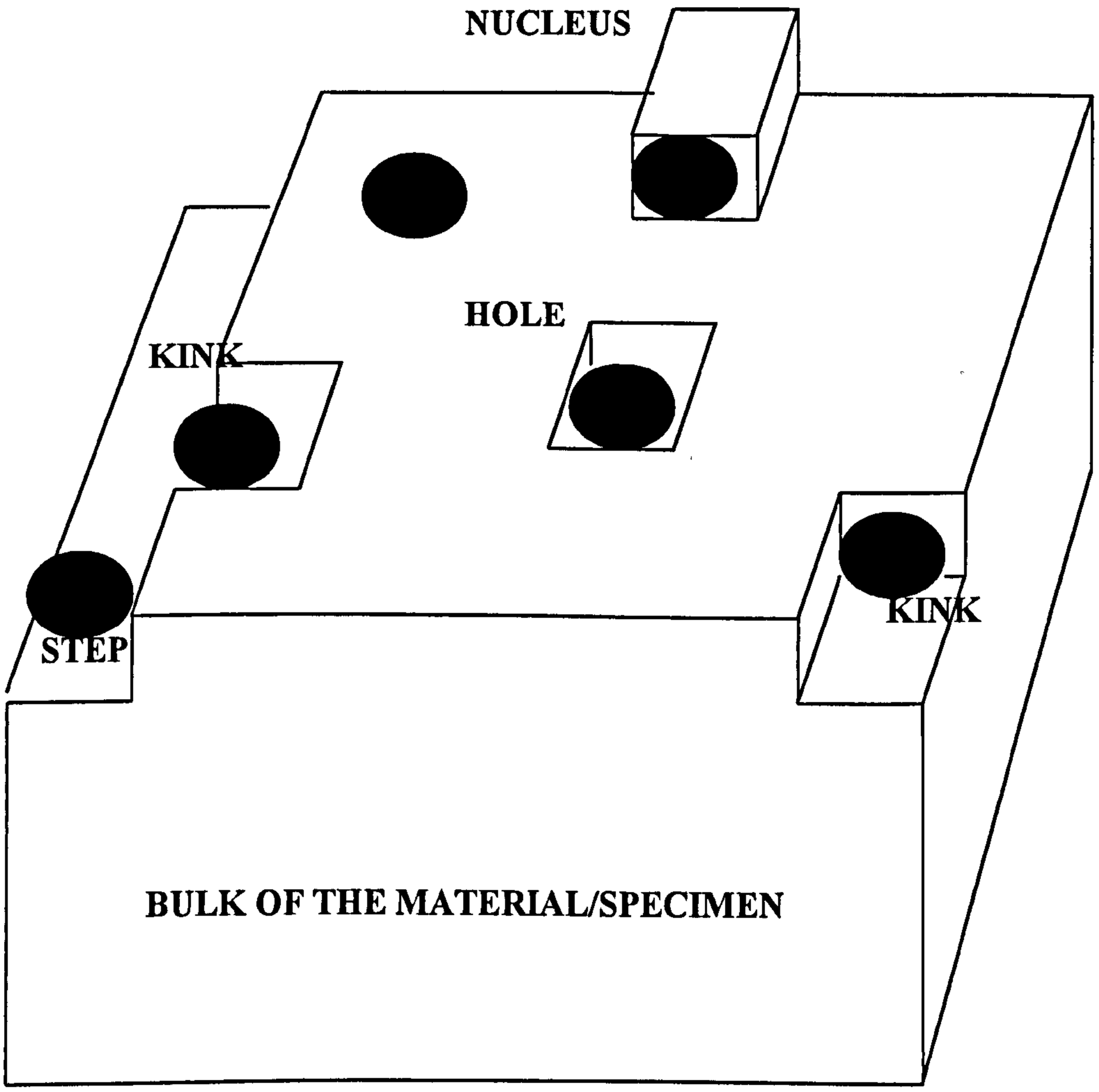

Figure 6.17 BCF model presenting a surface that posses different types of surface sites (step, kink, hole, nucleus) with adsorbed ions, after Burton, Cabrrera and Frank.

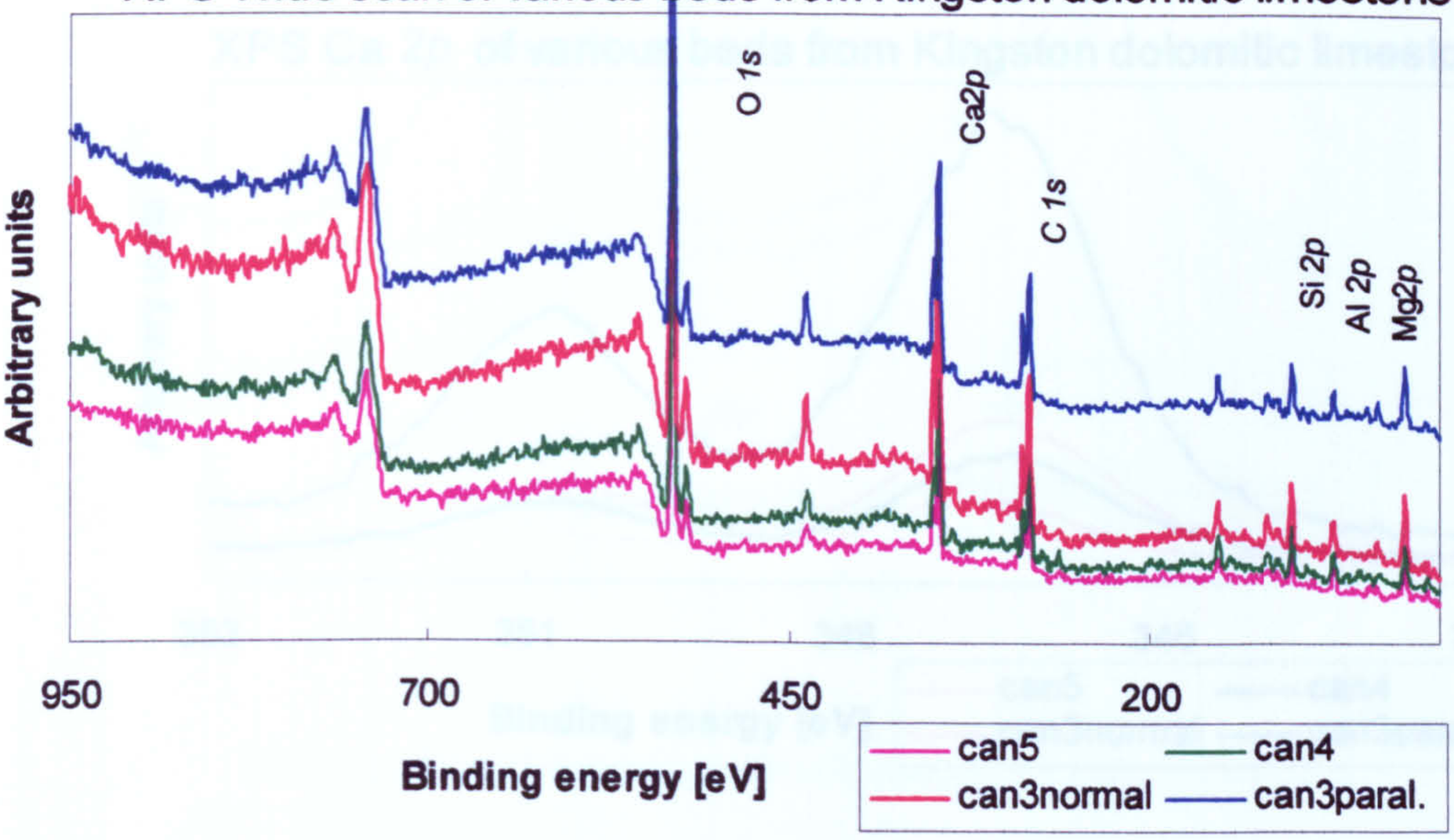
XPS Wide scan of various beds from Kingston dolomitic limestone
Arbitrary units
O 1s
Ca2p
C 1s
Si 2p
Al 2p
Mg2p
950
700
450
200
Binding energy [eV]
can5
can4
can3normal
can3paral.

a)

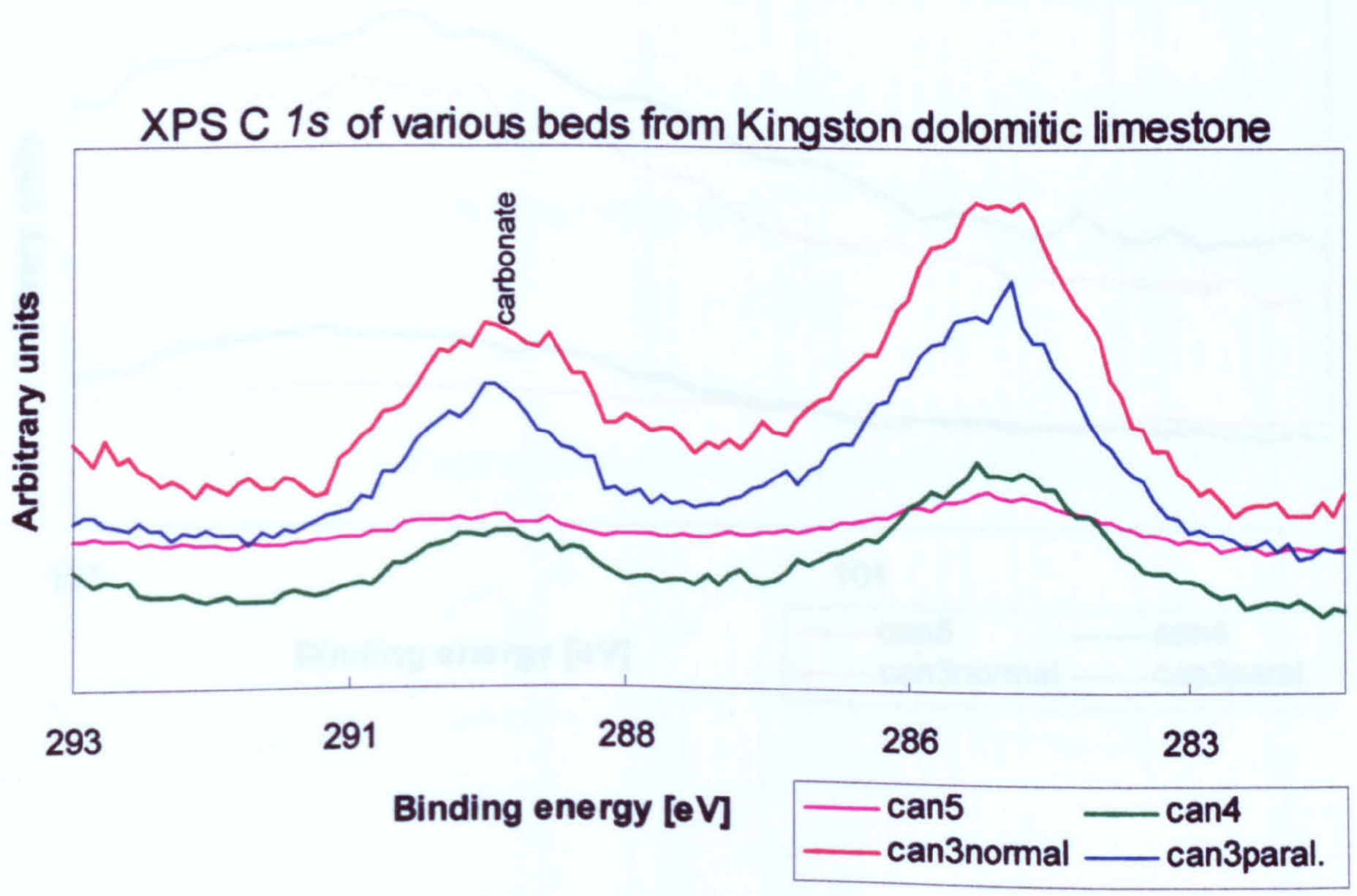
XPS C 1s of various beds from Kingston dolomitic limestone
Arbitrary units
carbonate
293
291
288
286
283
Binding energy [eV]
can5
can4
can3normal
can3paral.

b)

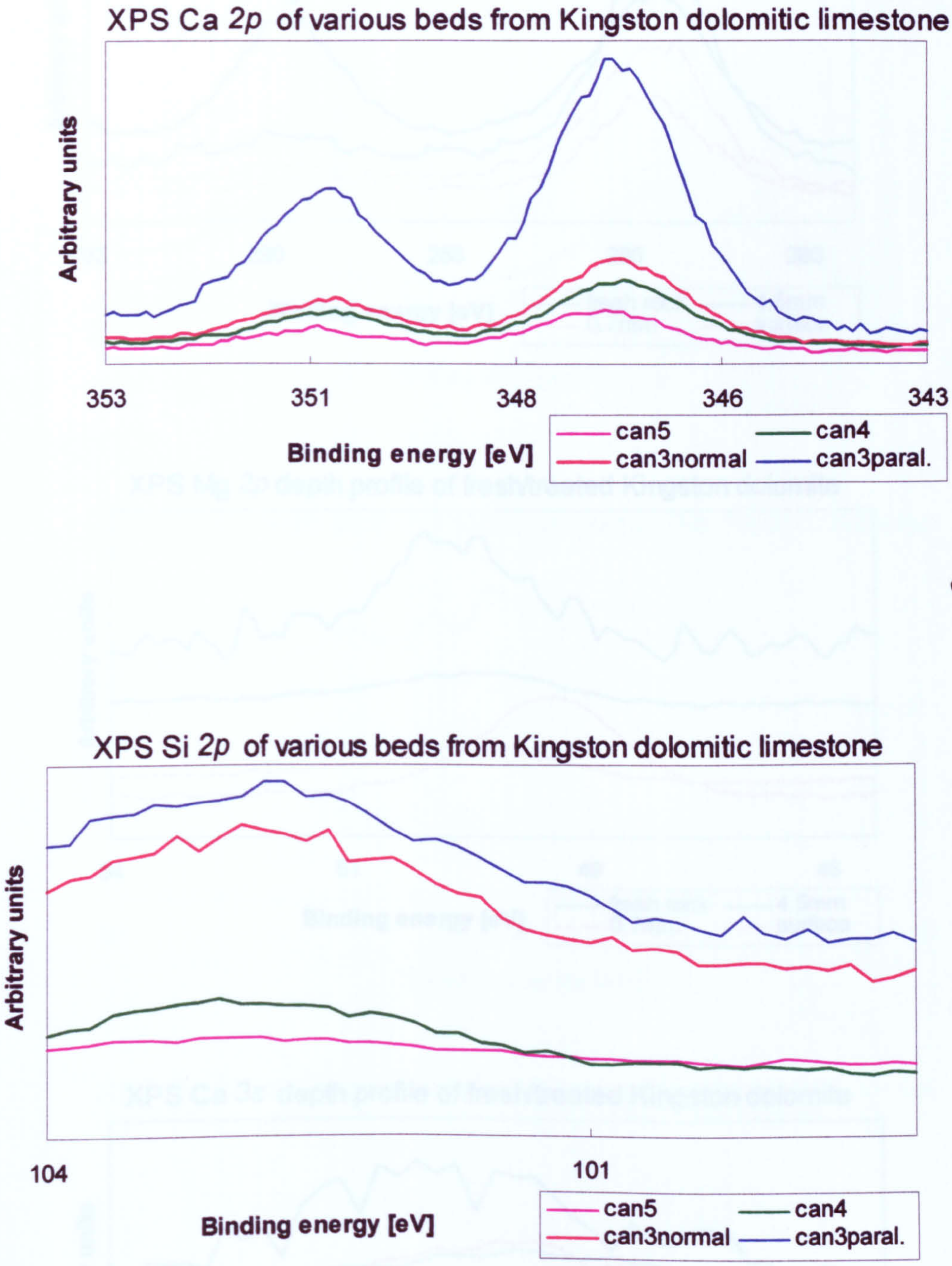

Figure 6.18 XPS spectra of alkali-induced changes in Kingston dolomite rock-cores from various beds of Pittsburgh Quarry. As can be observed there are no differences in chemical state of main elements in expansive and non-expansive samples for cores drilled parallel to the bedding and perpendicular to it.

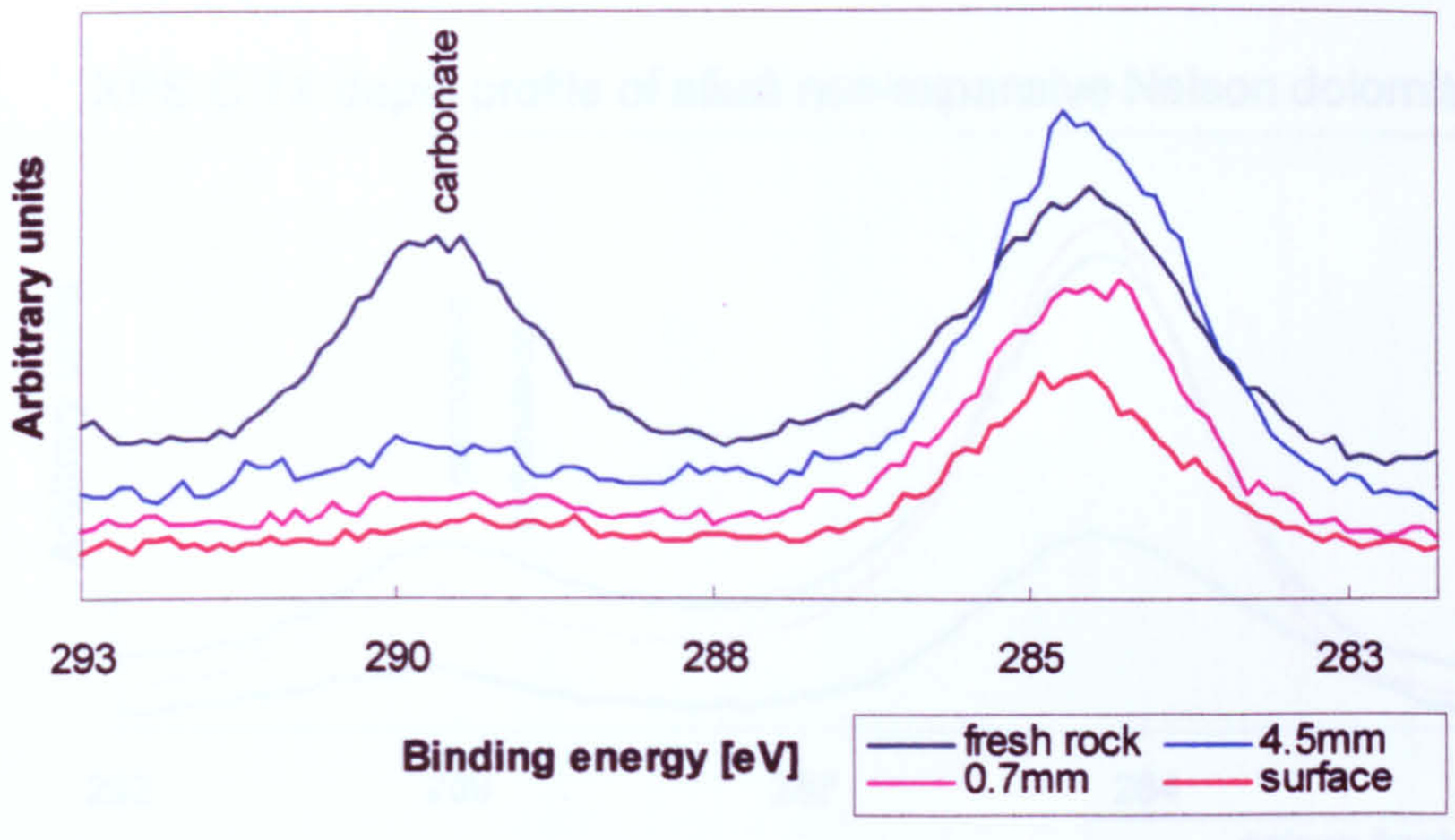

a)

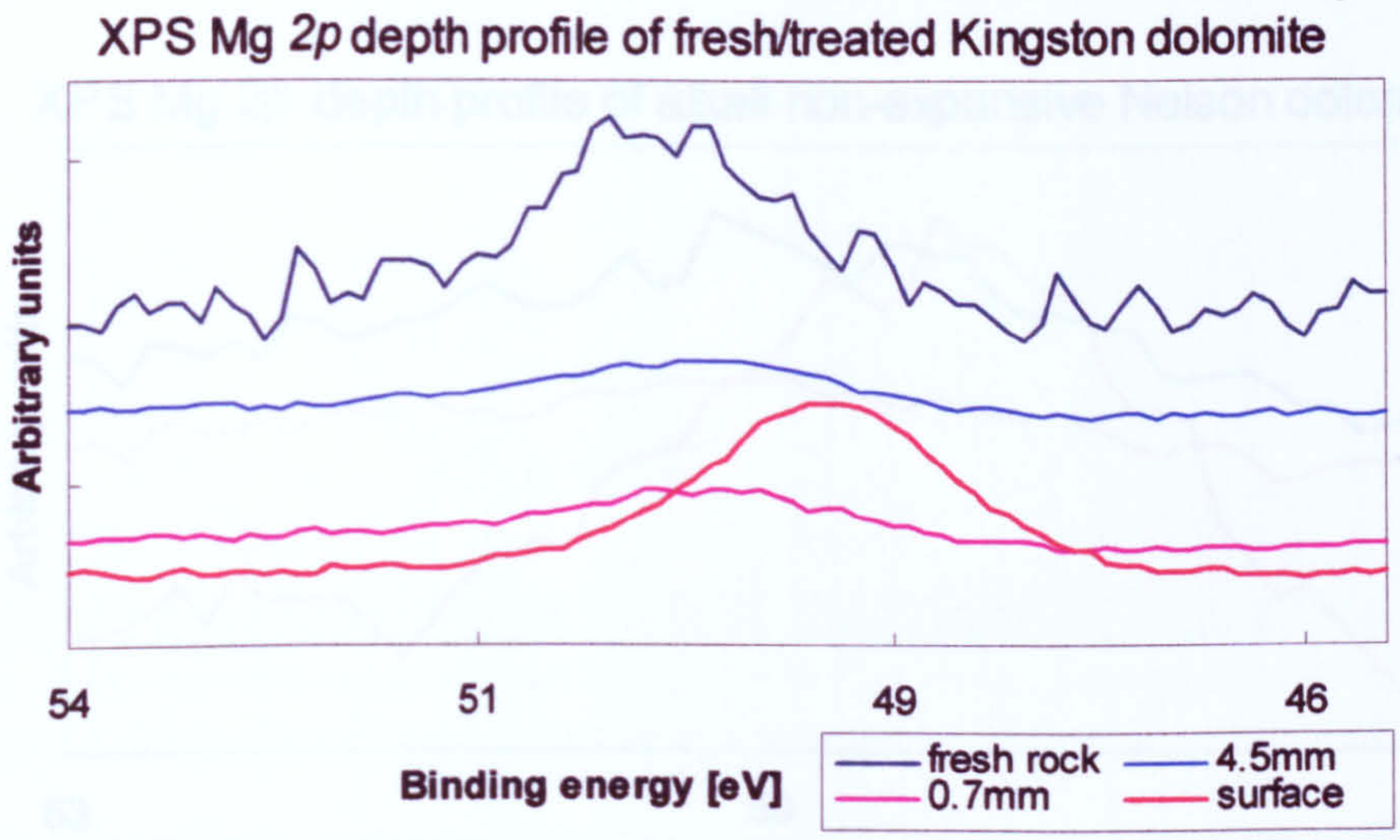

b)

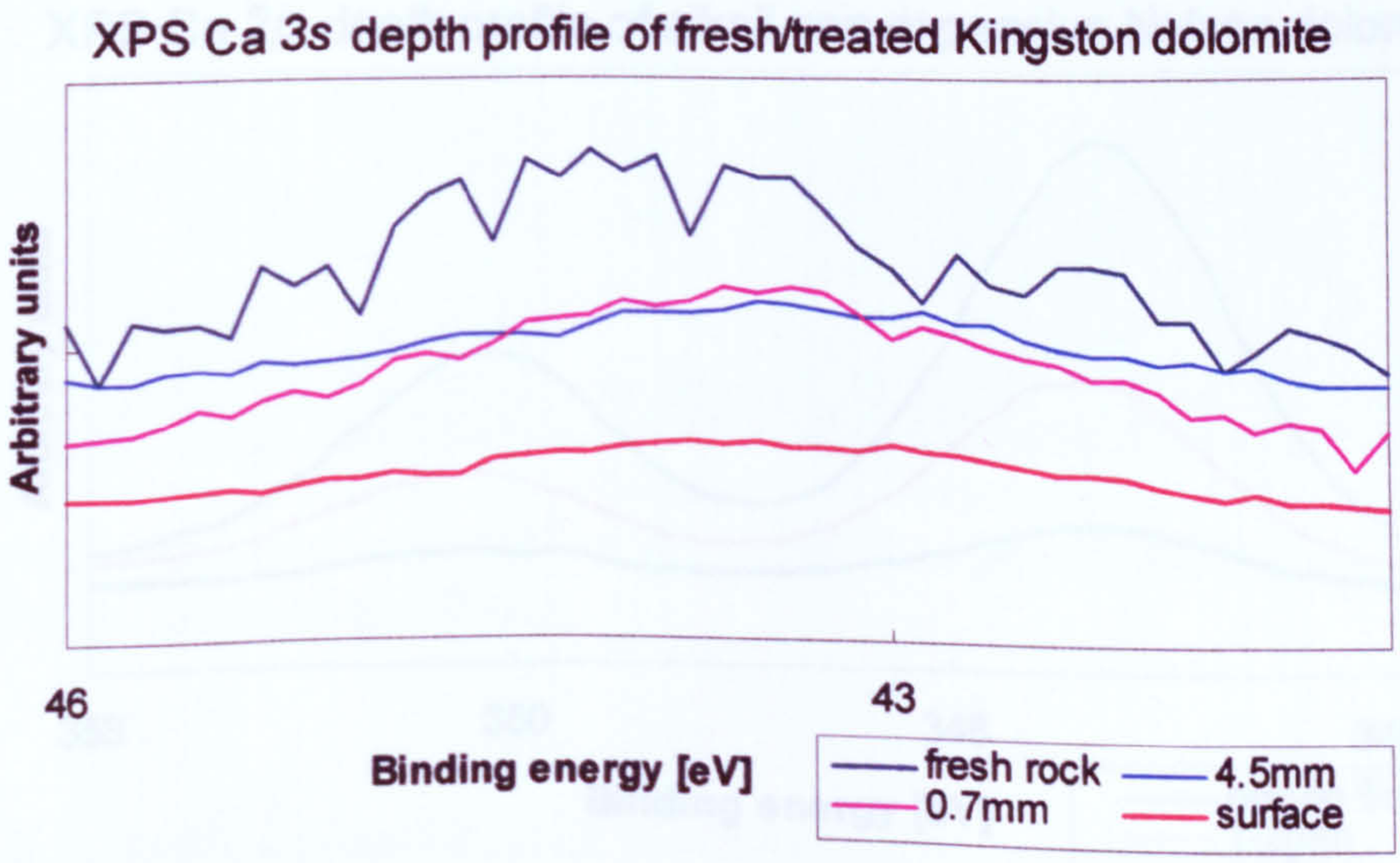

c)

Figure 6.19 XPS spectra of depth profile across rock-core, showing the change of chemical states of the elements present, induced by alkaline treatment.

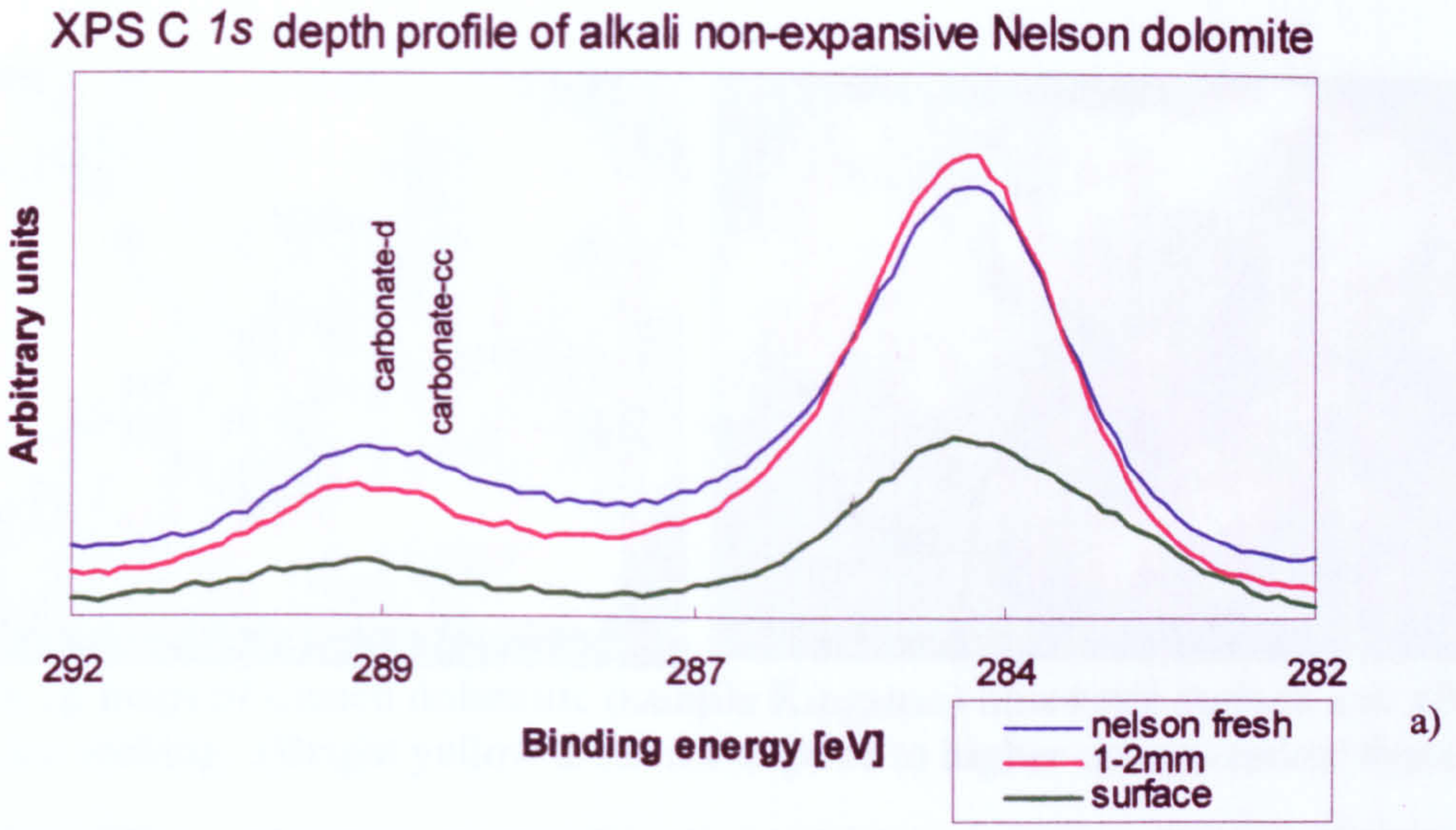

a)

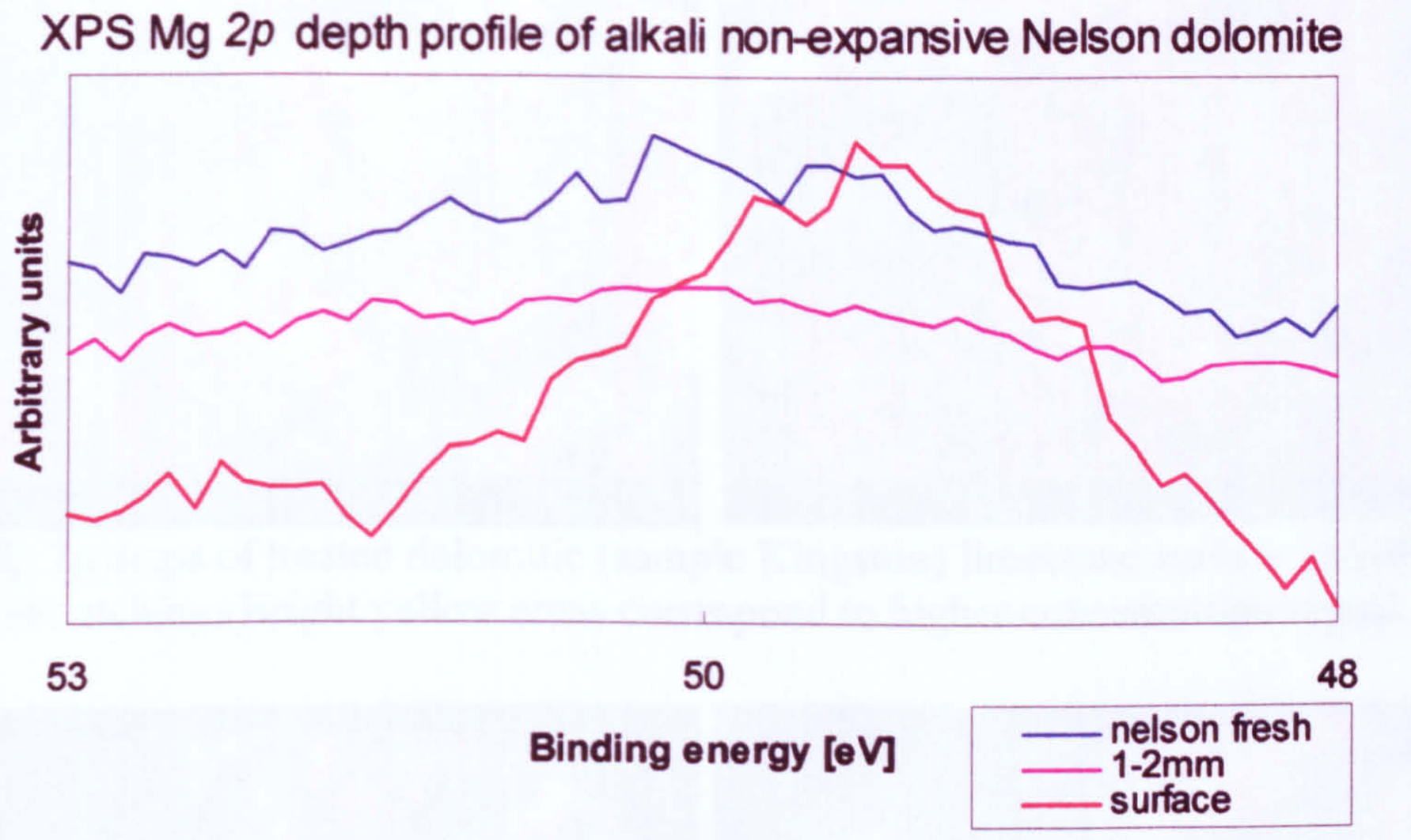

b

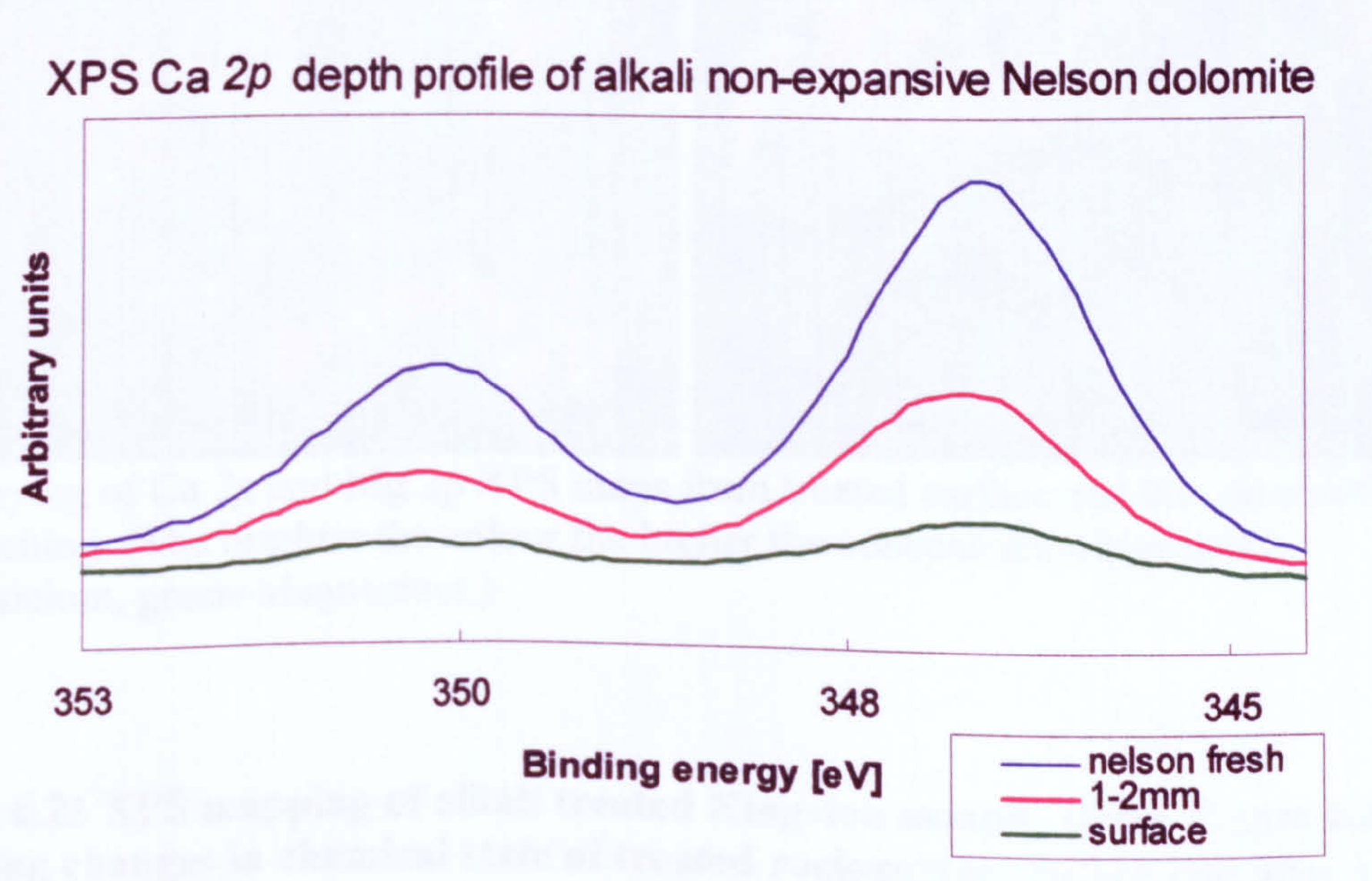

c)

Figure 6.20 XPS spectra for alkali treated Nelson dolomite (depth profile).

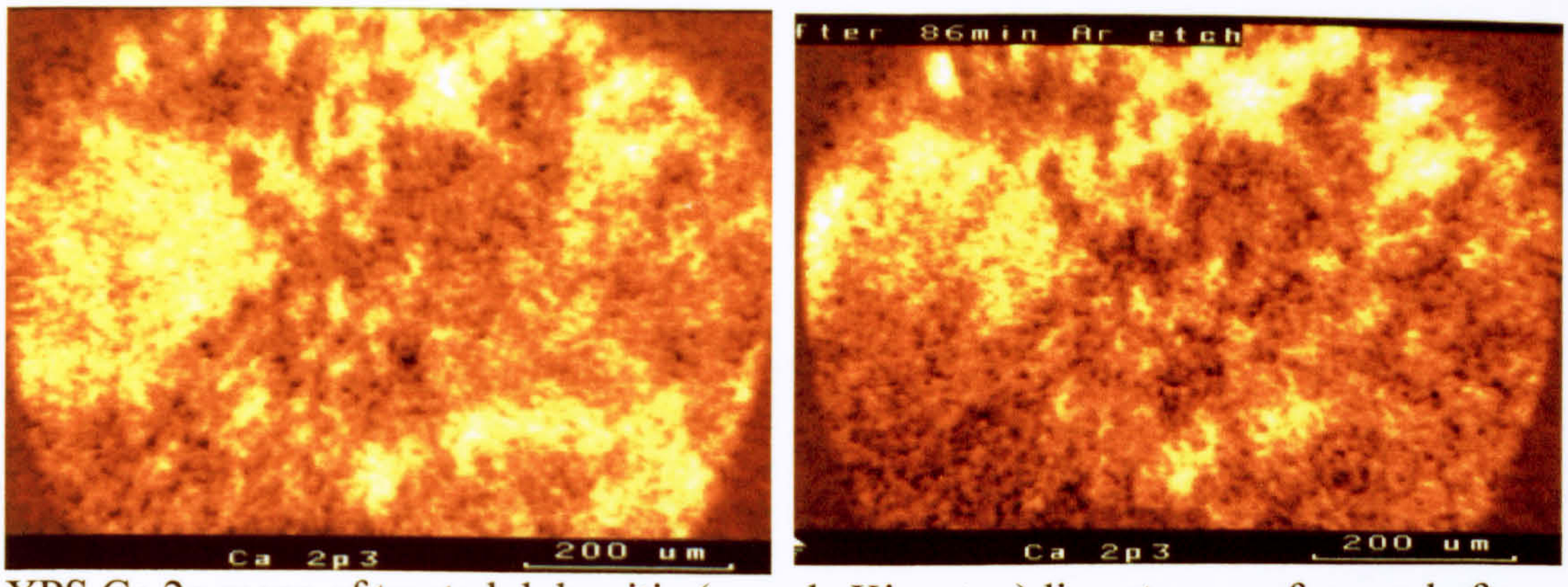

XPS Ca 2p maps of treated dolomitic (sample Kingston) limestone surface and after 86min ion etching. .(Bright yellow areas correspond to higher concentration/signal.)

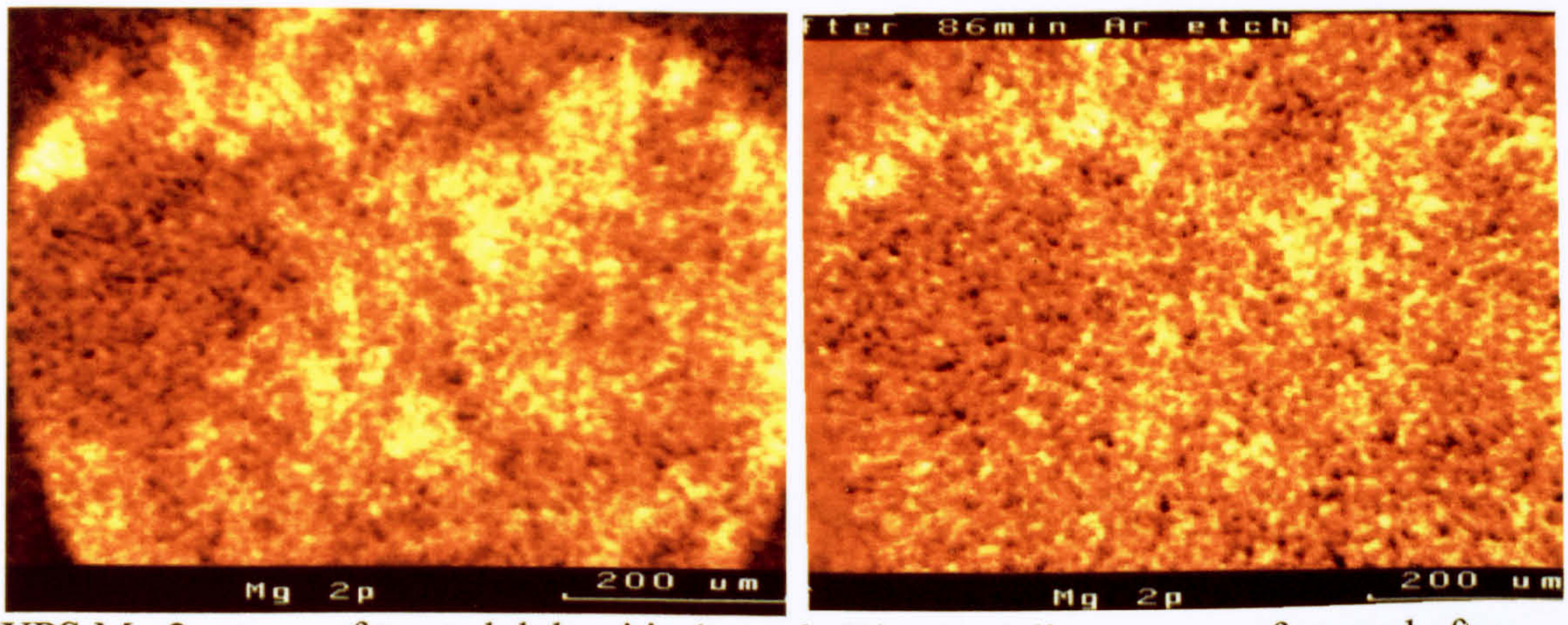

XPS Mg 2p maps of treated dolomitic (sample Kingston) limestone surface and after 86min ion etching.(Bright yellow areas correspond to higher concentration/signal.)

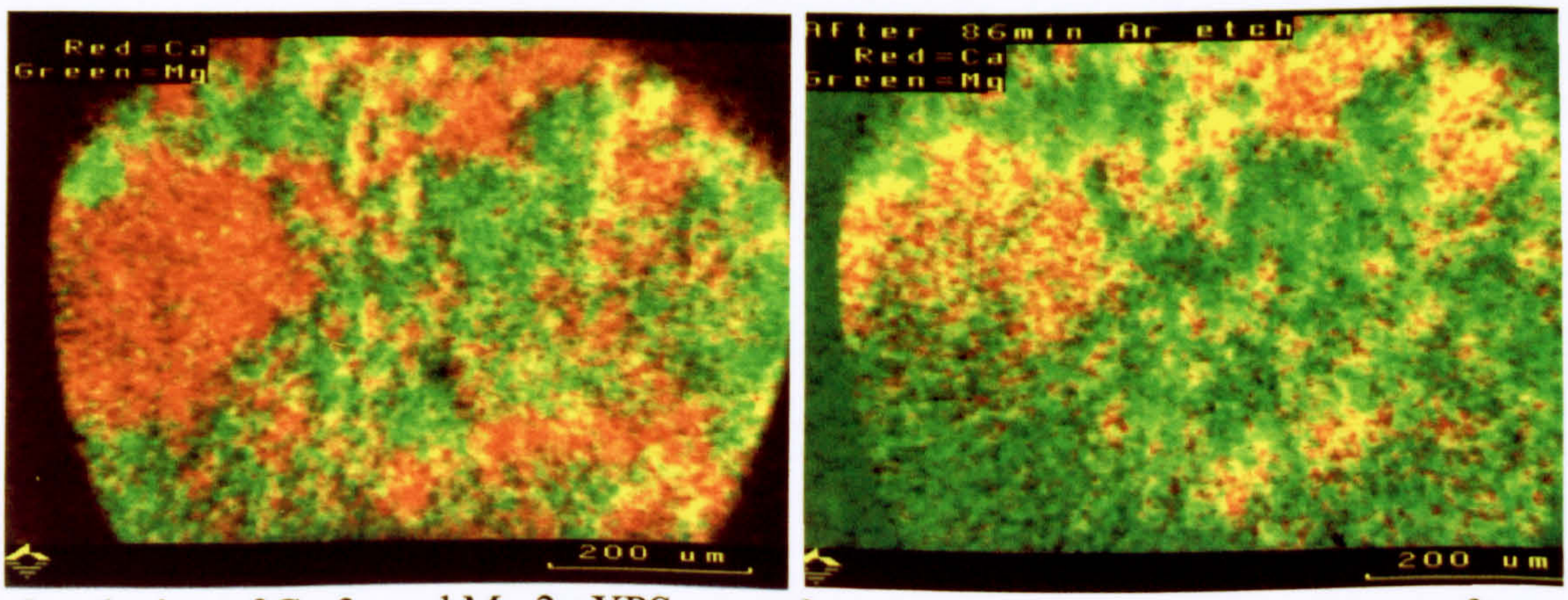

Overlaying of Ca *2p* and Mg 2p XPS maps from treated surface and the same surface after etching. (The brighter the colour the higher the concentration/signal is.) (red-Calcium, green-Magnesium.)

Figure 6.21 XPS mapping of alkali treated Kingston sample, (from Figure 6.20) revealing changes in chemical state of treated rock-surface before and after ion etching.

Single element maps showing the abundance of Ca, Mg, Si and Fe, yellow-high conc.

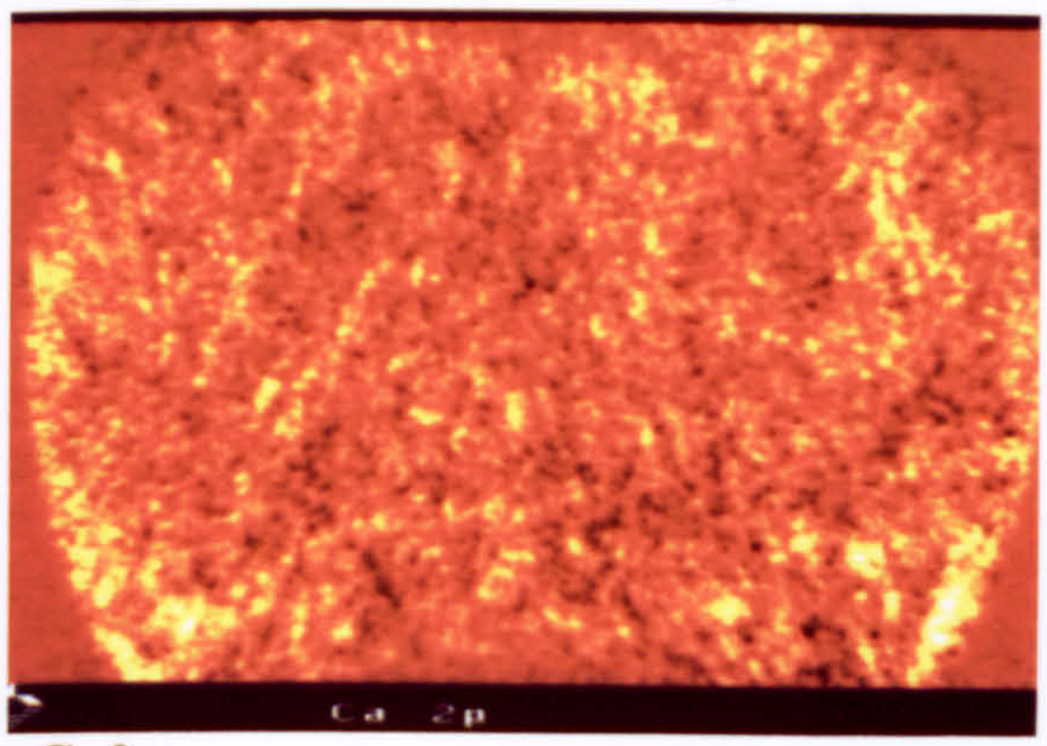

Ca2*p*

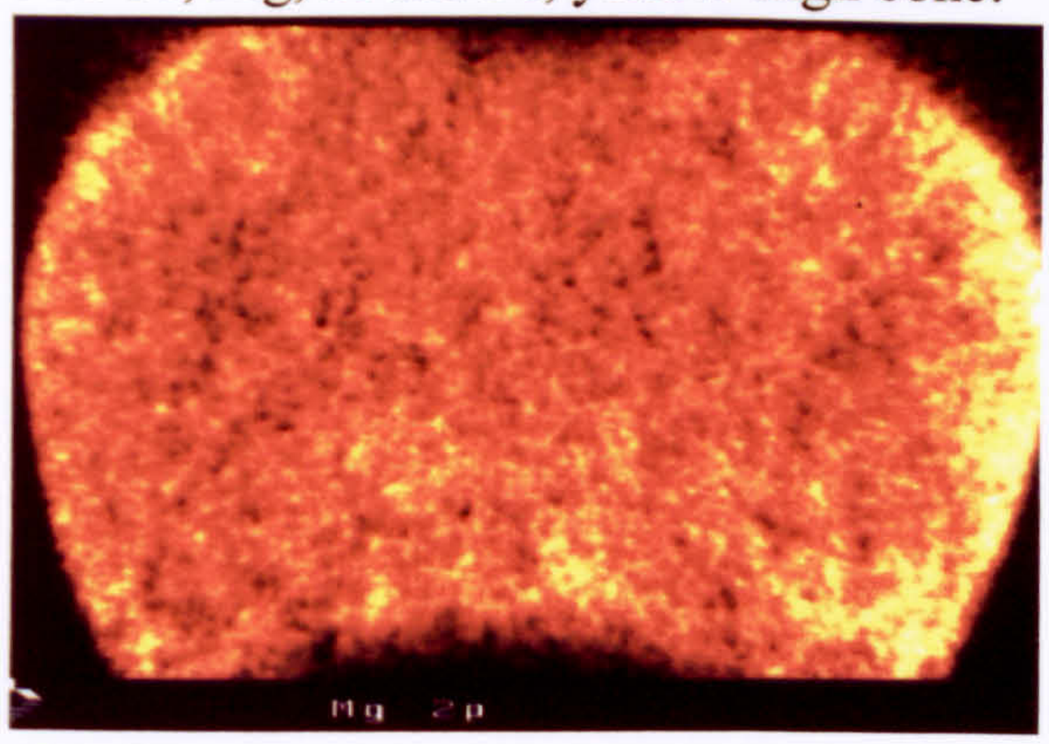

Mg2*p*

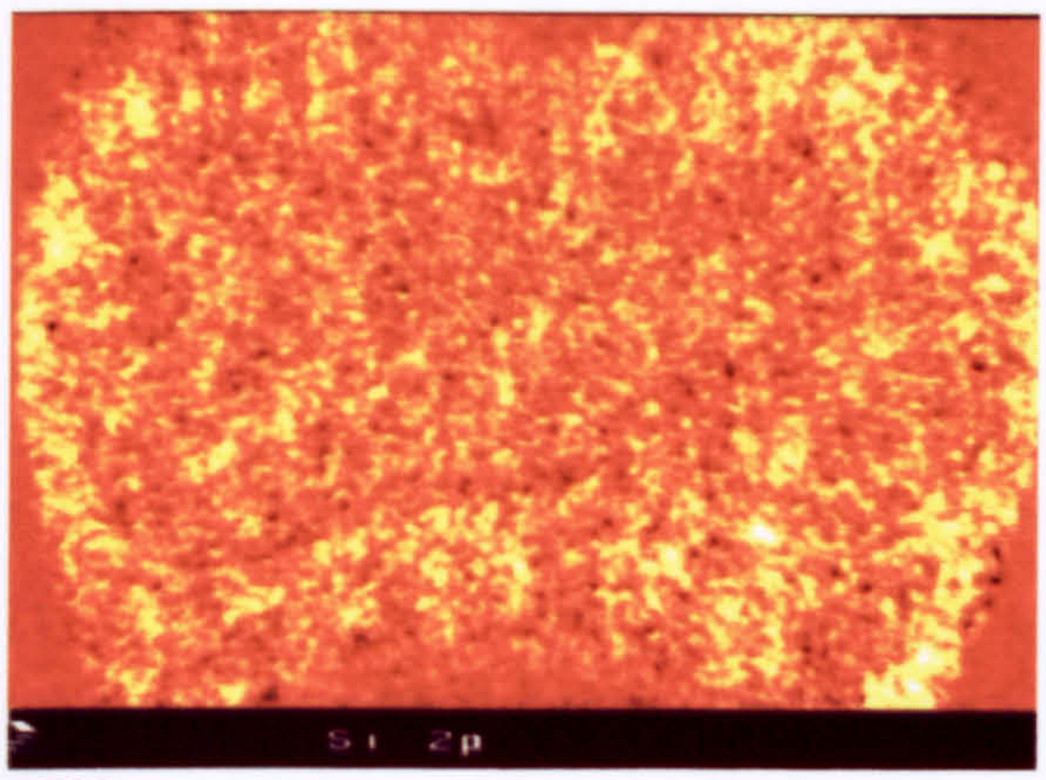

Si2*p*

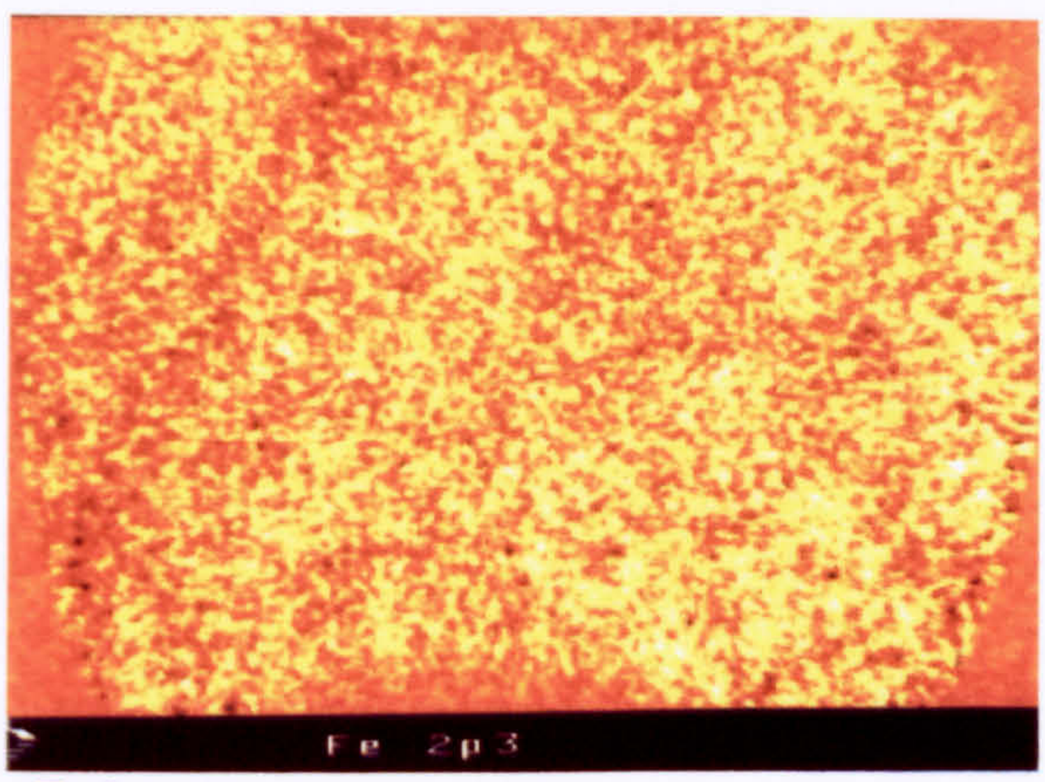

Fe2*p*

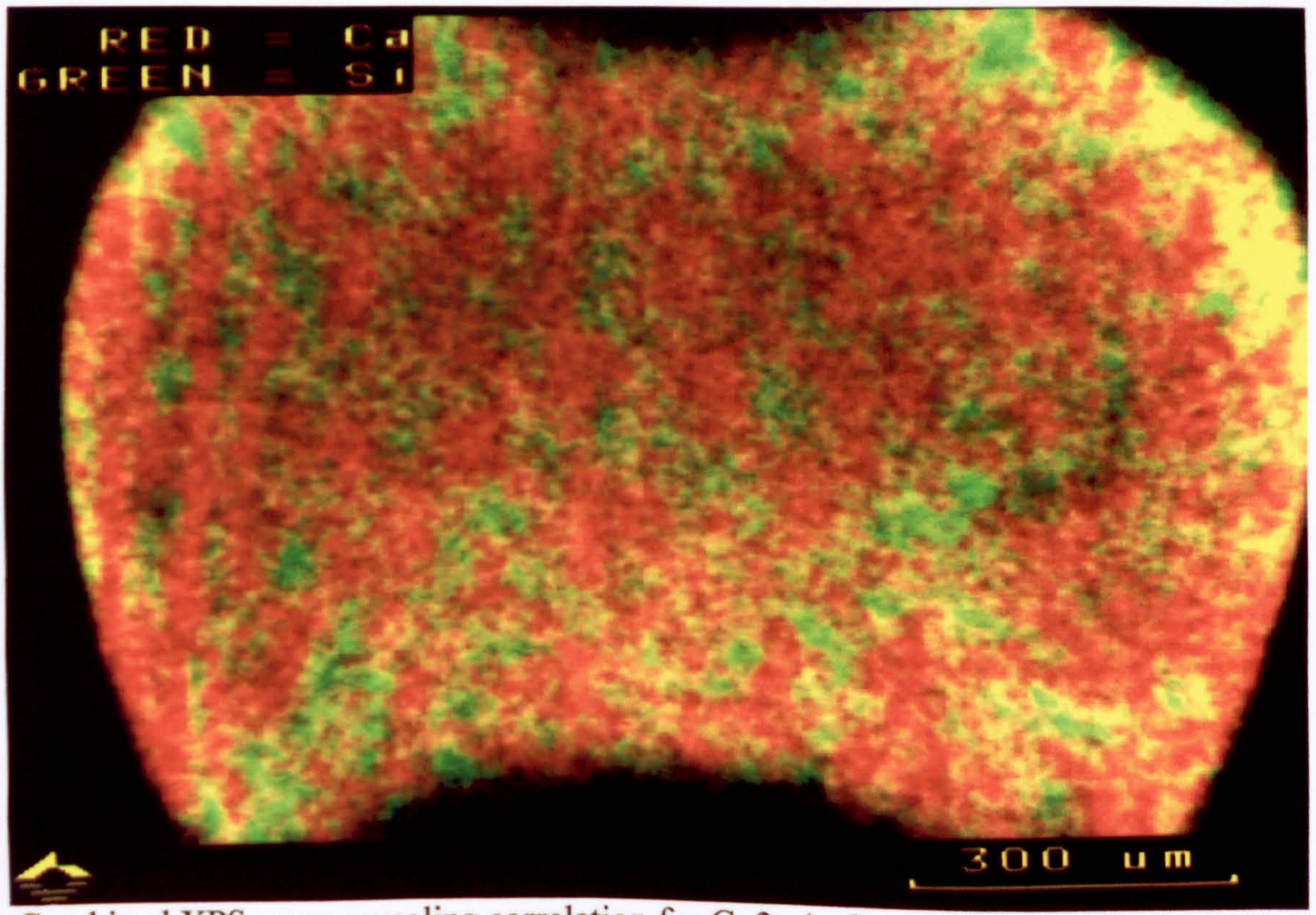

Combined XPS maps revealing correlation for Ca2*p* (red) and Si2*p* (green) distribution

Figure 6.22 XPS maps revealing the change in chemistry of a rock-tablet of Kingston dolomite immersed in 1N NaOH solution.

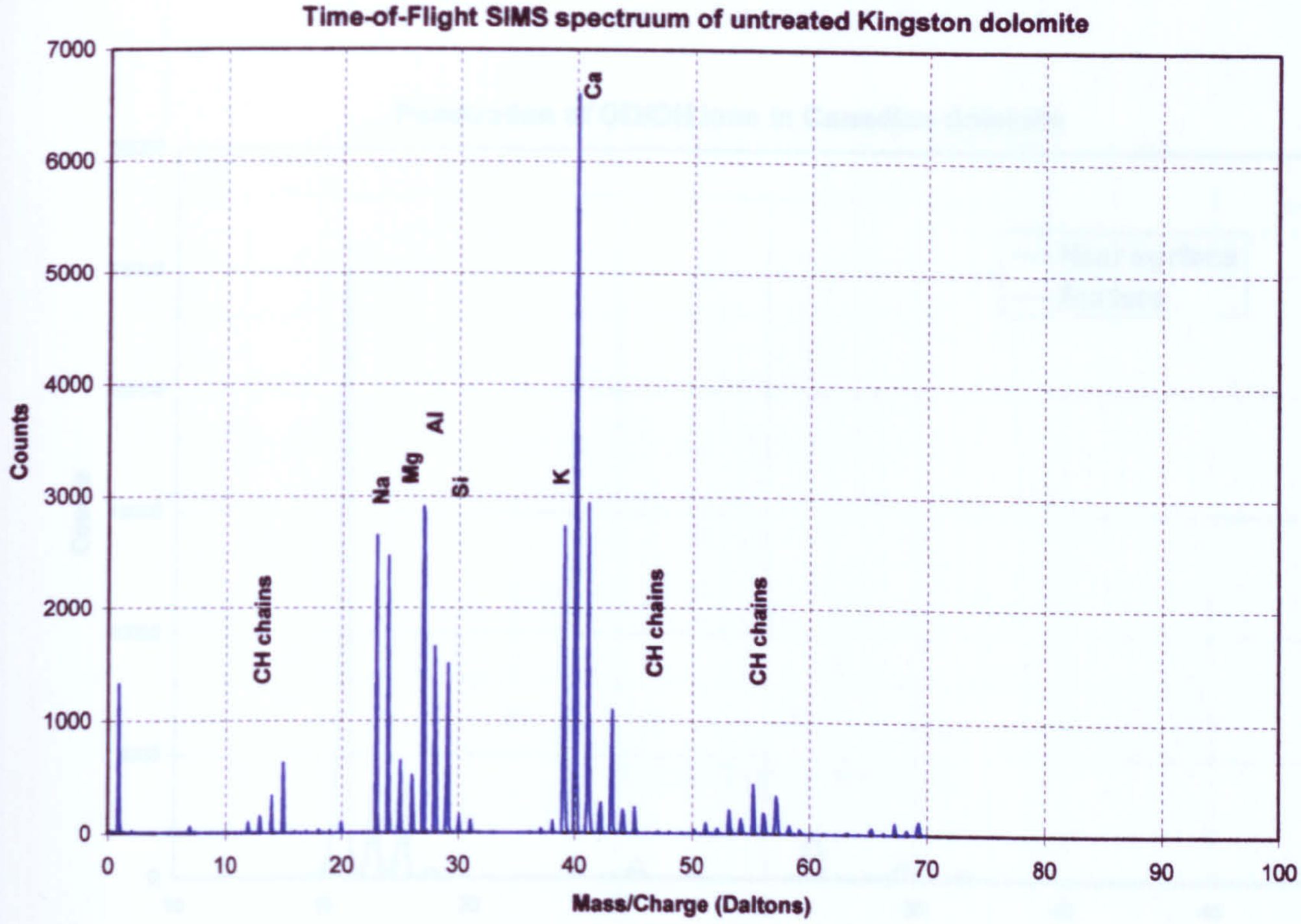

Figure 6.23 TOF-SIMS spectra of untreated Kingston dolomite from different samples.

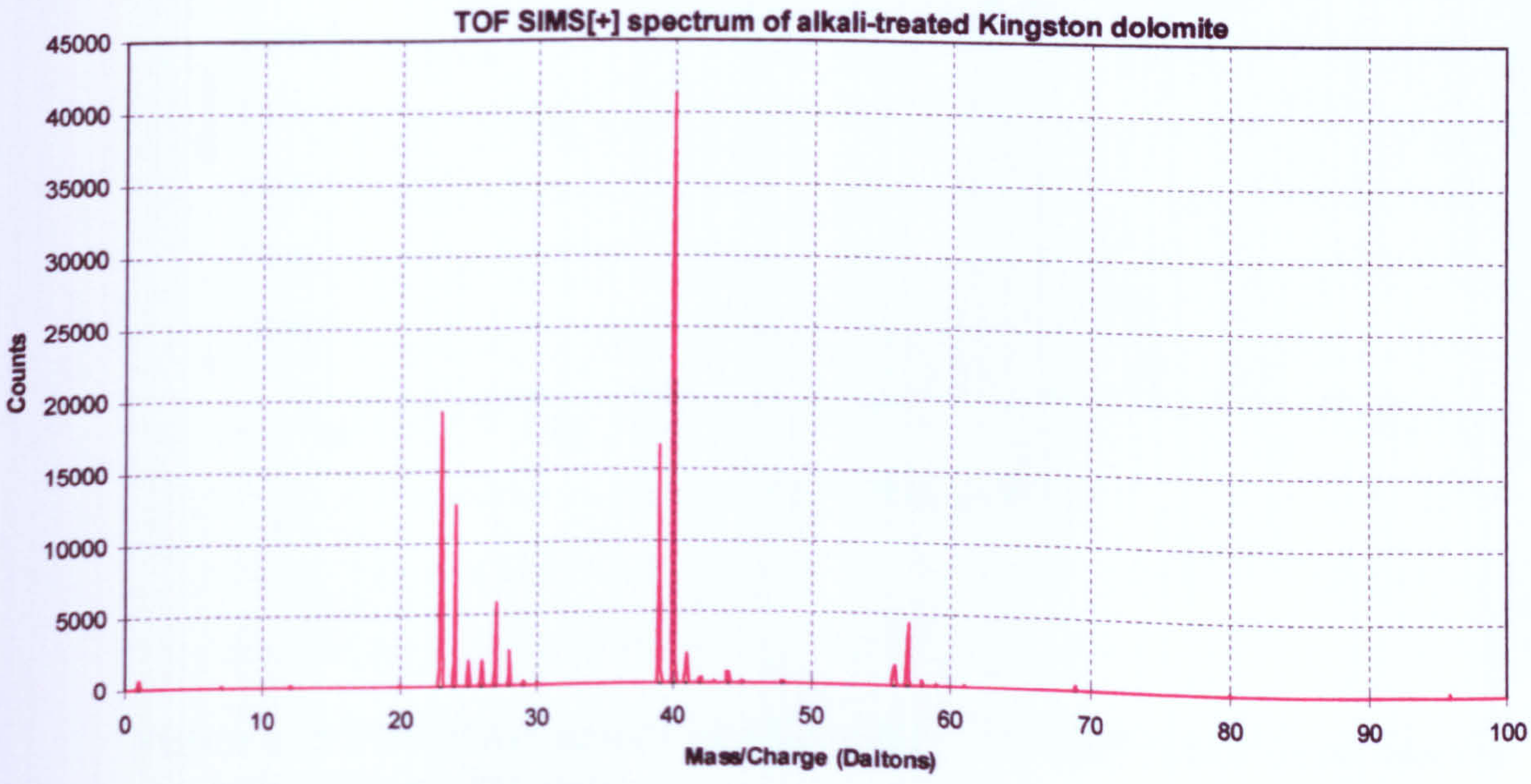

Figure 6.23 TOF-SIMS spectra of alkali-treated Kingston dolomite.

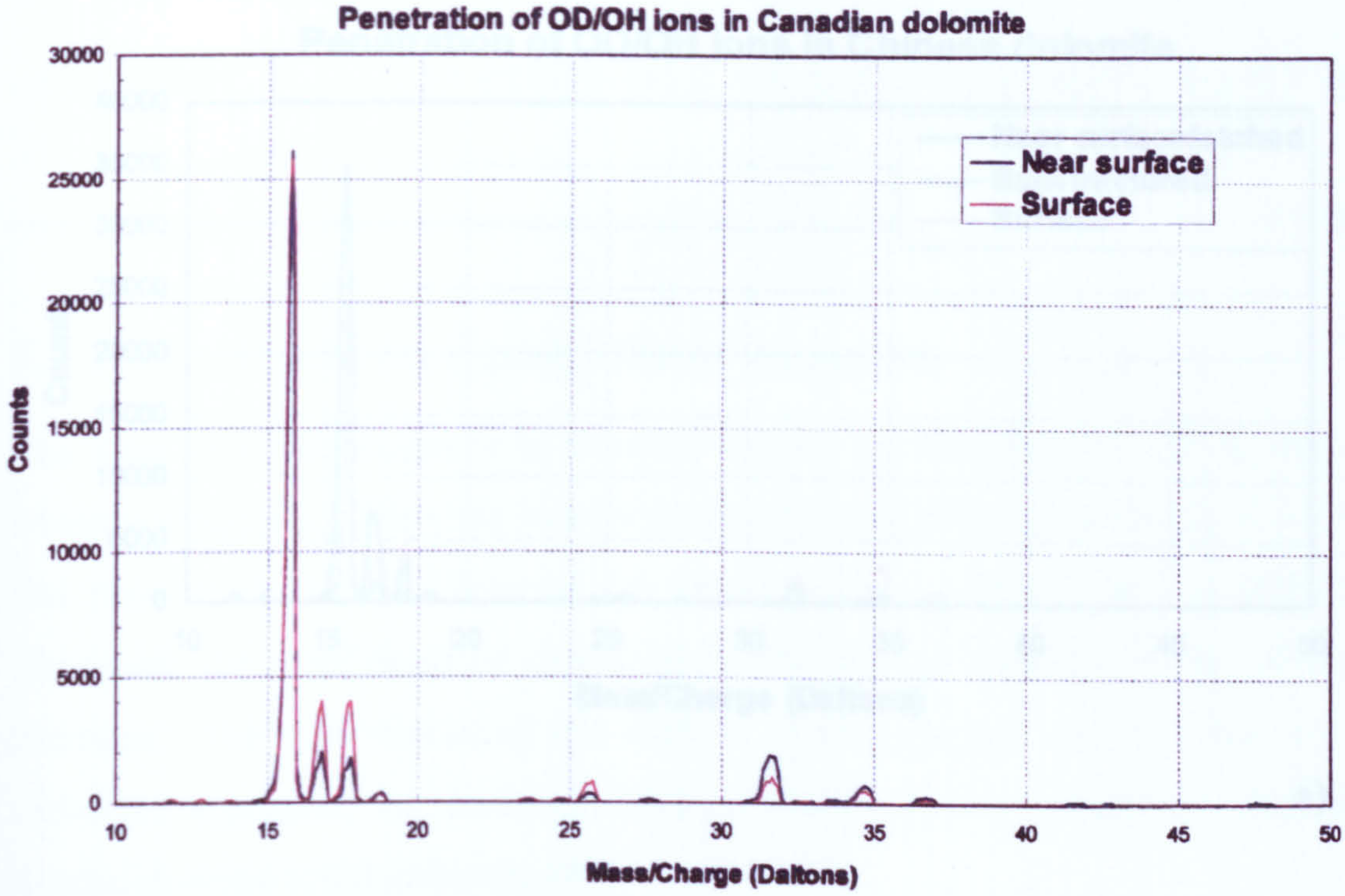

Figure 6.24 TOF-SIMS spectra for detection of the penetration level of OD^- ions into the Kingston dolomitic limestone. It also demonstrates the effect of porosity of the carbonate rock on its susceptibility to ACR.
(Peaks positions of O=16, OH^-=17 and OD^-=18)

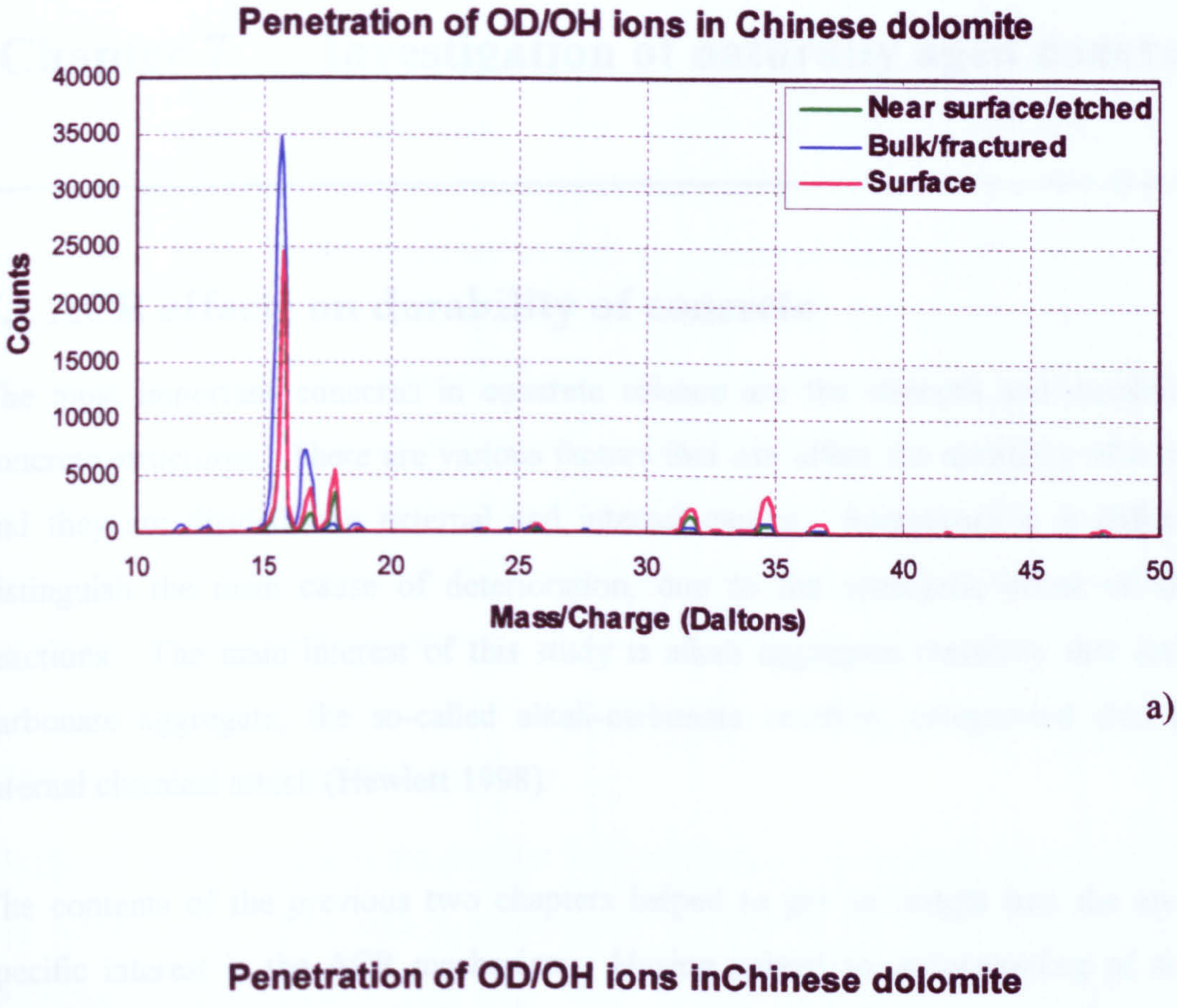

Figure 6.25 TOF-SIMS spectra revealing the level of OD^- penetration into the expansive Chinese dolomite.
(Peak positions: O=16, OH^-=17 and OD^-=18)

Chapter 7 Investigation of naturally aged concrete

7.1 ACR effects on durability of concrete

The most important concerns in concrete science are the strength and durability of concrete structures. There are various factors that can affect the durability of concrete and they are divided into external and internal causes. Sometimes it is difficult to distinguish the main cause of deterioration, due to the synergetic effect of several reactions. The main interest of this study is alkali aggregate reactivity that involves carbonate aggregate, the so-called alkali-carbonate reaction, categorised also as an internal chemical attack (Hewlett 1998).

The contents of the previous two chapters helped to get an insight into the areas of specific interest in the ACR mechanism. Having gained an understanding of simpler systems in mineral/solution and rock/solution reactions, will help in the identification and differentiation between various reactions and their products in concrete, which is a complex material. The characterisation of ACR rims developed around aggregate particles in concrete affected by this reaction has been reported by various researchers, from observations of thin sections under an optical microscope to more advanced SEM and EPMA studies (Gillott 1995). In section two of this chapter, results obtained in this study and their correlation with present-day knowledge are presented, with the additional expansion into a novel field of the environmental scanning microscopy. Sample preparation plays a vital role in obtaining an accurate and clear understanding of chemical and physical processes in a multi-component material such as concrete, especially because of the different hardness of various components. The complementation of observations from fractured and polished surfaces provided data on the internal microstructure, which consequently determines mechanical properties of concrete. Secondary phase growth at grain boundaries and within the interfacial transition zones, diffusion of various chemical components such as Si and H_20, which may affect the properties of concrete parallel to any changes in aggregates, were expected to be detected in micro analysis.

7.2 Microscopic observation of fractured concrete surfaces

In order to avoid potential contamination of samples due to polishing, fractured surfaces of concrete samples were observed. These samples also provided microstructural and morphological characterisation of aggregates, bulk cement paste and the transition zone between the two. Freshly fractured as well as weathered surfaces of aggregate grains removed from the concrete were Au or C coated prior to SEM imaging, using SE mode. Although the morphology of fractured surfaces did not allow accurate EDX analysis due to the topological effects, the information was still valuable. The data obtained will be classified based on the location of analysis within the concrete sample, since changes caused by ACR were expected to have had an impact on the aggregate, mainly in the aggregate/cement transition zone.

7.2.1 Aggregate/cement interface

Alkali-aggregate reaction in the simplest form refers to the interaction between aggregate and cement-paste. Therefore it is important to observe the changes at the interface involving these two phases. The importance of the transition zone (TZ) is not only in that of strength and bonding between aggregate and cement, but also because of increased porosity. The latter makes the TZ vulnerable to pore solution migration, as demonstrated by Mehta (1986) in his representation of a TZ in concrete (Figure 7.1a). Another schematic presentation of a TZ using a reinforcing fibre/cement-paste interface was given by Bentur (1986) (Figure 7.1b). The development of a TZ is shown in Figures 7.2 & 3.

The type of bonding between aggregate and cement paste depends on the nature of the rock/aggregate, presence of admixtures in the cement paste, mix design and curing conditions. The influence of each of these factors has been studied, mainly from a strength and durability point of view. One of the aspects is the distribution of water and its impact on the width of a TZ, Zimbelmann (1987) (Figure 7.2). Another important factor in the formation of a TZ is as reported by Scrivenner (1996) related not just to the water but to the grain size and placement of aggregate. Perhaps the most relevant for this study is the role of aggregate on the formation of the TZ. De-bonding zones between different rocks placed in Portland cement paste were observed by Odler and Zurz (1988), from which it was concluded that, with carbonate aggregates, a weak zone developed during cleaving under stress is within the cement paste. Finally, the

importance that admixtures can have on the properties of a TZ, was described by Goldman and Bentur (1989), presented the change in nature of a TZ induced by addition of silica fume to Portland cement, with the development of extra CSH at the boundary with aggregate.

Results

The features described and presented in the diagrams of Figures 7.(1-3) and their manifestation in the study of ACR will be presented in this section of Chapter 7. The SEM images shown in Figure 7.4 taken from a fractured ACR-affected concrete sample (Table 3.3). It reveals a typical TZ with all three components: the aggregate (bottom left), transition zone as labelled and bulk cement paste (top right). As can be observed the fracture plane is through the cement side of the TZ, not at the actual boundary as predicted for carbonate aggregates.

Another important detail is the texture of the TZ (approximately 80-100μm) with clearly oriented grains distinguished from bulk cement by their flaky appearance due to higher porosity (a type of texture seen in metamorphic rocks). Higher magnification SEM images were acquired for more detailed microstructure of the TZ (Figure 7.5a), showing a interface rich in a hexagonal platy crystals, most likely Portlandite according to their crystal habit as well as EDX analysis (Figure 7.5b). The complexity of this very important rim is further illustrated in Figure 7.6. The aggregate side is rich in Na, Mg, Si and Ca, crystals in a form of extrusion from dolomite surface. The cement paste side of the transition zone shows needle-like crystals growing perpendicularly from the substrate, what look like bridging of micro-cracks (Figure 7.6.b).

7.2.2 Aggregate

Aggregate particles as participants in ACR were expected to show some changes in microstructure that are not typical for original rock and would resemble the structures developed in rock immersed in alkaline solution. The SEM analysis on fractured concrete samples, with a focus on aggregate surfaces were carried out. Higher magnification SEM images suggest that there is more than one process to which aggregates are subjected while embedded in cement paste. One of first targets was to look for evidence of the dolomite to calcite transition. Growth of calcite grains, 2-5μm in size, on the surface of a 50μm dolomite crystal was observed on the fractured surface

of the 10 year old ACR affected concrete sample from Canada (samples Table3.3), (Figure 7.7.a, b). These new crystals were growing in a preferential orientation as observed in low magnification, micrograph in Figure 7.7.a. The shape and clear appearance only of one corner of the crystals (cubic corners) which appear from the dolomite substrate suggest that the morphology of these crystals is probably a distorted, elongated cuboid (Figure 7.7.b). These types of crystals can be formed by ionic exchange due to chemically/crystalographically heterogeneous dolomite layers. The crystal structure of dolomite is of a layered nature with Ca/Mg consecutive layers (Figure 5.1), so it is expected that any disorders or presence of foreign ions would act as potential nucleation sites.

Another important discovery on a fractured, control sample of the Kingston rock, was the confirmation of the existence of planes such as cleavage planes that could potentially have an active role in mineralogical transformation (Figure 7.8.a low and 7.8.b show higher magnification micrographs of layered structures within dolomite). These structures are the evidence of cleavage planes within dolomite crystals, so it is possible that calcite nucleation is related to those cleavage planes. When Figures 7.7 and 7.8 were compared, it was obvious that the growth orientation of calcite had the same trend as the orientation of cleavage planes in the same rock. This lead to a conclusion that ionic exchange was taking place along these layered structures due to an easy access of the reactive species from the solution. Examination of another fractured dolomite sample from an ACR-affected aggregate, gave another evidence for presence of foil-like crystals (Figure 7.9) along the cleavage planes, an the crystal habit suggests they are some form of silicates.

7.2.3 ESEM study of aggregate extracted from a 10 year old concrete

An aggregate surface previously attached to cement-paste was examined under high, relative humidity in an ESEM immediately after extraction from concrete specimen. The micrographs obtained have not been altered by sample preparation or coating, and at the same time not subjected to carbonation, migration of elements due to high vacuum (HV). High concentration of fine elongated crystals were observed growing at dolomite grain surfaces as presented in Figure 7.10.a, b.

As can be seen at higher magnification in some cases, dolomite crystals have been almost totally replaced by radiating needles. The composition of these needle-like crystals appears to be of Ca, Si, and Al, as shown by EDX spectra (Figure 7.11.a). Much finer crystals were observed on altered dolomite grains (Figure 7.12), EDX spectra of which reveal a degree of different composition as shown in Figure 7.11.b, with main constituents Mg, S, and Ca. This could be result of the skirting effect in ESEM EDX, where due to gaseous environment in the chamber, the X-ray can be giving signals from areas around the area perceived to be analysed.

Another type of crystals observed in ESEM analysis of ACR aggregate detached from cement paste were phases shown in Figure 7.13.a,b. The oblique crystals in Figure 7.13.a,b are in their habit similar to ettringite, pointed by blue arrows. It is not uncommon to observe ettringite growth in an ACR-affected dolomite, and it is most likely that its formation adds to the overall expansion. The sponge-like substrate looks like a blanket of intersected crystals, typical for brucite (see also Fig.5.5) pointed by red arrows, Figure 7.13.b.

The importance of ESEM study of aggregate grains of Kingston dolomite freshly detached from cement paste, was to be able to assess the level of interference that sample preparation for conventional SEM involved have on the fidelity of the acquired data. As has been demonstrated, the most important advantage of ESEM is the ability to observe very fine deposits that would be probably destroyed during drying, or under vacuum conditions, encapsulating, sectioning.

7.3 Qualitative and quantitative analyses of polished concrete

Microstructural characterisation of fractured surfaces of concrete samples gave an insight into the texture, competing growth of various crystals, development of micro-cracks and the entire micro-architecture of the grain boundaries of different phases. However, the complete understanding requires also an accurate chemical description of the established changes, which can only be obtained from flat, polished surfaces. The next stage was to produce samples from the same material (10 years old ACR-affected concrete samples which contained Kingston dolomite as aggregate) suitable for BEI and EPMA chemical

analysing. Samples of concrete previously embedded in epoxy resin were sequentially polished with a selection of diamond pastes to the finest of 0.25μm and carbon coated before analysed. The aim was to attempt to confirm the results obtained from fractured surfaces and if possible gain some extra information, such as establishing the presence of microcracks, change in porosity. A further aim was to identify Mg-and Fe-rich phases, easily distinguished from calcite/dolomite because of difference in atomic numbers (ΔZ), Table 7.1. The morphology of the surface had no impact on the signal since the samples were polished to 0.25μm.

Table 7.1 Mean atomic numbers of minerals observed in this study (Reed, 1996)

Mineral	Atomic number	Mineral	Atomic number
Dolomite	8.9	Periclase	10.4
Aragonite	12.4	Quartz	10.8
Calcite	12.4	Magnetite	21.0
Siderite	16.5	Haematite	20.6
Gypsum	12.4	Pyrite	20.7

* Other factor that can affect the signal is a morphology of the sample surface, higher areas –high counts.

7.3.1 EPMA study of chemistry of concrete

An EPMA study was conducted in order to establish more accurate data about the chemical and mineralogical changes involved in the ACR reaction. A further aim was to monitor the changes occurring in minor constituents (Mn, Fe and Sr), as they could also be indicative of transformations in the mechanism of reaction. It was also aimed to differentiate the pseudocalcite crystals, which would contain some of the original ions from parental dolomite such as Mn, Fe, from primary calcite. EPMA was also used for elemental analysis line profiles to establish the penetration of alkalis or other form of elemental redistribution of aggregate's constituents. These observations were collected from the cross section of aggregate grains as well as the adjacent and bulk cement paste. Use of BEI mode enabled determination of different forms of grain boundaries not just at the aggregate/cement interface but also at carbonate/silicate boundaries within aggregate.

7.3.2 EPMA analysis of the aggregate/cement interface

The boundaries between aggregate particles and cement paste were analysed using SEM in BE mode, which, due to the difference in domain atomic numbers, produced clear images of grain boundaries, impurities and defects present within different phases. As is evident in Figure 7.14, some of the grain boundaries involving carbonate aggregate are sound with no obvious reaction rims or alterations. The aggregate in this case (top right corner of the image) is dolomitic limestone with an evenly distributed dolomite fraction in a calcite matrix, with pyrite (bright areas) and with no physical disturbances. To a certain degree, a similar interface can be observed in Figure 7.15.a, b where the boundary is clear, with no phase alterations of aggregate. The crack developed through the grain is due to the physical application of pressure or a result of mixing of concrete.

In Figure 7.16.a a type of aggregate/cement interface can be observed, with evident migration of elements across the boundary, with the reaction rim developed between the aggregate and cement-past e (outlined area labelled reaction). This micrograph contains in the border region some dolomite and calcite crystals in the transformation stage that distinguishes them from intact dolomite grains. In its appearance this type of reaction rim is not associated with crack formation and it seems to have been formed more at the expense of cement paste than aggregate. When the aggregate particle is dolomite enriched and with a texture where dolomite clusters give a patchy appearance to the rock in BEI, the aggregate/cement boundary is not so clear, (Figure 7.16.b). From the same micrograph it can also be noted that the calcite rich area (central bright zone in the image) can be the result of the dedolomitisation reaction, as traces of a relict dolomite grain can be seen within the reaction zone.

Figure 7.17.a reveals another reaction rim, which also contains relicts of dolomite crystals (pointed in yellow), as the result of transformation of the dolomite fraction.. These types of reacted regions were further examined by acquiring elemental maps using WDX and EDX detectors in order to establish spatial distribution of elements in cement paste, aggregate adjacent to it including the TZ and the reaction rim developed. Figure 7.17.b contains the Back-scattered image of the area mapped in Figure 7.18. The description of the area is established by using the cross-polar as the orientation. The aggregate is in the top right quadrant (also pointed by blue arrows), the cement paste in

the remaining three quadrants (pointed by red arrows). The bright, central area in the middle is the reaction rim, which stretches from the top left to the bottom right corner of the BEI. Accompanying maps of Ca, Mg, Al, Si, Fe, S, and K are presented in Figure 7.18, with the reaction rim outlined with red lines. The data shows that Ca is the dominating element in reaction rim (Ca map), with enrichment in Fe (Fe map) and unexpected Mg phases other than dolomites in the aggregate (Mg map). Moreover, it is noted that this type of reaction rim is depleted of Si, compared with the neighbouring regions of cement on one side and aggregate on the other. The Si in the pore solution is a result of dissolution of pozzolans in OPC environment.

An example of a different boundary between aggregate and cement-paste appears in Figure 7.19, where the BEI (field of view 600 by 600μm) shows a reacted interface (outlined) but not in the form of a compositionally independent reaction rim. The aggregate/cement reaction is evident more as inter-growth of aggregate (top area of the image) and cement (bottom area of the micrograph), revealing dissolution of aggregate, new deposits and a difference in cement paste composition near and further from the interface. BE image also provides information on the difference between dolomite crystals in the eroded zone of the aggregate attached to the cement or present as relicts surrounded with calcite (marked as dedolomitisation) and those un-reacted dolomite within the aggregate (marked D). Some of the larger, well-developed dolomite grains were only affected in the outer regions, showing darker boundary rims. However, the majority of the dolomite mineral fraction contains some small calcite inclusions. These crystals also have a zoned appearance in BEI as a result of different compositional bands in the crystal structure. More detailed information is established with elemental maps of the area (Figure 7.20). Comparing the image with individual elemental maps shows that the boundary is Ca/Si rich, and in agreement with previous sets of maps, this data also confirms the presence of Mg rich phases (brucite) outside the dolomite aggregate region.

The impact of cement pore solution on the formation of Si rich reaction rim is present since the pozzolanas in concrete mixture will dissolve and become available. According to the EDX / WDX line analysis of the region, the composition of this rim is very similar to the ASR gel suggesting synergism between ACR and ASR. Table 7.2 gives the composition of dolomite grains, altered and intact calcite matrix, highly porous and non-porous and finally the reaction rim components, within the 60-100μm transition zone

containing tertiary calcite. Another point from this table is that the dolomite relicts within the reaction rim are of the same composition as the reminder of the dolomite fraction in the aggregate, as they probably are of the same origin. The analysis of the calcite fraction reveals that one possible method to distinguish between primary and secondary/tertiary calcite is the absence of minor components such as Fe and Si in the newly formed phases. The chemistry and composition of cement-paste as a medium for ACR was also considered. As can be seen in the set of maps in Figure 7.21 (at lower magnification and the field of view several hundred microns) Fe, Al and Mg are present as almost single phases (bright white areas on maps). At the same time Ca and Si are forming more complex phases (resulting in signal from almost entire mattrix), with sulphur concentrated around larger hydrated cement grains. Although the aggregate particles in this example are fine, therefore less susceptible to ACR, there is no evidence for re-distribution of elements from the bulk cement paste towards the interface.

Table 7.2 Results from quantitative EPMA

Analysis	MgOwt%	CaO wt%	SiO_2 wt%	FeO wt%
Aggregate / Cement-Paste Reaction Rim				
Reaction rim 40μm	0.95	51.9	12.3	0.32
Reaction rim 10μm	0.23	36.9	35.9	0.01
Change In Dolomite Fraction				
Intact dolomite grain	17.2	33.1	0.13	0.08
Relict dolomite in a rim	17.1	32.2	1.32	0.56
Difference In Composition Of Calcite Fraction				
Primary calcite matrix	0.71	50.3	2.47	0.27
Secondary calcite(dd)	0.47	54.4	0.00	0.00
Calcite in reaction rim	0.07	51.9	0.80	0.01

7.3.3 Carbonate/silicate boundary within aggregate

Most dolomitic-limestones contain silicates as minor constituents within the matrix or as inclusions in dolomite and calcite minerals. In the case of ACR this might be of importance as the compaction and the texture of rock can play a vital role in the

behaviour of such rock when used as aggregate. As it can be seen (Figure 7.22) dolomites are tightly packed in a surrounding matrix, allowing very little space for an additional crystal growth at the dolomite crystal surfaces. The same Figure (7.22) supports previous findings as the elemental mapping suggest the silicate phase almost attached to the dolomite grains, (see Si map). This Figure 7.22 also reveals the presence of mineral inclusions (silicates/quartz) as well as fine calcite.

7.3.4 Intra-crystals boundaries within dolomite

The fine calcite inclusions (Figure 7.22) present in dolomite grains are manifested as Ca-rich areas in the map they are bright regions on Ca map. It is possible that the aggregate used contained these features prior to its embedding in cement, in which case it might explain that the dolomite of such composition will be more prone to instability, as they already possess Ca-rich seeds for the dedolomitisation reaction. This type of dedolomitisation would be a continuation of a dedolomitisation that the original rock was subjected to. However, it is clear that Ca is predominantly present in the matrix in the form of calcite.

On the other hand Si is present in high concentrations in an immediate proximity to dolomite grains, creating a confined space, and occasional quartz inclusions within the dolomites. The role of Fe was considered since it is present instead of Mg in the dolomite lattice (Fe rich rims), and from the map it can be seen that the amount increases in peripheral regions of dolomite crystals. Fe rich dots are pyrites common in Kingston dolomite. However it is rather unexpected to observe a higher Mg signal from dolomite crystals, suggesting that the Ca/Mg ratio is probably close to ideal value of 1. As can be seen individual dolomite grains are zoned and rich in imperfections, demonstrated by different atomic numbers in BSE image (top image) which is also supported by individual maps of Ca, Mg Si and Fe.

7.4 Surface Chemistry as a tool for ACR presence

An average XPS spectrum of the fresh rock is presented in Figure 7.23.a wide spectra 0-1100keV and b)-h) with chemical elements of interest as separate regional spectra and the binding energies summarised in Table 5.2. The same settings were used for the acquisition of data from the alkali treated rock tablets and the data is presented in Figure

7.23 as a rock/NaOH line in each spectrum. These two sets are compared with the data obtained from an ACR affected aggregate grain that was removed from the 10 years old concrete sample and subjected to the same analysis. The comparison between the lines representing different samples reveals that the changes induced by alkaline solution are more severe than those produced in concrete, as all line shifts are more apparent for rock/NaOH samples than for the concrete sample.

First, there is a chemical shift in C*1s* peak, meaning that there is a another type of carbonate on the surface different from the dolomite carbonate measured from a control sample (Figure 7.23.b). A similar trend is observed in Ca*2p* (Figure 7.23.c). The data from previous rock/NaOH experiments also produced larger shift in binding energies of Mg*2p* and Ca*2p* than ACR aggregate. The regional spectrum for Mg*2p* Figure 7.23.d shows the shift observed in a single dolomite crystal study of Mg carbonate change to Mg hydroxide chemical state, (values in Table 5.2). This type of change in binding energy is less obvious in the Si*2p* region suggesting the minor role of Si in this reaction, in another word Si-phase present is almost chemically-inert (Figure 7.23.e). The change in Al*2p* is probably the most extensive but it also shows the greatest diversity between aggregate and alkali-treated rock samples (Figure 7.23.f), probably due to the presence of greater amounts of water. In order to confirm the results for Mg*2p*, spectra for Mg*3s* and also Ca*3s* are shown in Figures 7.23.g&h, and, as expected in both cases, there is the same trend as those mentioned earlier.

7.5 Conclusion

1) In comparison with untreated samples of Kingston dolomite, the same rock when used as aggregate in concrete for 10 years exhibited the following changes brought forward by alkaline environment of OPC: formation of brucite, secondary calcite and needle-like crystals, and in some cases map cracking. It seems that in some of the expanded samples there has not been much disturbance, and what can be observed is a competitive crystal growth, perhaps re-crystallisation.
2) As earlier postulated by Poole and French, this work also established as shown above, that Mg had a tendency to migrate and redeposit further from the aggregate leaving an enriched Ca zone within the aggregate. Furthermore, this type of reaction belt is

characteristic for its uneven morphology and dissolution of aggregate with a system of microcracks radiating from cement paste towards the aggregate. In spite of all the above, it is difficult to determine if the Ca rich zone is formed after dolomite, as some of the grains have rhomboidal form, where the others are fine grained (amorphous) build-up of Ca-rich mass within the interface belt.

3) The Back Scattered Imaging from flat polished samples of the same 10 year old concrete from Canada shows clearly the transformation of dolomite grains to relict dolomite and pseudomorphs of secondary calcite.

4) In addition to the dedolomitisation process, another reaction product was observed at the aggregate/cement boundary. BEI mode showed that this type of boundary consists of a low porosity phase containing primarily Ca and Si.

5) An example of an intact aggregate/cement boundary within the same ACR reactive aggregate from Kingston, Canada was also observed. The question here is whether a particle is undergoing dedolomitisation from within, as it appears to have a clear boundary with surrounding cement. There is no evidence of micro-cracking. However, it is clear from BEI that this particular boundary involves aggregate with predominantly calcite component and very low dolomite content of finely grained and evenly dispersed grains.

6) XPS results showed that the use of the ASTM C586 standard produces much harsher conditions than concrete. This increased alkalinity will probably speed the reactions, causing chemical shifts to be more apparent in NaOH / rock samples than in concrete aggregate.

7) Comparing the layered structure of dolomite with the orientation and a deposition of new phases it can be seen that there is a similarity, of orientation of those layers and the orientation of secondary calcites formed during dedolomitisation. Furthermore, the same orientation was observed in calcites formed in dolomite of ACR-affected aggregate.

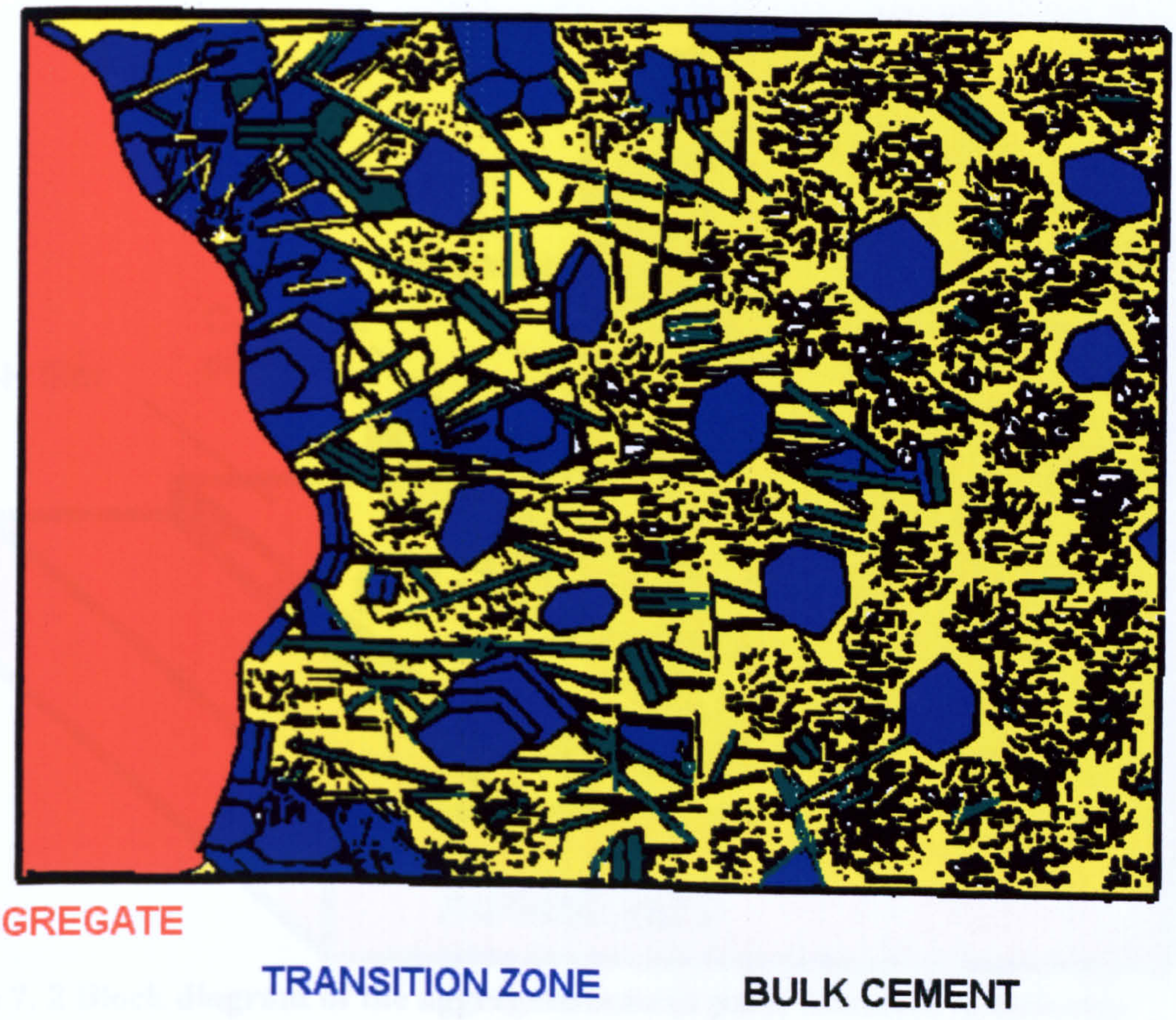

Figure7.1a Aggregate/cement paste boundary

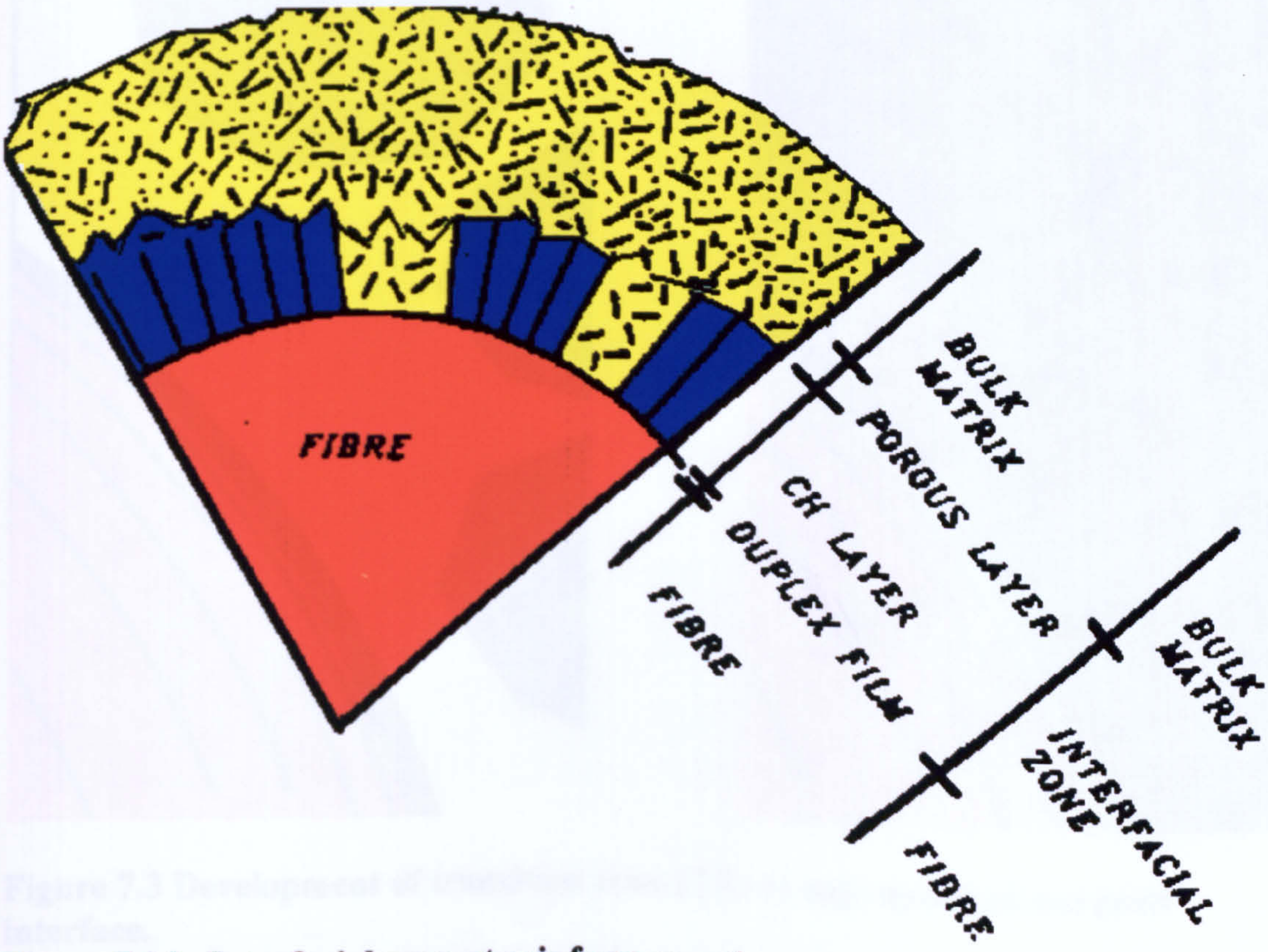

Figure 7.1.b Interfacial zone at reinforcement/cement paste

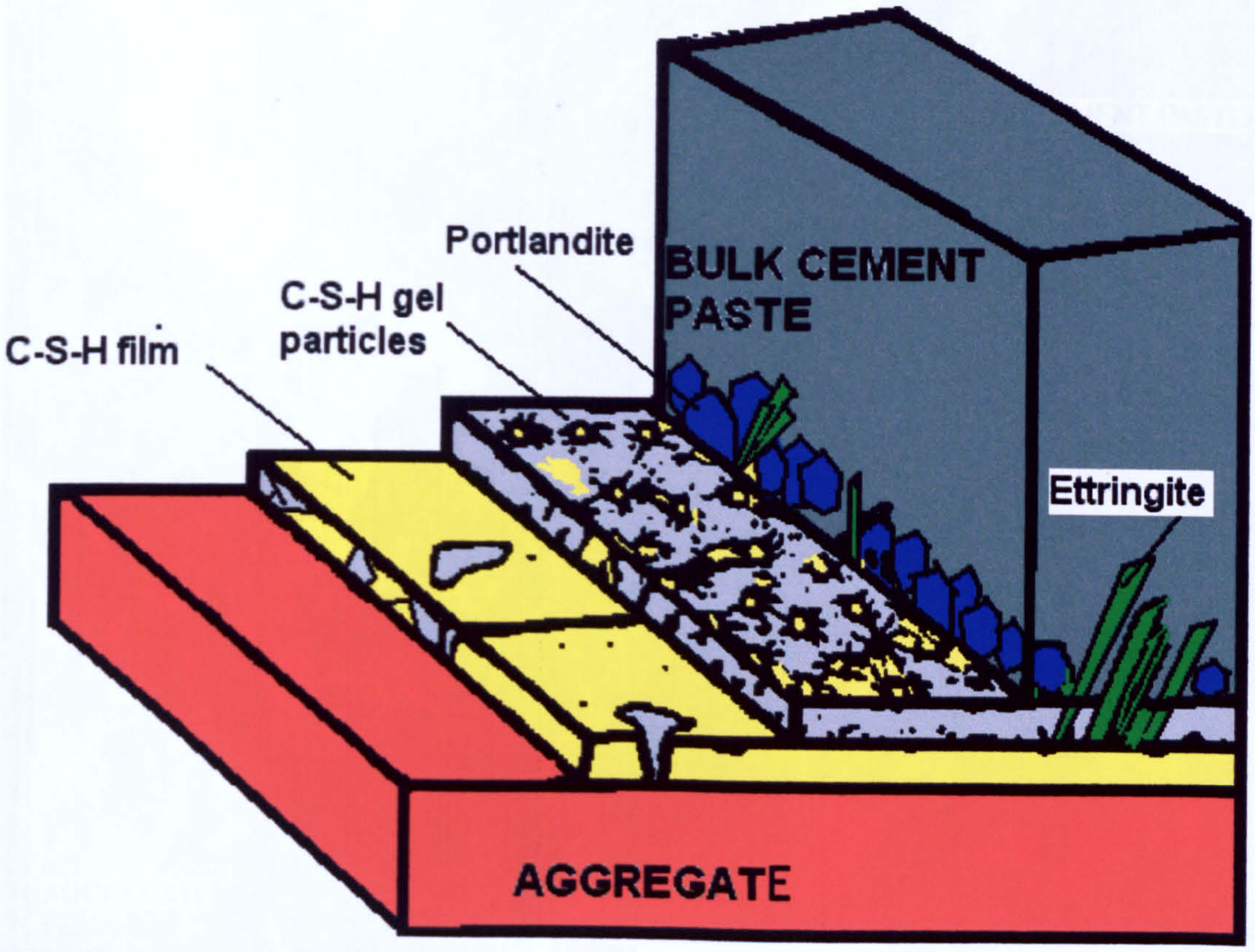

Figure 7. 2 Block diagram of the aggregate/cement paste interface in concrete.

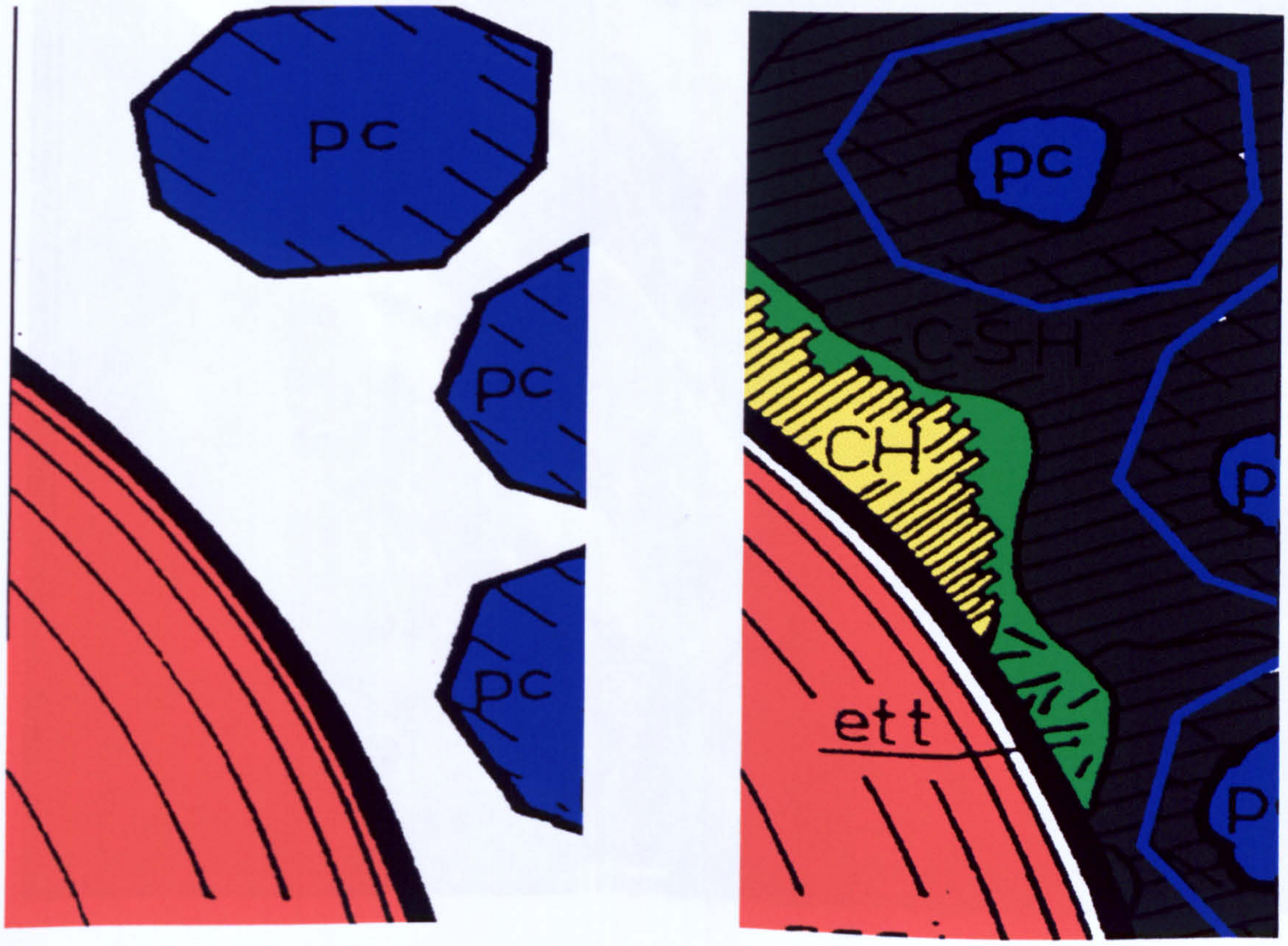

Figure 7.3 Development of transition zone (TZ) at aggregate/cement paste interface.

[red = aggregate, blue = un-hydrated portland cement particles, yellow = portlandite, green = ettringite, gray = C-S-H gel]

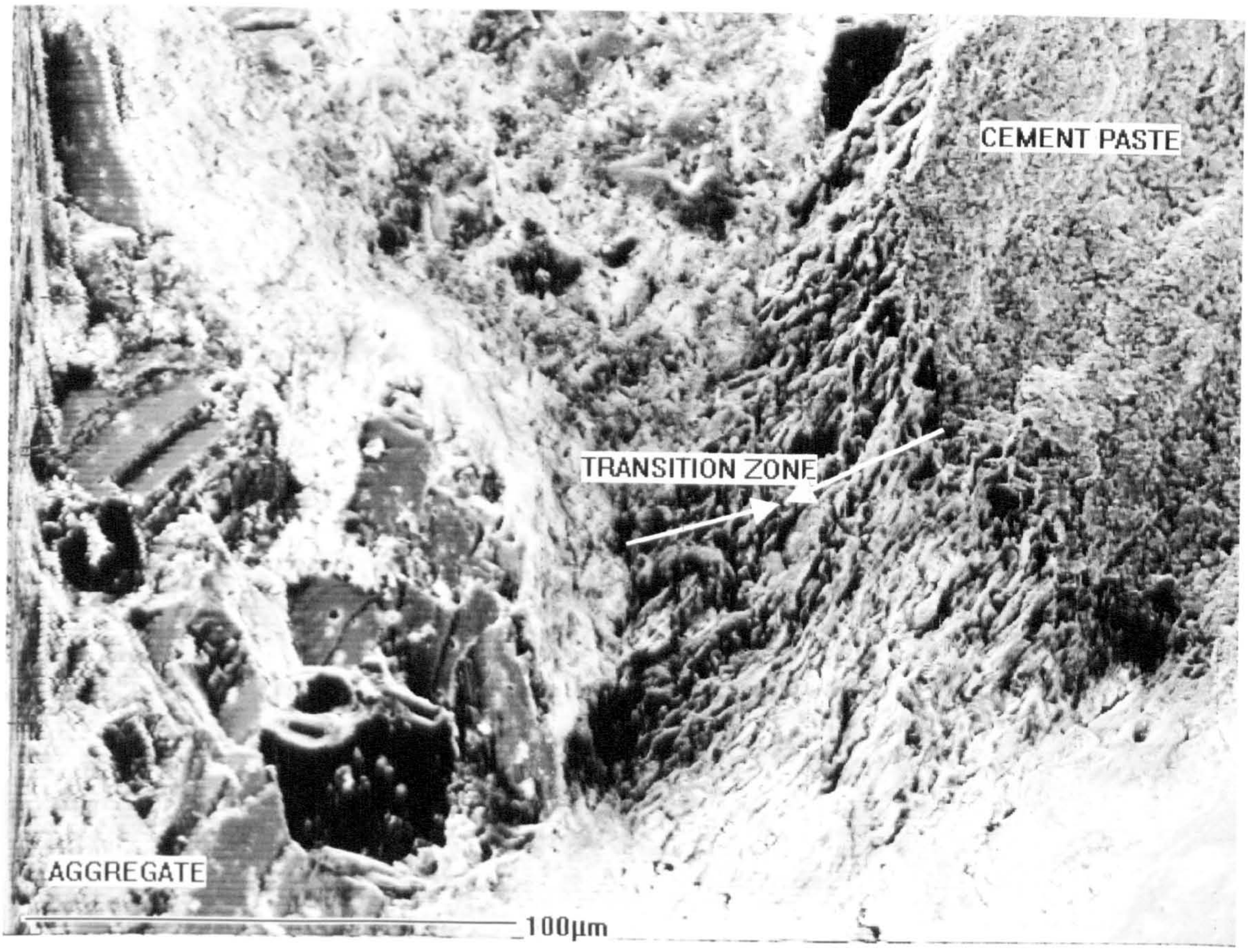

a)

b)

Figure 7.4 Transition zone of a fractured surface of ACR concrete sample with Kingston aggregate, lower image at a higher magnification, focused on the aggregate side.

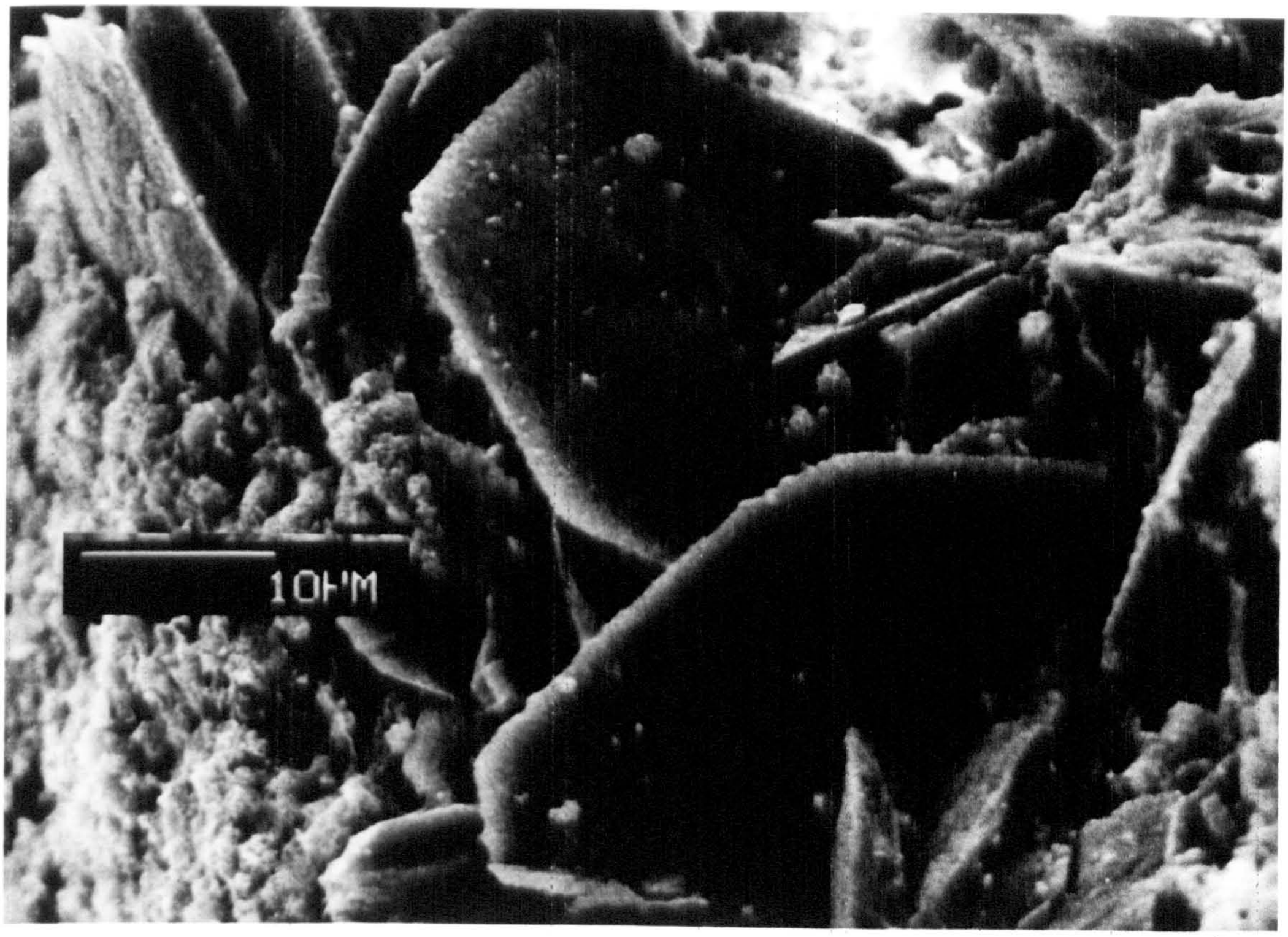

a)

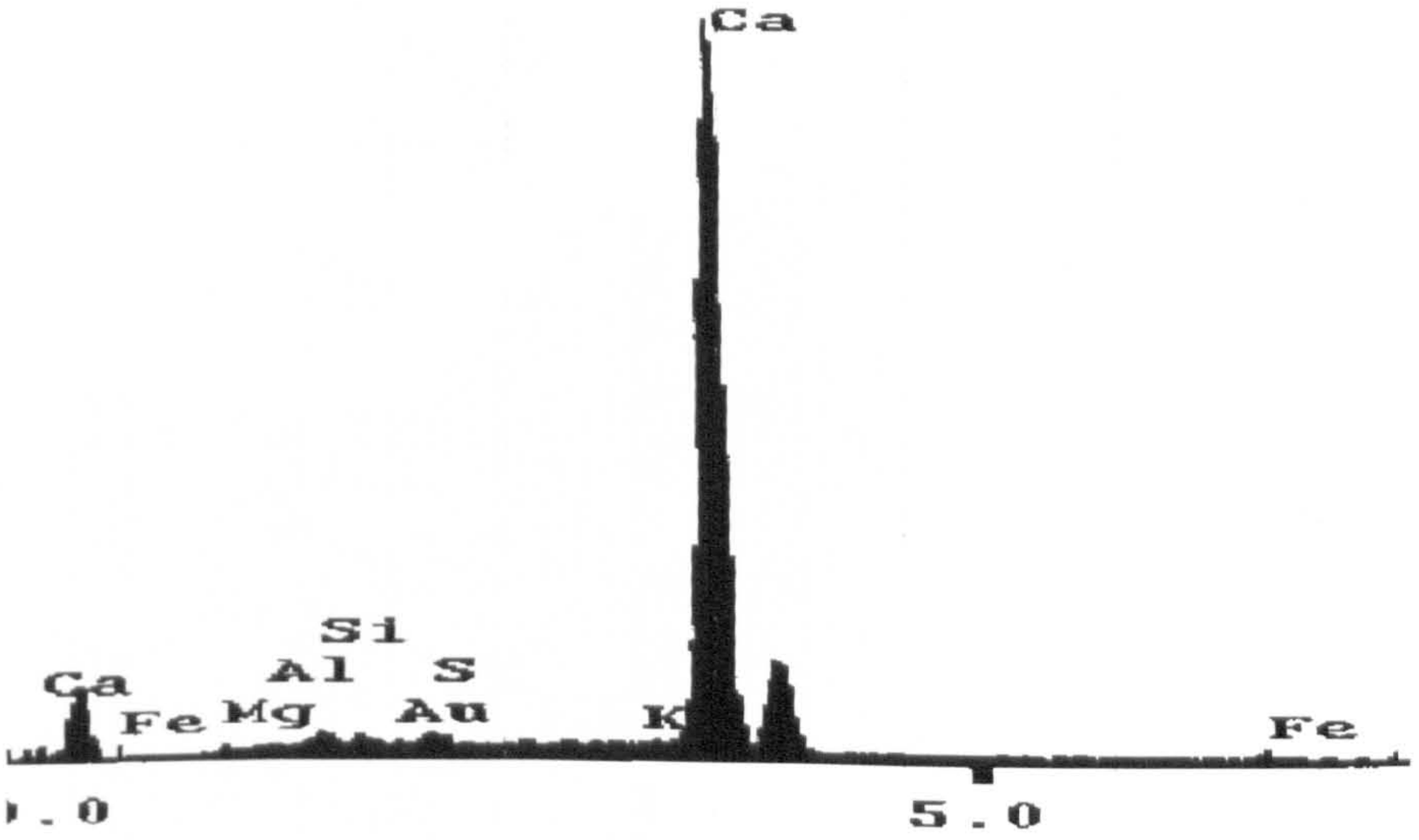

b)

Figure 7.5 SEM image of a fractured surface of aggregate/cement interface revealing platy Portlandite crystals (a). This is supported by the EDX spectrum dominated by Ca (b).

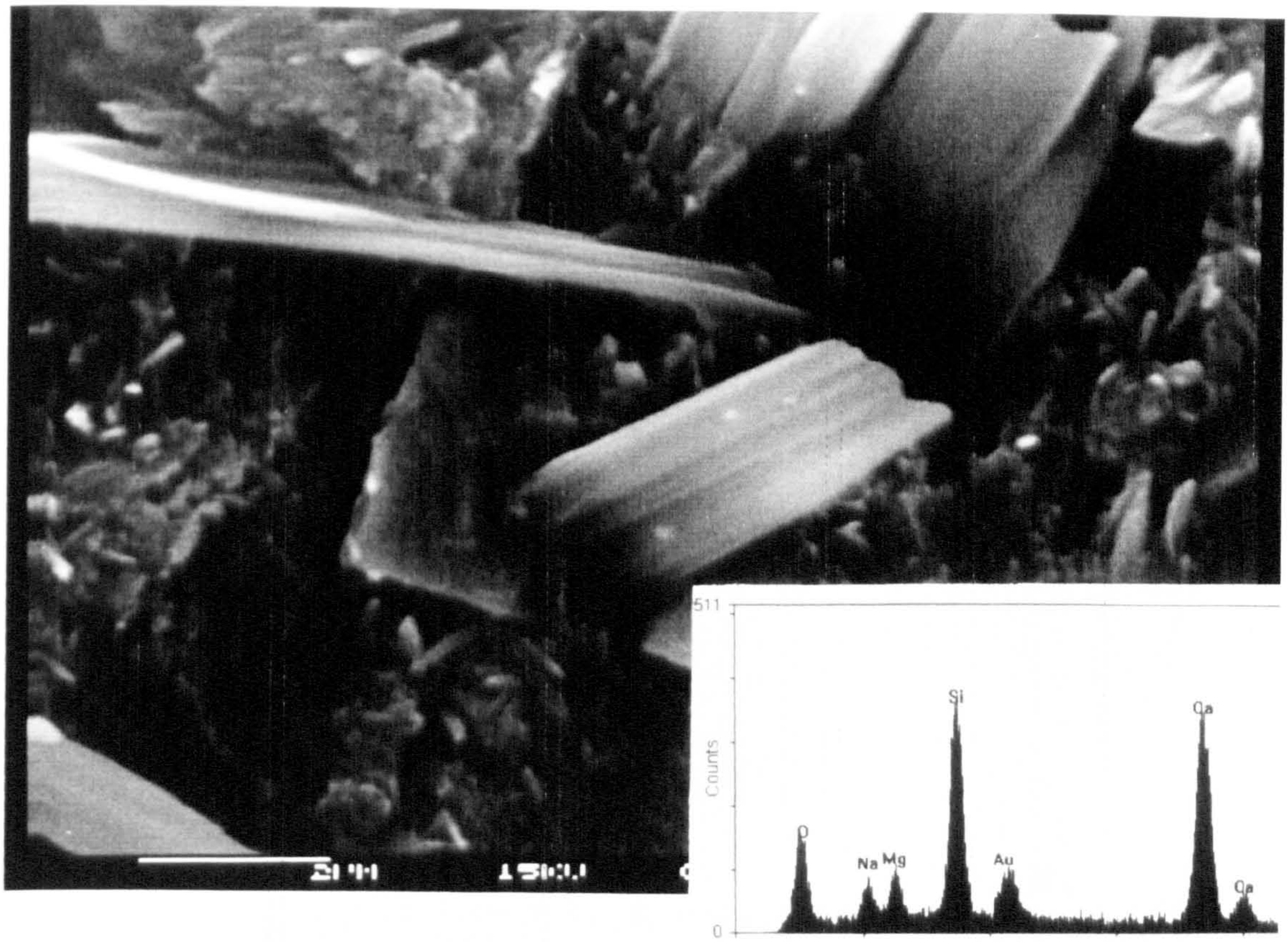

a)

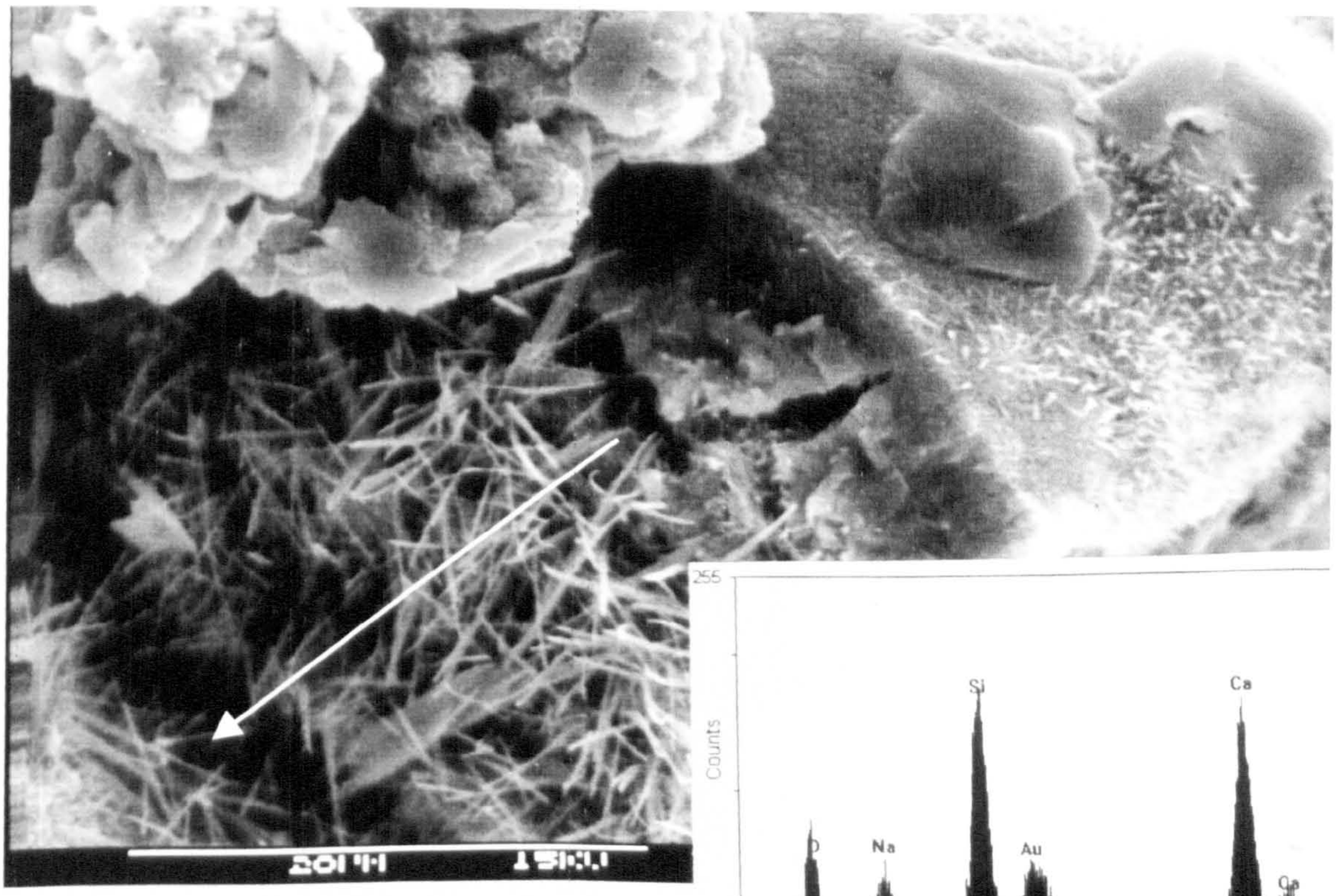

b)

Figure 7.6 SEM image of a fractured ACR concrete sample, revealing phases at the mineralogical complexity of concrete.
(Arrow points at the crack filled with fine needle-crystals, some sort of ettringite and C-S-H combination).

a)

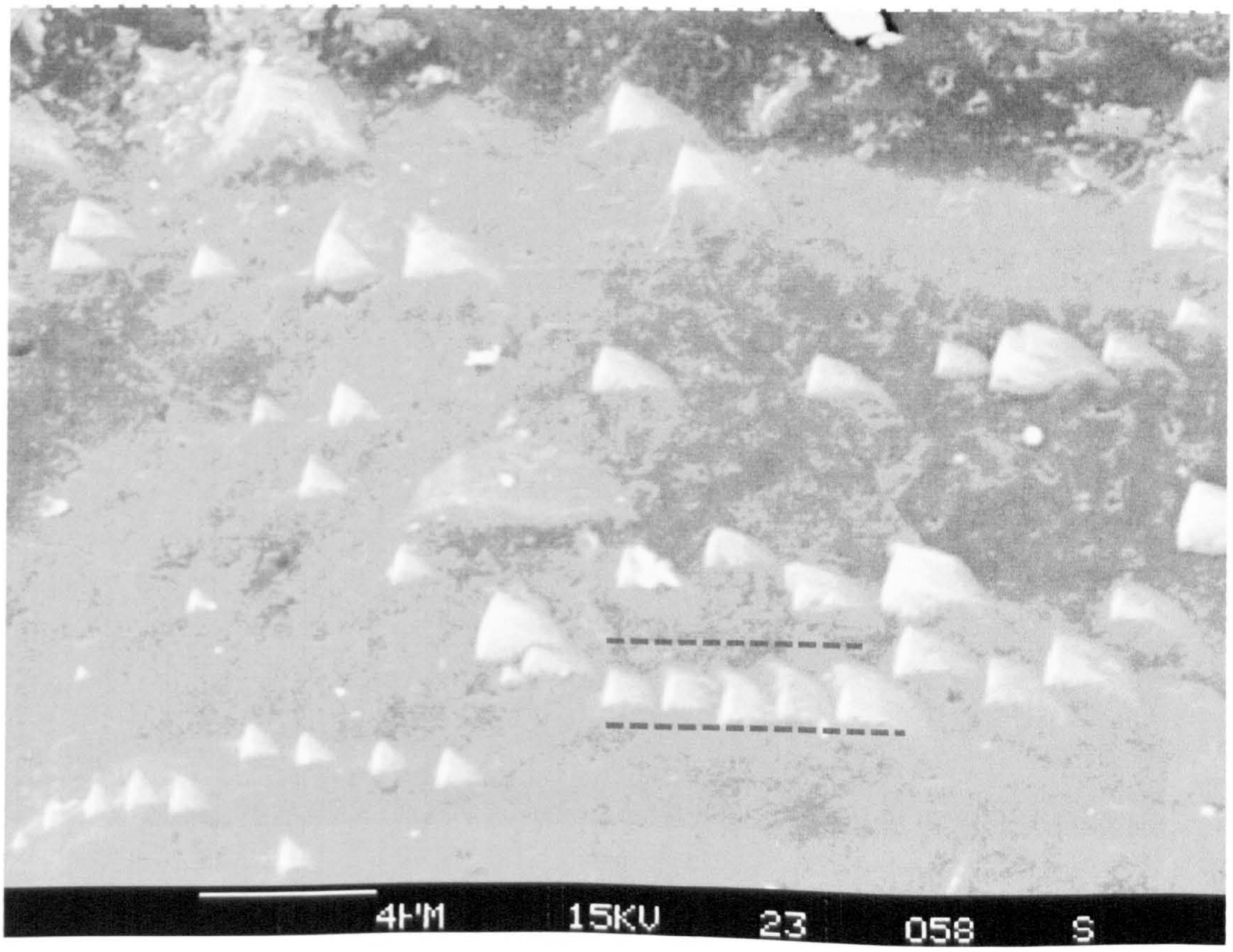

b)

Figure 7.7 Calcite growth (outlined) on a dolomite grain in an ACR affected aggregate, a) low magnification revealing the orientated growth and b) higher magnification for crystal habit. (The image was acquired from a fractured dolomite grain within 10yrs ACR concrete from Canada, (Table 3.4)).

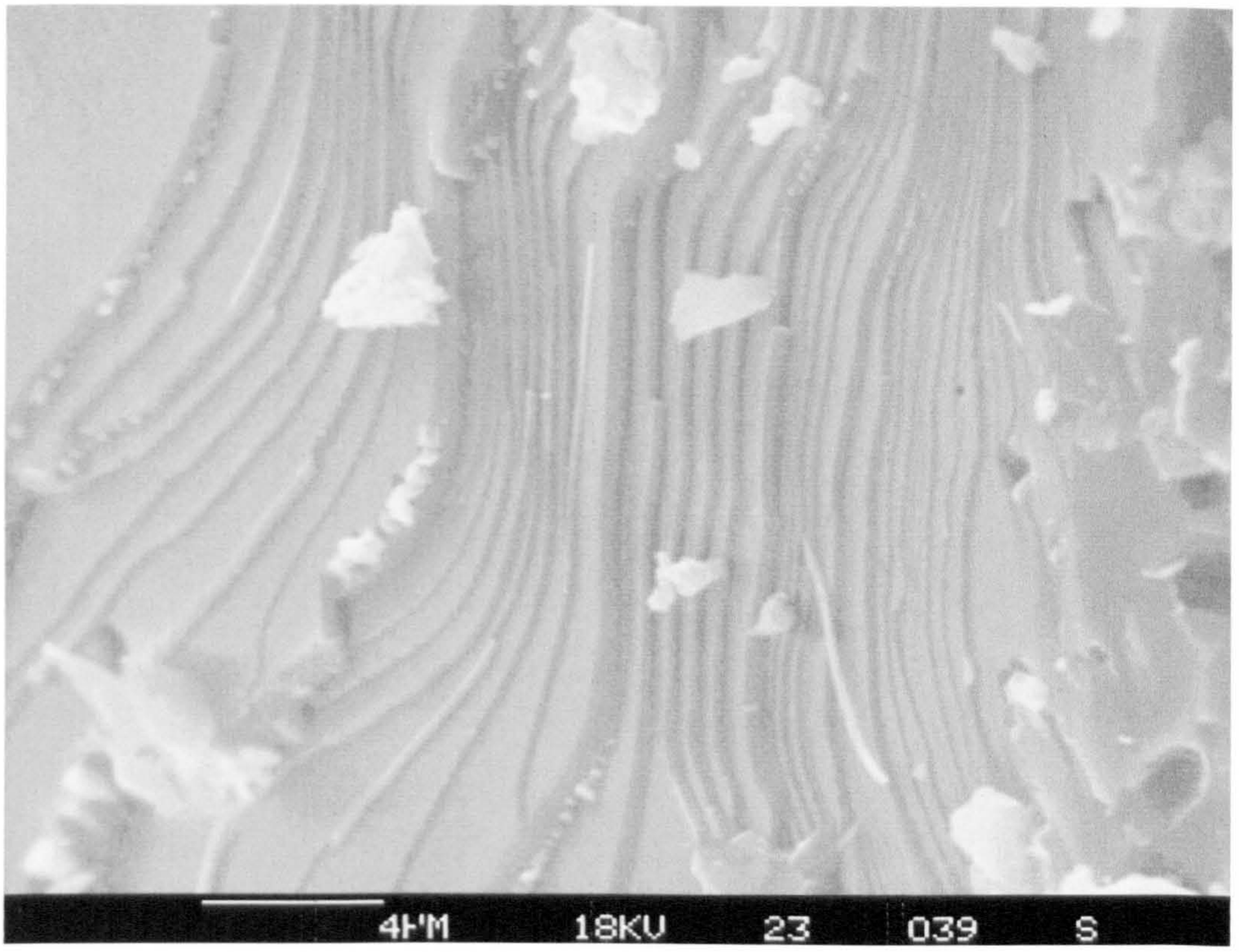

a)

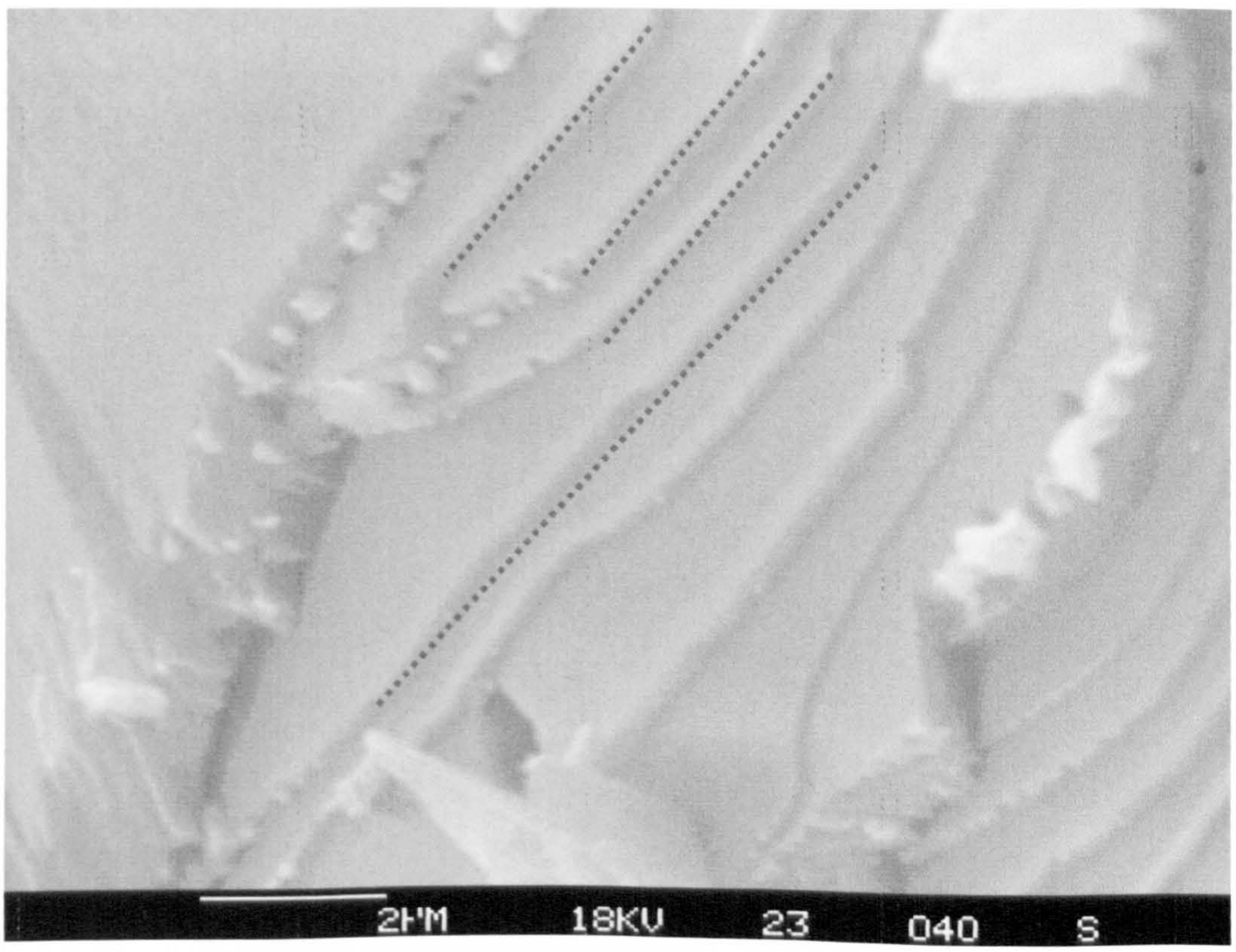

b)

Figure 7.8 SEM image of a fractured surface of control sample of Kingston argillaceous dolomite, revealing layered structure of dolomite grain. These are potential areas for ion-exchange and dedolomitisation, which is why the orientation of calcite in Fig. 7.7 is almost identical with orientation of these, most likely cleavage planes (outlined). (b is a close up of a).

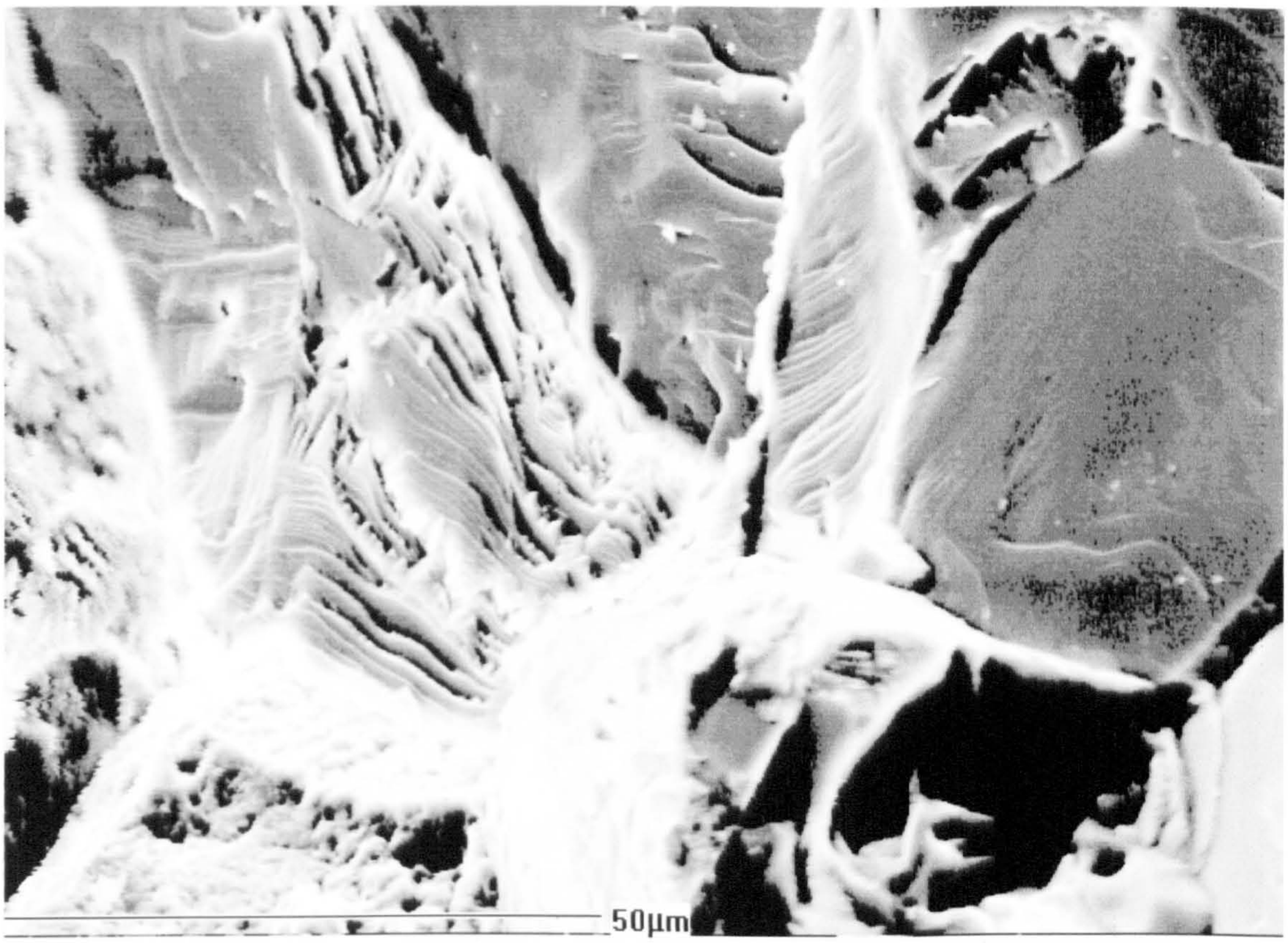

Figure 7. 9 a SEM image of fractured fraction of dolomite aggregate revealing layered structure.

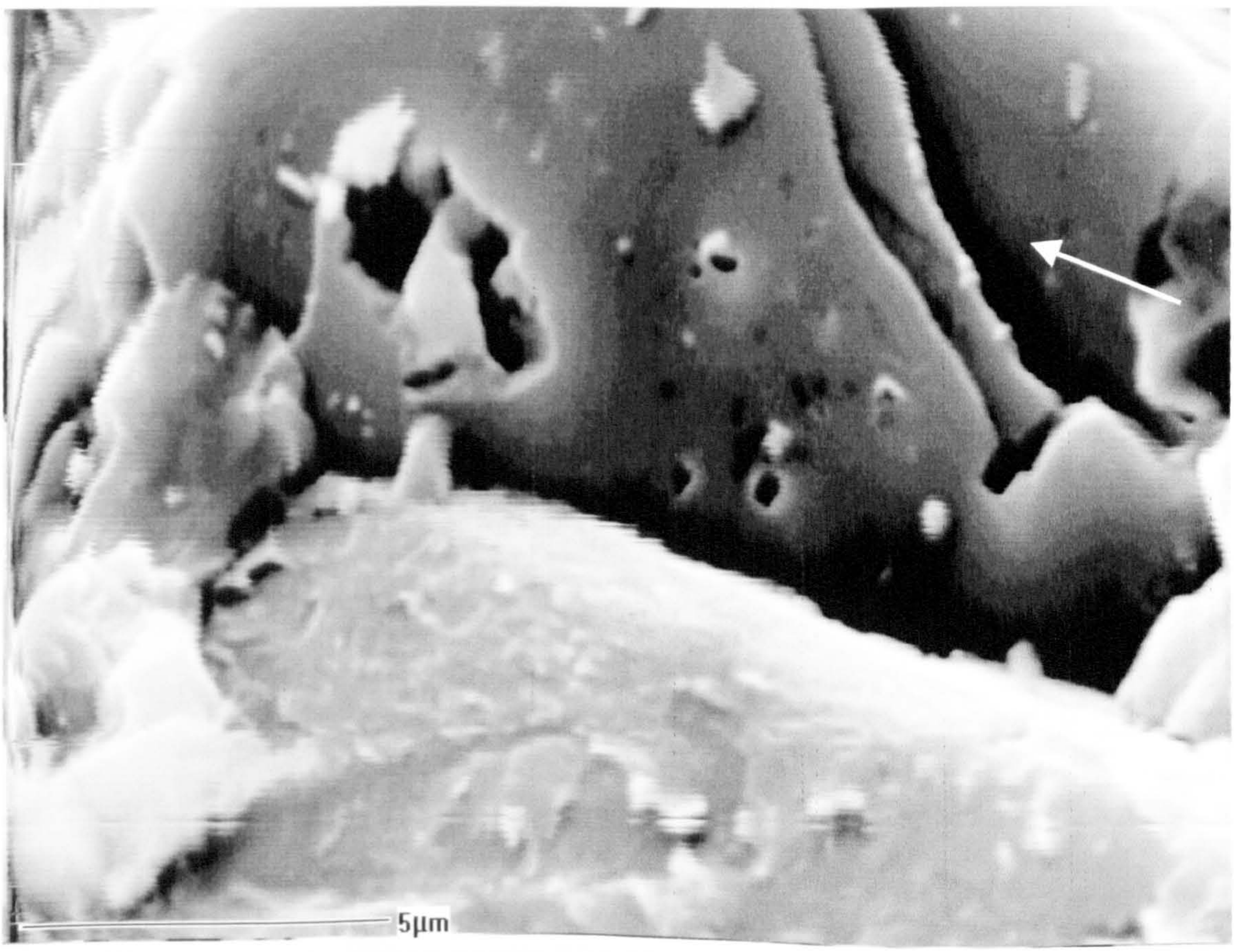

Figure 7.9.b Higher magnification presence of clays, in Kingston dolomite, bottom image.

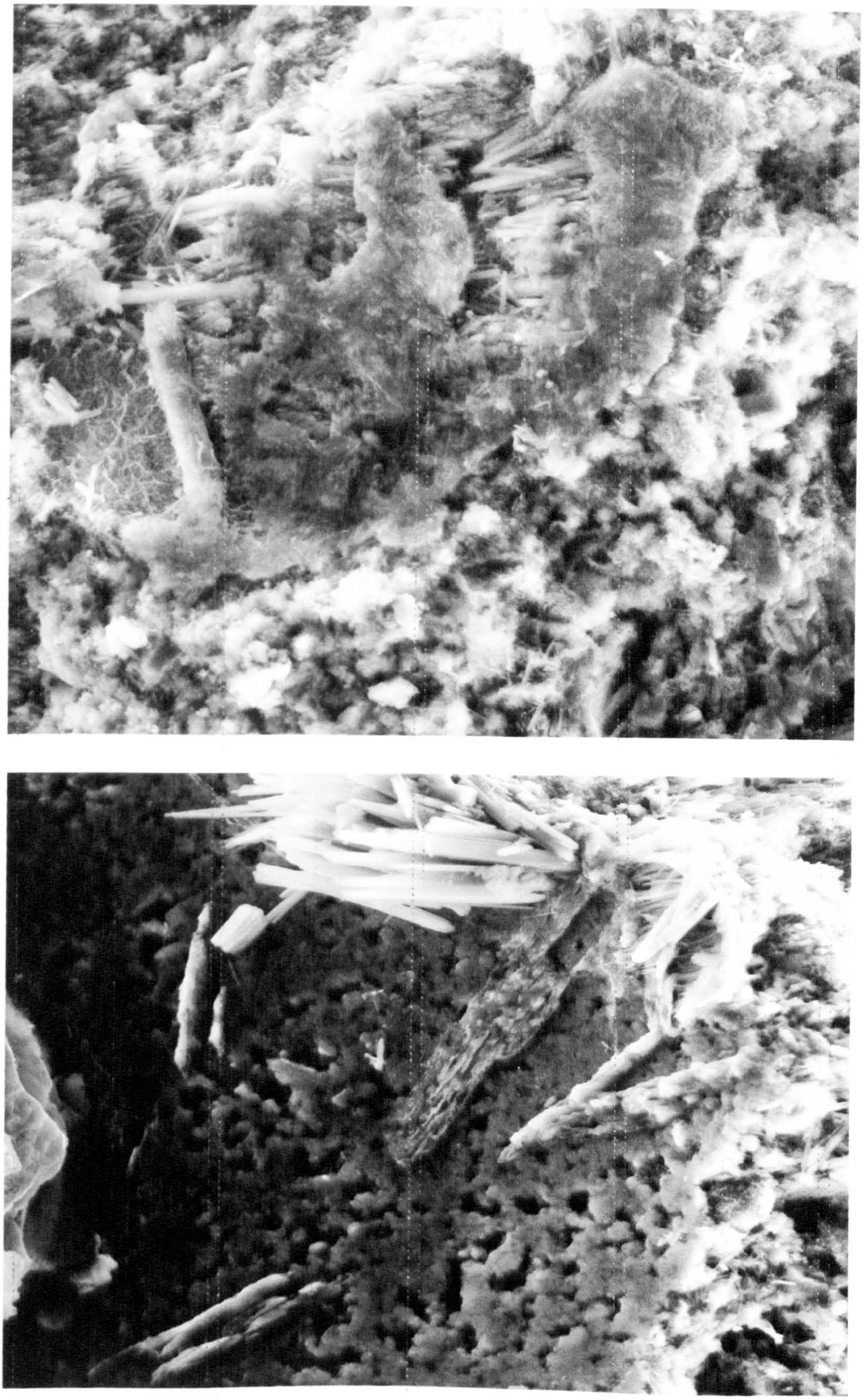

a)

b)

Figure 7.10 ESEM micrographs of a freshly peeled off aggregate from cement in an ACR concrete, revealing needle like crystal growth on dolomite surface. These needles are ettringite with microcrystalline C-S-H in the background.

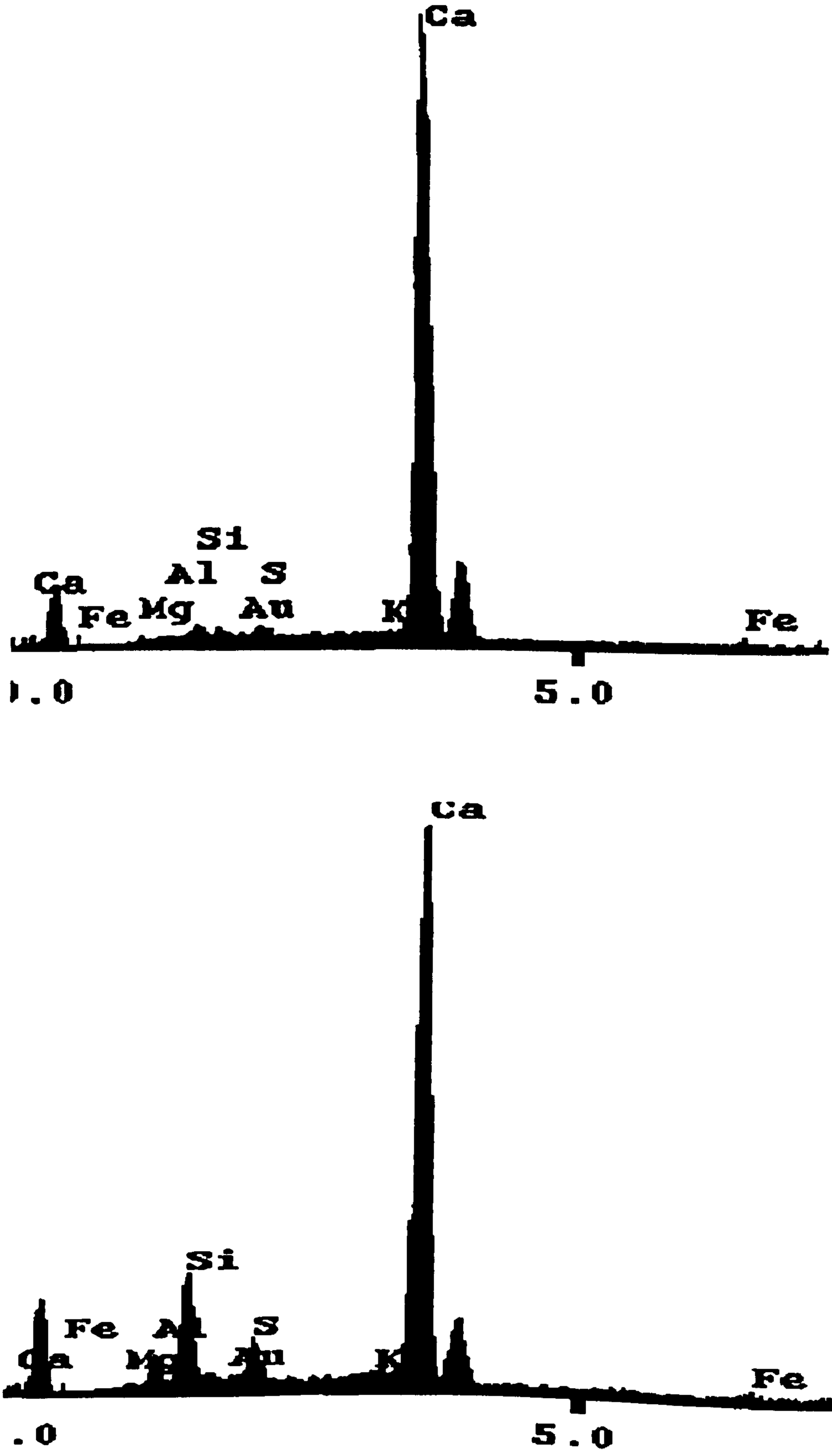

Figure 7.11 EDX spectra of ACR affected dolomitic aggregate, and the reaction rim.

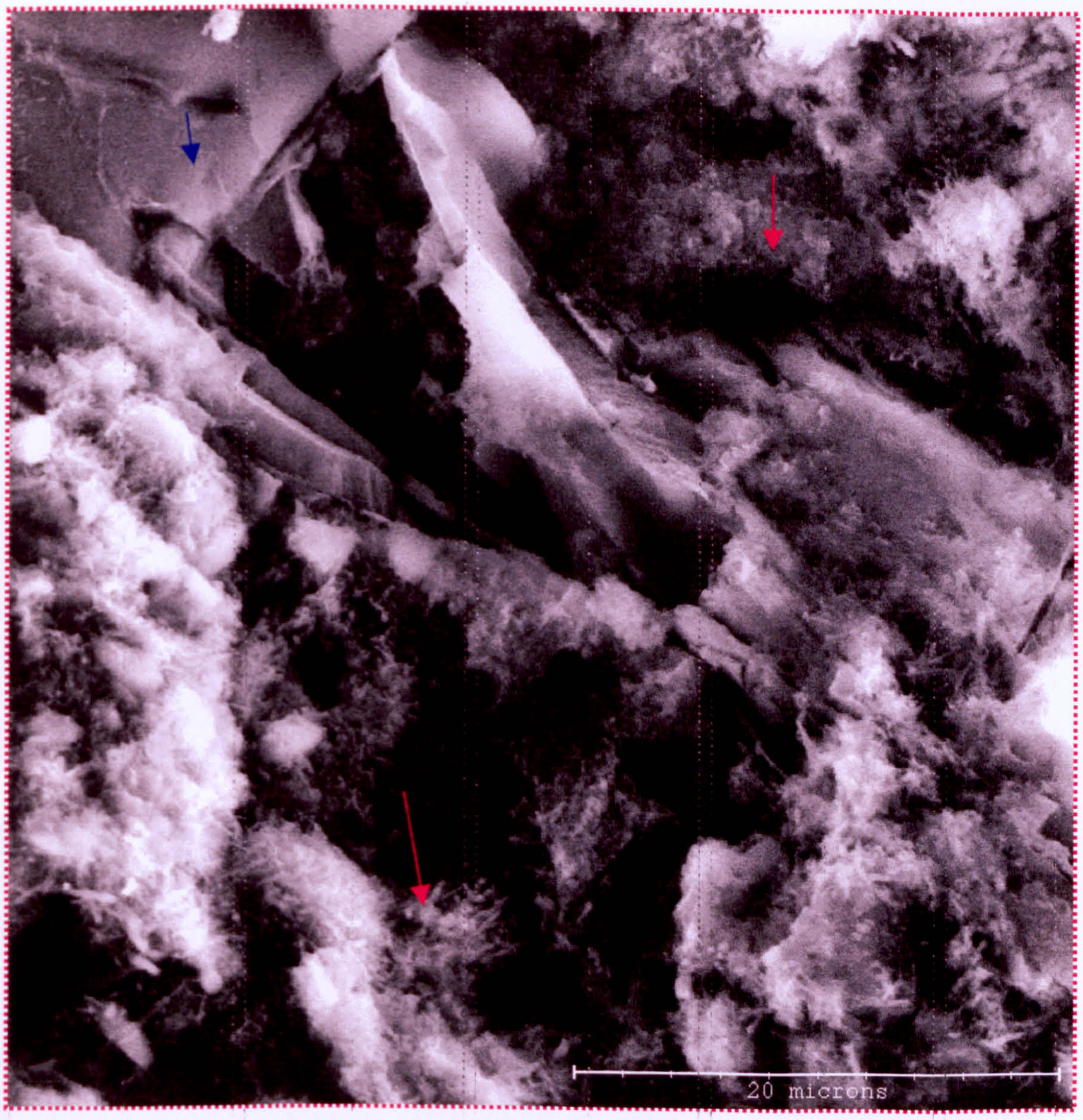

Figure 7.12 ACR affected concrete sample from Canada with Kingston dolomite as aggregate, ESEM enabled detection of a very fine deposits.

[Red arrows point to brucite and blue to carbonates.]

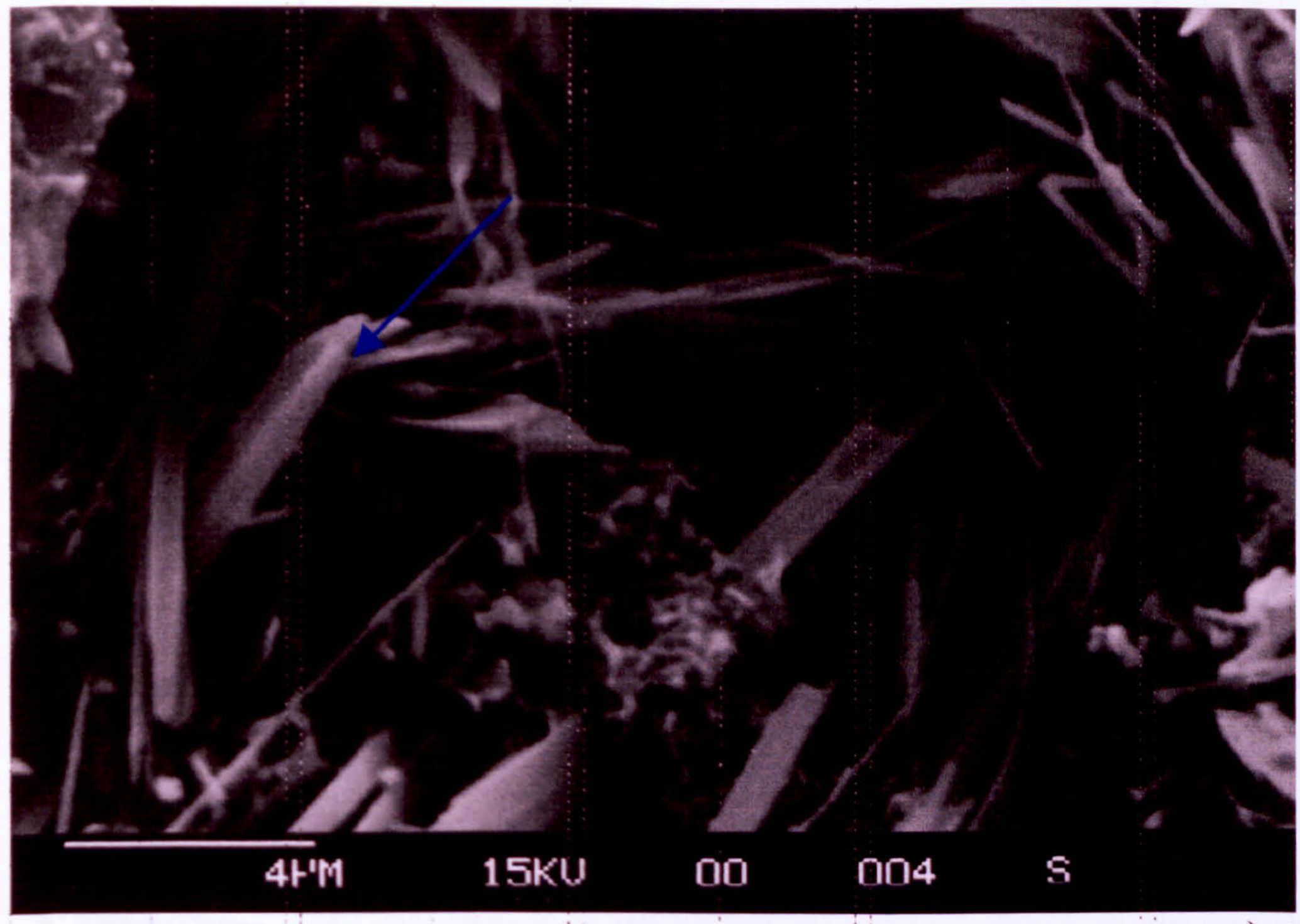

a)

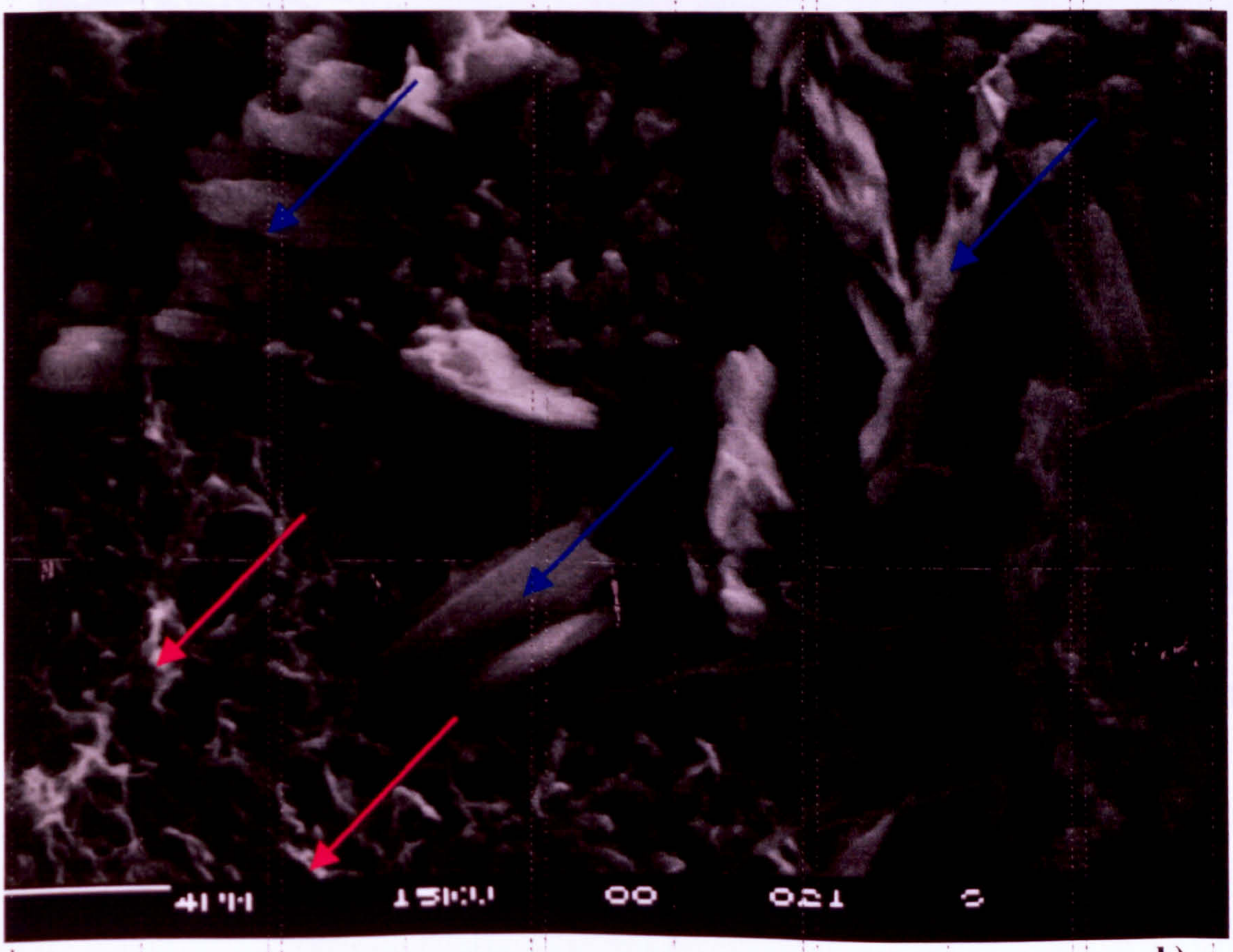

b)

Figure 7.13 ESEM image of an aggregate surface extracted from ACR concrete, showing the growth of ettringite from dolomite substrate that was adjacent to the cement-paste a) and the presence of a fine brucite layer with a typical blanket of intersected crystals in b). (red arrows-brucite, blue arrows-ettringite)

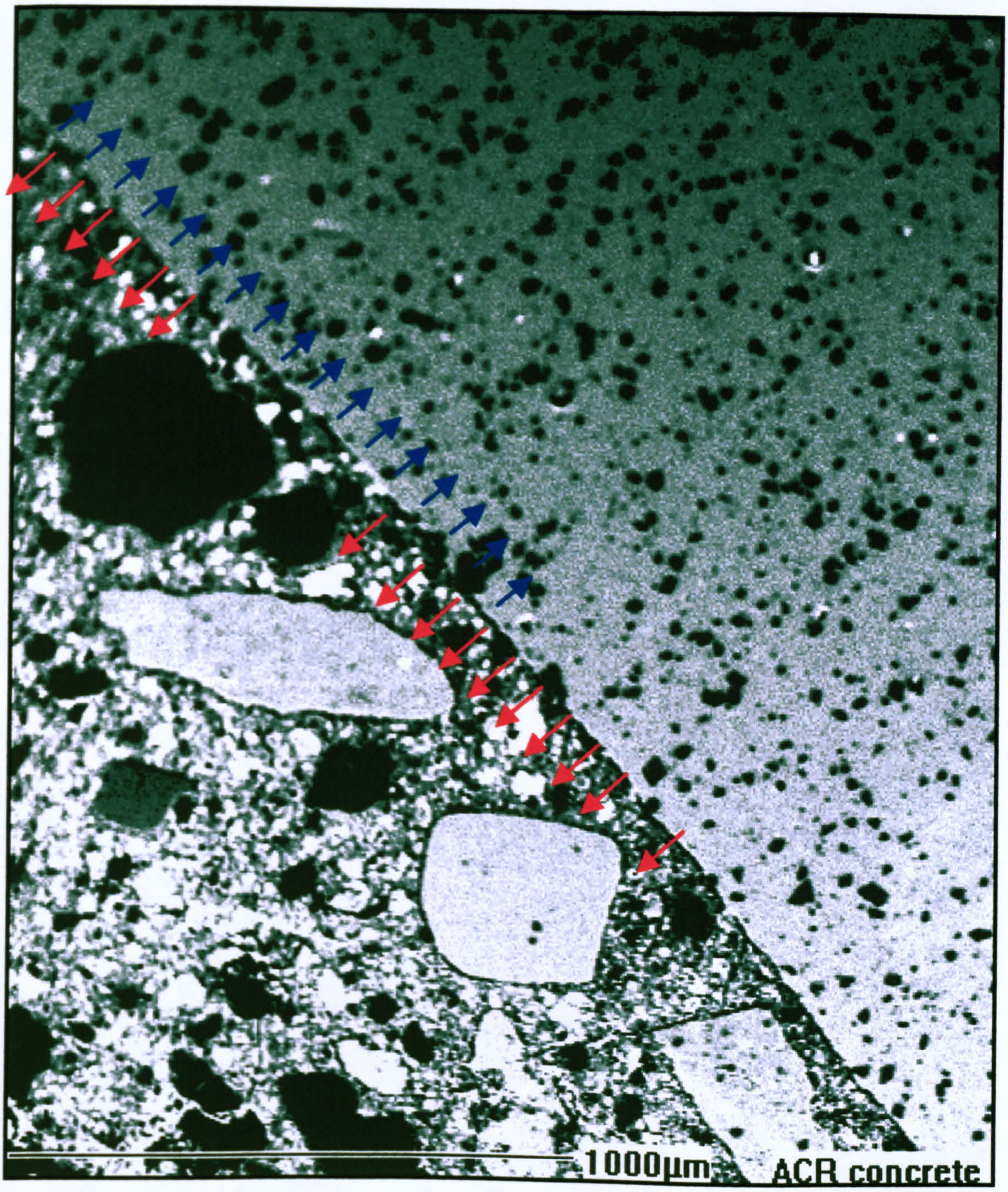

Figure 7.14 ACR affected concrete sample from Canada containing Kingston dolomite as aggregate. Revealing a sound aggregate/cement boundary.

[Aggregate pointed out by blue and cement-paste pointed out by red arrows, with the TZ between.]

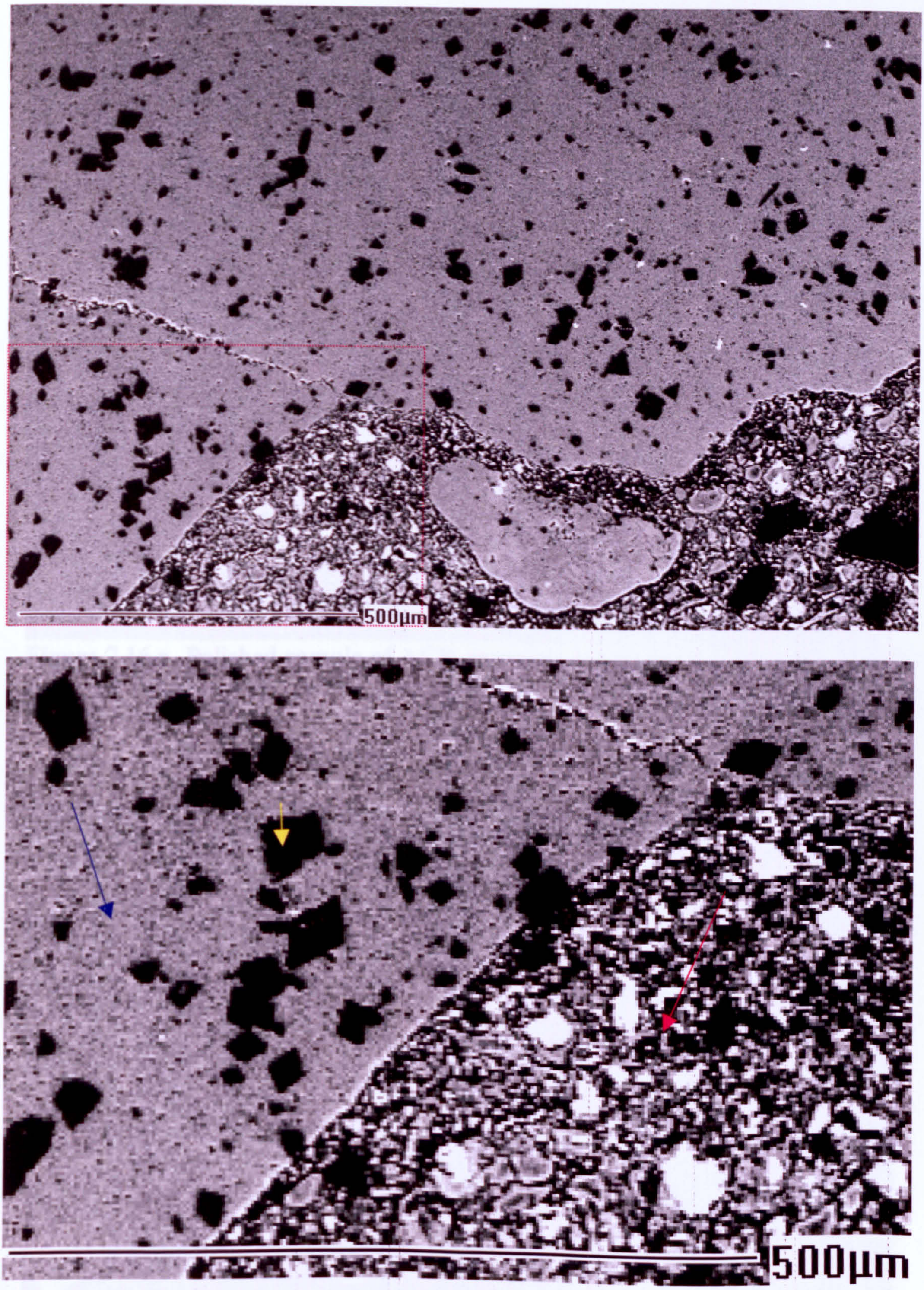

Figure 7.15 BSE image of an aggregate cement paste boundary that has not been affected by any chemical reactions; at low and high magnification. Sample of 10yrs old ACR concrete from a pavement in Kingston contains expansive aggregate.(Table 3.4).

[blue-calcite matrix in aggregate, yellow-dolomite grains in aggregate, red-cement]

* Irregular crack is a result of physical force during sample preparation or mixing.

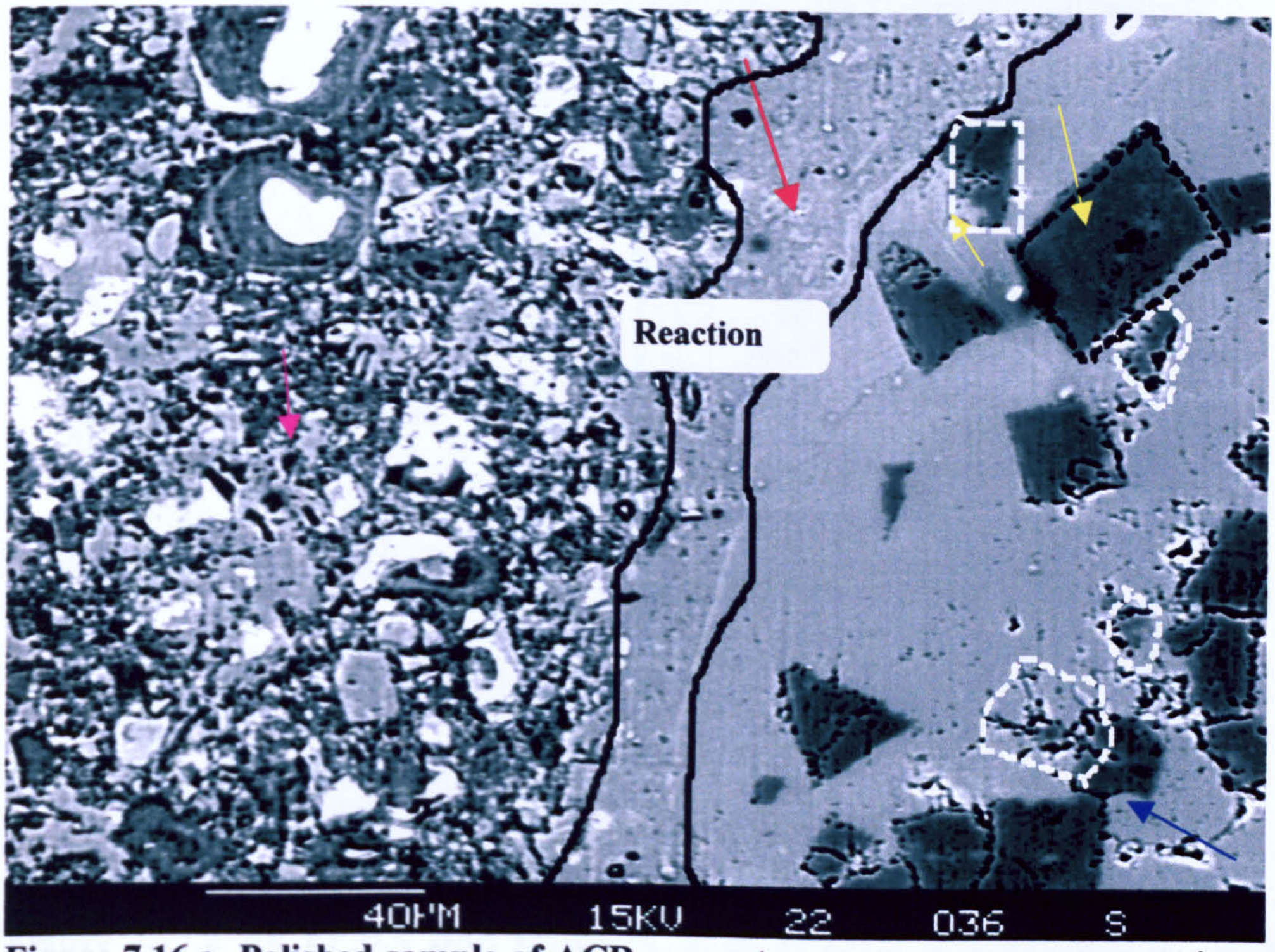

Figure 7.16.a Polished sample of ACR concrete, aggregate cement-paste interface with the reaction rim rich in silica. The source of Si is a pozzolana added to concrete mixture.

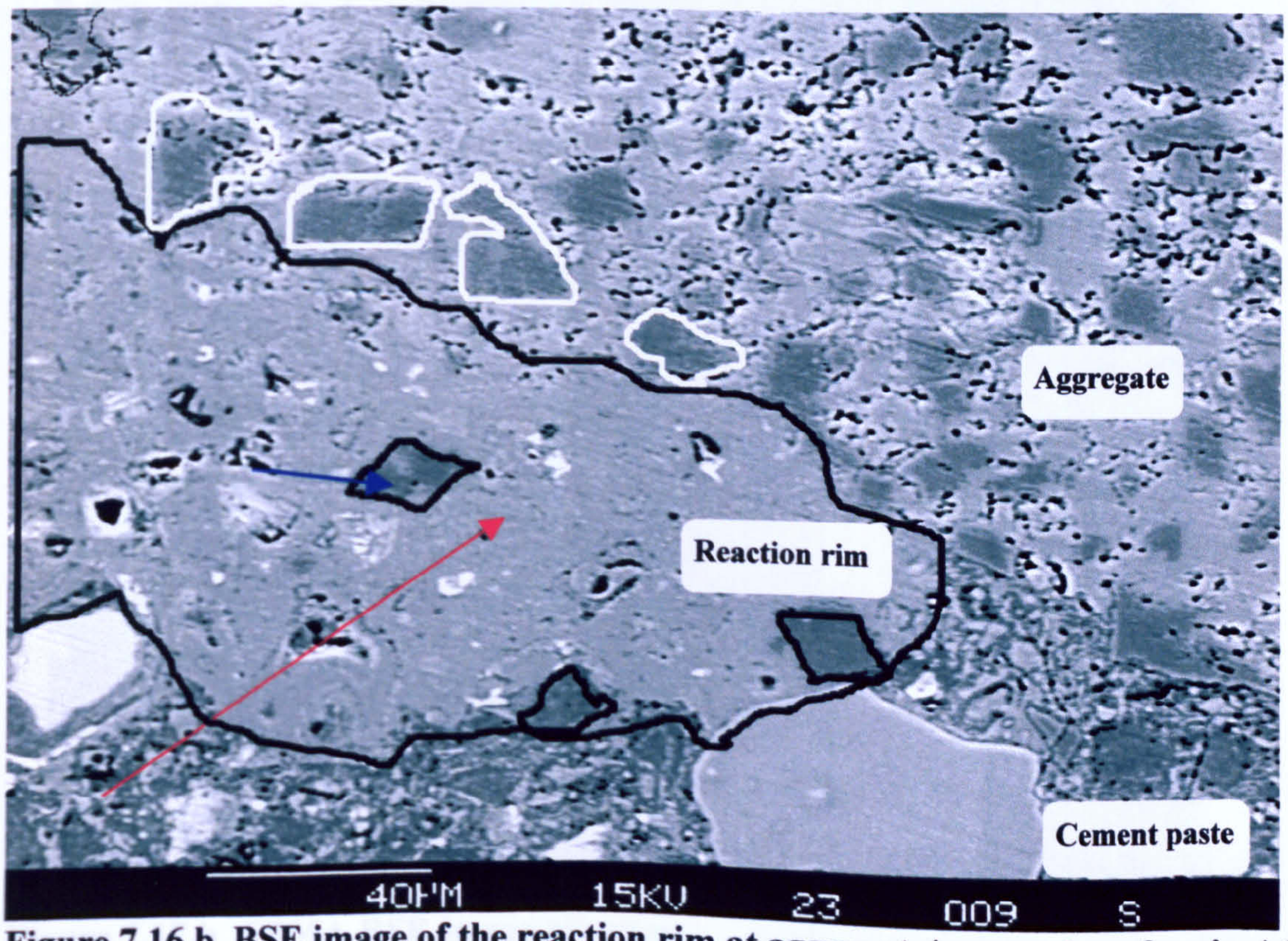

Figure 7.16.b BSE image of the reaction rim at aggregate/cement interface in ACR 10yrs old concrete from Canada. It shows dissolution of dolomites with a typical relict dolomites (pointed in blue) in the reaction rim (pointed in red).

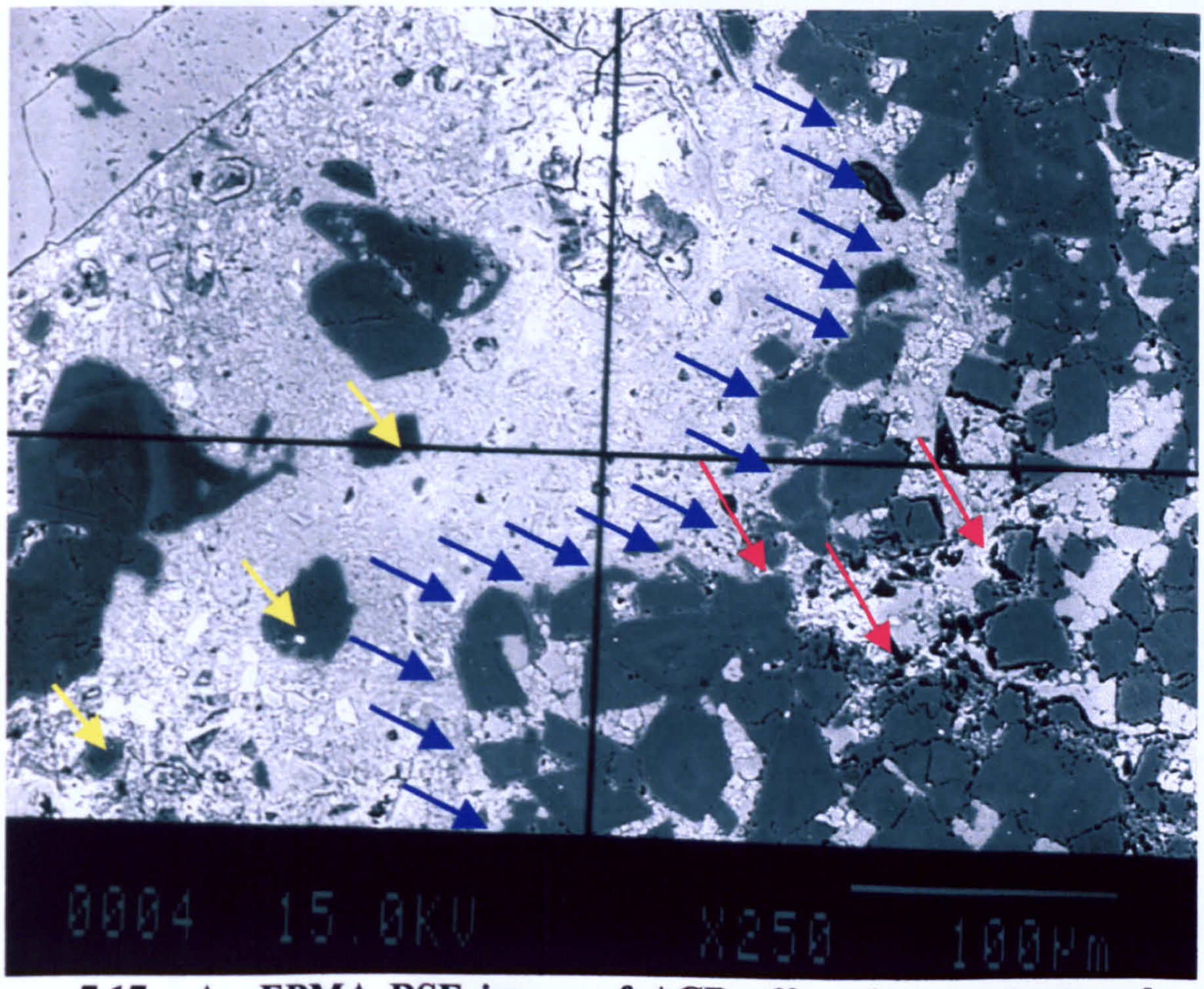

Figure 7.17.a An EPMA BSE image of ACR affected concrete sample, showing zoned, reacted dolomite grains (red arrows) **with unclear aggregate/cement boundary** (blue arrows) **and dolomite relicts** (yellow arrows).

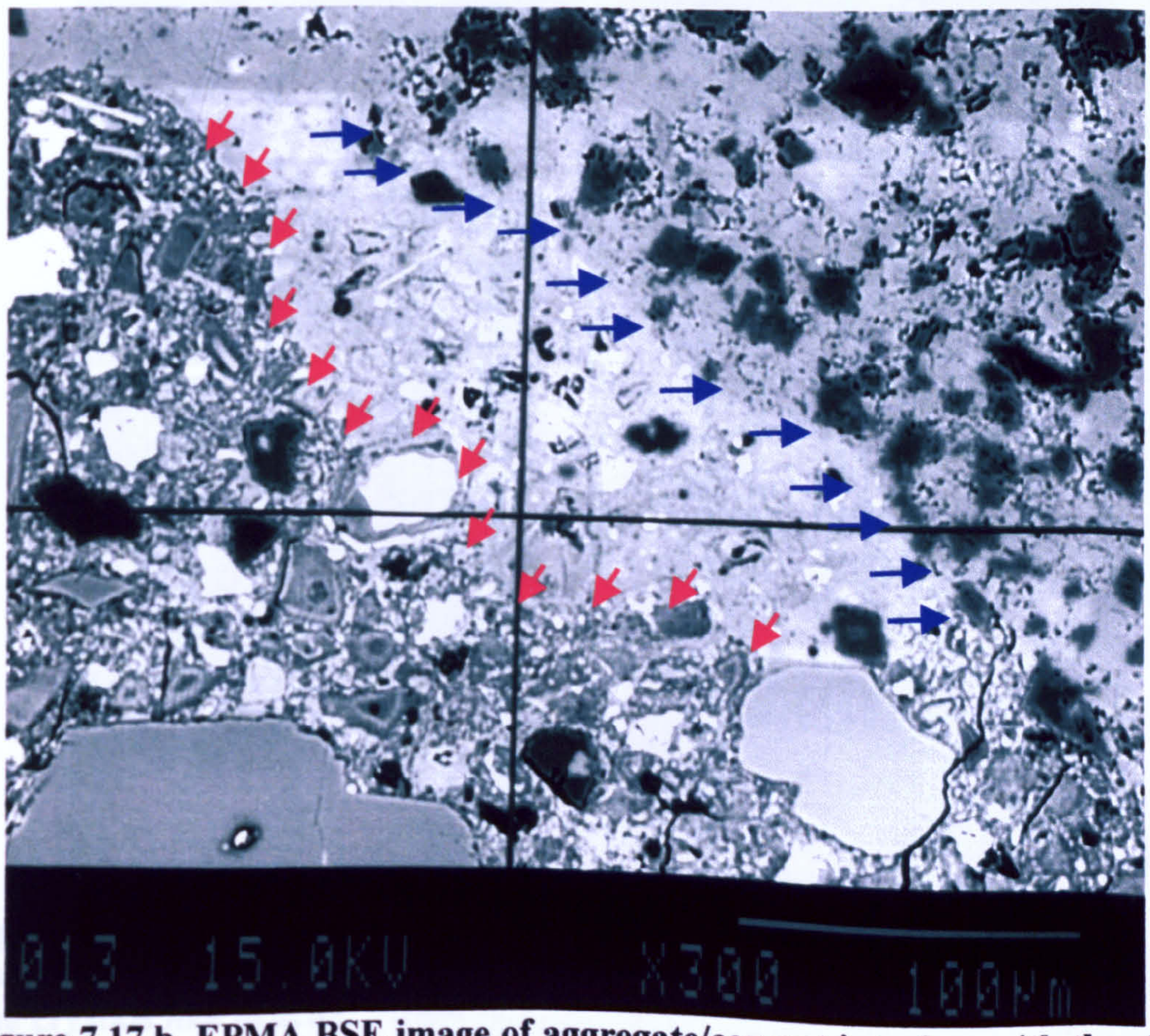

Figure 7.17.b EPMA BSE image of aggregate/cement interface with the elemental maps presented in Figure 7.18. Blue arrows point the aggregate, the cement-paste is pointed by red arrows, with the reaction rim between them.

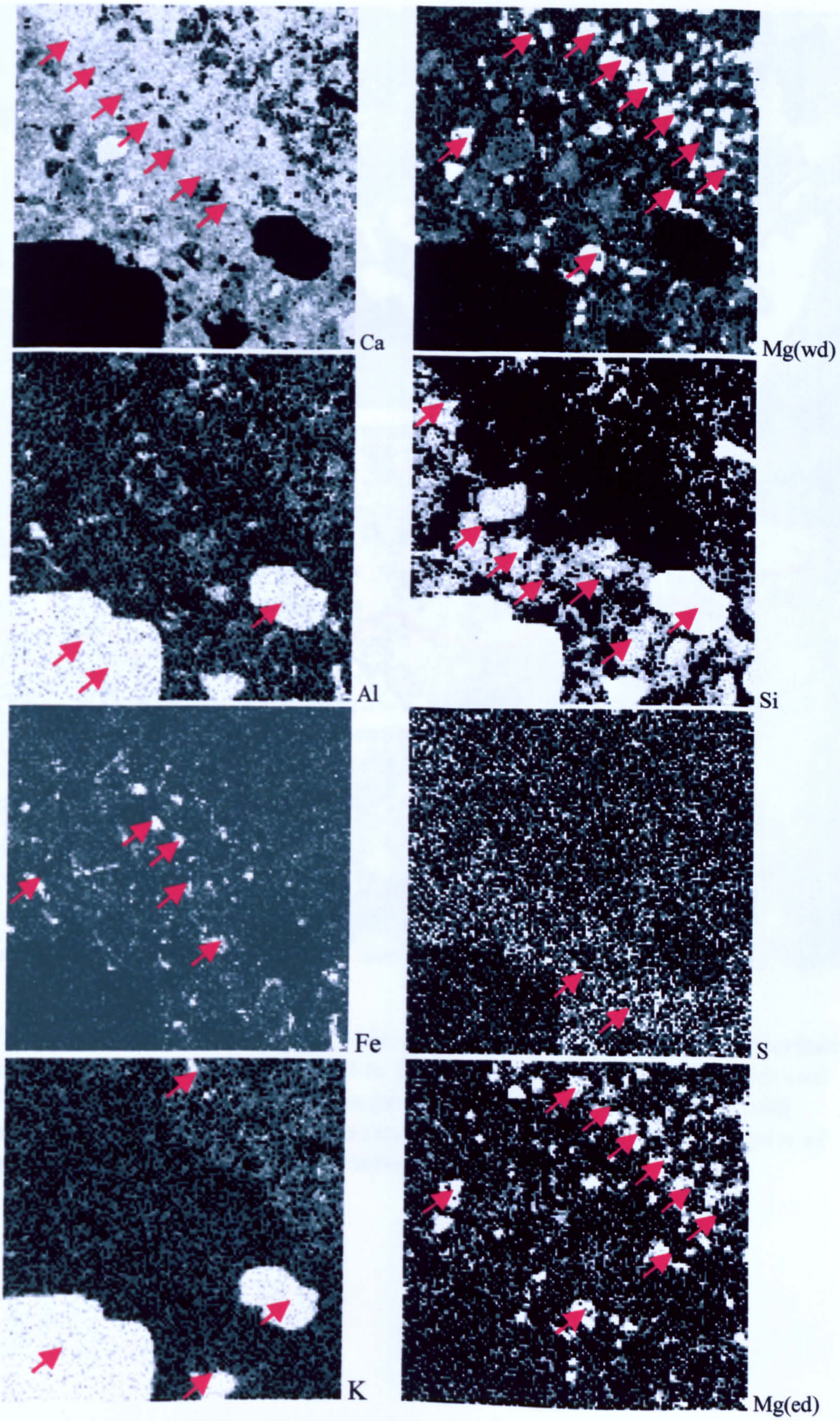

Figure 7.18 EPMA mapping of the transition zone of an ACR affected concrete, also illustrates sensitivity difference between wd and ed of particular interest for fine crystals like brucite. Areas of high concentration of each element are pointed with red arrows. The BSE image of the mapped area is shown in Figure 7.17b.

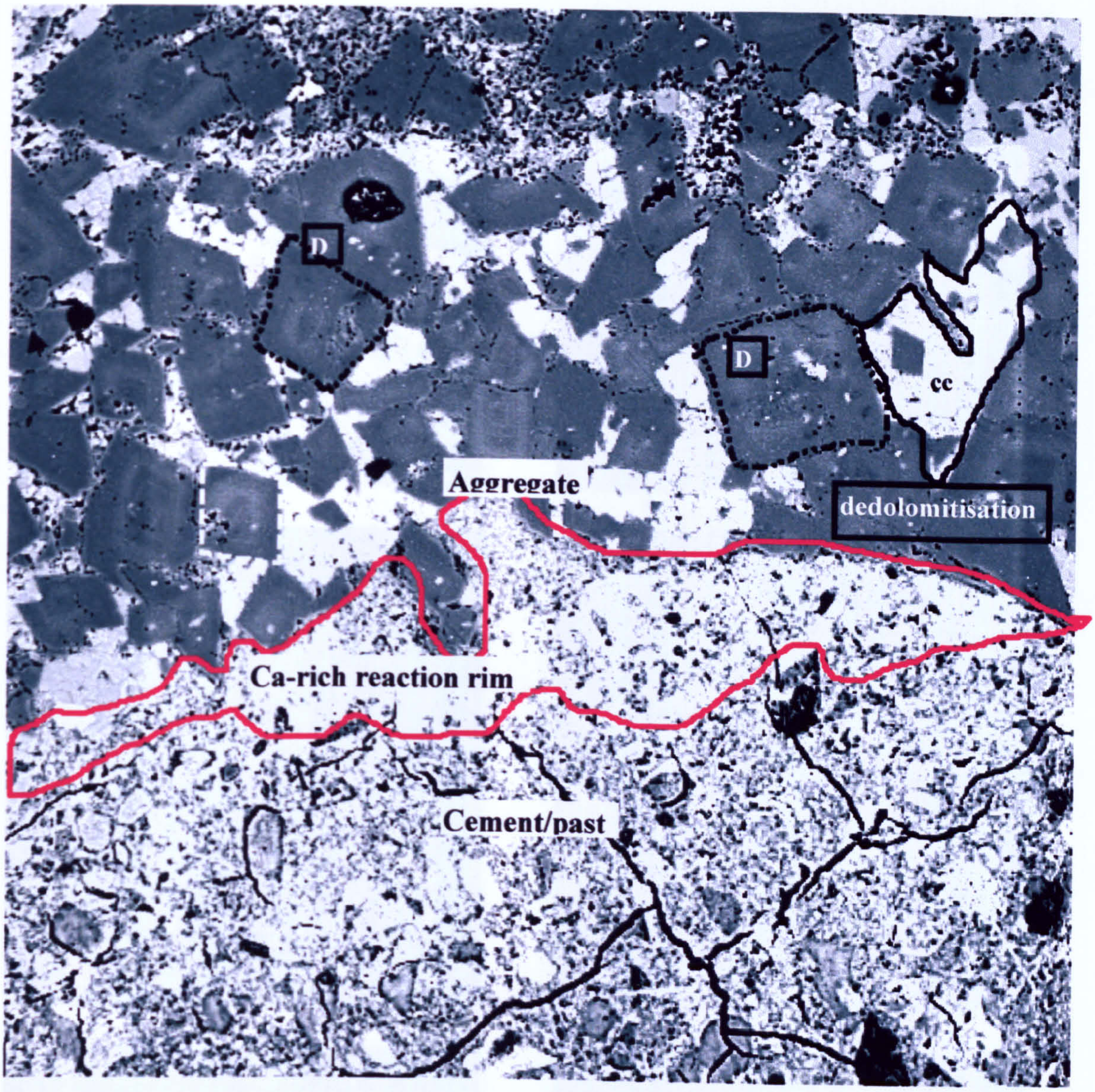

Figure 7.19 Back scattered electron image of an aggregate cement-paste interface, impregnated in epoxy resin and ground to 1micron fine surface. Image obtained using EPMA. The top part of the image presents the dolomite aggregate with reacted dolomite crystals. The reaction rim is outlined in red. The lower part of the image shows the cement and fine microcracks.

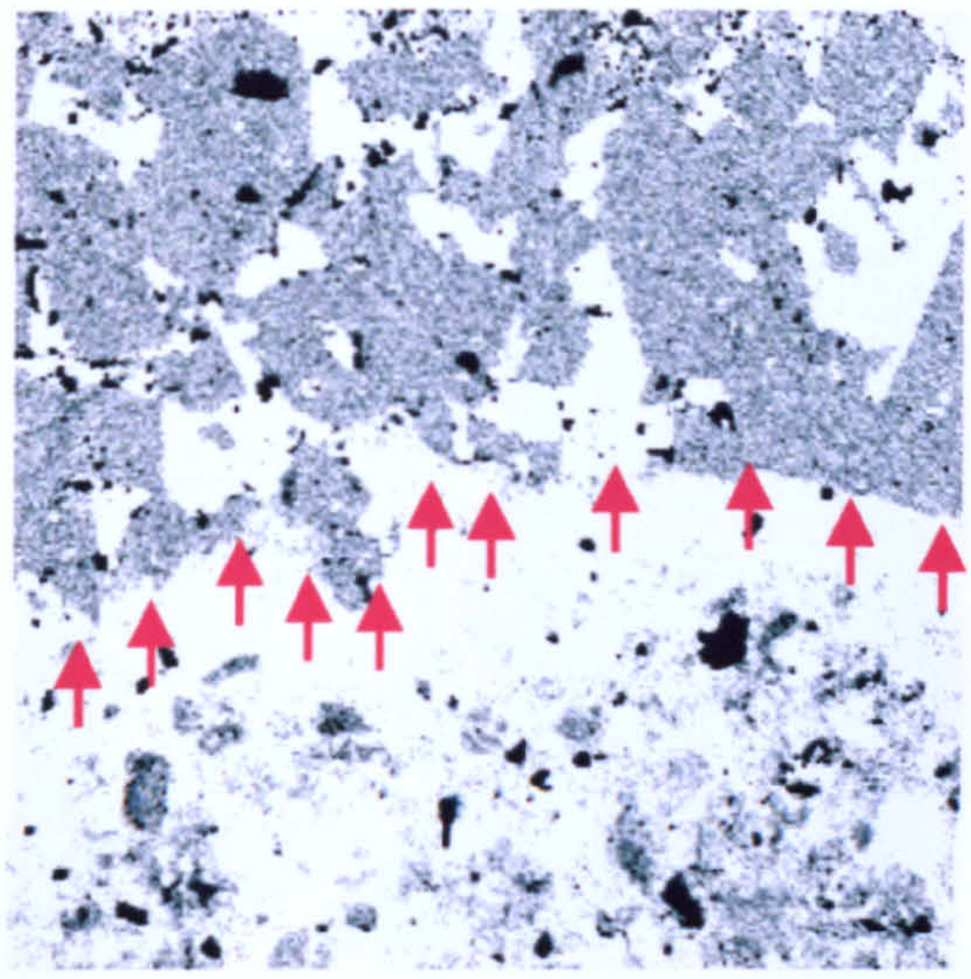

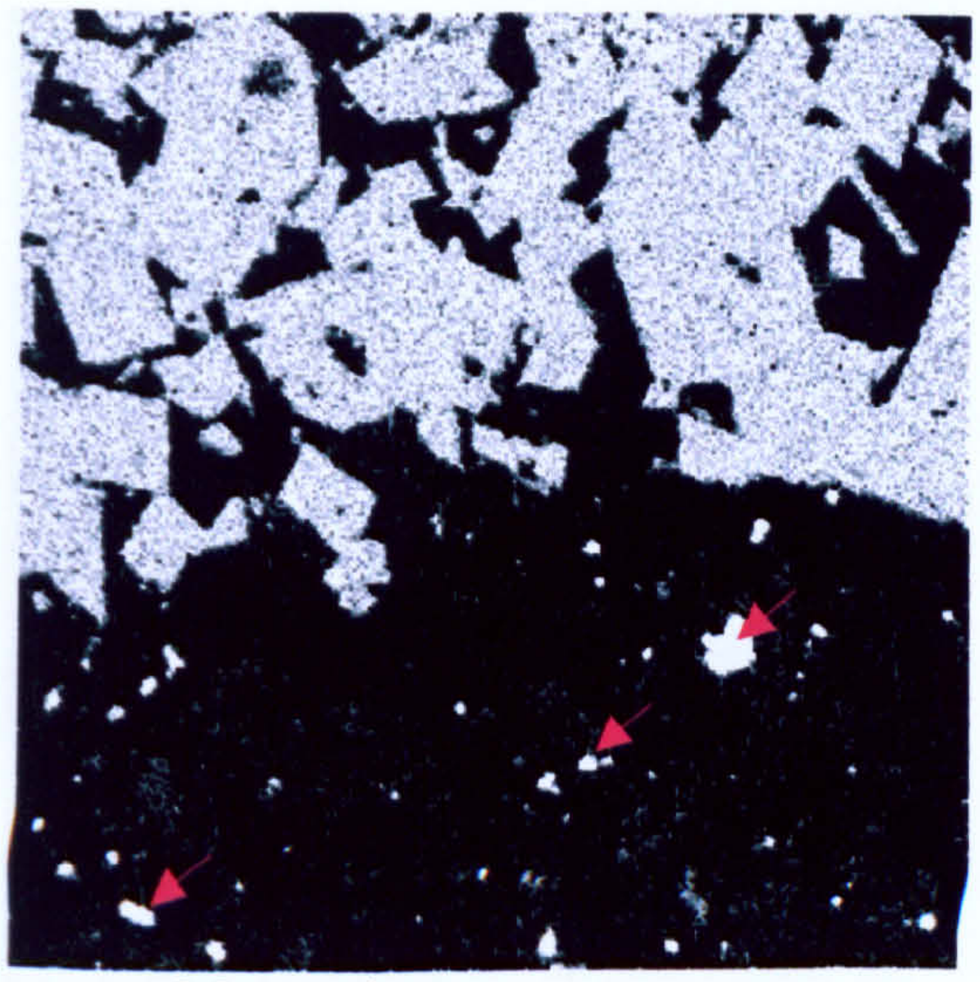

Calcium

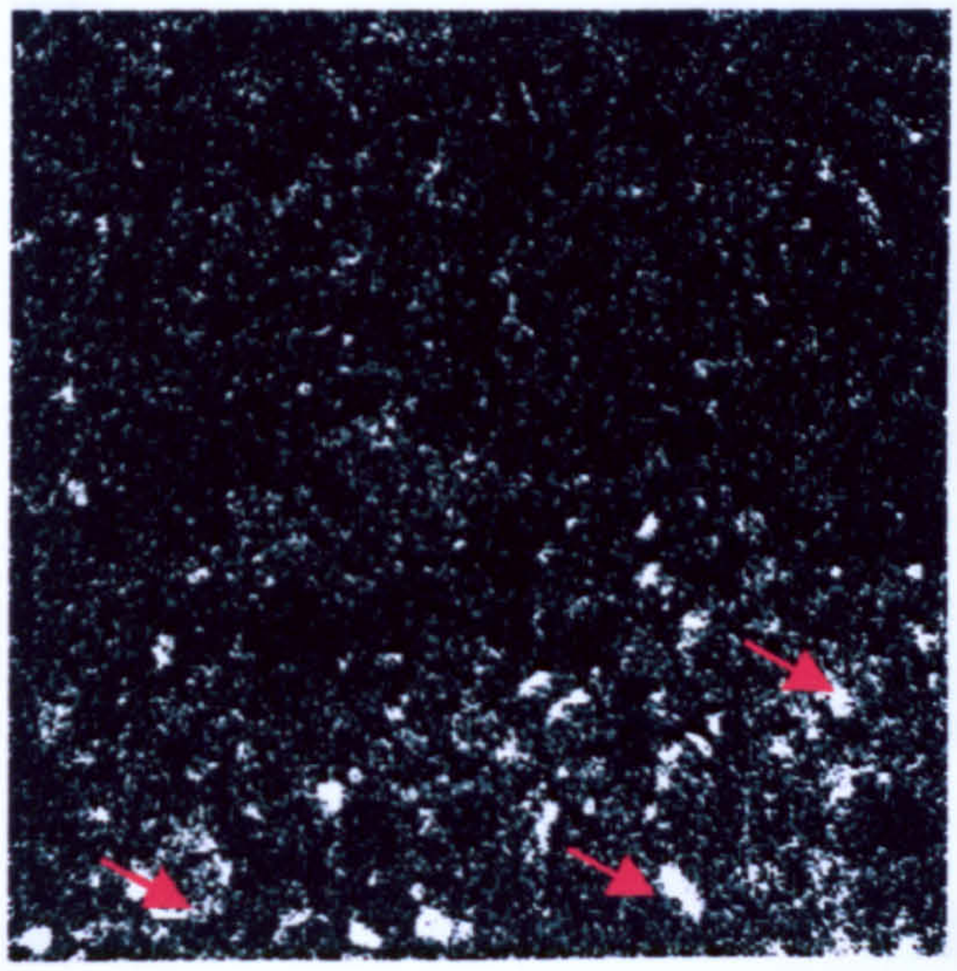

Magnesium

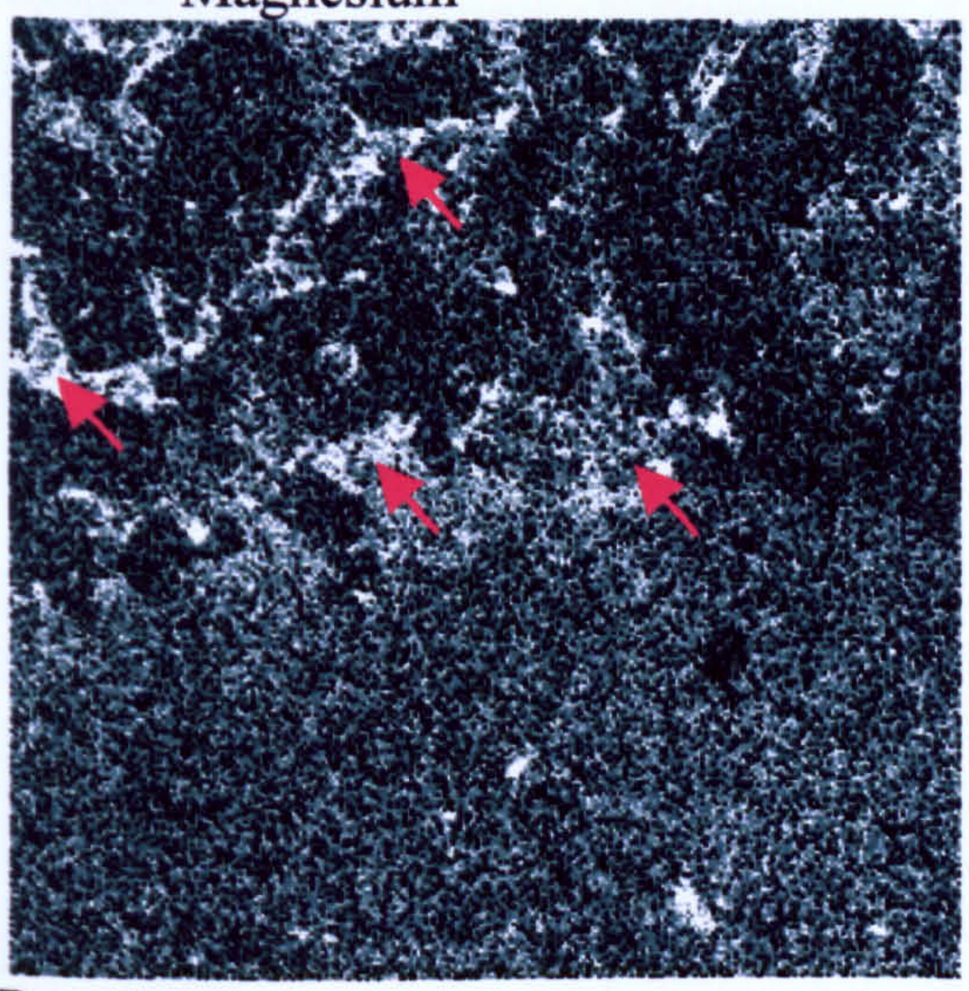

Iron

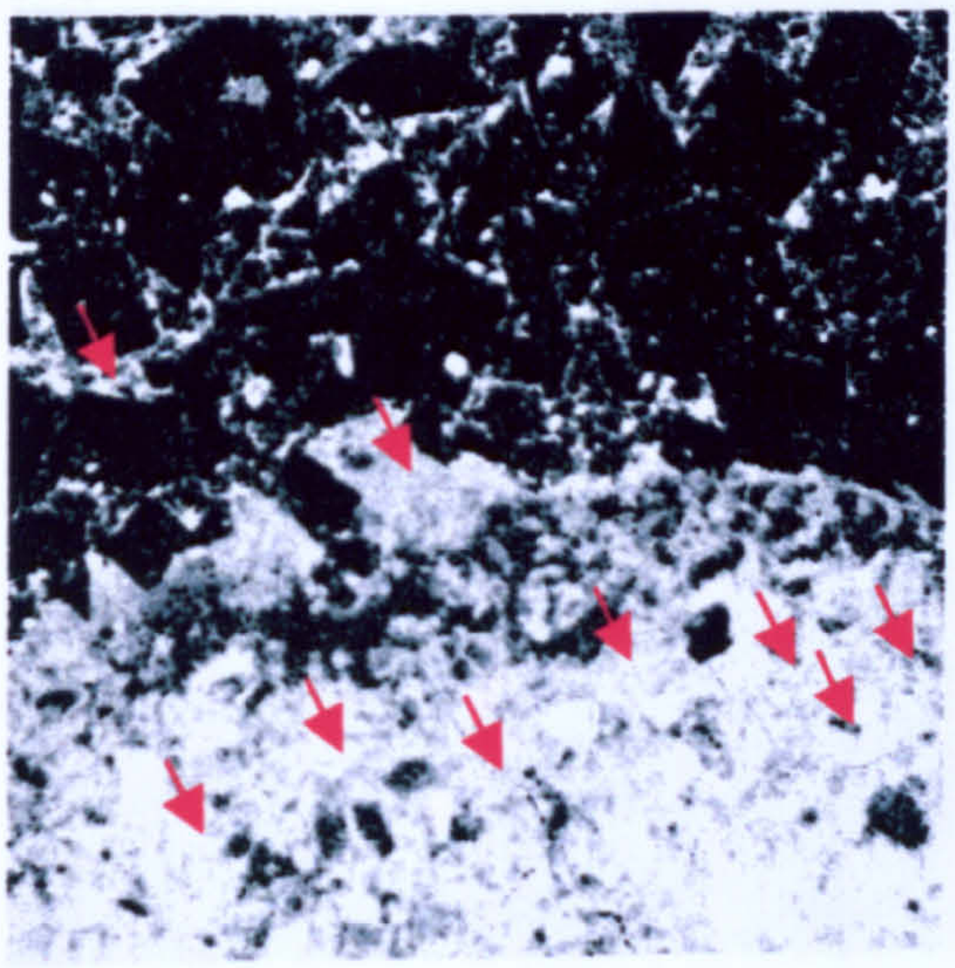

Potasium

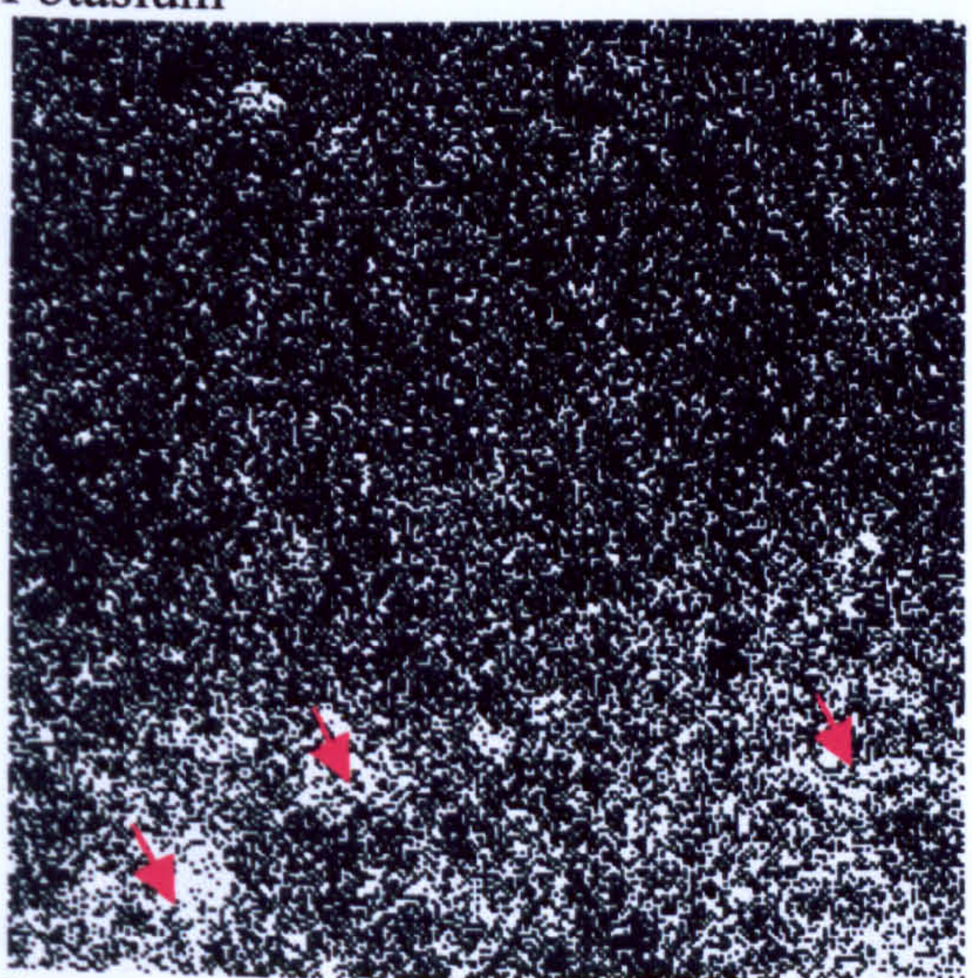

Silicon

Sulphur

Figure 7.20 Elemental distribution of major elements at aggregate cement interface, aggregate undergone ACR, mapped area from Figure 7.19.
(red arrows point at increased concentration of element relevant to each map)

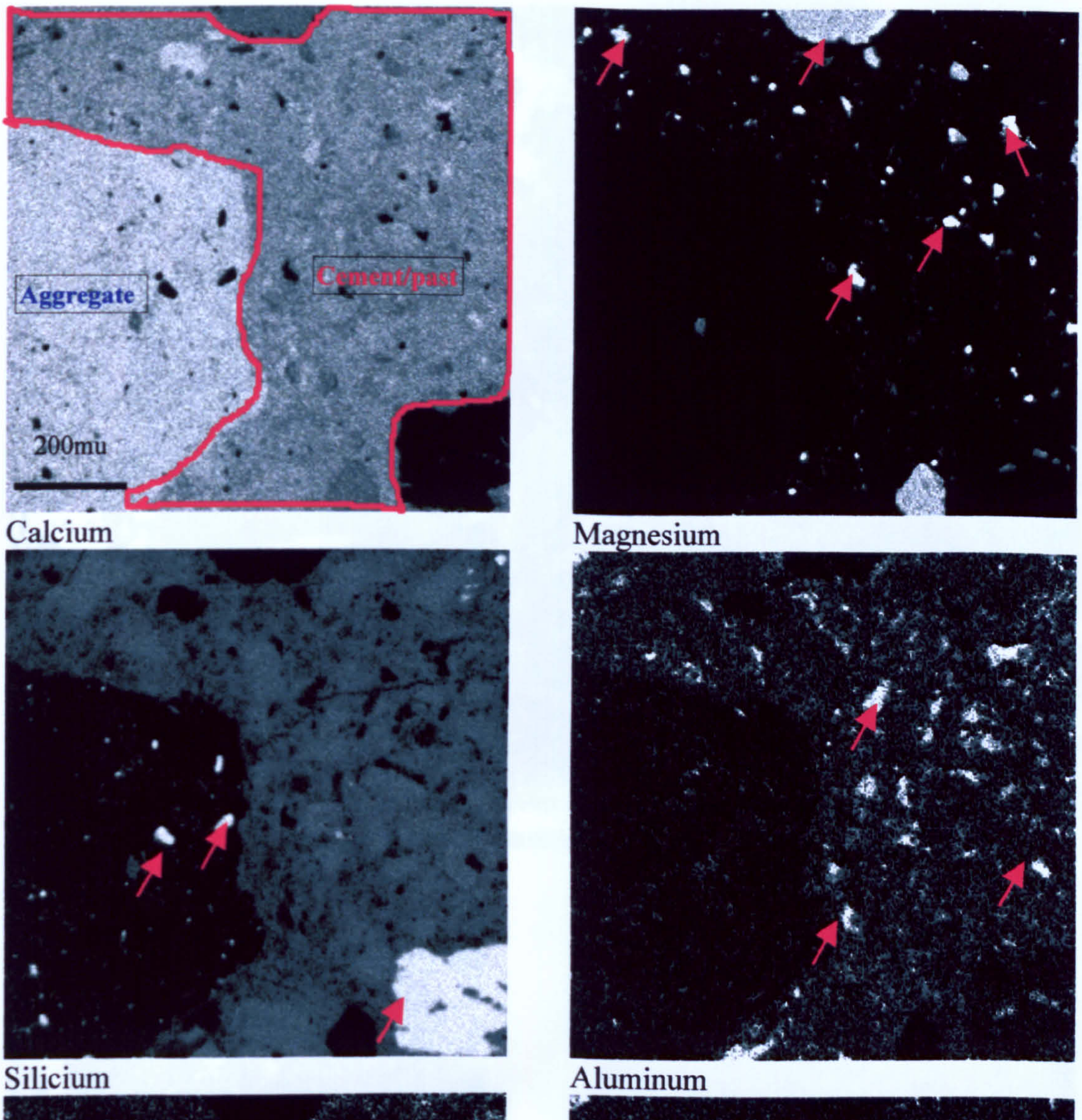

Figure 7.21 EPMA mapping revealing spatial elemental distribution within cement paste (outlined in red), and high concentrations of each element are pointed with red arrows.

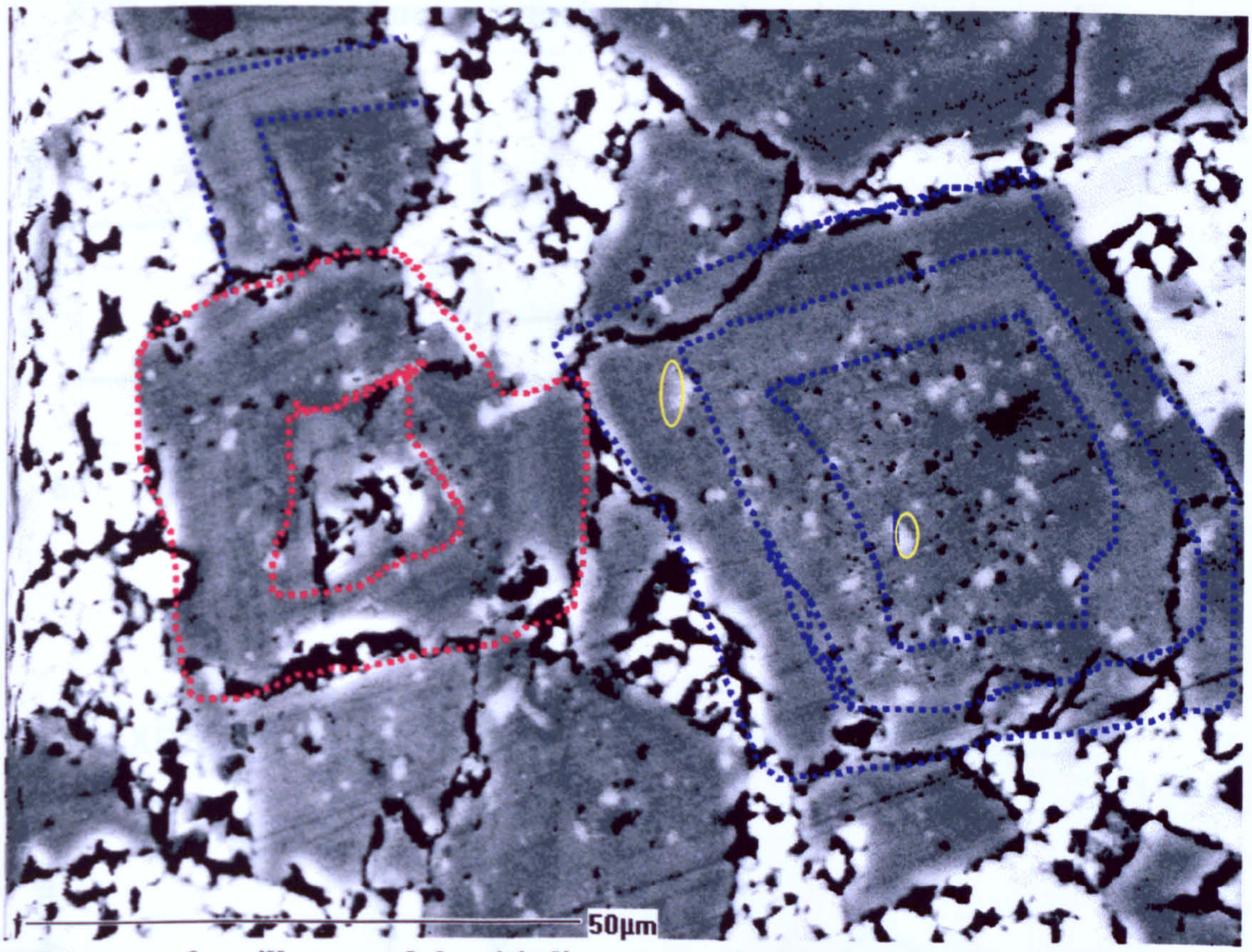

BE image of argillaceous dolomitic limestone after 3yrs in NaOH solution.

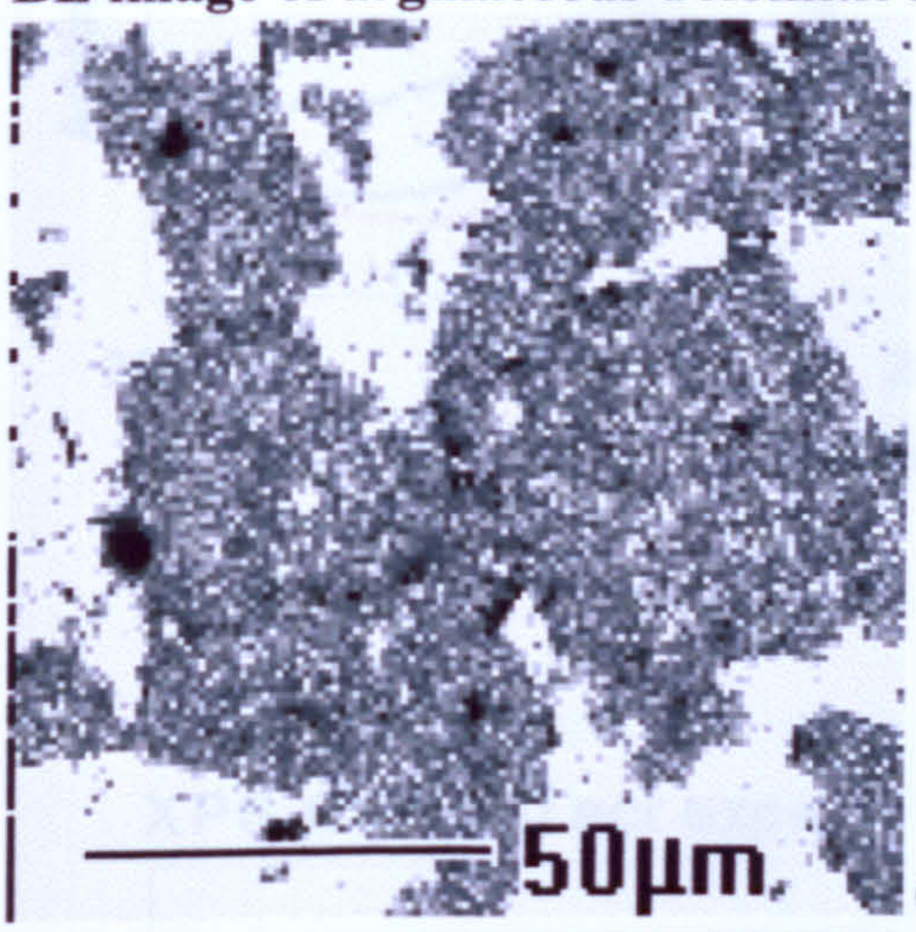

Ca

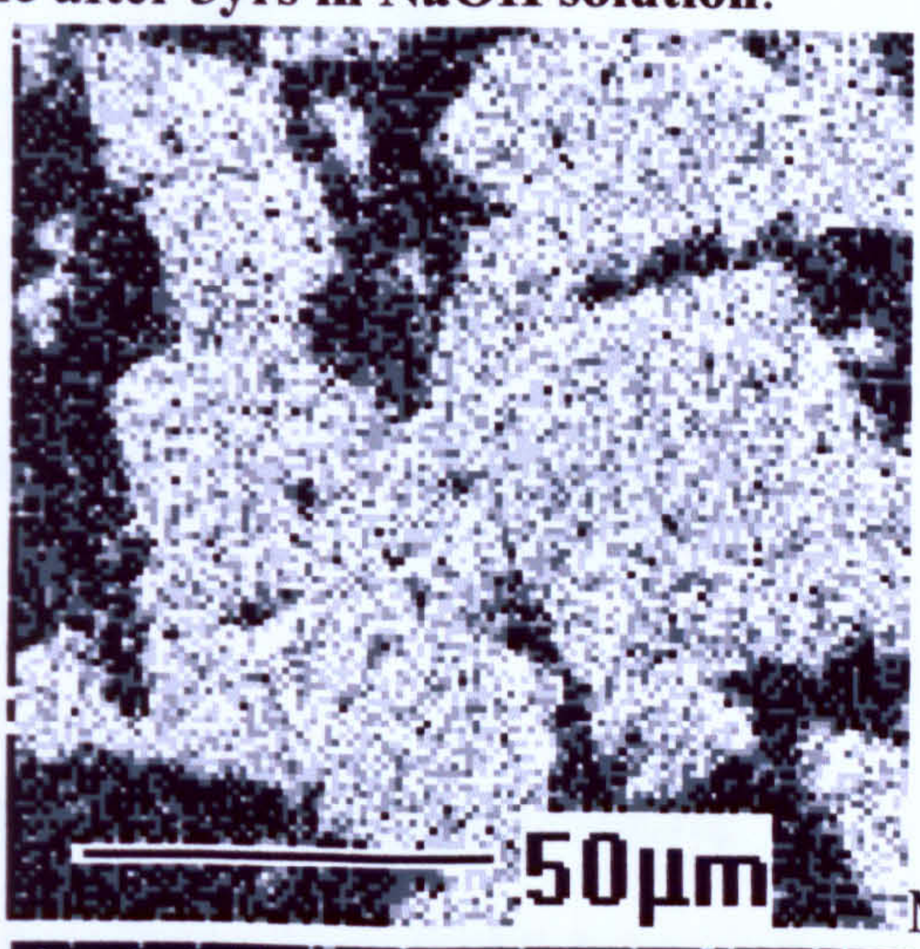

Mg

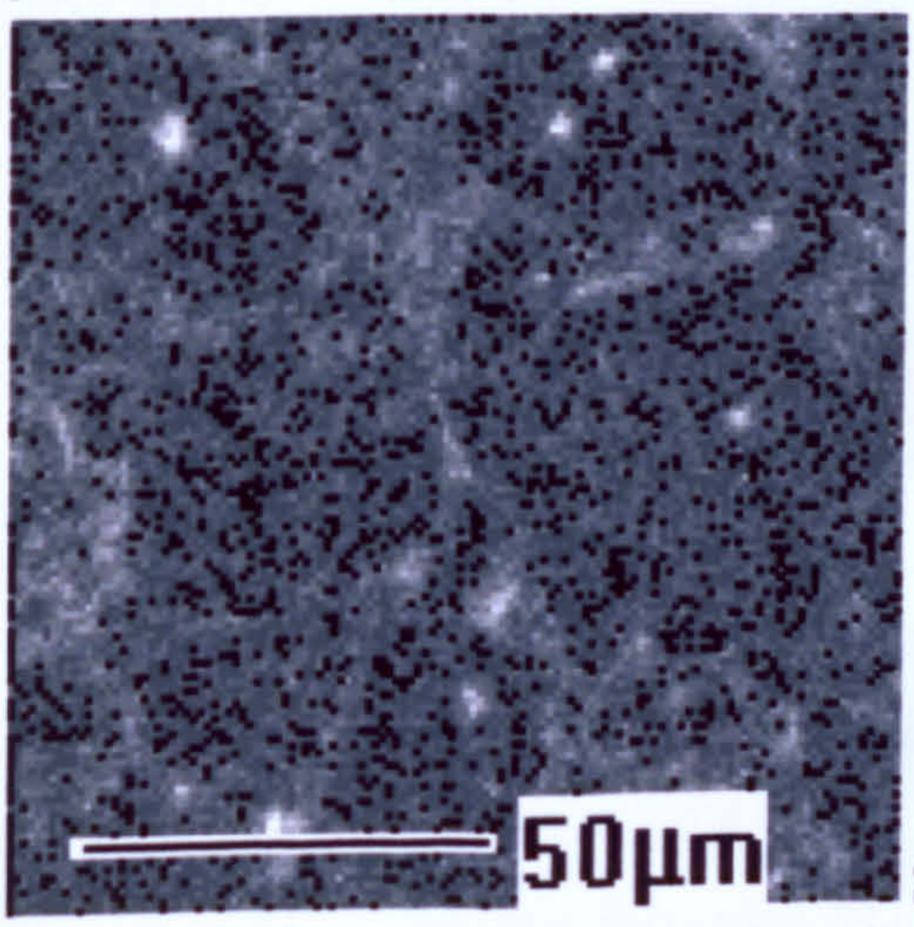

Si

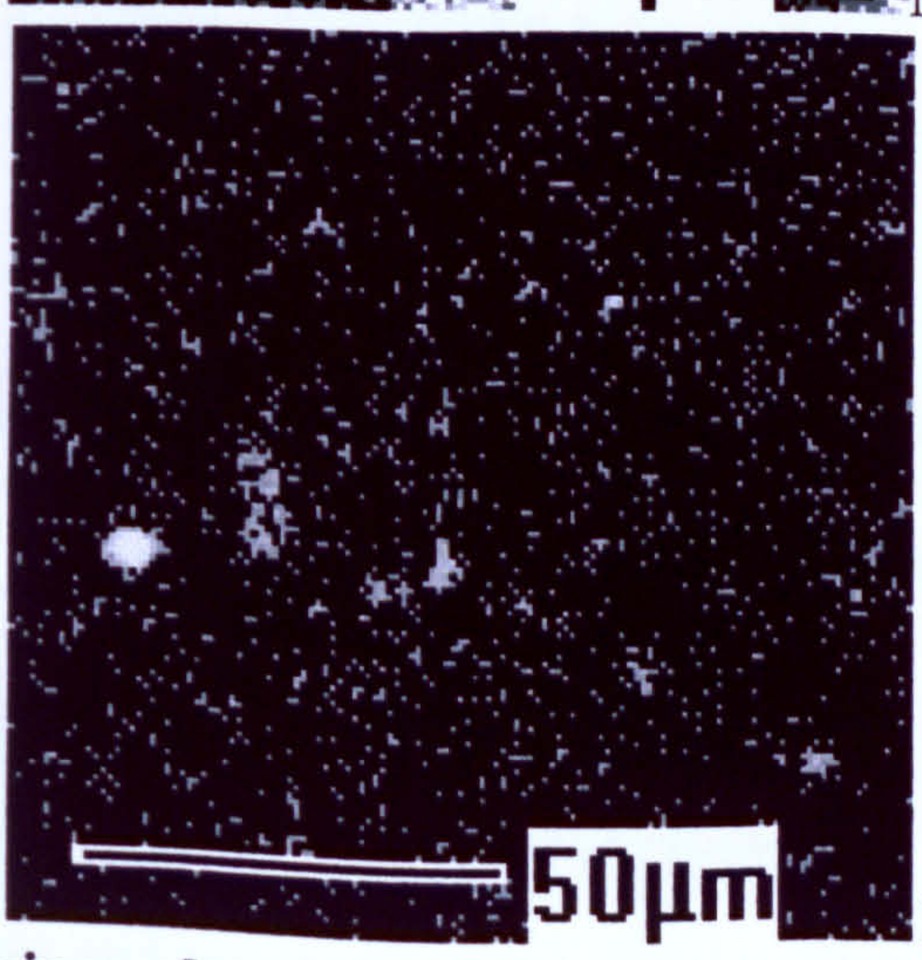

Fe

Figure 7.22 Distribution of major and minor chemical components in dolomite crystals after NaOH treatment and excessive expansion, (zoning outlined, inclusions)

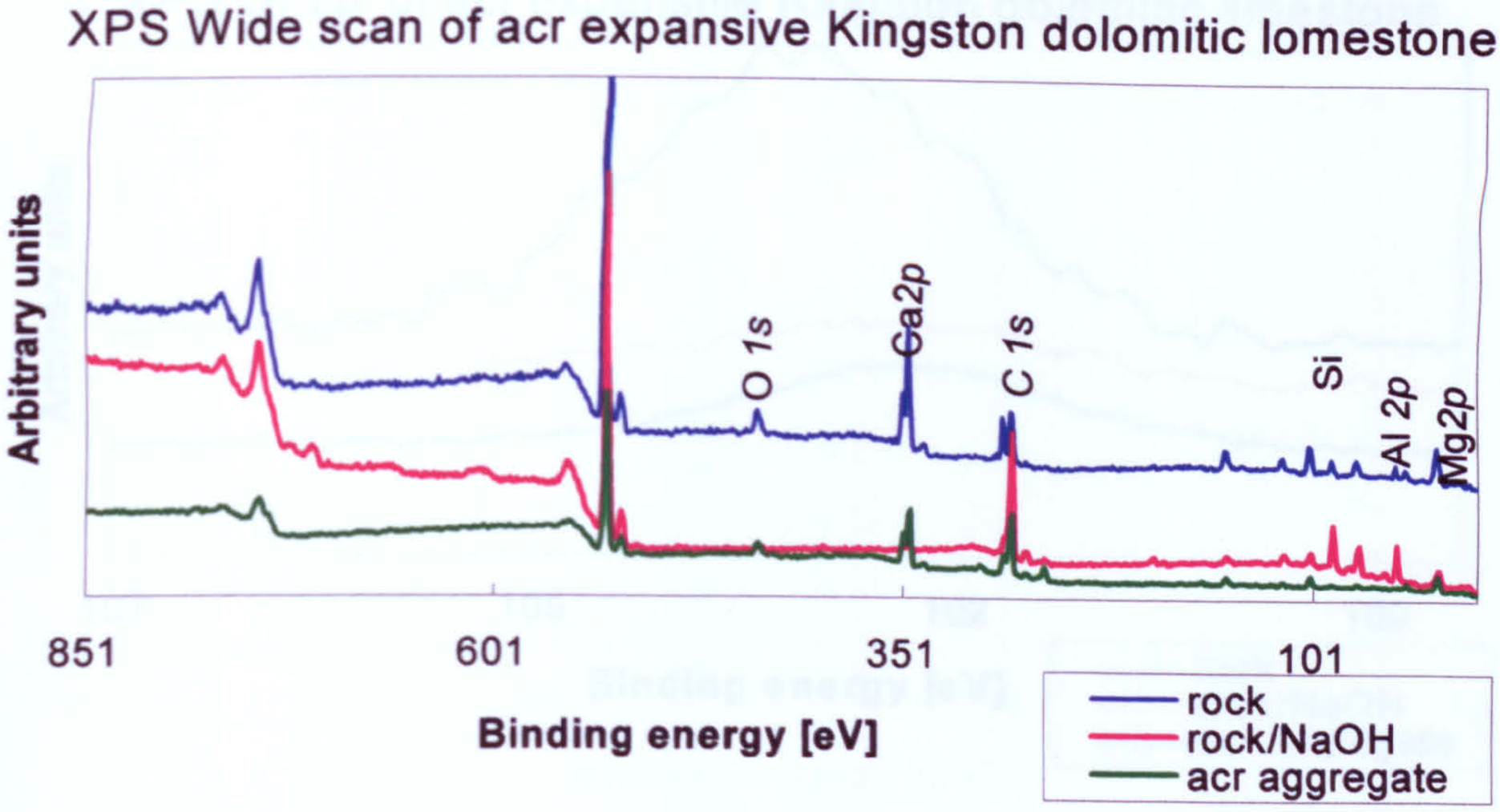
XPS Wide scan of acr expansive Kingston dolomitic lomestone
Arbitrary units
O 1s
Ca2p
C 1s
Si
Al 2p
Mg2p
851
601
351
101
Binding energy [eV]
rock
rock/NaOH
acr aggregate

a)

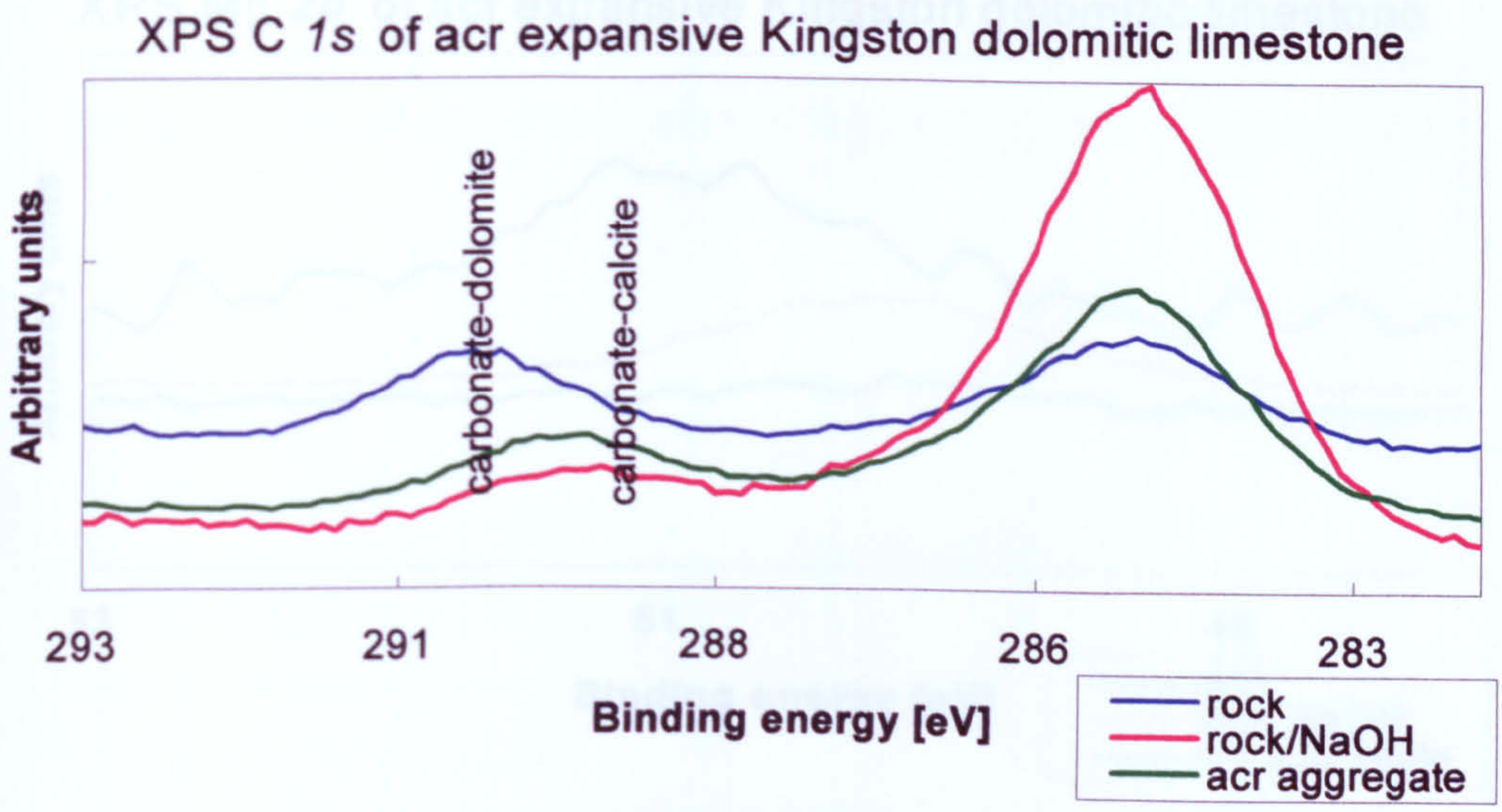
XPS C 1s of acr expansive Kingston dolomitic limestone
Arbitrary units
carbonate-dolomite
carbonate-calcite
293
291
288
286
283
Binding energy [eV]
rock
rock/NaOH
acr aggregate

b)

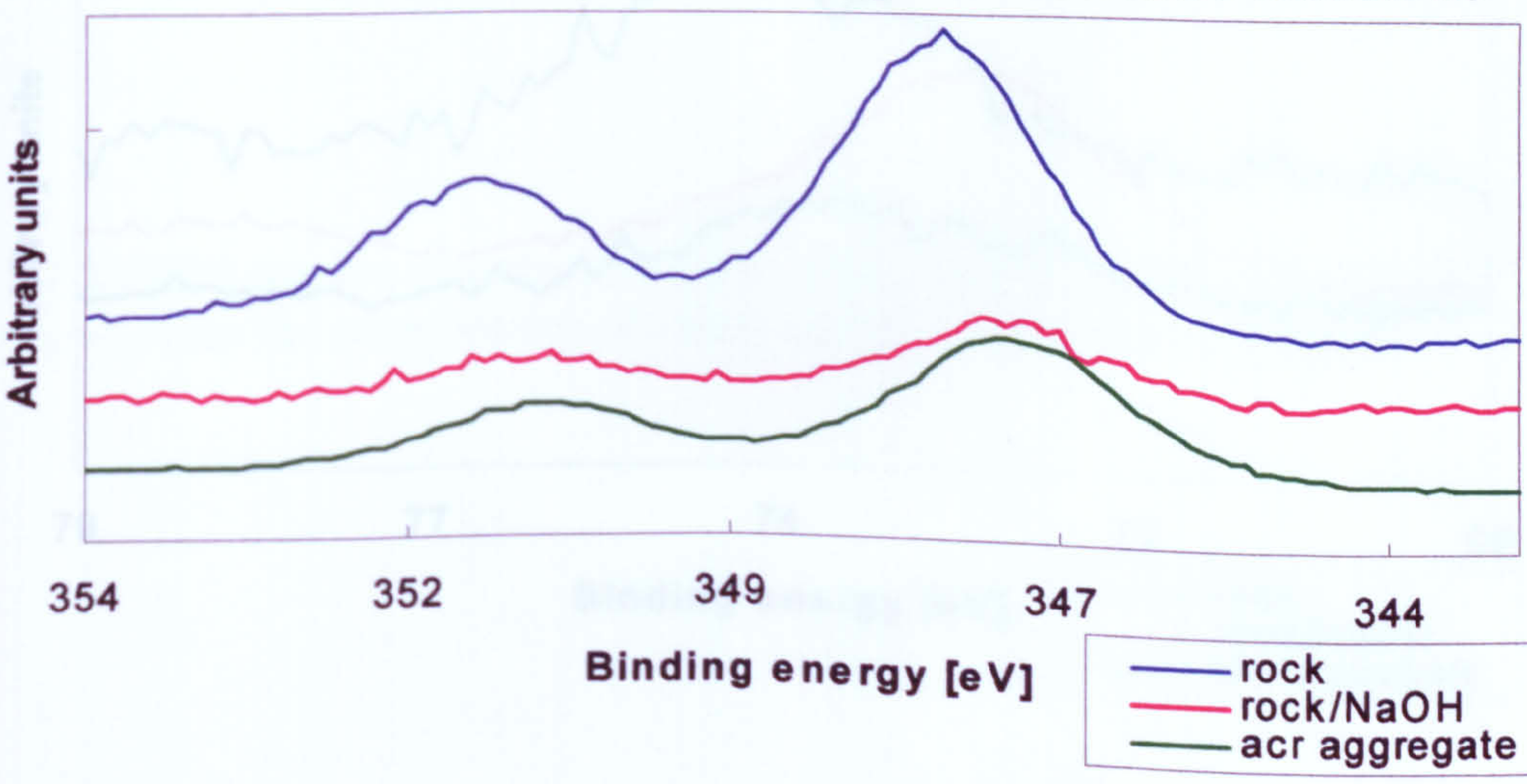
XPS Ca 2p of acr expansive Kingston dolomitic limestone
Arbitrary units
354
352
349
347
344
Binding energy [eV]
rock
rock/NaOH
acr aggregate

c)

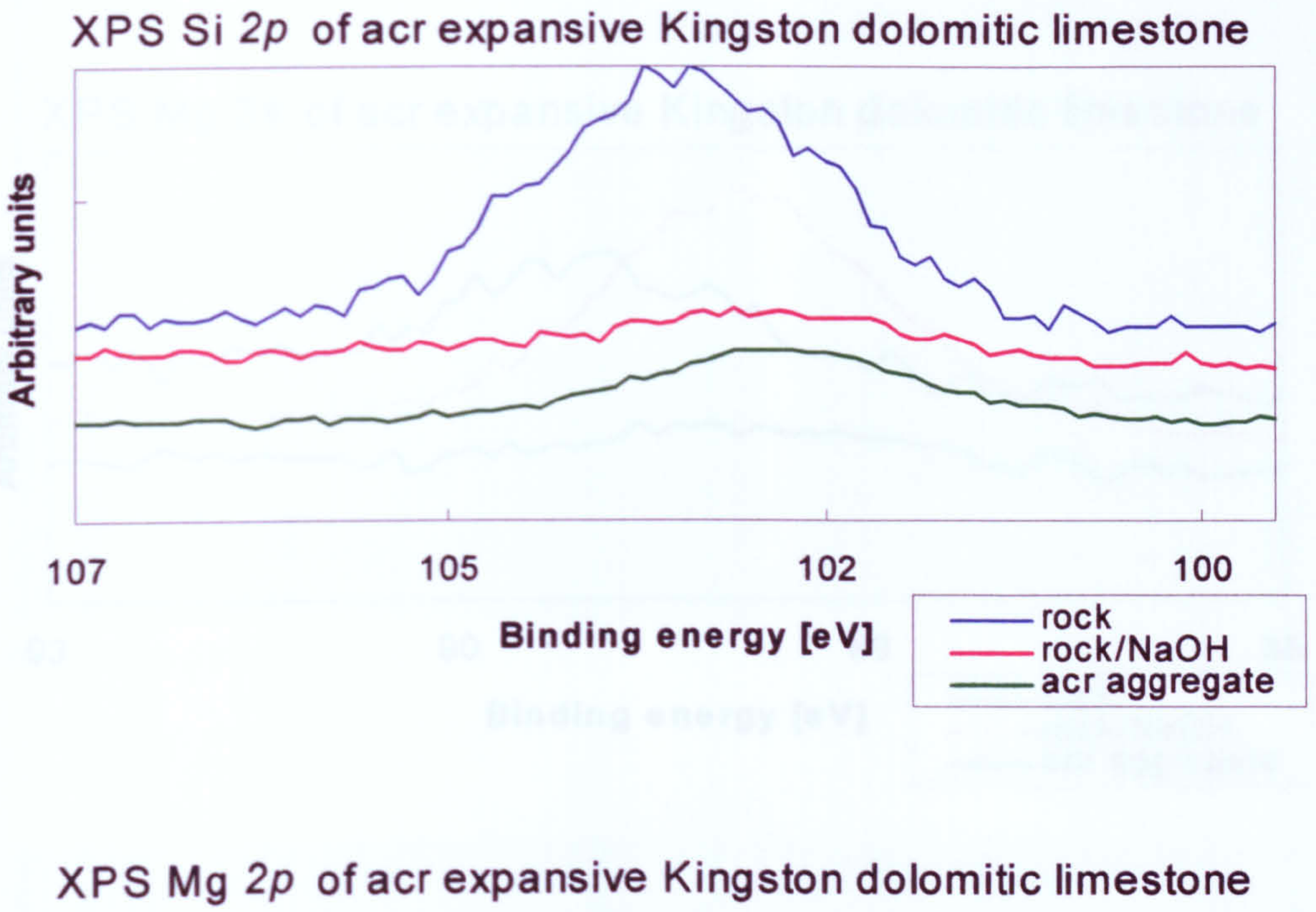
XPS Si 2p of acr expansive Kingston dolomitic limestone
Arbitrary units
107
105
102
100
Binding energy [eV]
rock
rock/NaOH
acr aggregate

d)

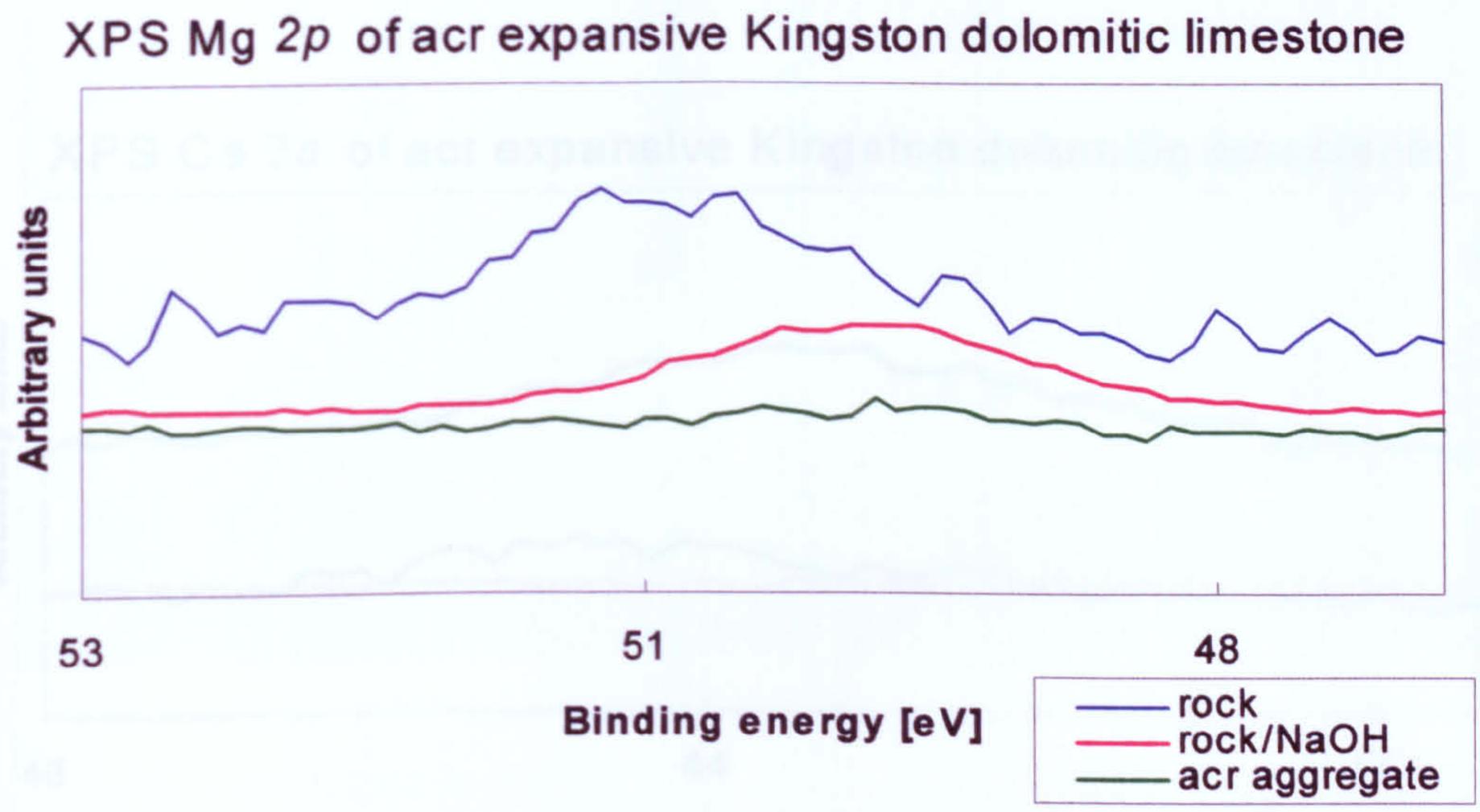
XPS Mg 2p of acr expansive Kingston dolomitic limestone
Arbitrary units
53
51
48
Binding energy [eV]
rock
rock/NaOH
acr aggregate

e)

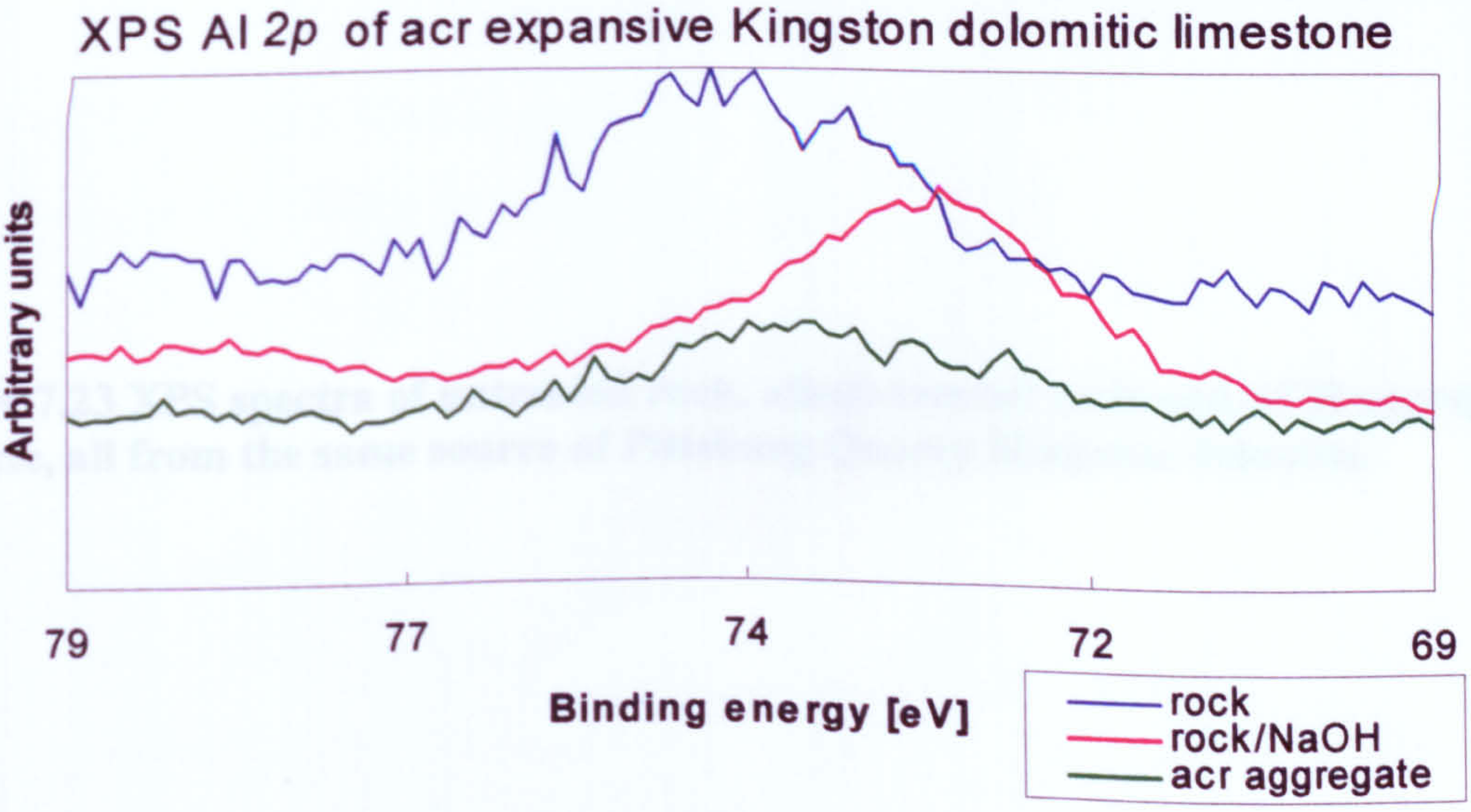
XPS Al 2p of acr expansive Kingston dolomitic limestone
Arbitrary units
79
77
74
72
69
Binding energy [eV]
rock
rock/NaOH
acr aggregate

f)

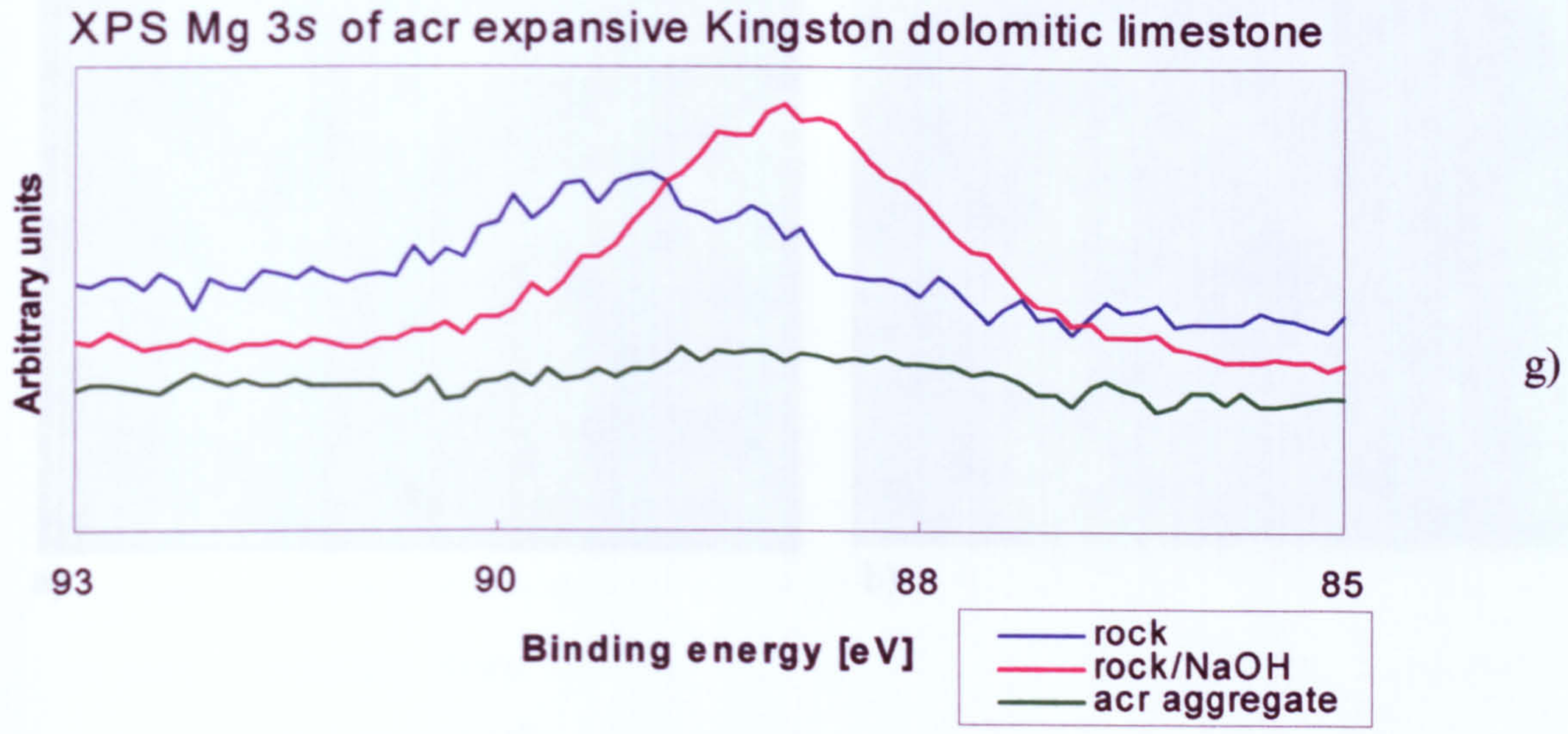

g)

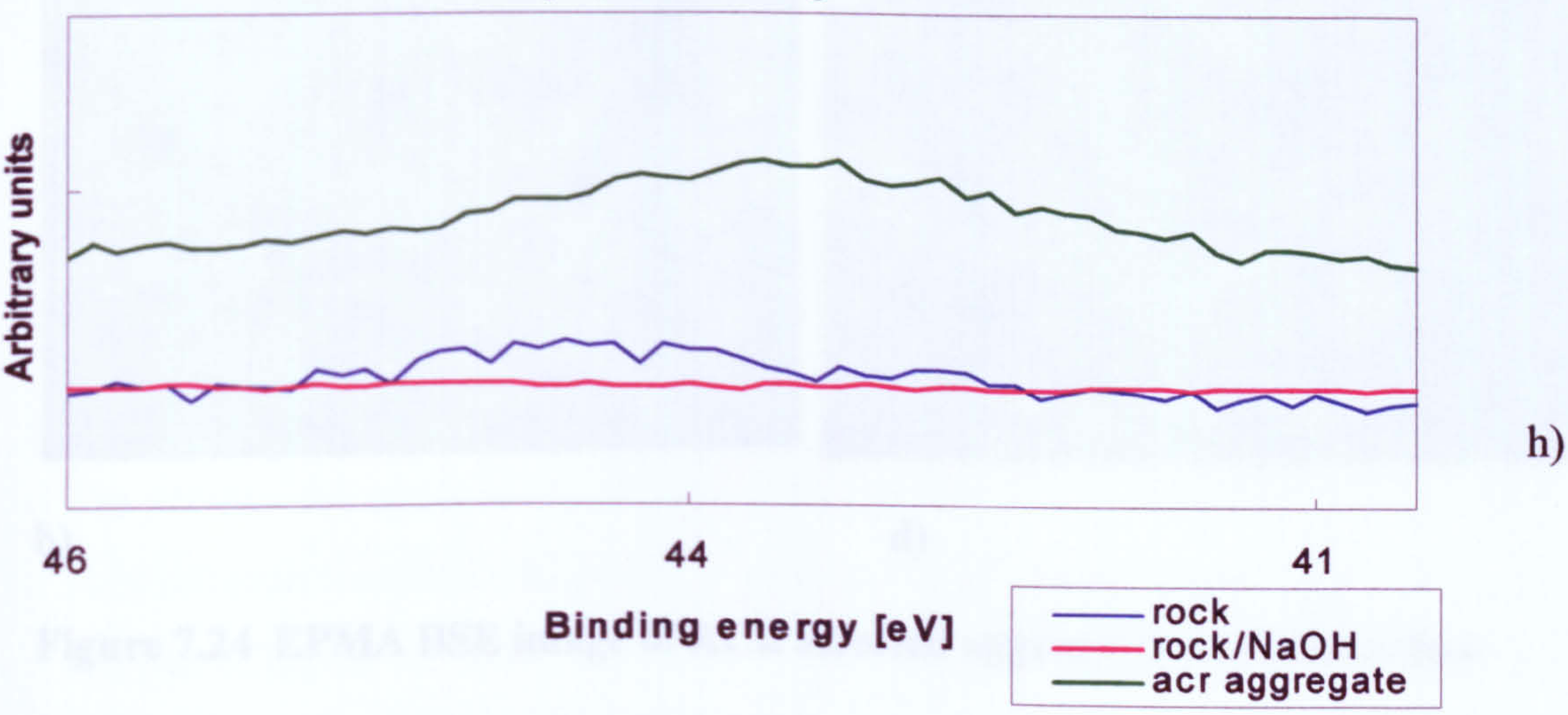

h)

Figure 7.23 XPS spectra of untreated rock, alkali-treated rock and ACR aggregate particle, all from the same source of Pittsburg Quarry Kingston dolomite.

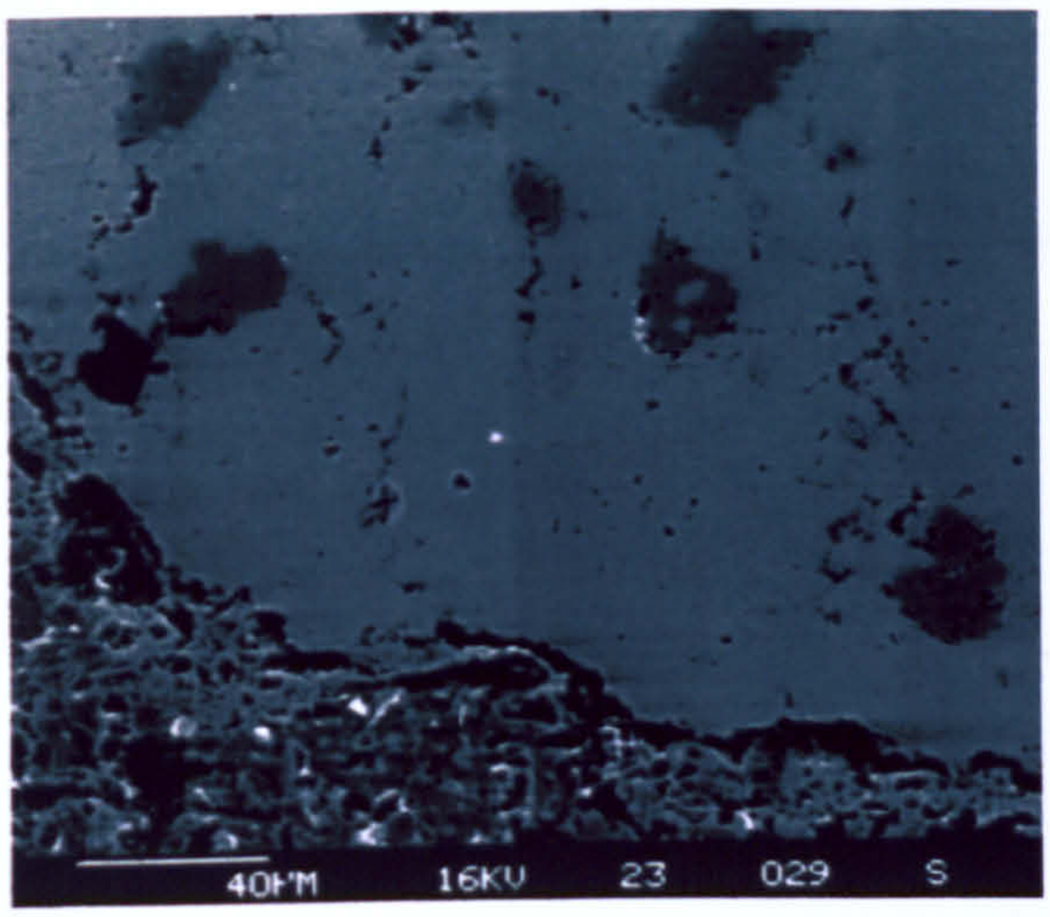

a)

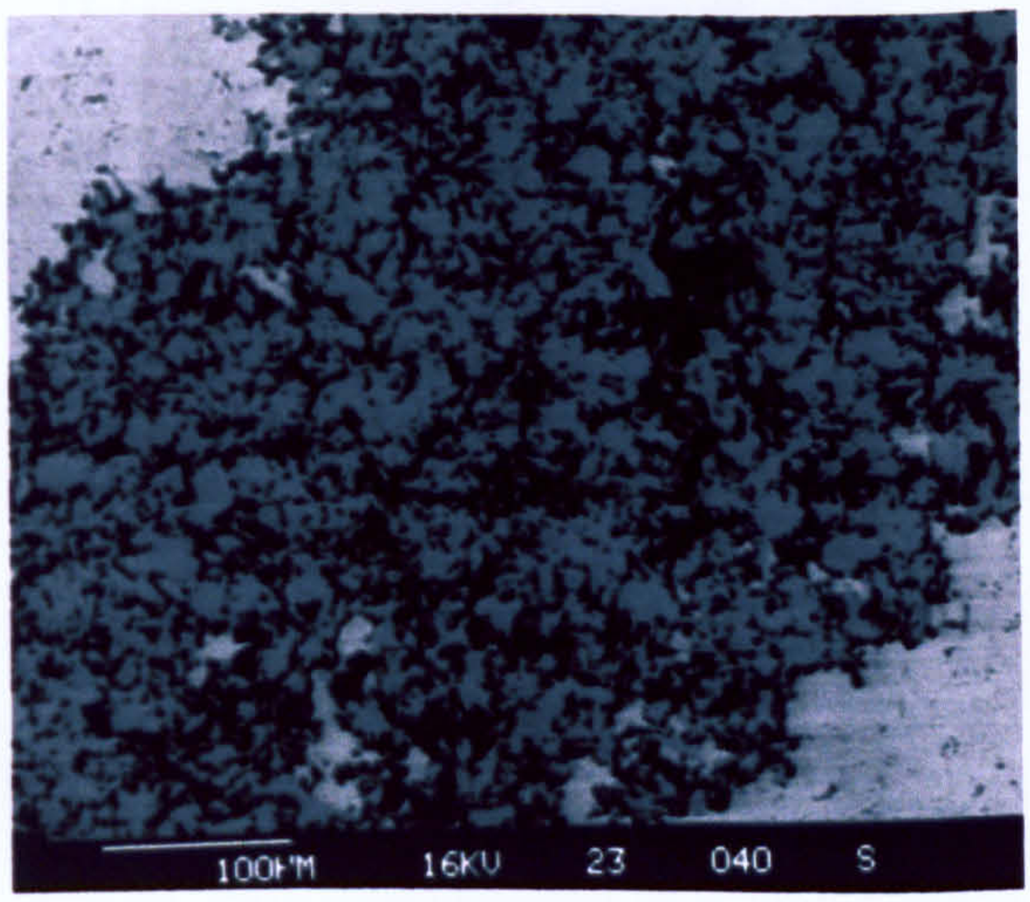

b)

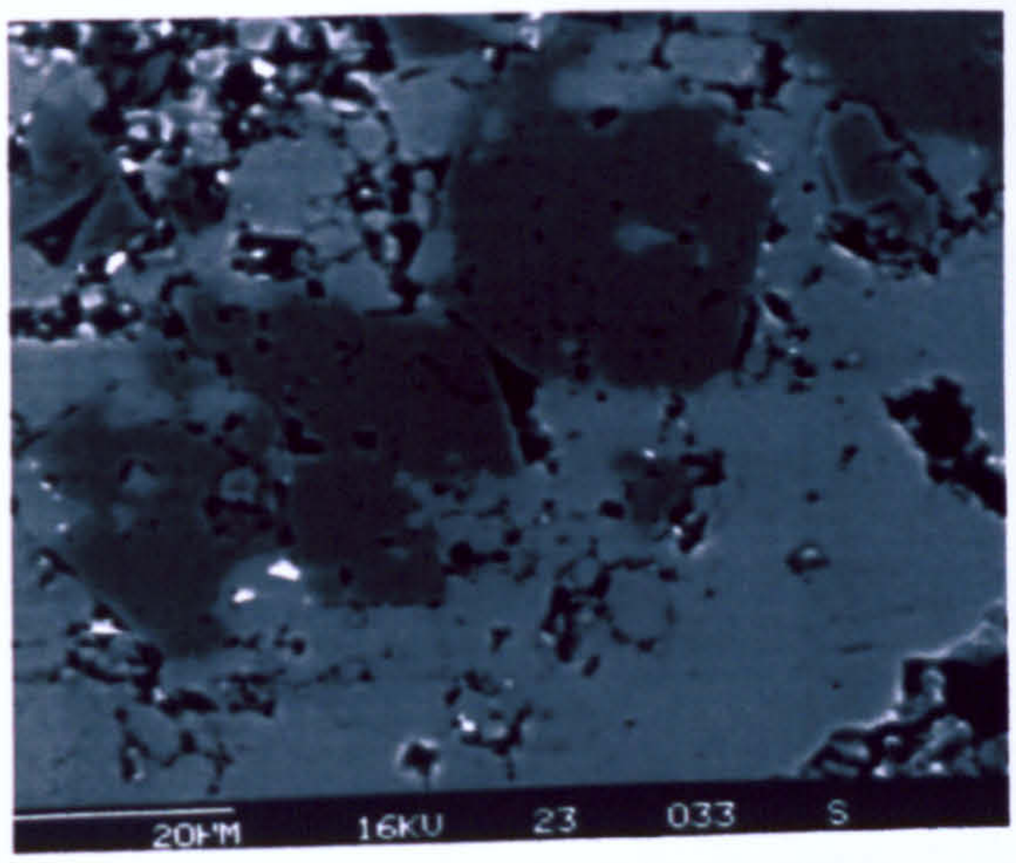

b)

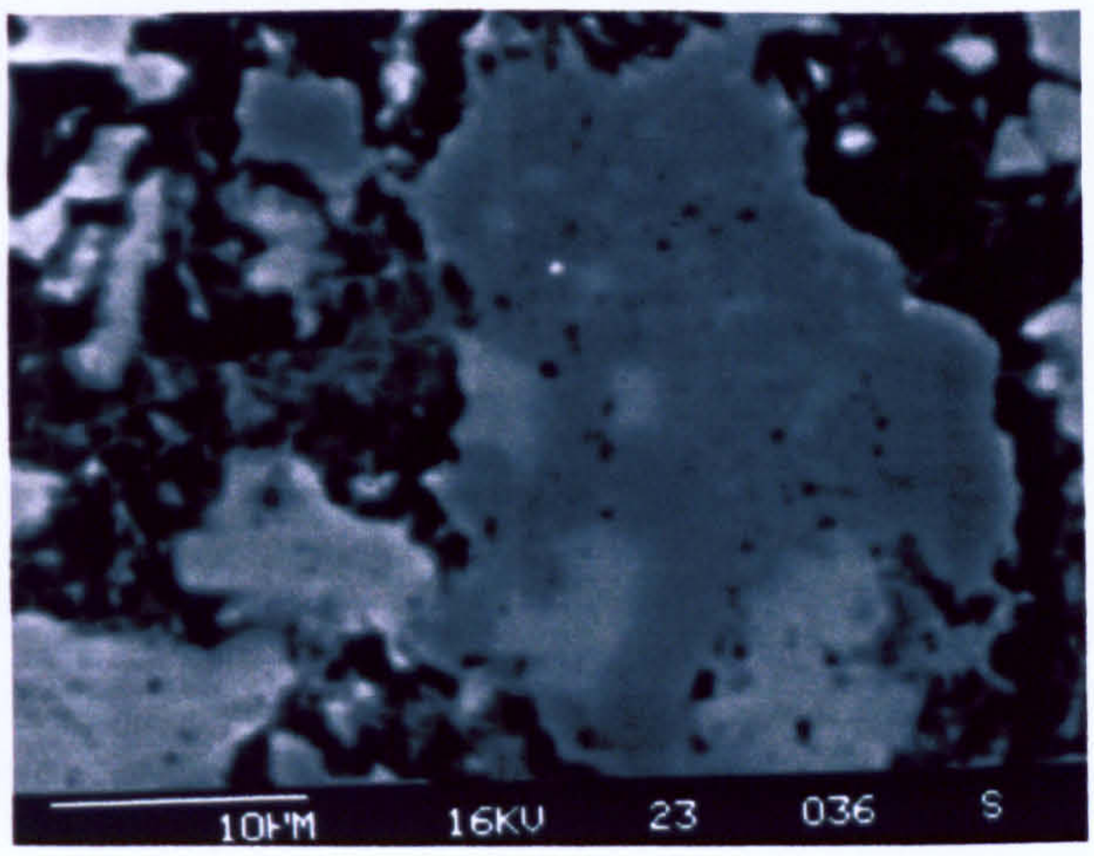

d)

Figure 7.24 EPMA BSE image of ACR affected aggregate/cement interface

Chapter 8 Discussion of the results

8.1. Introduction

The alkali-carbonate aggregate reaction is a physico-chemical process involving the dolomite fraction of carbonate aggregate and the high-alkaline concrete pore solution. The nature of this reaction required that the study presented in this thesis be carried out on three resolution levels (surface, near surface, and bulk) involving three different constituents (minerals, rocks, and concrete).

The approach adopted in this study was to analyse the minerals and to observe the physical and chemical changes induced by the alkaline solution using AFM and surface analytical techniques XPS and SIMS. The results are presented in Chapter 5. The next step included a study of surface reactions and microstructure with additional bulk analysis (XRD, EPMA) of carbonate rocks containing dolomite after immersion in an aqueous alkaline medium, as shown in Chapter 6.

The validity and applicability of the experimental results concerning mineral-solution and rock-solution reactions could only be confirmed after the study of ACR affected concrete samples (Chapter 7). Thus, this Chapter attempts to draw the results together in order to gain an overall view of the mechanism of ACR supported by thermodynamic calculations of the phases concerned and comparisons between the molar volumes of reactants and products that lead to the expansion observed.

8.2 Manifestations of the dedolomitisation reaction at an atomic surface level

'*The boundary is the best place for acquiring knowledge*' quoted Vaughan and Patrick (1995). In this study the combination of microscopic and spectroscopic studies on the surfaces of dolomite minerals enabled the gathering of complementary data on their chemical composition and micro-topography. My work also shows the necessity of an interdisciplinary approach for a study of complex materials, where each technique provides information on a different part of the puzzle.

ACR encompasses mainly the transformation of dolomite to calcite. Dolomite is a perfect example of a crystalline substance, which is found as a conglomerate of small crystals, known as poly-crystals. These are referred to as grains, and the term grain boundary is used for the interface were grains meet. The bonding between atoms lying at grain boundaries is not as perfect as it is in the interior of a grain. Hence the grain boundary can be considered as a zone of inherent imperfection (Cotterill 1986). Atoms at the surface of a mineral are not fully co-ordinated, resulting in dangling bonds. The structure also relaxes, causing a change in surface free energy and hence the mineral's stability.

In this study ESEM and AFM data revealed that the dolomite structure was susceptible to ion exchange reactions. The reaction involving dolomite transformation was further enhanced by the high rate of diffusion of NaOH solution through the carbonate minerals. In addition the BSE images identified calcite particles and quartz inclusions together with chemical impurities in the form of Fe atoms and high Ca content in the dolomite crystal, observed as zoned dolomite crystals. The results from the study of unexposed dolomite crystals revealed their susceptibility to solution induced changes due to chemical imperfections (ferroan dolomite where Fe replaces some Mg). This feature is known as dolomite zoning and can be demonstrated with observation of cathodoluminescence (Figure 8.1, Dickinson 1984). A comparison of cathodoluminescence image of zoned dolomite (Figure 8.1) with the EPMA maps from individual dolomite grains of reacted Kingston dolomite extracted from ACR concrete, in Figure 7.22, of Chapter 7, reveals identical trend. This suggests that chemical impurities reflected as the dolomite zoning are also preferential sites for mineral's instability.

AFM studies were conducted on as received and alkali-treated samples of single dolomite crystals to characterise the ordering of atoms within the top atomic layer. Contact mode AFM observations on unexposed dolomite crystal (sample MR03) revealed two types of atomic ordering within the surface layer (see Figure 5.7 & 8). Figure 5.7 shows a random display of atoms in the mono-layer, while Figure 5.8 depicts the segregation of atoms with finite angles and orientation. After exposure to an alkaline aqueous environment for 3-4 weeks, AFM analysis by contact mode produced unexpected results. This was attributed to 'contamination' of the probe, which picked up newly formed brucite crystals during scanning. This occurred solely because of the

nature of brucite growth. For this reason, AFM tapping mode was used to continue the analysis (Figure 5.9 &10.) These observations showed that brucite grows perpendicular to the dolomite substrate, forming a fine network layer of crystals.

In contrast to ESEM studies of alkali treated dolomite crystals, where brucite growth was detected only after 3 months exposure (Figure 5.3, 4 & 5), the AFM studies identified the same reaction products after 3 weeks (Figure 5.9 & 10). The formation of a brucite layer created a large surface area which was susceptible to moisture uptake, resulting in the requirement of greatly increased volume per metal atom, a phenomenon well demonstrated with AFM phase imaging (Figure 5.11). At the same time XPS data indicated that an alkali-treated brucite mineral was almost identical to brucite developed in rock/solution studies. This suggests that brucite can undergo further reaction with the alkaline medium and is supported by both AFM phase imaging studies and identical measured Mg*2p* binding energies in X-ray photoelectron spectroscopic measurements from alkali-treated brucite and brucite formed as a product during a laboratory observed dedolomitisation reaction.

Another product of the dedolomitisation process observed in this study was $CaCO_3$, which was detected after 3-4 months of dolomite immersion in NaOH solution. ESEM was used to examine the dolomite surface without any surface treatment (in near *in-vivo* conditions). Confirmation of the presence of brucite and the oriented growth of calcite gave further experimental evidence for the alkali-induced dedolomitisation process on one hand and demonstrated the spatial distribution of newly formed phases. AFM and ESEM analysis also gave an insight into the chronology of mineralogical transformation during the dedolomitisation process, where brucite forms first and calcite second.

Based on these findings a dedolomitisation model which suggests that the presence of chemical impurities in the layers of the dolomite crystal can react with an alkaline solution in the following sequences:

1) Adsorption of the anionic OH^- species from solution at the mineral surface, where adsorption presents the interfacial accumulation of sorbate as a surface complex without development of 3-dimensional molecular ordering (Zachara *et al.* 1991). The principal of an adsorption reaction is via exchange with Ca^{2+} or Mg^{2+} in

exposed lattice sites or by complexation to carbonate groups bound in a disordered hydrated surface layer (Davis *et al.* 1987, Koss and Moller 1974).

2) Migration or diffusion of the OH^- ions to the sites of high free energy such as Mg^{2+} or Fe^{2+} in the dolomite crystal structure coupled with an outward diffusion of Mg and Fe.

3) Mass transport and leaching of FeOOH first and than $Mg(OH)_2$ at the surface of individual dolomite crystals, resulting in Ca-enriched regions within dolomite lattice. These Ca-rich regions subsequently act as nucleation sites for the formation of secondary calcite, and in addition to internal sources (from the crystal lattice of non-stoichiometric dolomite) Ca^{2+} supply is further enhanced by Ca^{2+} from OPC pore solution.

Ostwald's step rule states that a reaction proceeds through a series of intermediate phases, each thermodynamically more stable than the preceding one (Ostwald 1897, referred to in Morse and Casey 1988). Since the dolomite solubility increases with the amount of excess Ca and decreases with the degree of cation ordering (Carpenter 1980) the experimental findings support the dedolomitisation model presented here. It has also been observed that the calcite to dolomite transformations are controlled by molar volumes and surface free energy-dominated nucleation kinetics (Nordeng and Sibley 1996), in agreement with the experimentally observed formation of brucite before calcite.

8.3 Inter-mineral changes in an alkaline aqueous environment

Alkaline solution has been shown to have varying effects on dolomite-containing carbonate rocks. Only certain types of dolomitic limestones are susceptible to expansive dedolomitisation while others, which undergo dedolomitisation show no expansion. These discrepancies have been attributed to textural characteristics and porosity of the carbonate rocks investigated. Permeability studies on sedimentary rocks have shown that the permeability values increase with increasing porosity, larger particle size homogeneity and decreasing inter-granular volume per surface area (Oelkers 1996).

The results obtained in this study are in agreement with studies carried out in different laboratories world-wide (Chapter 2). The XRD and EPMA data have suggested that the

dedolomitisation reaction is not always associated with a volume change. The dissolution of dolomite crystals well-embedded in carbonate/silicate matrices do not appear to provide sufficient space to accommodate the growth of secondary deposits (brucite, calcite or hematite), which as observed in Chapter 5, had a tendency to precipitate at the dolomite surface/alkaline-solution interface. Consequently mineral growth proceeded in a confined space, causing a joint generation of expansive forces from the perpendicular crystal growth and their large surface areas that are easily hydrated.

The main aim of the carbonate rock/solution study was to establish the impact of other carbonate minerals and silicates as well as the rock texture present on the rate of dedolomitisation and degree of expansion. EPMA measurements were carried out on alkali treated dolomite rocks that showed different levels of expansion (Kingston, Nelson and Massachusetts dolomite, Table 3.3). As summarised in Figures 6.10, 6.14 & 6.15, where the first 150 EPMA point-analysis are from reacted Kingston dolomite, points 150-200 are from the same but unaltered rock, and points 200-250 represent the calcite matrix. For comparison a less-expanded semi-altered Massachusetts dolomite is shown in points 300-500 EPMA line analysis. In these rocks the difference lies in the amount of silicates and the Ca/Mg ratio, where Kingston dolomite has Ca/Mg = 2/1 and Massachusetts dolomite has the Ca/Mg = 1/1. This is in agreement with De Groot's dedolomitisation model (Chapter 2) which shows that the rate of dedolomitisation is driven by higher Ca/Mg ratio.

The conclusion from this data is that it is the rate of dedolomitisation rather than its occurrence which has the greatest impact on the expansive nature of dolomitic rocks or in other words the amount of secondary products (brucite and calcite) formed in confined intra-granular spaces.

The chemical exchange reaction in dolomite/alkali systems proceeds if the Ca/Mg and Ca/Fe ratios of dolomite and ordering are not in equilibrium. Since dolomites used in this study had above mentioned characteristics, this suggests that the thermodynamic equilibrium of those crystals would be readily upset by alkaline solution. The quantification of common ratios (Ca/Mg, K/Na, Fe/Mn, Ti/Al) in dolomite is often undertaken in geochemical studies (Bhatt 1976). The argillaceous dolomitic limestone used in this study would be categorised as a highly dolomitised limestone (Mg

distribution greater than 10 % mole), most likely due to the selective dolomitisation of fine materials during the rock formation (Schmidt 1965).

The rock/solution study also showed that in the Kingston dolomitic limestone (ferroan dolomite) the presence of Fe could have a significant role in the expansion and deterioration. This was supported by EPMA analysis, which detected phases with the composition displayed in Table 8.1. These weight percentages of almost single elements was attributed to the presence of newly formed dedolomitisation products (brucite, goethite or hematite and calcite).

Table 8.1 EPMA quantitative analysis revealing the composition of newly formed phases in rock/solution system.

Mineral suggested	EPMA quantitative analysis
CaCO3	~60 wt % CaO
Mg(OH)2	~60-70 wt % MgO
FeOOH/Fe2O3	~40-50 wt % FeO

*These phases were not present in the unexposed Kingston dolomitic limestone, only after immersion in 1N NaOH for 3yrs.

Since laboratory conditions in alkali-treated single dolomite crystal involved only NaOH aqueous solution with no extra supply of Ca or Mg, it may be concluded that the Ca/Mg ratio is the key factor for formation of brucite and secondary calcium carbonate. However the same laboratory conditions for dolomitic rock samples will have a variety of solution species due to the possibility of matrix solubility. It is for example well known that carbonates, quartz, and silicates are soluble in high pH environments.

Observations from experiments with D_2O (deuterium-oxide was used instead of water for solution), clearly demonstrated the rapid incorporation of OH^- ions into the carbonate rock. The rate of permeability of porous material is a measure of the pore fluid flow. The overall value of the penetration is the combination of flow through the pore space, microcracks and grain boundaries of the bulk material (Oelkers 1996). The tracer experiment therefore confirmed the impact of the texture of the rock on its expansive nature. Both rock samples used in this study were known to be very expansive.

8.4 Mineral changes in ACR affected concrete aggregate

The results described in Chapters 5 and 6 (summarised in sections 8.2 and 8.3), were confirmed in the study of concrete samples undergone ACR. Firstly, an oriented growth of secondary calcite was observed in fractured dolomite grains removed from concrete samples (Figure 7.7), in an almost identical form to the orientation of secondary calcite crystals observed on the alkali-treated single dolomite crystal (Figure 5.4). This further suggested that the dissolution of dolomite was the initial reaction, leading to further mass transport-related changes identified by EPMA mapping of the aggregate/cement paste interface (Figure 7.19). As it can be observed in Figures 7.18&7.20, the Mg-rich phases were un-expectedly deposited within the cement paste, far from the reacted aggregate and the transition zone. Its smaller ionic radius and ionic activity probably encouraged the migrations of Mg as well as their affinity towards environmental species present enabling ion-exchange (high pH and availability of OH^- ions).

Another important result of this study is the comparison of the degree of deterioration in alkali treated rock and ACR affected aggregate. XPS data from both materials revealed that the chemical shift for Mg*2p* from carbonate (dolomite) to hydroxide (brucite) was much more apparent in laboratory-induced rock/solution studies than ACR field concrete samples. This is an important consideration when ASTM C586 and other chemical rock test data is used for predicting aggregate reactivity. The alkali-induced expansion is more extreme and could lead to a questionable assessment on whether a rock-aggregate will have good performance concrete.

8.5 Thermodynamic calculations confirmation

In order to establish the reactivity of dolomite and ferroan dolomite in alkaline solution as well as the stability of newly formed dedolomitisation products, thermodynamic calculations (using Geochemists Work-bench, Bethke 1993) were carried out for indicative purposes only.

Both dolomite/alkaline solution and dolomite + siderite/alkaline solution systems were considered. Figure 8.2.a represents the reaction of a 184gr s of dolomite and 1N NaOH alkaline solution system. It reveals that the only three phases present are brucite, calcite and dolomite where brucite and calcite follow an identical plot. The formation of brucite and calcite is at the cost of dolomite, and it is favoured to the point of saturation where

their concentration becomes static. At this stage re-precipitation of dolomite is initiated, and is manifested the increase of dolomite present (Figure 8.2).

However, when a ferroan dolomite and quartz mixture are treated with the same solution Figure 8.2b, brucite and calcite behave quite differently. Once calcite and brucite saturation is reached brucite becomes an unstable phase, suggesting that in the presence of iron, brucite will react with the alkaline solution and precipitate in the form of dolomite. This could be one of the main explanations for the reactive nature of the Kingston ferroan dolomite in comparison to other Fe-free dolomitic limestones. In relation to AAR problems these thermodynamic equilibrium calculations could also explain the difference between ASR and ACR. While alkali-silica reaction continues only until the alkali is consumed, the alkali-carbonate reaction proceeds indefinitely, possibly due to the renewed production of OH^- from brucite.

Therefore, the conclusion from the thermodynamic modelling is that the dolomite/solution equilibrium shown in Figure 8.2a is representative of an ordered, stoichiometrically ideal dolomite in an alkaline environment. However, Figure 8.2b presenting the mixture (dolomite, siderite and quartz) stability in alkaline solution, is more representative of an expansive feroan dolomitic rock such as Kingston dolomite.

8.6 Expansion as a consequence of the synergistic reactions

Whether or not a crystalline phase can establish itself depends on the probability of a sufficient number of atoms simultaneously arranging themselves in the crystalline configuration to produce a nucleus. The difference between the free energies of the liquid and crystalline phases is proportional to the volume of transformed material, whereas the energy of misfit between a crystalline region and the surrounding fluid is proportional to the surface area of the interface. Since volume increases at a faster rate than area, the volume-related factor must predominate if the crystalline region is greater than a certain critical size.

In concrete there are many simultaneous reactions taking place, from a hydration of cement to various aggregate/cement-paste related processes and changes within the aggregate itself. Some of these reactions can cause a solid volume change, whether

volume reduction or an increase in volumetric occupancy, as presented in Table 8.2 (Liang and Tang 1995).

8.2 Solid volume changes of selected chemical reactions in concrete

Process	Physico-chemical reaction	Solid volume change %
CaO Hydration	$CaO + H_2O = Ca(OH)_2$	102
MgO Hydration	$MgO + H_2O = Mg(OH)_2$	119
Sulphur expansion	$M_2SO_4+Ca(OH)_2+2H2O = CaSO_4.2H_2O+MOH$	123
Ice formation	H_2O (liquid) = H_2O (solid)	9
Carbonation	$Ca(OH)_2 + CO_3^{2-} = CaCO_3$	11.7
Dedolomitisation	$CaMg(CO_3)_2 + 2OH^- = CaCO_3+Mg(OH)_2+ CO_3^{2-}$	-4.3
Alkali-magnesite	$MgCO_3+2OH^- = Mg(OH)^2$	-12

As can be observed in Table 8.2 dedolomitisation may be presented as a solid volume reducing reaction (-4.3%). Based on the dedolomitisation model and empirical data of this study there are two types of dedolomitisation process occurring in ACR concrete:

Table 8.3 Change of molar volumes during the dedolomitisation reaction

*using SUPCRT 92 for calculating volumes (Johnson *et al.* 1992)

1) Argillaceous dolomitic limestone in a Ca rich alkaline environment of Portland cement pore solution behaving as follows:

$CaMg(CO_3)_2 + Ca^{2+} + 2OH^- = 2CaCO_3 + Mg(OH)_2$ {Volume change for solids is 52.9% and Molar volume change of reaction is 169.8%}
$CaMg(CO_3)_2 + Ca(OH)_2 = 2CaCO_3 + Mg(OH)_2$ {Volume change=1.1%}
$CaMg(CO_3)_2 + Ca^{2+} + 2H_2O = 2CaCO_3 + Mg(OH)_2+ H^+$ {Volume change for solids is 52% and Molar volume change of reaction is 19.88%} ΔGr = -14336 kcal/mole

2) Ferroan dolomitic limestone transforms in alkaline environment forming:

$Ca(Mg,Fe)(CO_3)_2 + Ca^{2+} + 2OH^- + H_2O + O_2 = 2CaCO_3 + Mg(OH)_2 + FeO(OH) + OH^-$ where FeO(OH) consequently ages to Fe_2O_3
$FeCO_3 + 2Ca^{2+} + 2H_2O + 0.5O_2 = 2CaCO_3 + Fe_2O_3 + 4H^+$ {Volume change for solids is 78% and Molar volume change of reaction is 79%} ΔGr = -15472 kcal/mole

The dedolomitisation process is of interest not just because of mineralogical and chemical changes but also because it is associated with the expansive nature of some dolomites. Measurements from a single dolomite crystal in this study did not involve measurements of volume change, but indicated that the reaction is of a surface character. Thus, it will require sufficient space to accommodate newly formed phases and taken together with the molar volume calculations it can be concluded that dedolomitisation can cause expansion.

It was necessary to investigate the physical consequence of the above reaction and its contribution towards the generation of expansive forces. Sedimentologists agree that there is an increase in volume during the reaction described as dedolomitisation type 1, but dedolomitisation in the alkali-carbonate reaction was considered to be the initiation reaction leading to expansion, rather than its source.

However, it is possible that the volume increase noted in sediments during the dedolomitisation process could also cause expansion in dolomitic aggregates in concrete, bearing in mind the high pH environment. The question remains: Why should this phenomenon be present only in selected dolomitic-limestones?

One of the reasons for expansion in argillaceous dolomitic rocks similar to Kingston type dolomite is related to the moisture requirement for this reaction. According to Gillott, the clay fractions would adsorb water once exposed to pore-solutions due to their large surface area. Another phase that will have similar effect is brucite with its layered structure and sufficient surface for reaction with alkaline medium. However, it is important to distinguish that the deposition of reaction products on the surface of brucite

plates itself will cause expansion. At the same time if this process is taking place at grain boundaries, there will be also a consequential physical process that also leads towards the generation of expansive forces within the confined spaces of the bulk material.

The presence of such reaction will result in the weaker OH-Mg-OH bonds in brucite in agreement with the observation of lower binding energy for the Mg*2p* in the XPS spectrum of a brucite mineral treated with alkalis, compared with the value of Mg*2p* for the same crystal before the treatment (Table 5.2). This reaction would be favoured first of all by the network-growth of brucite crystals during dedolomitisation, creating the large surface area with capacity to be enveloped by a high number of water molecules; and secondly by the layered structure of crystalline brucite itself. This was experimentally supported by AFM phase imaging of brucite formed on a single dolomite crystal surface after 3 weeks in NaOH, Chapter 5.

Aspects of particular importance for the ACR study are changes within carbonate rocks that involve processes of solution and precipitation at solid-liquid interfaces, and possible solid state transformations. Impurities in the original rock quarried for aggregate are also important. The expansion mechanism of ACR may be associated with the presence of pyrite crystals (a source of Fe phases seen in EPMA) in alkali-reactive dolomitic-limestone. The oxidation of iron sulphide may cause expansion by the formation of iron-oxy-hydroxides when situated at or near concrete surfaces. The Fe is also present as chemical impurity in the dolomite lattice (Kingston rock is known to be close to feroan dolomite), and as a result of that when replaced by Ca in dedolomitisation will form another expansive phase hematite.

Another contaminant, which may have a deleterious effect on the aggregate's durability, is the presence of clays. The principal detrimental effect of clays in concrete is to increase the water demand of concrete, or if present as sub-micron inter-granular inclusions in dolomite, they may react with alkaline pore solutions (Smith and Collis 1993). It should be noted however that latter was not supported by observations in this study.

8.7 Grain Boundaries and interfaces in concrete

The so-called transition zone (TZ) between aggregate and cement-paste has been always an object of mystery for concrete researchers, for two reasons. The first is its vital role on the strength and durability of the aggregate/cement bond. The second is because it was almost impossible to study it without alteration of the zone by drying, cutting, polishing or by the analysing conditions (UHV-high vacuum).

The use of ESEM enabled the observation of the interface in its intact form, offering a more accurate description of the phase-boundary than hitherto. Concrete samples, which were known to have undergone ACR, showed an unexpectedly large amount of needle-like crystals at the aggregate/cement boundary. These deposits are very similar to ettringite needles. This may be an additional previously un-encountered reason for the expansive nature of ACR, in this type of aggregate. The explanation for the ettringite formation is the supply of sulphur from pyrite or cement-paste, and Al from silicate matrix in rock or cement paste.

A reacted dolomite aggregate surface after 10 years embedded in concrete, showed dolomite crystals almost entirely covered by elongated crystals (Chapter 7). It is not clear whether this was a final stage of ACR or merely a transition phase leading to the subsequent formation of pseudo-calcites identified in many XRD studies of ACR altered aggregate.

8.8 Ancient materials - indicator of reaction kinetics

The data obtained in this and other studies can be compared with observations from an ancient 'Masada' mortar, ≈ 2000 years old from Israel, where lime-mortar was used to protect a water reservoir made within dolomite rock. In Figure 8.3 dissolution of the dolomite substrate rock is identified by SEM images of calcite growth on the surface of dolomite. In this case although a plentiful supply of moisture was present, the secondary calcite crystals are of only few μm in diameter.

Nevertheless the dolomite surface is evenly coated with tightly packed calcite crystals growing perpendicularly to the dolomite substrate. It may be concluded that the dedolomitisation reaction is a very slow process in natural environments. The difference between concrete dedolomitisation and dedolomitisation in the Masada sample is that the latter involved changes on a free surface, where as in concrete the changes occur in aggregates embedded in rigid cement paste. This also supports earlier conclusions on the importance of free space for crystal growth as well as the necessity for very sensitive techniques to monitor the kinetically slow reactions.

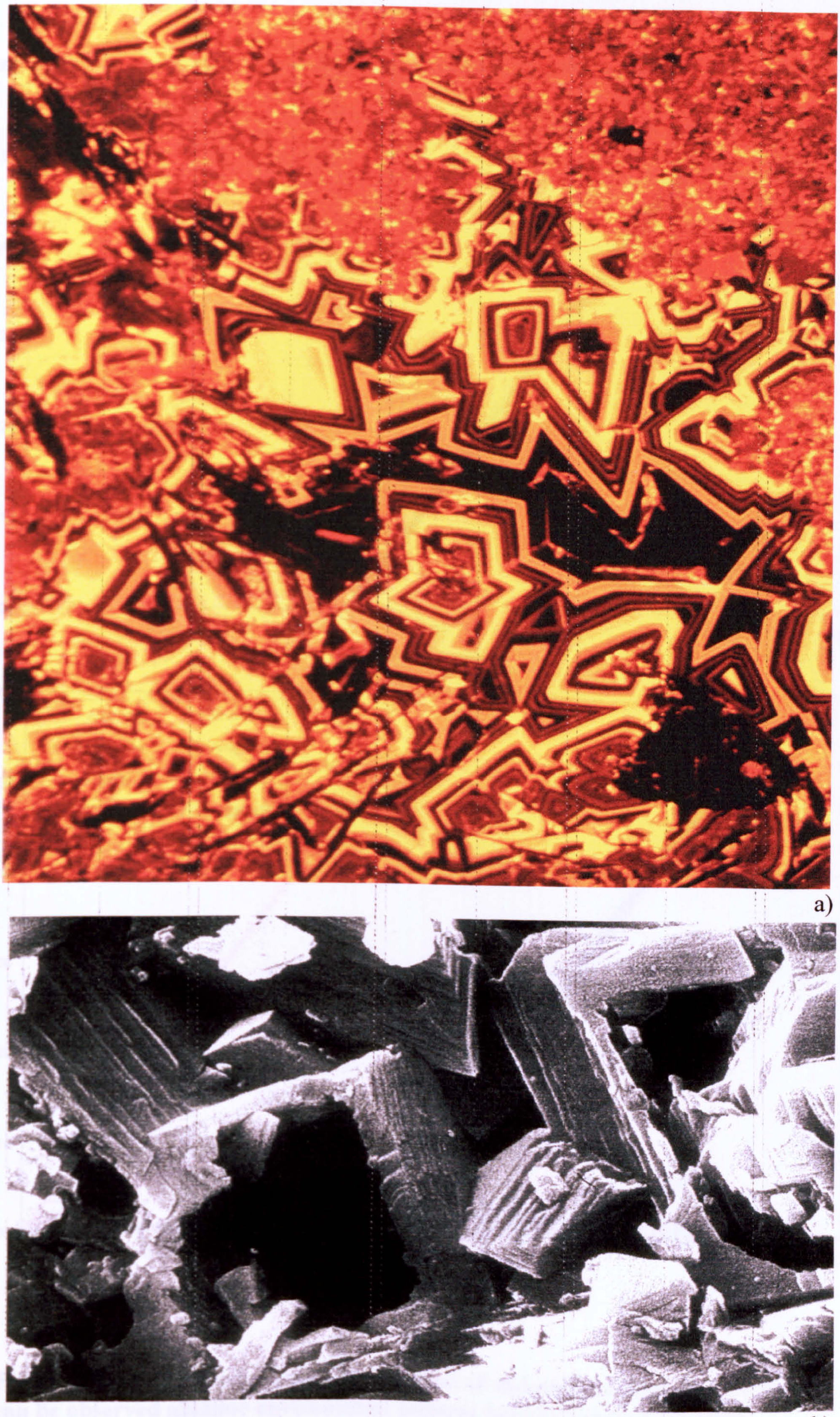

a)

b)

Figure 8.1 Cathodoluminescence micrograph of a thin section of zoned calcite [orange-black] and dolomite [red] from the Daldrian, Scotland, a), (after A.D. Dickinson), **and a SEM image of selective dolomite dissolution, in b).**

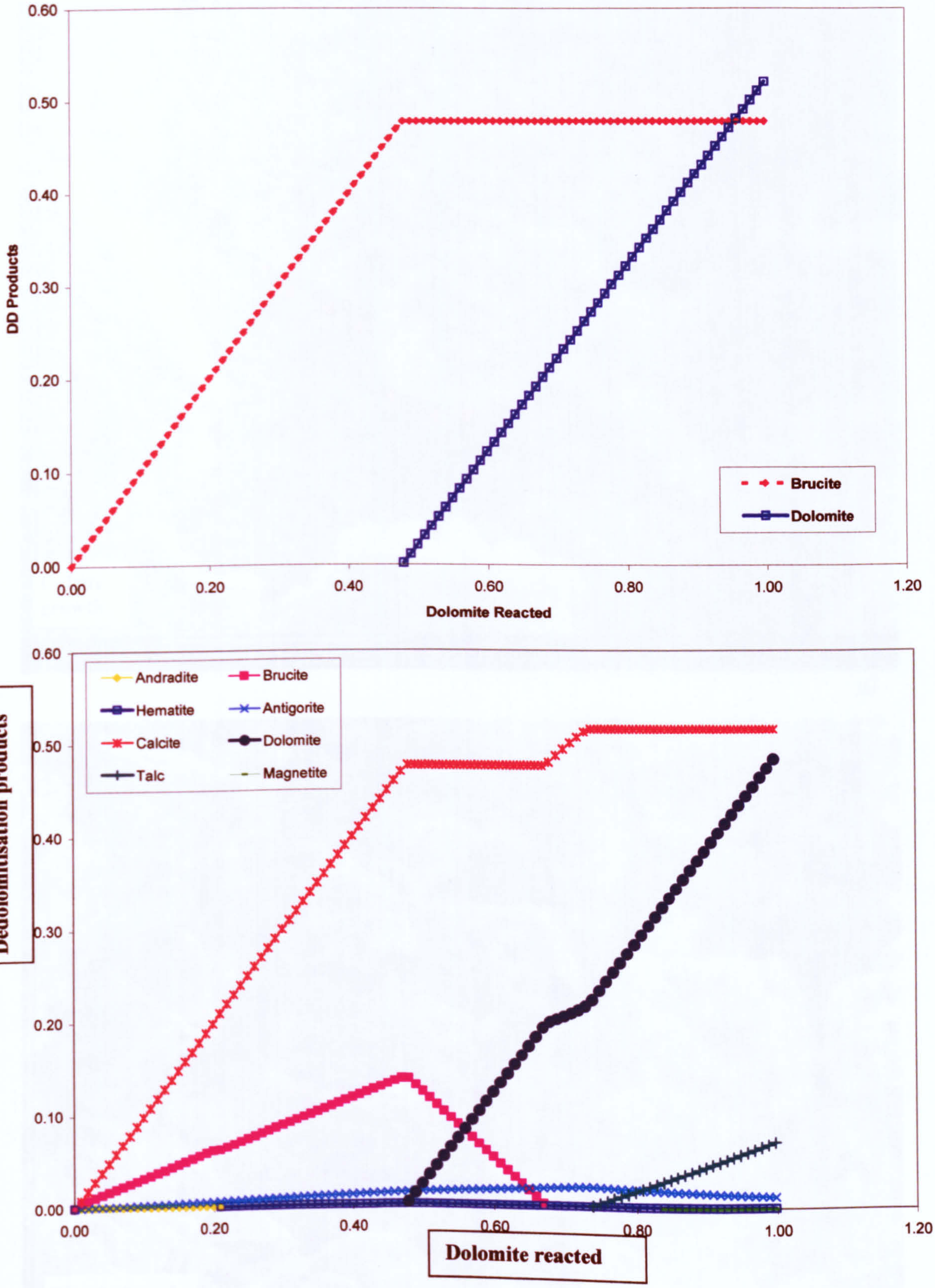

Figure 8. 2 a) Thermodynamic calculations of dolomite stability in 1N NaOH. As can be observed alkaline environment induces brucite/calcite formation.
b) Dolomite and siderite mixture in 1N NaOH solution, showing different products and stability and the thermodynamic equilibrium is of a different nature regarding reactants-products.

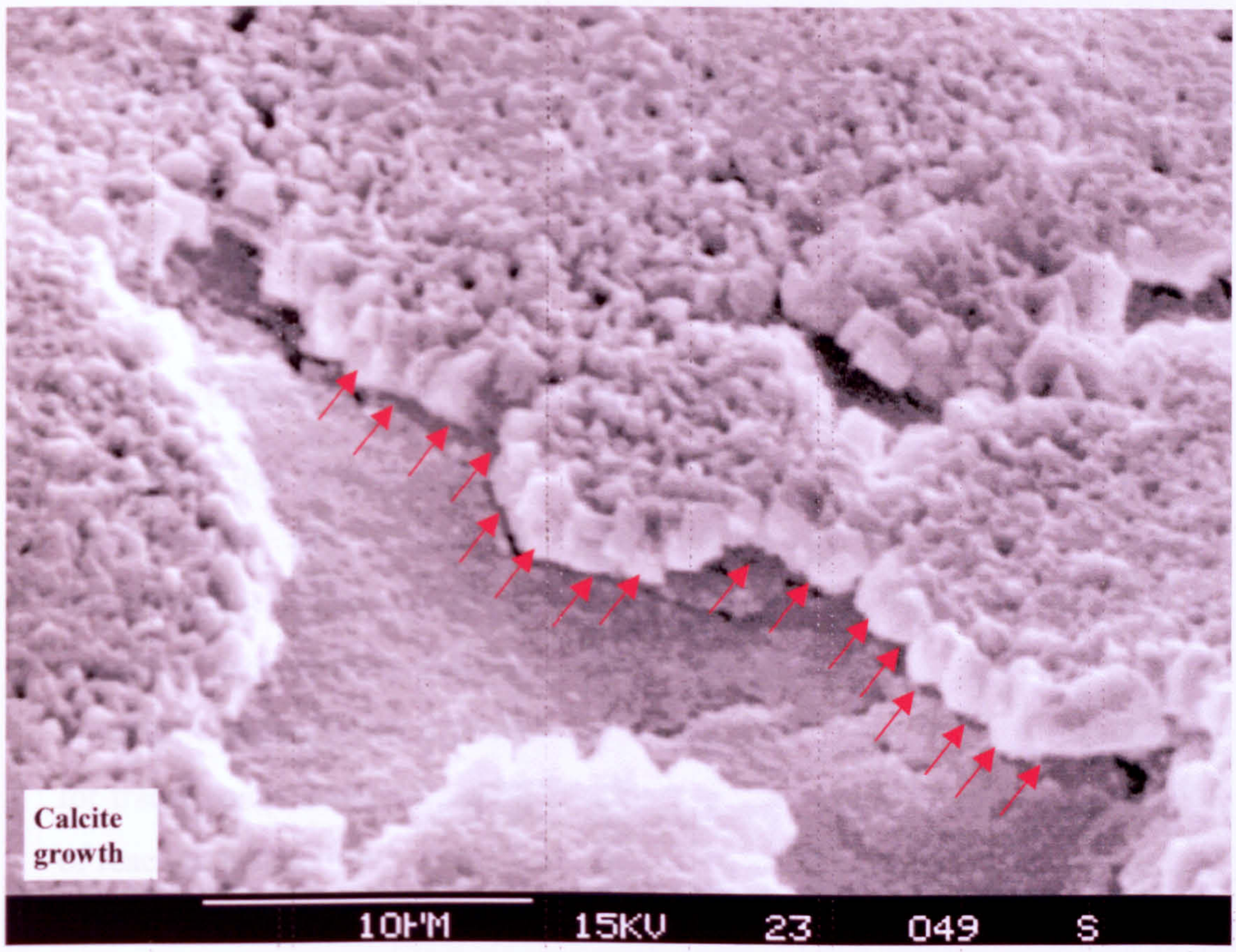

a)

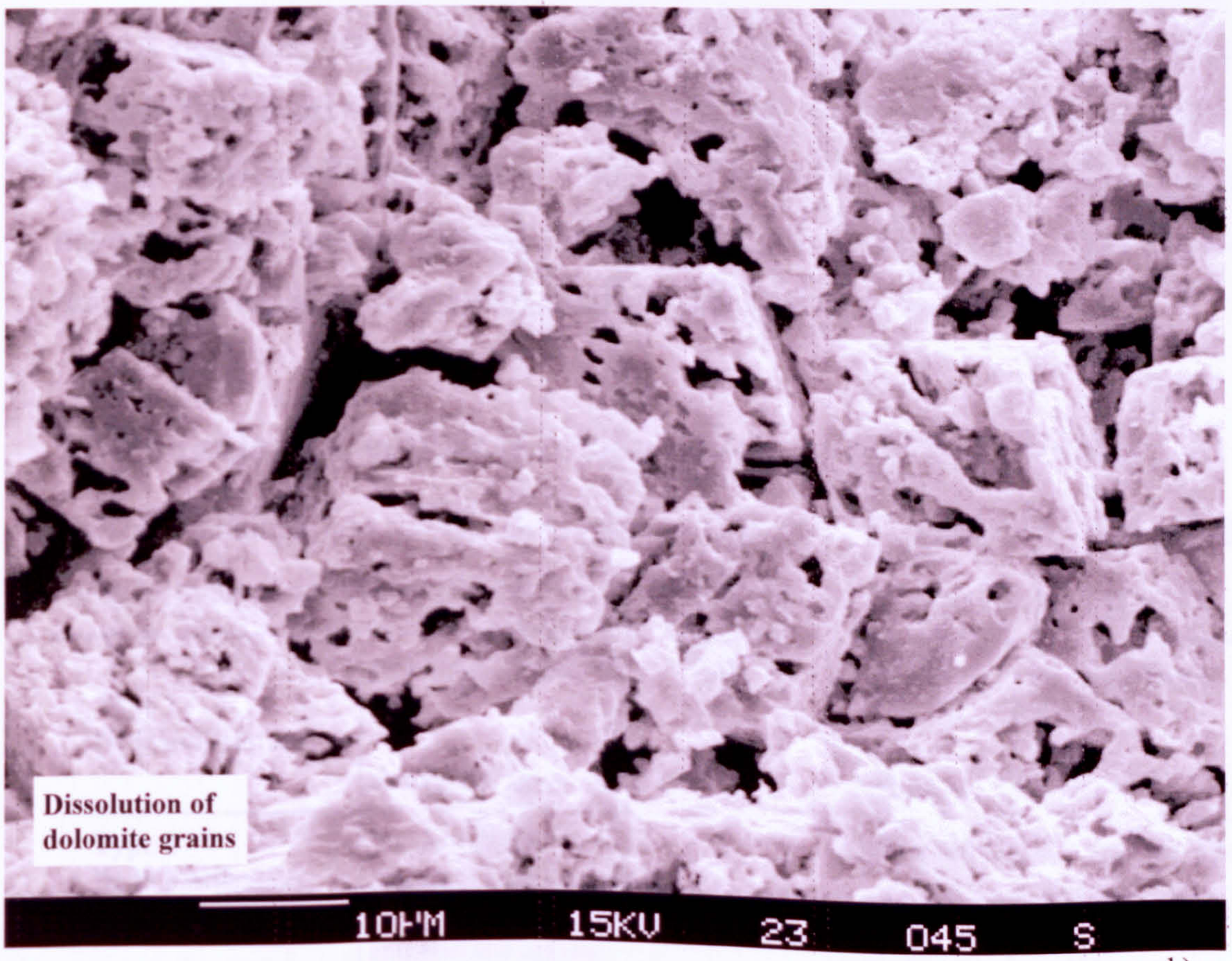

b)

Figure 8.3 A SEM image of the mortar sample from Masada (2000 yrs old) with dolomite aggregate, showing the calcite growth (outlined in red) **on the surface of dolomite a), and fine grained dolomite dissolution as a part of dedolomitisation b).**

Chapter 9 Concluding remarks and future prospects

9.1 Novel techniques in studies of cementitious materials

This study has demonstrated how much might be gained from the joint use of spectroscopic and surface techniques in studies of concrete chemistry and microstructure. The spectroscopic techniques XPS and TOF SIMS, widely used in materials science, have been applied to the study of the mechanism of ACR, to investigate mineralogical and chemical changes. The ability to carry out depth profiles for tracer components such as D_2O has also shown great potential for an understanding of reaction mechanisms. A novel approach of the work described here is also the use of ESEM, which offered the opportunity to monitor reactions in real time. A knowledge of the kinetics of chemical processes is essential for an understanding of the mechanisms of various reactions. This study has shown that ESEM can provide the type of analysis required for a more accurate description of the complex synergetic reactions which take place in concrete. Finally another 'young 'surface technique AFM, has also provided an important insight into the changes occurring at the top atomic layers, in their initial stage reducing the experimental time required for such reactions.

9.2 The role of Dedolomitisation in the mechanism of ACR

The new findings and models proposed here for the mechanism of ACR reveal the complex synergetic nature of the process. The following stages have been identified:

Type 1 Dedolomitisation	[dolomite] ⇔ [calcite + brucite] and further brucite hydration	$CaMg(CO_3)_2$ + alkaline solution ⇔ $CaCO_3 + Mg(OH)_2$ $Mg(OH)_2 \Leftrightarrow Mg(OH)_2.nH_2O$
Type 2 Dedolomitisation	[ferroan dolomite] ⇔ [calcite + goethite + brucite] and goethite ageing	$Ca(Mg,Fe)(CO_3)_2$ + alkaline solution ⇔ $CaCO_3 + FeOOH + Mg(OH)_2$ $FeOOH \Leftrightarrow Fe_2O_3 + H_2O$
Hydration	phases with large surface area react	hydrated brucite,

Additional to this it was observed:

- The development of various reaction rims around the aggregate or within the aggregate have also been identified using XPS, EPMA, EDX and BEI, showing Ca, Si, Fe and Mg enrichments confirming the results from single mineral studies in the more complex materials rock and concrete.

- AFM has been used to ascertain the volume changes by topological characterisation, the nature of brucite growth and its susceptibility to water uptake.

- The chronological order of dedolomitisation- induced mineralogical transformation has also been established by AFM, showing that brucite is the first reaction product followed by calcite which was detected with ESEM.

- The introduction of tracers such as D_2O has been used in TOF-SIMS studies to monitor chemical reactions and in particular the role of hydroxyl ions in the ACR mechanism. It was observed that the penetration rate in reactive expansive carbonate rocks is very large, enabling free access of OH^- ions to the reaction sites and brucite formation.

- Thermodynamic calculations were used to support experimental data, showing the transformation of dolomite to brucite and calcite and the possible re-precipitation of dolomite. Other important information was obtained for dolomite, siderite and silicate mixtures in aqueous alkaline environments showing the relative change in brucite and calcite stability.

- Molar volume calculations for reactants and products from the types of dedolomitisation present, suggested that they are volume increasing reactions.

- Finally, the mechanism of ACR and its expansive nature was a result of several simultaneous processes rather than just one single reaction.

9.3 Future Work

Empirically based suggestions for further research to introduce novel techniques and a combination of different scientific fields. Surface chemistry and spectroscopic techniques may be used to monitor changes at much shorter experimental exposure times by detecting alterations at the earliest stages.

XPS could be used to identify chemical changes in concrete including hydration of cements, alkali-aggregate reactions, ettringite formation, carbonation sulphate attack, corrosion of reinforcement. The ability to monitor the chemical state of species present could be used to provide detailed chemical information on reactions involving admixtures. Moreover, XPS could give a valuable information on the most desirable phases for the aggregate/cement bond in high strength concrete.

In the future AFM and ESEM can be used to monitor dynamic changes and *in-situ* experiments in solutions, elevated temperatures that are important for designing curing conditions for specific purpose cementitious materials. AFM can also provide the data for establishing the nucleation sites in various reactions. In case of dedolomitisation it would be ideal to run a real time AFM monitoring experiment in which a dolomite crystal is immersed in alkaline solution. It is expected that during the first 24-48 hours this experiment could reveal the form of the initial nucleation for brucite growth.
TOF-SIMS and tracer experiments with D_2O could also be used at much greater extent not just in alkali-aggregate reaction mechanisms but in hydration reactions with cement or lime binders.

The results of this study suggest further experimentation with surface analytical techniques combined with ESEM for the characterisation of cementitious materials. The range of applications vary from the development of preventive measures for unwanted reactions such as AAR, to achieving specific properties of concrete produced for novel conditions and purposes including the storage of nuclear waste or high strength structures. The tallest concrete building in the world today at the end of 20^{th} Century is after all 'only' 452m, whereas proposed underground tunnels for radioactive waste are the depth of a km or more.

References

Agarwal, B.K., X-ray Spectroscopy, 2nd Edition, Springer, Berlin, 1991.

Al-Hashimi, W.S. and Hemingway, J.E., Journal of Sed.Petrology, vol.43, No.1, pp.82-91, (1973).

American Standards for Testing Materials ASTM C-586, Annual Book of Standards, Vol.04.02, (1981).

Bentur, A., Gray, R.J. and Mindess S., Developments in Fibre Reinforced Cement and Concrete, RILEM , Vol.2, paper 6.1, (1986).

Bentur, A. and Odler, I., In "Interfacial Transition Zone in Concrete", RILEM Report 11, (ed.Maso, J.C.), pp.18-44, (1996).

Berkowitz, J., Photoabsorption, "Photoionization and Photoelectron spectroscopy", Academic Press, New York, (1979).

Berner, R.A., Geochem.Cosmochim.Acta, Vol.39, pp.489-504, (1975).

Berry, F.J., "Chemical Bonding and Spectroscopy in Mineral Chemistry", Chapman and Hall, (1985).

Bethke, C.M., "The Geochemists Workbench", Univ. of Illinois, Champagne, ILL, (1992).

Bhatt, J.J., "Introduction to Geochemistry and Geology of South Wales' Main Limestone", Modern Press, US, (1976).

Binnig, G., Quate, C.F.,Gerber, C., Physics Rev. Letters., Vol. 56, No. 930, (1986).

Brady, P., Krumhasnil, J.L. and Papenguth, H.W., Geochemica et Cosmochimica Acta, Vol. 60,No.4, pp. 727-731, (1996).

Briggs, D., Brown, A., Vickerman, J.C., "Handbook of Static SIMS", John Wiley&SonsLtd., Chichester and New York, (1989).

Briggs, D., Seah, M.P., "Practical Surface Analysis", 2nd Edition, Volume 2 "Ion and Neutral Spectroscopy", Wiley&Sons, New York (1992).

Burns, S.J. and Baker, P.A., Sedimentology and Geochemistry of Dolostones, SEPM Spec.Publ.No.43, (1988).

Burton, W.K., Carbrera, N. and Frank, F.C., Phil.Trans.Roy.Soc., A243, pp.299-358, (1951)

Bye, G.C., "Portland Cement Composition, Production, and Properties", Institute of Ceramics, Pergamon Press, Oxford UK, (1983).

Calvert, W.L., (ed.) Carbonate Rocks 1, AAPG reprint series No.4, (1972).

Carles-Gibergues, A., Ollivier, J.P., Fournier, B. and Berube, M.A., Proc.8th. Int. Confrence.on AAR, pp.161-166, Kyoto, Japan, (1989).

Carpenter, A.B., SEPM Special Publication 28, The Society of Economic Palaeontology and Mineralogy, pp.111-121, (1980).

Chou, L., Garrels, R.M. and Wollast, R., Chemical Geology, Vol. 78, pp. 269-282, (1989).

Compton, J. S., Sedimentology and Geochemistry of Dolostones, SEPM Special Publication No.43, The Society of Economic Palaeontology and Mineralogy, (1988).

Cotterill, R., "The Cambridge Guide to the Material World", Cambridge University Press, pp.124-129, (1986).

Coyne, L.M., McKeever, S.W.S., Blake, D.F., (eds), Spectroscopic Characterization of Minerals and Their Surfaces, Amer.Chem.Soc.Symp. Ser.415, (1989).

Czernin, W.," Cement Chemistry and Physics for Civil Engineers", translated by Amerongen, C., 2nd English ed., George Godwin Ltd, London, UK for Bauverlag Gmbh, Wiesbaden, Germany, (1980).

Danilatos, G.D., Journal of Microscopy, Vol. 162, pp. 391-402, (1991).

Danilatos, G.D., Advances in Electronics and Electron Physics, No. 78, pp.1-102, (1990).

Danilatos, G.D., Bibliography of Environmental Scanning Electron Microscopy, Microscopy Research and Technique, No.25, pp.529-534, (1993).

Danilatos, G.D., Microscopy Research and Technique, No.25, pp.354-361, (1993).

Davis, J.A. and Hayes, K.F., (eds) Geochemical Processes at Mineral Surfaces, Amer.Chem.Soc.Washington, (1986).

Davis, J.A., Fuller C.C. and Cook A.D. Geochemica Cosmochim. Acta 51, pp.1477-1490, (1987), in Brady *et al.* 1996.

Davis J.A. and Kent D.B. in Mineral Water Interface Geochemistry, Reviews in Mineralogy, Min. Soc. Of America, No.23, pp.177-260, (1990).

Deer, W., Howie, R. and Zussman, J., "An Introduction to the Rock Forming Minerals", 2nd Edition, Longman, (1995).

DeGroot, K., Journal of Sedim. Petrology, Vol.37, pp.1216-1220, (1967).

Deng, M. and Tang, M.S., Cem.and Con. Res., Vol.23, pp.1397-1408, (1993a).

Deng, M., Han, S.F., Lu, Y.N., Lan, X.H, Hu, Y.L., Tang, M.S., Cem. Con. Reasearch, vol. 23, pp. 1040-1046, (1993).

Dolar-Mantuani, L., "Handbook of Concrete Aggregates - A Petrographic and Technological evaluation", Noyes Publications, New Jersey, USA, (1983).

Dolar-Mantuani, L., In "Engineering Geology of Eastern-Southern Ontario", Glass, D.J., (ed.), 24th Int.Geological Congress, pp.23-2, 7(1972).

Dhir, R.,(ed), Proceedings Concrete in Service of Mankind, Dundee, Scotland, vol.1, Chapman and Hall, London, UK, (1996).

Ewamy, B.D., Sedimentology, vol. 2, pp. 164-170, (1963).

Feldman, L.C., and Mayer, J.W., Fundamentals of Surface and Thin Film Analysis, North Holland, New York, (1986).

French, W. and Poole, A.B., Concrete, January (1976).

French, W. and Poole, A.B., Cem. and Concr.Research ,Vol.4, pp.925-937, (1974).

Fournie, B., Proceedings of 7th Int. Conference on AAR, pp. 23-29, Ottawa, (1986).

Galliher, E.W., Recent Marine Sediments, AAPG, pp. 513-515, (1939).

Garboczi, E.J., via Internet (1998) and in "Interfacial Transition Zone in Concrete", RILEM Report 11, (quoted in Chapter 1 of the book) (1996).

Gillott, J.E., ASTM, Special Technical Report 600, (1976).

Gillott, J.E., Canadian Journal of Earth Sciences, Vol.1, pp.121, (1964).

Gillott, J.E., Clay Minerals, Vol.21, pp.261-278, (1986).

Gillott, J.E., Eng. Geology, Vol.23, pp.29-43, (1986a).

Gillott, J.E., Q.J.E.G., Vol.13, pp.289-303, London, (1980).

Gillott, J.E., Vol.74, pp.759-778, Geol. Soc. of America Bull., (1963).

Gillott, J.E. and Swenson, E.G., Q.J.E.G., Vol.2, pp.7-23, (1969).

Gillott, J.E, Journal of Materials in Civil Engineering, pp. 278-282, Nov. (1995).

Gillott, J.E., Personal communications from 1995-1998.

Grattan-Bellew, P.E., Proceedings of 4th Int.Conf. on the effects of alkalies in Cement and Concrete, Purdue University, Publication No. CE-MAT-1-78, (1978).

Grattan-Bellew,P.E., Personal communications at the 10th AAR conference in Australia and via email (1996).

Groves and Richardson, Personal communications at the Cement and Concrete Science Conference, (Institute of Materials), Aberdeen, Scotland, (1995).

Goldman, A. and Bentur, A., ACI Materials Journal, Vol. 86, No.5, (1986), (from Chapter 2 of the RILEM Report 11, 1996)

Goldstein, J.I.I., Newbury, D.E., Echlin, P., Joy, D.C., Fiori C. and Lifshin, E., "Scanning Electron Microscopy and Analysis", 2nd Edition, Plenum Press, (1991).

Hadley, D.W., Vol. 40, pp.462-474, Highway Research Board Proceedings, (1961).

Hadley, D.W., Symposium on Alkali-Carbonate Rock Reactions Record No.45. Highway Research Board, pp.1-20, (1964).

Heinrich, K.F.J. and Newbury, D.E., (editors), "Electron Probe Quantitation", Plenum Press, New York, (1991).

Heinrich, K.F.J., "Electron Beam X-ray microanalysis", Van Nostrand Rheinhold, New York, (1981).

Hertz, 1880, Hallwachs 1888, Thompson JJ 1899 Steinhardt and Serfass 1951, Planck 1905 and Berkowitz 1979 in Holmes N.R. PhD Thesis: "The characterisation of Uranium oxide surfaces", University of Bristol (1988).

Hewlett, P.C., (ed) "Lea's Chemistry of Cement and Concrete", 4th Edition, Arnold Publications, UK, (1998).

Hochella, Jr M.F., and White, A.F., (eds), "Mineral-Water Interface Geochemistry", Reviews in Mineralogy 23, Min. Soc. of America, Washington, US, (1990).

Hochella, Jr. M.F., "Spectroscopic Methods in Mineralogy and Geology", Reviews in Mineralogy 18, Min. Soc. Of America, Washington, US, (1988).

Jennings, H.M. and Sujata, K., Materials Research Symp. Proc., Vol.245, pp.243-252, Materials Research Society, (1992).

Katayama, T., Proceeding 9th Int. Conference on AAR in Concrete, pp.508-518, Concrete Society Publish., CS 104, Slough, England, (1992).

Kjellsen, K.O. and Jennings, H.M., Advanc. Cem. Based Materials, Vol.3, pp.14-19, Elsevier Sci. Inc, Amsterdam, (1996).

Lane, W.C., SEM Proceedings 3rd Annual SEM Symposium IITRI, Chicago, US, pp.41-48, (1970).

Lea, F.M., "The Chemistry of Cement and Concrete", Edward Arnold & Co., London (1935) and 3rd Edition (1970).

Legget (1960) in The Field Guide to Alkali-Carbonate Reactions in Kingston, Canada, by Rogers, CA., Ministry of Transportation of Ontario, (1991 and 1992).

Liang, T., Personal communications, (1995).

Liang, T. and Tang, M.S., Cement and Concrete Composites, submitted in (1995).

Liang, T. and Tang, M.S., Cem.and Con. Research, Vol.25, pp. 470-476, (1995).

Liang, T. and Tang, M.S., Cement, Concrete and Aggregates, subbmitted in (1995).

Mackenzie, F.T., Bischoff, W.B., Loijens, M., Schoonmaker, J., and Wollast, R., "Carbonates: Mineralogy and Chemistry", pp.97-144, Min. Soc. Of America, (1983).

Manning, D.A.C., "An introduction to industrial minerals", 1st edition, Chapman & Hall, London, UK, (1995).

Mather, K., Buck, A.D., and Luke, W.I., Highway research board 4, pp.79-109, (1964).

Mehta, P.K., "Concrete: Structure, Properties and Materials", Prentice-Hall, US, (1986).

Mehta, P., 66th Annual Technical Conference of the Society of Petroleum Engineers, pp.445-449, Dallas, (1991).

Mehta, P.K., Proceedings, Concrete in the Service of Mankind, Vol.1, Dundee (1996).

Michaelis, W., (1893, 1867) referenced in Lea's Chemistry of Cement and Concrete 4th ed., Chapter 1 Hewlett (ed.), (1998).

Milanesi, C.A. and Batic, O.R., Cem. Con. Research, Vol.24, pp.1073-1084, (1994).

Milanesi, C.A., Marfil, S.A., Batic, O.R., and Maiza P.J., Cem. Con. Research, Vol.26, pp.1579-1591, (1996).

Moore, C.H., "Carbonate diagenesis and porosity", Developments in Sedimentology No. 46, Elsevier Science Publishers, Amsterdam, The Netherlands, (1989).

Morse, J.W. and Mackenzie, F.T, "Geochemistry of Sedimentary Carbonates", Developments in Sedimentology 48, Elsevier Science Publishers, Amsterdam, The Netherlands, (1990).

Morse, J.W., "Carbonates: mineralogy and geochemistry", Vol.11, Min. Soc. of America, Mineralogical Reviews, 2nd, (1990).

Mucci, A. and Morse, J.W., Amer. J. Science, Vol. 285, pp.306-317, (1985).

Neville, A. M., "Properties of Concrete" 3rd and 4th editions, Longman Scientific, London, UK, (1988 and 1995).

Newlon, H. H., Ozol, M.A and Sherwood, W.C.,An evaluation of several methods for detecting ACR, Report No.5, Virginia Highway Research, 71-R33, (1972).

Newlon, H. H. and Sherwood, W.C., Bulletin No.35, Highway Research Board, pp.27-44, US, (1962).

Nordeng, S.H. and Sibley, D.F., Geochem. Cosmochim. Acta 58, pp.191-196, (1994).

Nordeng, S.H. and Sibley, D.F., mentioned by Brady in personal communications at University of Bristol (1996).

Oelkers, E.H., (ed.), "Reviews in Mineralogy" Vol.34. Min. Soc. of America, pp.131-191, (1996).

Pagano, M.A. and Cady, P.D., Cem.and Con. Research, Vol. 12, pp.1-12, (1982).

Poole, A.B. and Sotiropoulos, P., Q.J.E. G., Vol.13, pp.281-287, (1980).

Poole, A.B., Proc. 5th Int. Conference on AAR, Cape Town, South Africa, (1981).

Potts, P.J., Bowles, J.F.W., Reed, S.J.B., and Cave, M.R., (editors), "Microprobe Techniques in the Earth Sciences", The Mineralogical Society Series, No.6, (1995).

Pray, L.C., Murray, R.C., (editors), "Dolomitization and Limestone Diagenesis", SEPM Spec. Publication 13, Tulsa, Oklahoma, USA, (1965).

Prince, W. and Perami, R., Proc. 9th Int. Conference on AAR, London, UK, (1992).

Prince, W. and Perami, R., the same paper as above published in Cement and Concrete Research (1992a).

Purser, B., Tucker, M., and Zenger, D., (edit), "Dolomite", Spec. Publication 21, Int. Association of Sedimentologists, (1994).

Pytkowicz, R.M., Journal of Geology, Vol.73, pp.196-199, (1965).

Rae A.M. Geochemistry, Mineralogy and Expansive properties of Carbonates from the Gull River Formation, Unpublished thesis from Brock University, St.Cathrines, Canada, (1984).

Radonjic, M., Allen, G.C., Ragnarsdottir V.K. and Livesey P., Proceedings of a 10th Int. Conference on AAR, pp.814, Melbourne, Australia, (1996).

Radonjic, M., Allen, G.C. and Elton, N., 20th ICMA, Proceedings, pp.221-231 Guadalajara, Mexico, (1998).

Reed, J.B., "Electron Microprobe Analysis and Scanning Electron Microscopy in Geology", Cambridge University Press, UK, (1996).

Reed, S.J.B., "Electron Microprobe Analysis", 2nd Edition, Cambridge University Press, (1993).

Reeder, R.J., "Carbonates: Mineralogy and Geochemistry", Reviews in Mineralogy, Vol.11, Min. Soc.of America, 2nd ed. (1990).

Reimer, L., "Scanning Electron Microscopy", Springer-Verlag, Berlin, (1985).

Robie, R.A. and Waldbaum D.R., Thermodynamic Properties of Minerals in Related Substances, Geological Survey Bull. 1259, US, (1968).

Robinson, V.N.E., 8th Int. Congress on SEM, Australian Academy of Science, (ed. Sanders and Goodchild) pp. 50-51, (1974).

Rogers, C.A. and Hooton, R.D., Proceedings. 9th Int. Conference on AAR, London, UK, (1992).

Rogers, C.A., Cement Concrete and Aggregates, Vol.8, No.1, pp.13-23, (1986a).

Rogers, C.A., Proceedings 7th Int. Conference on AAR, pp.5, Ottawa, Canada, (1986).

Rogers, C.A., Report EM-31, Ministry of Transportation, Canada, (1979).

Rogers, C.A., Report EM-92, Ministry of Transportation Ontario, (1990).

Russ, J.C., "Fundamentals of Energy Dispersive X-ray Analysis", Butterworths, London, UK, (1984).

Schmidt, V., SEPM Special Publication No.13, pp.180, Oklahoma, US, (1965).

Scott, V.D. and Love, G., "Quantitative Electron Probe Microanalysis", 2nd ed., Ellis Horwood, Chichester, UK, (1994).

Scrivener, K., "Interfacial Transition Zone in Concrete", RILEM Report 11, Chapter 1 of the report, (1996).

Shukla, V. and Baker, P.A., (eds), Sedimentology and Geochemistry of Dolostones, SEPM Spec. Publication No.43, Tulsa, US, (1988).

Sims, I., and Poole, A.B., Concrete 14 (5), pp.27-30, (1980).

Smith, M.R., and Collis, L., (eds), Aggregates, 2nd edn, Geol. Soc. Spec. Publication, No 9, The Geological Society, London, UK, (1993).

Smith, P., Highway Research Board Record, No. 525, pp.23-27, US, (1964).

Stanley, C.C., Highlights in the History of Concrete, Cement and Concrete Association, Pub. No. 97.408, London, UK, (1979).

Stanton, T.E., Engineering News Record vol. 170, pp.59, US, (1940).

Stanton, T.E., Porter, O.J., Meder, L.C., and Nicol, A., Journal of ACI, vol.13, No.3, pp. 209-236, US, (1942).

Stanton, T.E., ASTM Proceedings, Vol. 43, pp.875-905, (1943).

St John, D.A., Poole, A.W. and Sims, I.,(eds.) "Concrete Petrography- A handbook of investigative techniques", Arnold Publishers, (1998).

Stumm, W., "Chemistry of the Solid-Water Interface: Processes at the Mineral-Water and Particle-Water Interface in Natural Systems", J.Wiley and Sons, New York, (1992).

Shah, J.S. and Beckett, Micron, Vol.10, pp. 13-23, and personal communications with Dr.Shah in Physics Dept., University of Bristol, (1979).

Swenson, E.G. and Gillott, J.E., Magazine of Concrete Research ,Vol.19, No.59, pp.95-104, (1967).

Swenson, E.G. and Gillott, J.E., Vol.45, pp.21-40, Highway Research Record, (1964).

Swenson, E.G., and Gillott, J.E., Highway Research Board, Bulletin No. 45, pp.18-31, (1960).

Swenson, E.G., American Society for Testing Materials, Bulletin 226, pp.48-51, (1957).

Tang, M.S., Su-fen, H., and Shi-hua, Z., Cem. Conc. Research, Vol.13., pp.417-422, (1983).

Tang, M.S., Proc.7th Int. Conference. on AAR, pp.286, Ottawa, Canada, (1986).

Taylor, H.W.F., "Cement chemistry", Academic Press, London, UK, (1990).

The Mathers (1950), in "Handbook of Concrete Aggregates", by Dolar-Mantuani L.,(1983).

Tucker, M., and Wright, P., "Carbonate Sedimentology", Blackwell Scientific Publication, Oxford University Press, (1990).

Tucker, M., Personal communications (1998).

Udowski, H., The formation of dolomite in Central Europe, "Recent developments in Carbonate Sedimentology in Central Europe", Miller, G. and Friedman, G.M., (eds.), Springer-Verlag, Berlin, (1968).

Vaughan, D.J. and Pattrick, R.A.D., (eds), "Mineral Surfaces", The Mineralogical Society Series No.5, Chapman and Hall, London, UK, (1995).

Vicat, L.J., "Treatise on Calcareous Mortars and Cements", translated with additions by Smith, J.T., London, (1837).

Vickerman, J. C., "Surface Analysis-The principal Techniques", 1st ed., Wiley, (1997).

Vickerman, J.C., Brown, A., Reed, N.M., (eds) Secondary Ion Mass Spectrometry, Principles and Applications, Oxford University Press, (1989).

Vitruvius, Vitruvius on Architecture, vol.2, translated by F. Granger, published by William Heinemann, London, (1962).

Von Merlot, A., Ueber Dolomit und seine kuenstliche Darstellung aus Kalkstein: HaidingerNaturwiss. Abhandl., Vol.1, p.305-315, (1847).

Walker, H.N., Significance of tests and properties of concrete and concrete-making materials ASTM STP, pp.722-743, (1978).

Walker, H.N., Cement-aggregate reactions, Record No. 5525, Transport. Research Board, US, (1974).

Waltham, A.C., "Foundations of Engineering Geology", Blackie Academic & Professional, an imprint of Chapman & Hall, London, UK, (1994).

Wenk, H.R., Barber, D.J. and Reeder, R.J., "Carbonates: mineralogy and geochemistry," reviews in Mineralogy vol. 111, Min. Soc. of America 2nd ed., (1990).

Weyl, P.K., EPR Publication No. 428, Shell Development Co., 1-59, (1965).

Williams, D.A., Rogers, C.A., Report MI-145, Eng. Materials Office, Ministry of Transportation, Ontario, Canada, (1991).

Williams, D.B., "Practical Analytical Electron Microscopy in Materials Science", Philips Electronic Instruments, (1984).

Woodruff, D.P., Delchar, T.A., "Modern Techniques of Surface Science", 2nd ed., Cambridge University Press, UK, (1994).

Zachara, J.M., Cowan, C.E. and Resch, C.T., Geochem.Cosmochim. Acta, Vol. 55, pp.1549-1562, (1991).

Zimbelmann, R., Cem. Con. Research, Vol.17, pp.651-660, (1987).

Point	Na_2O	MgO	K_2O	CaO	FeO	MnO	SiO_2	Al_2O_3	SO_3
1	1.9084	11.927	.1235	45.636	.4211	.0055	2.6477	.3307	.0597
2	1.8067	19.504	.0650	39.867	.5056	.0000	1.1899	.2234	.1157
3	.4516	19.355	.0319	36.105	.1338	.0020	.1029	.0587	.2535
4	.5402	19.076	.0092	36.423	.0893	.0522	.0000	.0119	.2233
5	1.2088	18.800	.0120	37.613	.2133	.0370	.0467	.0218	.2745
6	.2961	19.505	.0256	36.539	.2122	.0086	.0000	.0000	.1805
7	.2772	18.831	.0000	35.121	.3066	.0766	.0000	.0342	.2015
8	.1799	18.599	.0095	36.616	.2136	.0010	.0000	.0000	.3024
9	.1575	18.121	.0204	37.177	.2707	.0217	.1311	.1086	.2560
10	.2041	18.298	.0307	37.156	.2538	.0018	.4243	.2338	.3587
11	.2848	17.434	.2225	38.355	.5064	.0471	1.6359	.6922	.2962
12	.3967	10.227	.2105	48.702	.3289	.0260	1.6829	.5033	.1637
13	.1832	7.7528	.1886	55.764	.2263	.0289	1.3408	.5777	.1710
14	.2388	13.078	.2057	48.124	.3600	.0000	1.6862	.6051	.1382
15	.2891	17.197	.1650	42.337	.6196	.0193	1.9129	.8456	.3141
16	.2198	18.016	.2089	37.147	.6694	.0179	1.7639	.9063	.2978
17	.2062	17.869	.1302	35.445	.7631	.0930	1.5593	.6238	.2588
18	.1674	18.546	.1721	38.518	1.1340	.0000	1.9271	1.0211	.2903
19	.2161	17.0049	.4614	34.0226	1.7629	.0768	6.5562	3.5996	.2535
20	.1437	18.2543	.2833	36.5601	1.1486	.0451	3.6312	1.6481	.3059
21	.1583	18.9305	.1677	38.1124	1.1925	.0099	2.4520	1.1612	.2644
22	.1873	19.6774	.1499	36.5820	1.1496	.0156	2.1592	.9852	.2618
23	.1044	18.2976	.1232	39.7649	1.1317	.1156	1.6000	.7581	.4230
24	.1503	19.1277	.0670	39.4204	1.1114	.0689	1.0658	.4311	.4667
25	.1102	21.0866	.0861	41.3706	1.1179	.0982	.8526	.2944	.3544
26	.1302	21.5742	.0276	41.8008	.8212	.0000	.2323	.0451	.2729
27	.0978	21.3137	.0361	41.2907	.9209	.0175	.5744	.2403	.3321
28	.0572	21.2034	.0089	42.7668	.7915	.0014	.4435	.2615	.2476
29	.0796	21.1850	.0454	41.2675	.6872	.0430	.6237	.2148	.2505
30	.0622	22.7544	.0548	40.8949	.6585	.0128	.5865	.2898	.2796
31	.0580	20.1831	.0541	39.9058	.7236	.0000	1.4039	.7572	.3920
32	.0761	20.0185	.0200	38.7767	.3825	.0000	.0519	.0032	.2280
33	.0254	23.2674	.0221	40.6906	.3768	.0806	.0000	.0153	.2549
34	.0431	22.7976	.0124	40.6447	.3780	.0538	.0000	.0178	.2573
35	.1315	20.8392	.0189	41.7083	.3806	.0138	.0000	.0066	.2731
36	.0271	21.9150	.0190	42.0996	.3589	.0000	.0000	.0234	.2389
37	.0967	21.0124	.0060	41.6502	.3462	.0370	.0000	.0475	.2962
38	.0388	20.8897	.0126	41.0894	.3406	.0000	.0270	.0268	.1712
39	.1144	21.1517	.0000	42.6761	.2365	.0000	.0171	.0415	.2131
40	.0723	21.1571	.0044	42.1136	.0712	.0000	.0370	.0021	.2478
41	.1130	21.6311	.0224	41.2234	.1816	.0576	.0229	.0088	.2580
42	.1148	21.0206	.0214	42.6364	.1686	.0214	.1052	.0197	.1863
43	.0490	22.0667	.0465	43.1751	.3561	.0430	.1277	.0514	.2038
44	.0868	20.7311	.0379	42.4679	.2541	.0411	.2987	.0499	.1746
45	.1660	21.1404	.0535	39.5122	.3781	.0831	.4448	.1432	.2049
46	.4442	18.2463	.0626	36.5875	.2996	.0000	.5748	.1639	.2142
47	.9436	13.8144	.1372	39.4833	.3967	.0000	2.3639	.5462	.1403
48	1.4556	17.4255	.2562	34.5052	1.0558	.0000	7.9688	1.8027	.1017
49	2.0622	18.2817	.2061	33.6856	.9606	.0000	5.0241	.9143	.1683
50	.9027	19.8887	.0994	37.1762	.3906	.0000	2.0693	.2983	.2170
51	.7112	18.0716	.0282	35.4926	.2480	.0000	.5236	.0443	.1874
52	.7300	17.8905	.0106	36.7278	.2947	.0000	.0440	.0000	.2569
53	.7292	18.6955	.0298	35.8066	.4024	.0234	.0000	.0000	.3068
54	.7322	18.9293	.0044	34.6128	.4134	.0000	.0156	.0000	.2130
55	.6235	18.8668	.0240	35.1214	.5847	.0587	.0000	.0000	.3278
56	2.6346	20.5062	.1162	36.1885	.3594	.0000	.5535	.2754	.1930

Table A1 EPMA analysis of semi-dissolved dolomite grains in Kingston rock Points 1-56, MR01

Point	Na2O	MgO	K2O	CaO	FeO	MnO	SiO2	Al2O3	SO3
57	2.4813	17.1947	.1123	39.0097	.8256	.0298	1.6263	.3308	.1068
58	2.0128	11.6126	.0959	39.0186	.5917	.0545	3.4245	.1253	.2207
59	1.8300	14.8067	.0871	35.3305	.5962	.0458	1.9047	.8642	.2369
60	1.4772	17.5149	.0900	35.1003	1.1956	.0341	3.9035	1.9156	.1827
61	3.5193	14.6889	.1432	25.4663	3.9479	.0315	14.6119	3.9133	.1096
62	3.9340	16.0685	.1260	29.8372	4.1574	.0590	8.7229	3.5935	.1105
63	2.3511	16.7989	.1528	36.9216	1.8334	.0373	2.0387	.8516	.1773
64	2.1510	16.5193	.1355	38.1957	1.0360	.0887	.9194	.4172	.2125
65	1.3631	14.9477	.1896	42.8939	.5654	.0000	1.1440	.3719	.1388
66	1.2384	11.1105	.1375	45.0986	.2548	.0392	.7409	.3196	.1349
67	1.3600	15.0554	.1420	38.8752	.2630	.0521	1.0437	.4997	.2332
68	1.6104	17.5304	.1149	38.6898	.2855	.0416	.7433	.4116	.4226
69	1.5200	17.7483	.1338	36.4881	.4846	.0008	1.0101	.4566	.2832
70	2.8123	15.7276	.1713	36.2895	.8849	.0000	1.7132	.5337	.2621
71	3.3776	17.9399	.2260	38.3829	1.0753	.0752	1.7653	.7336	.2581
72	5.6873	17.4233	.3762	33.7022	1.7698	.0823	3.3380	1.2582	.1867
73	5.0904	14.3397	.3679	28.0556	2.9799	.0652	7.9035	2.3383	.0914
74	7.0110	14.0259	.5471	26.2706	4.1141	.0621	12.1214	4.3431	.1153
75	4.2512	16.8438	.2599	31.2191	2.3310	.0222	6.0438	2.4187	.0651
76	4.4708	16.0105	.1500	30.2672	2.4746	.0992	8.0980	2.9161	.2540
77	5.6405	14.7774	.1559	32.7761	1.8194	.0100	6.7262	1.7664	.2505
78	5.2958	16.4612	.2031	37.8845	1.3295	.0405	4.0162	1.0619	.2652
79	6.3700	14.3338	.2201	36.7605	.8166	.0774	4.3435	1.0609	.1925
80	7.4989	15.9109	.3280	32.9915	1.0232	.0628	13.0633	2.1109	.2159
81	4.6926	13.5074	.6081	19.5260	2.0770	.0838	28.9748	3.8489	.1595
82	5.1321	13.0469	.6006	20.9981	2.2096	.0000	25.2272	3.5105	.1101
83	2.8504	16.7470	.3057	31.8630	1.0341	.0631	10.3940	1.3866	.1737
84	4.4852	16.8117	.1730	35.2334	.6011	.0568	2.3031	.5608	.2955
85	4.9570	16.3870	.1179	38.3976	1.0119	.0738	1.3532	.3826	.2011
86	2.2938	16.7951	.1677	36.3611	1.0850	.1418	1.4691	.3920	.2371
87	1.9079	15.7681	.1169	36.3604	.5896	.0148	.9826	.3431	.2109
88	1.7231	16.3094	.1536	37.4541	.6936	.0830	1.1023	.3996	.5047
89	1.0695	15.0073	.1708	37.2320	.6352	.0257	1.9030	.8282	.3570
90	.9679	15.3029	.1456	36.7567	.6588	.0953	1.8381	.8039	.3323
91	1.2060	16.1388	.1870	36.1658	1.0008	.0055	2.0206	1.0175	.1827
92	2.7778	16.4004	.2022	40.0070	.8584	.0717	1.7362	.8696	.5009
93	1.0265	15.4729	.1877	35.7721	1.7023	.0588	2.8650	1.0038	2.6954
94	.8765	11.9153	.1526	29.5772	6.8292	.0773	7.3862	2.3299	9.4372
95	.4407	11.0901	.0715	24.9121	17.7477	.0815	4.5298	1.4979	31.94
96	.5445	14.4687	.0502	25.7505	15.6239	.0890	1.6623	.3796	22.525
97	1.5738	17.2549	.0410	30.3042	6.4652	.1762	3.0453	.1646	5.7948
98	2.1100	17.8723	.0412	30.2329	4.3001	.1136	1.5993	.1349	.6377
99	3.3252	15.9697	.0424	31.5543	4.2403	.1322	.5909	.0000	.2610
100	2.1471	15.4362	.1413	32.7629	4.2681	.1333	.8484	.4099	.0891
101	2.2496	13.3251	.5518	32.0120	4.1373	.0559	3.5717	1.7836	.0619
102	2.0508	9.7661	1.7196	24.7112	3.1212	.1262	12.0043	7.9535	.0266
103	1.1872	12.6422	1.3433	30.5613	3.6453	.0839	8.8694	5.0994	.0796
104	1.1446	14.3796	.6349	31.5117	4.3276	.0804	3.2088	1.9676	.0000
105	1.7590	16.2467	.3844	33.7008	4.0626	.1243	1.7976	.9944	.0049
106	1.1609	15.2606	.2137	36.5753	1.8119	.0625	1.3997	.6057	.1603
107	.5386	17.7379	.1495	35.6788	.5954	.0642	1.5325	.5648	.1571
108	.3035	16.8729	.1754	35.5519	.3672	.0308	1.8185	.6302	.2284
109	.4360	17.0035	.2257	37.5979	.2998	.0227	1.7772	.7177	.2925
110	.2173	17.5468	.4948	34.6209	.5616	.0343	3.2943	1.3048	.1967
111	.8758	17.9711	.1304	36.3070	.2063	.0000	1.5475	.4719	.2388
112	2.0831	14.4998	.2263	25.5462	.4907	.0301	14.5269	1.1530	.1845
113	2.4931	13.6723	.2751	32.2537	1.4634	.1244	9.0120	1.2679	.1668
114	2.8770	12.5672	.5396	29.3832	3.2357	.1431	11.7189	2.7731	.0741
115	1.4799	11.8411	.4237	27.9559	3.7533	.0342	13.6226	4.2706	.0739

116	1.0242	9.1729	.4309	30.7360	1.8278	.0121	10.8550	2.4068	.1299
117	1.6701	14.2088	.4086	32.3808	2.1486	.0000	9.0669	2.3997	.1176
118	1.3653	13.6243	.4718	31.9381	1.8015	.0631	9.5231	1.9919	.1544
119	2.6485	12.5895	.5525	32.4763	1.5700	.0144	9.3097	2.2676	.1580
120	4.1804	12.1460	1.0383	29.7974	2.5694	.0230	11.1988	4.5605	.1213
121	1.6748	15.9851	.5940	34.5058	1.7095	.0561	6.8014	2.4589	.1051
122	1.2334	14.0417	.5656	32.1763	1.3753	.0100	7.7084	2.1988	.1377
123	1.9460	15.3573	.3852	36.0282	.7203	.0366	4.3557	1.2676	.1668
124	.7887	15.7603	.2413	36.5567	.5636	.0000	3.5794	.9440	.2645
125	1.4296	14.6852	.3871	35.4961	.9373	.0101	3.7274	1.5776	.1577
126	1.2783	10.0833	2.2562	25.2198	2.9175	.0310	18.6176	8.6235	.0640
127	1.0071	4.9529	3.5305	14.7167	2.5964	.0586	37.4198	17.8201	.0125
128	.8799	2.4069	2.4377	29.6814	1.3243	.0525	28.8193	13.5957	.0496
129	.8578	1.4981	2.1985	39.1219	.9501	.0000	20.6119	10.4596	.0124
130	.6336	1.4305	1.8915	43.4343	.9007	.0000	17.8267	10.1030	.0806
131	.6977	1.3910	1.2962	47.9952	.8910	.0000	13.2510	7.2106	.0000
132	.5231	2.1967	.8649	49.2795	1.0347	.0000	9.4857	4.9529	.0074
133	.5618	6.0029	.9490	34.7918	2.3044	.1816	13.1221	6.4546	.0758
134	.6184	15.2298	.3531	32.2609	4.0863	.0459	8.1966	4.0282	.0000
135	.5513	16.3317	.1615	37.2964	2.7291	.0284	1.4734	.6846	.0634
136	.3583	16.4527	.1278	34.0531	2.0899	.1488	.7138	.2765	.1119
137	1.6707	18.1772	.1431	35.4886	.8079	.0347	2.2171	1.0807	.1740
138	3.2742	17.9444	.1892	26.0656	4.0187	.0341	12.6815	5.4735	.0932
139	4.3809	12.7467	.5036	18.6588	6.9693	.0443	21.0952	9.2393	.0564
140	3.1291	3.5026	.9421	42.2696	2.0261	.0179	12.2997	6.3299	.0121
141	1.0973	1.0811	.7168	51.8407	.6175	.0000	6.2181	3.2370	.0151
142	1.3437	1.2085	1.377	47.5206	.9115	.0795	10.3604	5.5631	.0568
143	1.0790	1.0778	1.235	46.7726	.5715	.0000	11.1276	5.4010	.0540
144	1.1157	.9893	.9199	50.8412	.3478	.0290	7.0780	3.2862	.0593
145	.8531	.6957	.5258	58.6721	.2422	.0000	3.3502	1.6603	.0692
146	.9271	.6807	1.025	51.6762	.4745	.0000	7.1659	3.7754	.0376
147	1.0257	1.1210	1.368	50.3687	.5874	.0000	10.3255	5.1500	.0250
148	.9173	2.4348	2.363	31.8304	1.6374	.0133	26.0567	11.7731	.0732
149	1.0724	1.7726	1.241	41.4111	1.2875	.1085	19.1417	6.9624	.0661
150	1.3937	1.2420	.6710	52.5338	.4491	.0358	8.6811	4.1351	.0566
151	1.2680	1.1237	.5999	54.7421	.2942	.0000	5.5365	2.9150	.0262
152	.6564	.9310	.7539	52.4296	.3914	.0000	5.6082	2.8234	.0614
153	.7742	1.0412	1.012	53.9386	.3624	.0000	7.1577	3.8357	.0441
154	.4636	.8482	3.437	44.1709	.3829	.0377	16.5116	7.0538	.0380
155	.3413	.4413	6.551	36.2059	.3560	.0162	30.0871	9.5493	.0270
156	.3236	.3141	8.7502	32.2264	.3038	.0000	31.9679	10.5937	.0063

Table A2, EPMA elemental analysis of a cluster of dissolved dolomite crystals within Kingston dolomitic limestone as a result of alkaline treatment (NaOH solution) Points 57-156 MRO1

Point	Na2O	MgO	K2O	CaO	FeO	MnO	SiO2	Al2O3	SO3
157	.0122	19.5779	.0000	42.4847	.1853	.0352	.0000	.0000	.2245
158	.0085	21.3315	.0009	45.2156	.3715	.0000	.0000	.0133	.1843
159	.0543	21.2130	.0000	44.0120	.2543	.0236	.0000	.0000	.1417
160	.0642	22.1556	.0000	45.4354	.3360	.0000	.0000	.0000	.1863
161	.0536	22.7920	.0186	46.4182	.4105	.0000	.0000	.0000	.1773
162	.0198	22.3432	.0100	45.9687	.4586	.0000	.0000	.0000	.2222
163	.0856	20.7156	.0070	44.5096	.3831	.0394	.0000	.0000	.2643
164	.0689	21.6226	.0039	44.5054	.3949	.0565	.0000	.0241	.2797
165	.0713	22.3017	.0009	44.0415	.4192	.0024	.0000	.0150	.2120
166	.0163	20.8781	.0108	45.1730	.6378	.0362	.0000	.0008	.2781
167	.0869	23.0641	.0194	42.9514	.9600	.0233	.0441	.0061	.1952
168	.0415	21.8002	.0000	43.6759	.9781	.0298	.0096	.0000	.1965
169	.0605	20.9742	.0049	44.3878	.6854	.0859	.0012	.1498	.2016
170	.0844	24.9106	.0272	52.0675	1.3544	.0000	.0000	.0000	.2457
171	.0749	20.0636	.0081	43.5144	.9698	.0812	.0174	.0000	.2092
172	.0797	20.6946	.0007	43.6259	.2858	.0769	.0000	.0023	.2520
173	.0788	20.5098	.0000	44.8811	.0976	.1170	.0000	.0000	.2467
174	.1167	20.1802	.0023	41.6382	.0357	.0000	.0359	.0246	.1852
175	.1246	20.6894	.0247	42.2981	.0175	.0964	.0000	.0414	.2454
176	.0584	20.5082	.0066	41.5923	.0558	.0272	.0742	.0289	.2134
177	.0406	21.2363	.0269	41.8293	.1354	.0038	.0000	.0401	.1546
178	.0381	19.9272	.0283	41.7570	.0213	.0081	.1434	.1184	.1430
179	.0609	19.8770	.0164	44.5532	.0439	.0000	.2735	.2197	.1868
180	.0505	18.6772	.0073	41.5840	.0829	.0094	.1916	.0682	.1882
181	.0354	20.1854	.0189	42.6971	.1789	.0404	.3504	.0877	.3113
182	.0382	19.9869	.0113	44.3875	.1046	.0351	.1785	.1107	.2495
183	.0598	20.1652	.0088	43.9155	.1894	.0069	.2704	.1429	.1762
184	.0276	20.1580	.0241	40.6643	.0975	.0413	.0252	.0661	.1395
185	.0945	20.0126	.0313	43.6942	.0289	.0000	.3280	.1203	.1841
186	.0840	20.8646	.0337	43.4207	.1007	.0261	.4285	.1804	.2078
187	.0820	20.0632	.0000	44.2201	.1462	.0000	.0911	.0000	.2031
188	.0648	20.8399	.0000	44.9828	.3830	.0277	.1258	.0432	.2312
189	.0734	20.2737	.0487	42.8730	1.0104	.0698	.4406	.1612	.2544
190	.0590	19.5760	.0300	42.9882	1.2643	.0677	.3610	.1141	.2406
191	.0230	21.0877	.0342	44.1176	1.3088	.0261	.4329	.2174	.2975
192	.0780	22.0323	.0424	44.3387	1.2879	.0347	.3019	.1073	.2470
193	.0442	20.5551	.0563	43.8853	1.1093	.0168	.4691	.2945	.2107
194	.0973	21.1339	.0562	44.4000	.9603	.0085	.2659	.0622	.1216
195	.1051	22.6685	.0269	44.0400	.8713	.0692	.0631	.0115	.3343
196	.1098	20.7555	.0000	45.1638	.5384	.0000	.0733	.0572	.2251
197	.2614	20.1130	.0702	42.4498	.4667	.0000	.7760	.3823	.2284
198	.4454	20.7477	.0969	41.1602	.4659	.0407	1.1426	.5603	.2850
199	.6267	20.7392	.0887	40.7455	.6190	.0000	1.3586	.4229	.2668
200	1.3433	20.3083	.2214	36.4709	.7264	.0094	3.8805	1.0222	.1994
201	3.1212	21.7674	.4248	32.4875	2.1961	.0346	10.5639	1.6727	.1441
202	2.3330	19.2591	.3533	29.3930	1.5352	.0042	15.9533	1.4303	.1911
203	1.6086	19.7725	.1645	36.3948	.7536	.0340	2.7355	.7141	.2265
204	1.5797	20.7248	.1526	38.1703	1.0446	.0010	1.4670	.5778	.1580
205	2.8422	20.8799	.0627	39.2498	.9494	.0634	.5288	.2298	.2229
206	2.3953	21.1495	.0422	40.2948	1.0756	.0941	.2941	.1009	.2564
207	2.0474	20.5210	.0574	38.0097	1.1378	.0341	.5155	.2395	.1131
208	1.4639	19.8997	.0421	37.7202	.7263	.0250	.1651	.0179	.1509
209	1.9249	19.8168	.0251	38.2400	.6762	.0179	.0725	.0749	.1735
210	1.9547	19.7202	.0274	38.0589	1.1155	.1203	.3558	.1418	.2886

Table A3 EPMA line profile showing the Chemical composition of an unaltered dolomite grain within Kingston rock
Points 156-211, MRO1,

Point	Na2O	MgO	K2O	CaO	FeO	MnO	SiO2	Al2O3	SO3
211	.9263	19.8996	.0209	38.0379	1.1144	.1212	.5384	.1521	.2813
212	.1929	1.2353	.0114	62.9885	.0000	.0252	.0175	.0176	.0000
213	.1613	.8227	.0000	62.8375	.0551	.0801	.0760	.0000	.0287
214	.0416	.1846	.0000	66.8653	.0117	.0610	.0051	.0217	.0000
215	.0419	.1235	.0000	72.0695	.0000	.0000	.0000	.0000	.0000
216	.0647	.1044	.0038	74.2876	.0921	.0318	.0000	.0000	.0062
217	.0364	.0835	.0020	66.9146	.0619	.0000	.0000	.0000	.0386
218	.0798	.1194	.0092	72.3106	.1079	.0593	.0026	.0260	.0107
219	.0349	.0638	.0234	69.7790	.0000	.0000	.0000	.0031	.0000
220	.0856	.0910	.0000	67.8901	.0479	.0989	.0188	.0298	.0410
221	.4924	.1043	.0105	69.2187	.0024	.0283	.0000	.0349	.0007
222	.5053	.0868	.0000	71.9992	.0371	.0000	.0160	.0000	.0555
223	.1812	.2251	.0000	70.5811	.0154	.0072	.0000	.0000	.0507
224	.0379	.2347	.0260	66.3011	.0324	.0610	.0000	.0000	.0114
225	.0457	.2621	.0000	67.6286	.0704	.0000	.0000	.0271	.0000
226	.0272	.2879	.0000	70.2328	.0000	.0127	.0000	.0000	.0214
227	.0554	.2724	.0000	63.2469	.0158	.0253	.0411	.0000	.0000
228	.0886	.2813	.0000	67.9488	.0094	.0457	.0000	.0000	.0000
229	.1065	.0000	.0054	69.7850	.0048	.0456	.0000	.0000	.0000
230	.0541	.2766	.0000	69.2611	.0154	.0448	.0000	.0000	.0065
231	.0346	.2952	.0041	71.6741	.0222	.0804	.0000	.0061	.0000
232	.0665	.2998	.0126	66.9897	.0112	.0000	.0000	.0000	.0000
233	.0832	.2830	.0073	72.7226	.0209	.0507	.0000	.0000	.0000
234	.0552	.3191	.0000	78.9432	.0000	.0000	.0000	.0000	.0010
235	.0536	.2782	.0001	73.1358	.0678	.1009	.0000	.0000	.0573
236	.0000	.2603	.0000	68.9326	.0000	.0206	.0000	.0000	.0304
237	.0492	.2355	.0000	68.4511	.0253	.0194	.0000	.0030	.0041
238	.0105	.2875	.0035	69.2282	.0557	.0490	.0000	.0000	.0073
239	.0120	.2988	.0000	70.8213	.0953	.0000	.0000	.0000	.0000
240	.0000	.2838	.0087	69.2376	.0000	.0269	.0000	.0035	.0197
241	.0360	.2514	.0010	69.6296	.0000	.0938	.0000	.0000	.0256
242	.0361	.3121	.0196	68.6758	.0000	.0018	.0000	.0000	.0055
243	.0290	.2733	.0000	68.6413	.0438	.0339	.0265	.0000	.0214
244	.0261	.2725	.0117	67.6370	.0000	.0551	.0000	.0000	.0024
245	.1488	.2810	.0178	63.1743	.0494	.0373	.0435	.0523	.0294
246	.2839	.2855	.0155	65.8722	.0000	.0000	.5773	.0168	.0336
247	.3019	.4364	.0281	62.3731	.0641	.0325	2.8037	.0005	.0311
248	.0658	.6755	.0010	63.7530	.0259	.0689	.8231	.0070	.0000

Table A4 Non porous calcite matrix within alkali-treated Kingston rock
Points 211-249, MRO1

Point	Na2O	MgO	K2O	CaO	FeO	MnO	SiO2	Al2O3	SO3
249	.1458	.6533	.0101	67.6718	.0310	.0000	.1272	.0044	.0163
250	.7560	.6700	.2378	59.3842	.2076	.0000	3.7250	.6887	.0438
251	3.0229	1.9850	.9853	33.0268	.9297	.0647	38.1569	3.0284	.1438
252	4.3906	.3964	.2132	29.1424	.1867	.0429	45.8747	.5367	.0931
253	1.4291	.1768	.1813	8.9195	.1428	.0619	84.2610	.3774	.0580
254	1.5927	.3023	.4991	17.6016	.2939	.0394	65.6955	1.1481	.0977
255	3.6789	.7706	.5647	28.5361	.6127	.0000	51.0374	1.4860	.1148
256	.5219	.2949	.4823	49.2938	.5059	.0392	8.9648	.7345	.0453
257	.2835	.6766	.2831	57.4331	.1340	.0125	2.5737	1.0752	.0651
258	.7449	.8440	.4088	60.6483	.1563	.0095	2.9051	1.2850	.0131
259	.5339	.9487	.3749	59.2256	.1317	.0377	2.6570	1.1016	.0694
260	.4980	.9523	.7485	53.8668	.2824	.0712	5.7187	2.6148	.0033
261	.7382	.9631	.7038	57.3258	.2748	.0000	4.2636	2.0324	.0435
262	1.3439	.9038	.2042	59.9470	.0413	.0145	1.0512	.5051	.0846
263	1.0162	.8106	.5146	56.4115	.2205	.0665	3.4459	1.5926	.0241
264	1.4216	.9503	.5161	57.0869	.2393	.0117	3.5650	1.5617	.0383
265	.6238	.9949	.6811	54.2131	.2940	.0663	5.3428	2.8551	.0539
266	.7011	.6896	.2670	57.3974	.1428	.0549	1.8576	.7909	.1242

Table A5 Elemental composition of porous calcite matrix and Mg-phases in alkali-treated Kingston rock
Points 249-266, MRO1

Point	Na2O	MgO	K2O	CaO	FeO	MnO	SiO2	Al2O3	SO3
267	.0810	18.4388	.3129	41.0650	.1599	.0000	1.4885	.6455	.1530
268	.0245	17.5929	.8796	42.1282	.3643	.0226	5.5586	1.9740	.3320
269	.0435	18.3619	.1104	44.8920	.3007	.0000	1.2353	.4426	.2433
270	.0410	19.1597	.0641	43.9264	.2732	.0146	.7553	.3210	.2758
271	.0535	18.4803	.0592	44.6174	.5938	.1274	.5004	.1786	.1704
272	.0349	15.8516	.0785	46.4792	.5696	.0453	1.1183	.3091	.2345
273	.1431	14.6571	.1189	42.1232	.7259	.0307	5.4443	.3154	.3178
274	.0869	9.7825	.0979	53.3107	.4691	.1497	1.1237	.3692	.2321
275	.0250	6.1942	.0714	59.2896	.3353	.0069	.7302	.2602	.1988

Table A 6 EPMA obtained chemical composition of inclusions in dolomite grain within Kingston rock
Points 267-275, MRO1

Point	Na2O	MgO	K2O	CaO	FeO	MnO	SiO2	Al2O3	SO3
276	.0624	17.4217	.0340	43.2081	.1183	.0664	.1418	.0793	.1778
277	.1858	19.5951	.0912	46.1171	.1566	.0559	.4639	.2060	.2244
278	.3285	17.3909	.1295	40.4811	.1703	.0138	.8818	.3532	.2046
279	.2016	16.8163	.2256	36.6238	.1212	.0062	1.4498	.7855	.1976
280	.1222	18.1558	.0822	37.0173	.0852	.0000	.3651	.1661	.2253
281	.1286	19.4694	.0768	40.4140	.3204	.0040	.6823	.3252	.1775
282	.1178	20.5219	.1278	38.8792	.7222	.0437	1.7991	.7009	.2619
283	.1331	18.6966	.1311	40.4169	1.0464	.0000	1.4799	.2284	.1202

Table A7 EPMA line profile across a single dolomite grain within alkali-treated Kingston dolomite, showing oscillation in the amount of Si, Fe, Ca and Mg. Points 276-283, MRO1

Point	Na2O	MgO	K2O	CaO	FeO	MnO	SiO20	Al2O3	SO3
293	.7667	9.2270	.7971	35.1019	.8700	.0077	15.3661	2.3158	.0827
294	1.2084	21.4372	.3045	34.1339	.3317	.0000	.1321	.0521	.1043
295	.9946	23.0204	.1851	31.8175	.0155	.0000	.0253	.0189	.0023
296	.1957	20.8649	.0379	33.0390	.2081	.0000	.1436	.0181	4.3608
297	.2961	18.3203	.1504	22.4354	.7547	.0494	.7794	.0823	.0327
298	.2087	9.5811	2.3446	18.5161	1.2345	.0960	18.2024	5.1976	.3900
299	.6664	10.7014	2.2853	21.7749	1.5464	.2817	15.2127	3.0944	.1422
300	.5955	10.8115	.5340	6.0616	36.7474	.0802	3.2085	12.1654	.0770
301	.8463	18.5919	.1852	23.4671	.5193	.0000	2.0570	.2755	.0437
302	1.0812	21.4456	.2570	28.9151	1.6461	.0029	.3888	.3979	.0257
303	2.7590	22.1028	.6599	29.2735	.2422	.0018	1.0828	.7394	.0000
304	.6056	18.8656	.1436	21.8895	.0692	.0180	.9145	.1726	.0542
305	.3936	18.4757	.0723	21.5640	.0859	.1169	.0000	.0579	.0000
306	1.0481	19.0767	.2887	25.8852	.0397	.0000	.0000	.0940	.0271
307	1.0754	17.7988	.2404	19.2128	.1445	.0000	.3380	.0000	.0159
308	2.3436	17.3523	.1989	17.9033	.0519	.0614	.0000	.0439	.0491
309	.0930	14.4602	.1876	24.0072	.2627	.0408	1.9787	.9738	.1212
310	.4524	20.9883	.0656	30.4619	.0021	.0330	.0000	.1042	.0000
311	.4257	21.0193	.0418	27.8308	.0576	.0350	.0452	.0179	.0000
312	.1621	12.9357	1.1428	22.3658	.2475	.0799	8.2563	.9420	.0082
313	1.4114	18.9630	.1228	22.9817	.0707	.0000	.0000	.1237	.0297
314	.0000	18.7207	.0030	24.9287	.0811	.0612	.1783	.0050	.0004
315	.0990	19.8672	.0164	25.5025	.0000	.0000	.0000	.0323	.0513
316	.4250	18.4054	.0630	21.5106	.0280	.0000	.1159	.0000	.0436
317	.5947	17.6686	.0935	19.8528	.0602	.0507	.4111	.0748	.0000
318	1.1596	19.0502	.2165	26.8748	.0000	.0755	.1730	.0000	.0710
319	.6682	20.4606	.1954	29.3749	.0137	.0552	.0521	.1088	.0000
320	.1377	21.9798	.0654	29.1124	.2526	.0203	.3667	.1124	.0583
321	.3199	17.0614	.0872	15.9878	.0000	.0000	1.6027	.1492	.0346
322	1.6715	18.4276	.1795	24.8348	.1455	.1289	.4255	.5017	.0399
323	2.6113	19.3559	.2147	22.2338	.0407	.0025	.0000	.1018	.0403
324	.1792	18.1388	.0196	22.6143	.0000	.0000	.0718	.2510	.0377
325	.1615	17.4491	.2671	28.9600	.7401	.2386	2.1053	.8661	.0771
326	.0335	18.5214	.2632	27.5479	.9618	.3779	3.5668	1.5413	.0127
327	1.3072	21.0765	.1650	25.9571	.1056	.0014	.3049	.0619	.0489
328	3.0125	18.1607	.0964	17.9134	.0463	.0000	.1501	.0361	.0418
329	.8392	17.3795	.1391	18.1297	.0000	.0000	.1235	.1951	.0463
330	.3749	17.3398	13.075	19.1023	.2404	.2737	53.1841	5.1967	.0099
331	.3080	.1338	12.635	.6096	.0000	.0697	48.9196	15.4977	.0000
332	.0000	17.5392	.0749	16.1012	.1588	.0732	.3496	.8419	.0310
333	.1868	14.7191	.3994	22.7275	.4371	.0000	4.3843	1.5454	.0706
334	.4248	14.9346	.1401	16.6659	.0353	.0148	.3849	.0808	8.0431
335	1.3882	15.7128	.0754	18.5544	.0503	.0073	.3917	.8849	.0000
336	2.1346	17.9659	.1764	18.8700	.1240	.0511	.5765	.1080	.0199
337	2.1606	17.5263	.3297	21.6285	.1074	.0000	1.6922	.2582	.0000
338	2.3572	16.0410	.1788	17.2318	.0920	.0249	.4415	.4713	.0000
339	.3305	17.2328	.2005	15.6612	.1080	.0070	.2090	.0416	.0317
340	1.2910	17.4781	.1026	17.6243	.0728	.0000	.7785	.1870	.0508
341	.1203	16.3699	.0167	17.0129	.0000	.0000	.0481	.1049	.0240
342	.1661	18.0278	.3100	22.0561	.4175	.0000	3.8933	.5862	.0242
343	.1105	17.1146	.0499	18.7077	.0206	.0390	.2920	.3381	.0426
344	.1046	17.5189	.0000	22.5319	.1079	.1787	.4906	.5313	.0727
345	.0799	20.3797	.0202	25.1567	.0158	.0000	.0591	.0000	.0184
346	.3410	12.3937	3.3525	17.6105	.8465	.0000	21.4688	3.6624	.0243
347	2.1902	19.0046	.1726	21.8212	.0000	.0184	.0000	.0000	.0000

348	.9655	20.1326	.2069	25.2285	.3982	.0371	.8236	.0000	.0069
349	1.6624	18.4411	.1097	21.4286	.0286	.0772	.0153	.0000	.0487
350	1.2156	18.8648	.1658	21.9255	.0114	.0310	.0000	.0479	.0621
351	2.2157	17.4685	.2163	16.9298	.0000	.0051	.2150	.1352	.0000
352	.6348	18.0098	.0882	19.7562	.0870	.0000	.0000	.0819	.0000
353	.1534	18.0607	.0181	21.3359	.0000	.0573	.0313	.0076	.0000
354	.0186	21.7029	.0000	35.9991	.0697	.0839	.0000	.1050	.0000
355	.0647	22.3406	.0029	36.7721	.1607	.0203	.0000	.0104	.0394
356	.0376	21.6001	.0084	35.6319	1.7035	.4548	.0000	.0000	.0057
357	.2400	12.5304	.3531	26.2028	1.8214	.8371	2.6695	.6801	.1509
358	.0394	20.3284	.0000	34.0657	2.2059	1.4192	.0647	.0000	.0030
359	.0028	18.5911	.0064	34.2302	1.4465	1.1208	.0000	.0142	.0000
360	.0207	22.5736	.0000	34.8583	.0136	.0244	.0000	.0033	.0429
361	.6686	22.5671	.1546	31.9319	.0648	.1435	.3334	.1040	.0569
362	.4486	21.2972	.1398	34.5260	.0918	.0053	.0000	.0000	.0106
363	.8213	18.4132	.0435	30.2740	.0399	.0226	.0000	.0000	.1075
364	.0769	15.7273	.0700	23.8480	.1743	.0326	.5164	.4581	.1102
365	.1966	18.6718	.0211	27.6645	.1315	.0000	.0948	.3379	.0236
366	1.9233	19.4845	.3808	31.7193	.0000	.0023	.3772	.1844	.0023
367	6.2922	22.8729	.8770	32.9403	.0343	.0000	.2223	.0137	.0100
368	.1261	21.1251	.2456	34.7767	1.9038	.5516	1.4954	1.1596	.0191
369	.0017	5.5343	.0000	18.5385	.6179	.1787	.0000	.0000	.0398
370	.0108	18.5374	.0000	19.7567	1.9205	.1446	.0000	.0000	.0441
371	.0127	19.3403	.0235	25.7165	.3217	.0722	.0000	.0000	.0432
372	.4619	17.5129	.0487	25.6998	.0779	.0000	.0189	.0597	.0876
373	.0875	18.2808	.0640	23.6013	.0696	.0000	.0000	1.1647	.0000
374	.6792	20.8114	.1691	25.3963	.1052	.0000	.0280	.0000	.0520
375	1.7023	21.0213	.3139	26.5293	.0267	.0370	.0000	.0000	.0077
376	.7497	19.4100	.0733	25.1525	.0165	.0292	.0000	.0185	.0027
377	6.9233	20.2664	.6688	22.9542	.2243	.0160	2.0658	.7185	.1494
378	.8121	18.8280	.1529	22.7607	.1617	.0453	.0689	.0258	.0000

Table A 8 EPMA line profile for elemental chemical composition across the rock core of alkali-treated dedolomitised but non-expansive Nelson dolomite
Points 293-378 MRO1

Point	Na2O	MgO	K2O	CaO	FeO	MnO	SiO2	Al2O3	SO3
379	.1012	18.5074	.0049	29.0200	.0697	.0335	.0199	.0132	.0224
380	.0481	18.3826	.0597	28.5003	.0696	.0069	.2944	.0402	.0558
381	.0278	19.3768	.0184	31.9591	.0235	.0462	.0674	.0787	.0163
382	.0367	19.3618	.0721	32.4490	.0000	.0510	.4160	.3422	.0564
383	.0191	17.4074	.1593	26.6336	.9810	.0468	.8927	.5324	.1468
384	.0119	18.5539	.0119	31.2008	.0399	.0000	.0000	.0176	.0000
385	.0628	19.1571	.0037	30.8016	.0865	.1064	.0000	.0000	.0284
386	.0215	19.1287	.0205	31.5409	.1810	.0158	.0245	.0000	.0186
387	.0612	18.7597	.0000	29.3234	.1000	.0000	.0000	.0000	.0220
388	.0405	18.2723	.0092	28.6690	.0987	.0000	.0000	.0338	.0803
389	.0773	18.2741	.0404	28.7798	.0966	.0224	.2715	.2501	.0683
390	.0474	18.5773	.0035	29.7288	.0974	.0705	.0000	.0133	.1666
391	.0595	19.5779	.0303	30.9693	.0000	.0070	.0000	.0622	.0538
392	.0855	18.6321	.0221	29.7043	.0469	.0000	.0000	.0447	.0231
393	.0785	20.0303	.0110	31.3822	.1598	.0569	.0000	.1324	1.5064
394	.0648	20.4283	.0002	33.1519	.0000	.0423	.0066	.0000	.0288
395	.0697	19.2062	.0078	32.2049	.0899	.0000	.0407	.0678	.0295
396	.0399	17.2834	.1032	26.5292	.1300	.0338	.9813	1.1846	.2000
397	.0496	19.8028	.0048	30.9356	.0340	.0000	.0380	.0120	.0239
398	.0840	19.0344	.0140	30.1059	.1068	.0000	.0000	.0353	.0549
399	.0611	19.4069	.0208	31.0677	.0372	.1185	.0040	.0737	.0367
400	.2069	13.9436	1.2060	21.4636	1.0987	.0477	9.3559	3.3522	.1622
401	.0408	17.9962	.0135	30.9574	.0234	.1133	.0847	.1006	.0487
402	.0559	18.2609	.0404	26.2883	.0771	.0000	.2570	.1719	.0515
403	.0725	18.4495	.0000	27.0780	.0303	.0273	.0000	.0288	.0069
404	.1124	17.2075	.1039	26.0183	.0732	.0278	.6520	.7684	.1432
405	.1694	17.5551	.1102	27.2545	.1467	.0077	1.0389	.3698	.0298
406	.0342	18.0810	.0109	28.1026	.0463	.0000	.0200	.0000	.0714
407	.0650	18.0578	.0781	28.1691	.1753	.0501	.6575	.2536	.1035
408	.5300	17.8463	.0723	26.5346	.0000	.0000	.1105	.0753	.0312
409	.7085	18.3879	.1258	24.6246	.0397	.0000	.3374	.3960	.0426
410	.8449	19.4117	.0739	24.4028	.0700	.0550	.5797	.0853	.0166
411	2.1698	18.2807	.0862	24.8472	.1347	.0000	.2892	.0000	.0000
412	.3560	18.5034	.0939	26.8855	.0936	.0000	.6914	.0939	.0130
413	.9216	12.1584	1.0169	14.1557	.7091	.4430	12.1871	4.3779	.0049
414	.0852	17.4727	.1252	22.8905	.0551	.0512	1.1831	.1409	.0000
415	.6381	18.0880	.0855	25.5765	.1483	.0666	.0552	.0000	.0000
416	1.2326	18.7807	.1839	27.2965	.1090	.1403	.0000	.0000	.0069
417	.5228	15.6745	.1356	24.3649	.0966	.0436	.3701	.1358	.0274
418	.1479	17.9302	.1302	25.7820	.0405	.0000	1.0397	.4553	.0230
419	.1968	16.9825	4.0649	28.7123	.7911	.0000	30.2181	.6053	.0000
420	.0130	16.0515	.4980	26.9783	.4243	.1235	3.6536	.5303	.1243
421	.1484	17.8025	.0634	24.0561	.0028	.0711	.0746	.0237	.0426
422	.7736	14.4704	.2440	24.2502	.0797	.0144	1.1902	.9483	.0294
423	.5795	16.7554	.1590	22.8417	.1154	.0162	1.1388	.5927	.0146
424	1.6847	18.3581	.0974	24.8903	.0303	.0000	.5771	1.2272	.0305
425	1.3681	17.8039	.1439	21.3328	.0667	.0000	.0000	.0630	.0452
426	1.0671	16.1844	.1845	21.1775	.0607	.0259	.0620	.0000	.0000
427	.6826	16.0445	.0170	21.5521	.0348	.0000	.0271	.0000	.0556
428	.5330	15.0815	.2337	19.9613	.0961	.0000	1.1194	.0000	.0000
429	.9659	16.1848	.0401	20.1899	.0543	.0436	.0000	.0434	.0000
430	1.0291	17.3736	.2076	23.0454	.0336	.0643	.0000	.0263	.0215
431	.9410	14.9696	.0446	20.0866	.0000	.0000	.1771	.0000	.0000
432	1.1844	11.4430	.2065	19.4396	.0686	.0000	1.1794	.3837	.0592
433	1.6470	14.4032	.3005	18.7274	.0098	.0316	.7288	.1777	.0390

434	2.4265	14.8992	.1130	18.9879	.0262	.0000	.1221	.0070	.0544
435	.7317	16.1083	.0583	19.6621	.0397	.0000	.2276	.0000	.0224
436	.8195	13.8372	.0238	15.5134	.0000	.0138	.0000	.0000	.0000
437	.9435	14.0768	.0170	16.2371	.0270	.0496	.0675	.0388	.0766
438	.2275	13.3722	.1124	14.6254	.0424	.0970	.7001	3.1707	.0228
439	.6599	12.0669	.5096	14.3914	.2047	.0174	5.6738	2.5115	.0769
440	2.3797	14.6621	.1465	20.2825	.1279	.0000	1.2272	.0000	.1215
441	.4545	.1826	.0316	.9665	41.5410	.0000	.0992	.0000	112.43
442	.3205	9.4835	.2198	9.8076	12.6150	.0300	3.9654	.8405	6.5134
443	.7671	13.9119	.2268	14.8762	.0412	.0803	2.3822	.2739	.0157
444	.1662	12.3865	.1836	13.4793	.1284	.0000	1.9333	1.5926	.1039
445	.1284	14.6151	.0667	18.2449	.0336	.0018	.3981	.1274	.0967
446	1.0270	15.1783	.1165	18.1859	.0574	.0212	.7653	.0000	.0283
447	.6974	13.2569	.1459	14.1814	.0000	.0140	.5019	.1390	.0510
448	.3777	14.2864	.0530	14.9132	.0000	.0175	.0000	.0040	.0311
449	1.8679	14.6066	.2758	17.0935	.0000	.0000	.0000	.1564	.1555
450	1.8091	13.2166	.0496	13.8076	.2296	.0183	.3474	.0567	.0640
451	1.8086	14.2666	.0137	16.3809	.0000	.0000	.1957	.0861	.0815
452	.3658	14.1981	.0514	16.1934	.1305	.0063	1.0886	.1896	.0109
453	.2322	11.0290	.7355	10.7726	.8586	.0531	9.1141	1.8623	.0694
454	.1219	18.0902	.2197	29.6424	.2702	.0430	1.2666	.6140	.0000
455	.3459	14.3801	1.2407	19.2290	1.5454	.3686	9.0738	5.5144	.3163
456	.1353	17.6467	.1109	29.1064	.1333	.0899	.9364	.4722	.1133
457	.1306	17.6833	.0358	29.3926	.0712	.0140	.0794	.0204	.0344
458	.1508	11.2496	.0495	15.3927	.0385	.0621	.0000	.0832	.0845
459	.2212	16.0732	.0579	19.1499	.0183	.0679	.0000	.0000	.0562
460	.0941	16.0296	.0051	19.4157	.0000	.0000	.0199	.0256	.0127
461	.1005	15.9829	.0192	23.6108	.0475	.0257	.0000	.1196	.0480
462	.0301	4.1565	.0099	21.2272	.3366	.1040	.0000	.0000	.0213
463	.0184	.1698	.0017	14.7088	.4650	.3340	.0000	.0000	.0366
464	.0030	4.2977	.0054	12.0420	.7470	.2596	.5571	.0461	.0850
465	.0352	16.8790	.0175	20.0544	.3267	.2097	.0027	.0076	.0077
466	.0745	16.1904	.0000	19.2926	.1858	.2082	.0125	.0000	.1083
467	.0133	4.4143	.0078	15.3980	.4604	.1897	.3227	.0719	.0715
468	.0000	11.8047	.0068	14.4578	.7757	.6369	.0439	.0000	.0000
469	.0252	19.4223	.0000	26.9167	.6032	.1820	.0000	.0000	.0000
470	.0153	9.3995	.0142	23.0421	.6303	.2210	.0000	.0381	.0408
471	.0230	20.3656	.0072	24.9738	.0769	.0439	.0000	.1690	.0635
472	.0934	15.1005	.0024	15.6074	.0621	.0000	.0000	.0000	.0097
473	.0876	15.7344	.0318	15.0429	.0535	.0241	.0000	.1688	.0133
474	.0894	16.7564	.0029	20.7356	.0000	.0777	.0000	.0000	.0081
475	.0253	15.8558	.0379	13.6151	.1652	.0000	.0000	.2275	.0055
476	.1222	14.8874	.0478	14.5452	.0414	.0346	.3530	1.0060	.8760
477	.2884	13.8054	.0219	13.0492	.0777	.0000	.0000	.0814	.0430
478	.1527	15.7387	.1680	18.4659	.1303	.1460	1.8621	.3536	.0226
479	.2841	14.8816	.0588	20.0473	.0006	.0179	.3010	.1166	.0368
480	.6854	5.9879	.6785	6.7258	.1569	.0075	6.3602	2.2301	.1409
481	1.7742	18.7666	.0846	21.4898	.0391	.0000	.1613	.0000	.0205
482	5.1190	14.9957	.0327	12.8444	.0381	.0000	.0267	.0000	.0578
483	.4900	11.5783	.0236	12.5692	.0103	.0315	.4714	.0000	.0000
484	.9403	13.9170	.0105	16.3953	.0009	.0000	.0282	.0162	.0038
485	.7729	18.3730	.1290	22.6652	.0387	.0457	.0000	.1131	.0554
486	1.0227	11.6753	.0795	9.2494	.0118	.0062	.5123	.2310	.0349

Table A9 EPMA line profile from un-altered region of Nelson dolomite to the dedolomitised white outer rim of the rock core after 3years in 2N NaOH solution Points 378-486, MRO1

Point	Na2O	MgO	K2O	CaO	FeO	MnO	SiO2	Al2O3	SO3
486	1.0227	11.6753	.0795	9.2494	.0118	.0062	.5123	.2310	.0349
487	3.0641	16.9258	.1423	25.6236	.0328	.0626	.5591	.1645	.0529
488	4.9702	15.7356	.2449	20.1607	.0432	.0000	.2241	.0000	.0000
489	.9425	14.6112	.1111	18.6320	.0280	.0087	.0369	.0000	.0035
490	.4523	18.1798	.0902	25.5482	.0000	.0000	.1065	.0748	.0084
491	.6594	16.4932	.2433	24.0488	.1851	.0014	1.3397	.7566	.0707
492	.5335	16.1708	.1615	23.2389	.0255	.0000	.7634	.1087	.0008
493	.3193	16.6043	.0470	22.3356	.0768	.0000	.2620	.0127	.0000
494	.2165	16.4818	.0386	25.4117	.0590	.0127	.0000	.0000	.0000
495	.1915	10.1812	.7999	14.3248	.2600	.1132	5.8657	7.2400	.1185
496	1.0717	17.0575	.1328	22.7817	.1856	.0164	1.0510	.0219	.0258
497	.7314	14.8800	.1145	21.0728	.1665	.1069	1.4370	.4484	.0189
498	2.2974	13.2116	.6933	20.5176	.3040	.0654	5.1014	1.3547	.0847
499	.9239	15.7350	.1569	19.9894	.0000	.0775	.0000	2.0312	.1342
500	1.4953	18.4059	.0622	25.5515	.0000	.0000	.0000	.0000	.0325
501	3.9650	16.0264	.2142	23.4539	.0705	.0000	.3004	.2614	.0427
502	2.3196	16.8868	.3135	25.4257	.0148	.0000	.0000	.0672	.0764
503	2.0191	16.3023	.1590	25.4549	.0345	.0000	.0000	.1903	.0629
504	.4235	16.1297	.1186	22.7887	.0000	.0000	.1468	.0727	.0218
505	.3988	15.1834	.1162	24.2019	.0496	.0000	.0000	.1354	.0398
506	.6815	17.3290	.0558	24.5020	.0000	.0173	.0023	.0487	.0000
507	.5111	17.4720	.1697	24.4971	.4518	.1186	.8285	.5846	.0822
508	1.0949	18.3282	.0508	25.8332	.0380	.0349	.1485	.0000	.0219
509	.6997	17.5243	.1345	25.8486	.0383	.0000	.1557	.0703	.0175
510	.6842	18.9524	.2734	27.4086	.0000	.0995	.0000	.0000	.0633
511	4.3558	18.2067	1.1272	25.3777	.0000	.0626	.0000	.0248	.0157
512	1.5545	21.1660	.4220	25.6480	.0349	.0368	.7612	.0706	.0394
513	.1263	19.1155	.0534	24.2227	.0842	.0000	.1522	.1433	.0465
514	.0000	19.7385	.0041	27.5137	.0719	.0000	.0000	.0797	.0615
515	.0641	19.0801	.0074	27.6755	.0000	.0102	.0000	.0000	.2870
516	.0441	21.0935	.0025	33.3626	.0237	.0000	.0000	.0190	.0398
517	.0253	20.0133	.0129	33.4306	.0191	.0896	.0000	.0203	.0079
518	.0368	20.1313	.0000	33.4782	.0572	.0452	.0383	.0094	.0216

Table A 10 EPMA line profile showing the chemical composition within intermediately reacted reaction rim of Massachusetts dolomite known to be semi-expansive when treated with alkaline solutions an as concrete aggregate Points 486-518, MRO1

Point	Na_2O	MgO	K_2O	CaO	FeO	MnO	SiO_2	Al_2O_3	SO_3
519	.0356	18.3649	.0006	32.0697	.0534	.0000	.0000	.0062	.0947
520	.0890	20.4990	.0062	34.3466	.1114	.0125	.0000	.0422	.0197
521	.0833	22.4994	.0141	37.1269	.0591	.0357	.0000	.0045	.0000
522	.0314	22.5620	.0047	37.3358	.0915	.0028	.0000	.0000	.0000
523	.0970	22.1775	.0150	36.8585	.1265	.0000	.0044	.0000	.0291
524	.0920	21.9786	.0000	36.7506	.1121	.0000	.0404	.0000	.0000
525	.0913	20.2277	.0169	35.3310	.1322	.0444	.0000	.0000	.0000
526	.1017	22.3593	.0000	37.3003	.0754	.0000	.0000	.0168	.0087
527	.0637	22.5161	.0000	37.4136	.1051	.0000	.0010	.0000	.0227
528	.0846	16.6171	.0086	33.3070	.2196	.0000	.0731	.0000	.0000
529	.1158	21.2283	.0062	36.4519	.1975	.0000	.0233	.0000	.0000
530	.0634	3.8270	.0207	29.8965	.0569	.0000	.8530	.1695	.0878
531	.2055	14.0834	.0178	30.8976	.1146	.0661	.1540	.0443	.0064
532	.2121	20.6331	.0038	35.0508	.1712	.0000	.2163	.0000	.0235
533	.0879	16.9173	.0103	35.7795	.1661	.0114	.3386	.0866	.0000
534	.1197	6.6171	.0000	30.9298	.1486	.0271	.0000	.0000	.0434

Table A 11 Chemical composition of non-porous dolomite grains within Massachusetts aggregate, Points 519-534.

Point	Na2O	MgO	K2O	CaO	FeO	MnO	SiO2	Al2O3	SO3
43	0	0	0	28.3466	0.0289	0	0.056	0.6278	0
44	0.0033	0	0.0054	31.9563	0.1176	0	0.0619	0.2353	0.0208
45	0.0018	0	0	32.2797	0.1567	0.0236	0	0.1891	0.011
46	0.0043	0.0053	0	31.8889	0.1245	0	0	0.1721	0
47	0.0015	0.0013	0	31.6888	0.1304	0	0.0633	0.0764	0
48	0.0062	0.0004	0	31.0797	0.1097	0.0149	0.1684	0.2081	0.0074
49	0.0175	0	0	31.1858	0.1355	0.0555	0.1356	0.249	0.0196
50	0	0	0.0013	31.4466	0.1689	0.0341	0.0955	0.2558	0
51	0	0	0	31.4028	0.0984	0.0519	0.0452	0.17	0
52	0.0024	0.0017	0.0024	32.0267	0.128	0	0	0.1539	0.0114
53	0.0192	0	0.0081	32.0713	0.1295	0	0	0.1377	0
54	0.0203	0	0.0026	31.9148	0.1536	0.0551	0	0.1541	0.0294
55	0	0.0017	0	32.4527	0.1173	0	0	0.1472	0
56	0	0	0	31.6543	0.1869	0	0.0091	0.1521	0
57	0	0	0	31.3032	0.0855	0	0	0.2939	0
58	0.0097	0	0	30.9225	0.0469	0	0	0.1104	0.0029
59	0	0.0009	0.0029	31.7117	0.122	0	0	0.1612	0
60	0.0144	0	0.0059	30.6827	0.1365	0.0192	0.0258	0.1742	0.0003
61	0	0.0005	0.03	20.4897	0.4233	0.049	1.3174	0.1261	0.1743
62	0	0	0	29.8773	0.1764	0.0003	0.1171	0.4786	0.0475
63	0.0125	0	0	31.4867	0.033	0.0652	0	0.1173	0.0322
64	0	0	0.0002	25.7441	0.1353	0.0103	0.1142	0.1078	0
65	0	0	0	28.6363	0.1172	0.0033	0.0039	0.1646	0.0554
66	0.0105	0.0022	0	29.7702	0.0683	0	0.0869	0.0837	0.0012
67	0.0046	0.0024	0.0034	27.521	0.1155	0	0.0916	0.6548	0.0272
68	0.0131	0	0.003	31.5326	0.1335	0.0541	0.0475	0.2518	0.0266
69	0	0.0025	0.0099	33.0553	0.0193	0.0815	0	0.2492	0.0181
70	0	0	0.0083	34.0705	0.0475	0.0434	0	0.061	0
71	0	0	0	33.3745	0.0838	0.0701	0	0.0525	0.0004
72	0.0154	0.0049	0	32.9306	0.0973	0	0	0	0
73	0	0.0052	0.0127	33.3324	0.0735	0	0	0.1016	0.0028
74	0	0.0038	0	33.5565	0.0374	0	0	0.143	0
75	0	0	0.0092	33.2105	0.1674	0.0801	0	0.1071	0
76	0	0.0026	0.0033	33.3461	0.0159	0	0	0.0953	0
77	0	0	0.0078	33.7895	0.1112	0	0	0.0262	0.0088
78	0	0.0017	0.0048	32.5724	0.2536	0.1283	0.1103	0.1444	0.0536
79	0.0225	0.0063	0	31.3265	0.0773	0.052	0.1031	0.1053	0
80	0.0036	0	0.0035	33.1528	0.0813	0.0489	0.0116	0.1359	0.0106
81	0.0203	0	0	33.9716	0.0538	0.0056	0	0.1006	0
82	0	0.0023	0	33.5719	0.0788	0.0781	0	0.0579	0.0341
83	0	0	0	32.7278	0.0263	0	0.0146	0.1252	0.0046
84	0.0055	0	0	32.859	0.1352	0.0001	0.0593	0.0224	0.0022
85	0	0.0053	0	32.2055	0.1957	0.0678	0	0.0087	0
86	0.0025	0	0.0004	33.3603	0.1365	0.0707	0	0.0581	0
87	0.0064	0	0	33.383	0.0325	0	0	0.1228	0
88	0.0003	0.0046	0	32.3849	0.02	0.0611	0.0926	0.1002	0
89	0.0015	0.0045	0	33.0979	0.2298	0	0	0.0446	0
90	0	0.0044	0	33.4234	0.0624	0.0017	0	0.0737	0.0008
91	0	0.0039	0	33.1592	0.0705	0	0.0055	0.1297	0.0317
92	0	0	0	33.1202	0.1235	0.0048	0	0.1137	0
93	0	0	0.0167	33.4944	0.0999	0.0352	0	0.0592	0.0295
94	0.0131	0.0039	0	33.479	0.1441	0.0178	0	0.1354	0
95	0	0.0065	0	33.2546	0.083	0.0522	0	0.0291	0.0217
96	0.0019	0	0.015	23.8114	0.143	0	1.9739	0.5116	0.1557
97	0	0	0.0109	16.3684	0.1139	0.059	0.0785	0	0.0045
98	0	0	0.0015	26.3235	0.0895	0	0	0.2516	0
99	0.0112	0.0061	0	22.9561	0.1244	0	0.1108	0.3397	0.0133
100	0	0.0054	0.0026	24.8558	0.1072	0.0218	0	0.2879	0.0481

101	0.0076	0.0027	0	24.0429	0.1325	0.0321	0.0113	0.4187	0
102	0	0.0025	0	23.9414	0.2669	0	0.5178	0.3789	0.0071
103	0	0	0.0087	24.7514	0.173	0	0.0455	0.4169	0.0071
104	0	0.0054	0.0106	22.4093	0.0966	0.0207	0.6734	0.4672	0.0177
105	0.0005	0.0053	0.0076	22.8522	0.2039	0.0542	0.4226	0.5131	0.0372
106	0	0	0	27.7364	0.1353	0.0057	0.622	0.3622	0.0148
107	0	0.0061	0	28.9028	0.1492	0	0.27	0.0271	0
108	0.0067	0	0.0137	25.2473	0.123	0	0.5982	0.3789	0.0191
109	0	0	0.0111	24.774	0.2142	0.044	0.9271	0.7353	0.0574
110	0.0143	0.0018	0.0194	23.8344	0.4649	0.0493	0.9217	0.7281	0.0954
111	0	0.0001	0	22.1155	0.3096	0	0.7716	1.0258	0.0942
112	0	0	0	31.34	0.0665	0.0117	0	0.1416	0
113	0.0015	0	0	31.9305	0.1922	0.089	0	0.1065	0
114	0	0	0	31.7924	0.1603	0	0	0.0821	0
115	0.0033	0.0013	0.0022	31.6799	0.0972	0.0094	0	0.0755	0.0342
116	0	0.0023	0.0014	31.7259	0.096	0	0	0.0595	0.0197
117	0	0.004	0	31.5383	0.0817	0.0295	0.0165	0.0553	0
118	0.0067	0.0029	0.0114	31.4904	0.1246	0.0395	0.0023	0.1049	0.0237
119	0	0.0007	0.0121	32.0767	0.0123	0.0241	0.0385	0.0746	0
120	0	0.0011	0.0076	32.2659	0.1518	0	0	0.0749	0
121	0	0	0.0063	31.7671	0.0854	0.0499	0	0.0438	0.0536
122	0.007	0	0	31.1003	0.1563	0	0.0384	0.1324	0
123	0.0019	0.0001	0.0056	31.643	0.078	0.105	0.023	0.0757	0.0027
124	0	0.0046	0	31.2927	0.0537	0.0355	0	0.0622	0.0123
125	0	0.0047	0	31.457	0.0964	0.0317	0.0202	0.0549	0.0059
126	0.0117	0	0	31.7805	0.097	0	0	0.0692	0
127	0	0	0	31.7759	0.0943	0.0474	0	0.0487	0.0017
128	0	0.0032	0	31.7866	0.1279	0.0252	0	0.0097	0.0114
129	0	0	0.0004	31.3749	0.0941	0.0904	0	0.0863	0
130	0	0	0.0109	31.7492	0.0915	0	0.0361	0.0615	0
131	0	0	0	32.0076	0.0359	0	0.0033	0.0717	0
132	0	0.0007	0	31.3115	0.0667	0.1044	0.2207	0.097	0.0141
133	0.014	0	0.0065	30.8171	0.0979	0.1056	0.099	0.1408	0.0171
134	0	0.002	0.0025	29.7468	0.0572	0	0.0544	0.1242	0
135	0	0	0.0067	31.3629	0.1254	0.0204	0.3196	0.1839	0
136	0.0042	0.0066	0.0089	31.1111	0.1313	0.0288	0.2531	0.1242	0
137	0	0.0068	0.0023	31.7786	0.1565	0.0648	0.0347	0.0492	0
138	0	0.0032	0	31.0272	0.1011	0.0306	0	0.0151	0.0236
139	0.0096	0.0318	0	32.0429	0.1561	0.0011	0	0.0193	0.0136
140	0.0149	0.0606	0.0123	32.2861	0.1475	0	0	0.0948	0.017
141	0	0.1068	0	31.8323	0.0481	0.0159	0.0258	0.0539	0.0221
142	0.0115	0.1411	0.0123	30.2486	0.0894	0.0068	0.0486	0.0347	0.0707
143	0	0.1965	0	29.6168	0.22	0	0.0548	0.0609	0.0524
144	0.0006	0.3993	0	26.2979	0.3352	0	0.2844	0.2558	0.0342
145	0.0343	0.3686	0.0029	21.5504	0.3385	0.0413	0.4559	0.1007	0.0385
146	0.0201	0.3659	0.0197	24.9122	0.3946	0.0192	0.1238	0.021	0.0689
147	0	0.5872	0	26.3784	0.2968	0.005	0.0996	0.0319	0.0659
148	0.0105	0.8027	0.0081	26.3027	0.1349	0.049	0.052	0.0472	0.0445
149	0	1.235	0	28.3496	0.2751	0	0.1199	0.0626	0
150	0.0111	1.8278	0.0087	29.8685	0.2872	0	0.037	0.0561	0.0948
151	0.033	2.1443	0.0041	27.2467	0.1566	0.0246	0.0768	0.0966	0.1032
152	0.0113	2.8676	0.014	26.8242	0.1401	0	0.0889	0.1372	0.0116
153	0.0279	2.9796	0	28.4993	0.1619	0.0716	0.0085	0.086	0.0587

Table A13 EPMA line profile of semi-reacted region within alkali treated Massachusetts dolomite
Points 44-153, MRO2

Point	Na2O	MgO	K2O	CaO	FeO	MnO	SiO2	Al2O3	SO3
1	0.008	8.564	0.0103	33.213	0.1163	0	0	0.0132	0
2	0	6.2711	0.014	32.515	0.0495	0.0591	0.0002	0.0048	0.0547
3	0.017	4.7794	0	33.205	0.1156	0	0.0099	0.0198	0.0248
4	0.0112	3.5146	0.0176	31.864	0.192	0.0689	0.1537	0.0506	0.0172
5	0	2.4621	0	32.151	0.0913	0	0	0.0352	0
6	0	2.0805	0.0057	32.2921	0.0671	0.0014	0	0.0658	0
7	0	1.5098	0.003	32.5141	0.151	0.0214	0	0.0433	0.0114
8	0.0081	1.266	0	30.3006	0.1245	0.0254	0	0.2026	0
9	0.0033	0.2603	0.0045	25.2207	0.021	0	0.0799	0.0165	0.0199
10	0	0.0721	0	26.3759	0.2933	0	0.2189	0.0183	0.0111
11	0	0.155	0	31.7768	0.0837	0	0	0	0.0132
12	0.0057	0.0442	0	30.9055	0.0659	0.0171	0.0011	0.0448	0.0339
13	0.0129	0.0087	0	31.6507	0.0699	0.0241	0.1032	0.1001	0
14	0.0001	0.0118	0	31.7214	0.0604	0	0	0.0229	0.0073
15	0	0	0	31.9076	0.1119	0	0.0404	0.0395	0
16	0.0005	0	0.0059	30.142	0.294	0.0025	0.0068	0.1929	0
17	0	0	0.0072	30.2992	0.2418	0.0582	0.0774	0.0439	0
18	0.0009	0	0.0021	31.8598	0.0587	0.065	0.0226	0	0
19	0	0	0	32.2224	0.0587	0	0	0.0337	0
20	0	0	0	32.3335	0.0887	0.0915	0	0.0343	0.0074
21	0	0.0051	0	32.5442	0.1209	0.0276	0	0.0146	0.0413
22	0.0117	0.0016	0.0013	30.784	0.1071	0	0.0751	0.0728	0.0286
23	0.0014	0.0002	0	32.1899	0.1145	0	0	0.0381	0
24	0.0005	0	0.0102	32.0846	0.0997	0.0661	0	0.0522	0.0609
25	0	0.0003	0	31.9888	0.1073	0.0224	0	0.1083	0
26	0.0163	0	0	32.5424	0.1067	0.0451	0	0	0
27	0.0039	0.0044	0	32.0969	0.0456	0.027	0	0.0768	0
28	0	0	0	32.1408	0.0304	0	0.0289	0.0571	0
29	0.0066	0.0052	0.0045	32.3885	0.0612	0	0	0.0962	0.0133
30	0	0	0	33.2242	0.0979	0.0474	0	0.1035	0
31	0.001	0	0.0059	32.9255	0.1743	0.0494	0	0.1052	0.0252
32	0	0	0.0059	30.8968	0.0993	0.0148	0	0.0627	0.0459
33	0	0	0.0194	23.7161	0.1033	0.1037	0.0831	0.5655	0.0655
34	0.0019	0	0.0008	29.9783	0.1618	0.0229	0	0.5217	0.0084
35	0	0.0058	0	30.7133	0.1985	0.0916	0.0206	0.2337	0.0438
36	0.0126	0.0016	0.0007	30.3648	0.058	0.0886	0.045	0.0765	0.0141
37	0.0024	0.0025	0	30.7932	0.0267	0	0	0	0
38	0.0019	0.0025	0.012	28.8983	0.151	0.0301	0.0831	0.0544	0.0174
39	0.0057	0	0	29.3571	0.1015	0	0	0.1295	0.0106
40	0	0	0	32.5272	0.1488	0.0425	0	0.0216	0.015
41	0	0.0024	0	31.6916	0.0113	0	0.0256	0.0932	0.0334
42	0.0188	0	0.0057	32.8149	0.1402	0.0222	0	0.1287	0.0094

Table A 12 EPMA line profile showing the chemical composition within peripheral dedolomitised rim of semi-reacted Massachusetts's rock after alkaline treatment
Points 1-43 MRO2

Point	Na2O	MgO	K2O	CaO	FeO	MnO	SiO2	Al2O3	SO3
154	0	4.642	0	29.762	0.0993	0	0	0.0842	0.0392
155	0.0027	22.8818	0.0027	31.7563	0.1763	0	0	0.0277	0
156	0.2506	22.971	0	28.9138	0.1461	0.0672	0.011	0	0.0732
157	0.0089	22.5787	0	33.8447	0.0865	0.0094	0	0.0458	0.0007
158	0.0641	21.973	0	33.196	0.1204	0	0	0.0131	0.0054
159	0.0128	22.1483	0	34.024	0.2017	0	0	0	0
160	0.0271	22.2805	0	34.198	0.0799	0.0087	0	0	0.002
161	0	22.1	0	33.7584	0.0658	0.0108	0	0	0
162	0.0111	22.0479	0.0112	33.7955	0.0742	0	0	0	0.0097
163	0.1674	21.0221	0.0154	32.5819	0.041	0.0021	0.0394	0.0376	0
164	0.4566	19.8737	0.0123	37.7995	0.062	0.008	0.0158	0	0.0465
165	0.037	22.3994	0	33.9033	0.0526	0.0208	0	0	0.003
166	0.1657	22.4005	0	33.3335	0.0968	0.0467	0	0.0326	0.0174
167	0.046	16.0137	0.0096	32.6058	0.0909	0	0	0.0126	0.0359
168	0.0078	24.3522	0	31.3614	0.0657	0	0.0317	0	0
169	0.0637	21.2332	0	30.0657	0.0554	0.0883	0	0	0.0131
170	0.016	15.8093	0	31.0919	0.1206	0.0952	0	0	0
171	0.0177	23.1631	0	33.0703	0.0873	0	0	0	0
172	0.0046	22.7168	0.0001	33.9867	0.1877	0.0525	0	0	0.005
173	0	22.2433	0	33.3746	0.1475	0	0	0	0
174	0.3789	7.9369	0.0113	37.8222	0.0587	0.0323	0.0115	0	0.0605
175	0.2932	17.8286	0.009	38.8872	0.1062	0	0	0	0.0684
176	0.1824	46.2162	0	23.142	0.2876	0	0.1412	0	0.0885
177	0.2485	20.7253	0.0142	38.5062	0.1587	0.092	0	0	0.0294
178	0.2588	24.1704	0	45.8261	0.092	0.0521	0.0641	0	0.0729
179	0.3966	2.8983	0	55.5892	0	0	0	0.0113	0
180	0.3736	22.043	0	45.509	0.082	0	0	0	0.067
181	0.2613	32.3697	0	35.1156	0.228	0.0029	0.0064	0	0.0111
182	0.3194	15.2063	0.0007	48.8695	0.1075	0.0368	0.0692	0	0
183	0.1407	19.1214	0.0029	48.7218	0.0786	0	0	0.009	0
184	0.2314	43.1142	0	33.6706	0.2577	0	0.0442	0	0.0108
185	0.2723	0.9882	0	56.1518	0.0144	0	0.0406	0	0
186	0.1383	64.3493	0	9.5608	0.4092	0.0742	0.0979	0	0.078
187	0.0601	73.2748	0.0034	11.598	0.401	0.0432	0.0422	0.0345	0
188	0.2766	23.3209	0.0116	42.3182	0	0.0505	0	0.0084	0.0399
189	0.302	6.0242	0.01	52.3163	0.0732	0	0	0.0139	0.0124
190	0.1569	53.793	0	25.8564	0.2868	0.0409	0	0	0
191	0.0894	58.662	0	12.2698	0.2937	0.0494	0.0474	0.0106	0.0366
192	0.0785	53.9347	0.0007	21.4115	0.2862	0.0871	0.0003	0	0.0105
193	0.1593	47.2277	0.0079	24.9038	0.3343	0	0	0	0
194	0.2623	23.6481	0.0055	39.2876	0.1938	0	0	0	0
195	0.2594	19.0276	0	44.4879	0.0642	0	0.0931	0	0
196	0.3841	10.6759	0.0048	51.565	0.0151	0.0804	0.0146	0	0
197	0.1749	29.059	0	35.3139	0.1785	0	0.0006	0.0149	0.0237
198	0.2778	41.588	0.0148	36.0216	0.1027	0	0.0505	0	0
199	0.2954	41.5252	0	32.8144	0.1742	0.0513	0.0423	0	0
200	0.2751	30.4256	0.005	36.0826	0.2779	0.0693	0.2046	0.0341	0
201	0.3175	18.4793	0	47.8602	0	0.0313	0.0041	0.0073	0
202	0.1959	9.4554	0	49.2319	0	0	0	0	0.0095
203	0.3863	11.8309	0	49.2963	0.059	0.038	0	0	0.0271
204	0.2181	23.8265	0.0046	42.7346	0.2583	0.0121	0	0	0.014
205	0.3384	4.7064	0.0134	55.1232	0	0.078	0	0.0013	0
206	0.3944	7.5439	0	53.2875	0.0386	0	0	0	0
207	0.285	21.4673	0	46.1954	0.0653	0.0205	0.0197	0	0.0531
208	0.3436	0.7481	0	57.6952	0.0406	0.0453	0	0	0
209	0.3158	15.6128	0.0033	48.7145	0	0.0563	0.0397	0	0.0223
210	0.2336	25.003	0.0044	37.9751	0.1266	0.1	0.0507	0.0023	0.0161
211	0.1674	22.3862	0.0115	35.75	0.1245	0.049	0.0346	0.0199	0.0442

212	0.1743	12.2916	0	51.4038	0.0148	0	0.066	0.0042	0
213	0.517	9.982	0.0187	52.917	0.0567	0.0189	0	0	0.0458
214	0.2915	40.5657	0.0132	24.8034	0.3378	0	0	0	0.0025
215	0.2717	36.9536	0	34.5324	0.1944	0	0	0.0128	0.0412
216	0.1911	28.5257	0.0052	36.4897	0.1487	0	0.007	0.0231	0.0545
217	0.2874	26.1313	0.0114	34.3438	0.135	0.0932	0.1216	0.0064	0.0816
218	0.2612	32.4263	0	37.8958	0.1855	0	0	0	0.0065
219	0.266	26.3424	0.0031	39.8975	0.2027	0	0.0583	0.0104	0.0733
220	0.3149	26.4179	0.0069	41.346	0.0987	0.0576	0	0.0171	0.0027
221	0.2752	19.8325	0	34.1355	0.1455	0.0332	0	0.0376	0
222	0.2367	39.8281	0.0051	29.95	0.2669	0.0321	0.0546	0.0145	0
223	0.2432	29.4296	0	39.447	0.0959	0.0483	0.0278	0.018	0.0268
224	0.3	22.9289	0	43.6713	0.03	0	0.0211	0	0
225	0.2799	48.263	0.0026	26.8171	0.3364	0.0849	0.0666	0	0
226	0.2598	26.9892	0	38.6911	0.1276	0.128	0	0	0.0146
227	0.2182	48.8263	0.0026	26.3384	0.2456	0	0.074	0	0
228	0.4108	18.3589	0	44.9454	0.0292	0	0	0.015	0
229	0.2339	14.4294	0.0009	47.8214	0.0668	0	0	0	0.0428
230	0.4913	18.9613	0.0195	43.5089	0.154	0.0073	0.0983	0.0714	0.063
231	0.0973	42.9295	0.0043	26.6756	0.2619	0	0.0417	0.0002	0.0457
232	0.2079	28.166	0	34.1079	0.2086	0	0	0.0176	0.0037
233	0.2109	17.3079	0	46.1223	0.1293	0.0671	0	0	0.0103
234	0.1558	45.1416	0	24.7973	0.251	0.0041	0.0771	0	0.0287
235	0.2151	21.2004	0.0059	40.2616	0.1309	0	0.0563	0.0113	0.0094
236	0.2139	30.5186	0.0089	38.3273	0.1289	0	0	0.0073	0.0336
237	0.2406	18.5364	0.009	45.9079	0.0505	0.0715	0	0	0.0117
238	0.3202	0.7783	0.0081	56.7823	0	0.0292	0	0.0165	0
239	0.2817	9.7003	0.0023	49.6434	0.1245	0	0.0507	0	0.0402

Table A14 Almost un-altered region within alkali-treated Massachusetts dolomite Points 154-239, MRO2

Point	Na2O	MgO	K2O	CaO	FeO	MnO	SiO2	Al2O3	SO3
240	0.2963	21.5427	0	43.4257	0.1601	0.0512	0.0392	0	0.0213
241	0.2298	17.0477	0	50.7479	0.0961	0	0	0	0.0412
242	0.2854	27.5152	0.0059	44.9106	0.1323	0.0437	0.0939	0	0.0109
243	0.2482	36.9791	0	34.5057	0.1255	0.0377	0	0.0095	0
244	0.3542	23.2003	0.0007	44.2211	0.108	0.0076	0.0408	0.0035	0.0154
245	0.4119	21.314	0	48.7448	0.0743	0.0639	0	0.0034	0.0148
246	0.3344	27.6273	0.0095	44.0222	0.0493	0.0777	0	0	0
247	0.2869	22.888	0	47.1788	0.0886	0.0113	0.0411	0	0.008
248	0.1965	45.0381	0.0021	29.9995	0.2474	0.1181	0	0.002	0.0118
249	0.1984	39.5908	0.0017	31.2904	0.1377	0.0138	0.0022	0.0401	0.0277
250	0.3439	9.7933	0.0298	52.7259	0	0.0423	0.0191	0	0.0465
251	0.3169	4.2104	0	58.0915	0.0475	0	0.0197	0	0
252	0.3417	5.9006	0	58.4071	0.0186	0	0	0	0.0031
253	0.2179	6.9765	0	58.6782	0.0037	0.1137	0	0.015	0
254	0.2908	9.6541	0	57.574	0.0516	0	0	0	0.0265
255	0.3161	27.6707	0	47.704	0.1762	0	0	0	0
256	0.1682	50.7758	0.0104	31.451	0.2877	0	0	0.0221	0
257	0.1941	39.6889	0.0222	35.8949	0.0992	0.0189	0	0	0.0542
258	0.3091	12.6667	0.0061	50.6598	0.0881	0.0154	0	0	0
259	0.3563	6.1477	0	56.243	0	0.0633	0	0.0098	0
260	0.3416	21.1562	0.0102	48.9333	0.1035	0	0	0.0068	0.0379
261	0.3027	17.0095	0.006	48.4866	0.0495	0.0224	0.0461	0	0
262	0.3451	11.0121	0.0107	51.1734	0.0381	0	0	0	0.0172
263	0.2259	18.2199	0.0011	51.7055	0.0941	0.0342	0.0461	0	0.019
264	0.2214	19.0306	0	50.258	0.004	0.026	0.0277	0.002	0
265	0.2475	33.8145	0	43.1589	0.1565	0	0.0061	0.0082	0.0826
266	0.2309	53.162	0.0131	26.6972	0.2477	0.0357	0	0	0
267	0.1787	37.002	0.0013	38.3204	0.0894	0.0683	0.013	0	0.0584
268	0.2861	14.7506	0.0014	54.325	0.1268	0.0514	0	0.0196	0.0461
269	0.347	25.1031	0	48.3667	0.1182	0	0	0	0.0051
270	0.3167	29.2938	0	41.7775	0.1739	0.0895	0.0338	0	0.0248
271	0.2272	37.0003	0	35.4064	0.0959	0	0	0.0365	0.0571
272	0.2401	36.7255	0.0146	32.8166	0.175	0.0182	0.0217	0.0368	0.008
273	0.2396	26.6344	0	39.5735	0.0888	0	0	0.0588	0.0235
274	0.3002	20.9329	0	47.8327	0.0479	0.0053	0.0397	0.0175	0.0655
275	0.1989	28.4345	0	41.8929	0.1524	0.1013	0.0679	0	0.0143
276	0.2426	13.1665	0	52.517	0.0016	0.0161	0.0257	0	0
277	0.1904	26.9217	0	47.2406	0	0.0477	0	0	0
278	0.1678	40.2647	0	31.2495	0.35	0	0	0	0.0282
279	0.2743	18.5762	0	50.4866	0.0963	0.0254	0	0	0.0254
280	0.2193	38.7228	0	35.7639	0.256	0.0057	0.0545	0	0.0233
281	0.2759	21.5773	0	47.7541	0.0409	0.0859	0.0179	0	0.0041
282	0.3025	19.6096	0.0077	49.697	0.1466	0.0465	0	0	0.0513
283	0.5163	13.2904	0	52.2254	0.0497	0.1026	0	0.0053	0.005
284	0.4298	13.9742	0	51.8327	0.1099	0.0053	0.0023	0.0067	0.0198
285	0.3952	28.2999	0	44.3003	0.1665	0.0658	0.0229	0	0
286	0.4856	13.105	0	55.0357	0.0209	0	0	0.0015	0.039
287	0.412	17.2029	0.0041	50.5279	0	0.0544	0	0	0.018
288	0.2584	24.0981	0	44.4102	0.065	0	0.0588	0	0.0254
289	0.2725	22.1784	0	44.0598	0.1135	0.0143	0.0421	0.0081	0
290	0.1944	19.1697	0	42.6026	0.0455	0	0.0131	0	0
291	0.3377	7.6244	0	53.4859	0.0285	0.0178	0.0099	0	0
292	0.1847	5.1869	0	58.4553	0.0584	0.016	0	0	0.0627
293	0.3006	5.2421	0	56.6025	0.006	0	0	0	0.0384
294	0.1194	2.7561	0	58.2455	0.0532	0	0.0141	0	0.0205
295	0.0815	6.9596	0.0002	56.4282	0.0726	0.0137	0.0453	0	0.0269
296	0.1649	2.7669	0	54.9404	0.67	0	0.1722	0.0556	0.0372
297	0.2852	2.2552	0.002	43.3312	1.8718	0.01	0.2794	0.0285	0.1246

298	0.0373	2.3682	0	40.7827	0.713	0	0.0252	0.0084	0.0167
299	0	0.8663	0.0033	41.1702	0.8881	0.0306	0.0339	0.0124	0.0021
300	0.0159	0.3733	0	40.134	0.1731	0.0869	0.0126	0	0
301	0.0073	0.3023	0	35.4554	0.6338	0	0.0024	0	0.0234
302	0.0033	0.7648	0	33.9195	1.0247	0.0205	0.014	0.0265	0.0035
303	0.1136	4.8676	0.0149	45.2719	0.52	0	0.0919	0	0.0244
304	0.1382	1.8457	0.0067	53.8947	0	0.0284	0	0.0265	0.0374
305	0.2008	0.5271	0.0005	56.3714	0	0	0	0	0
306	0.1676	0.3606	0	58.4808	0.0611	0.001	0	0	0
307	0.1162	0.1837	0	59.5289	0	0	0	0.0012	0
308	0.1911	2.1444	0	58.5588	0	0.024	0.0026	0	0.0124
309	0.1681	17.4204	0	51.2549	0.3072	0.0396	0	0.006	0.029
310	0.1429	19.5106	0	47.9178	0.1336	0	0.1703	0	0
311	0.134	16.3064	0.0015	48.6406	0.2045	0.0037	0.0696	0.0357	0
312	0.0646	35.0275	0.0048	24.6723	0.5318	0.0669	0.1829	0.0125	0.0203
313	0.075	41.9157	0	10.9217	0.5647	0	0.1528	0	0.0349
314	0.0567	44.3131	0.0037	11.3967	0.7057	0.0113	0.0684	0.0572	0.0666
315	0.1321	63.4657	0	12.3658	0.4725	0.0936	0.0701	0.0952	0.0623
316	0.175	60.4886	0.0124	20.5	0.3161	0.1133	0.0922	0	0.1168
317	0.2498	35.0518	0.0078	34.0452	0.184	0.1471	0.0484	0	0.0736
318	0.27	27.844	0	33.6097	0.1495	0	0.0818	0.0255	0.1182
319	0.2412	27.3805	0.0133	34.8979	0.2656	0	0.116	0.0507	0.0379
320	0.2256	29.4096	0.0035	35.038	0.1974	0	0.1382	0.0119	0.0401
321	0.2764	27.1314	0	38.4796	0.1802	0	0.0761	0	0.0278
322	0.2157	27.9723	0	42.1056	0.1105	0.0036	0	0.0153	0.0505
323	0.339	24.4259	0	43.4082	0.1769	0	0	0.0067	0.037
324	0.3948	11.5625	0	51.2809	0.1186	0.0166	0	0	0.0471
325	0.3833	3.0096	0.0111	55.8491	0	0.1087	0	0	0.0066
326	0.2389	2.9124	0	59.6696	0	0.0218	0.0098	0	0.0533
327	0.444	35.8945	0	36.1241	0.213	0.0883	0.0398	0	0.0226
328	0.2527	44.43	0.0013	27.5188	0.2128	0.0541	0	0	0.0191
329	0.3459	20.7528	0	45.4148	0.0457	0	0	0	0.0003
330	0.2949	17.2468	0	50.2071	0.0865	0.0061	0	0	0.0274
331	0.3261	8.8285	0	53.5896	0.0087	0.0713	0	0	0
332	0.318	8.436	0.0153	53.4838	0.0524	0.0454	0	0	0.017
333	0.2892	23.8913	0.0101	45.8932	0.191	0.0501	0	0	0.0167
334	0.2681	27.5976	0	43.9218	0.0571	0.0172	0	0	0
335	0.3285	24.6785	0	45.0677	0.0781	0.0419	0.0476	0.0098	0.0537
336	0.2609	24.3156	0	43.4446	0.1474	0	0	0	0.0793
337	0.266	13.9647	0	50.0523	0.069	0.0553	0	0.006	0.0627
338	0.2886	5.3261	0.0135	56.7776	0	0	0	0	0.0335
339	0.2232	9.7268	0	54.6643	0	0	0	0	0
340	0.2666	16.1209	0.0107	51.4459	0.1363	0.0049	0	0.0117	0
341	0.3386	9.8742	0	53.935	0.0545	0.024	0	0	0.0023
342	0.3156	2.1313	0.5083	9.5399	1.1804	0.4113	9.6806	2.2362	0.1792
343	0.1099	0.4596	7.7002	0.9094	0.1932	0	37.1969	11.1007	0.0078
344	0.4658	5.5352	1.2193	7.8912	1.0327	0.1034	10.2593	3.6173	0.2356
345	0.3522	5.4083	0.7574	10.6744	1.2541	0.2044	9.9353	3.5407	0.2438
346	0.0571	6.7168	0.0584	15.3597	0.1732	0	0.2891	0.1025	0.0622
347	0.0679	7.0183	0.0342	15.5309	0.0132	0.0509	0.393	0.1912	0.0714
348	0.037	6.7543	0.01	15.7067	0.1704	0.0347	0.0574	0.0633	0
349	0.0718	6.2484	0.0172	15.1656	0.2001	0.0036	0.3742	0.1508	0.045

Table A 15 EPMA line profile showing the chemical composition of porous fibrous material within discoloured reacted rim in Massachusetts dolomite
Points 239-349 MRO2

Point	Na2O	MgO	K2O	CaO	FeO	MnO	SiO2	Al2O3	SO3
401	0.0462	8.7244	0.0395	19.285	0.0604	0.0094	0.2692	0.194	0.0377
402	0.2536	4.2513	2.6331	5.7943	1.9479	0.0362	11.4078	4.4509	0.1444
403	0.1041	9.0172	0.0605	16.7864	0.3096	0.1397	1.9329	0.3638	0.0746
404	0.1018	8.3496	0.139	16.9583	0.4101	0.0556	2.2209	0.5628	0.076
405	0.0425	9.1147	0.0276	19.3306	0.0584	0	0.079	0.0496	0.0436
406	0.2255	6.1781	0.3225	16.7453	0.3431	0.0985	3.2857	1.6034	0.083
407	0.2043	6.828	0.9516	14.407	0.4938	0.0901	7.5473	3.5458	0.0936
408	0.0241	8.8745	0.0328	18.7941	0.066	0.045	0.069	0.0511	0.0265
409	0.0499	7.4077	0.0198	17.7998	0.0973	0.0789	0.0813	0.0289	0.025
410	0.0366	8.8301	0.0131	19.7892	0.0522	0	0.0313	0.0423	0.0577
411	0.1266	8.1648	0.1266	18.4792	0.5141	0.0568	1.656	0.5407	0.0483
412	0.0623	7.921	0.0428	18.4301	0.2719	0.0743	0.4308	0.2439	0.0812
413	0.0842	8.5442	0.0485	19.0043	0.153	0.0387	0.1803	0.0838	0.0362
414	0.1687	1.8343	0.8763	17.4744	0.7516	0.3668	12.9924	3.8477	0.173
415	0.0083	4.3294	0.0149	17.4358	1.6496	0.7167	0.0829	0.0506	0
416	0.0227	4.8658	0.0082	17.8623	0.8322	0.2801	0.0784	0	0.0706
417	0.0002	6.4321	0.0154	18.4177	0.7639	0.1296	0.0085	0.0126	0
418	0.0423	8.454	0.0122	19.2723	1.8492	1.1678	0.0393	0.0199	0
419	0.0291	8.6034	0.0561	18.6943	0.1005	0	0.3479	0.1914	0.0471
420	0.0453	9.001	0.0335	19.3373	0.1192	0.0706	0.1076	0.0524	0
421	0.269	8.439	0.4786	25.0089	0.4677	0.094	14.3494	2.4473	0.0824
422	0.3719	3.2238	0.4162	38.96	0.8185	0.0367	21.3813	2.7641	0.1379
423	0.3304	1.047	0.3661	45.4466	0.4454	0.0363	9.022	1.5819	0.1096
424	0.5567	0.9352	0.4624	46.937	0.7528	0.0094	6.9977	1.0642	0.0389
425	0.7707	0.6837	0.2886	46.5631	0.1211	0.0171	2.4126	1.1841	0.065
426	0.452	0.7352	0.2736	47.2304	0.1681	0.0012	2.7311	1.5426	0.0688
427	0.2874	0.848	0.6599	40.2941	0.967	0.0267	5.5466	1.6618	0.1011
428	0.2839	0.7738	0.304	44.2548	0.3326	0.0682	3.1001	1.6246	0.0801
429	0.2214	1.1386	0.5284	40.3647	0.6423	0	7.4194	4.2323	0.1233
430	0.241	1.1048	0.48	42.4629	0.7828	0.0949	8.6988	4.2951	0.1202
431	0.2539	1.4129	3.5954	21.9108	1.0574	0	24.5706	10.2265	0.0716
432	0.2998	0.7501	1.9198	28.0389	0.7731	0	13.5538	5.0386	0.1396
433	0.2556	0.5478	0.751	29.53	0.4899	0.0099	9.7534	5.1138	0.0991
434	0.38	0.5264	0.3592	33.911	0.5365	0.0869	7.9066	4.208	0.0262
435	0.4762	0.6567	0.4284	39.3952	0.3881	0.0645	3.8863	3.427	0.0054
436	0.3325	0.519	0.3493	44.3561	0.3638	0.0249	3.2338	2.3126	0.0559
437	0.8206	0.6045	0.228	46.7542	0.016	0.0477	1.4838	0.702	0.106
438	0.5803	0.7148	0.263	49.5772	0.1781	0	2.2111	1.1158	0.064
439	0.594	0.8753	0.4052	47.5157	0.3713	0.0796	4.3373	1.6782	0.0429
440	0.4235	0.8751	0.3676	48.3156	0.4007	0	6.21	2.4857	0.042
441	0.4818	0.9363	0.1563	48.1163	0.082	0.0888	0.761	0.5295	0.0758
442	0.4501	0.966	0.1479	51.4731	0.0856	0	1.5805	0.9348	0.0269
443	0.5093	0.7637	0.0685	49.6886	0.044	0	0.305	0.2324	0.0391
444	0.5586	0.7303	0.0578	51.2625	0.0062	0	0.3392	0.1941	0.0959
445	0.3253	0.7024	0.0947	48.7466	0.05	0.0692	0.2156	0.1839	0.095
446	0.2608	0.8251	0.0887	50.2843	0.0886	0	0.4783	0.2039	0.0731
447	0.3137	0.9432	0.0835	50.5848	0	0	0.2028	0.2137	0.093
448	0.3033	0.9777	0.0604	52.4591	0.0299	0	0.1316	0.1851	0.0772
449	0.2586	0.7474	0.0661	47.8269	0	0	0.1202	0.0987	0.0788
450	0.2123	0.8465	0.0837	51.551	0.0204	0.0529	0.3582	0.1292	0.0267
451	0.2195	0.95	0.082	52.8951	0.0011	0	0.3176	0.1166	0.1044
452	0.2389	0.7936	0.0481	53.4327	0.0127	0	0.1743	0.0322	0.039
453	0.2288	0.6391	0.0761	54.3589	0.0163	0.0249	0.3121	0.1392	0.1077
454	0.256	0.8411	0.081	55.4605	0.0275	0.0725	0.2529	0.1462	0.0957
455	0.3634	0.8609	0.0739	53.6539	0	0.0079	0.1701	0.1277	0.0251

456	0.2943	0.8914	0.0904	53.1855	0.0755	0.0155	0.4203	0.186	0.0489
457	0.3281	1.1883	0.2385	53.9657	0.0429	0.0299	1.1214	0.3068	0.0833
458	0.1681	0.5288	0.0334	49.0933	0.0994	0	0.0004	0.0061	0
459	0.0715	0.3229	0.031	51.2181	0.0237	0	0.0257	0.0574	0
460	0.0724	0.5117	0.016	54.7807	0.0458	0.0106	0.0629	0.015	0.07
461	0.0476	0.4577	0.0129	56.1021	0	0.0535	0	0.0424	0.0265
462	0.0971	0.576	0.0383	52.0284	0	0.0707	0.0485	0.0344	0.0499
463	0.1204	0.7029	0.0248	54.4026	0.0492	0	0	0	0.0594
464	0.0719	0.6318	0.018	55.4596	0.0919	0	0	0.005	0.011
465	0.0745	0.6789	0.0275	55.7632	0	0.0303	0	0	0.1231
466	0.1217	0.6763	0.0302	55.9033	0.1116	0	0.0918	0.0406	0.0471
467	0.6972	0.6214	0.0159	54.8981	0	0.0091	0.0511	0.0514	0.0696
468	1.0945	0.5726	0.0297	55.5107	0.0712	0	0.0318	0.0256	0.0222
469	3.0228	0.0732	0.0207	56.2561	0.0362	0	0.0404	0.0789	0.0286
470	0.0962	0.4102	0.0135	47.0656	0.1109	0	0.0172	0.0036	0.0435
471	0.1694	0.5136	0.0076	48.2015	0.0504	0.0079	0.0788	0	0.0454
472	0.0781	0.5197	0.0273	49.4923	0.1366	0	0.0482	0.023	0.0564
473	0.1269	0.593	0.0255	50.1496	0	0.0625	0.0199	0.0383	0.0166
474	0.1079	0.6675	0.0595	50.9733	0.0575	0	0.2231	0.0511	0.0182
475	0.0836	0.7647	0.0233	53.0873	0.0796	0.009	0	0.0014	0.0351
476	0.1074	0.7877	0.0221	53.2248	0.0371	0.0375	0.0559	0.0021	0.0804
477	0.0587	0.8166	0.0249	53.1205	0	0	0.0798	0	0
478	0.0925	0.7864	0.0283	53.2561	0.0674	0	0	0	0
479	0.1858	0.8719	0.0176	55.3728	0.0154	0	0.0382	0.0347	0.0853
480	0.1028	0.8169	0.0185	55.5835	0.0703	0.0075	0.004	0.0269	0.0274
481	0.0871	0.7241	0.0215	55.8665	0.025	0	0	0.0464	0.0429
482	0.1262	0.5806	0.0234	48.2413	0	0.0185	0.0109	0.0078	0.0741
483	0.1511	0.5959	0.0154	46.9066	0.0111	0.0406	0.0029	0.0335	0.1033
484	0.1071	0.6129	0.0214	48.5103	0.0469	0	0.0805	0.0167	0.0473
485	0.1713	0.6727	0.0189	50.7251	0.0987	0	0	0	0.0469
486	0.0509	0.6749	0.009	53.1142	0.0172	0	0	0.0002	0.0917
487	0.0667	0.7304	0.0071	54.2937	0	0.0403	0.0282	0	0.058
488	0.0772	0.5435	0.0365	52.1378	0.0405	0.0378	0	0.0201	0.0555
489	0.0617	0.3656	0.0203	48.7961	0.0087	0.0043	0	0.0361	0.0764
490	0.1034	0.4939	0.0136	47.6104	0.0539	0.0141	0.0386	0	0.0645
491	0.0933	0.505	0.0183	50.3311	0	0	0.0127	0	0.06
492	0.0929	0.5352	0.0035	51.8581	0.029	0.0554	0	0.0037	0.0213
493	0.0472	0.4247	0.01	51.067	0	0.0084	0.0074	0	0.0273
494	0.0871	0.4372	0.02	52.7247	0.1202	0	0.0246	0.0301	0.024
495	0.0599	0.6025	0.0081	52.4396	0	0.0044	0	0.0068	0.0417
496	0.0642	0.3953	0.0118	49.1039	0.0633	0.0682	0	0	0.0182
497	0.0793	0.5084	0.0092	51.6643	0	0	0	0	0.057
498	0.0485	0.5416	0.0246	52.9261	0.0149	0.0011	0	0	0.0716
499	0.0572	0.5247	0	53.5706	0	0	0	0	0.0372
500	0.1179	0.5941	0.0113	50.2805	0.0736	0.0329	0	0.0424	0.0547
501	0.0804	0.5527	0.0102	51.4599	0.0029	0	0	0	0.021
502	0.1142	0.6227	0	52.3855	0.0256	0	0	0	0.0423
503	0.087	0.5919	0	52.2905	0	0	0	0.0566	0.0463
504	0.1241	0.6377	0.0015	53.4217	0	0	0	0.0086	0.0562
505	0.0943	0.5662	0	52.5122	0.0766	0	0.0113	0.0195	0.0728
506	0.0914	0.4849	0.0132	49.8761	0.1348	0	0	0.0245	0.074
507	0.0878	0.5959	0.01	50.9163	0.0498	0	0	0.004	0.0484
508	0.0727	0.6265	0.0128	48.8088	0.1449	0	0	0	0.0104
509	0.094	0.7489	0.0062	51.4363	0.0332	0	0.0151	0.0137	0.0428
510	0.1266	0.6818	0.0037	50.9055	0.117	0	0.1147	0	0.021
511	0.0569	0.7176	0.0178	52.2507	0	0.0473	0	0	0.0275

512	0.0764	0.484	0	50.3862	0	0.0043	0	0	0.0309
513	0.0414	0.4344	0.0228	51.8255	0.0197	0.0252	0	0.0293	0.0416
514	0.0389	0.6589	0.0133	51.94	0	0	0	0	0.0319
515	0.0958	0.5732	0.0029	51.2322	0.0148	0.097	0	0.0226	0.0431
516	0.0481	0.6588	0.0053	51.1822	0	0.0266	0.0096	0.0122	0.042
517	0.0882	0.5671	0	52.5889	0.0675	0.0483	0	0.0023	0.0914
518	0.0663	0.6522	0.0129	52.8762	0.0485	0	0	0	0
519	0.0825	0.6232	0.0157	52.3253	0	0.0178	0	0	0.0132
520	0.0701	0.5806	0	52.2161	0.0748	0	0	0	0.0183
521	0.0867	0.5441	0	51.4613	0.0645	0.0591	0	0	0.0778
522	0.0762	0.6209	0.0118	52.2466	0.0954	0	0.0099	0	0.1102
523	0.0891	0.5888	0.0029	52.1005	0.1187	0	0	0.0147	0.018
524	0.0848	0.5435	0.0266	52.6554	0.0018	0.0033	0	0	0.0284
525	0.0619	0.5189	0.0164	51.7582	0.046	0.0127	0	0	0.0118
526	0.0711	0.4849	0.0229	53.4538	0.0846	0.0793	0	0.0208	0.0352
527	0.1421	0.5922	0.013	52.281	0.0388	0	0.0398	0.0022	0.0226
528	0.1088	0.5413	0.008	52.2693	0.0513	0	0	0	0.0376
529	0.0979	0.5391	0.009	51.1779	0.0097	0.0632	0	0.0746	0
530	0.1049	0.4826	0.0089	52.9541	0.087	0.0957	0	0	0.038
531	0.1321	0.629	0.0038	52.4602	0.0771	0	0.0153	0	0
532	0.1852	0.7736	0.0244	50.7685	0	0	0	0.0262	0.032
533	0.126	0.7057	0.0159	52.2891	0.055	0	0	0.0533	0.0338
534	0.1191	0.682	0	54.197	0.0458	0.0714	0	0.0061	0.0174
535	0.0796	0.5162	0.0047	49.4668	0.1828	0	0	0.0444	0.0544
536	0.1245	0.6669	0.0038	52.9572	0.0556	0	0.0478	0.0806	0.0626
537	0.0869	0.5891	0	53.3363	0.0858	0.0421	0	0.0047	0.0357
538	0.0679	0.5798	0.0203	53.7073	0.1376	0	0	0.0266	0.0125
539	0.0642	0.5802	0	53.9586	0.0121	0	0	0	0.0373
540	0.0842	0.7425	0.0045	54.1431	0.0599	0	0	0.0055	0.0458
541	0.0584	0.6098	0.0147	52.4013	0.0506	0	0	0	0.0777
542	0.0357	0.4589	0	52.4427	0.1724	0	0.011	0	0.0074
543	0.0749	0.5877	0.0038	52.3749	0.0466	0	0	0	0.0459
544	0.0367	0.4307	0.0038	50.6122	0	0.0635	0	0.0043	0.0534
545	0.027	0.5382	0.0199	49.8214	0	0.0575	0	0.0144	0.035
546	0.0463	0.5841	0.0115	53.0141	0.0306	0	0	0	0.0079
547	0.0317	0.6209	0.0044	54.4137	0.0381	0	0	0.0097	0
548	0.0708	0.5501	0	56.0358	0.0165	0.0522	0.044	0	0.0878
549	0.0613	0.6245	0.0177	55.7675	0.1195	0	0	0.0489	0.0394
550	0.1328	0.5951	0	45.4573	0	0.0252	0	0.017	0.0768
551	0.0789	0.5241	0.0074	47.3631	0.0065	0.0478	0	0	0.0338
552	0.1087	0.5323	0	50.2828	0.0405	0.0085	0	0.0339	0.0585
553	0.086	0.5407	0.0059	51.584	0.0322	0.0039	0	0.0058	0.0261
554	0.0239	0.3708	0.0173	50.982	0.0614	0.0047	0	0	0
555	0.1952	0.1179	0.0157	39.2804	0.0064	0.03	0.0058	0.0894	0.0125
556	0.1867	0	0.009	50.5206	0.0184	0	0	0	0.0625
557	0	0.8127	0.0022	52.1395	0	0	0	0	0.0379
558	0.1481	1.4773	0.0092	52.8946	0.031	0	0	0.0029	0
559	2.4578	1.7403	0.0111	52.0388	0	0	0.1193	0.0168	0.0434
560	0.0559	0.5267	0	50.4261	0.0339	0.0116	0	0.0272	0.0909
561	0.023	0.5613	0.0162	50.7707	0.0486	0	0	0	0.1027
562	0.1032	0.5389	0	44.2666	0.1243	0	0	0.0759	0.1071
563	0.0655	0.4798	0.0055	47.3429	0	0	0	0.0642	0.0359
564	0.0675	0.5296	0	49.1668	0.0307	0.0546	0	0	0.0081
565	0.0429	0.5145	0	49.4815	0.0279	0	0	0	0.0462
566	0.1051	0.6008	0.0059	49.5845	0.0482	0.0363	0	0	0.0824
567	0.0155	0.5914	0.0024	51.3711	0	0.022	0	0	0.0746

568	0.0863	0.6013	0.022	52.191	0.0012	0.0755	0	0	0
569	0.0097	0.5819	0.0165	53.3698	0	0.0271	0	0	0
570	0.0897	0.5573	0.012	51.6302	0.0409	0	0.0508	0	0.0155
571	0.1051	0.4914	0.0128	52.5123	0.0837	0.0096	0	0	0.0845
572	0.0536	0.3717	0.0062	47.939	0.0094	0.0592	0.029	0	0.0486
573	0.1141	0.4613	0.0079	44.7163	0.1169	0.0339	0.0625	0	0.0189
574	0.132	0.5105	0.0047	47.2425	0.1183	0	0.0362	0	0.0355
575	0.1153	0.4602	0.007	48.2268	0	0.0203	0	0	0.0382
576	0.0618	0.535	0.0135	49.8743	0.0631	0.0128	0	0.0238	0
577	0.0987	0.5336	0.0097	50.9753	0.0134	0.0567	0	0.0412	0.0418
578	0.0474	0.6773	0.0109	54.3711	0.0093	0	0	0.0265	0
579	0.0998	0.4799	0	45.665	0.0617	0.0145	0	0.0437	0.0309
580	0.0678	0.4687	0	45.3495	0.0524	0	0	0.0711	0.0929
581	0.0685	0.3805	0.0025	44.6549	0.134	0.0065	0	0.1203	0.0537
582	0.0617	0.4672	0.0059	48.6947	0.1105	0	0	0.0518	0.0832
583	0.0309	0.3817	0.0152	48.6263	0.0288	0	0.0076	0.0267	0.0529
584	0.0476	0.4272	0	49.8344	0	0	0	0	0.0378
585	0.0444	0.5107	0.008	50.5113	0.0482	0	0	0	0.0117
586	0.0547	0.636	0.0001	50.0255	0.0756	0.0917	0	0.0321	0.0384
587	0.1299	0.4995	0.0129	45.2913	0.0231	0.0633	0	0	0.0072
588	0.0554	0.4881	0.0135	42.1635	0.0111	0.0137	0	0.0383	0.021
589	0.2421	0.5867	0.0228	48.3255	0.0183	0.0043	0	0.034	0.0694
590	0.0618	0.684	0.0054	53.6761	0	0.0178	0	0.0224	0.0407
591	0.0555	0.7027	0.0056	55.37	0	0.0304	0	0	0.0291
592	0.6436	0.3001	0.0061	43.1461	0	0	0	0	0.0298
593	0.0853	0.6661	0.015	56.7533	0.0233	0.0487	0	0	0.0542
594	0.1266	0.5501	0.0105	43.2465	0	0.0405	0	0.0073	0.0241
595	0.1811	0.5445	0.0221	45.8863	0.0173	0.0071	0	0	0.0341
596	0.0617	0.2793	0.0174	46.9414	0.1176	1.4399	0	0.0478	0.004
597	0.5346	0.5701	0.0245	48.8328	1.4463	0.2751	0	0	0.0579
598	0.106	0.5668	0.0075	53.2008	0	0	0.0115	0.0087	0.0355
599	0.0368	0.7147	0.0047	55.5989	0.0186	0.0755	0	0.1104	0.072
600	0.29	13.3374	0.0147	29.747	0.1854	0.0269	0	0.0611	0.2603
601	0.3206	13.3273	0.02	31.2473	0.2275	0	0	0.0684	0.2848
602	0.2107	13.3855	0.0211	29.0554	0.2924	0.0344	0	0.055	0.3253
603	0.3002	12.6793	0	25.8356	0.5314	0	0.1188	0	0.2881
604	1.0618	14.1528	0.0017	29.3209	0.7676	0	0	1.9489	0.2789
605	0.0369	14.3343	0.0142	34.4822	0.4663	0.0195	0.0008	0.0428	0.1936
606	0.0034	14.3475	0	32.8662	0.7302	0.0803	0.0008	0.0408	0.31
607	0.0291	14.0998	0.0108	34.9041	0.9186	0.0952	0	0	0.1123
608	0.0453	13.6072	0.0014	34.3681	0.2081	0.0093	0	0.0037	0.1227
609	0.9091	11.7759	0.0849	30.3009	0.7699	0.0531	0.7796	0.4796	0.0193
610	0.1551	0.4624	0.0002	51.07	0	0	0	0.0044	0
611	0.0231	0.5234	0.009	46.5311	0.0649	0	0	0.0161	0
612	2.8549	0.3823	0.0077	46.3195	0.0574	0.0328	0.0311	0.1634	0
613	1.1827	0.5341	0.0083	47.2397	0.1529	0.0086	0	0.042	0
614	1.4223	0.4874	0	47.816	0.0307	0.0544	0.2806	2.2126	0.0818
615	0.602	0.526	0	51.6447	0	0.0336	0	0.0581	0.0475
616	0	0.4914	0	51.5847	0.1442	0	0	0.0112	0
617	0.0255	11.8205	0.008	33.852	0.3963	0	0.1708	0.0303	0.1094
618	0.053	15.3171	0.0057	34.9288	0.2022	0.0878	0	0.0161	0.2311
619	0	12.3158	0	35.3733	0.8646	0.0962	0	0.0294	0.2087
620	0.0578	15.8653	0.0125	34.9133	0.0405	0	0.042	0.042	0.2829
621	0.0315	15.7609	0.0083	33.5184	0.0388	0.0549	0	0.0613	0.2205
622	0.0041	13.3358	0.0011	35.289	0	0.0048	0.1113	0.0228	0.2271
623	0.023	14.4	0.0515	32.7662	0.4057	0.054	0.9342	0.4134	0.1797

Y

624	0.0342	13.6932	0.0042	34.4553	0.5185	0.0046	0.0171	0.0619	0.2811
625	0.0308	13.3143	0.0708	33.1525	0.5473	0.0739	1.0199	0.5817	0.2771
626	0.2554	11.2277	0.0879	27.5071	0.1072	0	0.7619	4.0222	0.1263

Tab A17 EPMA line profile showing the elemental distribution within discoloured dedolomitised white outer rim (Ca rich), within alkali-treated non-expansive Nelson dolomite
Points 401-626, MR02

UNIVERSITY OF BRISTOL LIBRARY